THE RARE EARTH ELEMENTS AS NATURAL ANALOGUES FOR THE ACTINIDES

CRAIG ALEXANDER FANNIN

A thesis submitted in partial fulfilment of the requirements of the Liverpool John Moores University for the degree of Doctor of Philosophy

1999

for my father, who didn't quite see this to the end

Acknowledgements

I would like to thank EPSRC and BNFL for the case award funding this project. Rob Edwards, Jack Pearce from LJMU and Eugene Kelly and Matt Randall from BNFl for their supervision and advice throughout the project. Art during the FIA development, (even though it would have been nice to have the option with the ICP). Nicola Dempster and her dream team for assistance with the XRD, FTIR and TGA analysis.

Dave Phillips at Lightworks for supplying the bits for a PC, without which all the modelling and preparation for Vail would not have happened. Nick Pearce and Richard White from Aberystwyth University for the offer and help with ICP-MS analysis, without which, this project would not have been completed.

Tim Dintinger, Graham, Bill and Chris for keeping me sane during my time in Liverpool particularly with the wine Keith supplied. Sarah for dragging me out of Liverpool, doc Dave for reading the intro in between beers, Becky for supplying info for the intro, then Stuart for bankrolling the odd event.

and finally my family and friends who had to put up with the endless complaints from the last few years which allowed me to finish

don't worry its not a train, just a candle in an alcove

Abstract

The Rare Earth Elements (REE) or lanthanides are a series of 14 elements which follow lanthanum in the periodic table, which form the M^{3+} ion in naturally occurring systems (except Ce, which can exist as Ce^{4+}, and Eu as Eu^{2+}). The group is characterised by a decrease in ionic radii across the series from La to Lu. The actinide elements, the series which follow actinium in the periodic table, have a similar though more significant ionic radii contraction with increasing atomic number, resulting in a similar ionic radii to the lanthanides in the same oxidation state. The actinides, which also occur in the M^{3+} state e.g. Am, Cm and Cf, have also been found to form the suite of solid phases as found for the lanthanides in the carbonate-pH system. Predictions about the chemical properties of the radioactive actinides Am and Cm, can therefore be drawn from a careful study of the lanthanides and be extrapolated to model actinide solubility over the lifetime of a nuclear waste repository (>10^5 years).

The REE-Na^+-K^+-CO_3^{2-}-OH^- and the REE-Na^+-K^+-SO_4^{2-}-OH^- systems were investigated in the laboratory using a combination of aqueous titrations and batch equilibrium techniques to determine the solubility limiting phases that precipitate. The solubility limiting phases were isolated and identified by XRD, FTIR and elemental analysis. The stability constants of the phases were determined by measuring the concentrations of REE in solution, after equilibrium, using flow injection UV , fluorescence and ICP techniques.

Stability constants for the following phases were determined, $REE_2(CO_3)_3.xH_2O$, $REECO_3OH$, $REE(OH)_3$, $NaREE(CO_3)_2.6H_2O$, $REE_2(OH)_4SO_4$, $NaREE(SO_4)_2$ and CeO_2. A study of the published stability constants showed a wide variation in data, primarily due to methods of preparation of the solid phases. The wide variation between published values for the REE hydroxy phases were of particular concern, although these can be explained in terms of crystallinity. The stability constants were used to construct stability field diagrams, and predict stable phases under conditions of pH, Eh, carbonate, sulphate and sodium activity. From these diagrams and associated aqueous data, REE solubility in aqueous solution was modelled.

Published solid phase and aqueous species databases, compiled for modelling nuclear waste aqueous reactions (e.g. using the programme PHREEQE), were critically reviewed. The two databases examined, NEA 9 and CHEMVAL 6, showed significant differences between REE solid phases and aqueous species. Some equivalent REE species to those of the actinide analogue, Am, are also omitted. Suggestions are made to improve the databases and model REE solubility in complex natural solutions.

Aqueous REE, below their solubility limit in carbonate or sulphate solution can be further removed from aqueous solution by sorption reactions with mineral surfaces.

Contents

Glossary

Actinide	**the 14 elements (Th-Lr) following actinium in the periodic table**
Am	**americium, element number 95**
An	**general symbol for any or all actinide elements**
Ce	**cerium, element number 58**
Cm	**curium, element number 96**
Eu	**europium, element number 63**
Lanthanide	**the 14 elements (Ce-Lu) following lanthanum in the periodic table**
Ln	**general symbol for any or all lanthanide elements**
Nd	**neodymium, element number 60**
PHREEQE/PHREEQC	**computer model for geochemical modelling**
REE	**rare-earth element(s), any of the elements from La to Lu, i.e. the lanthanides, often includes the Group 3 element Y, but not Sc**
TIC	**total inorganic carbonate**

Chapter 1

Introduction

1.1 The hazards posed by transuranic elements in nuclear waste

Uranium is the heaviest naturally occurring element, however transuranic elements (i.e. elements with atomic numbers greater than 92) can be produced from uranium by neutron capture followed by β-particle decay to produce a heavier element in a nuclear reactor. The nuclear industry has expanded dramatically since the 1950s as nuclear power was thought to be a clean efficient method of power generation that did not require vast quantities of fuel. Nuclear reactors were also used to produce Plutonium for national weapons programmes. The nuclear industry has been beneficial to many nations (e.g. Japan) that do not have access to large quantities of fossil fuels to supply the needs of modern industrial economies, where over 20% of the world-wide electricity is generated by nuclear power (Seaborg, 1993). Even though radionuclides are generally considered as hazardous, they do have some beneficial uses apart from energy generation. Since radioactive isotopes can be detected at concentrations well below that of all other analytical techniques, small quantities of radioisotopes (tracers) can be introduced to a system to monitor a reaction at trace concentration levels. The use of short-lived radiotracers has also found widespread medical applications (Hughes & O'Riordan, 1993) including X-rays as diagnostic techniques which reduce the extent of invasive surgery.

Nuclear reactors are powered by uranium fuel rods that produce heat by the controlled nuclear fission of the uranium. The build up of fusion and fission products (e.g. ^{241}Am, ^{243}Am, ^{244}Cm, ^{242}Cm, ^{144}Ce, ^{155}Eu, ^{60}Co, ^{90}Sr and ^{137}Cs) within the fuel rod results in an efficient life-time of between 5 to 7 years, after which they must be replaced. The spent fuel rod can be reprocessed and reused in the preparation of new nuclear fuel rods (Quiñones *et al.*, 1996). Thus, 96% of the fuel rod is returned to the nuclear fuel cycle as uranium. Plutonium forms a further 1% of the spent fuel, which can be separated either for use in reactors or military projects. However 3% of the initial fuel rod is left as waste fission products. In addition there has also been overproduction in the amount of

Plutonium required for military and civilian use, which will ultimately be treated as nuclear waste if alternative uses cannot be found (Krauskopf, 1988).

Nuclear power was originally promoted as a clean power source as the nuclear waste products are contained within the reactor, whereas the burning of fossil fuels fossil fuels emits chemicals into the atmosphere causing acid rain, smog and greenhouse effects,. However, the fission products (e.g. ^{60}Co, ^{90}Sr, ^{137}Cs, ^{144}Ce and ^{155}Eu), are themselves radioactive and produce significant amounts of heat from γ and β-particle decay. These radioactive emissions can also cause a wide range of biohazards as excessive exposure breaks can lead to the promotion of free radical reactions, resulting in carcinogens, cell damage and mutations (including genetic mutations). Exposure to radiation is however a natural hazard (e.g. from the exposure to radon gas near granite bodies in S. W. England or cosmic radiation), but nuclear waste poses a more significant concentrated, unwarranted hazard. Radioactive wastes must therefore be disposed of safely and isolated from the biosphere to prevent any direct health risks.

The skin does form an effective barrier that stops the absorption of radionuclides into the body, however radionuclides can enter the body through open wounds, inhalation and ingestion (Smith, 1992). Once in the body, radionuclides continue to undergo spontaneous fission reactions, releasing energy through the production of α and β particles and γ-radiation (Table 1.1). β and γ radiation is highly penetrative and will pass through body tissues. Exposure to β-γ emitters in the environment will therefore be hazardous without being ingested, emissions from ingested β–γ will also pass out from the body, causing less damage than if all the energy and particles were entirely absorbed by body tissues. Alpha particles are too large to pass through the skin and consequently are significantly more hazardous than β-γ emitters, if an α-emitter has been ingested all α-particles are absorbed by body tissues.

All of the transuranic elements are part of decay series in which each daughter product also emits α-particles (Figures 1.1 and 1.2). If transuranic nuclides are ingested most will pass out of the body relatively quickly, depending upon their chemical speciation and solubility in bodily fluids, however a portion of the ingested transuranic elements are retained to varied extents within body tissues; 90% of the absorbed Am and Pu is retained within the liver and bones, the remaining 10% is distributed throughout the body. When Am and Pu are retained within body tissues, they have retention half-lives' of at least 40 years and the continued ingestion of even trace quantities of radionuclides will be an accumulative hazard.

Even if all anthropogenic nuclear activities ceased immediately, there is still a significant volume of waste products (including the decommissioning of all related buildings) that must be disposed of securely in an environment that prevents significant contamination of the environment by hazardous radioisotopes. Most of the spent reactor fuel is composed of U and Pu isotopes with lighter fission products, however the neutron bombardment process that forms Pu can produce further fusion reactions that gives rise to the formation of even heavier elements such as Am and Cm. These heavier transuranic elements, are not naturally occurring and all have unstable isotopes.

Figure 1.1 The decay series of some Am and Cm isotopes

1. $^{245}Cm \longrightarrow {}^{241}Pu \longrightarrow {}^{241}Am \longrightarrow {}^{237}Np \longrightarrow {}^{233}U \longrightarrow {}^{229}Th \longrightarrow$
2. $^{242}Am \longrightarrow {}^{242}Cm \longrightarrow {}^{238}Pu \longrightarrow {}^{234}U \longrightarrow {}^{230}Th \longrightarrow {}^{226}Ra \longrightarrow$
3. $^{243}Am \longrightarrow {}^{239}Pu \longrightarrow {}^{235}U \longrightarrow {}^{231}Pa \longrightarrow {}^{227}Ac \longrightarrow$

after Allard *et al.*, (1984)

The nuclear fusion and fission products that form as waste products from the spent nuclear fuel can be long-lived, with half-life's in the order of 10^4 to 10^6 years (Table 1.1). Even though Am and Cm are produced directly in nuclear reactors they can be continuously produced e.g. from the β-decay of ^{241}Pu to

^{241}Am (Figures 1.1 and 1.2). Thus, the radiological hazard of some transuranic elements will increase over a 10^2 to 10^4 year time period. In addition to the hazards of each transuranic element, each daughter product will continue to be radiologically hazardous, until a stable isotope forms at the end of each decay series. Most of the daughter products are also heavy metals (e.g. Pb, Bi and Po) and therefore although a minor factor, compared to the radiological hazard they are likely to be toxic.

Figure 1.2 The production and decay series of ^{241}Am (Greenwood & Earnshaw, 1984)

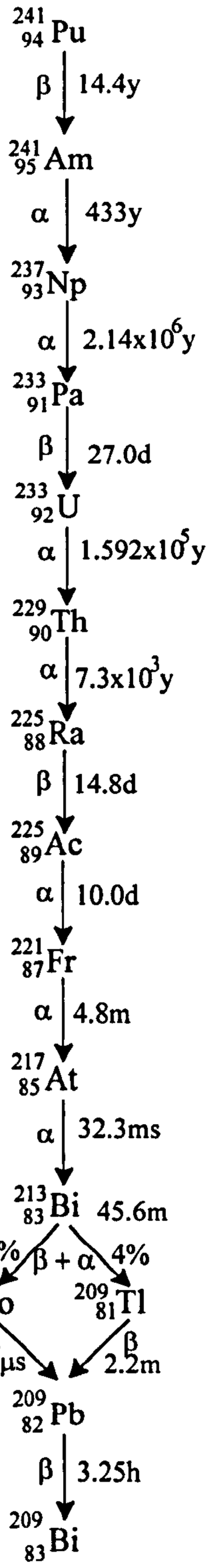

Table 1.1 Summary of the activity of varied radioisotopes

Isotope	½-life	Decay constant	Annual limit intake[1]		Solution activity per dm^3		Decay products		
					10^{-10}M	10^{-7}M			
	years	λ/s^{-1}	Bq	[2]Conc/M	[3]Bq	[4]Bq	MeV		γ (KeV)
^{241}Am	433	1.04×10^{-10}	5×10^{4}	8.02×10^{-10}	6.24×10^{3}	6.24×10^{6}	α	5.4	60
^{243}Am	7370	6.08×10^{-12}	5×10^{4}	1.36×10^{-8}	3.66×10^{2}	3.66×10^{5}	α	5.3	75
^{243}Cm	28.5	1.57×10^{-9}	7×10^{4}	7.39×10^{-11}	9.48×10^{4}	9.48×10^{7}	α	5.8	278
^{244}Cm	18.11	2.48×10^{-9}	9×10^{4}	6.04×10^{-11}	1.49×10^{5}	1.49×10^{8}	α	5.8	43
^{245}Cm	8500	5.28×10^{-12}	5×10^{4}	1.57×10^{-8}	3.18×10^{2}	3.18×10^{5}	α	5.4	175
^{239}Pu	24000	1.87×10^{-12}	2×10^{5}	1.78×10^{-7}	1.13×10^{2}	1.13×10^{5}	α	5.2	52
^{240}Pu	6470	6.93×10^{-12}	2×10^{5}	4.79×10^{-8}	4.17×10^{2}	4.17×10^{5}	α	5.2	45
^{241}Pu	14.4	3.11×10^{-9}	1×10^{7}	5.33×10^{-9}	1.88×10^{5}	1.88×10^{8}	β	0.02	149
^{234}U	2.45×10^{5}	1.83×10^{-9}	4×10^{5}	3.63×10^{-6}	1.10×10^{1}	1.10×10^{4}	α	4.8	53
^{235}U	7.04×10^{8}	6.37×10^{-17}	5×10^{5}	1.30×10^{-2}	3.84×10^{-3}	3.84	α	4.4	186
^{238}U	4.47×10^{9}	1.00×10^{-17}	5×10^{5}	8.28×10^{-2}	6.04×10^{-4}	6.04×10^{-1}	α	4.2	50
^{135}Cs	3.00×10^{6}	1.49×10^{-14}	4×10^{9}	4.44×10^{-1}	9.00×10^{-1}	9.00×10^{2}	β	0.2	0
^{137}Cs	30.17	1.49×10^{-9}	4×10^{6}	4.47×10^{-9}	8.95×10^{4}	8.95×10^{7}	β	0.5	6.62
^{90}Sr	28.8	1.56×10^{-9}	1×10^{6}	1.07×10^{-9}	9.38×10^{4}	9.38×10^{7}	β	0.5	0
^{60}Co	5.27	8.51×10^{-9}	2×10^{7}	3.90×10^{-9}	5.12×10^{5}	5.12×10^{8}	β	0.3	332
^{144}Ce	284.8 days	5.75×10^{-8}	8×10^{6}	2.3×10^{-10}	3.46×10^{6}	3.46×10^{9}	β	0.3	134
^{155}Eu	4.96	9.04×10^{-9}	6.25×10^{7}	1.15×10^{-8}	5.44×10^{6}	5.44×10^{8}	β	0.1	87

[1]Limits for intakes of radionuclides by workers by oral ingestion. *Annals of the ICRP. Publications 68 (1994) vol 24 N^0 4 & 30* (1979) vol 2 N°3/4 Pergamon Press, Oxford
[2]aqueous concentration of each isotope required for ALI assuming oral ingestion of 1dm^3 contaminated water
[3]activity per dm^3 for 10^{-10}M contaminated aqueous solution
[4]activity per dm^3 for 10^{-7}M contaminated aqueous solution

If nuclear waste is disposed of in a closed repository, the distribution and mobility of radionuclides will be controlled by reactions with the aqueous system. The most serious biological hazards are from the ingestion of water contaminated by the radionuclides, or from food sources similarly exposed. Other hazards are caused by contamination from the direct exposure to radiation in the vicinity of a waste repository and the possibility of inhalation of gaseous radionuclides, such as ^{3}H and ^{121}I. Restricting access to the repository site can reduce these factors. For the most active waste, deep burial has been proposed, using a geological barrier to isolate the waste from the biosphere (Chapman, 1995).

The activity of an isotope is described in becquerels (Bq) defined as the number of disintegration's per second (equation 1.1)

$$\text{activity(Bq)} = \lambda \,.\text{N}^{o} \text{ of atoms} \qquad (1.1)$$

$$\text{activity/dm}^3 = \lambda \,.(6.022\text{x}10^{23}).(\text{concentration/mols dm}^{-3}) \qquad (1.2)$$

$$\lambda = \frac{\text{Ln2}}{\text{half-life(seconds)}} \qquad (1.3)$$

where λ is the decay constant for that isotope.

An isotope with a short half-life will be more active than an isotope with a long half-life (Table 1.1). Thus a smaller concentration of the short half-life isotope, will be required for the same activity as a longer lived isotope. However, the shorter lived isotopes will decay faster and if containment is required for 10 half-lives (Chapman, 1995) then for example, ^{60}Co, ^{90}Sr and ^{137}Cs will have decayed to levels that are no longer biologically hazardous in under 500 years, whilst longer lived transuranic elements remain hazardous for at least 10^6 years.

The Annual Limit on Intake (ALI) for radiation workers, and the aqueous concentrations required to contain the ALI by ingesting one litre of solution are shown in Table 1.1 (and calculated from equation 1.2) for selected isotopes. The ALI for ^{243}Am and ^{245}Cm (half-life's 7370 and 8500 years respectively) would be contained within one litre of a 10^{-8}M solution, this reduces to 10^{-10}M solution for isotopes with half-life's of less than 450 years, e.g. ^{241}Am and ^{243}Cm. These

concentrations are at or below the detection limit for most analytical techniques (e.g. ICP-MS, with a detection limit between 10^{-8}-10^{-9}M for Nd) and are not routinely considered in water quality analyses. The ALI can also be reached by ingestion of larger quantities of more dilute solutions, i.e., only a total of 10^{-8} moles of ^{241}Am can be ingested annually without any serious health risks.

1.2 Nuclear Waste Disposal

Nuclear waste is usually segregated into three types, (i) High Level Waste (HLW) from the actual spent reactor fuel rods, including fission products such as Co, Sr, Cs and some lanthanides. (ii) Intermediate Level Waste (ILW) is material which was directly exposed to HLW, typically the fuel rod cladding used in the storage and transport of the HLW, or used in the production and refinement of Pu. Pu itself is classified as ILW. (iii) Low Level Waste (LLW) can include short-lived isotopes and any other material that has been exposed to a radiation source other than that directly produced in reactors. Typically low level wastes are derived from medical sources and laboratory debris. ILW and LLW may include transuranic elements as radioactive waste is classified by the total activity per tonne, (Bq/tonne) (Table 1.12). Thus Pu, Am and Cm must be considered in all models of waste containment and dispersal.

LLW was initially stored in shallow trenches or bunkers with a soil cap, or has been mixed with other domestic waste in landfill sites assuming that health risks would be minimal except from long term exposure. However, these systems have proven to be unsatisfactory especially for the volume of waste currently produced, and purpose built LLW repositories have become necessary (Chapman, 1995). There are currently no HLW or ILW repositories, which are still in the design and potential site characterisation stage, but some surface LLW repositories (e.g. The British Nuclear Fuels plc LLW repository at Drigg in Cumbria UK) are in operation.

Table 1.2 Classification of radioactive waste, after Chapman (1995)

High Level Waste (HLW)
Generate significant heat from radioactive decay Spent fuel or products from the immobilisation of highly active liquid wastes from fuel reprocessing Activity range 10^{16}-10^{18} Bqt^{-1}
Low Level Waste (LLW)
Less then $4x10^{9}$ Bqt^{-1} α-activity; less than $12x10^{9}$ Bqt^{-1} β-γ activity Most bulk waste, with lower activities than the α and β activity levels set for the LLW limits
Intermediate Level Waste (ILW)
All waste with activity levels between HLW and LLW

The disposal of radioactive waste is currently considered a two stage process. Firstly, concentration and isolation from the environment and groundwater system in a multi-barrier containment system (the near field) until a significant amount of the radioisotopes have decayed, and secondly, the slow dispersal and dilution, when the near-field containment system fails, through a geological barrier (the far field). Most of the LLW inventory will contain isotopes with half-lives of less than 10^{2} years that will decay before the repository (near field containment) has been breached. Thus, the majority of the LLW inventory is considered to have decayed to safe levels, So the geological barrier is not required for LLW disposal.

A multi-stage containment system has been proposed for the near field containment system (e.g. Angino, 1977, Bennet & Doyle 1997 or Chapman, 1995). HLW may be vitrified into a borosilicate glass, then mixed with a grout in steel containers. ILW and LLW may be immobilised directly into a cement-based grout and compacted to reduce the volume of waste without the vitrification stage. The initial stage immobilises the radionuclides into a solid matrix contained in steel containers, which are resistant to degradation and also shields

the effects of radiation. The steel containers and supporting matrix (of concrete) are contained in reinforced concrete silos with further engineered barriers composed of clay layers interspersed with crushed rock and sand layers. The concrete consists of an aggregate phase of flyash or gravel mixed with ordinary Portland cement (OPC), composed of calcium hydroxide and hydrated calcium silicates and calcium aluminates. The concrete structurally supports the steel waste containers and maintains a high pH environment around the waste, initially minimising the corrosion of the steel containers and ensuring a low aqueous solubility of the radionuclides after corrosion has occurred.

In near surface LLW repositories the emphasis is upon limiting the infiltration of water into the near field environment by a combination of barriers. Low permeability layers such as compacted clay are interspersed with conductive barriers, such as a permeable sand layer that use capillary forces to divert water away from and around the waste. A vegetation layer can further control water percolation and the engineered geometry of the capped system can enhance surface run off. In surface LLW repositories drainage channels are commonly built beneath the repository to channel any infiltration water, allowing any initial radioactive discharge to be monitored before back filling of the drainage system and final closure of the system.

Long lived isotopes of U and Pu will form the dominant proportion of ILW. Isotopes of these elements have half-life's (from 10^5 to 10^9 years), thus the near-field containment system can be expected to be breached before the radionuclide inventory has decayed to safe levels. Intermediate level waste repositories will require an effective far field barrier, ideally formed by a stable geological environment with little or no fluid flow. The geological barrier must be deep, with low ground water flow rates that ensure any radionuclides released from the near-field environment are sufficiently retarded, so when dispersed throughout the far field they do not pose a significant threat to the biosphere over time periods greater than 10^7 years.

The long-term stability and low groundwater flow rates at the far-field environment are considered more important than rock-type alone. A range of rock types have been considered, these include; (i) hard rock environments that can be shown as stable over the time periods required, from constructional and engineering considerations. (ii) Argillaceous rocks (clay sediments and metasediments) have low fluid flow rates, that may be by diffusion therefore enhancing the sorption capacity of the host and (iii) evaporite deposits such as halite which have little internal structure and fractures are self sealing.

Another factor to consider is that high and intermediate level waste and their fission and decay products contain α, β and γ emitters that produce large amounts of heat, therefore unlike LLW, HLW must be allowed to cool down before any processing and disposal can begin to be considered. Significant heat generation will continue throughout the lifetime of a repository with HLW and ILW, so elevated temperatures must be considered when modelling disposal scenarios.

1.3 Characterising the chemical properties of radioisotopes

The elements U, Th, Cs, Sr, Co, Pb and H occur naturally as stable isotopes (or in the case of U and Th the isotopes are unstable but have half-lives of the order of 10^9years). Their chemical properties can be easily determined from short term laboratory and field experiments or by the examination of geochemical conditions in geological regimes (Menger *et al.*, 1994, Read *et al.*, 1991) to characterise the long term processes these elements will undergo in potential disposal systems. These natural systems are not readily available for the transuranic elements (except for the Oklo Natural Reactors, Hidaka *et al.*, 1994) as they have only existed in significant quantities for a half-century. They are present in the environment in minute quantities, as by-products of atmospheric nuclear weapons testing (Allard *et al.*, 1984, Simpson *et al.*, 1980 & 1982) and therefore their geochemical properties are largely unknown. There has been some field studies based on leakage from existing nuclear waste storage and repositories (e.g.

Guillamont, 1994, Saunders, 1995 or Stockman, 1998). The transuranic elements are α-particle and γ-emitters, thus laboratory experiments are hazardous, so by necessity experiments must be on a small scale using only trace quantities in dilute solutions (e.g. for Am and Cm).

The comparison of trends between elements across the periods and within each group of the periodic table has shown that the chemical properties of the transuranic elements can be inferred by comparisons with other elements with similar properties such as outer electronic structure, oxidation state and ionic radii. The rare-earth elements (REE) are a naturally occurring group of 14 elements that follow lanthanum in the periodic table. All the REE form the M^{3+} oxidation state in aqueous solutions and have a similar ionic radii to Am and Cm when in the same oxidation state. Therefore the REE can be considered as natural analogues to the M^{3+} transuranic elements (e.g. Choppin, 1986, Come & Chapman, 1987, Krauskopf, 1986 and Lepel *et al.*, 1989).

1.4 The REE as chemical analogues for Am and Cm

The terms rare-earth elements (REE) and lanthanides (Ln-any/mixture of lanthanides) are almost synonymous and are used to describe the fourteen f-block elements Ce to Lu which follow the group 3 metal lanthanum, but before group 4 (Hafnium) of the Periodic Table (Figure 1.3). However traditionally the term REE also includes the group 3 metals La and Y. The REE were first isolated by leaching from phosphate minerals, to leave a mixed REE oxide (or earth). The REE were also originally mistakenly thought to be rare compared with other elements, this was mainly due to initial analytical difficulties, and because the REE predominantly occur at trace quantities within most primary mineral phases. However they cannot accurately be described as rare, as Ce is in fact the 26th most abundant element (Greenwood & Earnshaw, 1984, Meucke & Möller, 1988 & Morteani, 1991).

Promethium (Pm), the fourth lanthanide element is the only REE not naturally occurring, but is found as a fission product in nuclear reactors. La and Y are often considered as REE in geochemical literature as they occur together in natural systems, have similar properties and same outer d^1 electron structure in the ground state. Sc, the first group 3 metal is not considered as a REE because of its significantly smaller ion (Table 1.3), Sc does not follow the general group trends. The term lanthanide is commonly used to describe the REE (especially in chemical literature), as La immediately precedes the series in the periodic table, and the symbol Ln has come into use to describe a general reaction applicable to any lanthanide element. Similarly the metals with a 5f structure following the group 3 metal actinium, are commonly called the actinides, with the general symbol An to describe a reaction or element applicable to any actinide element.

Table 1.3 The ionic radii of selected (6 co-ordinate) M^{3+}, group 3, lanthanide (4f) and actinide (5f) ions (Greenwood & Earnshaw, 1984):

Group 3	4f	5f
Sc 74.5pm	Ce 103.2pm	U 102.5pm
Y 90pm	Nd 98.3pm	Pu 100pm
La 103.2pm	Pm 97pm	Am 97.5pm
Ac 112pm	Eu 94.7pm	Cm 97pm
	Lu 86.1pm	

Figure 1.3 The Periodic Table of the Elements, indicating atomic number, (Greenwood & Earnshaw, 1984)

1	2	3	4	5	6	7	8	9	10	11	12	13	14	15	16	17	18
^{1}H																	^{2}He
^{3}Li	^{4}Be											^{5}B	^{6}C	^{7}N	^{8}O	^{9}F	^{10}Ne
^{11}Na	^{12}Mg											^{13}Al	^{14}Si	^{15}P	^{16}S	^{17}Cl	^{18}Ar
^{19}K	^{20}Ca	^{21}Sc	^{22}Ti	^{23}V	^{24}Cr	^{25}Mn	^{26}Fe	^{27}Co	^{28}Ni	^{29}Cu	^{30}Zn	^{31}Ga	^{32}Ge	^{33}As	^{34}Se	^{35}Br	^{36}K
^{37}Rb	^{38}Sr	^{39}Y	^{40}Zr	^{41}Nb	^{42}Mo	^{43}Tc	^{44}Ru	^{45}Rh	^{46}Pd	^{47}Ag	^{48}Cd	^{49}In	^{50}Sn	^{51}Sb	^{52}Te	^{53}I	^{54}Xe
^{55}Cs	^{56}Ba	^{57}La	^{72}Hf	^{73}Ta	^{74}W	^{75}Re	^{76}Os	^{77}Ir	^{78}Pt	^{79}Au	^{80}Hg	^{81}Tl	^{82}Pb	^{83}Bi	^{84}Po	^{85}At	^{86}Rn
^{87}Fr	^{88}Ra	^{89}Ac															

The Lanthanide and Actinide series (see also Tables 1.4 and 1.5)

^{58}Ce	^{59}Pr	^{60}Nd	^{61}Pm	^{62}Sm	^{63}Eu	^{64}Gd	^{65}Tb	^{66}Dy	^{67}Ho	^{68}Er	^{69}Tm	^{70}Yb	^{71}Lu
^{90}Th	^{91}Pa	^{92}U	^{93}Np	^{94}Pu	^{95}Am	^{95}Cm	^{97}Bk	^{98}Cf	^{99}Es	^{100}Fm	^{101}Md	^{102}No	^{103}Lr

1.4.1 General chemical and physical properties of the lanthanides and actinides

The REE(III) have almost identical properties. Any fractionation (e.g. caused by slight differences in chemical properties) within the group is attributed to the "Lanthanide contraction" which is the decrease in the ionic radii across the series from Ce(III) to Lu(III). The f-block elements of the periodic table are unique in that the maximum of the 4f-charge density functions is well within the outermost $5s^2$ and $5p^6$ electrons, thus the 4f-electrons are shielded from the surrounding environment. The 5s and 5p-orbitals however penetrate the 4f sub-shell and consequently are not shielded from the increasing nuclear charge along the series, resulting in an ionic size contraction from Ce to Lu (Cotton 1991). Most of the 4f-electrons remain towards the core of the atom and do not take part in any bonding or ionising events. In the ground state the 5d electron may become incorporated into the 4f orbitals, but will generally be available with the outer 6s electrons to form the Ln(III) ion. These three electrons are available for bonding or forming ions thus, the REE all have very similar chemical properties, i.e. there is a strong tendency to form Ln(III) ions, rather than covalent compounds, which differ only slightly in their densities and ionic radii. It is probably this factor more than any other that has contributed to the 4f and 5f-block elements being considered as analogous. The elements with 5f electrons behave in a similar manner to the 4f-electrons although there is a much larger contraction than for the lanthanides due to the presence of filled 4f-orbitals. The Actinides are consequently of almost identical size as the Lanthanides (Table 1.4) in the M(III) oxidation state (Seaborg, 1993).

The general similarity in the physical properties (charge and ionic radii) of the 4f and 5f elements (Tables. 1.4 and 1.5, Greenwood and Earnshaw, 1984) means that the chemical properties are generally regarded as identical for the same oxidation state (Choppin, 1995 or Johannesson *et al.*, 1996b). Pm and Am have almost identical ionic radii, of 97pm and 97.5pm respectively, but Pm is also radioactive with no stable isotopes, thus Nd is considered the closest REE

analogue to Am (Petit 1992). The actinides with atomic numbers greater than 96 (Cm) are also assumed to form as An(III) ions (and so may be considered analogous to lanthanides with similar ionic radii), although their extremely low abundance means that they are generally ignored in waste disposal scenarios.

The lanthanide contraction is the controlling factor in all lanthanide chemistry. All lanthanides form Ln(III) ionic compounds and they naturally occur as a mixture of phosphates, carbonates and fluorides. The lanthanides have little or no covalent properties, unlike d-block elements where overlapping partially filled, d-orbitals are involved in bonding allowing some covalent characteristics.

Other oxidation states do occur for lanthanides under specific conditions, but not to the same extent as seen in the actinides (e.g. U^{VI} and Np^{VII} occur). The variation in oxidation states for the lanthanides is attributed to the Tetrad effect (McLennan 1994) which suggests that Ln(IV) and Ln(II) compounds do exist under appropriate redox conditions. These form due to a slight increase in stability by minimising electron-electron repulsion when the f-orbitals are empty, $\frac{1}{4}$-filled, $\frac{1}{2}$-filled, $\frac{3}{4}$-filled, or completely filled . For example Ce(IV) has a $4f^0$ structure (empty f-orbital) compared with Ce(III) with a $4f^1$ structure. Eu(II) has a $4f^7$ structure (1/2-filled f-orbital) whilst Eu(III) has a $4f^6$ structure. Ce and Eu are the only naturally occurring examples of the tetrad effect, although other examples can be synthesised under laboratory conditions. LnO_2 (solid) has been isolated for Ce(IV), Pr(IV) and Tb(IV) by heating under oxygen. CeF_4 is the only lanthanide(IV) fluoride known, and there are no known $LnCl_4$ as the chloride is oxidised to Cl_2. There is also a range of aqueous Ln(IV) complexes such as $Ce(CO_3)_3^{2-}$ and $Ce(NO_3)_6^{2-}$. Eu(II) and Yb(II) $4f^{14}$ structure are formed under reducing conditions but are not stable in aqueous solutions where they are easily oxidised to Ln(III).

Table 1.4 Oxidation states and ionic radii of the Lathanides (or REE) and Group 3 elements (Greenwood & Earnshaw, 1984)

	Oxidation state	0	II	III	IV		
Atonic number	Electronic configuration/ ionic radii(pm)	$6s^2 5d^0 4f^n$		$6s^0 5d^0 4f^n$		RAM /$gmol^{-1}$	comments
58	Cerium (Ce)	$5d^1 4f^1$ 181.8		$4f^1$ 102	$4f^0$ 87	140.12	
59	Praseodymium (Pr)	$4f^3$ 182.4		$4f^2$ 99.0	$4f^1$ 85*	140.907	*stable in water
60	Neodymium (Nd)	$4f^4$ 181.4	$4f^4$ 129	$4f^3$ 98.3		144.24	
61	Promethium (Pm)	$4f^5$ 183.4		$4f^4$ 97.0		(147)	
62	Samarium (Sm)	$4f^6$ 180.4	$4f^4$ 129*	$4f^5$ 95.8		150.35	* readily oxidized
63	Europium (Eu)	$4f^7$ 208.4	$4f^7$ 117	$4f^6$ 94.7		151.96	
64	Gadolinium (Gd)	$5d^1 4f^7$ 180.4		$4f^7$ 93.8		157.25	
65	Terbium (Tb)	$4f^9$ 177.3		$4f^8$ 92.3	$4f^7$ 76	158.924	
66	Dysprosium (Dy)	$4f^{10}$ 178.1	$4f^{10}$ 107	$4f^9$ 91.2		162.5	
67	Holmium (Ho)	$4f^{11}$ 176.2		$4f^{10}$ 90.1		164.93	
68	Erbium (Er)	$4f^{12}$ 176.1		$4f^{11}$ 89.0		167.26	
69	Thulium (Tm)	$4f^{13}$ 175.9	$4f^{13}$ 103*	$4f^{12}$ 88.0		168.934	* stable in aq carbonate soln
70	Ytterbium (Yb)	$4f^{14}$ 193.3	$4f^{14}$ 102*	$4f^{13}$ 86.8		173.04	* stable in aq carbonate soln
71	Lutetium (Lu)	$5d^1 4f^{14}$ 173.8		$4f^{14}$ 86.1		174.97	
21	Scandium (Sc)	$4s^2 3d^1$ 162		74.5		44.96	
39	Yttrium (Y)	$5s^2 4d^1$ 180		90.0		88.91	
57	Lanthanum (La)	$6s^2 5d^1 4f^0$ 187		$4f^0$ 103.2		138.91	
89	Actinium (Ac)	$7s^2 6d^1 5f^0$		112		227.03	

$4f^n$ stable under environmental conditions

$4f^n$ stable under extreme artificial conditions

Table 1.5 Oxidation states and ionic radii of the Actinides (Greenwood & Earnshaw, 1984)

	Oxidation state	0	II	III	IV	V	VI	VII	RAM
Atomic N°	Electron structure/ ionic radii(pm)	$7s^2 6d^0 5f^n$	$6s^0 5d^0$						$gmol^{-1}$
90	Thorium (Th)	$6d^0 5f^2$ 179		$5f^1$ 108	$5f^0$ 94				232.038
91	Protactinium (Pa)	$6d^1 5f^2$ 163		$5f^2$ 104	$5f^1$ 90	$5f^0$ 78			(231)
92	Uranium (U)	$6d^1 5f^3$ 156	$5f^5$ 110	$5f^3$ 102.5	$5f^2$ 89	$5f^1$ 76	$5f^0$ 73		238.03
93	Neptunium (Np)	$6d^1 5f^4$ 155		$5f^4$ 101	$5f^3$ 87	$5f^2$ 75	$5f^1$ 72	$5f^0$ 71	(237)
94	Plutonium (Pu)	$6d^0 5f^6$ 159		$5f^5$ 100	$5f^4$ 86	$5f^3$ 74	$5f^2$ 71		(242)
95	Americim (Am)	$6d^0 5f^7$ 173	$5f^7$ 126	$5f^6$ 97.5	$5f^5$ 85				(243)
96	Curium (Cm)	$6d^1 5f^7$ 174		$5f^7$ 97	$5f^6$ 85				(247)
97	Berklelium (Bk)	$6d^0 5f^9$ 170		$5f^8$ 96	$5f^7$ 83				(247)
98	Californium (Cf)	$6d^0 5f^{10}$ 186±2		$5f^9$ 95	$5f^8$ 82				(249)
99	Einstenium (Es)	$6d^0 5f^{11}$ 186±2		$5f^{10}$					(254)
100	Fermium (Fm)	$6d^0 5f^{12}$		$5f^{11}$					(253)
101	Mendelevium (Md)	$6d^0 5f^{13}$	$5f^{13}$	$5f^{12}$					(256)
102	Nobelium (No)	$6d^0 5f^{14}$	$5f^{14}$	$5f^{13}$					(254)
103	Lawrencium (Lr)	$6d^1 5f^{14}$		$5f^{14}$					(257)

$5f^n$-most stable occurring state

$5f^n$-stable occurring state under natural redox conditions

$5f^n$-stable only under correct redox conditions only

1.5 REE geochemistry

The study of REE geochemistry has mainly examined the relative changes to each REE in geological samples and aqueous environments. A general decrease in natural abundance along the 4f period is observed in conjunction with the Oddo-Harkins effect (Harkins, 1950) which reflects the existence of higher concentrations of those elements with even atomic numbers. Direct REE comparisons between samples is achieved by normalising each rare earth concentration using the primordial abundance found in chondritic meteorites (Table 1.6), for primary (crystallised from a molten source) rare earth material, or by normalising with shale composites for secondary (altered) rare earths. The normalisation results in a smooth profile of the REE, so their relative fractionation (due to ionic radii) can be compared directly between samples (Figure 1.4) independently of actual elemental abundance's.

Table 1.6 REE abundance's (ppm) commonly used for normalisation:

	Ce	Pr	Nd	Sm	Eu	Gd	Tb	Dy	Ho	Er	Tm	Yb	Lu
i	.865	-	.630	.203	.077	.276	-	.343	-	.225	-	.220	.0339
ii	73	7.9	33	5.7	1.24	5.2	0.85	-	1.04	3.4	0.50	3.1	0.48

i, average chondrite, Nakamura (1973)
ii, North American Shale Composite (NASC), Haskin *et al.*, (1968)

Applying the chondrite normalisation represents changes relative to the bulk earth content, while applying the shale normalisation gives changes relative to the crustal REE composition, showing elemental differentiation through time. Most geological studies involving the REE use these normalised profiles to show the relative enrichment (or depletion) of the Light REE (LREE) La-Eu, compared to the Heavy REE (HREE) Gd-Lu. This provides a general indication of the source depositional or solution conditions involved, for example Eu anomalies indicate

feldspar involvement when Eu(II) substitutes for Ca into plagioclase feldspar (Wilson, 1989).

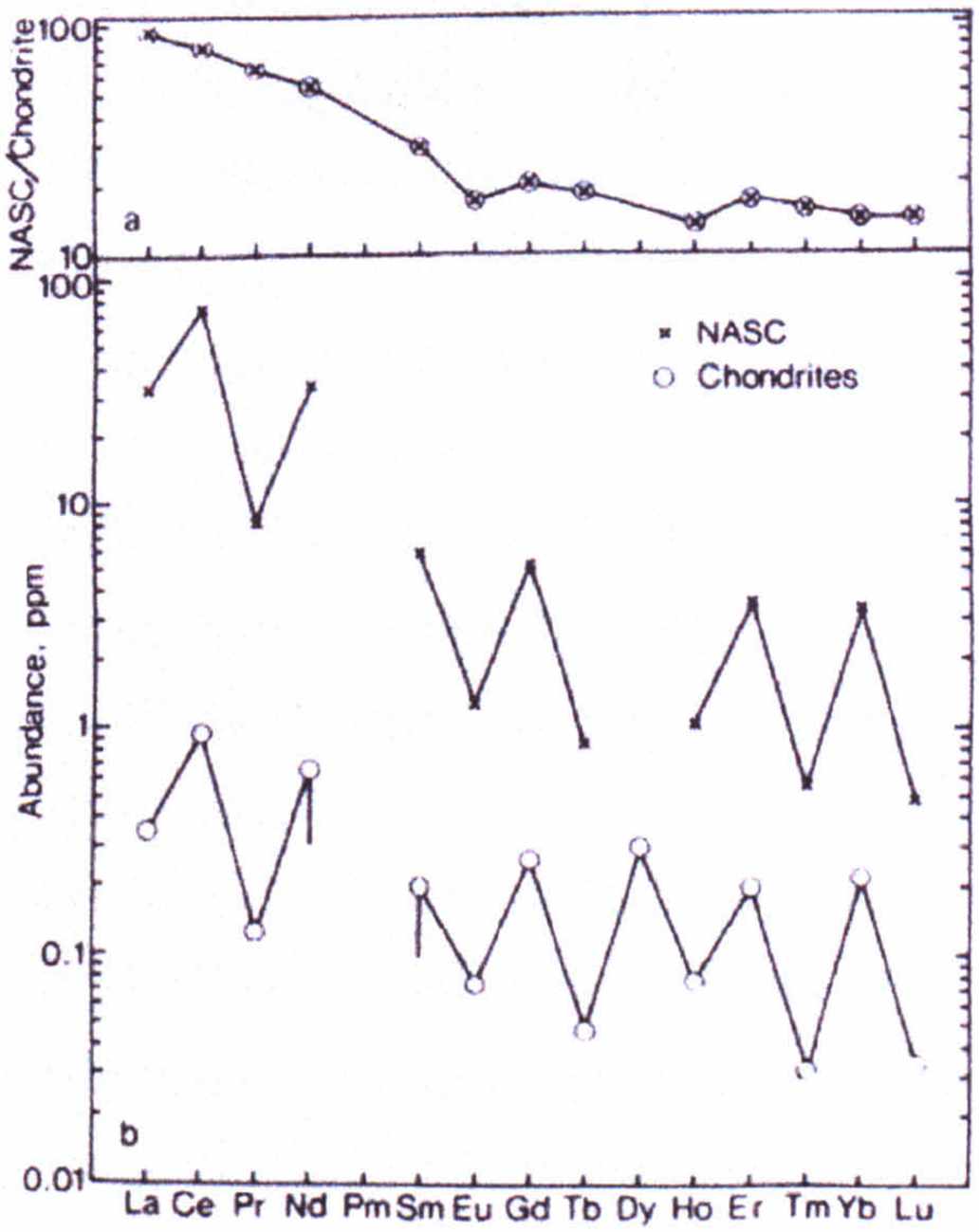

Fig 1.4

a, REE NASC/Chondrite profile indicating that the total REE is enriched especially the LREE during weathering and alteration processes.

b, Chondrite and NASC (shale) REE abundances. After Nakamura, (1973) and Haskin *et al.*, (1968)

The REE ^{147}Sm isotope (half-life of 1.06×10^9 yrs) is naturally occurring and decays to ^{143}Nd. Sm-Nd isotope data has also been used as a primary source indicator, as the isotopes are assumed not to be fractionated during alteration processes. However this premise has recently been questioned after in-depth studies of mineral phases (Wilson, 1989). Interest in the REE has increased with the widespread application of ICP-MS techniques, that can analyse all the REE in a single sample. The results of which indicate relative enrichment or depletion of REE related to environmental changes.

Geological studies have concentrated on the presence of either mineral phases or solution species, without trying to link them, or considering both factors within models, (unless in very loose or general terms). Mineral assemblages are studied at temperatures of formation from 100° to 800°C, e.g. during hydrothermal,

magmatic or metamorphic events where assemblages are readily available (e.g. Klinkhammer *et al.*, 1983 & 1995, Lehmann *et al.*, 1994 or Pan *et al.*, 1994). Solution studies are mostly used to determine the common surface conditions of rivers, lakes and oceans, although some theoretical extrapolation from low to high temperatures can be found in the literature (Haas *et al.*, 1995, Michard, 1989 or Wood, 1990b). Geological rock and solution studies commonly involve the analysis of REE, but the data are often presented as normalised profiles to indicate partition between crystals, melts and solutions. These studies are aimed at showing fractionation between the REE due to the slight size difference in ionic radii. For example, the HREE tend to partition into crystals from a melt to a greater extent than LREE to leave the melt relatively enriched in LREE, but the HREE are also more soluble in aqueous solutions than the LREE. The actual relative partitioning will depend on the actual mineral phases involved e.g. Eu^{2+} for Ca^{2+} in feldspars, HREE into garnets and zircons, MREE into clinopyroxene and LREE into feldspars and apatitite. Such normalised profiles have little bearing on absolute concentrations within phases. For example, Ce, the most abundant REE, often has the highest concentration of all phases present even though the normalised profile indicates depletion relative to other REE, especially in seawater (Elderfield & Greaves, 1982).

1.5.1 REE mineralogy

REE can be found as substituted cations in most mineral phases, but specific REE minerals do exist mostly as secondary alteration or hydrothermal minerals (Burt, 1989). Primary monazite ($LnPO_4$) can be found in granites and remains stable during weathering processes to accumulate as monazite sands of ore quality. REE substitution is dependant upon the co-ordination number of the host mineral which controls the fractionation between the REE, as the LREE have co-ordination numbers from 7-12, while the HREE have co-ordination numbers from 6-9 as a result of ionic radii contraction.

The LREE commonly substitute for Ca(II) and Th(IV) requiring the co-substitution of Na to charge balance the system. This is demonstrated by co-leaching of REE and Na from apatites (Lieftink *et al.*, 1994). The HREE substitute for Y, Mn(II) and Fe(II). HREE dominated minerals are actually Y based due to their similar size and chemical properties. Most REE bearing minerals thus tend to be either LREE or HREE enriched. This is more commonly the case for the most simple minerals, such as phosphates, where two end-member Ce and Y minerals do exist; monazite-(Ce) (9-co-ordinate) which is LREE enriched and xenotine-(Y) which is HREE enriched (Figure 1.5).

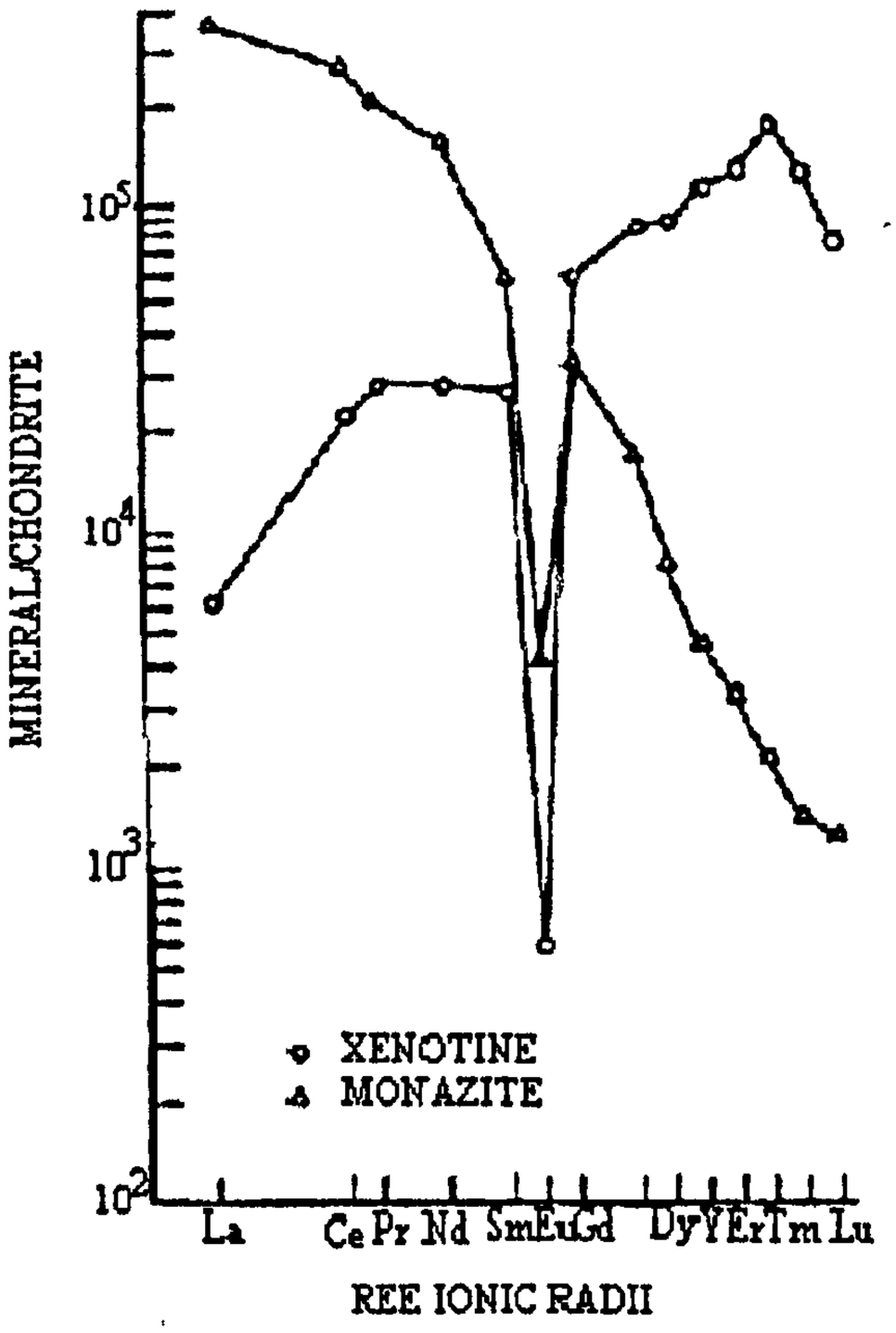

Fig 1.5
Comparison of the REE content between two (chondrite-normalised) REE phosphates ($LnPO_4$). Monazite LREE enriched Xenotine HREE enriched both minerals show a strong negative Eu anomaly

The negative Eu anomaly represents the reduction of Eu(III) to Eu(II) in the source environment and preferential extraction into feldspars e.g. by substituting for Ca^{2+}, subsequently Eu is unavailable when the other REE phosphate minerals crystallise (Bau, 1991). Eu geochemical properties are therefore strongly dependent on the redox conditions.

More complex REE minerals include at least two cations in different oxidation states, charge-balanced by differing amounts of Al and Si. Over 90 REE minerals are known (not including those formed by substitution into other mineral phases such as garnets and epidote). The substitution within minerals is often coupled, and takes place over all co-ordination sites by different elements (not just the REE), these minerals are less discriminating between the LREE and HREE, but rather reflect the total chemistry and conditions of formation.

Primary REE minerals tend to comprise REE substituents in the common rock forming and accessory minerals, such as zircon, apatite, allanite (epidote) and aegrine (pyroxene). These minerals do form a core to other more exotic specific REE minerals produced during alteration processes, (Bogoch *et al.*, 1992)

The most common secondary REE minerals are the fluorocarbonates (Table 1.7). William-Jones and Wood, (1992) have developed stability fields and solid solution series for the Ca-REE-CO_3^{2-}-F^- system, involving the minerals bastnaesite (the main REE-ore), parisite, synchysite, fluocerite and fluorite and are the most common REE rich ores, usually associated with calcite. Their calculations from thermodynamic data and field observations show pressure, pH, and Ca activity (with minor contributions from the F^--CO_3^{2-} activities) dominate.

Table 1.7 REE/Ca and REE/anion ratio for the common REE minerals

Mineral	Formula	Ln	Ca	CO_3^{2-}	F^-
Synchysite	$LnCa(CO_3)_2F$	1	1	2	1
Parisite	$Ln_2Ca(CO_3)_3F_2$	1	1/2	3/2	1
Bastnaesite	$LnCO_3F$	1	0	1	1
Fluocerite	LnF_3	1	0	0	3

Ln-any lanthanide/REE

If free $CaCO_3$ (calcite) is present then bastnaesite is not expected in the assemblage. Instead parisite and synchysite are found adjacent to the wallrock (a

possible source of Ca), while bastnaesite is usually found in the centre of veins where calcite is depleted or is not present. However, bastnaesite is more thermally stable than parasite and synchysite, and is found in higher temperature formations. Substitution is possible for all REE, calcium and fluoride ions within the minerals. Most minerals have a REE content in the order of Ce>Nd~La with a minor contribution from the remaining REE, reflecting their natural relative abundances (Table 1.6).

The system is further complicated as the decreasing ionic radii of the REE present, decreases the thermal stability of the mineral. For hydroxybastnaesite, $LnCO_3OH$, the pure La-endmember is stable above 550°C whilst for the Er-endmember there is a maximum thermal stability of only 400°C before decomposition.

1.5.2 REE in geological systems

Geological case studies of REE are based upon observing mineral assemblages within rocks and veins and inferring the conditions of formation. However, it is difficult to determine exact fluid constraints and these have largely been ignored, except in general terms of the bulk chemistry of the fluid involved.

In primary igneous systems the REE substitute into all the major mineral phases to a small degree, but especially into pyroxenes, amphiboles and garnets. Any remaining REE partition into the accessory minerals such as apatite $Ca_5(PO_4)_3F$ and monazite $(Ce,La)PO_4$, (which concentrate the LREE), and xenotine YPO_4 (which concentrates the HREE). However, even when extreme fractionation occurs each mineral will contain a mixture of all REE. The extent of partitioning is defined as the K_d value (equation 1.4) and shown in Table 1.9

$$K_d = \frac{\text{Concentration in mineral}}{\text{Concentration in Liquid}} \qquad (1.4)$$

In most of the rock forming minerals the REE are incompatible (i.e. $K_d < 0.1$) except for garnet (Table 1.8), which can strongly control REE release into mantle melts giving LREE enriched basalts. In most igneous rocks the REE are mainly found in trace amounts in all minerals but concentrate slightly into the last crystallising fraction to form accessory minerals such as apatite, monazite or zircon. Primary zircons are found in chondrites but only with Ce in the Ce(III) state (Ireland & Wloztka, 1992). Terrestrial zircons do have a small amount of Ce(IV) substituting for Zr(IV) to give strongly enriched Ce anomalies if formed in an oxidised environment (Henderson, 1984).

Table 1.8 Typical K_d for some rock forming and accessory minerals

		Ce	Eu	Eu*	Yb
Olivine		0.001	0.002	0.002	0.002
Clinopyroxene	B	0.1	0.2	0.3	0.28
	A	0.5	1.6	1.8	1.6
Garnet	B	0.02	0.32	0.35	4.0
	A	0.4	1.5	6.5	40
Plagioclase	B	0.10	0.3	0.06	0.03
	A	0.3	2.1	0.1	0.1
K-Feldspar		0.04	1.1	0.01	0.01
Apatite		35	30	60	25
Zircon		2.5	3	8	300

after Hanson 1977 (B-basaltic, A-intermediate/acidic, Eu*-Eu interpolated from adjacent REE)

The normalised REE fractionation profile is an important tool for determining changes in the source environment of mineral phases. Kerr, (1995) uses whole rock REE profiles in basalts related to the Iceland plume from Greenland to Skye, to determine the fractionation within the mantle source for these related Tertiary basalts. The REE normalised profiles are similar over the entire sample area as primary basalt chemistry is very source dependent. The REE are further concentrated into any subsequent re-melting or fractionation, shown by the

increased concentration of REE in minerals in acidic igneous rocks compared with the same mineral in basaltic rocks. The normalisation constants from chondrite to shales do indicate that significant fractionation does occur. The relative proportion of accessory minerals also increases, as these minerals tend to melt first and crystallise last therefore concentrating in the partial melt fractions. REE within granites become concentrated almost entirely into single mineral phases , to the extent that feldspars contain 80% of the total Eu and monazite up 75% of the LREE in the Carnmenellis granite of SW England (Smedley, 1991).

Primary REE ores are rare and are only seen in carbonatites which have high concentrations of incompatible elements. Their mineralogy is dominated by carbonates, phosphates and fluorides. Carbonatites mostly form as pods within other silicate bearing rocks, thus allanite (Ce-bearing epidote) often occurs with bastnaesite monazite and other rare earth minerals. REE carbonatite mineralization often occurs with enrichment of other incompatible elements such as phosphates, resulting in REE strongly partitioning into the carbonate phase (Woolley *et al.*, 1991).

Weathering and diagensisis can also enrich or fractionate the solid phase REE content (Condie *et al.*, 1995, Macrae, 1992) as the bulk of weathered REE are contained in alteration products (clays). REE are even removed from solution by adsorption reactions to be incorporated within clays with HREE enriched by 100-200% (Walter *et al.*, 1995). The REE are then transported in particulate form to be deposited as shales without going into solution (Sholkovitz, 1992). REE bearing sandstones contain monazite as the REE host (as substitution with quartz does not take place).

Late stage fluid action is a common method of mineralization e.g. in the Rodeo de Los deposit Argentina (Lira & Ripley, 1991) the host monzogranite is altered to fenite by Na-K rich fluids through a process of removal of Ca^{2+} and H^{+} with concordant replacement by K^{+} and Na^{+}. The original feldspars are replaced/altered to perthite and albite whilst biotite is destroyed. The Ca^{2+} is

found in localised enriched pods (syenites) with much of the REE mineralization. This mineralisation takes place in three stages as the fluids cool.

1. allanite, britholite and aegrine in quartz veins. T>450°C
2. alteration of britholite to bastnaesite with calcite-fluorite veining.
   271<T<340°C.
3. Late stage calcite-fluorite veining, with alteration of earlier assemblages.
   T<200°C

REE concentration is mainly achieved through hydrothermal fluid action typically at temperatures between 100° and 400° C, although primary ores are still found in carbonatites, where precipitation of the REE minerals bastnaesite, synchysite and parisite occurs through fluid interaction with wallrock. These enriched REE solutions can be observed from hydrothermal vents at mid ocean ridges (Michard *et al.*, 1983). The exact REE mineralogy that forms is dependent upon the variations in calcium and carbonate activities. Ngwenya, (1994) suggests that because only synchysite forms in veins hosted by apatite within the Tundulu Complex Malawi then there is an excess of Ca present, and bastnaesite predominates in areas of ankerite ($Ca(Mg,Fe)(CO_3)_2$) carbonatites, i.e. the reduction in available Ca determines the REE minerals formed. Field relations show this depletion within the solution as veins form in the order Synchysite-Parisite-Bastnaesite from the wallrock to the centre of the vein, indicating depletion of calcium and carbonate within the solution. The Bayan-Obo REE-Fe-Nb ore deposit (Chao *et al.*, 1992) is also dependent upon the host rock, as where carbonate bands contain both monazite and bastnaesite ores, quartzite hosted ores are mostly aegrine-bastnaesite and biotite zones containing REE within biotite and magnetite. Sedimentary (beach and dune) placer deposits of monazite bearing sandstones were, until 1965, the main source of bastnaesite.

The above examples do indicate that REE are mobile under certain conditions. Under most metamorphic conditions, where fluid/rock ratios are greater than 1, REE are relatively immobile and tend to be incorporated into the newly forming metamorphic minerals. Greenstone belts (altered from seafloor basalts) tend to

have similar REE profiles to modern basalts, with the REE included in chlorite and other clay phases formed during the alteration process (Menzies *et al.*, 1979).

REE are mobile under hydrothermal conditions, or where large water/rock ratios are involved, but even then in quantities much smaller than found in the host rock. The type of fluid can also be important in fractionating and redistributing REE. Na based alteration has been observed at temperatures between 65-120°C and at depths of 2-5Km in the North Sea Basin (Munz & Wayne, 1994) which suggests that the temperature of the fluid is not the only controlling factor, as fluid content and volume are also important. HREE are susceptible to complexing in CO_2 rich fluids. McLennan and Taylor, (1979) found HREE are enriched in U ores. Fluid inclusion data show these mineralisation conditions were oxidising, below pH 7 and less than 100°C. The HREE enrichment is attributed to complexing with carbonates where U is oxidised to the soluble U(VI) form. Mineralisation takes place when the ore fluid is degassed on entering cavities in the sedimentary host.

Most geological studies can not determine the distance REE travel in solution before deposition, though altering greenstones and fenites do indicate whole rock REE content does not vary (Martin *et al.*, 1978). Some studies suggest source material can be derived from large areas. Bouch *et al.*, (1995) examined diagenic francolite (carbonate-apatites) overgrowths around detrital apatite grains in sandstones and found Ce-enrichment (up by 1 wt% Ce_2O_3), in the francolite which cannot be explained by dissolution of the apatite cores. These near surface alterations suggest a strong complexing agent in solution. Organic complexing has been suggested due to the lack of suitable inorganic anions. In extreme water/rock ratio conditions, such as during dehydration of pelites, then anion content is important (F^-, CO_3^{2-}, OH^-), and often controls the preferential removal of the HREE.

These studies give an indication of some of the conditions at the fluid-rock interface (studies of fluid inclusions and mineral assemblages give the

temperature and pressure regimes), but they do not indicate the fluid source, distance travelled, time in equilibrium with the hostrock or the fluid content before mineralization.

1.6 REE in aqueous systems

1.6.1 REE aqueous species

The behaviour of REE in solution has been reviewed in a series of papers on "The aqueous geochemistry of the REE and Y" by Wood (1990a & b, 1993), Gammons *et al.*, (1996) and by Millero (1992) using thermodynamically measured and calculated data. These studies are based upon single metal components in solution, with a variety of inorganic anions, to produce stability constants for each of the common complexes formed in the natural system. Table 1.9 shows the generally agreed, complex stability for the common complexes in natural systems:

Table 1.9 Typical log K stability constants for the formation of the common aqueous Ln(III) species at 25°C

	$Ln(CO_3)_2^-$	$Ln(HPO_4)_2^-$	$Ln(CO_3)^+$	$LnOH^{2+}$	$LnSO_4^+$	LnF^{2+}	$LnNO_3^{2+}$	$LnCl^{2+}$
Ce	11.50	8.34	6.95	5.60	3.29	3.28	0.69	0.31
Eu	12.24	9.10	7.37	5.83	3.37	3.63	083	0.28
Lu	13.20	10.05	7.70	6.24	3.01	4.05	0.56	-.03

(Ln any lanthanide or REE(III) Log K data from Millero 1992)

Table 1.10 The dominant aqueous lanthanide species in natural solutions

pH <3	$Ln^{3+}/LnSO_4^+$
pH 3-6	$Ln^{3+}/LnSO_4^+/LnF^{2-}$
pH 6-9	$LnCO_3^+$
pH >9	$Ln(CO_3)_2^-$

The Log K values show that some fractionation between the REE is possible in solution especially when carbonate solutions are involved. The actual complex found will depend upon the pH of the solution and can range from pH 2 for acid mine waters to pH10 in some alkali fluids (e.g. ophiolite complexes) (Figure 1.6). The *aquo* ion, sulphate and fluoride phases dominate in acidic conditions and carbonate species are dominant above neutral pH values (Table 1.10).

Fig 1.6 The relative REE speciation in natural waters (after Wood 1990).

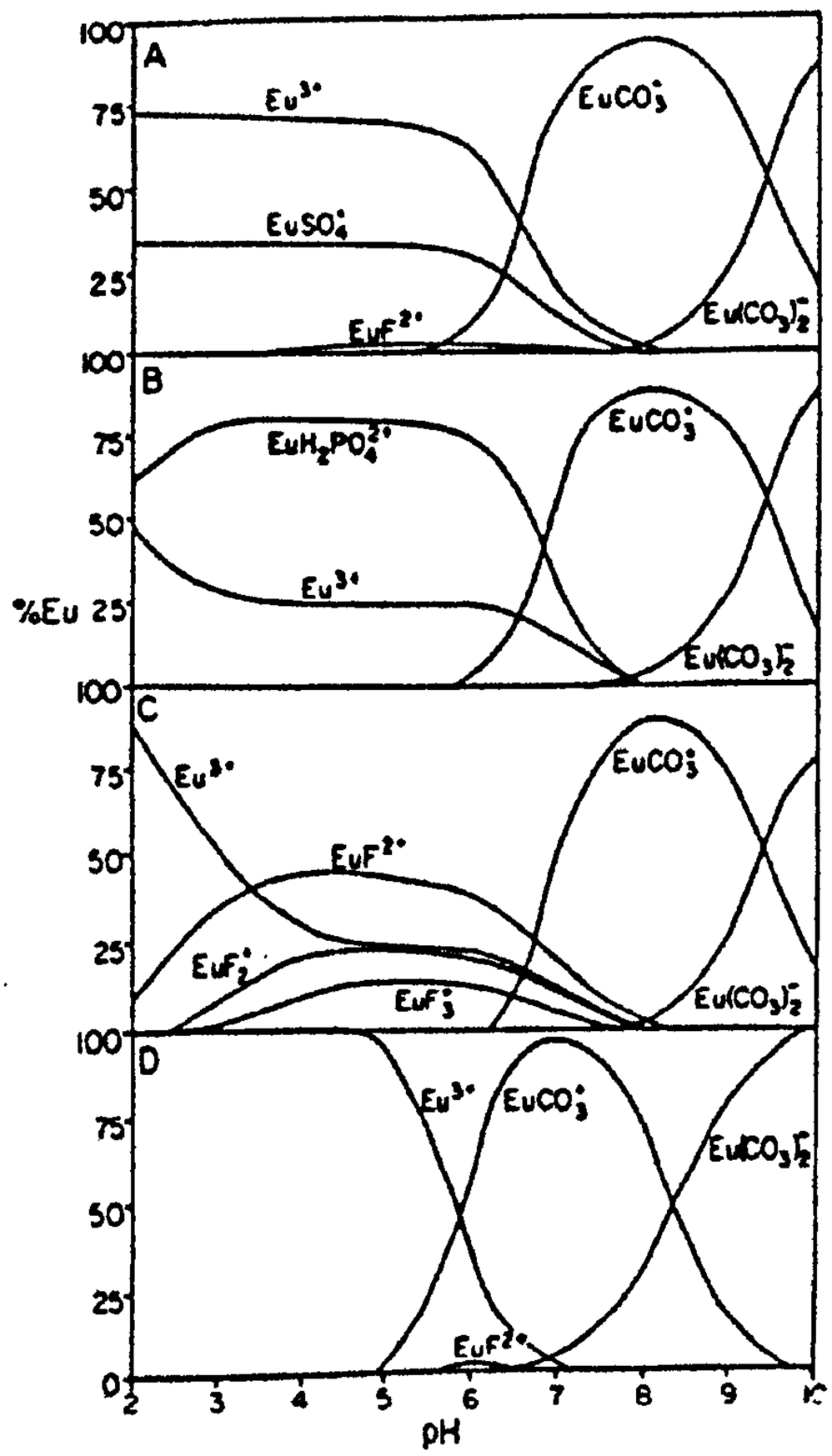

A- modal composition.
(total concentrations)
$[Eu] = 10^{-7}M$, $[F^-] = 10^{-6}M$
$[Cl^-] = 2x10^{-4}M$, $[SO_4^{2-}] = 10^{-4}M$
$[PO_4^{3-}] = 10^{-6}M$, $[CO_3^{2-}] = 10^{-4}M$
$[NO_3^-] = 10^{-4}M$

B-high phosphate, low sulphate.
$[PO_4^{3-}] = 0.01M$, $[SO_4^{2-}] = 10^{-6}M$

C-high fluoride, low sulphate.
$[F^-] = 10^{-4}M$, $[SO_4^{2-}] = 10^{-6}M$

D-high carbonate, low sulphate.
$[CO_3^{2-}] = 10^{-3}M$, $[SO_4^{2-}] = 10^{-6}M$

The activity of each anion will control the relative amount of each REE complex, e.g. the fluid and complexes are chloride dominated in salt brines, carbonate dominated in limestone hosted regions and fluoride from granitic groundwaters.

The total carbonate content must be less than 10^{-3}M for effective competition between the free *aquo* ion and carbonate species, unless pH constraints make the carbonate species unviable, e.g. at pH<6 HCO_3^- is present as the dominant carbonate species and does not compete with the stabilities of lanthanide sulphate, fluorides and aquo-ions.

The presence of REE-organo complexes cannot be ignored (although it has been in most studies) as EDTA is commonly used to decontaminate radioactive areas, as EDTA forms strong complexes with many radioisotopes which are readily washed away. This suggests that natural organic complexes (e.g. acids) are important in REE transport in weathering soil horizons and organic rich deposits, such as oil rich sediments, as they will act in a similar manner, i.e. inhibiting sorption onto particulate matter (Means *et al.*, 1978a).

1.6.2 REE in natural solutions

The concentration of REE in natural solutions are typically less than 10^{-12}M, however high concentrations of up to 10^{-6}M have been detected under specific conditions (Smedley, 1991).

Natural solution studies have concentrated upon

i, ocean waters

ii ,lakes

iii, ground/meteoric waters

River studies have shown that the bulk transport of REE was in the colloidal fraction (Moulin, 1992), within fine clay minerals or adsorbed to mineral surfaces and not as aqueous species (Lipen & Mackay, 1993, Sholkovitz *et al.*, 1994).

1.6.2.1 REE within oceans

Ocean and sea waters are assumed to be in a steady state with localised variations due to (i) river input, (ii) hydrothermal vents related to oceanic volcanism and (iii) aeolian material. Studies have been based around concentration with ocean depth and the relative proportion of each dissolved species. The total chemistry and pH of seawater are the controlling factors in REE speciation(Schif *et al*, 1991, Zhang *et al.*, 1994). Between pH 6-9 and a total carbonate concentration of approximately 10^{-3}M, 99% of REE exist as $REE(CO_3)^+$ complexes with a small amount of the aquo-ion. The majority of the REE added to the ocean system is in particulate form (within clay minerals) and does not become involved with the aqueous phase. Within the water column there are cycles of sorption onto particles (usually Fe/Mn) near the surface followed by re-solution at depth, but some REE are removed from the water column by sorption. The REE then become incorporated into each successive growth ring of Fe and Mn oxide minerals. This process is more dramatic for the LREE than the more soluble HREE which form more stable carbonate complexes, which are less likely to be sorbed onto particles.

Table 1.11 Typical REE concentrations (pmols/dm^3) within an oceanic water column (after Elderfield & Greaves, 1982)

Element	Ce	Nd	Gd	Yb
Surface	66.3	34.3	5.59	3.15
100m	13.0	12.8	3.41	3.55
4500m	55.1	45.8	8.27	5.16

In general a profile of the water column (Table 1.11) shows REE concentration increasing with depth. Elderfield and Greaves (1982) have shown initial enrichment at the surface, then a minimum at ~100m, followed by a steady increase with depth. Within the ocean basin there can be extrema within the

column when waters mix e.g. at 1000m in the Atlantic where the Mediterranean waters mix.

When ocean waters are shale normalised there is a slight negative Ce anomaly, but a prominent negative Eu anomaly due to the effects of changing redox states. The Eu is thought to be a relic effect from Eu inclusion in feldspars, whilst the Ce(III) becomes oxidised to Ce(IV) to co-precipitate with Fe oxide minerals. There is a general enrichment in the shale normalised HREE patterns compared with the LREE within the surface mixing zone (upper 100m), when the LREE are scavenged from solution compared to the HREE. In the rest of the water column there is a smaller relative enrichment of the HREE compared with the LREE, probably as a result of a stronger REE-carbonate aqueous complexes for the HREE than the LREE (Elderfield & Greaves, 1982).

REE profiles in ocean basins reflect inputs at the surface and bottom of the water column, followed by scavenging from solution. The surface source is probably aeolian. Elderfield and Greaves, (1982) found Mid Atlantic surface waters were comparable with the North Atlantic (Sahara) marine aerosols and Saharan desert soils. They attributed the early scavenging to oxidation of Fe and Mn and surface sorption of (predominantly) LREE onto particles within the mixing zone (upper 100m). The Ce anomaly develops over the top 500m of the water column and is thought to be due to the oxidation of Ce(III) to the less soluble Ce(IV) form, in concert with in-situ Mn(II) oxidation to Mn(IV)to form particulate oxyhydroxides (Sholkovitz *et al.*, 1994). However, Moffett, (1990) suggests Ce (IV) is generated through microbial oxidation.

The bottom source is the release of interstitial waters during diagenesis. Precipitation within sediments is shown to be in equilibrium with the ocean waters as ferromanganese nodules have the same Nd isotopic values as oceanwater. Scavenging is partly due to REE-anion co-precipitation of insoluble complexes when the REE becomes saturated with respect to each anion. Byrne

and Kim, (1993) suggest phosphate saturation may remove some dissolved REE from solution as precipitates.

Hydrothermal vents (the source of massive sulphide deposits) are a major influx of REE compared with average seawater content. Ce concentrations in the order of $5{,}800 \times 10^{-12}$ mol/Kg have been observed in upwelling plumes (to ~ 300m) above active vents (compared with typical values of 50×10^{-12}M in Table 1.12). German *et al.*, (1990) found that solution of these REE only takes place only after hydrothermal precipitates which scavenge REE within the plume have settled to the seafloor, as the maximum REE/Fe ratios for suspended particles around the plume are approximately 10 times lower than for the hydrothermal sediments at the vent. REE from the seawater are also thought to be scavenged from solution to a solid phase. The ^{3}He isotope signature of the fluids suggests a mantle derived component as does the very high REE content compared with that expected from hydrothermal fluids of ocean origin leaching material as fluids circulate. Michard *et al.*, (1983) found LREE enrichment at the East Pacific Rise with a large positive Eu anomaly compared with the local basalts, suggesting that solutions are not derived by simple dissolution of host basalt material from a hydrothermal field.

1.6.2.2 REE in lake systems

REE lake studies have mainly concentrated on anomalies in the major element chemistry and conditions in the lake. e.g. saltbrines, alkali or acid waters. In extreme conditions some lake waters have a much greater REE content than that found even in hydrothermal solutions.

The alkaline lakes from the Great Basin Western USA have a pH range from pH 8.48-9.78 and a total REE content up to 8,030 pmol/Kg with the Ce content alone up to 2,355 pmol/Kg in the highest pH Lakes. Johannesson *et al.*, (1994) attribute the stability of REE in solution to the formation of $Ln(CO_3)_2^-$ and the cerium is

oxidised and forms $Ce^{(IV)}(CO_3)_2^0$ to give a positive shale normalised Ce anomaly; almost all the REE (over 99%) is found as carbonate complexes. Lake Van in Turkey also shows an enhanced Ce anomaly (Moller & Bau 1993) due to the high alkalinity (pH 9.6) derived from constant volcanogenic hydrothermal Ca and CO_2 inputs. Seawater cannot stabilise $Ce^{(IV)}(CO_3)_2$ due to the oceans lower total dissolved carbonate content. Any Ce oxidised to Ce(IV) becomes sorbed onto Mn and Fe oxyhydroxide particles and removed from the system giving a negative shale normalised Ce anomaly.

Colour Lake NW Canada (Johannesson and Lyons, 1995) has contrasting conditions to the alkaline lakes. A permanent 1.8m thick ice cover gives reducing conditions thus Ce(IV) is not produced. The Lake does not have any measurable carbonate content but, is instead is dominated by sulphate ions (between 2.15-3.69mmol/Kg) and resulting in pH 3.6 to 4.74. Acidity is partly generated from groundwater seepage and precipitation of iron hydroxides. The REE exist as an almost equal mixture of sulphate and free aquo ions with a small percentage as fluoride species. The REE content is dependent upon pH as maximums for Ce content (31,790pmol/Kg) are found at areas of lowest pH. The sulphate complexes are particularly stable for the mid-REE compared with the other REE and are seen enriched in normalised profiles.

1.6.2.3 REE in groundwater systems

The REE content of groundwaters are dominated by source host rocks. Clear differences can be observed between granites and host metasediments. The granite hosted fluids are typically between pH 4-7 dominated by Na-K-Ca-Cl. Sediment hosted waters are Na-Ca-Mg-SO_4-CO_3 fluids and generally have a higher total dissolved salt (TDS) content than granitic waters, due to much more varied host materials. In low temperature fluids the total REE content is dependant upon the dissolution of REE hosted minerals and the effects of anions in solution. The exact amount of REE is determined by the extent of weathering

and host-rock REE content. The granite hosted fluids of Carnmenellis SW England have up to $1.6x10^{-6}$M total REE (Smedley, 1991); Ce alone is up to 24,621pmol/Kg; concentrations only found in extreme pH conditions (though much lower than the REE content in the host granite). The major source of REE is the dissolution of monazite, the bulk host of REE in mineral form. Organic and colloid content is also an important transport mechanism of REE transport in river or groundwater (solution or colloidal) systems. In the Mississippi River the LREE are mainly transported as colloids, while the HREE are transported as dissolved species due to the greater stability of the HREE- carbonate complex compared to the LREE-carbonate complexes.

Chloride complexes are only found associated with salt brines like those in the Palo Duro Basin USA (Gosselin *et al.*, 1992). The $LnCl^{2+}$ species exists, even though it has negative stability constant, due to the abnormally high chloride content of 1.3-3.0 mol/Kg which is 3-5 orders of magnitude higher than the total carbonate and total sulphate content of the brines. The dominant dissolved REE species is still the aquo-ion and like other groundwaters REE content is controlled by host-rock dissolution. The REE content of chloride-rich solutions is often lower than other chloride-poor groundwaters. The REE content depends upon the host-rock and is maximised by the controlled dissolution in localised areas, of lower chloride content (normally associated with slightly increased sulphate and carbonates in solution).

1.7 Summary of the REE geochemical properties

The rare earth elements are not rare or earths (i.e. oxides) and are found as trace elements in most silicate phases or as carbonate and phosphate minerals. REE tend to partition into the melt fraction and the REE content can be enriched through successive partial melts and subsequent crystallisation as final stage minerals. However the REE do not readily partition into an aqueous phase.

The low temperature geochemistry of REEs is dominated by solid phase alteration reactions, as the REE tend to remain in the solid phase, i.e. the decomposition or alteration of silicate minerals to clay minerals increases the REE content at the expense of other more soluble elements during weathering and metamorphic processes. Thus the REE can effectively be constrained into a solid matrix for time periods of greater than 10^6years. The normalised REE profile of Archean greenstones is similar to the normalised REE profile from modern basalts, indicating that the REE are immobile over 10^9 years. As REE stay in the particulate phase during alteration, only a small proportion is released into solution and mass transport of REE is in the particulate phase as fine clay minerals which form the final silicate weathering product. The presence of mineral grade monazite from placer sands also emphasises that REE minerals are stable and that REE mobility is through the physical erosion and mass transport of solid phases.

Even though aqueous REE do exist in all systems, concentrations are relatively low (typically below 10 pmol dm^{-3}) compared to most other elements. Higher aqueous concentrations can be found under extreme pH conditions, carbonate and high temperature environments (Table 1.12), but these levels are significantly lower than most other metals in similar systems.

Table 1.12 Extreme natural aqueous Ce concentrations

[Ce]/pmol dm^{-3}	pH	Source	Reference
55	7.5-8.5	ocean	Elderfield & Greaves (1992)
5800		Hydrothermal	German et al., (1990)
8030	8.5-9.8	Alkali lakes	Johannesson *et al.*, (1992)
31790	3.6-4.8	Reducing lakes	Johannesson & Lyons (1995)

The aqueous REE speciation is dependent upon relative anion composition and pH of the solution (Johannesson *et al.*, 1996a & 1996b), though stability fields

do increase with temperature (especially for high-temperature chloride fluids). Carbonate is one of the most soluble anions at low temperatures and the dissolved REEs dominantly form carbonate species above pH 6, even from phosphate rich source materials, (which are not as readily soluble as carbonates). Below pH 6 the free *aquo* ions, F^-, PO_4^{3-} and SO_4^{2-} aqueous species dominate.

When REE are released into solution they are normally scavenged from solution by surface reactions with organic and colloidal mineral phases, although the HREE form stronger aqueous carbonate complexes than the LREE and therefore fractionation across the group will occur.

1.8 Americium and curium environmental chemistry

Am and Cm are the most abundant actinides that dominantly form as a M^{3+} ion. The other (more dominant) actinides form a range of oxidation states (Table 1.4); e.g. Th and Pu form stable M(IV) ions, U as M(VI) and Np as M(VII) ions, the chemical properties of most actinides are therefore dependent upon the redox state of the system. Even though Am does not form naturally there are trace quantities of Am in the environment (e.g. as a Pu decay product) from atmospheric nuclear weapons tests (i.e. Mono Lake California, Anderson *et al.*, 1982, Choppin, 1989 and Johannesson *et al.*, 1995b) and the deep-sea disposal of radionuclides from old nuclear powered ice breakers and submarines (e.g. in the Kara sea, Furhmann *et al.*, 1997) or other accidental releases from nuclear power stations (von Gunten and Benes, 1995). The bulk of the Am produced has still to be disposed.

The published work on the chemistry of Am has recently been reviewed by Silva *et al.*, (1995), who have identified the thermodynamic properties of Am and produced a consistent set of Am aqueous thermodynamic constants, from often contradictory sets of data. Am will form as M(IV) ions, but only under strongly oxidising conditions, which require strong complexing anions (i.e. carbonate and normally form as mixed oxy ions) to stabilise an aqueous Am(IV) ion. These

higher oxidation state species are unlikely to form for Am in any potential disposal regime isolated from the atmosphere. The aqueous chemistry of Am is therefore dominated by Am(III) species.

The chemical properties of Am have been identified from linear free-energy calculations, by inference from other (less active) Actinide(III) species, comparisons with the lanthanides and from some direct measurements (e.g. Nitsche *et al.*, (1992) have determined the formation constant for $AmCO_3^+$ from Am^{3+} by a shift between the strong absorption bands at 505.3nm and 502.8nm respectively by varying the carbonate activity). There has been considerably more work on Am aqueous speciation (funded by the need to characterise nuclear waste disposal), than for the lanthanides, where until recently studies have focused on the relative (normalised) variations between each lanthanide or on the aqueous speciation in geochemical systems e.g. seawater. The inference from other actinides has lead to the postulation of a number of mixed americium oxy and hydroxy species (e.g. $Am(OH)_2CO_3^-$) which have no lanthanide analogue.

Americium chemistry in seawater and simulated groundwaters (above pH 7) is dominated by the formation of simple carbonate species ($AmCO_3^+$, $Am(CO_3)_2^-$ and $Am(CO_3)^{3-}$) or hydroxy species($AmOH^{2+}$, $Am(OH)_2^+$ and $Am(OH)_3^0$) at low carbonate activities (Allard *et al.*, 1984, Bidoglio, 1983, Choppin & Du 1992 or Fuger 1992). Apart from $Am(CO_3)_3^{3-}$ all these species lanthanide analogues have been proposed. However, the lanthanide speciation has usually been determined from seawater and groundwaters where the pH and carbonate activities are too low to support the formation of a $Ln(CO_3)_3^{3-}$ ion (e.g. Wood 1990a).

Experimental environmental aqueous americium chemistry is almost exclusively limited to the carbonate-pH system where solubility limits for Am are assumed to be controlled by the precipitation of the carbonate, hydroxycarbonate or hydroxide phase, dependent upon the actual pH and carbonate activity (or $pCO_{2(g)}$) of the equilibrium phase (Vitorge, 1992). The alpha particle and X-ray emissions from Am increases the hazard during the routine production of Am

solid phases used for solubility product determination and solid phase characterisation. Further, the radiation from the decay of Am interferes with X-ray analytical techniques and will have a destabilising effect upon the crystal structure.

Despite the hazards, Am solid phases and their solubility products have been determined directly (e.g. Morss and Williams, 1994). However Am solid phases are routinely determined assuming that a comparable Nd and Eu preparation will produce the equivalent Am solid phase, and that the remaining Am in solution can be relatively easily measured. Self irradiation will however destroy a crystal structure, for example, Silva *et al.*, (1995), note that crystalline $^{244}Cm(OH)_3$ is completely degraded in 24 hours, whilst $^{241}Am(OH)_3$ shows initial damage after 2 weeks and complete degradation after 5 months in water.

The removal of Am from solution by sorption processes is rapid, and partition from solution onto a surface phase (such as clay minerals, oxides and sulphides e.g. Degueldre *et al.*, 1994) is almost entirely complete (i.e, above 99.99%) for neutral and high pH solutions. Thus, most of the environmental Am is associated with the sedimentary phase. Steady state sorption of Am onto mixed ocean sediments in solutions at pH 7 is obtained in under 50 hours with K_d values of above 10^5ml/g (e.g. Furhmann *et al.*, 1997). Americium mobility can be enhanced by this strong sorption process on to mobile colloidal phases, for example the dominant Am(III) and Cm(III) isotopes transported at the Nevada test sites are associated with humic and fulvic colloids, (von Gunten & Benes, 1995). Sorption experiments can be measured directly for Am, but the sorption process must be examined below the solubility limit under the required solution conditions to eliminate any interference from the precipitation of solid Am phases. Thus sorption experiments are usually carried out using radiotracers concentrations below the Am solubility limit, and commonly below the detection limit of the lanthanides by standard analytical techniques. Similar experiments for the lanthanides would also require radiotracers.

1.9 Immobilising REE

Lanthanide elements can effectively be fixed into mineral phases in an initial solid matrix. When the lanthanides (and their analogues Am and Cm) are initially contained in a borosilicate glass, over 98.5% of the lanthanides are retained in the alteration products on the glass surface under flowing conditions, possibly as a co-precipitate with a silica gel (Ménard *et al.*, 1998). However they can be mobilised by sorption onto colloids. Barret, (1992) has shown that the lanthanides, La and Sm, can be fixed in a tricalcium silicate matrix (as a simplified cement analogue) when modelling the initial cement hydration. Ca^{2+} is displaced from the tricalcium silicate matrix by the lanthanides, which also accelerates the hydration process. When $Ca^{2+}$and the more soluble Na^{+} and K^{+} ions are released into the pore waters, ensuring a high pH (above pH 12), any remaining REE precipitate as the hydroxide. CO_2 will also be consumed by the formation of $CaCO_3$(s) and the partial pressure of CO_2 could decrease to as low as 10^{-10} bar (Diakonov, 1998). Nd will also react with the solid calcite phase (Caroll, 1993) by displacing Ca^{2+} ions by the adsorption of Nd carbonate and hydroxycarbonate phases, and will form a solid solution series within a calcite structure. The lanthanides (and therefore Am and Cm) will be effectively fixed during the alteration of the primary matrix and only released very slowly from the primary containment area.

The chemical properties and speciation of each element and not the radiological effects of each isotope will control the chemical mobility, although the actual elemental composition will change as the decay produces different elements which may have significant different chemical properties. The mobility of the lanthanide ions over time will be primarily controlled by the dissolution rates of the solid matrix, which can be expected to be low as the REE tend to remain in the solid phase upon mineral dissolution and alteration. The maximum lanthanide mobility will then be constrained by the precipitation of secondary minerals in equilibrium with the pore water solutions. The composition of this solution will be controlled by the dissolution of the concrete matrix and possibly be in

equilibrium with calcite. The secondary lanthanide minerals that may precipitate in an evolving pore water solution must be identified, characterised and their solubility products determined to quantify the solubility limit as the maximum amount available for aqueous transport. A direct comparison of the lanthanides can then be made with Am to determine the exact chemical similarities between these elements for future predictions of Am mobility in a disposal environment. Other immobilisation factors can also be considered to reduce the mobility further, e.g.. sorption processes on to mineral particles which the fluid must diffuse through or flow past to leave the disposal environment. These mineral surfaces will include corrosion products of the initial steel containers, the concrete matrix components, oxide and sulphide minerals and clay and other silicate minerals in the multi-barrier system. There may be the further filtering effects from diffusion through each barrier, which can trap colloidal particles and their associated adsorbed surface ions. The rate of radionuclide diffusion towards the biosphere will ultimately be constrained by the localised hydrology and flow rate within the system.

1.10 Characterising REE solubility

The lanthanides are ideally suited to model the solubility of the An(III) metals Am and Cm at levels approaching the solubility limits and any possible solid phase, lanthanide analogue experiments at levels considerably lower than the solubility levels (in particular adsorption to mineral surfaces) are less useful as radiotracer experiments are required to determine the amount remaining in solution and the radioactivity of Am and Cm can therefore be an asset. The chemistry of the REE is further worth considering as ^{152,154,155}Eu and ^{141,144}Ce have been found as fission products already in the environment in the Nevada test sites and as "hot particles" released from the Chernobyl reactor (von Gunten and Benes, 1995) and will therefore be included in any disposal inventory.

This project will consider the factors that may affect the chemical solubility of lanthanides (and if comparisons with Am and Cm are possible) in a post-disposal environment, particularly in a LLW repository. Potential near-field solutions to those found in the wider geosphere must therefore be considered. Biological and organic aspects of lanthanide mobility will not be considered. The radioactivity of Am and Cm will not directly affect their aqueous chemistry, but will slowly change their total concentration over time, however α-particle release will probably inhibit the transition from amorphous to crystalline phases, these phases would also include possible incompatible elements from the decay products.

The speciation of a metal determines the chemical reactivity, whilst the activity controls its solubility (Millero, 1992), these factors will be determined from the bulk solution composition and must be completely characterised to make meaningful comparisons with the actinides to predict their properties, including solubility limits and radionuclide mobility below the solubility limit. Studies on groundwater systems and the dissolution of concrete matrixes have shown that the bulk solution composition is dominated by Ca^{2+}, Mg^{2+}, Na^{+} and K^{+} cations with CO_3^{2-}, SO_4^{2-}, PO_4^{3-}, F^{-} and Cl^{-} anions in solution further controlled by the pH and Eh of the system. Lanthanide phosphate, fluoride and chloride aqueous ions are only dominant below pH 6 at 25°C (Figure 1.5) and therefore phosphate and fluoride activities are unlikely to be significant in a neutral or high pH disposal regime.

The lanthanide elements do form as carbonate minerals and aqueous lanthanide ions are dominantly associated with carbonate in most natural environments. This study will initially investigate the effects of carbonate ions upon lanthanide solubility and all the phase changes which may occur across the pH range from pH 3 to 12. This pH range will include all natural solutions from acid mine waters (pH 2-5), through seawater (pH 7-8) and highly alkaline groundwater solutions from carbonatites and ophiolites (up to pH 12). The dissolution of concrete has shown that the solution pH may be as high as pH 11.5, in a high ionic strength CO_3^{2-}, Cl^{-}, Na^{+}, K^{+} and Ca^{2+} solution. Some SO_4^{2-} ions may also

be present from the dissolution of the aggregate content, although the proportion of SO_4^{2-} to S^{2-} will be dependent upon the redox state of the system over time. The investigation of lanthanide solubility will therefore examine the possible effects of lanthanide solubility on the solubility-limiting phase from an initially high pH environment to a solution in equilibrium with the potential host groundwater and ultimately to a marine environment. The subsequent addition of other ions can then be included (e.g. SO_4^{2-} and Ca^{2+}) to characterise lanthanide chemical properties in an aqueous environment.

1.11 References

ALLARD, B., OLOFSSON, U., and TORSTENFELT, B., (1984) Environmental actinide chemistry. *Inorgan. Chim. Acta* **94** 205-221

ANDERSON, R. F., BACON, M. P., and BREWER, P. G., (1982) Elevated concentrations of actinides in Mono Lake. *Science* **216** 514-516

ANGINO, E. E., (1977) High-level and long-lived radioactive waste disposal. *Science* **198** 885-890

BARRET, P., (1992) Short term processes of radionuclide immobilization in cement: A chemical approach. *App. Geochem.(Supp. Issue)* **1** 109-124

BAU, M. (1991) REE mobility during hydrothermal and metamorphic fluid-rock interaction and the significance of the oxidation state of europium. *Chem. Geol.* **93** 219-230

BENNETT, M. R., and DOYLE. P., (1997) Environmental geology. *Wiley Chicester*

BIDOGLIO, G., (1983) Characterization of Am(III) complexes with bicarbonate and carbonate ions at groundwater concentration levels. *Radiochem. Radioanal. Letts.* **53** 45-60

BOGOCH, R., WEISSBROD, T., and BARMATTHEWS, M., (1992) Significance of REE-mineral inclusions in aegrine from an alkali syenite, Negev, Israel. *Eur. J. Mineral.* **4** 1337-1346

BOUCH, J. E., HOLE, M. J., TREWIN, N. H., and MORTIN A. C., (1995) Low-temperature aqueous mobility of the rare-earth elements during sandstone diagenesis. *J. Geol. Soc.* **152** 895-898

BURT, D. M., (1989) Compositional and phase relations among REE minerals. . *Mineral.* **21** 259-307

BYRNE, R. H., and KIM, K., (1993) Rare-earth precipitation and co-precipitation behaviour: The limiting role of phosphate on dissolved REE concentrations in seawater. *Geochim. Cosmochim. Acta* **57** 519-526

CARROLL, S. A., (1993) Precipitation of Nd-Ca carbonate solid solution at 25°C. *Geochim. Cosmochim. Acta* **57** 3383-3393

CHAO, E. C. T., BACK, J. M., MINKIN, J. A., and REN, Y. C., (1992) Hostrock controlled epigenic hydrothermal metasomatic origin of the Bayan Obo REE- Fe-Nb ore deposit, Inner Mongolia, PRC. *App. Geochem.* 7 443-458

CHAPMAN, N. (ed)(1995) The scientific and regulatory basis for the geological disposal of radioactive waste. *J. Wiley & Sons* Chichester

CHOPPIN, G. R., (1986) Speciation of trivalent f-elements in natural waters *J. Less-Common Metals* **126** 307-313

CHOPPIN, G. R., (1989) Soluble rare earth and actinide species in seawater. *Mar. Chem.* **28** 19-26

CHOPPIN, G. R., (1995) Comparative solution chemistry of the 4F and 5F elements. *J. Alloys and Compounds* **223** 174-179

CHOPPIN, G. R., and DU M., (1992) F-element complexation in brine solutions. *Radiochim. Acta* **58/59** 101-104

COME, B., and CHAPMAN, N. A., (eds) (1987) Natural analogues in radioactive waste disposal. *Graham and Trotman for CEC(EUR11087EN)*

CONDIE, K. C., DENGATE, J., and CULLERS, R. L., (1995) Behaviour of rare-earth elements in a palaeoweathering profile in the Front Range Colorado USA. *Geochim. Cosmochim. Acta* **59** 279-294

COTTON, S., (1991) Lanthanides & Actinides. *Macmillan Education Ltd.*

DEGUELDRE, C., ULRICH, H. J., and SILBY, H., (1994) Sorption of ^{241}Am onto montmorillonite, illite and hematite colloids. *Radiochim. Acta* **65** 173-179

DIAKONOV, I. I., TAGIROV, B. R., and RAGNARSDOTTIR, K. V., (1998) Standard thermodynamic properties and heat capacity equations for rare earth element hydroxides. *Radiochim. Acta* **81** 107-116

DILL, H. G,. (1994) Can REE patterns and U-Th variations be used as a tool to determine the origin of apatite in elastic rocks. *Sed. Geol.* **92** 175-196

ELDERFIELD, H., and GREAVES, M. J., (1982) The REE in seawater. *Nature* **296** 214-217

FUGER, J., (1992) Thermodynamic properties of actinide aqueous species relevant to geochemical problems. *Radiochim. Acta* **58/59** 81-91

FUHRMANN, M., ZHOU, H., NEIHEISEL, J., SCHOONEN, M. A. A., and DYER, R., (1997) Sorption/desorption of radioactive contaminants by sediment from the Kara Sea. *The Science of the Total Environment.* **202** 5-24

GERMAN, C. R., KLINKHAMMER, G. P., EDMONDS, J. M. MITRA, A., and ELDERFIELD, H., (1990) Hydrothermal scavenging of REE in oceans. *Nature* **345** 516-518

GREENWOOD, N. N., and EARNSHAW, A., (1984) Chemistry of the elements. *Pergamon Oxford*

HAAS, J. R., SHOCK, E. L., and SASSANI, D. C., (1995) Rare earth elements in hydrothermal systems: Estimates of standard partial molal thermodynamics properties of aqueous complexes of the rare earth elements at high pressures and temperatures. *Geochim. .Cosmochim. Acta* **59** 4329-4350

HARKINS, W. D., (1950) Special and magic numbers as factors in nuclear stability and abundance. *Phys. Rev.* **79** 724-725

HASKIN, L. A., HASKIN, M. A., FREY, F. A., COLLINS, K. A., and WILDMAN, T. R., (1968) Relative and absolute abundances of the rare earths. In: L. H. Aherns (Ed.) Origin and Distribution of the Elements, *Pergamon*, New York, p889-912

HELLMAN, R., EGGLESTON, C. M., HOCHELLA, M. F., and CERRAR, D. A., (1990) The formation of leached layers on albite surfaces during

dissolution under hydrothermal conditions. *Geochim. Cosmochim. Acta* **581** 267-1281

HENDERSON, P., (Ed) (1984) Rare-earth element geochemistry. *Elsevier*

HIDAKA, H., TAKAHASHI, K., and HOLLIGER, P., (1994) Migration of fission products into micro-minerals of the Oklo Natural Reactors. *Radiochim. Acta* **66/67** 463-468

HUGHES, J. S., AND O'RIORDAN, M. C., (1993) Radiation exposure of the UK population- 1993 Review. **NRPB-R263** *HMSO*

IRELAND, T. R., and WLOTKZA, F., (1992) The oldest zircons in the solar-system. *Earth Plt. Sci. Letts.* **109** 1-10

JOHANNESSON, K. H., LYONS, W.B., and BIRD, D. A., (1994) REE concentration and speciation in alkaline lakes from the Western USA. *Geophys. Res. Letts.* **21** 773-776

JOHANNESSON, K. H., and LYONS, W. B., (1995a) REE geochemistry of Colour Lake, an acidic freshwater lake on Axel Heiberg Island NW Territories Canada. *Chem. Geol.* **119** 209-223

JOHANNESSON, K. H., STRETZBACH, K. J., and HODGE, V. F., (1995b) Speciation of the rare-earth element neodymium in groundwaters of the Nevada test site and Yucca mountain and implications for actinide solubility. *Appl. Geochem.* **10** 565-572

JOHANNESSON, K. H., LYONS, W. B., YELKIN, M. A., GAUDETTE, H. E., STETZENBACH, K. J., (1996a) Geochemistry of the rare-earth elements in hypersaline and dilute acidic natural terrestrial waters: Complexation behaviour and middle rare-earth element enrichment. *Chem. Geol.* **133** 125-144

JOHANNESSON, K. H., STRETZENBACH, K. J., HODGE, V. F., and LYONS, W. B., (1996b) Rare earth element complexation behaviour in circumneutral pH groundwater. Assessing the role of carbonate and phosphate ions. *E. Plt. Sci. Letts.* **139** 305-319

KERR, A. C., (1995) The melting process and composition of the North Atlantic (Iceland) plume: geochemical evidence from the Early Tertiary basalts. *J. Geol. Soc.* **152** 975-978

KLINKHAMMER, G., ELDERFIELD, H,. and MITRA, A., (1995) Geochemical implications of REE patterns in hydrothermal fluids from M.O. Ridges. *Geochim. Cosmochim. Acta* **58** 5105-5113

KLINKHAMMER, G., ELDERFIELD, H., and HUDSON, A., (1983) REE in seawater near hydrothermal vents. *Nature* **305** 185-188

KOEPPENKASTROP, D., DECARLO, E. H., and ROTH, M., (1991) A method to investigate the interaction of rare earth elements in aqueous solutions with metal oxides. *J. Radioanal. Nuc. Chem.* **152**, 337-346

KRAUSKOPF, K. B., (1988) Radioactive waste disposal and geology. *Chapman & Hall, London*

KRAUSKOPF, K. B., (1986) Thorium and rare-earth metals as analogues for actinide elements. *Chem. Geol.* **55** 323-335

LEHMANN B., NAKAI, S., HOHNDORF, A., BRICKMANN, J., DULSKI, P., and HEIN, U. F., (1994) REE mineralization at Gakara, Burundi-evidence for anomalous upper mantle in the western Rift Valley. *Geochim. Cosmochim. Acta* **58** 985-992

LEPEL, E. A., LAUL, J. C., and SMITH, M. R., (1989) Rare-earth element patterns in briny groundwaters (Analogue study). *Radio. Waste Mange. Nuc. Fuel Cycle.* **13** 367-377

LIEFTINK, D. J., NIJLAND, T. G., and MAIJER, C., (1994) The behaviour of rare-earth elements in high-temperature Cl-bearing aqueous fluids: Results from the Odegardens Verk natural laboratory, *Can. Mineral.* **32** 149-158

LIPEN, B. R., and MACKAY, G. A., (eds) (1993) Geochemistry and mineralogy of rare-earth elements. *Min. Soc. Am. Rev. Mineral.* **21**

LIRA, R., and RIPLEY, E. M., (1992) Hydrothermal alteration and REE-Th mineralization at the Rodeo-De Los-Molles deposit Argentina. *Cont. Mineral. Petrol.* **110** 370-386

MACRAE, N. D., (1992) Developments of a positive Eu anomaly during diagenesis. *Earth Plt. Sci. Letts.* **109** 585-591

MARTIN, R. F., WHITLEY, J. E., and WOOLLEY, A. R., (1978) An investigation of Rare-earth mobility: Fenitized quartzites, Borralan Complex, NW Scotland. *Contrib. Mineral. Petrol.* **66** 69-73

MCLENNAN, S. M., (1994) Rare-earth element geochemistry and the Tetrad effect. *Geochim. Cosmochim. Acta* **58** 2025-2032

MCLENNAN, S. M., and TAYLOR, S. R., (1979) REE mobility associated with Uranium mineralization. *Nature* **282** 247-250

MEANS, J. L., CRERAR, D. A., BORCSIK, M. P., and DUGOID, J. O., (1978a) Radionuclide adsorption by manganese oxides and implications for radioactive waste disposal. *Nature* **274** 44-47

MEANS, J. L., CRERAR, D. A., and DUGUID, J. O., (1978b) Migration of radioactive wastes: Radionuclide mobilisation by complexing agents. *Science* **200** 1477-1481

MENARD, O., ADVOCAT, T., AMBROSI, J. P., and MICHARD, A., (1998) Behaviour of actinides (Th, U, Np and Pu) and rare earths (La, Ce and Nd) during aqueous leaching of a nuclear glass under geological disposal conditions. *App. Geochem.* **13** 105-126

MENGER, M. T., HEATH, M. J., IVANOVICH, M., MONTJOTIN, C., BARILLON, R., CAMP, J., and HASLER, S. E., (1994) Uranium migration/retention processes in core profiles from El Berrocal (Spain): Implications for matrix diffusion in fractured granite. *Radiochim. Acta* **66/67** 475-483

MENZIES, M., SEYFRIED, W., and BLANCHARD, D., (1979) Experimental evidence of REE mobility in greenstones. *Nature* **282** 398-399

MEUCKE, G. K., and Möller, P., (1988) The not-so-rare earths. *Sci. Amer.* **258** 285-298

MICHARD, A., (1989) Rare-earth element systematics in hydrothermal fluids. *Geochim. Cosmochim. Acta* **53** 745-750

MICHARD, A., ALBARDE, F., MICHARD, G., MINSTER, J. F., and CHARLOU, J. L., (1983) REE and U in high -T solutions from E. Pacific Rise hydrothermal vent field (13°N). *Nature* **303** 795-797

MICHARD, A., BEAUCAIRE, C., and MICHARD, G., (1987) Uranium and rare-earth elements in CO_2-rich groundwaters from Vals-les-Bains (France). *Geochim. Cosmochim. Acta* **51** 901-909

MILLERO, F.J., (1992) Stability constants for the formation of rare earth inorganic complexes as a function of ionic strength. *Geochim. Cosmochim. Acta* **56** 3123-3132

MOFFETT, J. W., (1990) Microbially mediated cerium oxidation in seawater. *Nature* **345** 421-423

MOLLER, P., and BAU, M., (1993) REE patterns with positive Cerium anomaly in alkaline waters from Lake Van, Turkey. *Earth Plt. Sci. Letts.* **117** 671-676

MORSS, L. R., and WILLIAMS, C. W., (1994) Synthesis of crystalline $Am(OH)_3$ and determination of its enthalpy of formation of the solubility-product constants of actinide(III) hydroxides. *Radiochim. Acta* **66/67** 89-93

MORTEANI, G., (1991) The rare-earths: Their minerals, production and technical use. *Eur. J. Mineral.* **3** 641-650

MOULIN, V., and OUZOUNIAN, G., (1992) Role of colloids and humic substances in the transport of radioelements through the geosphere. *Applied Geochem.* **Issue No 1** 179-186

MUNZ, I. A., and WAYNE, D., (1994) Retrograde fluid infiltration in the high-grade Modum Complex, South Norway: evidence for age, source and REE mobility. *Contrib. Mineral. Petrol.* **116** 32-46

NAKAMURA, N., (1973) Determination of REE, Ba, Fe, Mg, Na and K in carbonaceous and ordinary chondrites. *Geochim. Cosmochim. Acta* **38** 757-775

NGWENYA, B. T., (1994) Hydrothermal rare-earth mineralization in carbonatites of the Tundulu Complex, process at fluid-rock interface. *Geochim. Cosmochim. Acta* **58** 2061-2072

NITSCHE, H., MULLER, A., STANDIFER, E. M., DEINHAMMER, R. S., BECRAFT, K., PRUSSIN, T., and GATT, R. C., (1992) Dependence of actinide solubility and speciation on carbonate concentration and ionic-strength in groundwater. *Radiochim. Acta* **58/59** 27-32

PAN, Y. M., FLEET, M. E., and BARNETT, R. L., (1994) Rare-earth mineralogy and geochemistry of the Mattaganni lake volcanogenic massive sulphide deposit Quebec. *Can. Mineral.* **32** 133-147

PETIT, J. C., (1992) Reasoning by analogy: rational foundations of natural analogue studies. *Applied Geochem.* **Suppl. Issue 1** 9-11

POITRASSON, F., PIN, C., and DUTHOU, J., (1995) Hydrothermal remobilization of REE and its effect on Nd isotopes in rhyolite and granite. *Earth Plt. Sci. Lett.* **130** 1-11

QUIÑONES, J., GRAMBOW, B., LOIDA, A., and GECKEIS, H., (1996) Coprecipitation phenomena during spent fuel dissolution. Part 1: Experimental procedure and initial results on trivalent ion behaviour. *J. Nucl. Mat.* **1996** 38-43

READ, D., HOOKER, P. J., IVANOVICH, M., and MILODOWSKI, A. E., (1991) A natural analogue study of an abandoned uranium mine in Cornwall England. *Radiochim Acta* **52/53** 349-356

SAUNDERS, J. A., and TORAN, L. E., (1995) Modelling of radionuclide and heavy metal sorption around low- and high-pH waste disposal sites at Oak Ridge, Tennessee. *App. Geochem.* **10** 673-684

SCHIF, J., DEBAAR, H. J. W., WUBRANS, J. R., and LANDINGS, W. M., (1991) Dissolved REE in the Black Sea *Deep-sea research Pt. A. Oceanographic research papers* **52** 805-823

SEABORG, G. T., (1993) Overview of the actinide and lanthanide (The F) elements *Radiochim. Acta* **61** 115-122

SHOLKOVITZ, E. R., (1992) Chemical evolution of REE-fractionation between colloidal and solution phases of filtered river water. *Earth Plt. Sci. Lett.* **114** 77-84

SHOLKOVITZ, E.R., LANDINGS, W. M., and LEWIS, B. L., (1994) Ocean particle chemistry: The fractionation of REE between suspended particles and seawater. *Geochim. Cosmochim. Acta* **58** 1567-1579

SILVA, R. J., BIDOGOLIO, G., RAND, M. H., ROBOUCH, P. B., WANNER, H., and PUIGDOMENCH I. (1995) Chemical Thermodynamics Volume 2. Chemical thermodynamics of americium. Elsevier (Amsterdam).

SIMPSON, H. J., TRIER, R. M., OLSEN, C. R., HAMMOND, D. E., EGE, A., MILLER, L., and MELACK, J. M., (1980) Fallout plutonium in an alkaline, saline lake. *Science* **207** 1071-1073

SIMPSON, H. J., TRIER, R. M., TOGGWEILLER, J. R., MATHIEU G., DECK B. L., OLSEN, C. R. HAMMOND, D. E. FULLER, C. and KU, T. L. (1982) Radionuclides in Mono Lake, California. *Science* **216** 512-514

SMEDLY, P. L., (1991) The geochemistry of REE in groundwater from the Carnmenellis area SW England. *Geochim. Cosmochim. Acta* **55** 2767-2779

SMITH, H., (1992) The detrimental health effects of ionizing radiation. *Nucl. Med. Comms.* **13** 4-10

STOCKMAN, H. W., (1998) Long-term modelling of plutonium solubility at a desert disposal site, including CO_2 diffusion, cellulose decay and chelation. *J. soil Contamination* **7(5)** 615-647

VITORGE, P., (1992) $Am(OH)_3$, $AmOHCO_3$ and $Am_2(CO)_3$ stabilities in environmental conditions. *Radiochim. Acta* **58/59** 105-107

VON GUNTEN, H.R., and BENES, P., (1995) Speciation of radionuclides in the environment. *Radiochim. Acta* **69** 1-29

WALTER, A. V., NAHON, D., FLITCOTEAUX, R., GIRAD, P., and MELFI, A., (1995) Behaviour of major and trace elements and fractionating of REE under tropical weathering conditions. *E. Plt. Sci. Letts.* **136** 591-602

WILLIAM-JONES, A .E., and WOOD, S. A., (1992) A preliminary grid for REE fluorocarbonates and associated minerals. *Geochim. Cosmochim. Acta* **56** 725-738

WILSON, M., (1989) Igneous Petrogenesis. *Unwin Hyman Ltd*

WOOD, S. A., (1993) The aqueous geochemistry of the REE- critical stability-constants for complexes with simple carboxylic -acids at 25°C and 1-bar and their application to nuclear waste management. *Eng. Geol.* **34** 229-259

WOOD, S. A., (1990a) The aqueous geochemistry of the REE and Y. 1: Reviews of available data for inorganic complexes and the inorganic REE speciation of natural waters. *Chem. Geol.* **82** 159-186

WOOD, S. A., (1990b) The aqueous geochemistry of the REE and Y. 2: Theoretical predictions of speciation in hydrothermal solutions to 350°C. *Chem. Geol.* **88** 99-125

WOOLLEY, A. R., BARR, M. W. C., DIN, V. K., JONES, G. C., WALL, F., and WILLIAMS, C. T., (1991) Extrusive carbonatites from the Uyaynah area United Arab Emirates. *J. Petrol.* **32** 1143-1167

ZHANG, J., AMAKAWA, H., and NOZAKI, Y., (1994) The comparative behaviours of yittrium and lanthanides in the seawater of the North Pacific. *Geophys. Res. Letts.* **21** 2677-2680

Chapter 2

Analytical Techniques

2.1 Introduction

REE are relatively insoluble in aqueous solutions and often difficult to analyse using standard techniques such as atomic absorption spectroscopy (AAS) which are typically used for aqueous transition metal determination. Graphite furnace AAS and the less sensitive flame AAS are not sensitive enough for lanthanide determination, and have detection limits above 10^{-4}M Ln^{3+} which is at least two orders of magnitude above that of colourimetric methods (Section 2.2) and above that found from the dissolution of many REE solid phases.

Aqueous REE are usually determined by ICP-MS analysis (detection limit 10^{-8}M aqueous lanthanide) (Section 2.4) or from ICP-AES techniques (detection limit approximately 10^{-5}M aqueous Ln). ICP techniques are independent of the solution pH or bulk composition and allow the rapid determination of multiple elements. Solutions can be easily preconcentrated upon strongly cationic resins (usually Chelex 100), before elution with strong acids (e.g. Greneva *et al.*, 1996 and Halicz *et al.*, 1996). ICP analysis was unavailable for most of the project and a colourimetric method was developed for the REE determination.

The solid phases prepared in the lanthanide-hydroxide-carbonate system typically have a single lanthanide and possibly Na or K present. Three methods of solid phase analysis were routinely used: X-ray diffraction (XRD) to determine the crystal type, infra-red (IR) to determine the functional groups present (e.g. CO_3^{2-}, OH^- and crystalline water) and thermogravimetric analysis (TGA) to calculate the formula of each solid phase.

The analytical techniques required for the experimental sections of Chapters 3, 4, 5, 6 and 8 are outlined in this chapter. The development of the Flow-Injection Analysis using an Ultra -Violet (FIA-UV) technique, during this study, for the determination of aqueous lanthanides is discussed in detail (Section 2.2). All other techniques utilised are established analytical techniques and only their general principles will be briefly described in Chapter 2.

2.2 FIA-UV Determination of REE using Arsenazo(III)

Nd^{3+} and Eu^{3+} can be analysed using UV-Visible spectroscopy, as they have absorbance maximas at 793.6nm and 393.4nm respectively (Runde *et al.*, 1992); the limits of detection are very high and only useful for Ln^{3+} concentrations below pH 7 when lanthanides are relatively soluble. The detection limit can be enhanced by the addition of a colourimetric reagent, since the formation of coloured complexes that strongly absorb UV light is a convenient method of trace metal analysis. There are three established colourimetric reagents used for lanthanide determinations, Arsenazo(I), Xylenol Orange and the most commonly used Arsenazo(III). The molar extinction coefficients for aqueous Nd increases from 10.81 to $5.5 \times 10^4 l.mol^{-1}cm^{-1}$ in the presence of arsenazo(III), due to the formation of an arsenazo(III)-Nd complex (Marcenzko, 1986).

Arsenazo(III) is the most commonly used colourimetric reagent for lanthanide determinations, as the free reagent does not possess an overlapping maximum absorbance with lanthanide-arsenazo(III), but also chloride and sulphates ions do not interfere with the complex absorbance. The effects of Fe^{3+} interference can be eliminated by adding a reducing agent (e.g. ascorbic acid), reducing any Fe^{3+} to Fe^{2+} (Marcenzko, 1986). The Ln-arsenazo(III) complex maximum absorption is in the limited acidic pH range of pH 2.3-2.8, which is fortuitous as the lanthanides are commonly concentrated and separated upon ionic resins that are eluted with acid. Xylenol Orange and Arsenazo(I) have their maximum lanthanide-complex absorbance between pH 5 and 8, which is too high for acid eluted solutions.

The UV determination of metal complexes often requires extensive pretreatment to each sample, e.g. the addition of the complexing reagent and buffer solutions before being introduced into the spectrometer. Alternatively, the pretreatment can be incorporated into a flow injection system (Havel *et al.*, 1994 and Gladilovich *et al.*, 1988), which introduces a precisely controlled sample volume into a continuous stream of the required buffers and reagents, immediately prior to being introduced to the spectrometer. Flow injection analysis allows a small

sample volume (typically 10-200μm) to be determined directly (possibly with an auto-sampler system for multiple sample determinations) by most analytical techniques e.g. UV-spectroscopy, ICP-AES, ICP-MS or fluorescence-spectroscopy.

2.2.1 Method Development

Lanthanide-arsenazo(III) sample preparation

The sample preparation of Marcenzko (1986) for total lanthanide determination using UV-spectroscopy and arsenazo(III) as a colourimetric reagent, was adapted from a single-cell UV technique to a flow injection technique. Aqueous lanthanide determinations after the method of Marcenzko (1986) requires extensive sample preparation (Table 2.1), before each individual sample is introduced into a UV-Visible spectrometer in quartz glass cells.

Table 2.1 Sample preparation for the UV-Arsenazo(III) determination of aqueous lanthanides, after Marcenzko(1986)

1. take a sample containing less than 40μg Ln^{3+} and acidify to pH ~1
2. add 1cm^3 of ascorbic acid as a reducing agent
3. allow sample to stand for 2-3 minutes
4. add 1 cm^3 of formate buffer (pH 3.5), prepared by adding 60 cm^3 of formic acid to 28g NaOH and diluting to 1 dm^3
5. add 2cm^3 of a 5% arsenazo(III) solution
6. dilute to ~20cm^3 with water
7. adjust sample pH to pH 2.6±0.1 with NaOH (0.1M)
8. dilute to 25cm^3 with water
9. transfer 2cm^3 to a quartz glass cell and measure the absorbance at 650nm against a reagent blank

Determination of the peak arsenazo(III) and lanthanide-arsenazo(III) absorbtion wavelengths

The wavelengths of the maximum absorbance of the arsenazo(III) and the lanthanide-arsenazo(III) complex were determined by preparing samples after Marcenzko (1986) and running UV-Visible electronic spectra were obtained over the wavelength range from 200nm to 800nm (Figure 2.1) upon a Hewlett Packard 8452A Diode Array Spectrophotometer, using quartz cells (1cm path length).

The red coloured reagent has a maximum absorbance at 540nm. The reagent changes colour to blue upon the addition of 10^{-5}M $LnCl_3$ with a distinct maximum absorbance at 652nm for Nd. The reagent blank has an absorbance approximately equal to zero at 652nm, and therefore will not significantly interfere with the lanthanide determination.

Figure 2.1 The determination of the peak lanthanide-Arsenazo(III) absorbance

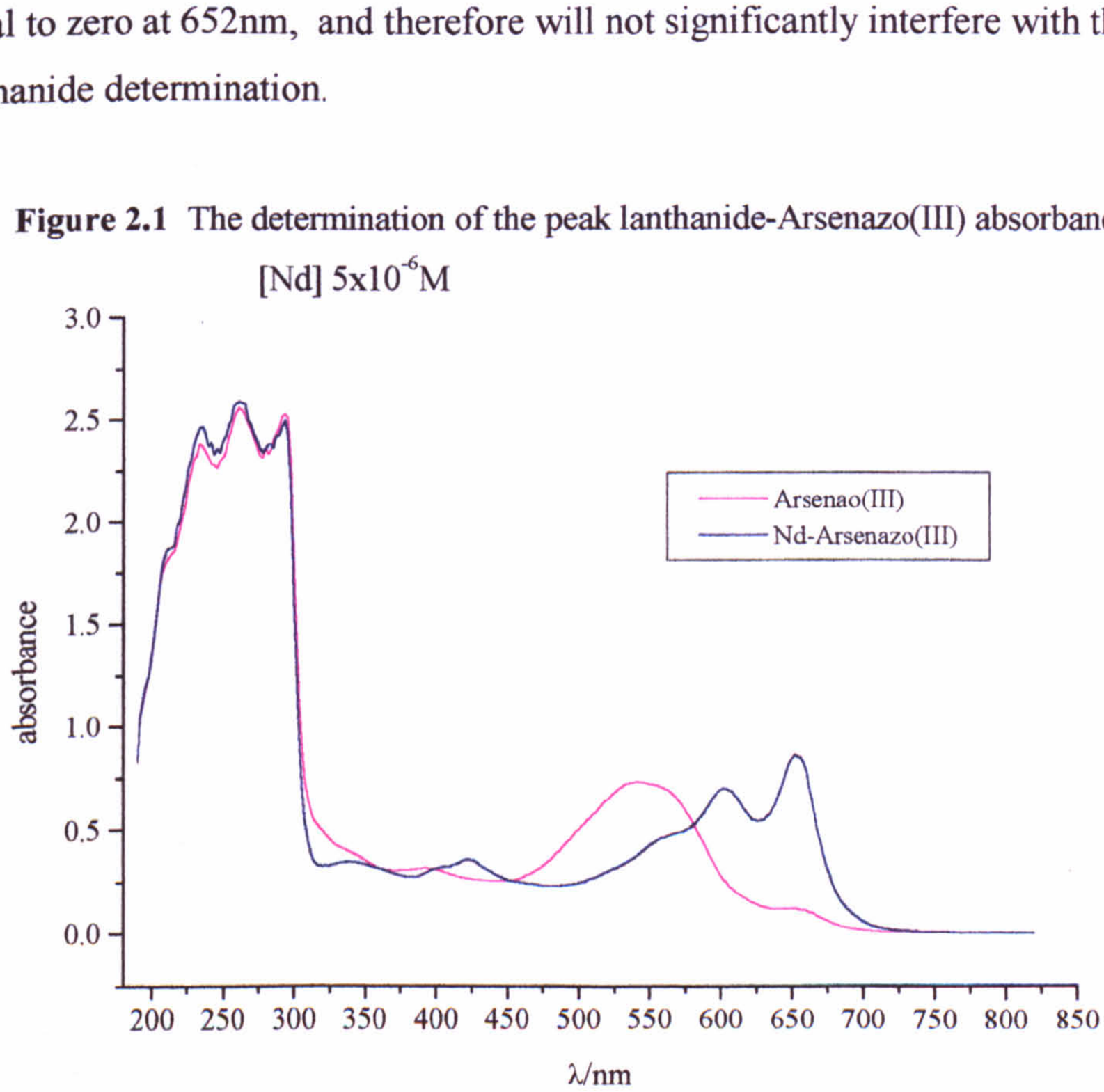

Flow Injection Systems

The sample preparation of Marcenzko(1986) for total lanthanide determination (Table 2.1) can be adapted from single-cell UV analysis, to a flow injection

method to allow the rapid repeated analysis of multiple samples. Flow injection systems mix a sample solution directly with a reagent solution (and buffer solutions if required) before introduction to a detector.

The FIA system (e.g. Figures 2.2 and 2.5) is composed of a peristaltic pump with peristaltic tubing of varied diameter to control the flow rate through the system. A precisely controlled sample volume is injected into a carrier stream. The carrier stream is then mixed with a reagent stream containing a buffer solution that controls the reaction pH, and the analytical reagent (e.g. arsenazo(III)). Further buffer solutions can also be added if the reaction is highly pH sensitive. The mixed solution then passes through a UV detector then to waste. The absorbance of the complex can be measured as peak height on a chart recorder as the injected sample passes through the detector.

Ideally the sample should register as a single sharp peak above a constant background signal. However the system has a number of variables that have to be optimised to maximise the sensitivity and reproducibility of the system. These include pH of the reaction, flow rate through the system, reaction time after mixing with the reagent stream, sample dilution from the reagent solution, carrier solution and any buffer solutions. Increasing the sample volume can significantly increase the system response; a large sample volume can broaden the peak response, instead of increasing peak height due to incomplete mixing or diffusion within the reagent stream.

The FIA-UV determinations were made with a Tecator FIA Star connected to a flat bed chart recorder as detailed below

1. Flow injection analyzer: Model 5010
2. Injection valve: Model V-100
3. Chemifold tray and chemifold type III
4. Spectrophtometer: Model 5023
5. Detector controller: Model 5032
6. Chart recorder: Model kipp and Zonen BD12

When the sample is injected directly into the reagent solution, the mixing and reaction time becomes critical as the stream is initially reagent-sample-reagent passing through the tubing which must mix and react before the detector. The system setup must therefore be a compromise between adding adequate buffers to homogenise each sample and dilution of the sample to minimse the detection limit.

2.2.2 The effects of reagent pH and ionic strength on absorbance

Experimental

The reaction between arsenazo(III) and lanthanides is dependant upon the solution pH. The pH of the reagent solution was altered with HCl or NaOH to give a range of solutions from pH 1-4. A 3-line manifold (Figure 2.2) was used to examine the effects of pH upon a 10^{-5}M Ln^{3+} solution, thus enabling the reaction pH to be adjusted by varying the pH of the minimum amount of solutions i.e. the buffer solution. When the most favourable analytical pH has been determined for the system, the buffer solution can be mixed with the reagent solution to reduce sample dilution at the detector.

A $NdCl_3$ (10^{-5}M) sample was injected into a carrier stream of HCl (0.1-0.5M) which was then mixed with a NH_4OH (0.1-0.5M) buffer solution at the same ionic strength , the NH_4OH buffer solution was mixed with NaOH (0.1M) to adjust the pH of the reacting mixture at the detector.

The carrier and buffer solutions were then mixed with the reagent solution before passing through a UV detector. The pH of the final solution was measured immediately after the detector. The effects of the solution pH on the reaction could be examined with that of the effects of 0.1M to 0.5M buffer solutions upon the sample.

Figure 2.2. FIA design of a three-line manifold for determining the optimum analytical pH for lanthanide-arsenazo (III) determinations

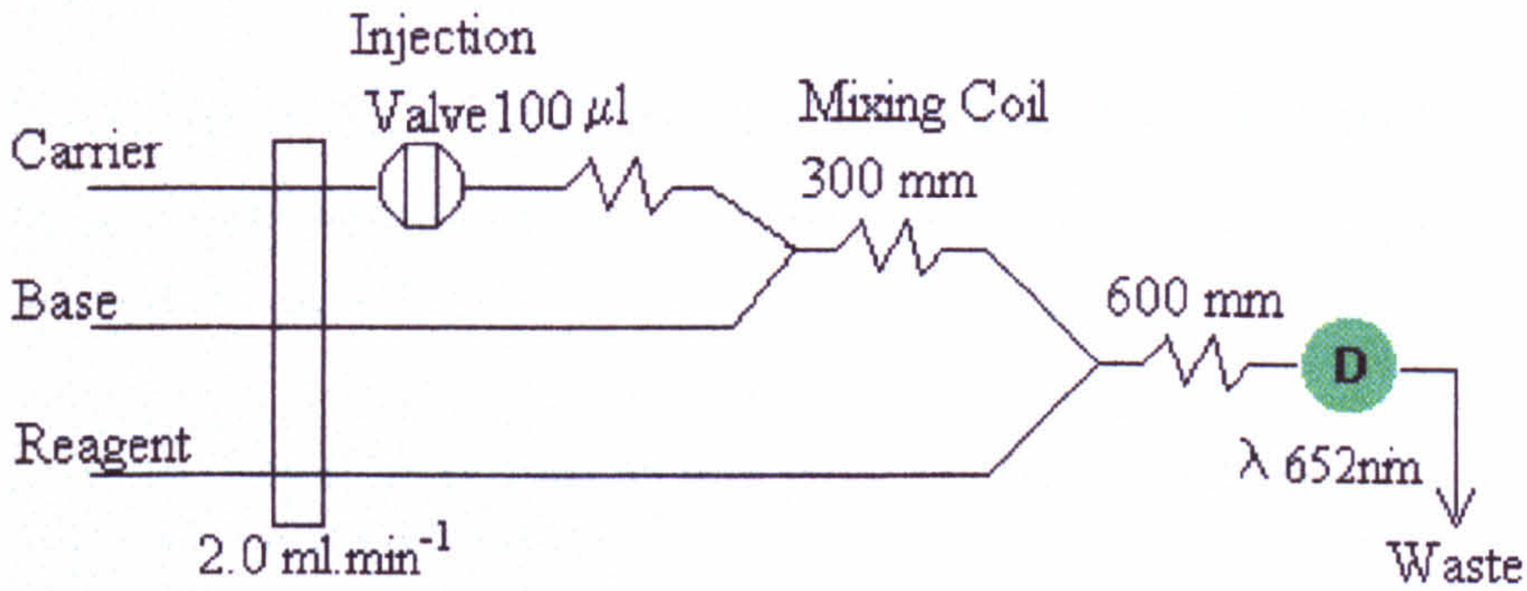

Carrier : 0.1-0.5 M HCl

Base : 0.1-0.5 M NH_4OH + x cm^3 of 0.1 M NaOH per 100 cm^3 of NH_4OH to adjust to the desired pH.

Reagent : Arsenazo(III) (0.005 % w/v)

Results

There is a sharp increase in absorbance from pH 1.2 to pH 2.4 (Figure 2.3). A significant colour change can be observed in the reacting solution as the blue Ln^{3+}-arsenazo(III) complex forms at pH 2.6. This colour change does not occur when the solution is acidified to below pH 1.8. A wavelength scan (Figure 2.4) shows the characteristic double peak of the Ln^{3+}-arsenazo(III) complex at pH 2.6 is significantly reduced and almost merges with the arsenazo(III) blank at pH 1.8, indicating the dissociation of the Ln^{3+}-arsenazo(III) complex.

The maximum absorbance decreases slightly when the pH is increased above pH 2.8, possibly due to increases in the absorbtivity of the reagent blank. A colour change from red to blue can be observed in the reagent when NH_3 is added to increase the reagent pH to pH 10 (Figure 2.4).

Increasing the ionic strength of the buffer solutions causes a slight decrease in the maximum absorbance of the complex. The decrease could be due to the high ionic strength of the solutions inhibiting complex formation or an increase in the detection pH as the sample is injected into the carrier stream, which may not mix

completely with the acid, before mixing with the NH_4OH solution then reacting with the reagent.

The effects of the buffer solution in controlling pH are more important when samples are preconcentrated upon an ionic resin in the carrier stream and are eluted by acid (section 2.2.6).

Figure 2.3 The effects of buffer concentration (HCl/NH_4OH) and pH upon peak height

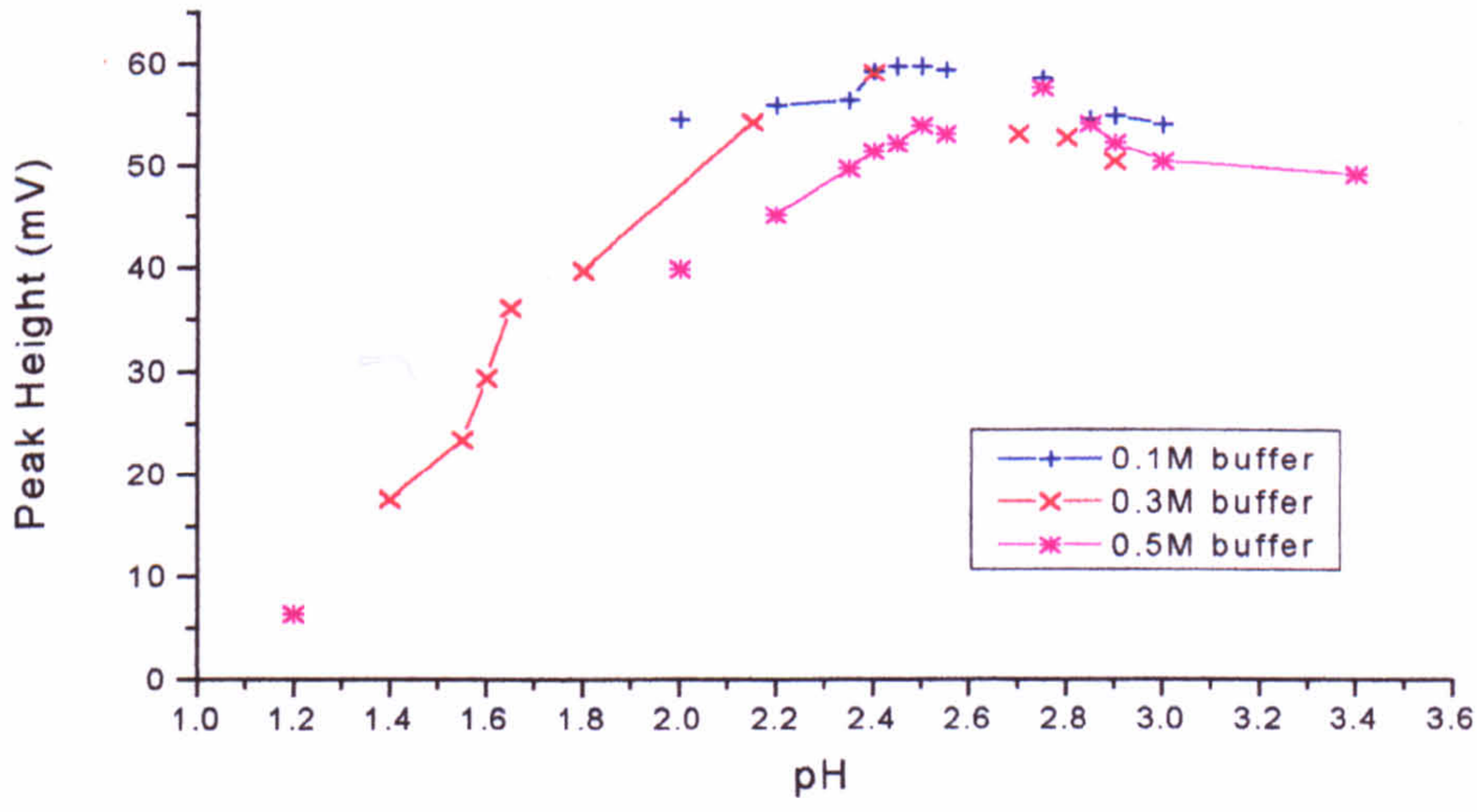

Figure 2.4 The variation in absorbance of arsenazo(III) and lanthanide-arsenazo(III) complexes with pH [Nd] $5x10^{-6}M$

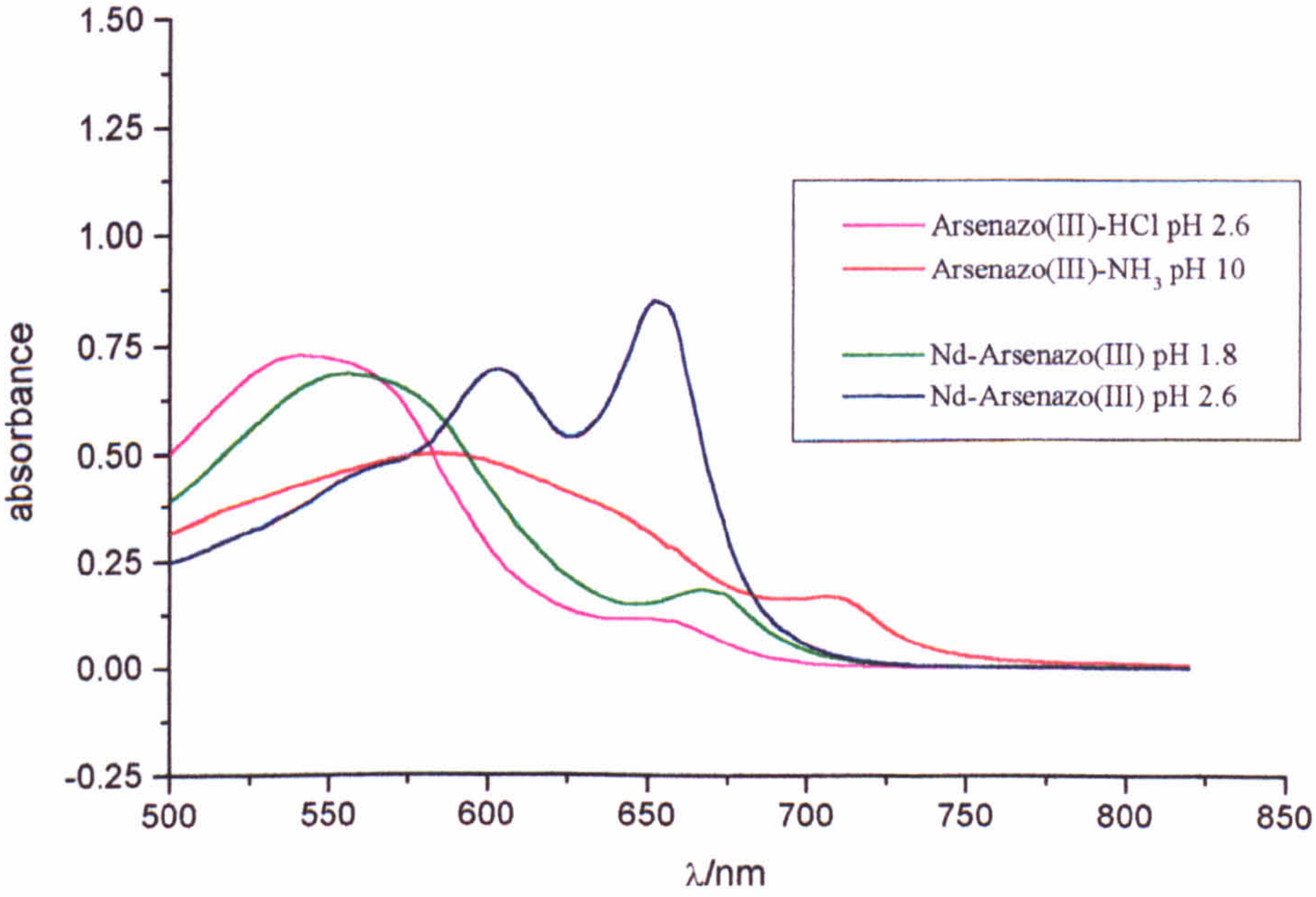

2.2.3 The effects of sample pH on lanthanide-arsenazo(III) analysis

Sequential dilution of the sample with numerous buffer and reagent solutions dilutes the sample and reduces the detection limit. Incorporating the buffer solutions into the reagent minimises the dilution effects. The minimum dilution would occur if the sample was injected directly into the reagent stream. The mixing time between the carrier-reagent solution and the sample then becomes critical as sufficient time is required for the reaction.. A two-line system of reagent solution (incorporating all required buffer solutions) and a carrier solution, which also acts as an analytical blank (e.g. H_2O for aqueous solutions) has two advantages over a single line system. A constant blank is measured between sample injections, and the sample will be mixed directly with the reagent in a 1:1 ratio when the sample and reagent streams combine.

Lanthanide solutions in the Na^+-K^+-SO_4^{2-}-CO_3^{2-}-OH^- system can vary from pH 0 to pH 13. The sample pH could therefore have a significant effect upon the absorbance, especially if the reaction pH is not sufficiently buffered. The zero absorbance was set for the injection of distilled water into a distilled water carrier stream, mixing with the reagent stream, before passing through the detector. The reagent stream alone must therefore be capable of buffering the reaction, especially as a strongly acidic sample could reduce the absorbance of the arsenazo(III) complex (Figure 2.4) to below that of the water-arsenazo(III) complex, resulting in an apparent negative absorbance of the complex or a high pH sample may not form a Ln^{3+}-arsenazo(III) complex.

Experimental

The FIA system (Figure 2.2), was reduced from a three-line manifold to a two-line manifold of containing a carrier solution and reagent solution (Figure 2.5). A distilled water carrier solution allows a continuous analytical blank to be monitored between each sample injection. The buffer solutions, required to adjust the reaction pH, were added to the reagent solution which forms the second solution line. The reagent solution was prepared from combining the formate buffer solution, ascorbic acid and the arsenazo(III), the pH of this

solution could be altered with HCl or NaOH to pH 2.6. The pH of a 10^{-5}M $LnCl_3$ sample solution was adjusted by the dropwise addition of HNO_3 or NH_3 to between pH 2 and pH 10.

The flow rate was adjusted to 1.5 cm^3/min and a 600mm mixing tube was added before the detector to allow time for the Ln^{3+} to react with the reagent but minimise the detected peak width (and maximise peak height). The wavelength of the maximum absorbance was checked by a sequence of injections on the FIA system from 600-700nm and the maximum absorbance was found at 652nm.

Figure 2.5 FIA Design for lanthanide-arsenazo(III) UV-spectroscopic analysis using a two line manifold

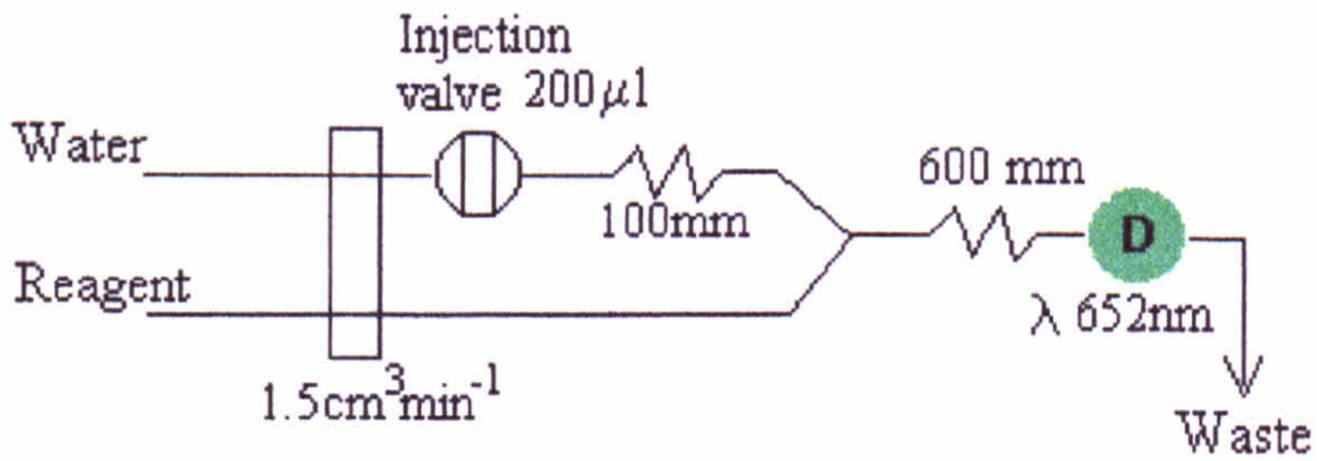

Results

There is a negative absorbance at pH 2 (i.e. less than the system blank), there was a steady increase in absorbance to a maximum at pH 4.5-5.0 (Figure 2.6). The absorbance reduces slightly from pH 5-8 then increases slightly at pH 8.5 to the same absorbance found between pH 4.5-5.0. The absorbance reduces sharply above pH 9, however this decrease could be due either to the precipitation of $Ln(OH)_3$ when the sample pH was adjusted or the complete breakdown of the Ln^{3+}-arsenazo(III) complex. The drop in absorbance from pH 5-9 is within the analytical error of the technique and not necessarily due to the sample pH.

The sample pH only has a significant affect at extreme low or high pH, however the slight variations in absorbance could be affected by the aqueous speciation in

the solution, therefore the pH of all solutions were adjusted before analysis to between pH 4-5.5, for the direct determination of total aqueous lanthanide.

Figure 2.6 The effects of sample pH upon absorbance

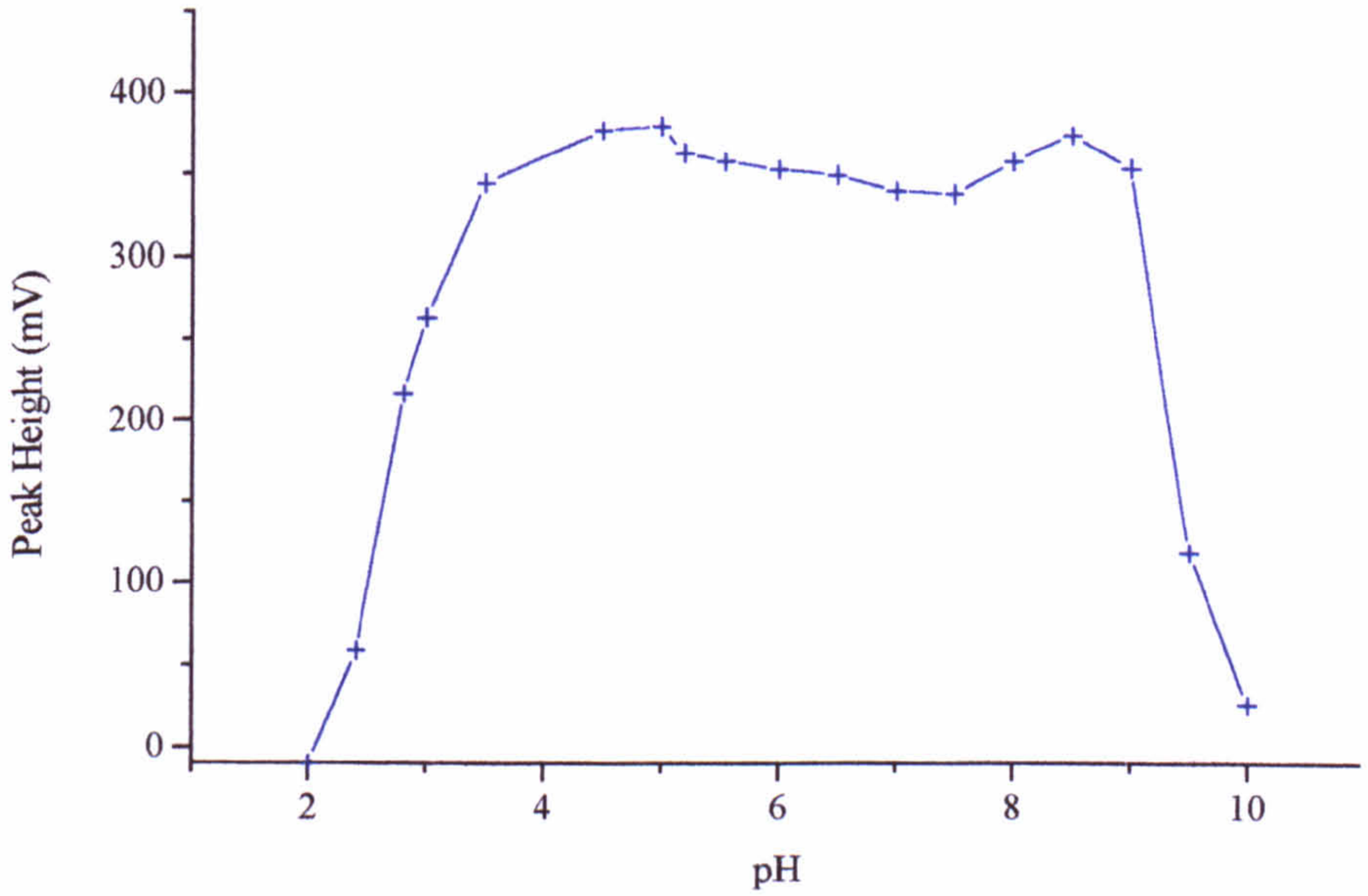

2.2.4 Ionic Interferences

The effects of interfering ions can be examined by spiking standard solutions with a variety of ions and comparing absorbance between the spiked solutions and standard solutions. There are a limited number of ions in the Na^+-K^+-CO_3^{2-}-SO_4^{2-}-OH^--Cl^- system, most of which are known not to interfere with the Ln-arsenazo(III) absorbance, however other ions may possibly interfere with the Ln^{3+} determination. Several potential interfering ions upon Nd-arsenazo(III) determination were investigated for their effect on peak response.

Experimental

A standard $NdCl_3$ (10^{-5}M) solution was injected to determine a standard peak height, a series of solutions were diluted to 10^{-5}M Nd^{3+} with varied concentrations of potential interferences.

Results

A species was considered to interfere with the determination if the ion had a greater than 10% effect upon the standard peak response. The level of interference required to affect lanthanide determination is shown in Table 2.2 Na^+, K^+, Cl^- and SO_4^{2-} have a minimal interference effect upon the lanthanide determination, however CO_3^{2-} increases the peak response due to the formation of CO_2 from acidifying the samples, causing an increase in the refractive index of the solution. Excessive bubble formation from degassing CO_2 can inhibit all lanthanide determinations in carbonate solutions as the reagent and lanthanide sample cannot mix before passing through the detector.

Table 2.2 Summary of the interference ions on the peak height of a 10^{-5}M Nd^{3+} solution

Interferent	[interferent]/[Nd]	%RE
Na^+, Mg^{2+}, Cl^-, SO_4^{2-}, NO_3^-	10,000	<10
Cu^{2+}	1,000	<5
K^+	500	<5
Ni^{2+},	200	<10
Cd^{2+}, Fe^{3+}	200	<5
Ba^{2+},CO_3^{2-}	50	<10
Ca^{2+}	50	<5
Co^{2+}	100	<10
V^{3+}	40	<10
Zn^{2+}, Al^{3+}	30	<10
Pb^{2+}	12	<10
EDTA	1	<5
Ti^{4+}	0.1	<10

2.2.5 Linear calibration range

Experimental

The FIA system for the determination of aqueous lanthanides using arsenazo(III) and UV-spectroscopy was optimised as a two-line system (Figure 2.5). The linear calibration range of the system was found by the repeated injection of a series of standards. The peak response was taken only after five duplicate peaks were obtained for each standard.

Each sample was acidified immediately after filtration to between pH 4 and 5.5, to homogenise the pH of each sample before analysis. The acidification also reduced the carbonate concentration of each sample by degassing a significant amount of $CO_2(g)$, which must be removed from the solution before analysis. A 200μl sample was injected for 15 seconds into a distilled water carrier solution, before mixing with the reagent solution, prior to passing through a UV-detector, that measured the absorbance at 652nm. The reagent solution composition and the FIA system parameters are given in Table 2.3 for the system calibration and sample determinations.

Table 2.3 The reagent solution composition and analytical procedure for the analysis and calibration of an FIA-UV system for the determination of aqueous lanthanides using arsenazo(III)

Carrier solution/System blank distilled water	FIA system parameters
Reagent solution Arsenazo(III) 0.05g Ascorbic Acid 5g (Formate Buffer) Formic Acid $12cm^3$ NaOH 6g Dilute to $1dm^3$ and adjust to pH 2.6 with HCl	Detector wavelength λ 652nm Injection time 15seconds Delay time 65seconds Flow rate $1.5cm^3$/min
Sample solution adjust to pH 4-5.5	Sample injection volume 200μl

Results

The two-line system has a linear calibration between $1x10^{-6}$M and $2x10^{-5}$M Ln^{3+} (Figure 2.7). Above $2x10^{-5}$M Ln^{3+} (by $3x10^{-5}$M Ln^{3+}) the calibration is not linear and the absorbance tapers off to a plateau (Figure 2.8).

Figure 2.7 Linear calibration range for Ln^{3+}-Arsenazo(III)

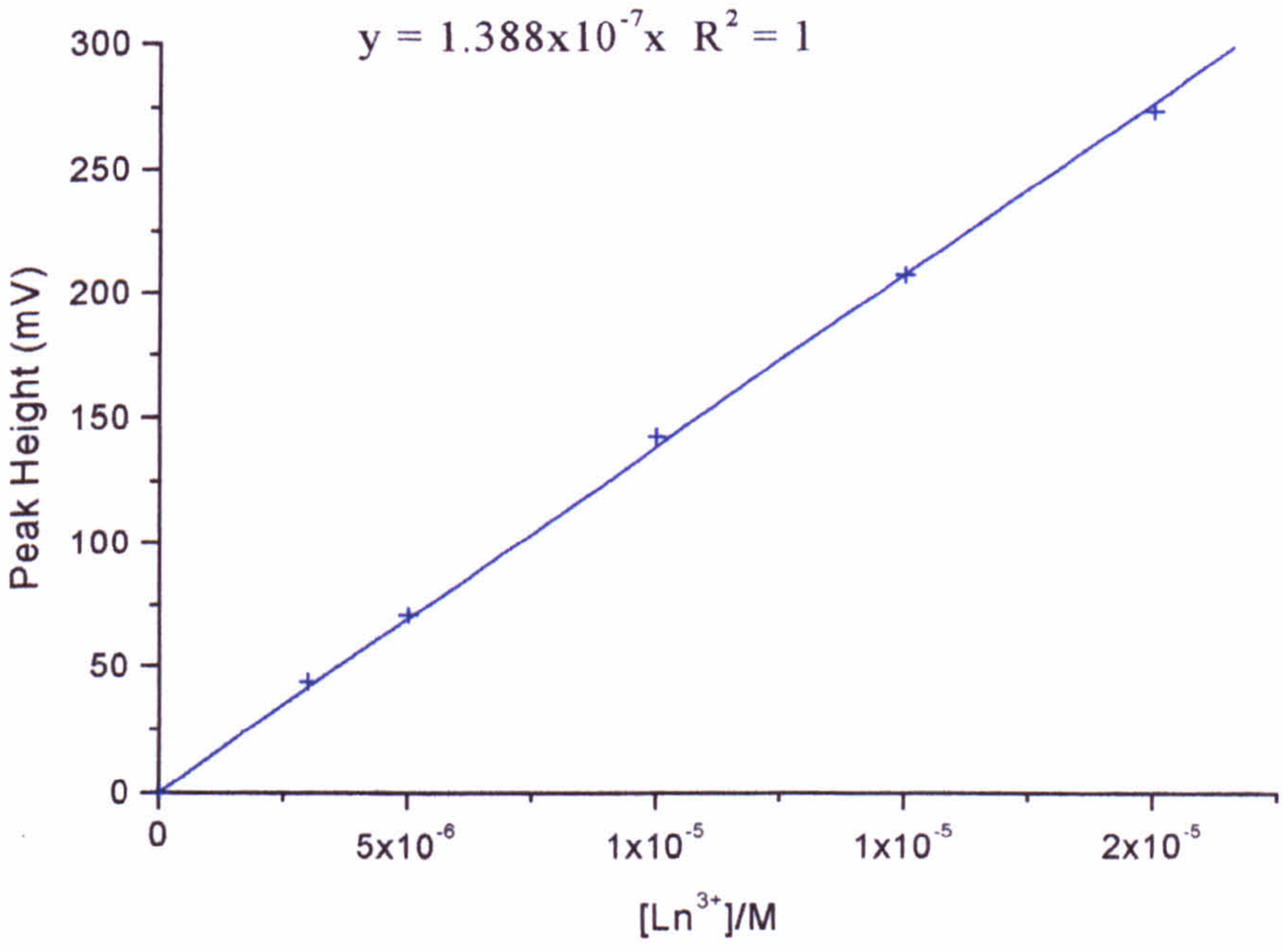

Figure 2.8 Calibration range for Ln^{3+}-Arsenazo(III) determinations with a two-line manifold

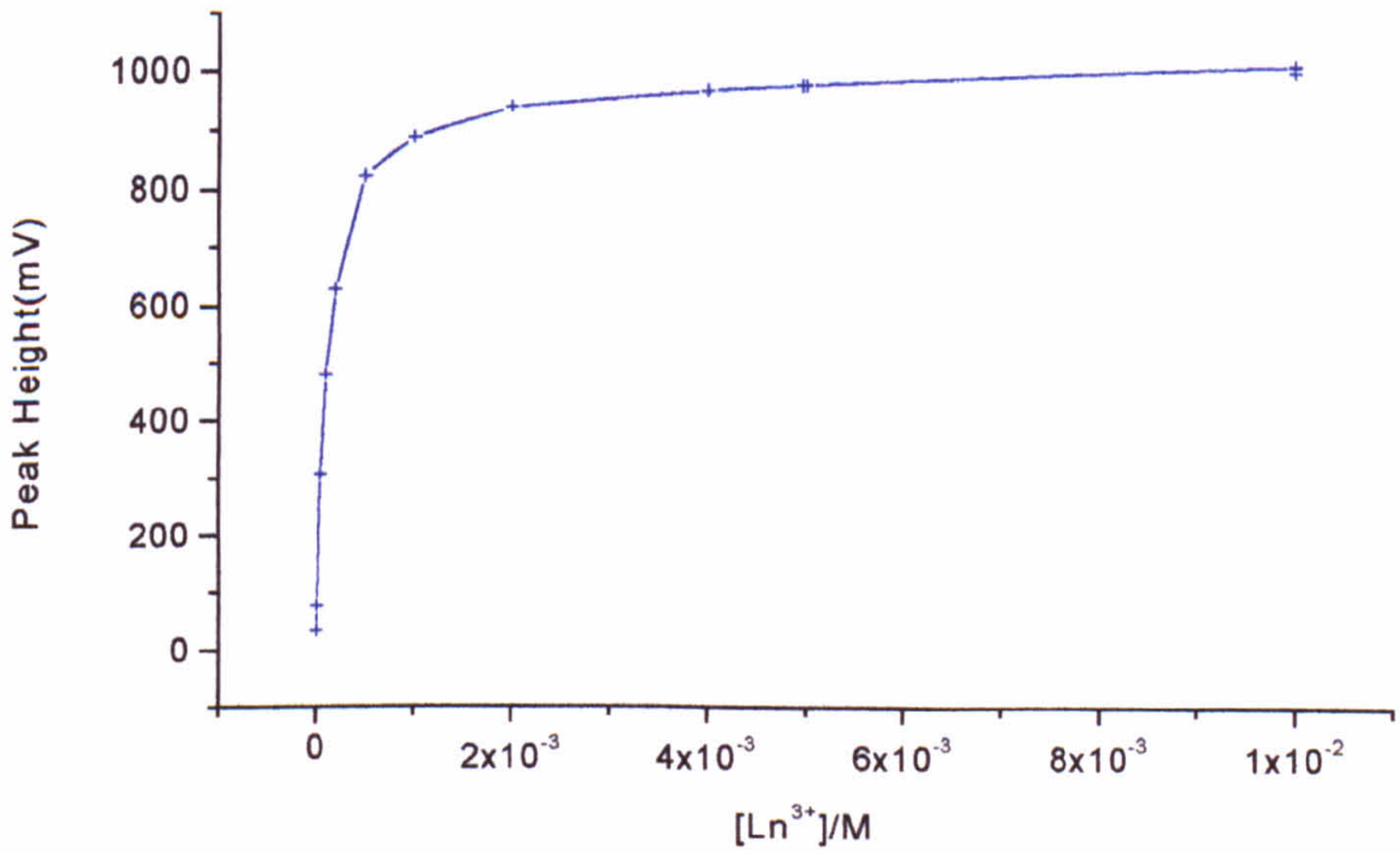

2.2.6 On-line preconcentration of lanthanides to lower the analytical detection limit

Solutions with less than $1x10^{-6}M$ Ln^{3+} can be analysed by preconcentration of the lanthanides on an ionic resin online in the FIA system, then eluted with acid, before mixing with the reagent then passing through the UV detector. The concentration (and separation) of lanthanides upon ionic resins is an established technique for on and off-line analytical methods especially for ICP and AAS determinations which are independent of the solution conditions (i.e. pH).

Experimental

The two-line FIA system (Figure 2.5) was adapted to include a column filled with an ionic resin inserted into the carrier stream after the injection loop (Figure 2.9). The sample in the injection loop was replaced with HCl to elute the column. A three-way tap was added to the carrier stream to switch between the sample solution and water. A HCl/NH_4OH (0.4M) buffer solution was added to the reagent to counter the effects of the eluting acid.

Figure 2.9 FIA design for the on-line preconcentration of lanthanides

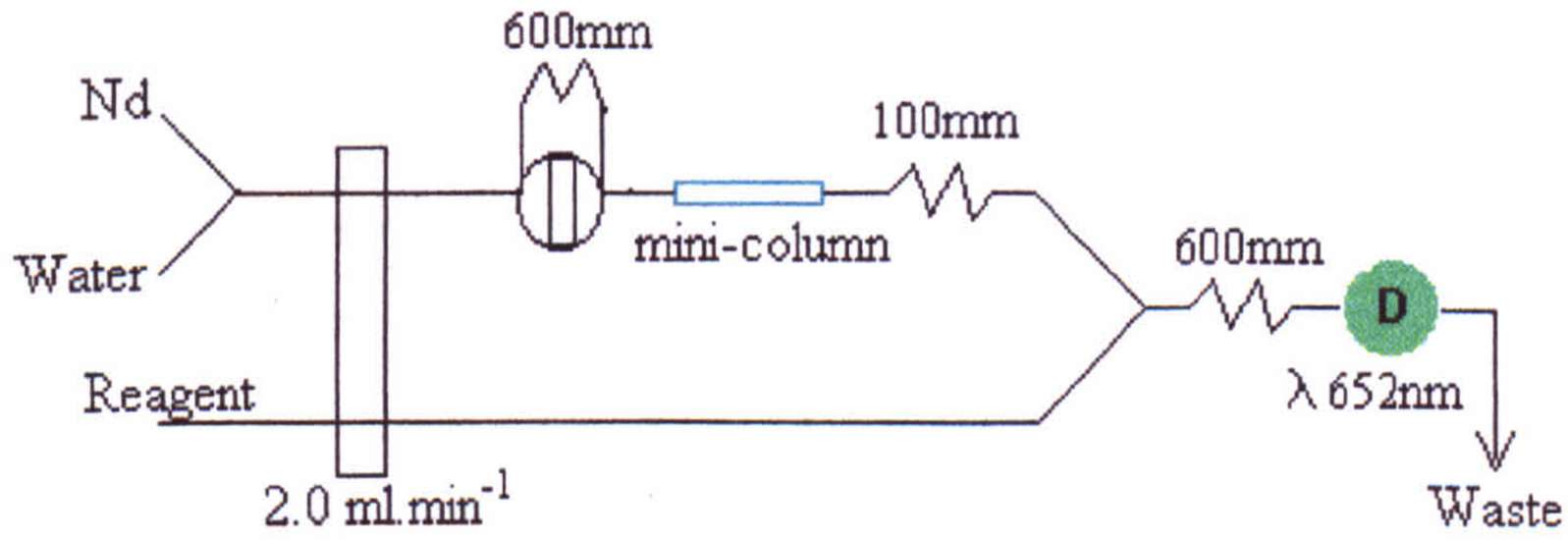

The carrier line and column was washed with acid to remove any Ln^{3+} in the system, then distilled water to remove the acid. The sample was loaded onto the column for a predetermined time, then the 3-way tap turned to wash all the remaining Ln^{3+} in the carrier stream onto the column. The efficiency of the column loading can be monitored from the amount of Ln^{3+} passing through the detector. When the column has been washed with water, acid was then injected

through the column to elute the concentrated Ln^{3+} from the column then through the detector as a sharp pulse. Two further acid injections determine the efficiency of the acid to elute the column and regenerate the column for the next sample. Standards are similarly preconcentrated to give a direct comparison with the samples.

Five resins, two column lengths and two acid concentrations were examined to determine the most suitable resin for preconcentration. The resins vary from the strongly cationic binding Chelex 100 (typically used for ICP-AES analysis) to the weakly cationic binding Amberlite IRC-50, were placed in glass tubing (internal diameter 4mm) to form resin filled columns, plugged with glass wool, 20mm or 50mm in length. The columns were then eluted with either 0.01M or 0.1M HCl. The column was eluted three times with acid to ensure complete removal of the lanthanide and to regenerate the column between samples.

Results

The peak responses (Figure 2.10) show that a 20mm Amberlite IRC-50 filled column is most appropriate when eluted with 0.01M HCl for arsenazo(III)-UV lanthanide determination.

The 50mm columns show a reduced response compared with the 20mm columns, indicating stronger acid was required to elute the Ln^{3+} from the column. However, increasing the acid concentration had a negative effect on the peak height (i.e. a smaller peak response) by decreasing the reaction pH between the lanthanide and reagent solution, which is highly pH sensitive reaction.

Chelex 100 is the favoured resin for preconcentration before ICP analysis (Grenva *et al.*, 1996), as the stronger resin is a more efficient aqueous metal concentrator, however the concentrated acid (above 2M) required to elute the column has a negative effect upon the arsenazo(III) reagent.

The 0.01M HCl used to elute the lanthanides from the amberlite IRC-50 column had the minimum effect upon the arsenazo(III), although there are slight negative peaks when the acid is injected through the empty column.

Figure 2.10 Peak responses for the FIA-UV arsenazo(III) determinations on the on-line preconcentration of lanthanides on various ionic resins, to determine the optimum ionic resin, column length and eluting acid concentration

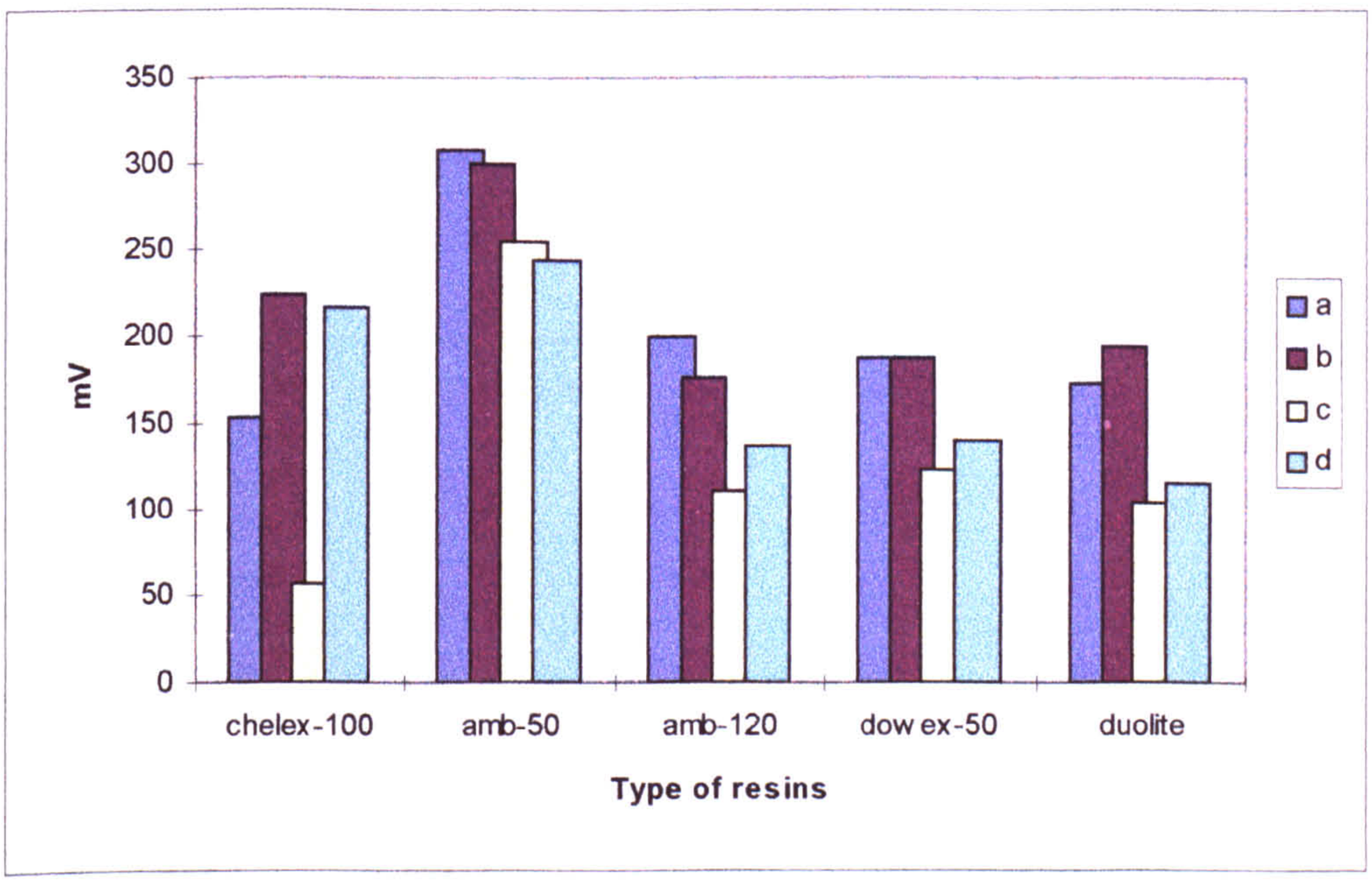

Where a = 2 cm column length and 0.01 M HCl

b = 2 cm column length and 0.1 M HCl

c = 5 cm column length and 0.01 M HCl

d = 5 cm column length and 0.1 M HCl

The optimum column ($2cm^3$ amberlite IRC-50) when loaded for 2 minutes has a linear calibration range up to $6x10^{-7}$M Ln^{3+}, above this concentration the column loading is less efficient resulting in a tapering of the calibration line (Figure 2.11). Lower concentrations can be determined by longer loading times.

Figure 2.11 The calibration range for the preconcentration of Ln^{3+} on a $2cm^3$ amberlite IRC-50 micro-column, after loading for 2 minutes, then eluting with HCl (0.01M)

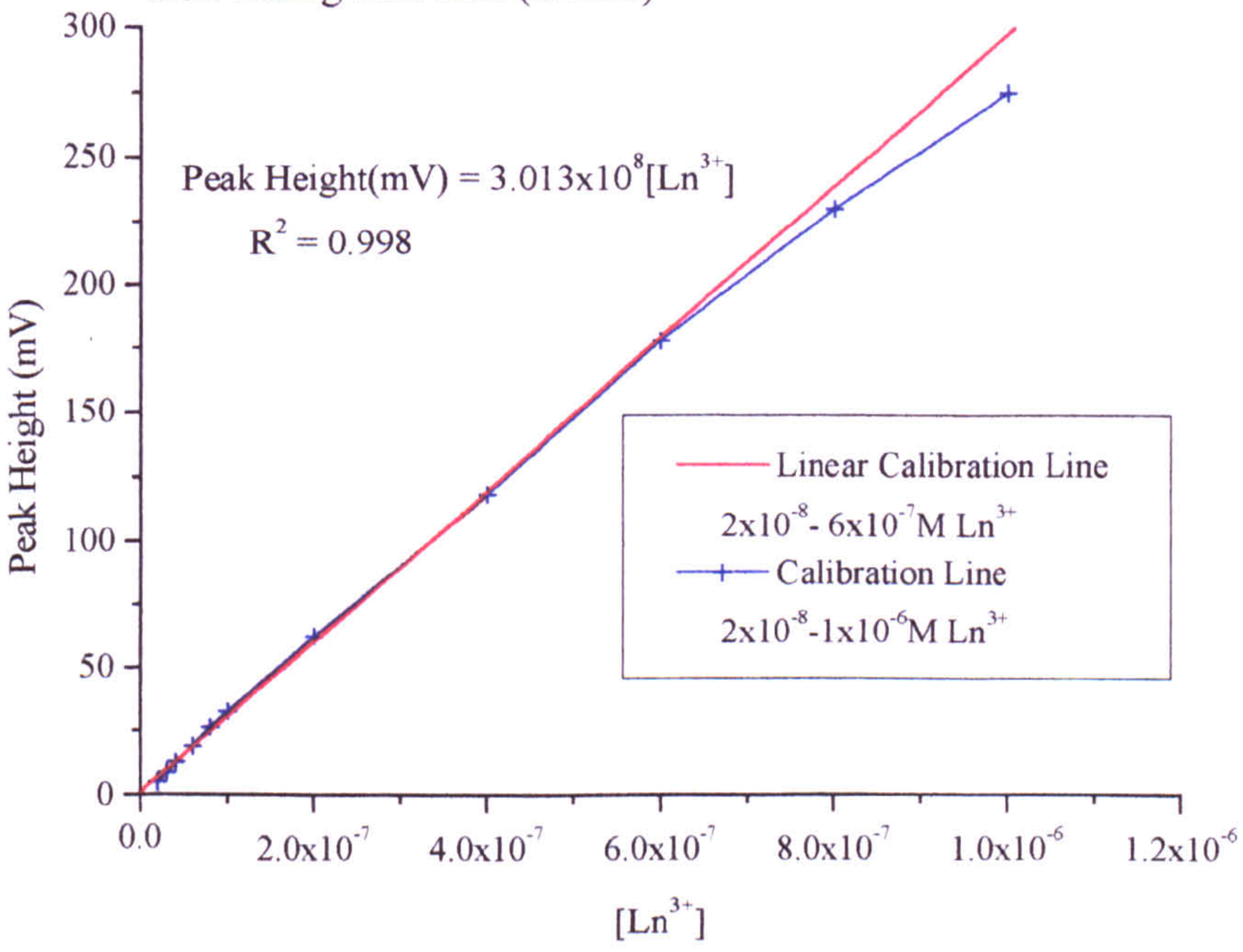

2.2.7 Effects of ionic strength and loading time on preconcentration

Ln^{3+} can be eluted from the column at pH below 3 and will load onto the amberlite IRC-50 column between pH 4 and 7. Below pH 4 the $LnCl_3$ solutions will be partially eluted and above pH 7 hydroxy complexes dominate aqueous lanthanides ions, which compete with the resin for the aqueous lanthanides, therefore the sample will not be retained sufficiently during the loading of the column.

Sample solutions primarily contain Na^+, K^+ and CO_3^{2-} ions in solution which compete with the lanthanides for the resin or can form aqueous lanthanide complexes with a negative charge that will inhibit adsorption to the resin.

The effects of excess Na^+ ions on column loading

The effects of ionic strength and competition for the resin can be examined by spiking standard solutions with NaCl, which do not affect the solubility of the

$LnCl_3$ standards. $LnCl_3$ ($1x10^{-5}$M to $8x10^{-5}$M) solutions were diluted by 100 with either 0.1M NaCl or distilled water then concentrated on the column.

Results

Figure 2.12 The effects of loading time and NaCl concentration (0.1M) on column efficiency

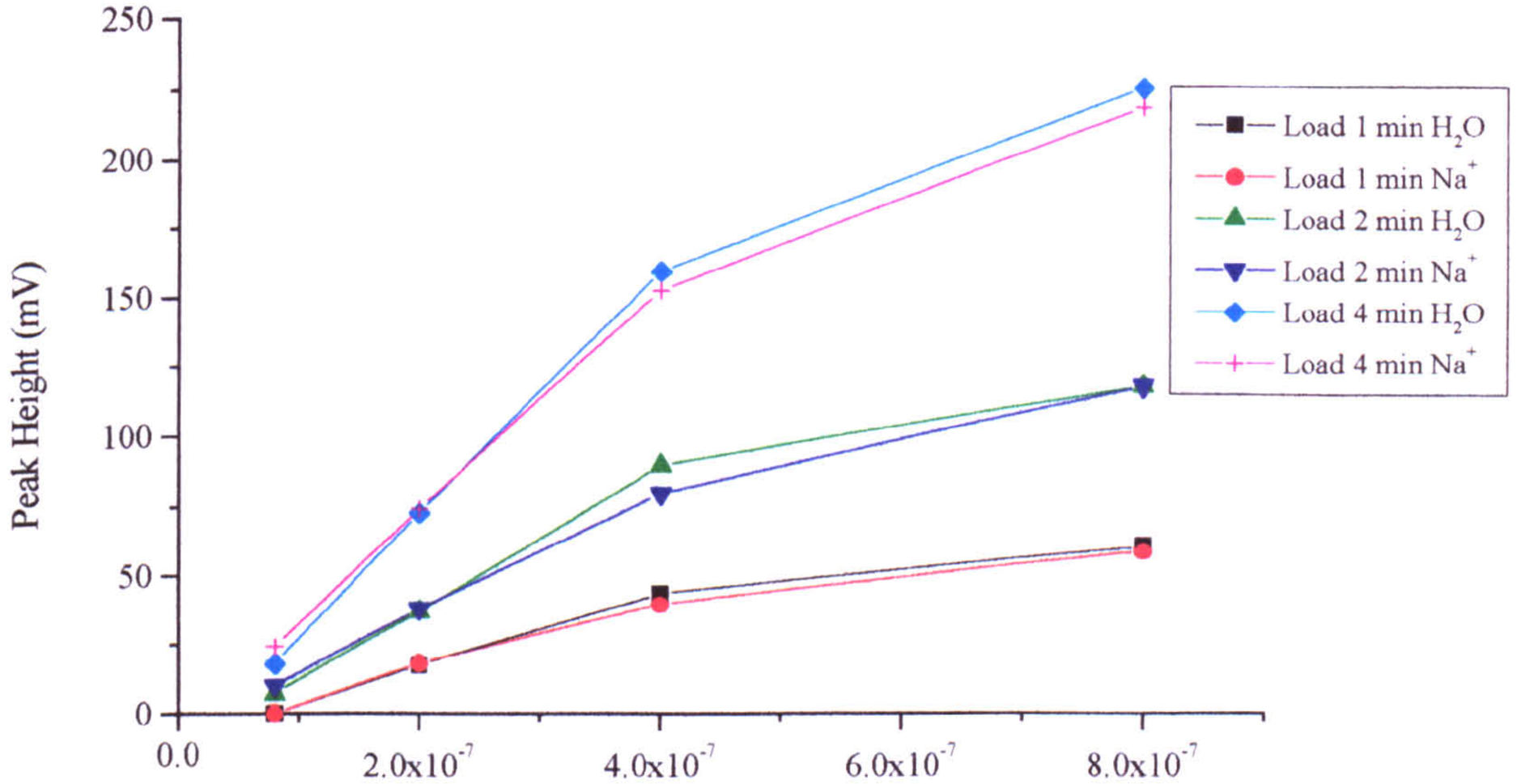

$[Ln^{3+}]$

NaCl (0.1M) has no apparent effect upon the preconcentration of lanthanide in solution at pH 5-7 (Figure 2.12). The Ln^{3+} ion is more strongly adsorbed than the Na^+ at weakly acidic pH, however there is a maximum aqueous concentration of Ln^{3+} (between $4x10^{-7}$M and $6x10^{-7}$M) that can be loaded efficiently onto the column to give a linear calibration (Figure 2.11 and 2.12), The maximum lanthanide concentration that can be loaded, appears to be independent of the loading period, however more concentrated solutions do not require preconcentration.

The interference of pH and anions on the loading of columns

There is a further problem on the actual loading of the column. If a lanthanide solution contains aqueous carbonate there is a definite effect upon sample loading. Carbonate samples adjusted to pH 5-7, show a peak response when the

lanthanide solution is loaded onto the column (Figure 2.13), the peak returns to the baseline when the column is washed with distilled water before eluting with acid.

Figure 2.13 The effects of lanthanide-carbonate complexes on loading the amberlite IRC-50 preconcentration column

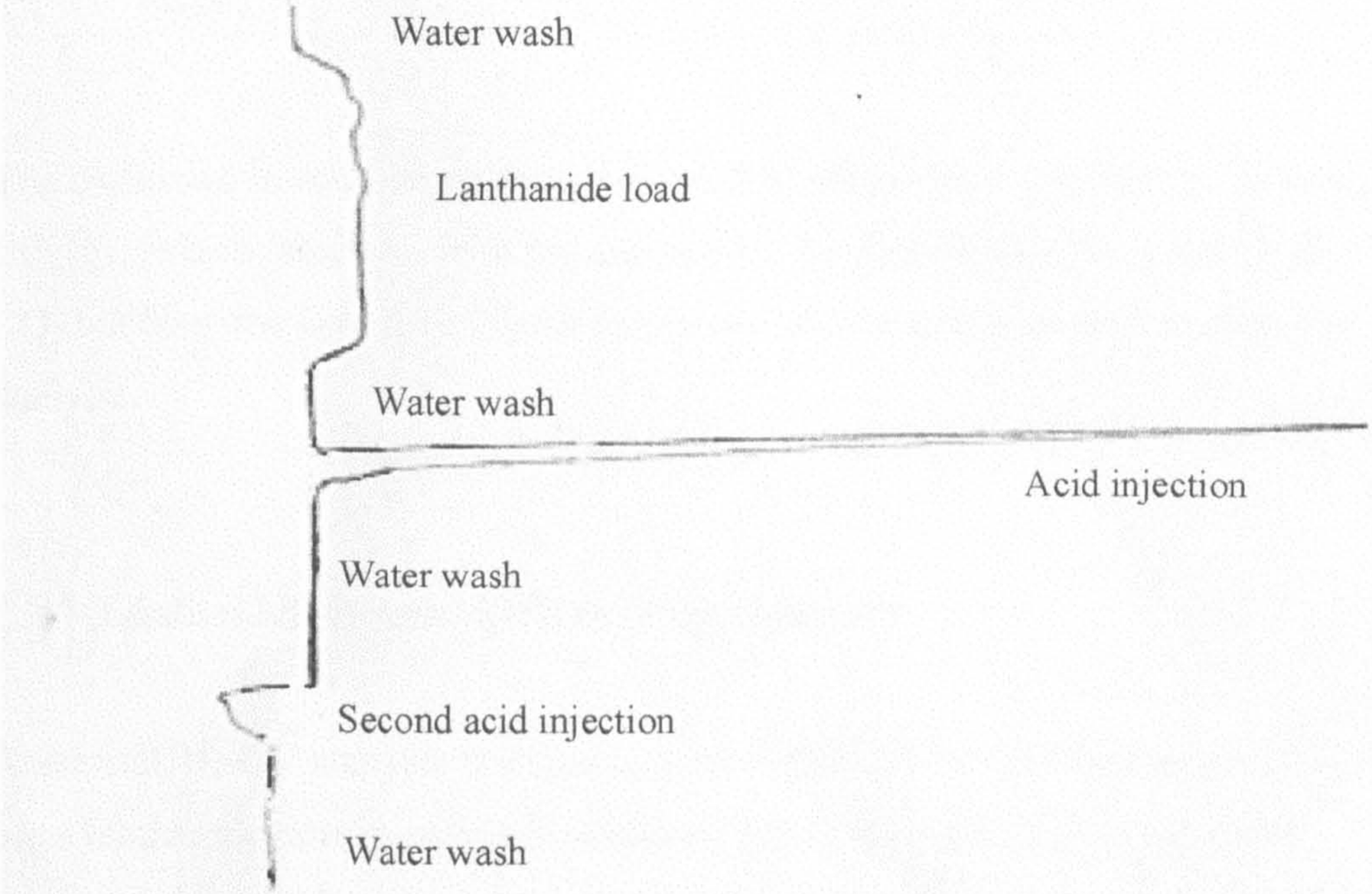

The lanthanide loading peak response is pH dependent and can be eliminated if the sample pH is altered to between pH 4-5. Typical sample solutions (Chapter 4) may contain between 10-50mM carbonate at pH 8-11. When the solution pH is at pH 5, Ln^{3+} is the dominant aqueous ion in a 20mM carbonate solution (Table 2.4). At the slightly higher pH of 7 a significant amount (above 80%) of the aqueous lanthanide is present as $LnCO_3^+$ or $Ln(CO_3)_2^-$, which are much larger and lower charged complexes than Ln^{3+}. Below pH 4 the solution is saturated in H^+ ions and Ln^{3+} ions are not loaded onto the column.

Table 2.4 The effects of pH on Nd aqueous speciation in carbonate solutions.

Solution composition		Nd speciation at pH 5		Nd speciation at pH 7	
Nd^{3+}	$5x10^{-7}M$	Nd^{3+}	$4.1x10^{-7}M$	$Nd(CO_3)_2^-$	$3.1x10^{-7}M$
Na^+	50mM	$NdCO_3^+$	$8.0x10^{-8}M$	$NdCO_3^+$	$1.9x10^{-7}M$
TIC	20mM	$NdCl^{2+}$	$5.9x10^{-9}M$	Nd^{3+}	$2.7x10^{-9}M$
Cl^-	10mM				

The carbonate in solution also has a secondary effect when acidified by degassing $CO_2(g)$, which interferes with the analysis by the formation of large volumes of CO_2 bubbles that alter the refractive index of the solution and interfere with the analysis.

2.2.7 Lanthanide-arsenazo(III) analysis summary

Arsenazo(III)-UV analysis is a cheap, simple method for the multiple analysis of trace lanthanide determination in solution, which does not require extensive sample pretreatment before analysis. The linear calibration range from $1x10^{-6}$ M to $2x10^{-5}$M, or from $2x10^{-8}$M to $6x10^{-7}$M total aqueous Ln^{3+} when preconcentrated on-line for 2 minutes on an amberlite IRC-50 resin, is significantly lower than standard flame or graphite furnace AAS techniques.

The only sample preparation required is acidification to pH 4.5-5.0 before analysis to reduce analytical errors due to the effects of sample pH upon the peak response. The pH ensures that the sample can be preconcentrated without further treatment if required.

The initial peak height reproducibility within samples is often poor , and a series of up to ten injections is required before a reliable average peak height can be calculated. The peak height usually starts as a maximum or minimum (independent of the previous sample or standard) before gradually levelling off to

a stable plateau of ±1mV from a set of at least five sequential injections, the variation in peak height is rarely random.

Calibration standards using the peak height of the plateau form a linear calibration line with an R^2 within the range of 0.9977-1.000. The peak heights from the initial injections of each sample or standard often bear no resemblance to the plateau peak height.

2.3 Ce Analysis by fluorescence spectroscopy

Fluorescence is the radiation emitted when an ion or molecule excited by the adsorption of radiation returns to the ground state. The wavelength of the emitted energy is displaced to a lower frequency than the exciting radiation due to a slight loss of vibrational energy to the surroundings. Most fluorescence occurs from organic molecules or biorganic compounds however some lanthanides, uranium and thorium are the only simple inorganic ions that fluoresce. In 1968 Cukor and Weberling suggested $Ce^{3+}_{(aq)}$ could be determined by fluorescence in solution without pretreatment and little inorganic interference. Nd^{3+}, Na^+, K^+, Cl^-, SO_4^{2-} and CO_3^{2-} do not significantly interfere with the fluorescence. The intense Ce^{3+} fluorescence is however influenced by pH. Below pH 4, the Ce^{3+}(aq) intensity is constant, but decreases (or quenched) as Ce^{3+} hydrolyses (Jianxin *et al.*, 1998).

NO_3^- and Fe(III) are notable exceptions to the simple common ions as they also adsorb the excitation energy required to promote Ce^{3+} fluorescence. The Fe(III) interference can be eliminated by reduction to Fe(II), but NO_3^- must be removed from the sample. The Ce^{3+} fluorescence is also quenched by oxidation to Ce^{4+}, this regular quenching has led to the indirect determination of other elements such as Eu^{3+}, As(V) and Fe^{3+} by Al-Sowdani and Townshend (1987) which oxidise Ce^{3+} to Ce^{4+}.

2.3.1 Determination of the optimum fluorescence excitation and emission wavelengths

Al-Sowdani and Townshend (1986) suggest the maximum fluorescence occurs with an excitation wavelength of 260nm and emission wavelength of 350nm. The emission and excitation wavelengths were confirmed by an emission and excitation scan from 200-800nm with $1x10^{-5}M$ $CeCl_3$, by holding the emission or excitation wavelength constant and varying the excitation and emission wavelength respectively upon a Kontron Instruments SFM25 Spectrofluorimeter.

The wavelength scans show an emission maximum at the excitation wavelength and 550nm for the Ce solution and the water blank and a peak due to Ce^{3+} alone at an emission wavelength of 360nm (Figure 2.14). The fluorescence maximum was found with an excitation wavelength of 259nm.

Figure 2.14 Ce^{3+} flourescene emission scan Excitation λ 274nm

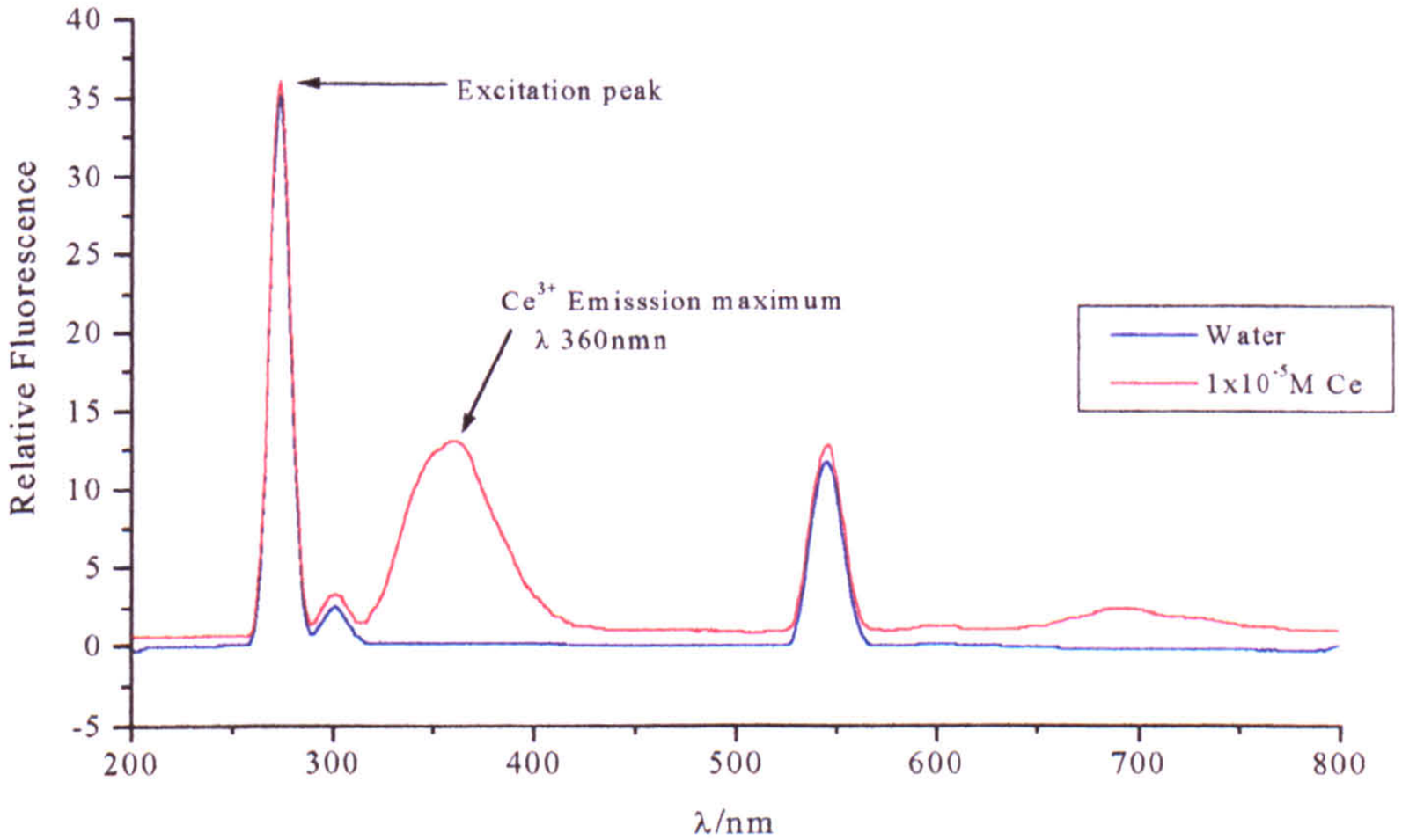

2.3.2 Ce^{3+}Calibration

The aqueous Ce^{3+} concentration in simple inorganic solutions was measured directly by the fluorescence emitted in a Kontron Instruments SFM 25 Fluorimeter. All sample and standard solutions were acidified with H_2SO_4, then

2 cm^3 of each aqueous solution was transferred to a quartz glass cell, and placed in the spectrofluorimeter. the sample was excited at 259nm and the relative fluorescence of the Ce^{3+} (aq) emission was measured at 360nm.

The aqueous Ce^{3+} concentration is directly proportional to the fluorescence emission peak height, which gave a linear calibration between $5x10^{-8}$M and $1x10^{-4}$M Ce^{3+} with an R^2 above 0.99 (Figure 2.15)

Figure 2.15 Ce^{3+} Fluorescene Calibration at Emission λ 259nm Excitation λ 360nm

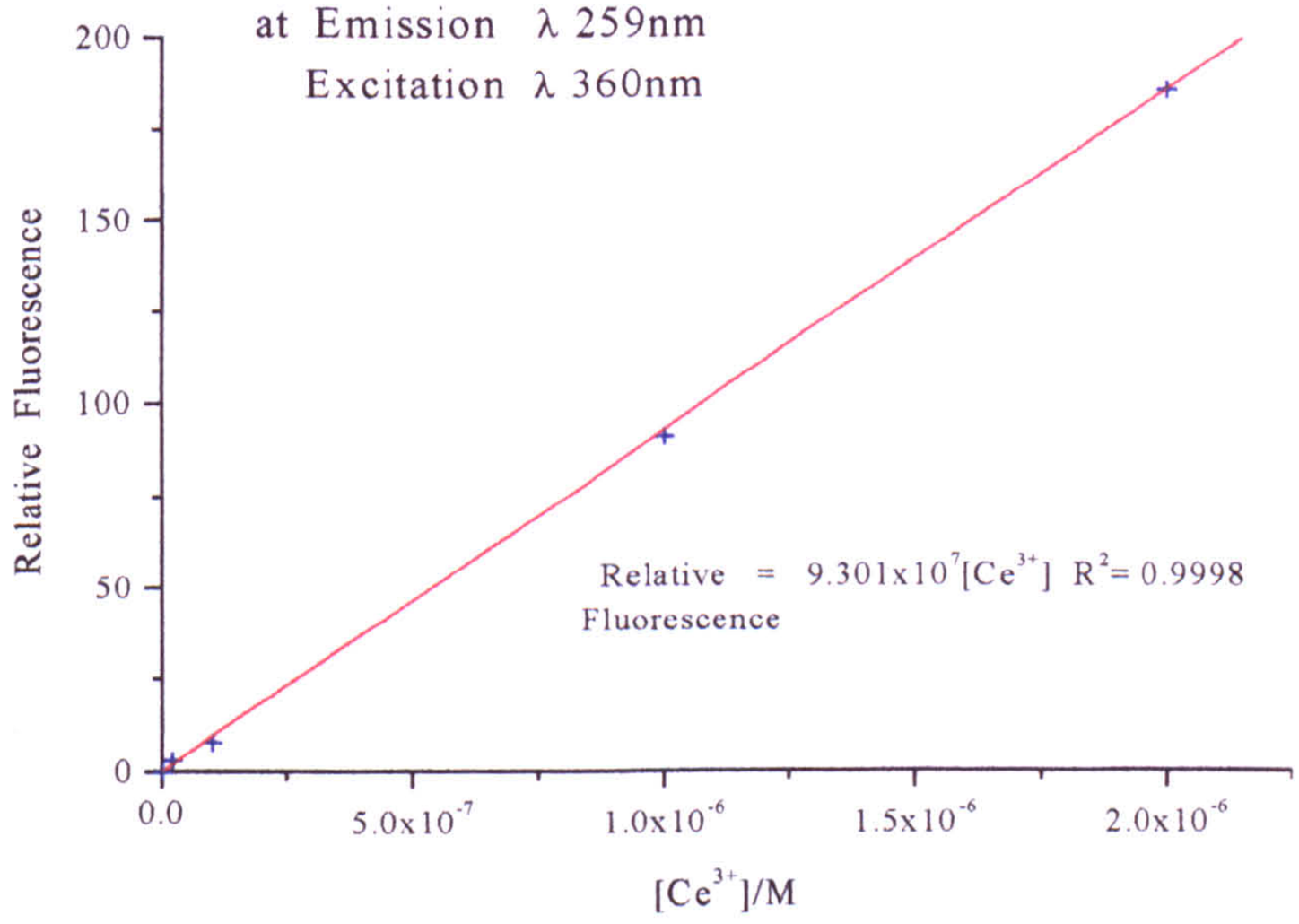

r

Figure 2.16 Comparison of the effects of acid on the quenching of Ce^{3+} fluorescence of aqueous $4x10^{-6}$ M $CeCl_3$ solutions

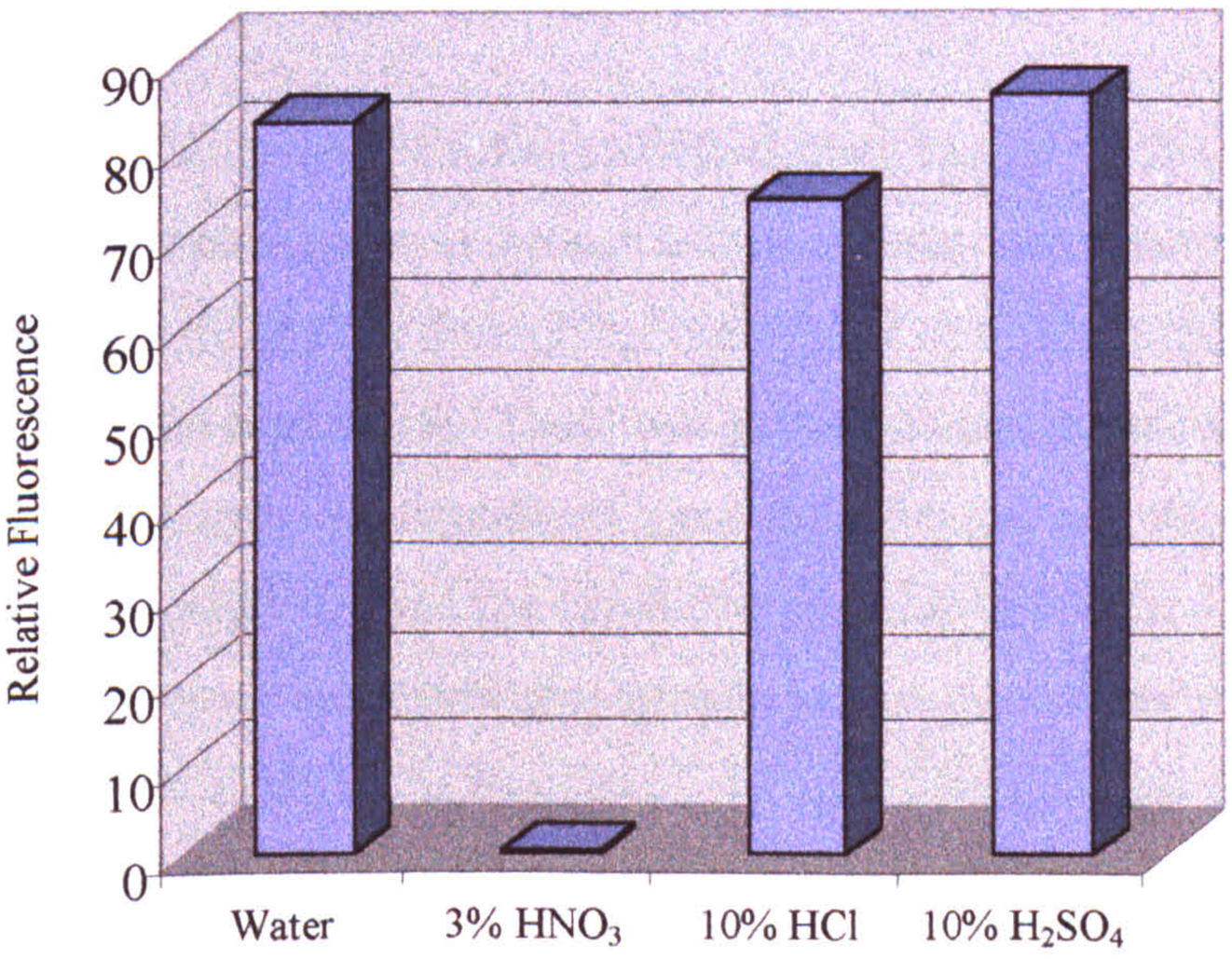

The effects of acid quenching on Ce^{3+} fluorescence

Care must be taken when acidifying the sample and standard solutions to below pH 4 without using HNO_3, the standard acid used to acidify samples, as the NO_3^- ion has a significant quenching effect (Figure 2.16). If other unknown nitrates were present in the sample, a similar quenching effect would occur.

2.4 ICP-MS analysis

Inductively Coupled Plasma (ICP) is a method of generating a high temperature environment (above 5000K), which is capable of ionising most elements (Evans, 1998). The plasma will ionise multi-element samples (or standards), which are usually introduced as aqueous solutions, before the successive determination of each element. The ionised elements are usually detected by one of two methods, Atomic Emission Spectrometry (AES) or Mass Spectrometry (MS). ICP-AES is not routinely used for lanthanide analysis as detection limits are higher than for ICP-MS techniques and the close emission lines from mixtures of lanthanides often interfere. In contrast the lanthanides are heavy metals, each of which has a unique stable isotope, which can be detected in mixed systems.

Plasma generation

The plasma is generated by coupling radiofrequency energy into a gas via a magnetic field which is induced through a two- or three-turn water cooled copper coil. Two Ar gas flows flow through the outer tubes of a concentric, three-tubed silicon torch in the copper coil. These two gas flows become turbulent as they merge within the torch. An introduced spark seeds the gas with electrons, which accelerate in the magnetic field and reach energies that ionise the Ar gas into a plasma. The plasma is self-sustaining through almost instantaneous collisions with other gaseous atoms. The magnetic field causes the ions and electrons to flow in the horizontal plane of the coil, heating the neutral argon by collisions that produce a plasma that ranges in temperature from 8000-10000K down to 5000-6000K in the tail flame.

The sample is introduced within an Ar gas flow through the central quartz tube into the plasma.

The plasma causes almost complete decomposition and ionisation to singly charged ions of most of the elements. Most elements are over 80% ionised with the notable exception of the halogens and noble gases.

Quadrupole mass analyser

Quadrupoles are four metal rods into which a combination of radiofrequency (RF) and direct currents (DC) are applied to each pair of rods to create an electric field between the rods which allow ions in a narrow mass/atomic number (*m/z*) range to pass through. Changing the RF/DC ratio allows the quadrupole to scan through a range of *m/z* for specific isotopes. The number of ions of each required isotope entering the detector per second is then counted.

Sample Preparation

The samples were analysed using a Fisons Instruments VG Elemental Plasma Quad 2^+ ICP-MS which was tuned to Pr (which exists as the single isotope ^{141}Pr). All the samples and standards were spiked with Rh (100ppb) as an internal standard, then acidified with 10% HNO_3, to stop precipitation of the Rh. The solution was then analysed for Rh, Ce, Nd and Eu. Each lanthanide has at least one unique isotope (Table 2.5) which can be analysed sequentially and a detection limit of approximately 10^{-8}M in aqueous solutions, using the appropriate lanthanide standards and a solution blank.

Interferences occur from the masses of Ar-air complexes, which occlude some elements i.e. C, S and the first transition period. This interference does not occur with heavier metals such as the lanthanides.

Table 2.5 Isotopes used for the aqueous lanthanide ICP-MS analysis

Element	Rh	Ce	Nd	Eu
Isotope	103	140	146	151
% Natural abundance	100	88.5	17.2	47.8

Figure 2.17 The ICP-MS calibration from $5x10^{-9}$M to $1x10^{-5}$M of aqueous Nd and Eu

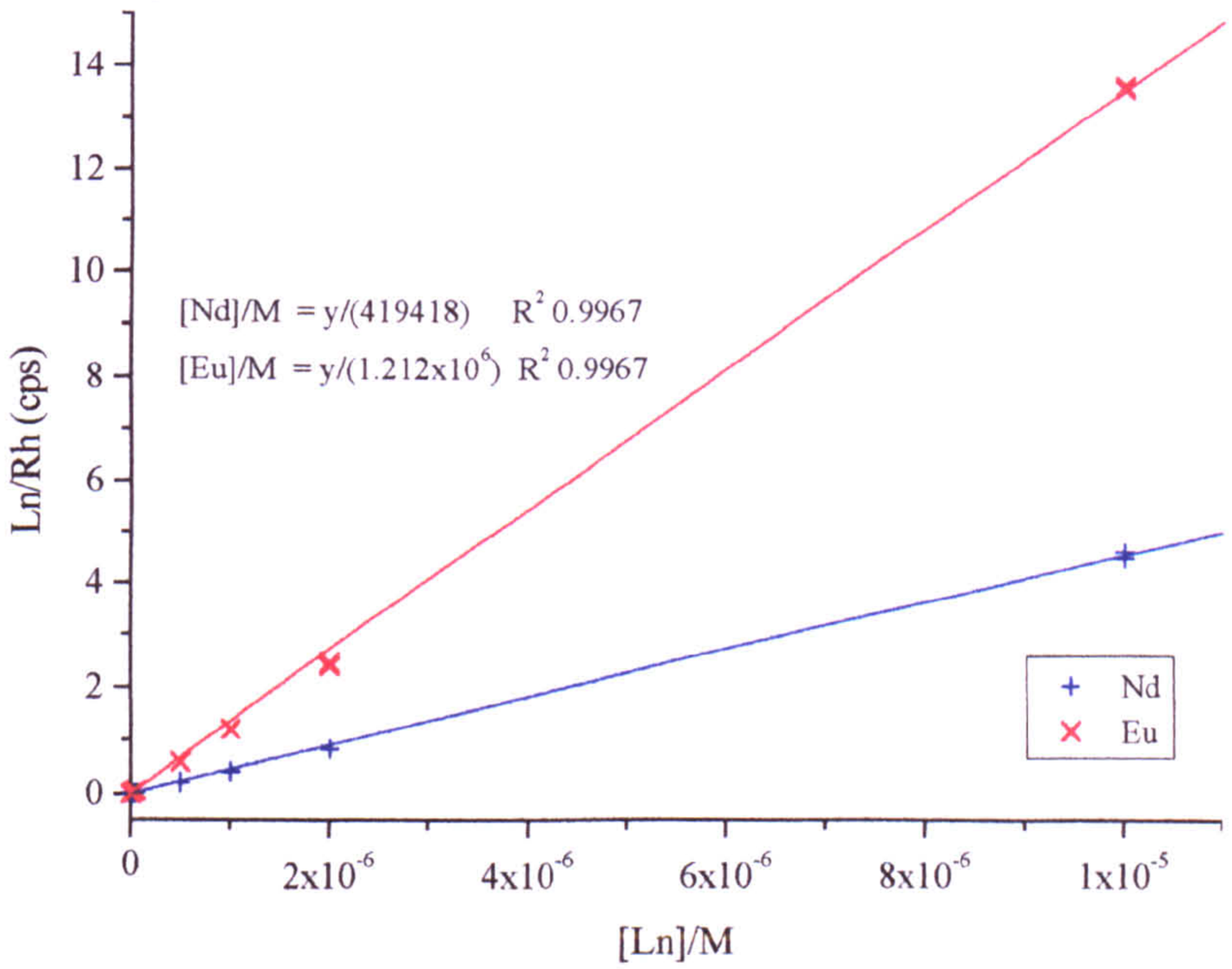

There is a greater response (and consequently lower detection limit) for Eu than Nd (Figure 2.17), due to the larger proportion of the Eu isotope used for the analysis (Table 2.5). Similarly Ce, would be expected to have an even lower detection limit than Eu.

2.5 Comparison of the aqueous lanthanide analytical techniques (FIA-UV, ICP-MS and fluorescence spectroscopy)

FIA-UV arsenazo(III) is a cheap simple convenient bench top analytical technique that does not require the facilities or expense required for ICP analysis, however detection limits for preconcentration with arsenazo(III) are similar to that of the

ICP-MS. There is a close agreement between the Arsenazo(III) and ICP-MS techniques (Table 2.6), for the determination of a set of Nd and Eu samples.

Table 2.6 Comparison of duplicate FIA-arsenazo(III) and ICP-MS analysis for Nd and Eu bearing samples

Sample	ICP-MS I	ICP-MS II	FIA I	FIA II
NdC 7a	2.9×10^{-6} M	2.8×10^{-6} M	2.2×10^{-6}M	4.3×10^{-6} M
NdC 7b	1.4×10^{-7}M	1.4×10^{-7}M	5.4×10^{-7}M	3.5×10^{-7}M
NdC 7c	2.8×10^{-7}M	2.7×10^{-7}M	6.5×10^{-7}M	8.1×10^{-7}M
NdC 7d	6.9×10^{-7}M	6.7×10^{-7}M	5.9×10^{-8}M	3.5×10^{-6} M
NdC 7e	5.3×10^{-8}M	5.1×10^{-8}M	8.3×10^{-7}M	3.2×10^{-6} M
NdC 7f	3.4×10^{-7}M	3.3×10^{-7}M	1.2×10^{-7}M	4.7×10^{-7}M
EuC 7a	4.2×10^{-5}M	4.3×10^{-5}M	4.0×10^{-5}M	
EuC 7b	3.6×10^{-5}M	3.8×10^{-5}M	2.1×10^{-5}M	
EuC 7c	1.3×10^{-6}M	1.6×10^{-6} M	6.3×10^{-7}M	
EuC 7d	3.1×10^{-5}M	3.3×10^{-5}M	1.7×10^{-5}M	
EuC 7e	4.2×10^{-5}M	4.4×10^{-5}M	3.5×10^{-5}M	
EuC 7f	5.0×10^{-6}M	5.2×10^{-6} M		

The ICP-MS has the advantage of the simultaneous determination of each lanthanide element, whilst the FIA-arsenazo(III) technique is not element specific, but determines the total lanthanide content, solutions of mixed lanthanides cannot therefore be determined. The FIA-arsenazo(III) technique is also dependent upon the solution composition, peak height can be reduced if the sample is not at the optimum pH and transition metals can complex with the arsenazo(III) and displace Ln^{3+} from the coloured complex.

Spectrofluorescence is the simplest of the aqueous analytical methods used with very low detection limits down to 5×10^{-8}M Ce^{3+}, however its use is restricted to Ce^{3+} analysis (or Eu^{3+} by interpolation) and therefore cannot be used for other REE analysis.

2.6 Aqueous sodium and potassium determination by flame photometry

The characteristic emission colour of group 1 metals upon heating in a flame is a convenient method of analysis for dilute Na and K solutions by flame photometry. When Na^+ or K^+ ions are aspirated into a flame the excited electrons emit radiation when they return to the groundstate at the characteristic wavelengths of 589.2nm and 766.5nm for Na and K respectively.

Figure 2.18 Linear calibration range of Na^+ flame emission spectroscopy

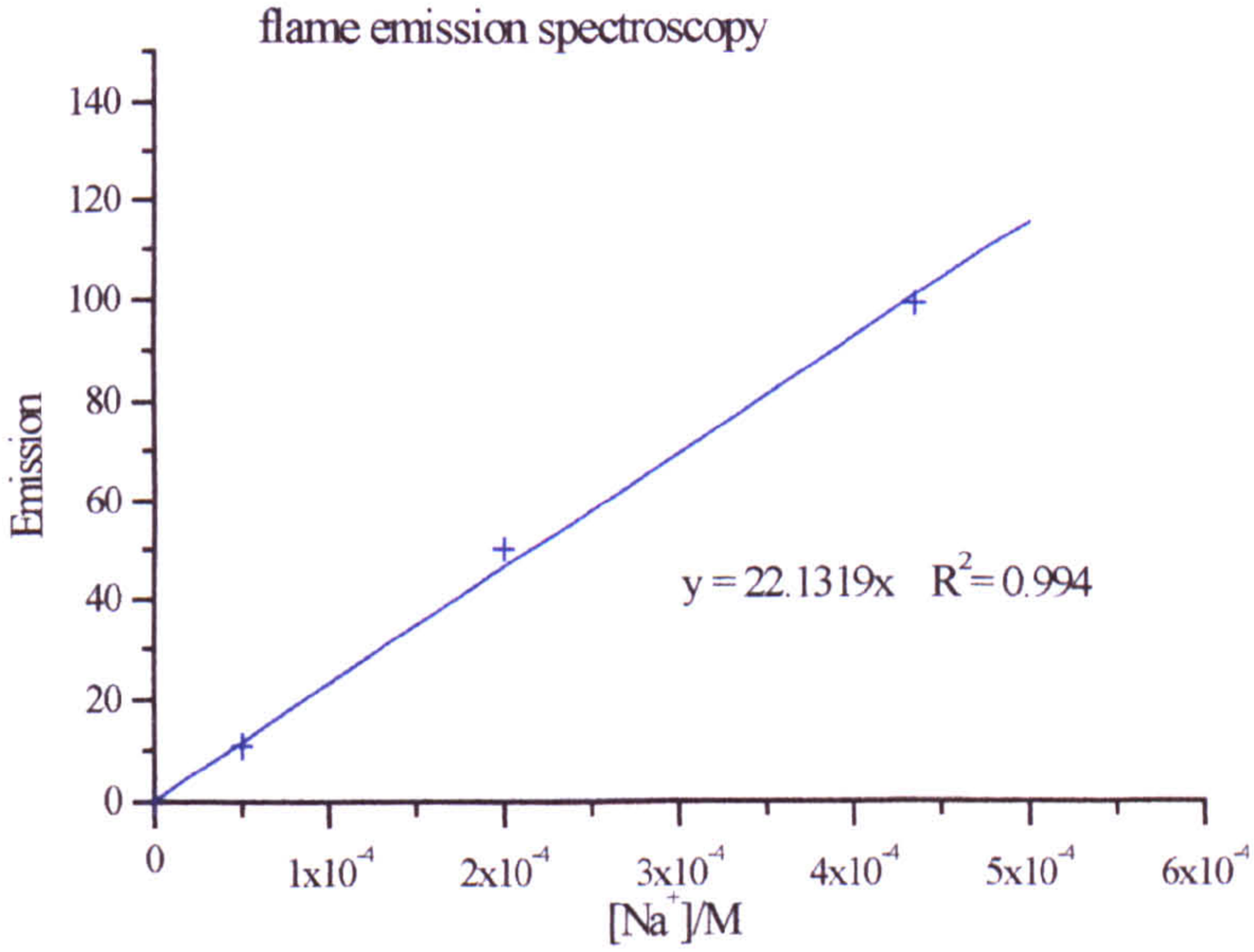

Figure 2.19 Na^+ flame emission calibration from 10^{-5}M-0.1M NaCl

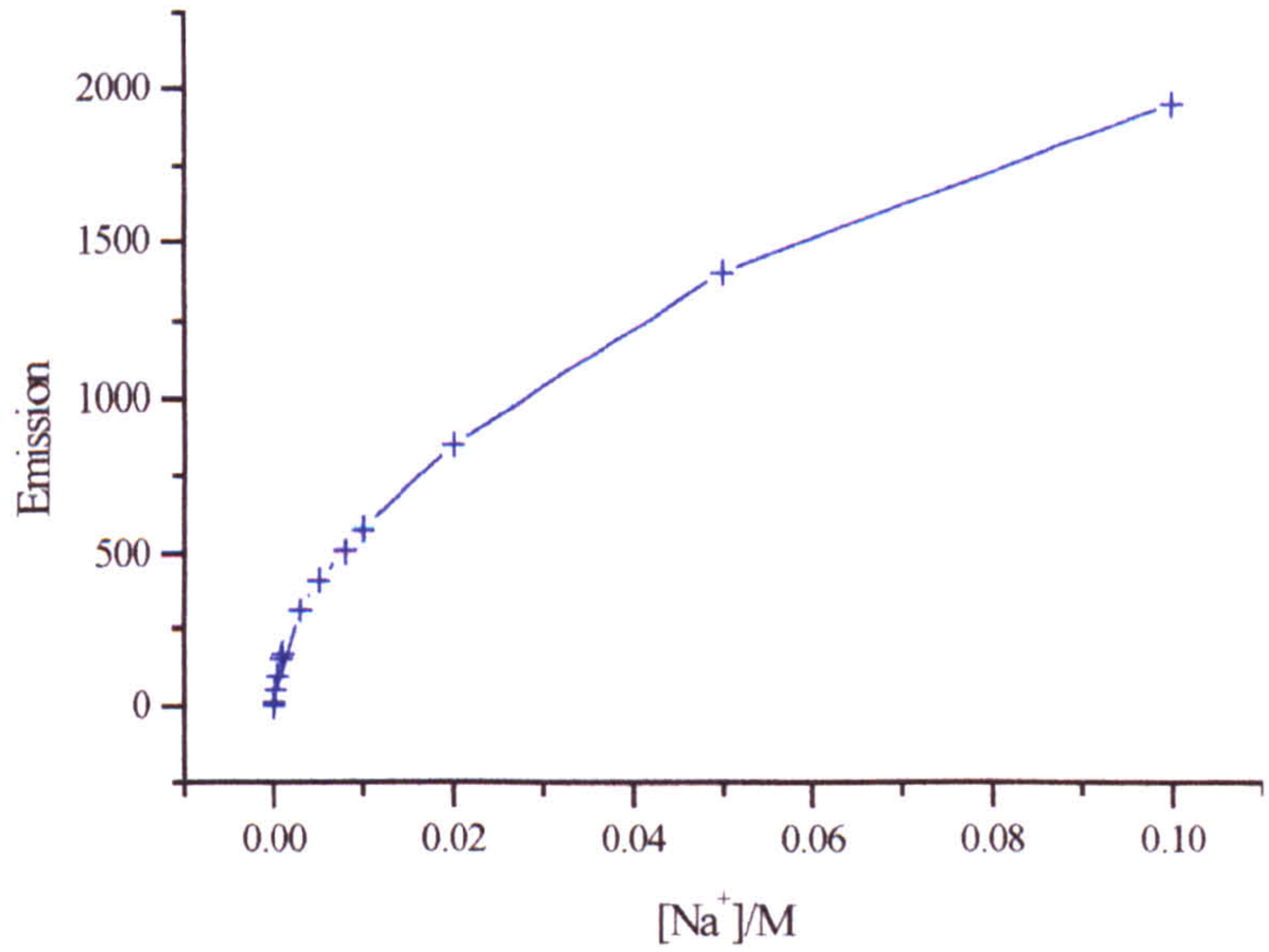

Each sample and standard was aspirated directly into the flame of a Jenway PFP7 Flame Photometer, without pretreatment. The emission was then measured at the appropriate wavelength for Na^+, then the process repeated for K^+. Calibrations have shown that the emission is linear in dilute solutions from $5x10^{-5}M$ to $5x10^{-4}M$ solutions, samples outside this range were diluted to within the linear calibration range. The calibration range for Na^+ is shown in Figures 2.18 and 2.19.

2.7 Powder X-Ray Diffraction (XRD)

Powder XRD analysis is an analytical technique that defines crystal structure. When a solid is placed in front of an X-ray source, most X-rays pass directly through without intersecting the nucleus of the constituent atoms, however a portion of the incident X-rays are diffracted. The diffracted X-rays follows a regular pattern as the X-rays are diffracted from the crystal planes (Battey, 1984).

The wavelength of x-rays used in XRD analysis is of the same order of magnitude as the distance between crystal lattice points. W. L. Bragg in 1912 showed that X-rays were reflected from the planes of atoms in the crystal structure. When X-rays strike a set of crystal planes the X-rays penetrate or are reflected by a plane. When the reflected X-rays are out of phase they interfere with each other and are destroyed, however when in phase from reflections of an even number of parallel crystal planes, constructive interference reinforces the number of X-rays reflected from a crystal plane.

The Bragg Law:

$$n\lambda = 2d\sin\theta$$

describes the condition for successful reflection where d is the crystal plane spacing, λ is the frequency of the X-rays and θ the defracted angle of the X-rays. From the Bragg condition (Figure 2.20) a set of planes of particular spacing (d) can reflect X-rays of a given wavelength at one angle of incidence only. The XRD will therefore construct a unique fingerprint for each crystal type.

Figure 2.20. The Bragg condition

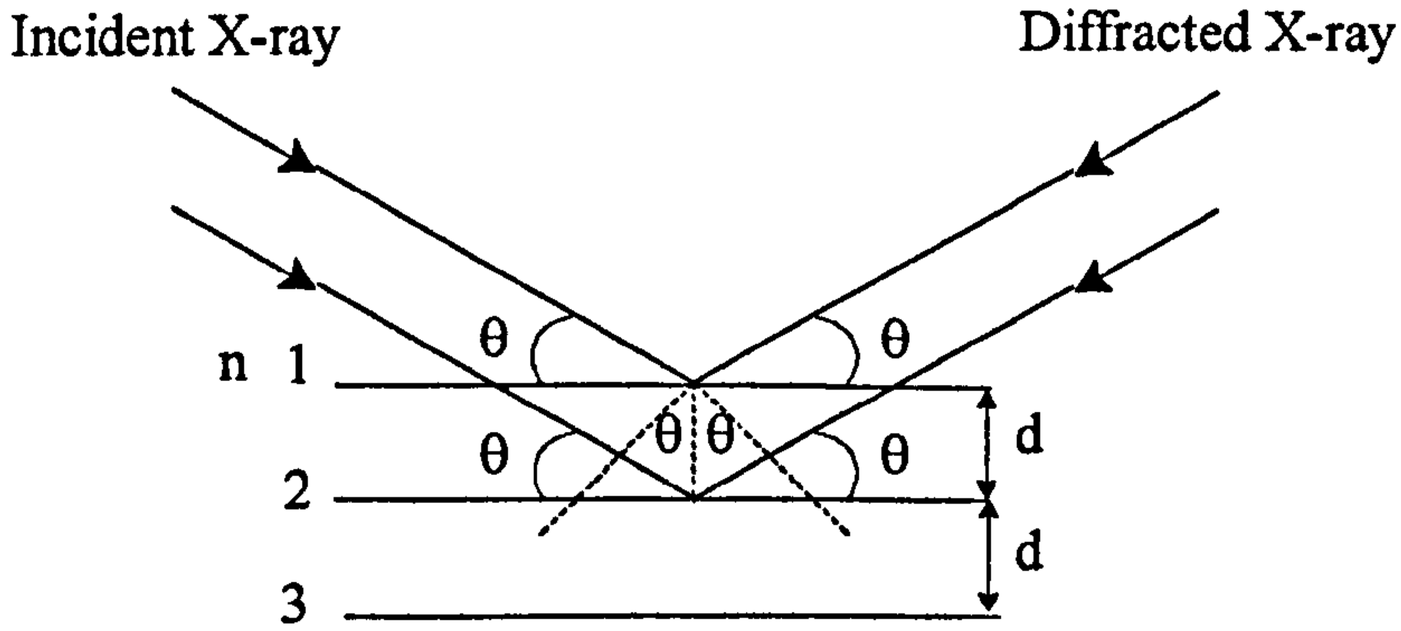

The crystal plane spacing (d) is unique to each crystal type and therefore even similar crystal structures such as $NdCO_3OH$ and $EuCO_3OH$ which have the same crystal type will have a uniquely identifiable pattern. Even though the pattern may appear the same, the systematic decrease in d-spacing from the small decrease in the Ln^{3+} ion size along the group results in an increase in 2θ. Amorphous samples cannot be identified as the lack of a crystal structure results in continuous destructive interference and therefore a continuous background signal.

Table 2.7 XRD analysis parameters

Tube Anode:	Cu
Generator tension [kV]:	40
Generator current[mA]:	30
wavelength [A]:	1.54060
Irradiated length [mm]:	12
Receiving slits [mm] :	0.2
Start angle [2θ] :	5.000
End angle [2θ] :	80.000
step size [2θ] :	0.040
Time per step [s] :	1.000

The XRD patterns were recorded upon a Phillips PW1710 Powder X-Ray Diffractor with the same analysis parameters shown in Table 2.7. The crystals are powdered to ensure that all the possible crystal planes are facing in all directions and to maximise the number of diffractions. The angle (°2θ) of the diffracted X-rays were recorded to determine the crystal spacing (d) and the number of X-rays (counts per second) for each value of 2θ, to give the peak intensity.

The unique crystal structure of the solids studied was then determined from comparisons with known patterns from literature data and the JCPDS database.

2.8 Infra-Red Analysis

The vibrational spectra of inorganic and organic compounds is an established technique to identify the functional groups present, however it is not sensitive to identify the actual metal in a complex. The technique is particularly useful in identifying the presence (and environment) of hydroxide, bicarbonate, carbonate, sulphate and hydrated water in a compound which are often difficult to determine by other means in a solid phase.

When molecules absorb energy from the infrared range between 100μm ($100cm^{-1}$) and 1μm ($10{,}000cm^{-1}$) bonds vibrate at frequencies characteristic of a particular vibration. These vibrations can be identified by identifying the frequency energy is absorbed by a sample when scanned across the infrared range.

The planar carbonate ion has a total of 6 vibrational modes, although only four are used to identify the presence of carbonate in a solid phase (Figure 2.21). The ν_1 symmetric stretch should not be infra-red active, as it does not affect the molecule's dipole moment. However, crystal lattice defects in the solid phase distort the molecular shape resulting in a minor peak. The ν_3 and ν_4 stretches form as doublets and the ν_3 stretch forms as a distinct doublet for the lanthanides even when trace quantities of CO_2 have contaminated the sample.

Figure 2.21 . Carbonate ion vibrations

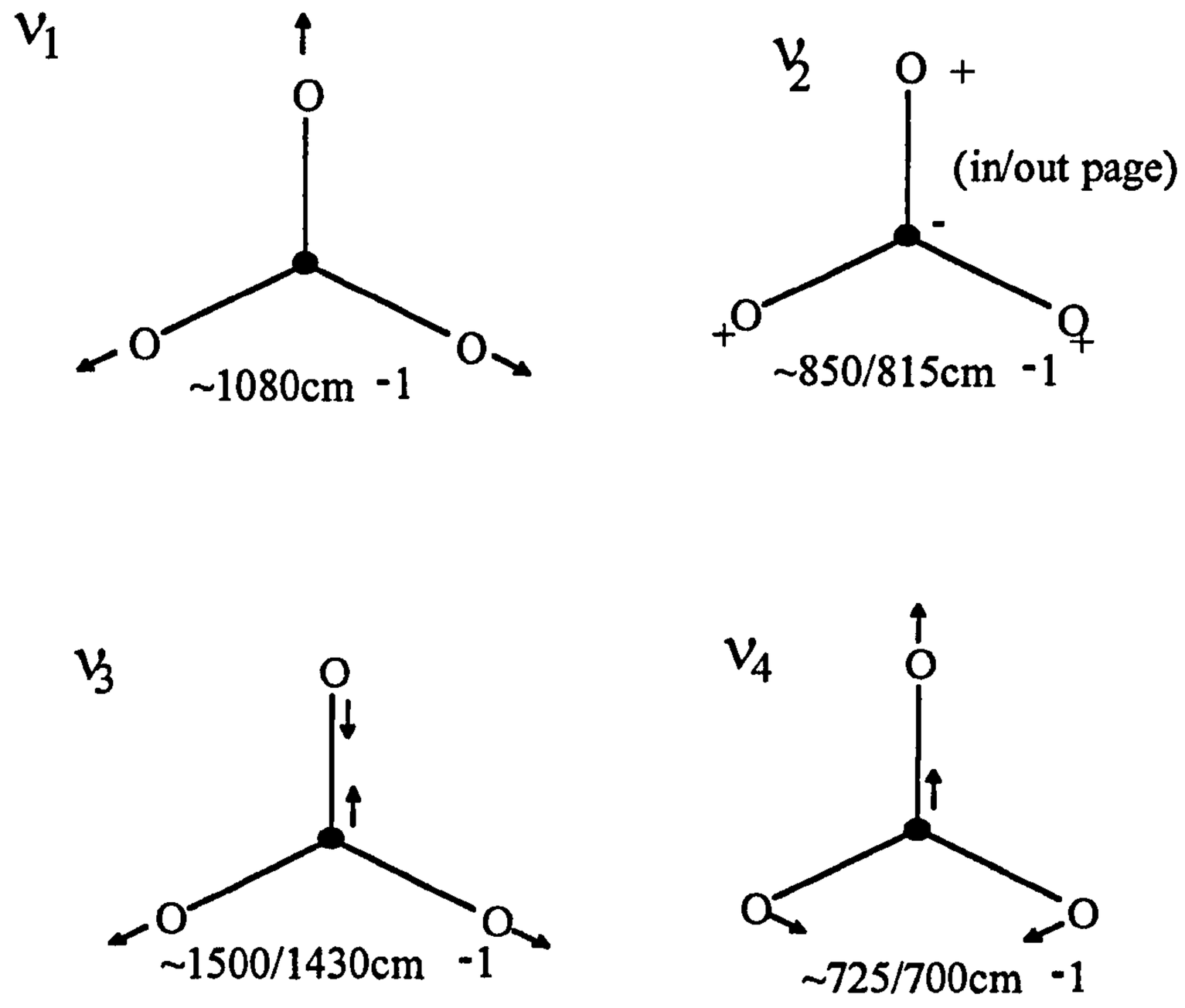

Figure 2.22 Sulphate ion vibrations

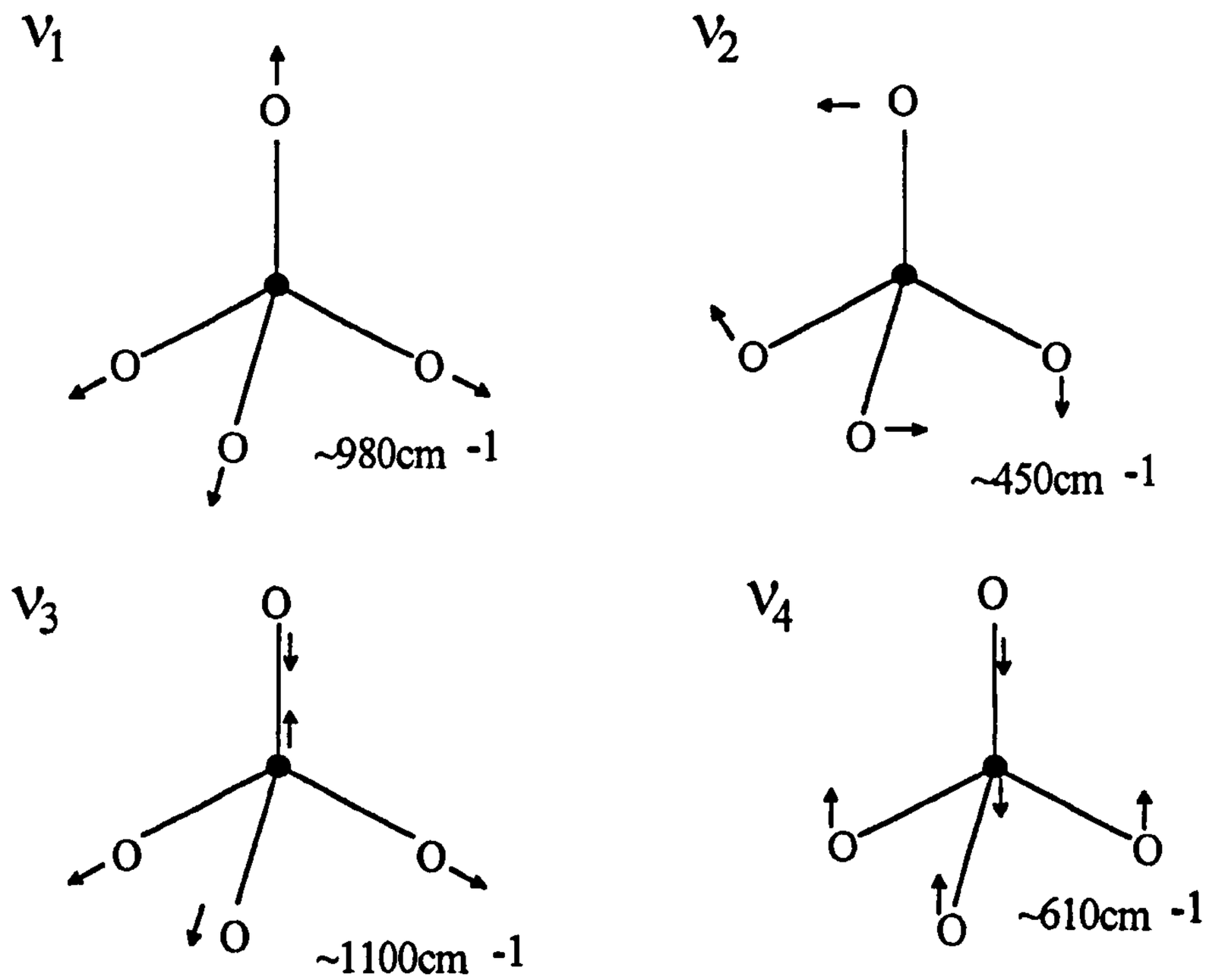

The tetrahedral sulphate ion is also characterised from four modes of vibration, although the sulphate molecule has a total of 9 vibrational modes (Figure 2.22), the most distinctive of which is the ν_3 asymmetric stretch at approximately 1100cm^{-1}. Crystal lattice defects will also distort the sulphate molecule in a similar manner to solid phase carbonates therefore the sulphate ν_1 symmetric stretch which should also be infra-red inactive can be determined.

Figure 2.23 Coordinated water vibrations

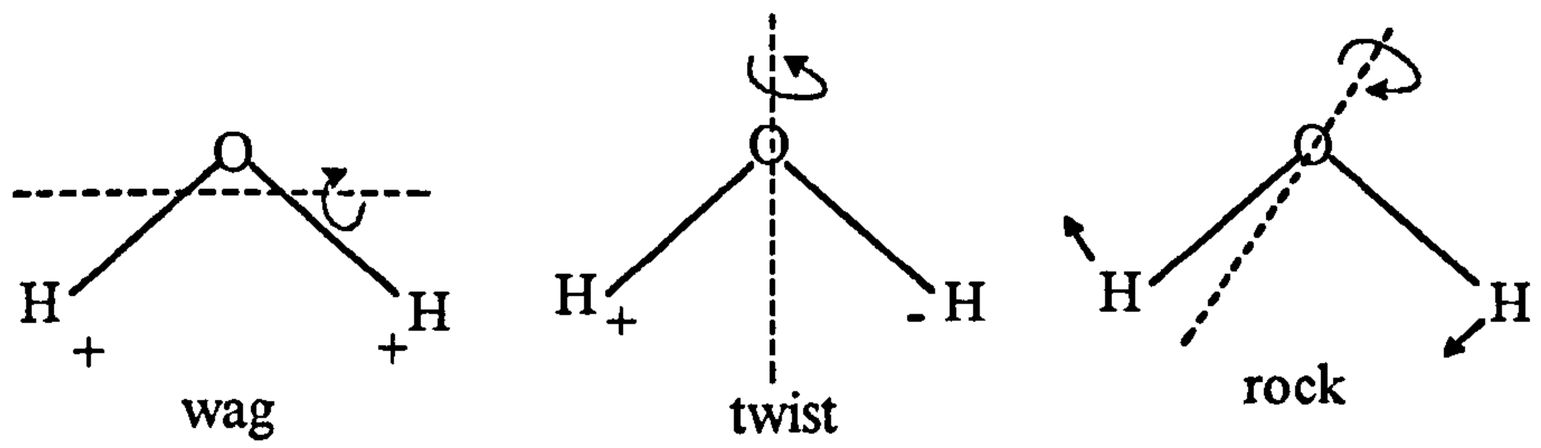

Lattice water absorbs between 3550-3200cm^{-1} as asymmetric and symmetric OH_2 stretching, normally as a broad band incorporating a variety of stretches which can only be properly distinguished at high resolutions (Nakamoto, 1986). H-O-H bending occurs between 1630-1600cm^{-1}. Coordinated water includes the lattice water vibrations plus three additional vibrations, wagging, twisting and rocking (Figure 2.23).

Hydroxyl groups (OH^-) have a single strong sharp stretch at ~3600cm^{-1} and a second vibration from M-O-H bending at ~680cm^{-1} for the lanthanides and americium (Morss and Williams 1994).

Most M-O and M-Cl vibrations occur below 450cm^{-1} and are not as distinctive or as strong as the OH^-, H_2O, CO_3^{2-} and SO_4^{2-} groups, therefore they have not been used to characterise the compounds.

Samples for infrared analysis were prepared as KBr disks made from a 100:1 ratio of KBr to sample and the spectrum recorded on a Perkin Elmer 1600 series FTIR between 4000cm^{-1} and 450cm^{-1} and the functional groups assigned from literature data.

2.9 Thermogravimetric Analysis

Thermogravimetric analysis (TGA) is the measurement of mass loss of a sample with the controlled increase in temperature due to thermal decomposition.
If the exact formula of the TGA end product can be established (generally a metal oxide), then back calculations can define the exact formula of a starting material (e.g. Haines, 1995 or Dodd and Tonge, 1987).

The technique is particularly useful to determine the exact CO_3^{2-}, OH^-, H_2O or SO_4^{2-} content within a sample as it decomposes to an oxide. Hydroxides and crystalline water decompose and evaporate as water vapour. Carbonates decompose in two stages, the formation of an oxycarbonate, then the oxide with the loss of $CO_{2(g)}$ (Table 2.8). Sulphates similarly decompose to oxysulphates and oxides with $SO_{2(g)}$ and $SO_{3(g)}$ evolved.

Thermal decomposition is carried out with a Perkin Elmer TGA 7 under a $N_{2(g)}$ atmosphere to stop the reaction with atmospheric oxygen. The thermal decomposition is limited to below the evaporation temperature of the metal components. The mass loss calculations assume all mass loss is due to the volatile species alone e.g. $H_2O(g)$, $CO_2(g)$ and $SO_3(g)$.

Table 2.8 The thermo-decomposition temperature range of hydrated lanthanide carbonates and hydroxides

25 °C-60°C	loss of adsorbed H_2O
60°C-120°C	loss of crystalline H_2O
370°C - 450°C	decomposition of CO_3^{2-} and OH^- as the loss of CO_2 or H_2O
>600 °C	loss of any remaining CO_3^{2-} as CO_2

2.11 References

AL-SOWDANI, K., and TOWNSHEND, A., (1986) Simultaneous spectrofluorimetric determination of cerium(III) and cerium(IV) by flow injection analysis. *Anal. Chim. Acta* **179** 469-473

BATTEY, M. H., (1984) Mineralogy for students. *Longman group Limited* (Harlow)

DODD, J. W. AND TONGE, K. H., (1987) Thermal methods. *Wiley, Chichester*

EVANS, E. H., (1998)An introduction to analytical atomic spectroscopy. *Wiley, Chicchester*

GLADILOVICH, D. B., KUBAN, V., and SOMMER, L., (1988) Determination of the sum of rare-earth elements by flow-injection analysis with arsenazo III, 4-(2-pyridylazo) resorainol, chrome azurols and 5-bromo-2-(2-pyridylazo)-5-diethylaminophenol spectrophotometric reagents. *Talanta* **35** 259-265

GRENEVA, O. N., KUZ'MIN, N. M., TSYSIN, G. I., and ZOLOTOV, Y. A., (1996) On-line-sorption preconcentration and inductively coupled plasma atomic emission spectrometry determination of rare earth elements. *Spectrochim. Acta* **B51** 1417-14523

HAINES, P. J., (1995) Thermal methods of analysis: principles, applications an problems. *Chapman & Hall, Glasgow*

HALICZ, L., GAVRIELI, I., and DORFMAN, E., (1996) On-line method for inductively coupled plasma mass spectrometry determination of rare earth elements in highly saline brines. *J. Anal. At. Spec.* **11** 811-814

HAVEL, J., VRCHLABSKY, M., and KOHN, Z., (1992) Fluorimetric determination of uranium(VI) in waters by flow-injection analysis after preconcentration on a silica gel microcolumn. *Talanta* **39** 795-799

JIANXIN, M., (1998) determination of formation constants of Ce^{3+} complexes by fluorescence. *J. Rare Earths* **16** 85-89

MARCZENKO, Z., (1986) Separation and spectrophotometric determination of elements. *Ellis Horwood Chichester*

MORSS, L. R., and WILLIAMS, C. W., (1994) Synthesis of crystalline $Am(OH)_3$ and determination of its enthalpy of formation of the solubility-product constants of actinide(III) hydroxides. *Radiochim. Acta* **66/67** 89-93

NAKAMOTO, K., (1986) Infrared and raman spectra of inorganic and coordination compounds. 4^{th} edition. *J. Wiley and Sons.* New York

RUNDE, W., MENRATH, G., and KIM, J. L., (1992) A study of solid-liquid phase-equilibria of trivalent lanthanide and actinide ions in carbonate systems. *Radiochim. Acta* **58/59** 93-100

Chapter 3

Titrations of lanthanide chlorides in the carbonate-hydroxide system with sodium and potassium

3.1 Introduction

The bulk composition of a solution depends on the host material through which the groundwater flows. Initially solutions are derived for example, from rainwater and contain very few trace anions and cations. As surface water percolates through the earth, Na^+ and Cl^- ions dissolve as the most soluble of the common elements. The ionic strength of the solution increases by the further dissolution of Ca^{2+}, Mg^{2+}, CO_3^{2-} and SO_4^{2-} ions whilst iron and silicate containing minerals tend to remain in the solid state or dissolve at a much slower rate except at extreme conditions of acidic pH or alkaline pH solutions in which Fe and Si respectively increase in solubility.

Clay-lined concrete repositories have been proposed for the long-term storage of nuclear waste to inhibit dissolution and transport of the waste. The pH of the incoming groundwater is buffered from the dissolution of concrete, by releasing Ca^{2+} and CO_3^{2-} ions into solution. The relative amount of other ions i.e. Mg^{2+}, K^+ and SO_4^{2-} will depend on the actual composition of the host material. This bulk solution composition can be significantly modified by the equilibrium with host rocks and mixing with other fluids away from the repository.

The solubility of a metal, e.g. Am or a lanthanide is limited by the thermodynamic reaction constant for the dissociation reaction of an equilibrium solid phase (Chapter 4) and the activities of all the component ions in equilibrium with the equilibrium solid phase. The equilibrium solid phase must be identified for the variations in groundwater chemistry and predicted repository compositions which may occur, to enable the calculation of the solubility limit of the target elements, e.g. the lanthanides Ce, Nd and Eu and ultimately to model the solution and mobility rates through a wide range of conditions. Initially within a waste repository the near field conditions are characterised by alkaline pH and high concentrations of Ca^{2+}, CO_3^{2-}, SO_4^{2-}, Na^+ and Cl^- ions in solution, which will change as a result of dilution and dispersion of the fluid away from the repository. A wide range of conditions must be examined to determine if there are any variations in the nature of the solubility limiting phase (i.e. the least

soluble phase under specific conditions) across a pH range from pH 6-12 with an increase in the ionic strength of the solution.

Carbonate and phosphate minerals are the most important natural source of REE e.g. bastnaesite, parisite, monazite and xenotine. REE minerals form as mixed Ca^{2+}-Ln^{3+}-CO_3^{2-}-F^--OH^- or Ca^{2+}-Ln^{3+}-PO_4^{3-}-F^--OH^- phases which crystallise from hydrothermal solutions or magmatic liquids. The mixed calcium-lanthanide minerals usually decompose when formed from solutions below 90°C to form lanthanide and calcium fluoro-carbonates or phosphates dependent upon their respective activities in solution (William-Jones and Wood, 1992).

Carbonate is the most common simple complexing ion which is abundant in groundwater systems and the mineral lanthanite, $Ln_2(CO_3)_3.8H_2O$, has been noted as a weathering product (William-Jones and Wood, 1992). The lanthanide-carbonate-hydroxide system will therefore be examined as F^- and PO_4^{3-} have a limited abundance in the environment. The effects of SO_4^{2-} ions will be examined in Chapter 5. Ca^{2+} ions are excluded as $CaCO_3$ could form as a solid phase within the system and its precipitation may interfere with the solution composition by removing Ca^{2+} and CO_3^{2-} ions and possibly induce co-precipitation of lanthanide phases or surface reactions, Carroll (1993). Literature data for lanthanides and their actinide analogue Am suggests that three main lanthanide phases can form; which are lanthanide carbonate, $Ln_2(CO_3)_3$, lanthanide hydroxycarbonate, $LnCO_3OH$, and lanthanide hydroxide, $Ln(OH)_3$, depending upon the pH and carbonate activity of the solution (Vitorge, 1992).

A series of titration experiments were designed to show how the Ln^{3+}-Cl^--OH^--CO_3^{2-} system changes due to the sequential addition of sodium hydroxide or sodium carbonate. Titrations were run to initially examine the reaction of $LnCl_3$ with NaOH. Following this, the carbonate ion was used in place of the hydroxide. The lanthanide, carbonate and hydroxide solutions used in the titrations were prepared from either the sodium or chloride salts as they are very soluble. Na^+ and Cl^- ions will also be present in all natural solutions and the potential effect of these elements must also be modelled.

The system is significantly affected by absorption of atmospheric CO_2. Therefore to prevent any carbonate contamination the titration solutions and any products formed all reactions were prepared using degassed distilled water; prepared by boiling distilled water under a nitrogen atmosphere and bubbling $N_2(g)$ through the water to displace any dissolved CO_2 and O_2. The water was allowed to slowly cool to room temperature whilst still bubbling $N_2(g)$ to saturate the water with N_2, to prevent the re-adsorption of CO_2.

Lanthanides typically form as Ln^{3+} ions and the expected endpoint of the titrations can be estimated from the reactions 3.1 and 3.2

$$Ln^{3+} + 3OH^- \longrightarrow Ln(OH)_3 \quad (3.1)$$
$$2Ln^{3+} + 3CO_3^- \longrightarrow Ln_2(CO_3)_3 \quad (3.2)$$

An excess of hydroxide or carbonate solution (4mmols) was therefore titrated against a constant amount of $LnCl_3$ (1mmol) where Ln = Ce, Nd, Sm or Eu, to allow a sufficient amount of precipitate to form and be characterised and ensure that any reaction was complete.

3.2 Experimental-General Titration Procedure

Stock solutions of $LnCl_3$ (0.2M, 5 cm^3), where Ln = Ce, Nd, Sm or Eu were prepared by dissolving $LnCl_3.6H_2O$ in degassed distilled water (Table 3.1).

A 5 cm^3 aliquot of the stock solution was diluted to 160 cm^3 with degassed distilled water to give a starting concentration of $6.25x10^{-3}$ M $LnCl_3$. The solution was placed in a 250 cm^3 three-necked round bottomed flask, which had been previously degassed with $N_2(g)$ to ensure an inert atmosphere. Nitrogen was continuously bubbled into the vessel through one side neck to ensure a positive N_2 atmosphere. A pH electrode (GK 2401C combined glass electrode) was fitted securely to the second side neck and the pH measured on a Radiometer PHM 85 Precision pH meter. A burette was placed in the centre neck. The solution was stirred with a magnetic stirrer.

Table 3.1 Chemicals and dilutions of the stock solutions used in the titrations

	F.W. ($gmol^{-1}$)	Dilution	conc^{n}
$CeCl_3.7H_2O$ (99+%)	372.59	18.6295g in 250 cm^3	0.2M
$NdCl_3.6H_2O$ (99.9%)	358.69	17.9345g in 250 cm^3	0.2M
$SmCl_3.6H_2O$ (99.9%)	364.80	18.240g in 250 cm^3	0.2M
$EuCl_3.6H_2O$ (99.9%)	366.41	18.3205g in 250 cm^3	0.2M
NaOH (Analar)	40.00	2.00g in 500 cm^3	0.1M
KOH (Analar)	56.11	2.8055g in 500 cm^3	0.1M
$NaHCO_3$ (Analar)	84.01	4.2005g in 500 cm^3	0.1M
Na_2CO_3 (Analar)	105.99	5.2995g in 500 cm^3	0.1M
K_2CO_3 (Analar)	138.20	6.910g in 500 cm^3	0.1M

The solution was titrated with a series of titre solutions of NaOH, $NaHCO_3$, Na_2CO_3 or K_2CO_3 (0.1M, 40cm^3). The titre solution was added dropwise using the burette. After each addition, the solution was allowed to equilibrate, which was indicated by a stable pH reading. The pH was then recorded prior to further addition. Each titration was repeated three times for each lanthanide chloride.

At the end of the titration, the contents of the flask were transferred to a 250 cm^3 HDPE Nalgene bottle under an atmosphere of N_2. The precipitate formed during the reaction was then filtered through a Whatman N°4 sintered glass crucible washed with water and then dried over silica gel in a vacuum dessicator. The solid phases were analysed by IR, XRD and TGA (Chapter 2).

3.3 Titrations of $LnCl_3$ with NaOH

3.3.1 Experimental

The titrations were carried out following the method outlined in Section 3.2, and NaOH (0.1M, 40 cm^3) was used as the titre solution.

3.3.2 Results

The starting solutions of lanthanide chloride were clear, Ce and Eu were colourless , Nd purple and Sm was slightly yellow at pH 4-6. On the addition of 0.1 cm^3 NaOH there was an initial increase in pH to pH~8 (Figure 3.1), the pH was then buffered during further titre additions. Each addition results in an immediate increase in pH which then slowly decreases to an equilibrium value.

The equilibrium pH increases by pH 0.005 units with every 5 cm^3 of NaOH solution. The buffer zone extends until 26 cm^3 of NaOH had been added at pH 8.75. A gelatinous precipitate forms at the end of the pH buffer zone, which is purple for Ce, lilac Nd, cream Sm and white Eu. The pH rises rapidly after 26 cm^3 of NaOH solution had been added and increases to pH 11 after the addition of 30 cm^3 of NaOH solution. This rise in pH is accompanied by a rapid precipitation causing the solution to become opaque at pH 11. The rate of pH increase then slows and approaches the pH of the titre solution. The purple Ce precipitate slowly changes colour at pH > 10 to yellow, the Nd, Sm and Eu gelatinous precipitates do not change colour

At the end of the titration, the precipitate was allowed to settle and the remaining solution was clear and colourless for each lanthanide system. All the lanthanide elements examined give almost identical titration curves. The end solution was filtered and the solid phase analysed by FTIR, XRD and TGA to characterise the precipitate.

Figure 3.1 Typical titration curve for 1mmol $NdCl_3$ with 4mmols NaOH

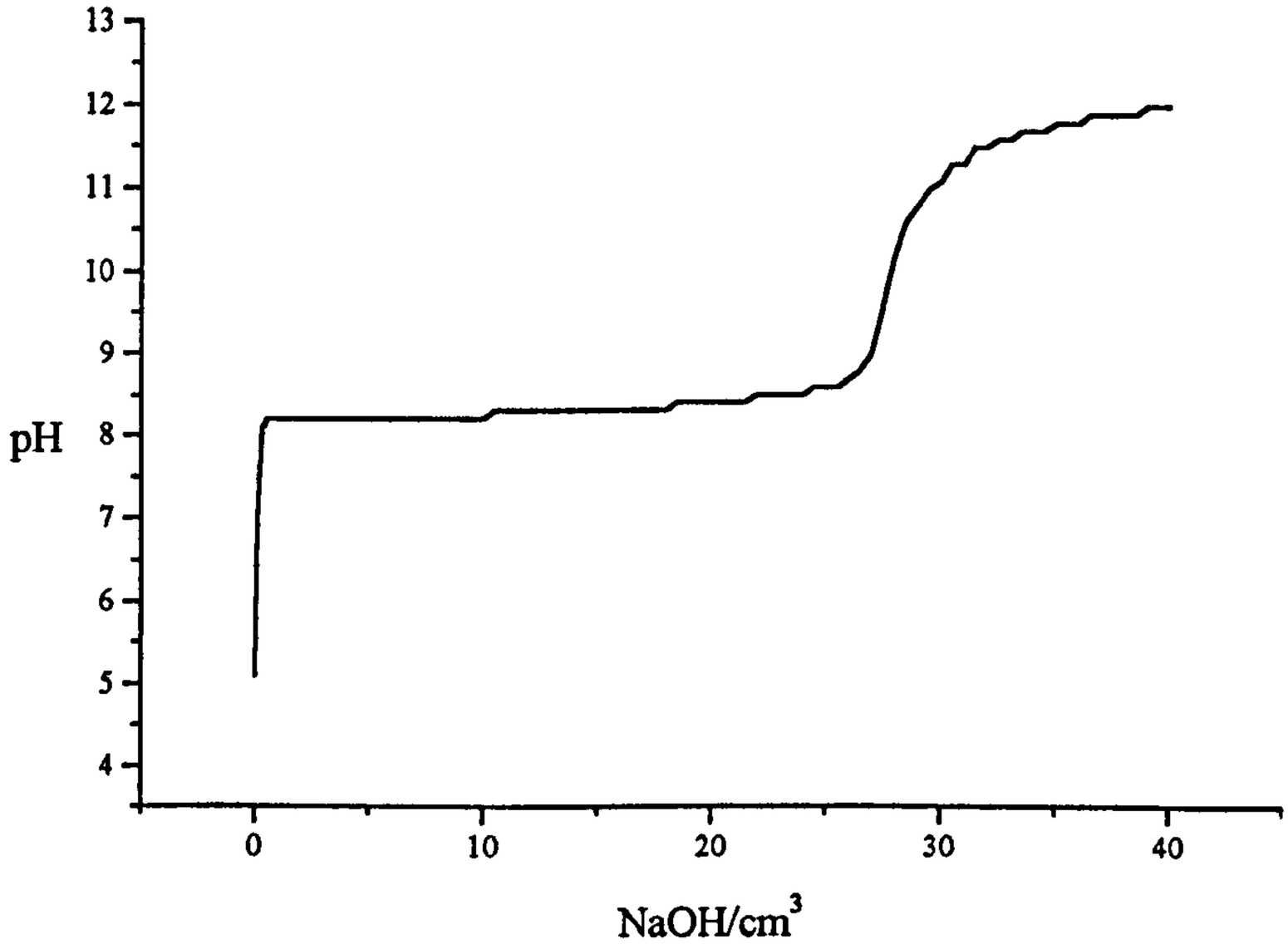

The Nd, Sm and Eu precipitates were characterised as $Ln(OH)_3$ (Section 3.3.3) and the reaction occurring can be written as equation 3.3, leaving Na^+ and Cl^- ions in solution.

$$Ln^{3+} + 3OH^- \longrightarrow Ln(OH)_3{}^0(aq) \longrightarrow Ln(OH)_3(s) \qquad (3.3)$$

An intermediate aqueous species must form to buffer the solution pH during the successive addition of NaOH as there was no visible precipitate to remove the OH^- from solution.

The Ce system follows a three-stage reaction. The first stage when pH was buffered to produce an aqueous $Ce(OH)_3{}^0$ complex (equation 3.4) then a second stage precipitate followed by a third stage redox reaction associated with the colour change (equation 3.5) possibly forming $Ce(OH)_4(s)$ as an intermediate phase, before altering to $CeO_2(s)$. However the identification of a $Ce(OH)_4(s)$ could not be confirmed as the purple precipitate altered to the yellow (CeO_2) phase upon drying.

$$Ce^{3+} + 3OH^- \rightarrow Ce(OH)_3(aq) \qquad (3.4)$$

$$Ce(OH)_3(aq) + H_2O\,(aq) \rightarrow Ce(OH)_4(s) + \tfrac{1}{2}H_2 \rightarrow CeO_2.2H_2O(s) \qquad (3.5)$$

purple → yellow

3.3.3 Characterisation of Precipitate

The dried precipitates were characterised using the techniques described in Chapter 2. The FTIR spectras (Figure 3.2, Table 3.2), XRD patterns (Nd and Eu shown in Figure 3.3 for Nd and Eu, Ce shown in Figure 3.4, Table 3.3) confirm the end precipitates are the lanthanide hydroxide, $Ln(OH)_3$, for Nd, Sm and Eu and Ce has been oxidised to form CeO_2. The crystal structures were confirmed by comparisons with reference patterns from the JCPDS database.

The IR hydroxide spectra is characterised by a strong very sharp O-H stretch at 3606 cm^{-1} next to a broad H_2O stretch between 3500 cm^{-1} and 3400 cm^{-1} There is a further O-H bend at 680 cm^{-1}. A doublet at 1500 cm^{-1} indicates there is slight CO_3^{2-} contamination which probably results from absorption of atmospheric CO_2 during the filtering and washing stages. Diakonov *et al.*, (1998) suggest that the CO_3^{2-} contamination is the result of surface layer alteration which can only be distinguished by infra-red analysis.

The FTIR spectrum of the Ce precipitate indicates that a hydroxide stretch was not present and the only IR stretch was from crystalline water. The XRD pattern of CeO_2 is significantly different from the $Ln(OH)_3$ pattern, although both patterns have a maximum peak height of 600 counts/second, indicating that the precipitates are poorly crystalline. The wet purple sample had no distinguishable crystal structure from XRD analysis and the broad water absorbance band from excess water in the sample occluded any possible OH^- stretch, therefore any confirmation of a formula could not be made.

Figure 3.2 FTIR Spectra of the end precipitate (CeO_2 and $Ln(OH)_3$) of the NaOH titrations

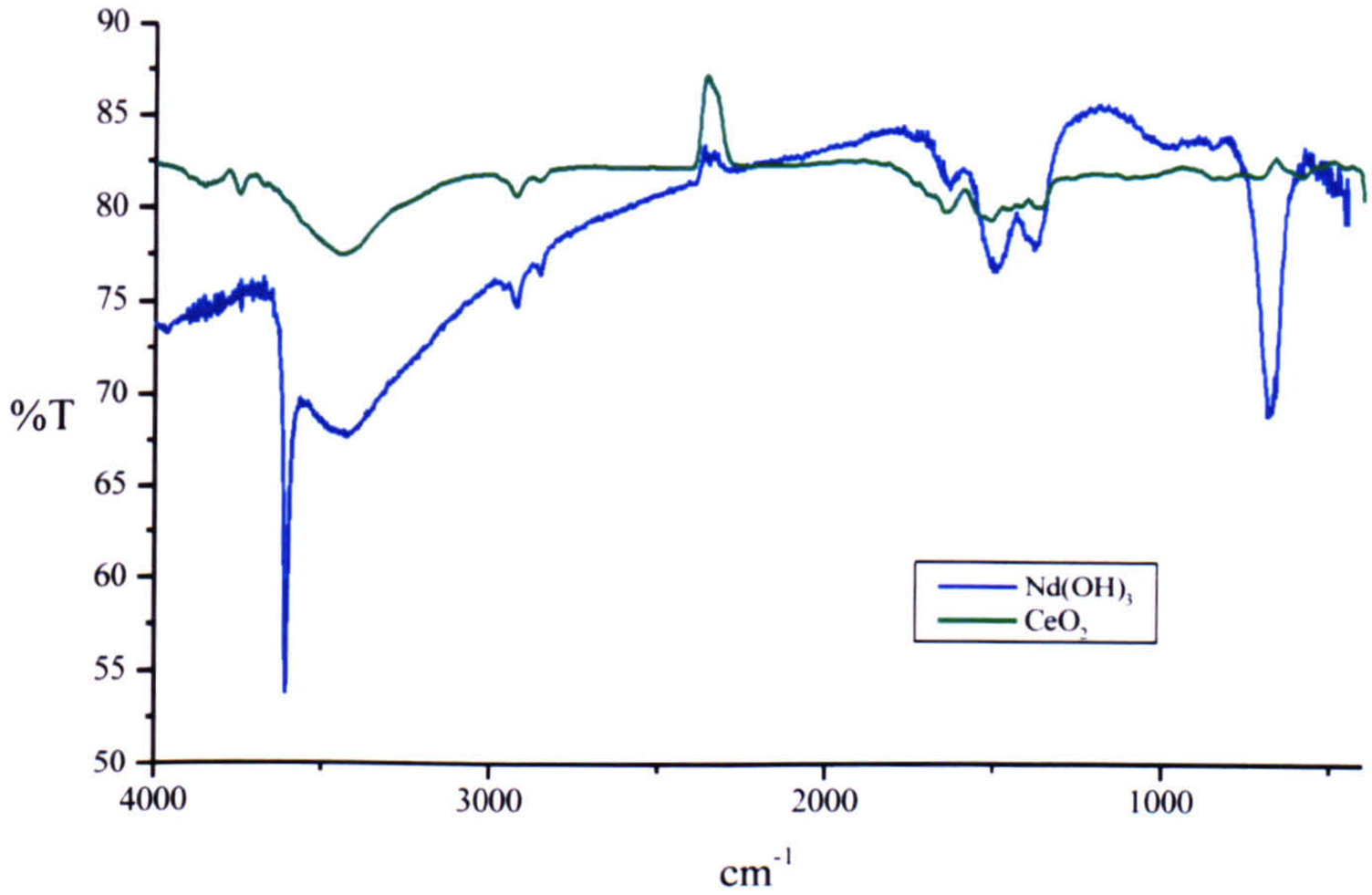

Table 3.2 FTIR stretches for hydrated $Ln(OH)_3$ and CeO_2

	Ce-ppt	$Nd(OH)_3$[1]	Nd-precipitate	$Sm(OH)_3$[1]	Sm-precipitate	Eu-precipitate
νO-H		3608±1	3609	3608±1	3608	3608
δO-H		673	688	692	696	701
νO-H_2	3340		3432		3420	3422
δO-H_2	1624		1633		1636	1638
$\nu_1CO_3^{2-}$			(1067)		(1064)	
$\nu_2CO_3^{2-}$			(850)		(845)	(848)
$\nu_3CO_3^{2-}$			(1504/1384)		(1506/1379)	(1507/1382)
$\nu_4CO_3^{2-}$						

[1]Merli et al (1997) ( ) minor peaks

Figure 3.3 XRD pattern of $Ln(OH)_3$ identified from JCPDS reference pattern 6-601

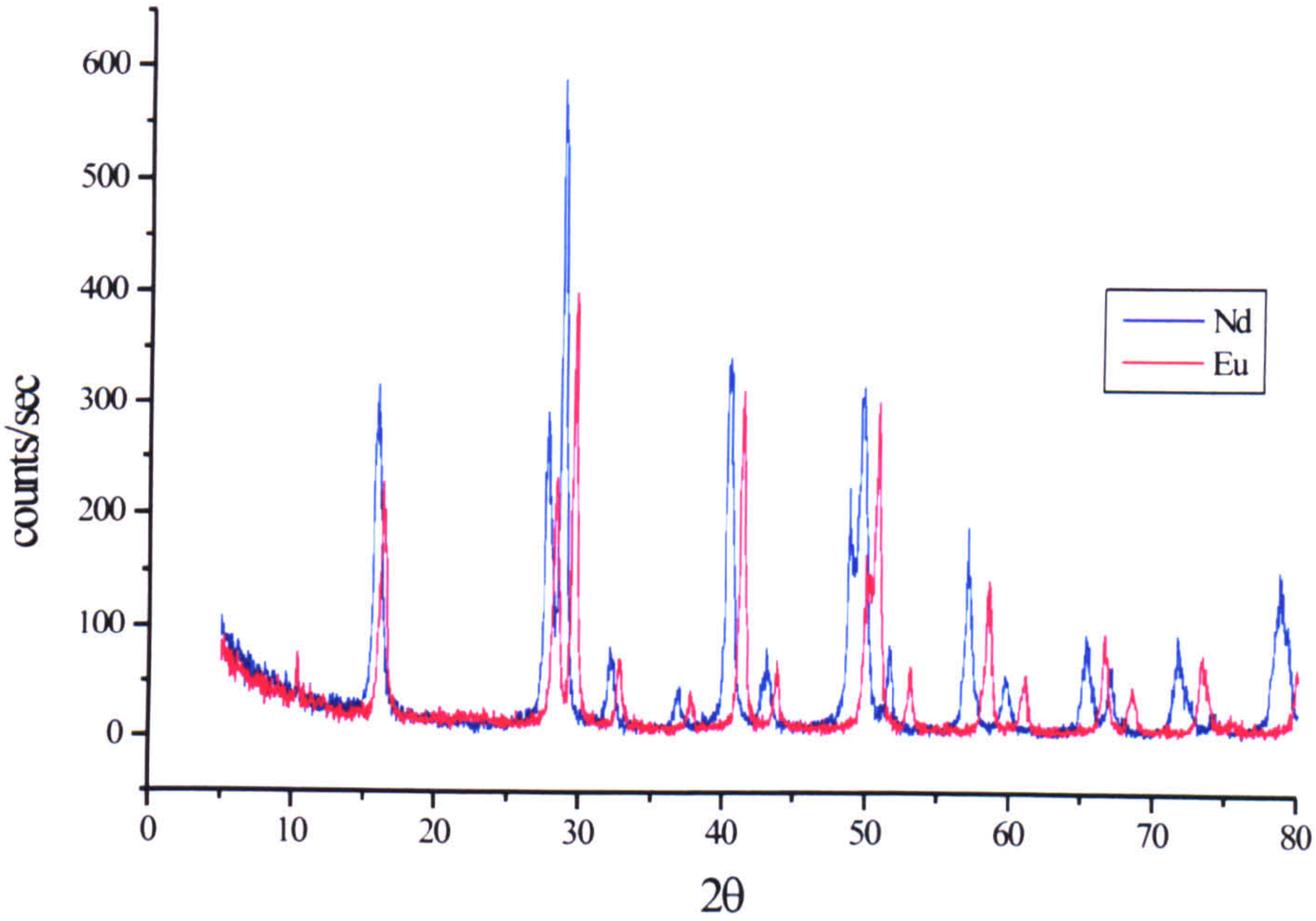

Figure 3.4 XRD pattern of CeO, identified from JCPDS reference pattern 34-394

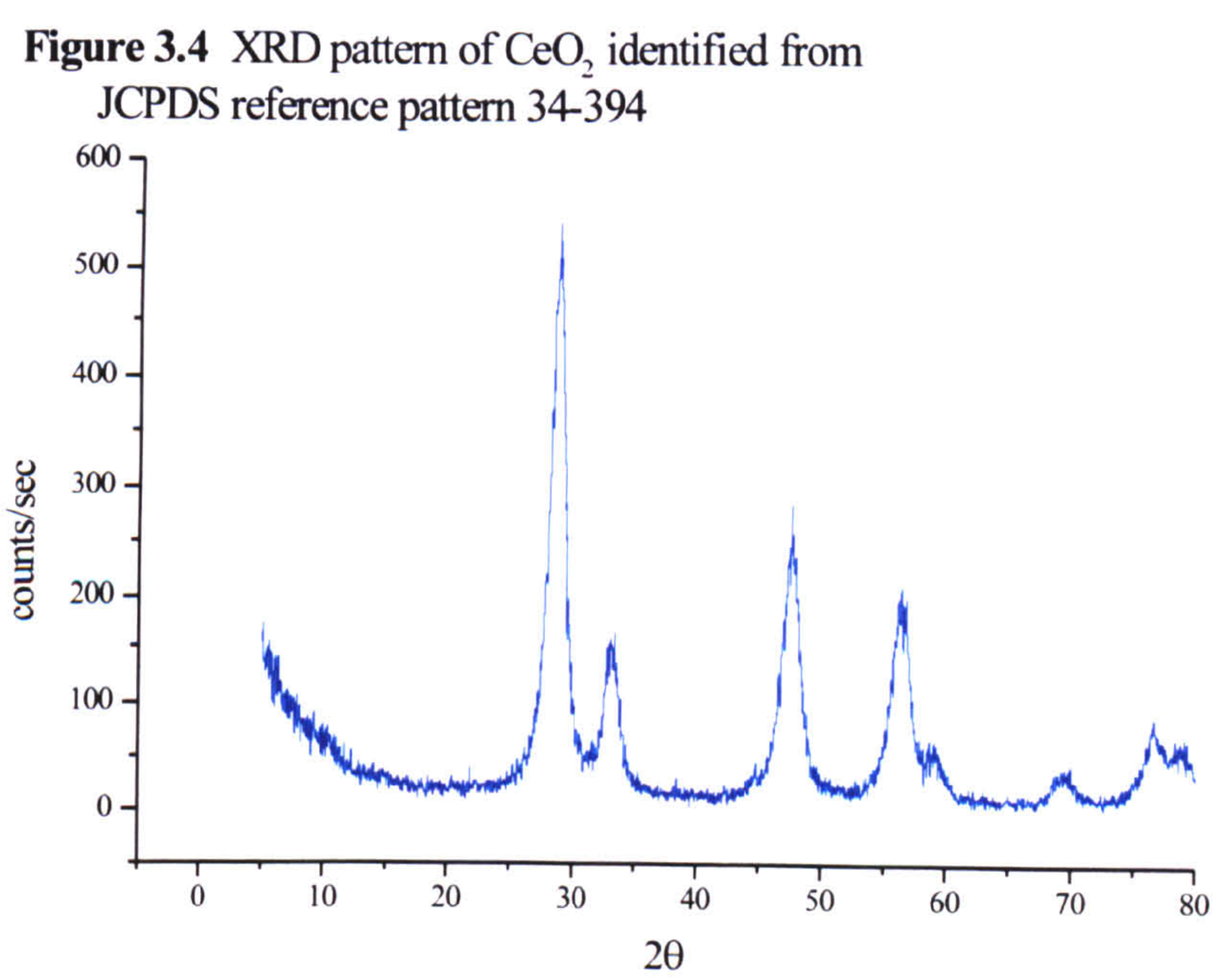

Table 3.3 XRD d-spacing for CeO_2 and $Ln(OH)_3$; End precipitates from the NaOH titrations

[1]CeO_2	Ce- precipitate		[2]$Nd(OH)_3$	Nd precipitate		Sm-precipitate		[3]$Eu(OH)_3$	Eu- precipitate	
d(Å)	d(Å)	2θ	d(Å)	d(Å)	2θ	d(Å)	2θ	d(Å)	d(Å)	2θ
3.128	3.1251	28.54	5.570	5.5366	16.00	5.3975	16.41	5.520	5.2668	16.82
2.705	2.6872	33.32	3.200			3.1642	28.18	3.180	3.1048	28.73
1.913	1.9011	47.81	3.080	3.0760	29.01	3.0240	29.52	3.050	2.9661	30.11
1.631	1.6335	56.27	2.768	2.7548	32.48	2.7254	32.84	2.757	2.6876	33.31
1.562	1.5704	58.75	2.450	2.4213	37.10			2.399		
1.353	1.3571	69.17	2.217	2.2138	40.73	2.1881	41.23	2.202	2.1588	41.81
			2.092	2.0930	43.19			2.080	2.0510	44.12
			1.848	1.8657	48.77					
			1.842	1.8268	49.88			1.837		
								1.828		
				1.7646	51.77	1.8043	50.55	1.810	1.7860	51.10
								1.733	1.7102	53.54
			1.605	1.6109	57.14	1.5896	57.97	1.589		
								1.585	1.5677	58.86
			1.540	1.5464	59.75			1.527		
						1.4568	63.85	1.524	1.3930	67.15
			1.417	1.4159	65.92	1.4106	66.20	1.410		
			1.392	1.3928	67.16			1.374	1.3625	68.86
			1.311	1.3139	71.79					
			1.290			1.2957	72.96	1.295	1.2855	73.63
								1.262		
				1.2127	78.87			1.201		
								1.194		
								1.189		
								1.171		

Literature values JCPDS Powder Diffraction Files [1]34-394, [2]6-601 and [3]17-781

3.4 Titrations of $LnCl_3$ with $NaHCO_3$

Preliminary titrations of $LnCl_3$ solutions with $NaHCO_3$ have shown that a precipitation forms after the first the first $0.5cm^3$ of titre is added. Therefore the titrations were repeated after the starting $LnCl_3$ solution was acidified with HCl to pH 2 to determine the point of the initial precipitate. The $LnCl_3$ titrations were carried out manually and using a Mettler DL70 Autotitrator.

3.4.1 Experimental

The titrations were carried out following the method outlined in Section 3.2, with $NaHCO_3$ (0.1M, $40cm^3$) as the titre solution.

The acidified $LnCl_3$ starting solution was prepared from a $5cm^3$ aliquote of $LnCl_3$ stock solution and HCl (0.1M, $5\ cm^3$) and diluted to $160cm^3$ with degassed distilled water. The solution was then titrated with $NaHCO_3$ (0.1M, $60\ cm^3$).

Titrations were also carried out with a Mettler DL70 Autotitrator. The titre solution was added as a constant volume ($0.05\ cm^3$) at 30 second time intervals, the reacting solution was therefore not allowed to equilibrate between each addition if equilibration took longer than 30 seconds.

After the final addition of $NaHCO_3$, the contents of the reaction vessel were transferred to $250cm^3$ HDPE Nalgene bottles and sealed under an atmosphere of N_2 to prevent any adsorption of CO_2. The precipitate formed during the reaction was then filtered through a Whatman N°4 sintered glass crucible washed with water and then dried over silica gel in a vacuum dessicator.

3.4.2 Results

The addition of a small amount of $NaHCO_3$ to the lanthanide chloride solution causes an initial rise in pH from pH 5.5 to 6.8, after which the pH remains constant until $1cm^3$ of titre is added (Figure 3.5). This initial rise in pH is accompanied by the formation of a precipitate. Further addition of $NaHCO_3$ to the reaction mixture causes an initial increase in pH which then slowly decreases to a steady value. The stable pH reading indicates that the solution has attained equilibrium.

To prevent immediate precipitation of the solid phase on addition of the first of $NaHCO_3$ titre, the starting solution was acidified. Acidifying the starting solution to pH 2 with HCl had no effect on the pH of the initial precipitation at pH

6·5-7·0. The first 5cm^3 of $NaHCO_3$ in the acidified titrations was used to neutralise the added HCl (Figure 3.6). No precipitation was observed during this "neutralising" stage. Further titre addition was marked by an immediate increase in pH followed by a slow decrease in pH until equilibrium was obtained. During this addition of $NaHCO_3$ solution precipitation of an initially amorphous phase is observed which is white for Ce and Eu, lilac Nd and a cream/yellow coloured Sm.

In both the acidified and non-acidified solutions, the titration follows the same pattern for all the elements studied. Although Ce exhibits slightly different behaviour in the initial stages of the titration when a pH maximum is reached for up to 5cm^3 of titre, then drops sharply by 0.5 pH units, before following the buffer pattern shown by Nd, Sm and Eu.

Precipitation continues until 24.5 cm^3 and 29 cm^3 of $NaHCO_3$ at pH~5.9 for the lanthanide and acidified lanthanide solutions respectively. At 30cm^3 and 35cm^3 for the lanthanide and acidified lanthanide solutions respectively the solution pH increases sharply on the addition of the next 5 cm^3 of $NaHCO_3$, and then starts to plateau towards the end of the titration at pH 8.5.

The lanthanide and acidified lanthanide titration curves can be superimposed on each other along the buffer zone and final pH rise when the 5cm^3 of $NaHCO_3$ used to neutralise the HCl is taken into account.

The maximum titration run of 100 minutes for the autotitrator restricts the total time for the titration , the solution cannot therefore achieve equilibrium between each addition, which may take over 10 minutes at particular points especially when precipitating along the buffer zone. There is therefore a small net gain in pH for the autotitrated runs compared to when the solution is allowed to come to equilibrium along the buffer zone. The net gain has little effect on the endpoint of the titration, shown by a rapid rise in pH towards the pH of the titre solution.

Figure 3.5 Manual titration curve for 1mmol $NdCl_3$ with 4mmols $NaHCO_3$

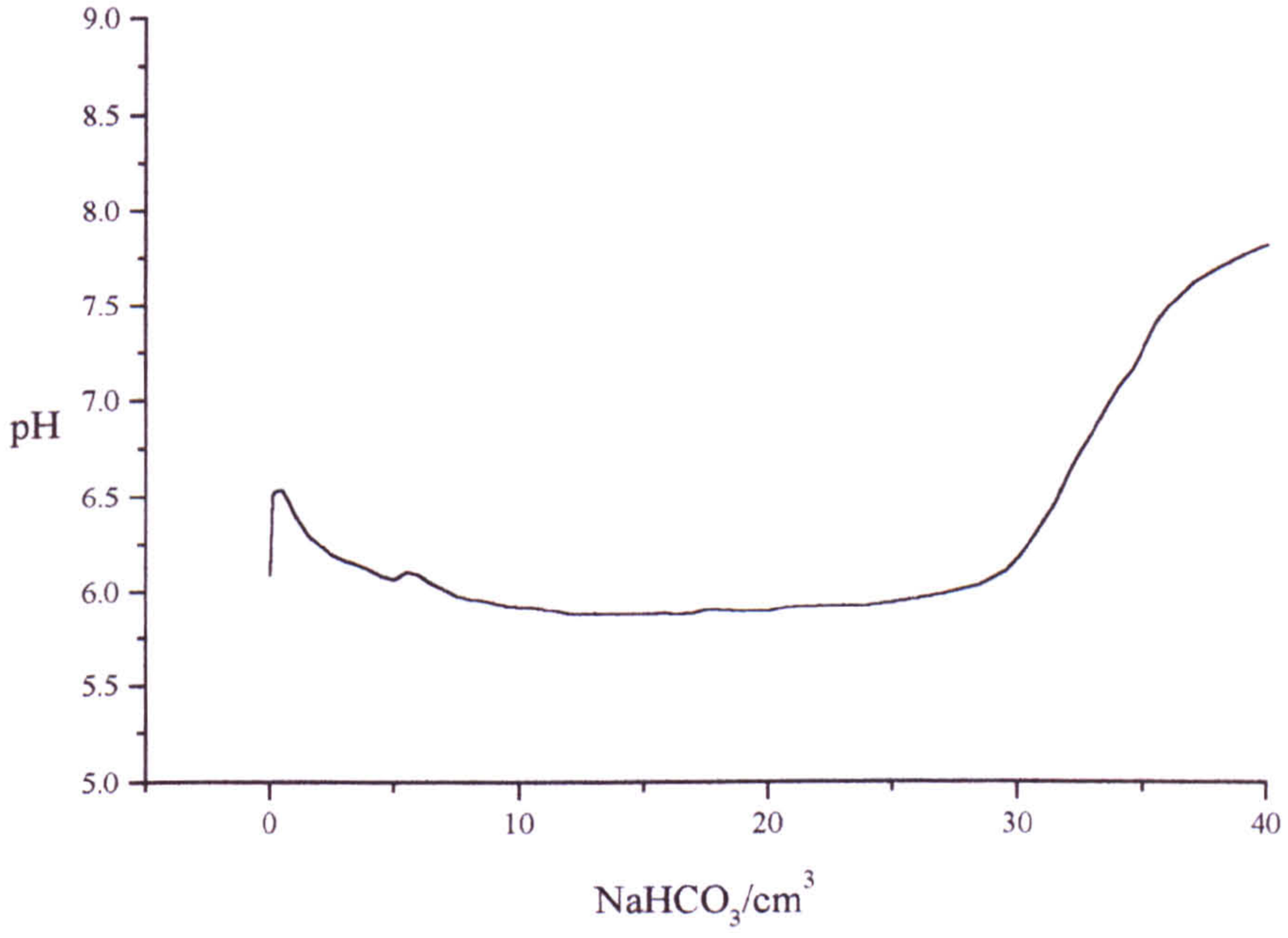

Figure 3.6 Autotitrated titration curve for

1mmol $LnCl_3$ + $^1/_2$mmol HCl with 6mmols $NaHCO_3$

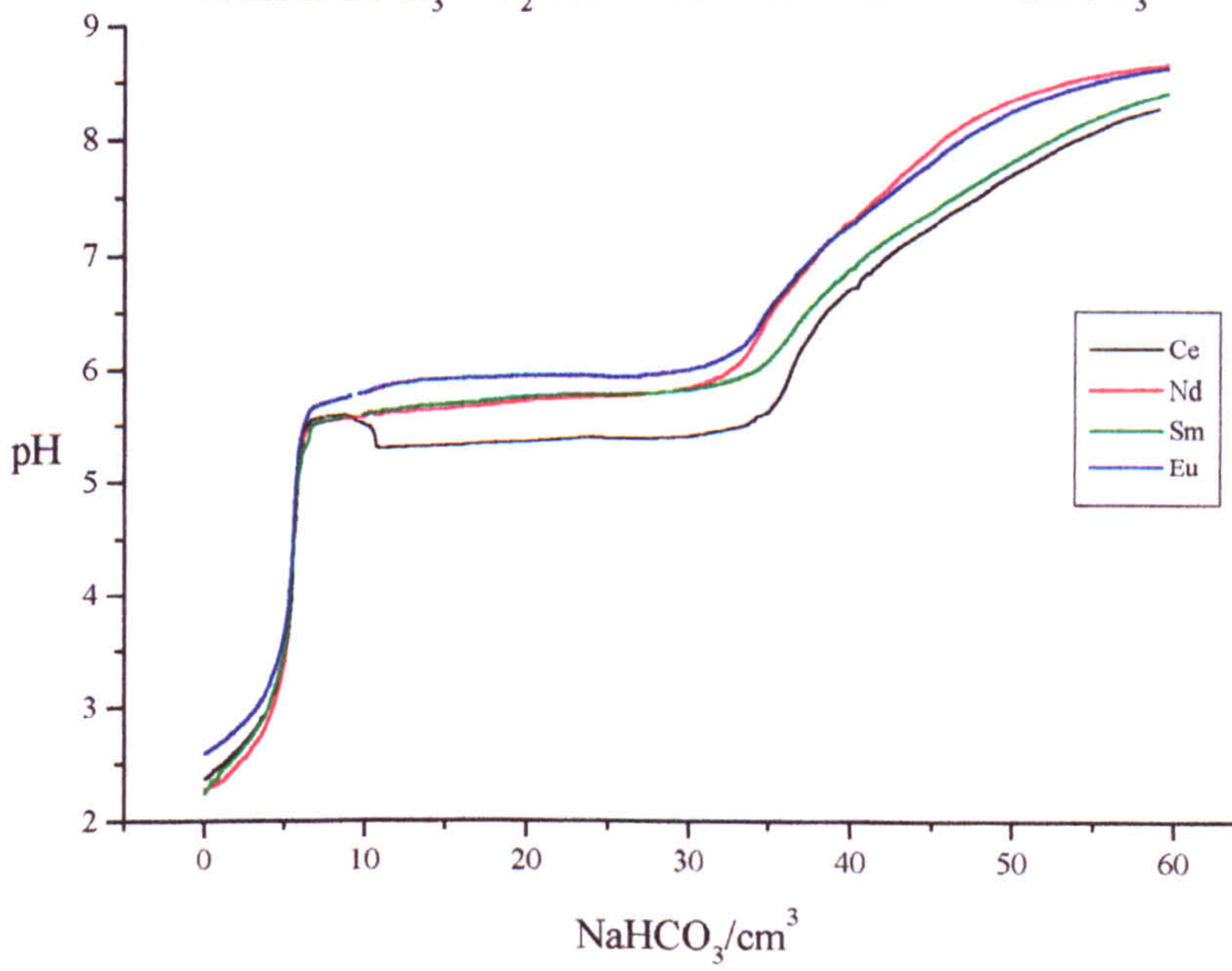

The reaction can be written in two stages. Initially neutralisation of the HCl (equation 3.6)

$$\underset{5cm^3(0.1M)}{\tfrac{1}{2}HCl} + \underset{5cm^3(0.1M)}{\tfrac{1}{2}NaHCO_3} \longrightarrow \tfrac{1}{2}NaCl + \tfrac{1}{2}H_2CO_3 \qquad (3.6)$$

followed by precipitation of $Ln_2(CO_3)_3$ (Section 3.4.3) along the buffer zone from pH 6-8 (equation 3.7)

$$\underset{5cm^3(0.2M)}{LnCl_3} + \underset{30cm^3(0.1M)}{3NaHCO_3} \longrightarrow \tfrac{1}{2}Ln_2(CO_3)_3(s) + {}^3/_2HCO_3^{2-} + {}^3/_2H^+ + 3Na^+ + 3Cl^- \qquad (3.7)$$

$30cm^3$ of $NaHCO_3$ are required for the complete reaction of the $LnCl_3$, the buffered pH of the solution is controlled by the remaining H^+ and HCO_3^- ions in solution. Further addition of $NaHCO_3$ after a 3:1 HCO_3^-- to Ln^{3+} ratio has been obtained increases the pH of the solution without further reaction.

3.4.3 Characterisation of Precipitate

FTIR and XRD analysis indicates that a solid hydrated lanthanide carbonate was present from all the $NaHCO_3$ titrations. Differences between the precipitates were due to the crystalline water content of each sample.

The FTIR spectrum (Figure 3.7, Table 3.4) indicates that a hydrated lanthanide carbonate is present for all the lanthanides examined. The ν_3 CO_3^{2-} doublet dominates the spectrum at approximately 1500 cm^{-1} and 1400cm^{-1}. The ν_1 stretch is weak, though the ν_2 and ν_4 CO_3^{2-} stretches are easily determined. The broad peak from 3400 cm^{-1} to 3200 cm^{-1} indicates that the sample is hydrated and a OH^- group is not present.

Figure 3.7 FTIR spectrum of $Nd_2(CO_3)_3.xH_2O$

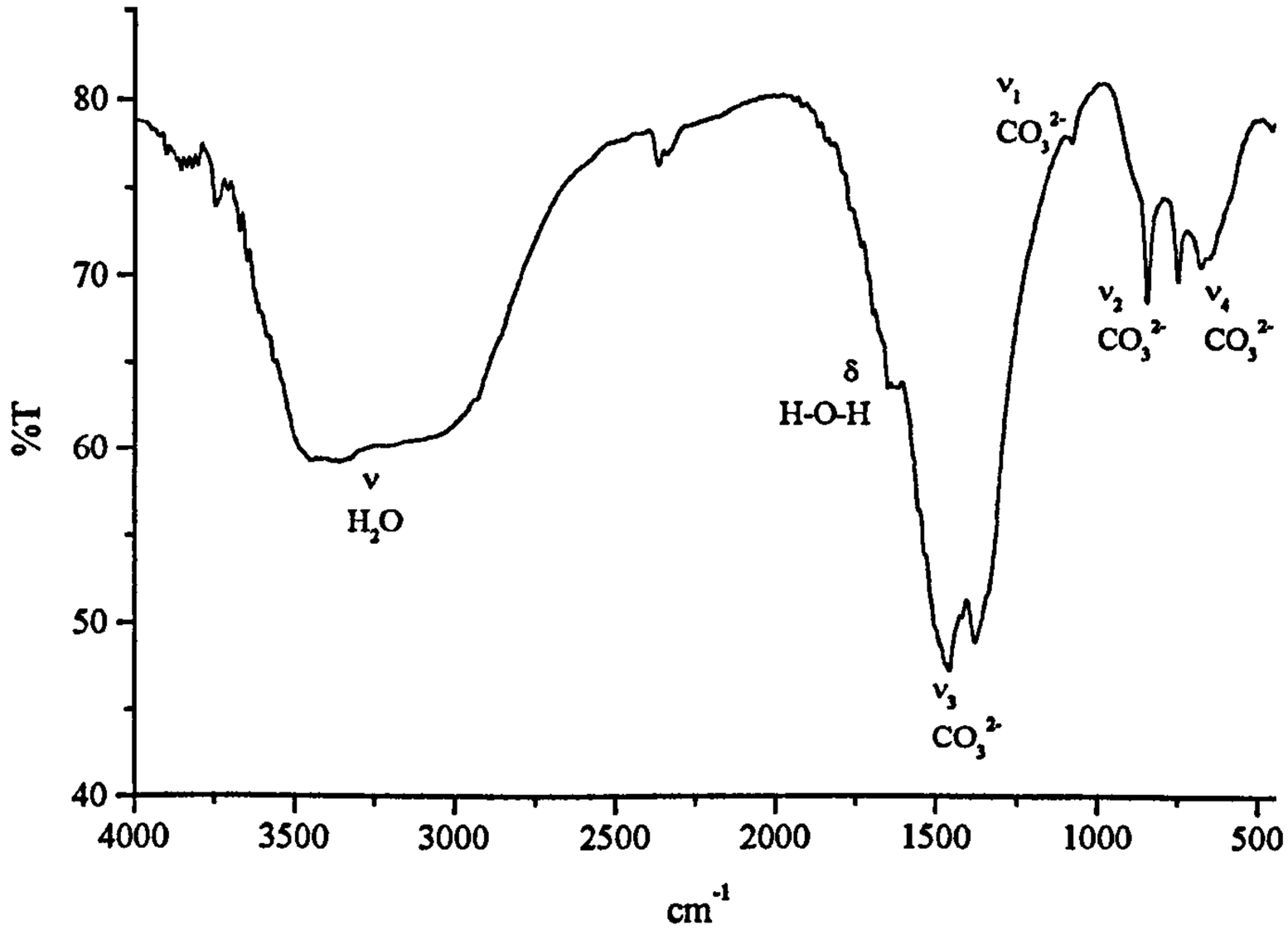

Table 3.4 FTIR peaks for hydrated $Ln_2(CO_3)_3.xH_2O$

	Ce-ppt	$Nd_2(CO_3)_3$ [1]	Nd-ppt	Sm-ppt	$Eu_2(CO_3)_3$ [1]	Eu-ppt
νO-H						
δO-H						
$\nu O\text{-}H_2$	3346	3420	3316	3404	3410	3396
$\delta O\text{-}H_2$	1654		1632	1631		1627
$\nu_1 CO_3^{2-}$	1077	1088	1083	1076	1089/1067	1093/1060
$\nu_2 CO_3^{2-}$	849	848	851	846	836/850	837/850
$\nu_3 CO_3^{2-}$	1476/1368	1491/1377	1488/1387	1506/1398	1499/1406	1498/1396
$\nu_4 CO_3^{2-}$	748/678	750/680	753/680	746/668	752/681	752/683

[1]Runde et al (1992)

The powder XRD spectra of Ce and Nd (Figure 3.8, Table 3.5) indicate that the lanthanite ($Ln_2(CO_3)_3.8H_2O$) is the dominant equilibrium crystal phase found, though $Ln_2(CO_3)_3.4H_2O$ has a similar XRD pattern and frequently forms. Sm and Eu tend to lose more crystalline water and can form with any amount of crystalline water down to $Ln_2(CO_3)_3.2{\cdot}85H_2O$ structure. The actual amount of crystalline water depends on the drying conditions of the sample and can vary from $Ln_2(CO_3)_3.8H_2O$ to completely dehydrated $Ln_2(CO_3)_3$. The $Ln_2(CO_3)_3.8H_2O$ precipitates are more crystalline than the $Ln(OH)_3$ precipitates, shown by the

intense diffraction patterns of the former, an increase from less than 500 counts per second for $Ln(OH)_3$ and CeO_2 precipitates compared with up to 18,000 counts per second for $Ce_2(CO_3)_3.8H_2O$.

Table 3.5 XRD d-spacing for $Ln_2(CO_3)_3.8H_2O$; End precipitate from the $NaHCO_3$ titrations

[1]$Nd_2(CO_3)_3.8H_2O$	Ce precipitate		Nd precipitate		Eu precipitate	
d(Å)	d(Å)	2θ	d(Å)	2θ	d(Å)	2θ
8.410	8.4345	10.48	8.3392	10.60	8.4025	10.52
4.710	4.7552	18.65	4.7039	18.85	4.5741	19.39
4.430	4.4669	19.86	4.4185	20.08	4.4393	19.99
4.150	4.2319	20.98	4.2012	21.13	4.2240	21.015
4.110	4.4160	21.42	4.1024	21.65	4.0298	22.040
3.910	3.9510	22.49	3.9132	22.71		
3.840	3.8712	22.96	3.8431	23.13	3.3466	26.62
3.230	3.2559	27.37	3.2230	27.66		
3.150	3.1647	28.18	3.1369	28.43	3.1027	28.75
3.020	3.0406	29.35	3.0493	29.26		
2.979	3.0071	29.69	2.9845	29.92	2.9178	30.615
2.909	2.9234	30.56	2.9044	30.76		
2.811	2.8243	31.65	2.8057	31.87	2.8252	31.65
2.681	2.6912	33.27	2.6896	33.29	2.7561	32.46
2.565	2.5827	34.71	2.5609	35.01	2.6013	34.45
2.412	2.4314	36.94	2.4129	37.24	2.4044	37.37
2.305	2.3193	31.80	2.3008	39.12		
2.266	2.2901	39.31	2.2677	39.72		
2.142	2.1595	41.80	2.1456	42.08	2.1256	42.495
2.118	2.1199	42.62	2.1062	42.91		
2.082	2.1008	43.02	2.0808	43.46		
2.055	2.0690	43.72	2.0503	44.14	2.0255	44.71
2.005	2.0400	43.37	2.0047	45.20	1.9975	45.37
1.953	1.9678	46.09	1.9520	46.49	1.9264	47.14
1.868	1.8833	48.29	1.8663	48.76	1.8872	48.18
1.815	1.8266	49.89	1.8137	50.27	1.7953	50.82

[1]$Nd_2(CO_3)_3.8H_2O$ JCPDS Powder Diffraction Files 29-918

Figure 3.8 XRD pattern of $Nd_2(CO_3)_3.8H_2O$

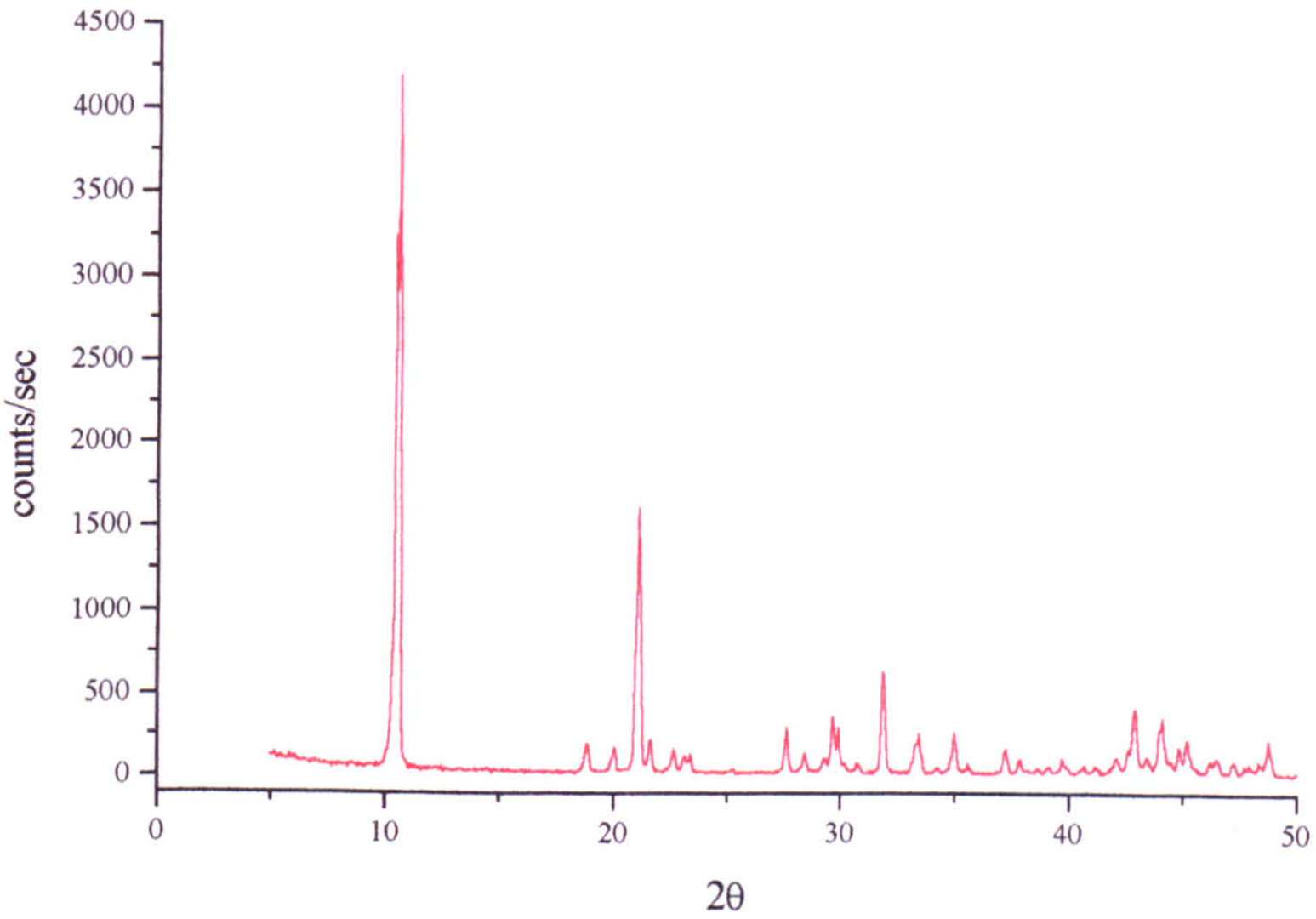

The actual amount of crystalline water can be determined from thermogravimetric analysis (Figure 3.9, Table 3.6). The thermal decomposition of $Ln_2(CO_3)_3.xH_2O$ takes place in 4 stages and is calculated in Table 3.6 from the decomposition profile shown in Figure 3.9. The calculations are based upon the following decomposition stages to give a formula of $Nd_2(CO_3)_3.4H_2O$

1. loss of adsorbed water 60°C
2. loss of crystalline water 120°C
3. initial decomposition of CO_3^{2-} as $CO_2(g)$ 400°C
4. final decomposition of remaining CO_3^{2-} 530°C

and a formula of $Nd_2(CO_3)_3.4H_2O$ with 0.8 adsorbed water molecules to the crystal structure can be calculated, even though the XRD indicates a formula with 8 crystalline water molecules.

Table 3.6 Thermal decomposition of $Nd_2(CO_3)_3.4H_2O$

End formula	Nd_2O_3 (RMM 336.48gmol^{-1})
	equivalent to 60.8% of the initial mass
therefore initial formula mass	553.4gmol^{-1}
1	loss of adsorbed water 60°C to 100°C
	100% -97.5% = 2.5% mass loss ≡ 13.8g ∴ $0.8H_2O$
2	loss of crystalline water 100°C to 300°C
	97.5%-84.8% = 12.7% mass loss ≡ 70.3g ∴ $3.9H_2O$
	$Nd_2(CO_3)_3.4H_2O \xrightarrow{\Delta H} Nd_2(CO_3)_3 + 4H_2O(g)$
3	initial decomposition of CO_3^{2-} 300°C to 450°C
	84.8%-68.1% = 16.7% mass loss ≡ 92.4g ∴ $2.1CO_2(g)$
	$Nd_2(CO_3)_3 \xrightarrow{\Delta H} Nd_2O_2CO_3 + 2CO_2(g)$
4	final decomposition of CO_3^{2-} 450°C to 950°C
	68.1%-60.8% = 7.3% mass loss ≡ 40.4g ∴ $0.9CO_2(g)$
	$Nd_2O_2CO_3 \xrightarrow{\Delta H} Nd_2O_3 + CO_2(g)$

Figure 3.9 TGA of hydrated $Nd_2(CO_3)_3$

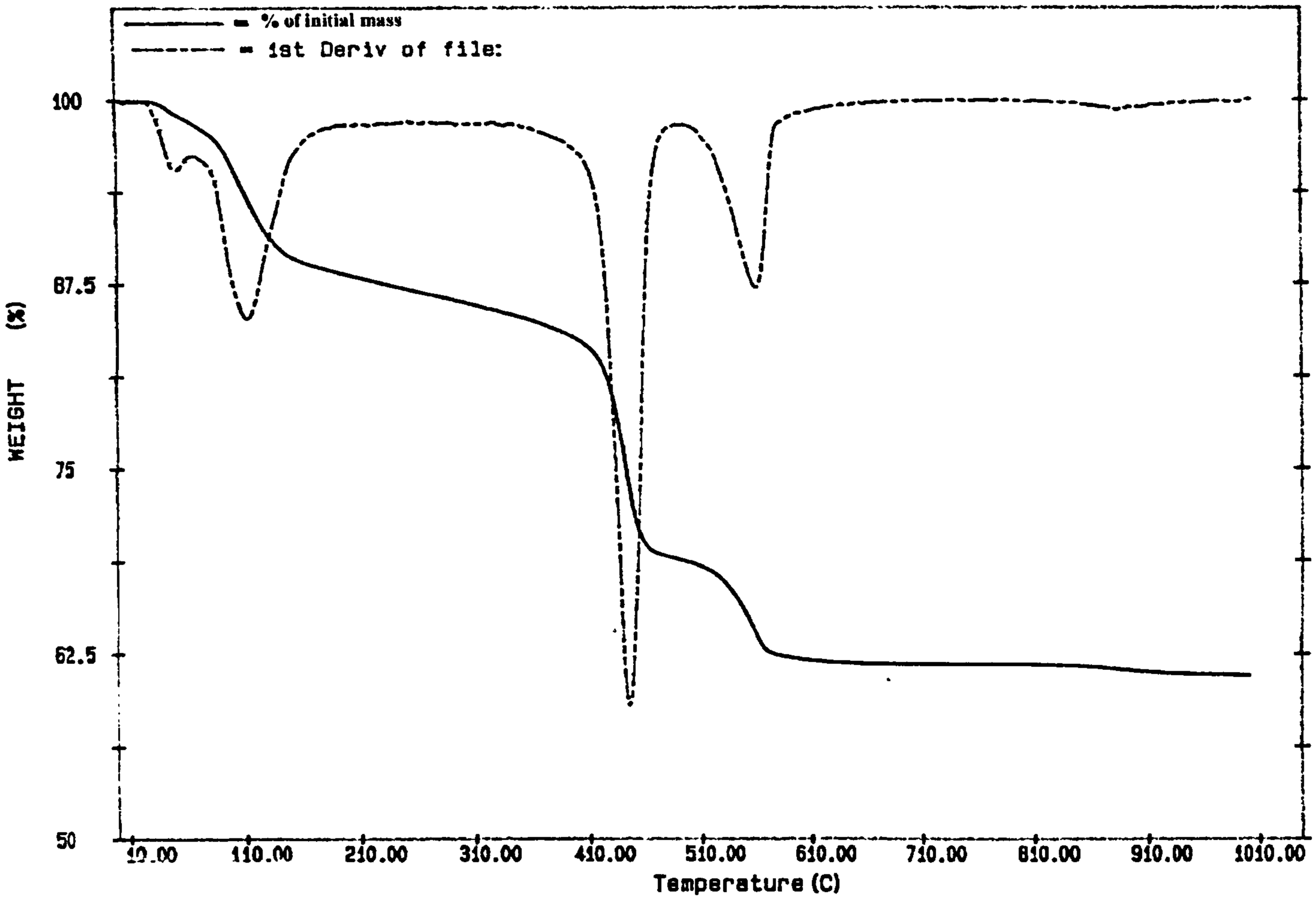

3.5 Titrations of $LnCl_3$ with Na_2CO_3

The effects of high pH cannot be examined with $NaHCO_3$ titrations or compared directly with the higher pH of the NaOH titrations. Na_2CO_3 allows a direct comparison between the carbonate and hydroxide systems above pH 10.

3.5.1 Experimental

The titrations were carried out following the method outlined in Section 3.2, with Na_2CO_3 (0.1M, $40cm^3$) as the titre solution.

3.5.2 Results

The effect of titrating lanthanide chloride solutions with a solution of Na_2CO_3 follows the same initial rise then drop in pH as precipitation of $Ln_2(CO_3)_3$ (characterised in Section 3.5.3) proceeds and the system equilibrates as observed in the $NaHCO_3$ system until $11cm^3$ of titre has been added (Figure 3.11). The addition of further Na_2CO_3 gradually to 15 cm^3 results in further reaction with the pH still buffered by the solution but there is a slight continuous rise in pH from pH 6.3 to 7.3. Between the addition of $15cm^3$ (pH 7.3) and $23cm^3$ (pH 9.3) of Na_2CO_3 there is an immediate rise then fall in pH with each addition. Further addition of titre solution after 23ml results in a slight continuous increase in pH. The end point of the titration is marked by the sharp rise in pH found at a $3CO_3^{2-}$ to $2Ln^{3+}$ ratio expected for the reaction (equation 3.8), when all available Ln^{3+} has reacted with the Na_2CO_3.

$$\underset{5\ cm^3(0.2M)}{2LnCl_3} + \underset{15\ cm^3(0.1M)}{3Na_2CO_3} \longrightarrow Ln_2(CO_3)_3 + 6Na^+ + 6Cl^- \qquad (3.8)$$

The end point is at a constant point for all replicate titrations and is comparable for each of the different lanthanide solutions studied.

Figure 3.10 Typical titration curve for 1mmol$NdCl_3$ with 4mmols Na_2CO_3

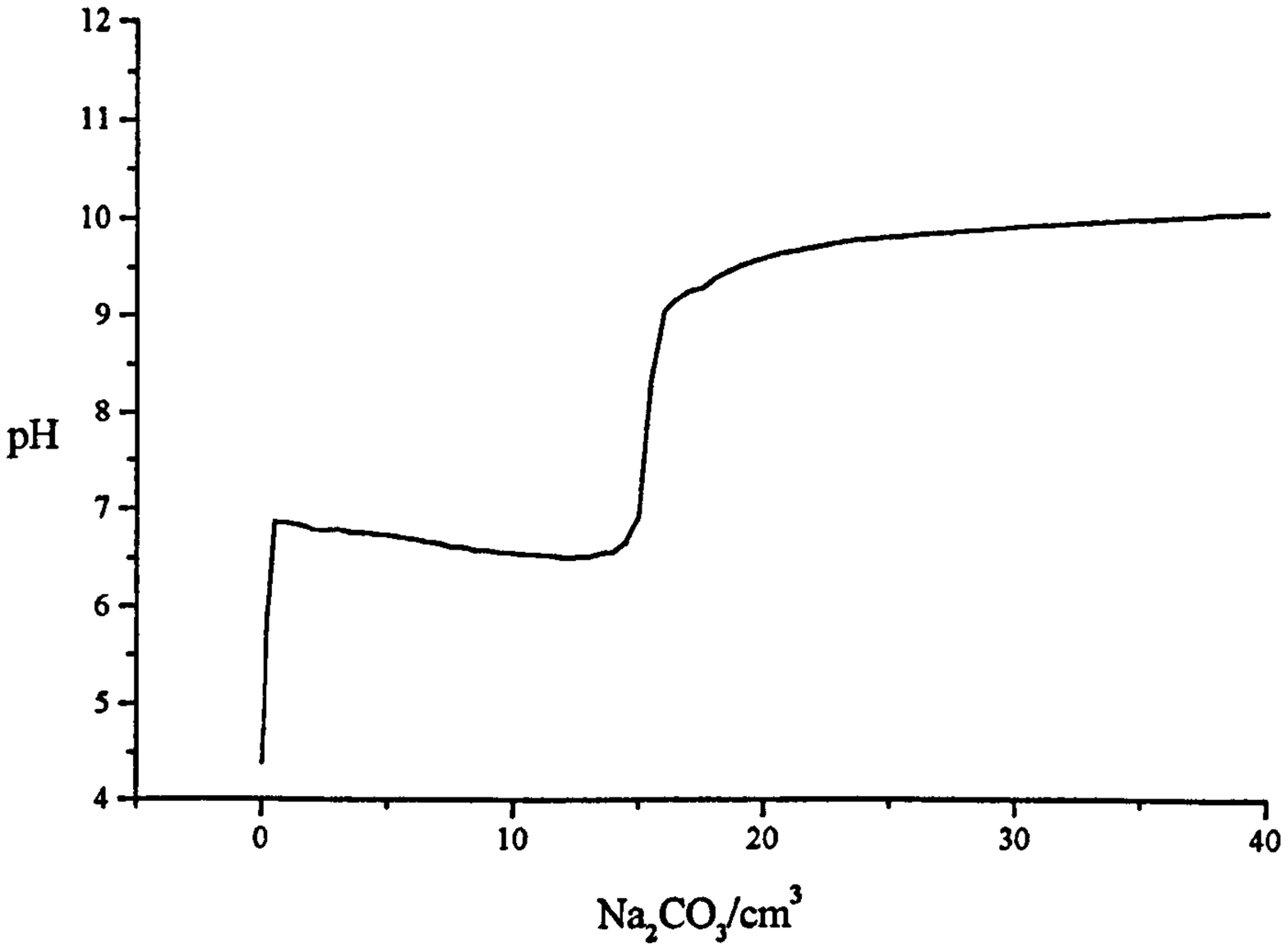

The end-point of the titration, after 15 cm^3 of Na_2CO_3 had been titrated is not the final reaction step even though the Nd, Sm and Eu precipitates do not visibly appear to alter further when excess titre solution was added. However, the end product of the Na_2CO_3 titrations with Nd, Sm and Eu was found to be the double salt $NaLn(CO_3)_2.6H_2O$ (characterised in Section 3.5.3), formed from the further reaction of Na_2CO_3 with the solid $Ln_2(CO_3)_3$ phase (equation 3.9).

$$\underset{10cm^3(0.1M)}{Ln_2(CO_3)_3 + Na_2CO_3} \longrightarrow 2NaLn(CO_3)_2 \qquad (3.9)$$

The Ce precipitate visibly alters after 15cm^3 of Na_2CO_3 had been titrated. The white $Ce_2(CO_3)_3$ precipitate alters to yellow CeO_2 above pH 9.5 (equation 3.10).

$$\tfrac{1}{2}Ce_2(CO_3)_3 + 2H_2O \xrightarrow{pH>9.5} CeO_2 + \tfrac{3}{2}CO_3^{2-} + \tfrac{3}{2}H^+ + \tfrac{1}{2}H_2 \qquad (3.10)$$

3.5.3 Characterisation of Precipitate

The initial and final precipitates were analysed by FTIR, XRD and acid dissolution of the precipitates then elemental analysis for Na and Ln^{3+} using the techniques described in Chapter 2. The initial precipitate formed below pH 8,

was identified as hydrated $Ln_2(CO_3)_3$, which originally precipitates as an amorphous phase, for all the lanthanides examined and have been characterised in Section 3.4.3. $Ce_2(CO_3)_3$ alters directly to CeO_2 (characterised in Section3.3.3) without an intermediate $NaCe(CO_3)_2$ phase or amorphous purple hydroxy phase as found during the hydroxide titrations.

FTIR analysis of the final product indicates crystalline water and carbonate stretches are present for Nd, Sm and Eu (Figure 3.13 and Table 3.7). The FTIR spectra is indistinguishable from the initial $Ln_2(CO_3)_3$ precipitate. However, elemental analysis (for Na^+ and Ln^{3+}) indicates that there is a 1:1 Na^+:Ln^{3+} ratio in the final product and a 0:1 Na^+:Ln^{3+} ratio in the initial $Ln_2(CO_3)_3$ precipitate.

Figure 3.11 FTIR spectrum of $NaNd(CO_3)_2.xH_2O$

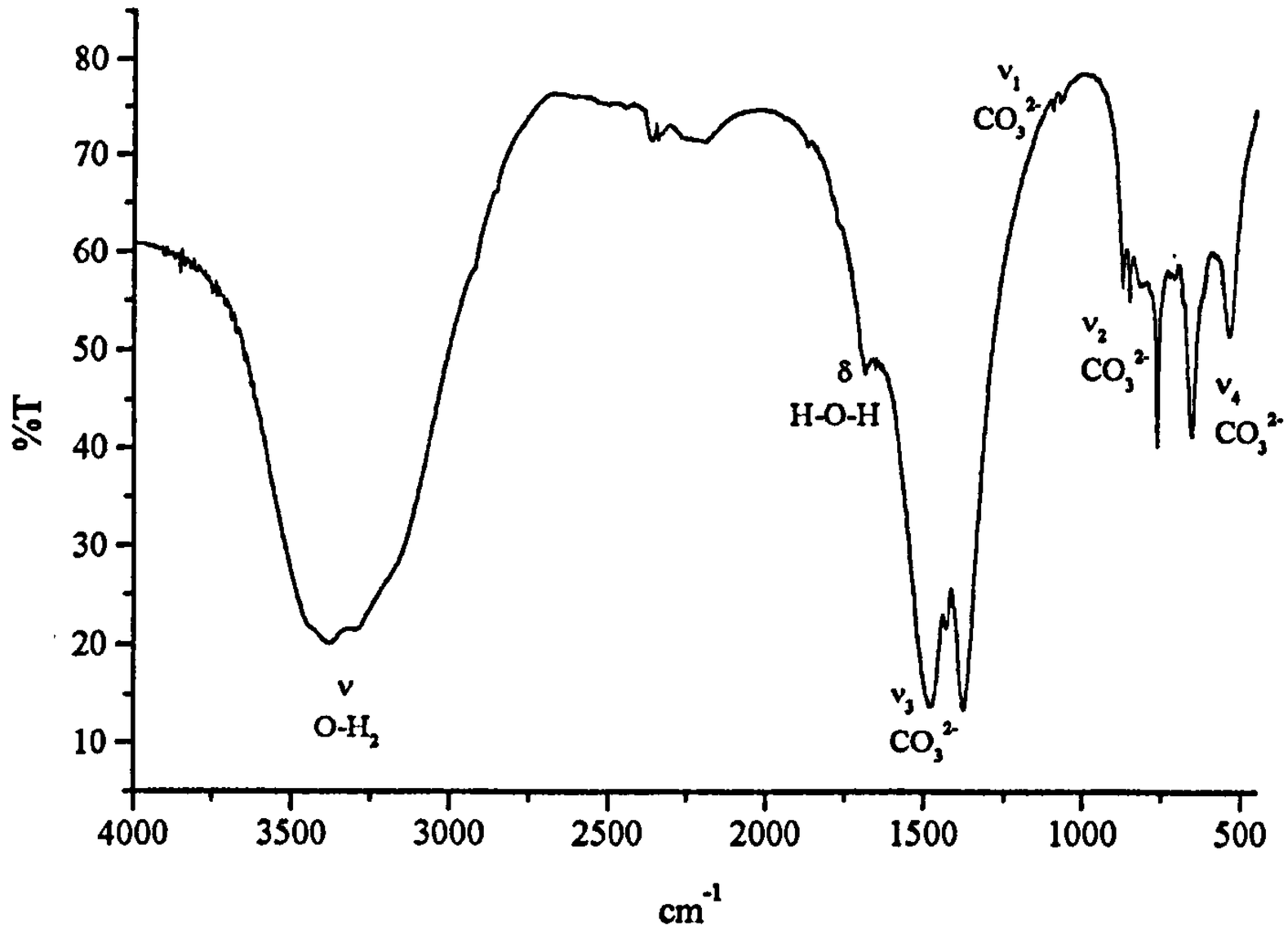

Table 3.7 FTIR stretches for hydrated $NaLn(CO_3)_2$

	Nd[1]	Nd-ppt	Sm-ppt	Eu-ppt
νO-H				
δO-H				
$\nu O\text{-}H_2$		3380	3384	3356
$\delta O\text{-}H_2$		1684	1646	1676
$\nu_1 CO_3^{2-}$	1070	1072		1066
$\nu_2 CO_3^{2-}$	875/850	872/850	854	
$\nu_3 CO_3^{2-}$	1530/1385	1477/1374	1498/1384	1522/1376
$\nu_4 CO_3^{2-}$		763/653	762/641	

[1]Mochizuki et al (1974)

Table 3.8 XRD d-spacing for $NaLn(CO_3)_2.6H_2O$; End precipitates from the Na_2CO_3 titrations

$NaNd(CO_3)_2.6H_2O$	Ce-precipitate		Nd-precipitate		Sm-precipitate		Eu- precipitate	
d(Å)	d(Å)	2θ	d(Å)	2θ	d(Å)	2θ	d(Å)	2θ
13.30	13.3448	7.16	13.3614	6.61	12.6812	6.97	12.0752	7.32
6.610	6.3660	13.90	6.5974	13.41	6.4258	13.77	6.2650	14.13
4.370	4.2834	20.72	4.3871	20.23	4.3009	20.64	4.2210	21.03
3.280	3.2299	27.60	3.2836	27.14	3.2806	27.16	3.2466	27.45
2.620	2.5914	34.59	2.6238	34.15	2.5889	34.62	2.5631	34.98
2.180	2.1665	41.66	2.1848	41.29	2.1595	41.80	2.1371	42.26
1.870	1.8203	50.07	1.8579	48.99	1.8510	49.19	1.8358	49.62

Literature values JCPDS Powder Diffraction Files [1]30-1223

$NaCe(CO_3)_2$ precipitate formed from a 1M $NaHCO_3$ solution (Chapter 4)

Figure 3.12 XRD pattern of $NaNd(CO_3)_2.6H_2O$ end product of the Na_2CO_3 titrations

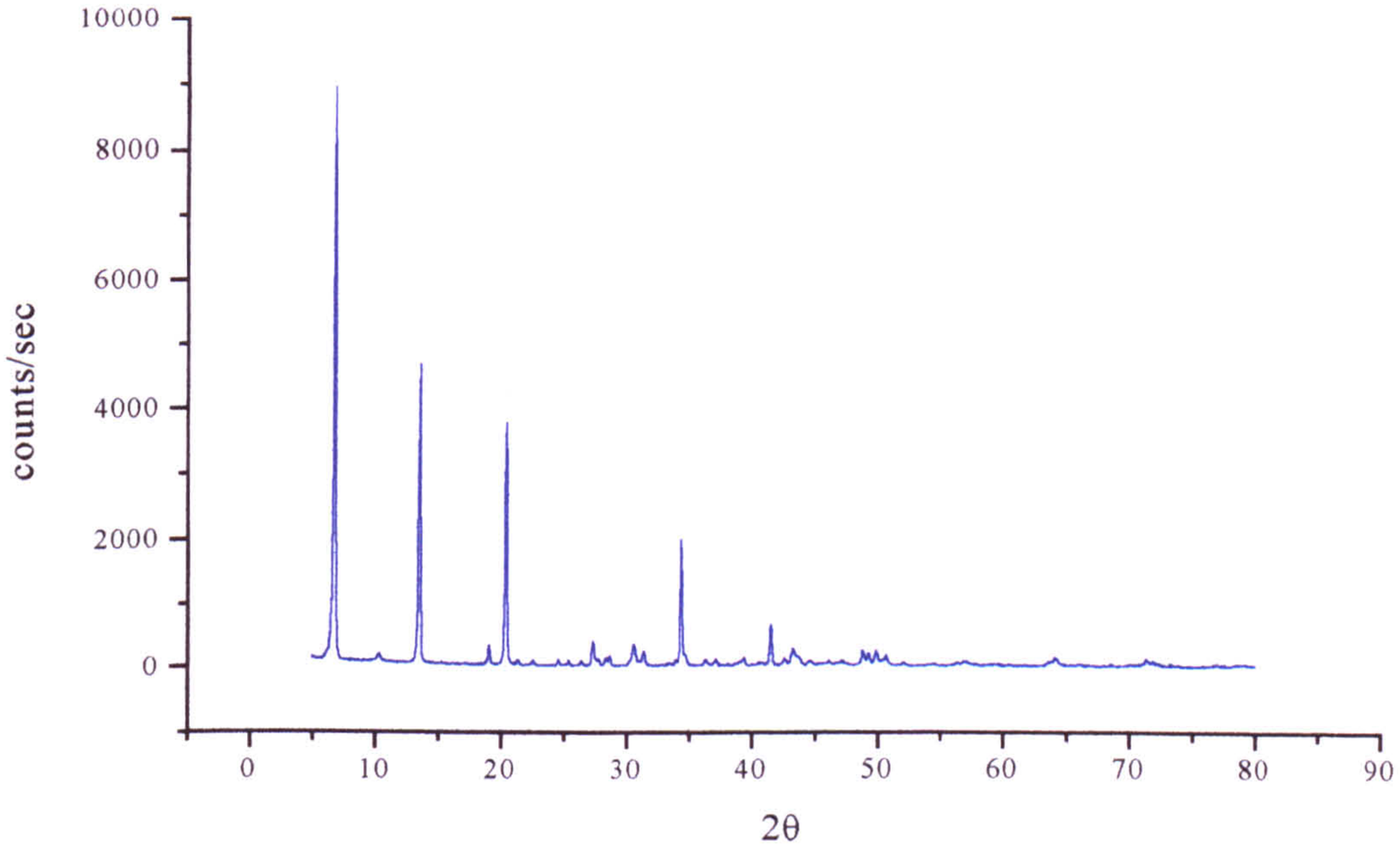

The identification of a $NaLn(CO_3)_2.6H_2O$ structure was confirmed by XRD analysis by comparison with the literature XRD pattern which has only 7 distinct crystal planes (Table3.8) from Mochizuki *et al.*, (1974). Nd, Sm and Eu have identical XRD patterns which are offset to a slightly higher value of 2θ, as the ionic radii decreases across the lanthanide series. The precipitates form as very crystalline specular Nd or fibrous Eu crystals and are characterised from their strong diffraction pattern (up to 22,000 counts per second)

The actual water content of the hydrated $NaLn(CO_3)_2$ structure can be determined by thermal gravimetric analysis. The thermal decomposition can be calculated from Figure 3.13 (showing the decomposition of $NaNd(CO_3)_2.xH_2O$), assuming that the sample is completely dehydrated to $NaNd(CO_3)_2$ with no breakdown of the carbonate to the oxy-carbonate at 550°C (Table 3.10). All mass loss below 550°C is assumed to be due to the loss of H_2O.

The thermal decomposition (Table 3.10) indicates there are actually seven crystalline water molecules that decompose in two equal stages after the initial loss of surface adsorbed water. The water loss occurs as three sharp bands in of

mass loss at 60°C, 150°C-200°C and 450°C shown from the derivative of mass loss curve. The decomposition of carbonate to the oxy-carbonate occurs as a sharper drop in mass than Mochizuki *et al.*, (1974) but only half a CO_3^{2-} molecule decomposes to CO_2(g). There was no further decomposition up to 850°C. If the initial CO_3^{2-} decomposition occurs with dehydration then the extra water molecule may account for the drop in CO_3^{2-} decomposition. The technique only determines the mass loss with temperature and further analysis of the evolved species would be required to determine the actual amount of CO_3^{2-} decomposition.

The decomposition stages cannot be followed by XRD analysis as there are as yet no intermediate $NaLnO(CO_3)$ reference patterns, and phases may be amorphous therefore undetectable with XRD analysis.

The hydrated $NaNd(CO_3)_2$ decomposition differs from the hydrated $Nd_2(CO_3)_3$ (Section 3.4.3) in that the sodium double carbonate is thermally stable at higher temperatures, decomposition of $Nd_2(CO_3)_3$ to Nd_2O_3 is complete by 600°C.

Mochizuki *et al.*, (1974) give a 3 stage decomposition (Table 3.10) from $NaNd(CO_3)_2.6H_2O$ to $NaNdOCO_3$ from 50°C to 650°C. The oxy carbonate is thermally stable until 700°C and no further decomposition was determined.

Table 3.9 Thermal decomposition of hydrated $NaNd(CO_3)_2$ from Figure 3.13

Start 100% mass $NaNd(CO_3)_2.6H_2O$ (from XRD analysis)

assume mass loss to 550°C from dehydration alone.

$NaNd(CO_3)$ RMM 284gmol^{-1} ≡ 60.2% of initial mass

∴ 100% mass ≡ 477.1gmol^{-1}

1 mass loss from 0-80°C adsorbed water

100%-86.4% = 13.6% ≡ 64.9g ∴ $3.6H_2O$ lost

2 loss of initial crystalline water from 80°C to 330°C

86.4%-73.3% = 13.1% ≡ 62.5g ∴ $3.5\ H_2O$ lost

3 loss of final crystalline water from 330°C to 550°C

73.3%-60.2% = 13.1% ≡ 62.5g ∴ $3.5H_2O$ lost

4 initial decomposition of CO_3^{2-} from 550°C to 730°C

60.2% -55.3%= 4.9% ≡ 23.4g ∴ $0.5CO_2$ lost

The decomposition reactions can be written as

1 loss of adsorbed water $\xrightarrow{\Delta H}$ $NaNd(CO_3)_2.7H_2O$

2 $NaNd(CO_3)_2.7H_2O \xrightarrow{\Delta H} NaNd(CO_3)_2.3{\cdot}5H_2O + 3{\cdot}5H_2O$

3 $NaNd(CO_3)_2.3{\cdot}5H_2O \xrightarrow{\Delta H} NaNd(CO_3)_2 + 3{\cdot}5H_2O$

4 $NaNd(CO_3)_2 \xrightarrow{\Delta H} NaNdO_{0.5}(CO_3)_{1.5} + 0.5CO_2(g)$

Table3.10 Thermal decomposition of $NaNd(CO_3)_2.6H_2O$ after Mochizuki *et al.*, (1974)

$NaNd(CO_3)_2.6H_2O \longrightarrow$	$NaNd(CO_3)_2.3H_2O + 3H_2O$	120-200°C
$NaNd(CO_3)_3.3H_2O \longrightarrow$	$NaNd(CO_3)_2 + 3H_2O$	370-450°C
$NaNd(CO_3)_2 \longrightarrow$	$NaNdOCO_2 + CO_2$	650°C

Figure 3.13 TGA decomposition of hydrated $NaNd(CO_3)_2$

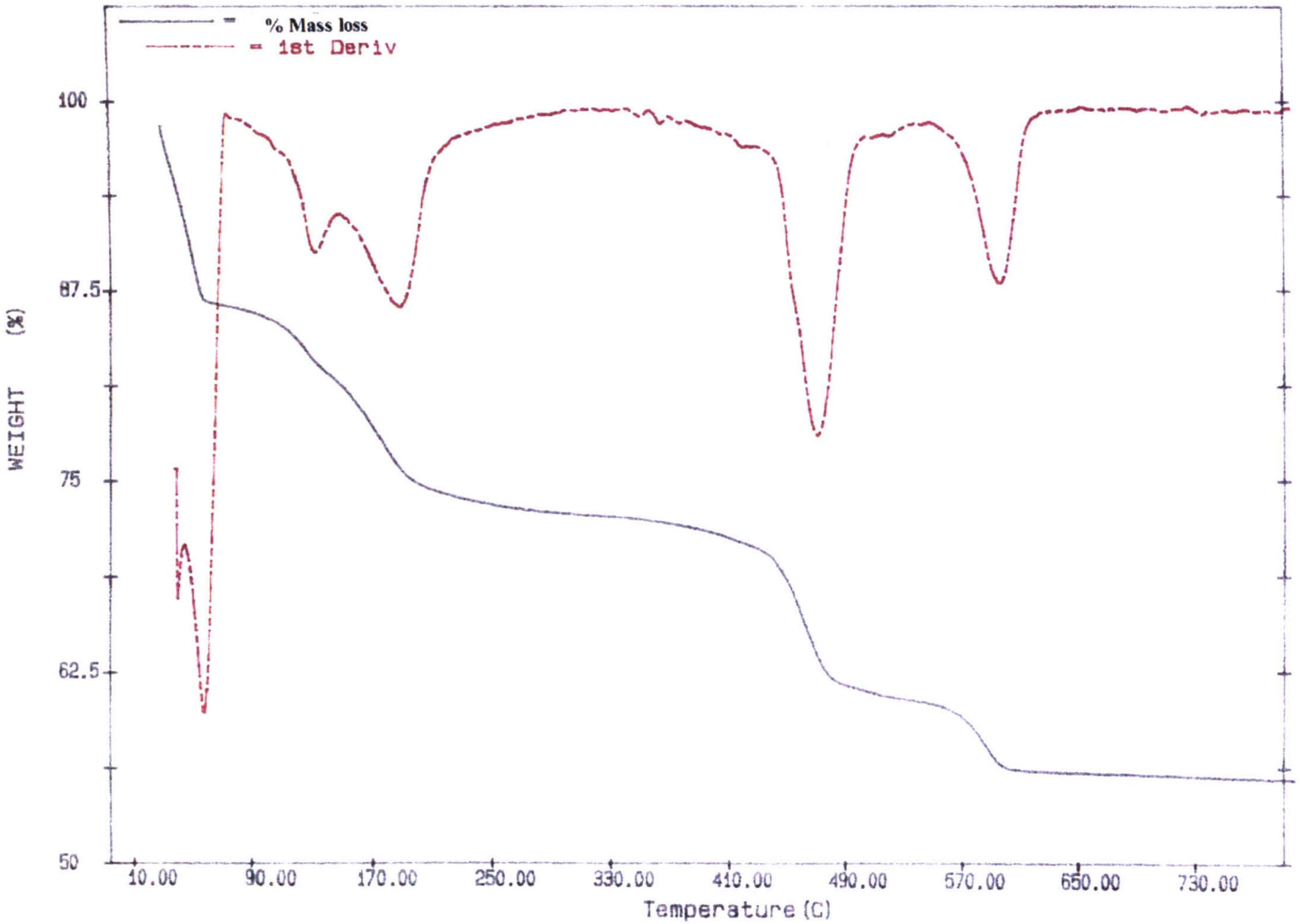

3.6 Titrations with K_2CO_3

The formation of , $NaLn(CO_3)_2.6H_2O$, found in the Na_2CO_3 titrations indicates that the Na^+ ion activity effects the system at high pH. Therefore to examine the effects of CO_3^{2-} and OH^- at high pH without the effects of Na^+, the Na_2CO_3 titre solution was replaced with K_2CO_3. This should also demonstrate if a comparable potassium lanthanide carbonate is formed, although no previous reports have indicated conditions for its formation.

3.6.1 Experimental

Titrations were carried out following the method outlined in section 3.2, with K_2CO_3 (0.1M, $40cm^3$) as the titre solution.

3.6.2 Results

Figure 3.14 Typical titration curve for 1mmol $NdCl_3$ with 4mmols K_2CO_3

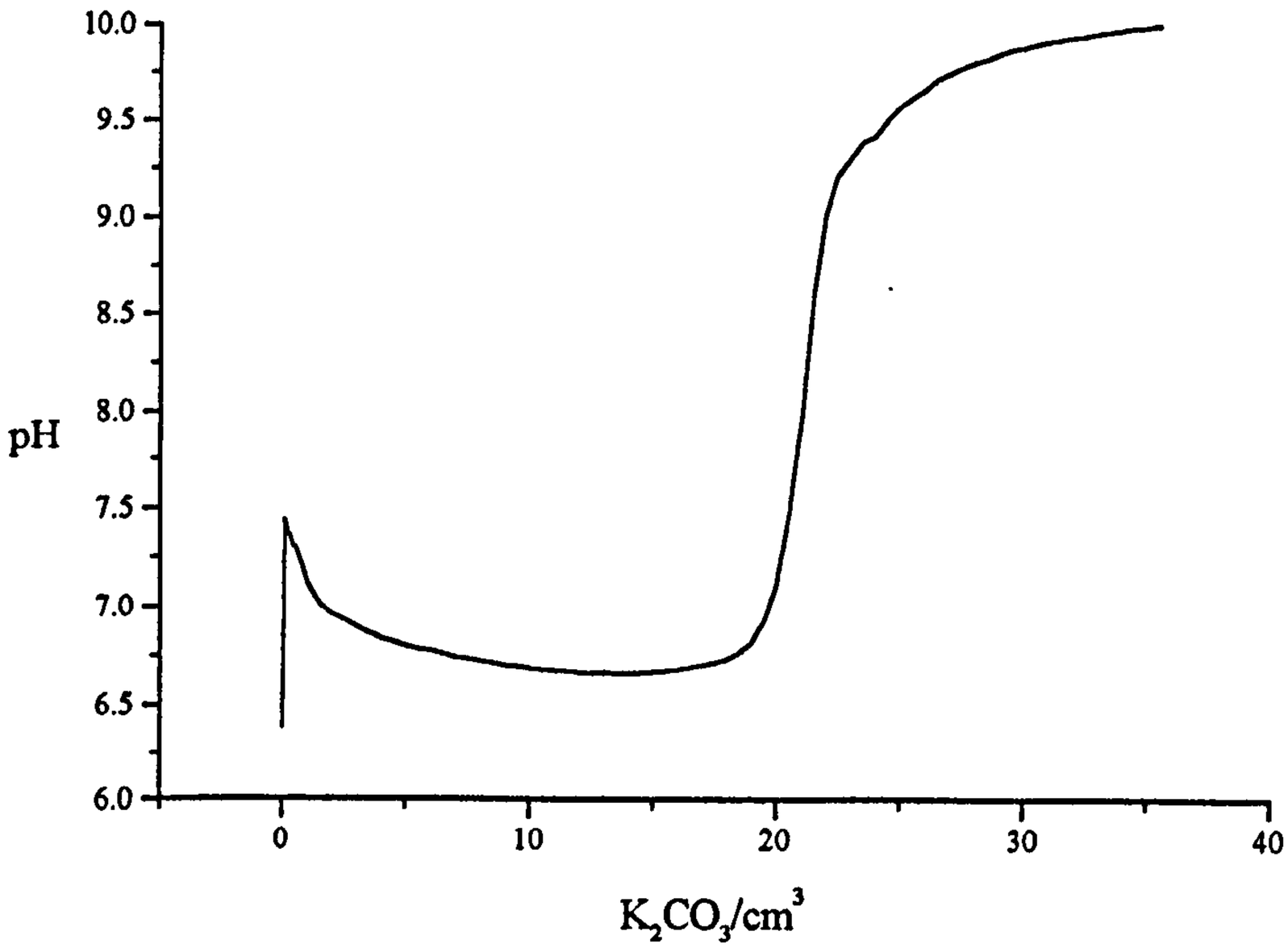

The titration follows the initial pattern seen with $NaHCO_3$ titrations. There is an initial rapid pH increase for 0.1-0.2cm^3 K_2CO_3 to pH 7.0 followed by a slight

decrease in pH with precipitation as the titration progresses (Figure 3.16). During the slow addition of K_2CO_3 between 0.5cm^3 to 19cm^3 the pH is stable (a slight decrease is apparent) and a precipitate is gradually formed. The pH increases sharply from pH 6.5 to 9.2 at 20 cm^3 of K_2CO_3. This is the 2:1 CO_3^{2-}/Ln^{3+} ratio. The pH then rises slowly with each successive addition of K_2CO_3. The colours of the precipitates initially mirror the $NaHCO_3$ system, but the Ce ion slowly alters to yellow above pH 9, indicating CeO_2 has formed.

The K_2CO_3 titrations follow a similar pattern to the Na_2CO_3 titrations of immediate precipitation of a hydrated $Ln_2(CO_3)_3$, followed by the alteration of the precipitate to $LnCO_3OH$ or CeO_2 at high pH.

The precipitation of $Ln_2(CO_3)_3$ (equation 3.11) occurs when the solution pH was buffered at pH 6, for the first 15 cm^3 of K_2CO_3 titre added.

$$\underset{5cm^3(0.2M)}{LnCl_3} + \underset{15cm^3(0.1M)}{^3/_2K_2CO_3} \longrightarrow \tfrac{1}{2}Ln_2(CO_3)_3(s) + 3K^+ + 3Cl^- \qquad (3.11)$$

The pH of the solution does not rise rapidly when all the lanthanide ions have precipitated as for the Na_2CO_3 titrations even though precipitation cannot buffer the solution pH further. The further addition of 5cm^3 K_2CO_3 to the solution did not increase the pH of the solution, there must then be a further reaction in solution or with the solid phase from 15cm^3 to 20cm^3 of titre.

A two stage reaction is possible initially producing OH^- ions (equation 3.12) which then react with the $Ln_2(CO_3)_3$ precipitate (equation 3.13) and prevents the pH increasing from pH 6 after 15cm^3 to 20cm^3 of titre.

$$\underset{5cm^3(0.1M)}{\tfrac{1}{2}K_2CO_3(aq)} + H_2O \longrightarrow K^+ + H_2CO_3 + OH^- \qquad (3.12)$$

$$\tfrac{1}{2}Ln_2(CO_3)_3(s) + OH^- \longrightarrow LnCO_3OH(s) + \tfrac{1}{2}CO_3^{2-} \qquad (3.13)$$

The oxidation of $Ce^{(III)}$ to $Ce^{(IV)}$ follows the hydrolysis reaction and the precipitate alters to CeO_2 (equation 3.14)

$$Ce_2(CO_3)_3(s)+4OH^- \xrightarrow{pH>9} 2CeO_2(s)+3CO_3^{2-}+2H^++H_2 \qquad (3.14)$$

Ce follows the same titration pattern as Nd and Eu K_2CO_3 titrations, though the phase change to yellow CeO_2 is not immediate and slowly occurs above pH 9 as a $CeCO_3OH$ reaction intermediate may form before the oxidation reaction but was not isolated.

3.6.3 Characterisation of Precipitate

The initial precipitates formed in the Ln^{3+}-K_2CO_3 titrations were all identified as hydrated $Ln_2(CO_3)_3$, however at high pH the precipitates had altered to CeO_2 (Figure 3.3)or $NdCO_3OH$ and $EuCO_3OH$ (Figures 3.15 and 3.16, Tables 3.11 and 3.12).

The precipitates formed at high pH can be identified as the hydroxy carbonates from their FTIR spectra. The hydroxide group has a sharp but tapering OH^- stretch instead of a broad water OH_2 stretch at about 3400cm^{-1}. This also indicates there are no crystalline water molecules in the hydroxycarbonate structure. The carbonate group has a strong infra red absorption doublet at approximately 1500cm^{-1} (Table 3.11).

Figure 3.15 FTIR spectra of $LnCO_3OH$: End product of the K_2CO_3OH titrations

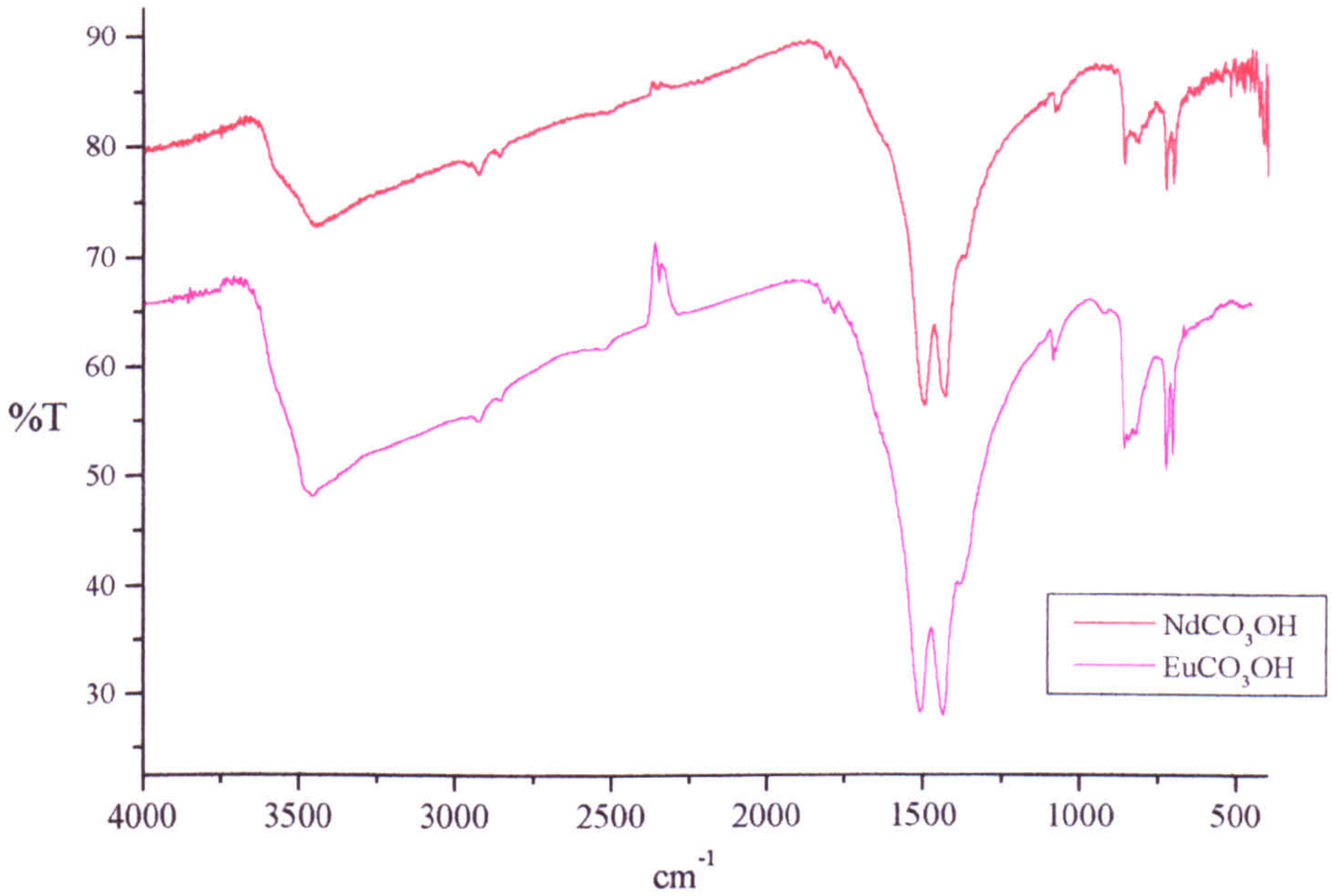

Table 3.11 FTIR stretches for $LnCO_3OH$

	Nd[1]	Nd-ppt	Eu[1]	Eu-ppt
$\nu O\text{-}H$	3450	3441	3479	3453
$\delta O\text{-}H$				
$\nu O\text{-}H_2$				
$\delta O\text{-}H_2$				
$\nu_1 CO_3^{2-}$	1080	1080	1089	1087
$\nu_2 CO_3^{2-}$	857/815	857	857/821	858/821
$\nu_3 CO_3^{2-}$	1498/1434	1497.3/1429	1510/1433	1509/1438
$\nu_4 CO_3^{2-}$	725/699	725/699	723/702	724/702

[1]Runde *et al.*, (1992)

The identification of the lanthanide hydroxy carbonate was confirmed from powder XRD analysis and comparison of the diffraction pattern with the JCPDS powder files 27-1295 and 27-1296 (Table 3.12). The results are in good agreement with the Runde *et al.*, (1992) preparation of $LnCO_3OH$ (Ln = Nd or Eu). The Nd, Sm and Eu $LnCO_3OH$ XRD patterns (Figure 3.16) can be superimposed upon each other with a slight peak shift to a higher 2θ with decreasing ionic radii (i.e. from Nd to Eu). The generally small peak heights of less than 700 counts per second reflect the almost amorphous nature of the $LnCO_3OH$ precipitates compared with the $Ln_2(CO_3)_3$ and $NaLn(CO_3)_2$ precipitates (with peak heights generally above 5000 counts per second).

Figure 3.16 XRD pattern of $LnCO_3OH$
Characterised from JCPDS reference pattern 27-1296 ($NdCO_3OH$)

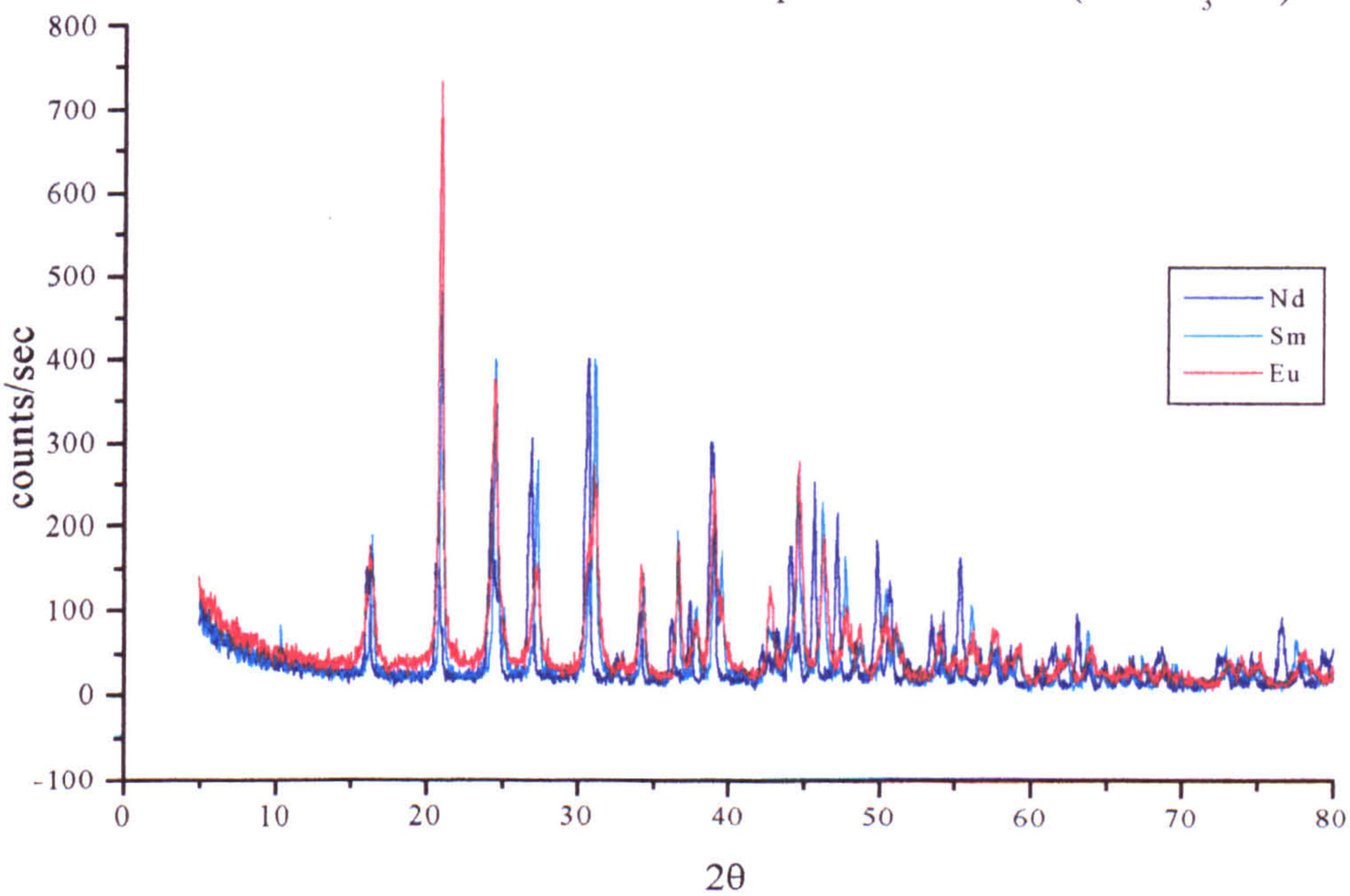

Table 3.12 XRD d-spacing for $LnCO_3OH$; End precipitate from the K_2CO_3 titrations

$NdCO_3OH$[1]	Nd- precipitate		Eu- precipitate		$NdCO_3OH$[1]	Nd- precipitate		Eu- precipitate	
d(Å)	d(Å)	2θ	d(Å)	2θ	d(Å)	d(Å)	2θ	d(Å)	2θ
5.500	5.4854	16.15	5.3975	16.41	1.691				
4.280					1.688				
4.240	4.2580	20.85			1.660	1.6596	55.31		
3.680	3.6688	24.24			1.620	1.6226	56.69		
3.650	3.6338	24.48			1.603	1.6020	57.48	1.5896	57.97
3.320	3.3142	26.88	3.1642	28.18	1.599				
2.940	2.9248	30.54	3.0240	29.52	1.580				
2.910					1.570	1.5715	58.71		
2.748	2.7425	32.63	2.7254	32.84	1.535	1.5345	60.27		
2.630	2.6145	24.270			1.515				
2.475	2.4692	36.355			1.502	1.5052	61.56		
2.400	2.3949	37.53			1.500				
2.323					1.472	1.4742	63.01	1.4568	63.85
2.310	2.3162	38.85	2.1881	41.23	1.458				
2.138	2.1359	42.28			1.438	1.4394	64.71		
2.122	2.1123	42.78			1.415	1.3994	66.80	1.4106	66.20
2.097					1.368	1.3723	68.30		
2.050	2.0439	44.28			1.305	1.3023	72.53	1.2957	72.96
2.030					1.282				
1.984	1.9859	45.65			1.272	1.271	74.54		
1.925	1.9258	47.16			1.245	1.2440	76.52		
1.880	1.8779	48.44			1.240				
1.830	1.8335	49.69			1.228	1.2261	77.84		
1.805	1.7993	50.70	1.8043	50.55	1.205				
1.715	1.7133	53.44	1.7323	52.81	1.197				

[1]Literature values JCPDS Powder Diffraction Files 27-1296

The thermal decomposition of the lanthanide hydroxycarbonate is shown for $NdCO_3OH$ in Table 3.13 and derived from Figure 3.17. The thermal decomposition indicates that there is a small amount of adsorbed water on the surface of the sample, which is lost below 100°C and crystalline water is not present. There is also an approximate CO_3^{2-}/OH^- ratio of 1.15 to 1, rather than the 1 to1ratio expected from the formula, $NdCO_3OH$, confirming that $Ln_2(CO_3)_3.xH_2O$ is not present. This interpretation is subjective as the actual evolved gas (H_2O or CO_2) and there proportions when mixed are assumed from the calculation and not actually confirmed analytically.

Table 3.13 Thermal decomposition of $NdCO_3OH$

Final product Nd_2O_3 (RMM 336.48g) identified from XRD analysis

Final product 71.7% of initial mass

Initial formula mass 469.3gmol^{-1}

1 Loss of adsorbed water below 120°C

100% -97% = 3% ≡ 14g ∴ $0.8H_2O$

2 Decomposition of initial decomposition of carbonate and hydroxide 420°C

97%-81.3% = 15.7% ≡ 73.7g ∴ $H_2O(g) + 1.3CO_2(g)$

Reaction

$$2NdCO_3OH \xrightarrow{\Delta H} Nd_2O_2CO_3 + H_2O(g) + CO_2(g)$$

3 Final decomposition of any remaining carbonate 500°C to 620°C

81.3% -71.7% = 9.7% ≡ 45.5g ∴ $CO_2(g)$

Reaction

$$Nd_2O_2CO_3 \xrightarrow{\Delta H} Nd_2O_3 + CO_2(g)$$

Figure 3.17 TGA decomposition of $NdCO_3OH$

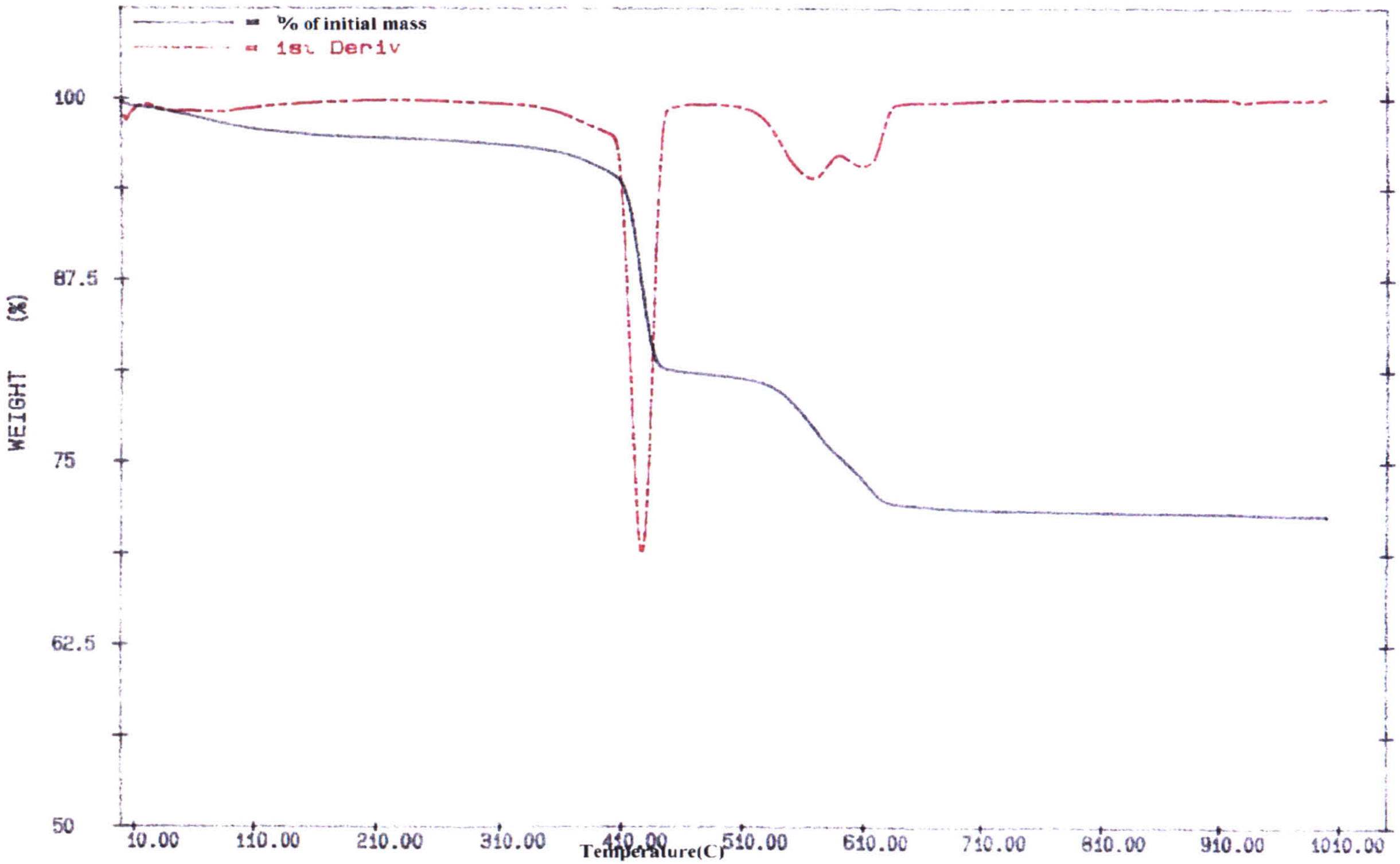

3.7 Titrations with $NaHCO_3$ and KOH

A titre solution with a formula of $NaKCO_3$ i.e. an intermediate between K_2CO_3 and Na_2CO_3 can be prepared by mixing equal concentrations of $NaHCO_3$ and KOH.

3.7.1 Experimental

The titrations were carried out following the method outlined in section 3.2, with $KOH/NaHCO_3$ (0.1M, $40cm^3$) as the titre solution prepared by dissolving KOH (2.8055g) and $NaHCO_3$ (4.2005g)in degassed distilled water ($500cm^3$).

3.7.2 Results

The mixed Na/K titration follows the initial pattern of the previous carbonate titrations (Figure 3.18) with an initial rise in pH then buffering of the pH by precipitation. The end point almost mirrors the Na_2CO_3 system and is intermediate between that of the Na_2CO_3 and K_2CO_3 titrations at $16cm^3$-$17cm^3$ of titre solution reflecting the formation of $NaLn(CO_3)_2$ from the solution.

The $Ln_2(CO_3)_3$ phase precipitates almost immediately as in all previous carbonate titrations, which then alters to the sodium double carbonate by the end of the titration.

Figure 3.18 Typical titration curves for $NdCl_3$ with $4CO_3^{2-}$

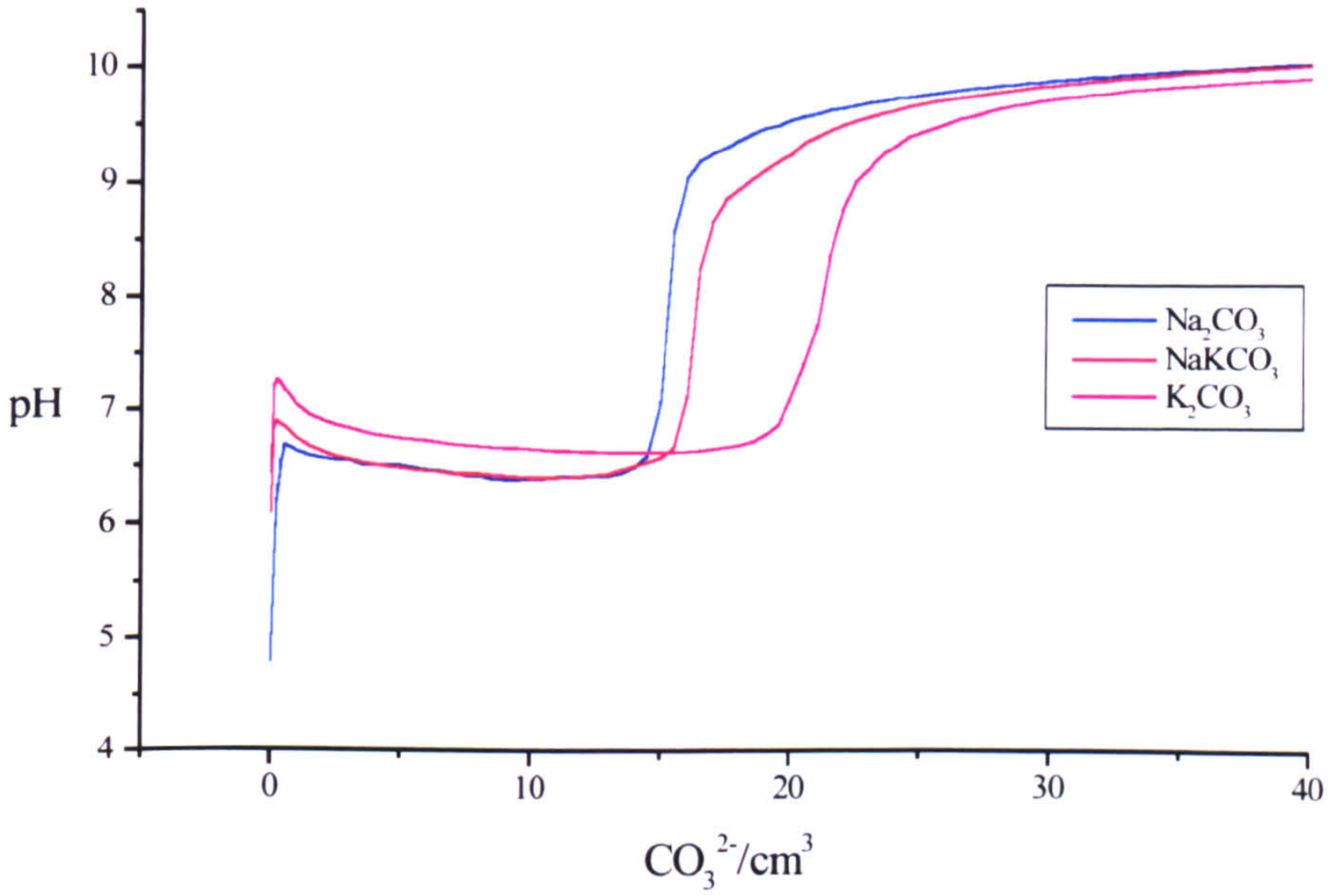

The precipitation of $Ln_2(CO_3)_3$ and alteration to $NaLn(CO_3)_2$ follows a two stage reaction. Initially there is the precipitation of $Ln_2(CO_3)_3$ (equation 3.15) at a 3:2 CO_3^{2-} to Ln^{3+} ratio

$$LnCl_3 + {}^3/_2NaKCO_3 \longrightarrow \tfrac{1}{2}Ln_2(CO_3)_3 + {}^3/_2Na^+ + {}^3/_2K^+ + 3Cl^- \qquad (3.15)$$

$5cm^3(0.2M)$ $15cm^3(0.1M)$

The second stage reaction requires more titre solution than the Na_2CO_3 titrations to inhibit the hydrolysis reaction that forms the hydroxy carbonate due to the lower Na^+ activity of the $NaKCO_3$ solution.

$$\tfrac{1}{2}Ln_2(CO_3)_3 + NaKCO_3 \longrightarrow NaLn(CO_3)_2 + K^+ + \tfrac{1}{2}CO_3^{2-} \qquad (3.16)$$

There may be some formation of a hydroxy phase as in the K_2CO_3 titrations (equations3.12 and 3.13) before the Na^+ and CO_3^{2-} activities increase enough to form the $NaLn(CO_3)_2$ double carbonate.

3.8 Titration Discussion

The titration of a lanthanide element with various titre solutions (Figure 3.19) have shown that there are four separate titration curves resulting in four equilibrium phases which form in the Ln^{3+}-CO_3^{2-}-OH^--Na^+-K^+ system (Table 3.13) for the lanthanides Nd, Sm and Eu. The phases formed are dependant on pH, carbonate and sodium activities up to 40mM and 80mM respectively.

Figure 3.19 Comparison of typical titration curves for 1mmol Ln^{3+} with 4mmols of titre solution

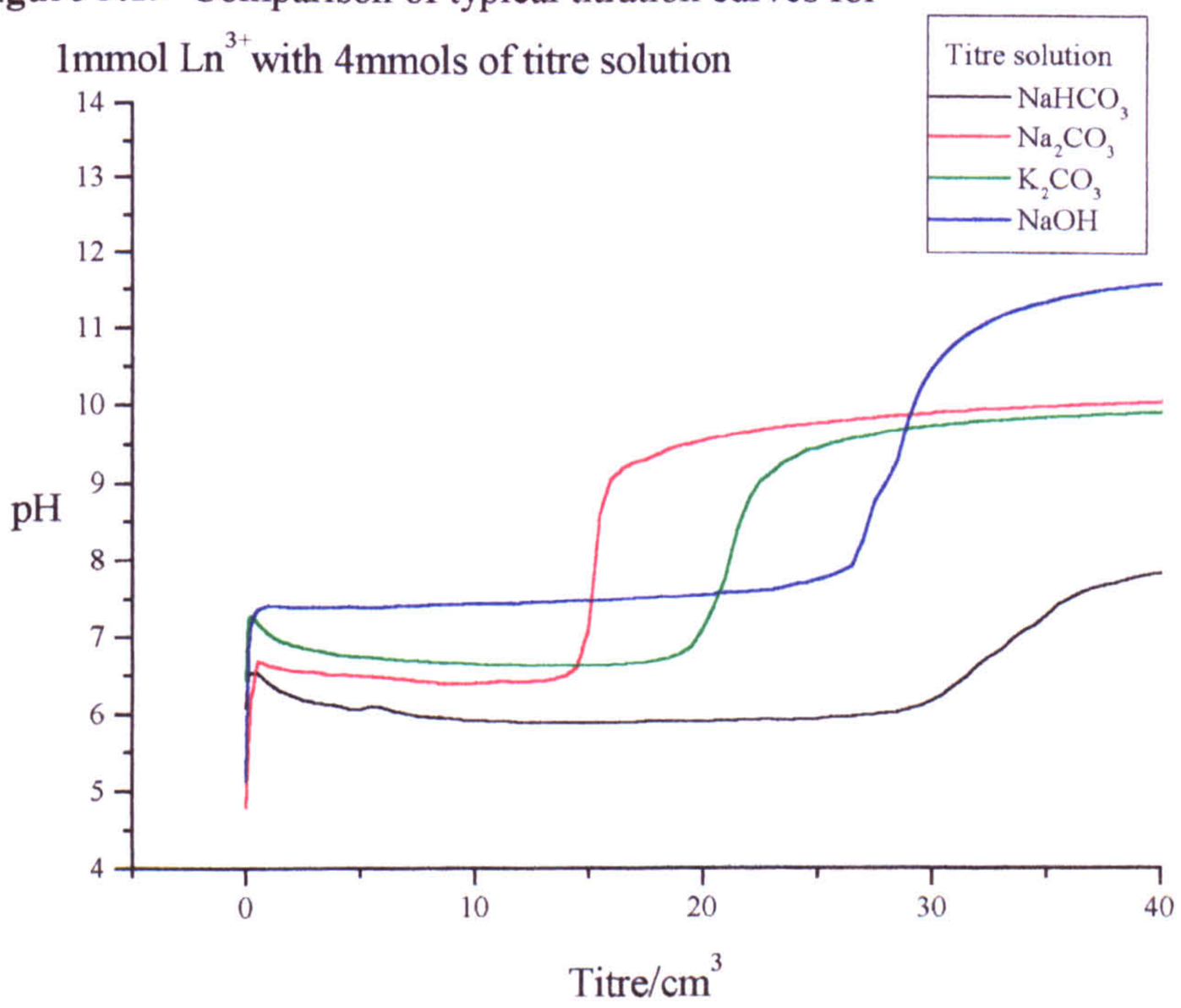

Table 3.13 Titration Summary

Titre solution	End point (TIC or OH^-) /Ln	First ppt pH5-7.5	Final ppt Ln = Nd/Sm/Eu		Final pH
Na_2CO_3	1.5	$Ln_2(CO_3)_3$	$NaLn(CO_3)_2$	CeO_2	10
K_2CO_3	2	$Ln_2(CO_3)_3$	$LnCO_3OH$	CeO_2	10
$NaHCO_3$	3	$Ln_2(CO_3)_3$	$Ln_2(CO_3)_3$	$Ce_2(CO_3)_3$	8.5
NaOH	2.7	None	$Ln(OH)_3$	CeO_2	12

The lanthanide carbonate, $Nd_2(CO_3)_3$, forms at low pH (below pH6.5), which then alters to the hydroxycarbonate at higher pH or a sodium double carbonate if

there is sufficient Na^+ in solution. The hydroxide forms at high pH (above pH 8.5) solutions with a low carbonate activity.

There are only two phases in the redox sensitive Ce-CO_3^{2-}-OH^--Na^+ system. Above pH 9 Ce^{3+} oxidises to $Ce^{4+}$with the formation of CeO_2 instead of any Ce^{3+} hydroxy phases. Cerium follows the group trends found from the other lanthanides examined with the initial precipitation of a $Ce_2(CO_3)_3$ phase in carbonate solutions or an aqueous buffering reaction during the Ce-NaOH titrations. Intermediate hydroxy phases may form before the redox reaction but these could not be identified. The end point of the Ce titration curves match those found from the other lanthanides examined.

Precipitation in the carbonate free system occurs at the end of the buffer zone when an excess of hydroxide ions have been added to the lanthanide solution. pH buffering therefore must occur by the formation of aqueous complexes and the end of the buffer zone is marked by all the Ln^{3+} forming $Ln(OH)_3^0{}_{(aq)}$. The addition of more OH^- will therefore increase the pH after all the Ln^{3+} has reacted, above pH 8.

The initial carbonate precipitate in all titrations, is $Ln_2(CO_3)_3$ and not the expected $LnCO_3OH$ phase, which would require a lower CO_3^{2-} activity to form. However, the first precipitate forms below pH 7 where the OH^- activity is too low to form a hydroxy carbonate precipitate at these carbonate activities. The initial rise in pH from the first titre additions increase the aqueous CO_3^{2-} activity to that required for $Ln_2(CO_3)_3$ precipitation. The hydroxy carbonate then forms after the increase in hydroxide activity by the end of the titration.

Ciavetta *et al.*, (1981) suggested that less than 1% of the Ln^{3+} ion can be transformed into aqueous carbonate complexes without the formation of solid carbonates, and confirmed by the almost immediate precipitation of an initially amorphous $Ln_2(CO_3)_3.xH_2O$ when only trace amounts of CO_3^{2-} have been added to a lanthanide solution, reflecting a lower carbonate solubility at intermediate pH of pH 5.5-8 solutions than the hydroxide which forms as stable relatively soluble aqueous complexes below pH 8.

$LnCO_3OH$ is the expected equilibrium phase at high pH in carbonate containing solutions from the alteration of $Ln_2(CO_3)_3$ (equation 3.17) due to the increase in OH^- activity with pH. If CO_3^{2-} is in excess of OH^- in solution, $LnCO_3OH$ would revert to $Ln_2(CO_3)_3$.

$$Ln_2(CO_3)_3 + 2OH^- \longrightarrow 2LnCO_3OH + CO_3^{2-} \qquad (3.17)$$

The presence of Na^+ in solution inhibits this reaction from the formation of $NaLn(CO_3)_2$ (equation 3.18)

$$Ln_2(CO_3)_3 + Na_2CO_3 \longrightarrow 2NaLn(CO_3)_2 \qquad (3.18)$$

Na^+ can be relativity easily incorporated to form the double carbonate as the Na^+ and Ln^{3+} ions are of a similar ionic radii (Table 3.14). K^+ ions do not inhibit the hydrolysis reaction (equation 3.17) as the K^+ ion is much larger and probably incompatible within the double carbonate structure at these relatively low potassium activities in the titrations.

Table 3.14 Ionic radii of selected ions

	Am^{3+}	Ce^{3+}	Nd^{3+}	Sm^{3+}	Eu^{3+}	Na^+	K^+	Ca^{2+}
pm	97.5	102	98.3	95.8	94.7	102	138	100

The $Ln_2(CO_3)_3$ phase requires a lower carbonate activity to form than the double carbonate, $NaLn(CO_3)_2$, (Table 3.15) and is consequently the first precipitate at low hydroxide activities. $NaLn(CO_3)_2$ only forms when there is an excess of carbonate ions in a Na^+ solution.

Table 3.15 Comparison of component ion ratios of the titration precipitates

	CO_3^{2-}/Ln^{3+}	Na^+/Ln^{3+}	OH^-/Ln^{3+}
$LnCO_3OH$	1	0	1
$Ln_2(CO_3)_3$	1.5	0	0
$NaLn(CO_3)_2$	2	1	0

Acid spiked titrations can be superimposed on the acid-free $NaHCO_3$ titrations from the initial precipitation along the buffer zone and the pH rise at the end of the titration. They indicate that any carbonate addition from pH 2-5 neutralises the acid and increases the solution pH without reacting with the aqueous lanthanide ions. Ln^{3+}-CO_3^{2-} aqueous complexes will only form at an intermediate pH above pH 5 if sufficient carbonate is present.

There was no reaction with the chloride in solution and the chloro-carbonate phase did not form as the chloro analogue to the $LnCO_3F$ mineral, bastnaesite. $CaCO_3$ titrations were not performed as the 0.1M titre solutions were above the $CaCO_3$ solubility limit.

The colour change and a slight shift in the XRD pattern to a smaller d-spacing between crystal panes with a decrease in the size of the lanthanide ion (i.e. from Nd to Sm , Table 3.16) were the only difference between the properties of the Ln^{3+} elements examined. As the lanthanides Nd, Sm and Eu had identical chemical properties, Am^{3+} could reasonably be expected to behave in a similar manner and follow any lanthanide group trends. The lanthanides may then not only predict the solubility limiting phase under specific aqueous conditions but also infer the actual Am^{3+} solubility.

3.9 References

Carroll, S. A., (1993) Precipitation of Nd-Ca carbonate solid solution at 25°C. *Geochim. Cosmochim. Acta* **57** 3383-3393

CIAVATTA, L., FERRI, D., GRENTHE, I., SALVATORE, F., and SPAHIU, K., (1981) Studies on metal carbonate equilibria. 3. The Lanthanum(III) carbonate complexes in aqueous perchlorate media. *Acta Chem. Scand.* **A35** 403-413

MERLI, L., LAMBERT, B., and FUGER, J., (1997) Thermochemistry of lanthanum, neodymium, samarium and americium trihydroxides and their relation to the corresponding hydroxycarbonates. *J. Nucl. Mat.* **247** 172-176

MOCHIZUKI, A., NAGASHIMA, K., and WAIKITA, H., (1974) The synthesis of crystalline hydrated double carbonates of rare-earth elements and sodium. *Bull. Chem. Soc. Jpn* **47** 755-756RUNDE, W., MENRATH, G., and KIM, J. L., (1992) A study of solid-liquid phase-equilibria of trivalent lanthanide and actinide ions in carbonate systems. *Radiochim. Acta* **58/59** 93-100

VITORGE, P., (1992) $Am(OH)_3$, $AmOHCO_3$ and $Am_2(CO)_3$ stabilities in environmental conditions. *Radiochim. Acta* **58/59** 105-107

WILLIAM-JONES, A. E., and WOOD, S. A. (1992) A preliminary petrogenic grid for REE fluorocarbonates and associated minerals. *Geochim. Cosmochim. Acta* **56** 725-738

Chapter 4

The Solubility of REE in Carbonate Solutions

4.1 Introduction

The REE or lanthanides are being modelled to test the assumption that they can be used as experimental analogues for the dominant actinides (americium and curium) in the M^{3+} oxidation state. The lanthanides can also be fission products from the decay process and therefore there is a need to determine their solubility limits within nuclear waste repositories to predict the maximum possible dissolution and dispersion rates. Solubility data can also be used to determine the actual conditions required to immobilise each target element in the solid phase.

If the REE are mobilised, their transport rate will be determined from equilibrium conditions with secondary minerals (determined in Chapter 3) formed by precipitation in equilibrium with the relevant solution conditions. The solution composition will change dramatically from the near-field source region (the actual repository) where the composition will be determined by carbonate minerals at a high pH in a concrete matrix. Dilution and dispersion away from the near-field environment will limit the effects of this matrix to buffer the solution pH and control composition. The solution composition will therefore vary from high pH, and possible high carbonate activity to a lower pH with a limited carbonate activity; other ions such as Ca^{2+}, Na^{+} and K^{+} may also be present in significant quantities.

Determining the solubility products of the carbonate and hydroxy phases (formed in Chapter 3) can be compared directly with the equivalent actinide data to justify the analogue assumption. If Am does react in a similar manner to the lanthanides it's properties should be based on the way Nd reacts, and its thermodynamic data, any variation will be between the limits of the properties of model Nd and Eu, which are lanthanide elements with larger and smaller ionic radii to Am respectively. The solubility products can then be used to predict the solubility of each target element under precise conditions.

The Gibbs free energy of formation (ΔG_f°) for any phase can be calculated from the solubility product, which in turn can be used to calculate the exact

relationship between two phases and a precise phase boundary, dependant on the solution parameters, For example: from the reaction of $Nd_2(CO_3)_3$ and water, (equation 4.1)

$$Nd_2(CO_3)_3 + H_2O = 2NdCO_3OH + 2H^+ + CO_3^{2-} \qquad (4.1)$$

an increase in the solution pH will favour the formation of the hydroxycarbonate, whilst an increased carbonate activity will favour the carbonate phase, (Le Chatelier's principle).

The prediction of the phase relationships between each solid phase will also allow the solubility limit of each target element to be calculated for each solid phase under all relevant conditions.

4.2 Experimental

The preparation of each solid phase was based on the conditions determined from the titration experiments (Chapter 3). $NaClO_4$ buffers were not used to maintain a constant ionic strength as Na^+ ions are a phase controlling species A standard amount of each lanthanide chloride solution (10mmols) was used to prepare each solid phase to ensure a large enough precipitate for full analysis. Only solutions in equilibrium with pure solid phases were used in solubility calculations

4.2.1 Preparation of $Ln_2(CO_3)_3$

A solution of $LnCl_3$ (0.5M, $2cm^3$) where Ln = Ce, Nd or Eu was mixed with $NaHCO_3$ (0.1M, $40cm^3$) and then diluted to $100cm^3$ with degassed distilled water in a $125cm^3$ HDPE Nalgene bottle. The reaction mixture was kept under N_2 in a waterbath at 25°C for at least 2 months to ensure complete reaction and equilibration. The pH of the solution was measured immediately prior to being filtered and analysed by FTIR and XRD spectroscopy. The filtrate was analysed for total lanthanide content by FIA-UV with arsenazo(III) and Ce^{3+} by

spectrofluorimetry. All other components were calculated from a knowledge of the starting materials and the amount removed by precipitation of the pure phase.

4.2.2 Dissolution of $Ln_2(CO_3)_3$

A sample of crystalline $Ln_2(CO_3)_3$ (~0.3g), where Ln = Ce, Nd or Eu, was placed in a 125cm^3 HDPE Nalgene bottle which was then filled with $HClO_4$ (0.1M), to exclude all atmospheric CO_2(g) from the bottle. The solution and solid phase were allowed to equilibrate for at least 2 months in a thermostated waterbath at 25°C. The pH of the solution was measured and then filtered through a Whatman N°4 sintered glass crucible.

The precipitate was analysed by FTIR and XRD spectroscopy to determine any changes in the solid phase from the start of the dissolution. The filtrate was analysed for total lanthanide content by FIA-UV. All other components were calculated from a knowledge of the starting materials and the amount removed by precipitation of the pure phase.

4.2.3 Preparation of $LnCO_3OH$

Two methods were used to prepare $LnCO_3OH$: The first followed the components in the K_2CO_3 titrations (Chapter 3) and the second method contained Na^+ as NaOH and Na_2CO_3 but restricted CO_3^{2-} to determine if a hydroxy-carbonate phase could form from a low carbonate high pH solution.
A solution of $LnCl_3$ (0.5M, 2cm^3) where Ln = Ce, Nd or Eu was mixed with K_2CO_3 (0.1M, 40cm^3) then diluted to 100cm^3 with degassed distilled water in a 125cm^3 HDPE Nalgene bottle. A second set of solutions were prepared by mixing $LnCl_3$ (0.5M, 2cm^3) where Ln = Ce, Nd or Eu, with Na_2CO_3 (0.1M, 10cm^3) and NaOH (0.1M, 10cm^3). The mixed solution was diluted to 100cm^3 in 125cm^3 Nalgene bottles .

The reaction mixtures were kept under N_2 in a waterbath at 25°C for at least 2 months to ensure complete reaction and equilibration. The pH of the solution was measured immediately prior to filtering and the precipitate analysed by FTIR and XRD spectroscopy. The filtrate was analysed for total lanthanide content by FIA-UV with arsenazo(III) and Ce^{3+} by spectrofluorimetry. All other components were calculated from a knowledge of the starting materials and the amount removed by precipitation of the pure phase.

4.2.4 Preparation of $Ln(OH)_3$ and CeO_2

A solution of $LnCl_3$ (0.5M, $2cm^3$) where Ln = Ce, Nd or Eu was mixed with NaOH (0.1M, $40cm^3$) then diluted to $100cm^3$ with degassed distilled water in individual $125cm^3$ HDPE Nalgene bottles. The reaction mixture was kept under N_2 in a waterbath at 25°C for at least 2 months to ensure complete reaction and equilibration. The pH of the solution was measured immediately prior to filtering and the precipitate analysed by FTIR and XRD spectroscopy. The filtrate was analysed for total aqueous lanthanide content by FIA-UV with arsenazo(III) and Ce^{3+} by spectrofluorimetry. All other components were calculated from a knowledge of the starting materials and the amount removed by precipitation of the pure phase.

4.2.5 Precipitation of $NaLn(CO_3)_2.6H_2O$

A solution of $LnCl_3$ (0.5M, $2cm^3$) where Ln = Nd or Eu was mixed with Na_2CO_3 (0.1M, $40cm^3$) then diluted to $100cm^3$ with degassed distilled water in a $125cm^3$ HDPE Nalgene bottles. The reaction mixture was kept under N_2 in a waterbath at 25°C for at least 2 months to ensure complete reaction and equilibration. The pH of the solution was measured immediately prior to being filtered and the precipitate analysed by FTIR and XRD spectroscopy. FTIR and XRD analysis was performed on a partially dry sample, as complete drying causes the phase to decompose (described fully in Chapter 5). The filtrate was analysed for the total lanthanide content by FIA-UV with arsenazo(III). All other components were

calculated from a knowledge of the starting materials and the amount removed by precipitation of the pure phase. The solid phase (~0.02g) was dissolved in HNO_3 (0.4M, 100ml) then analysed for Na^+ and K^+ by flame photometry and FIA-UV for Ln^{3+}.

4.2.6 Preparation of $NaCe(CO_3)_2.6H_2O$

A solution of $CeCl_3$ (0.5M, $2cm^3$) was mixed with either $NaHCO_3$ (1M, $98cm^3$) solution or a mixed $NaHCO_3$/NaCl (1M HCO_3^-,1M Cl^-, $98cm^3$), in $125cm^3$ HDPE Nalgene bottles. The reaction mixture was kept under N_2 in a waterbath at 25°C for at least 2 months to ensure complete reaction and equilibration. The pH of the solution was measured immediately prior to being filtered and then the precipitate analysed by FTIR and XRD spectroscopy. The filtrate was analysed for total lanthanide content by FIA-UV with arsenazo(III) and Ce^{3+} by spectrofluorimetry. All other components were calculated from a knowledge of the starting materials and the amount removed by precipitation of the pure phase.

4.2.7 Preparation of $KNd(CO_3)_2$

A solution of $NdCl_3$ (0.2M, $5cm^3$) was mixed with K_2CO_3 (0.1M, $195cm^3$) in $250cm^3$ HDPE Nalgene bottles. The reaction mixture was kept under N_2 in a waterbath at 25°C for at least 2 months to ensure complete reaction and equilibration. The pH of the solution was measured immediately prior to being filtered then analysed by FTIR and XRD spectroscopy. The filtrate was analysed for total Nd content by FIA-UV with arsenazo(III). All other components were calculated from a knowledge of the starting materials and the amount removed by precipitation of the pure phase. The solid phase (~0.02g) was dissolved in HNO_3 (0.4M, 100ml) then analysed for Na^+ and K^+ by flame photometry and FIA-UV for Ln^{3+}.

A pure phase of $KLn(CO_3)_2$ was only isolated for Nd, a mixed phase of $KEu(CO_3)_2$ and $EuCO_3OH$ could only be made under all the conditions studied.

$KNd(CO_3)_2$ was characterised from an XRD pattern almost identical to $NaNd(CO_3)_2$ (Section 3.5.3, Fig 3.12) with only a slight shift in the diffraction peaks and a 1:1 K^+/Nd^{3+} ratio from elemental analysis.

Figure 4.1 XRD pattern of hydrated $KNd(CO_3)_2$

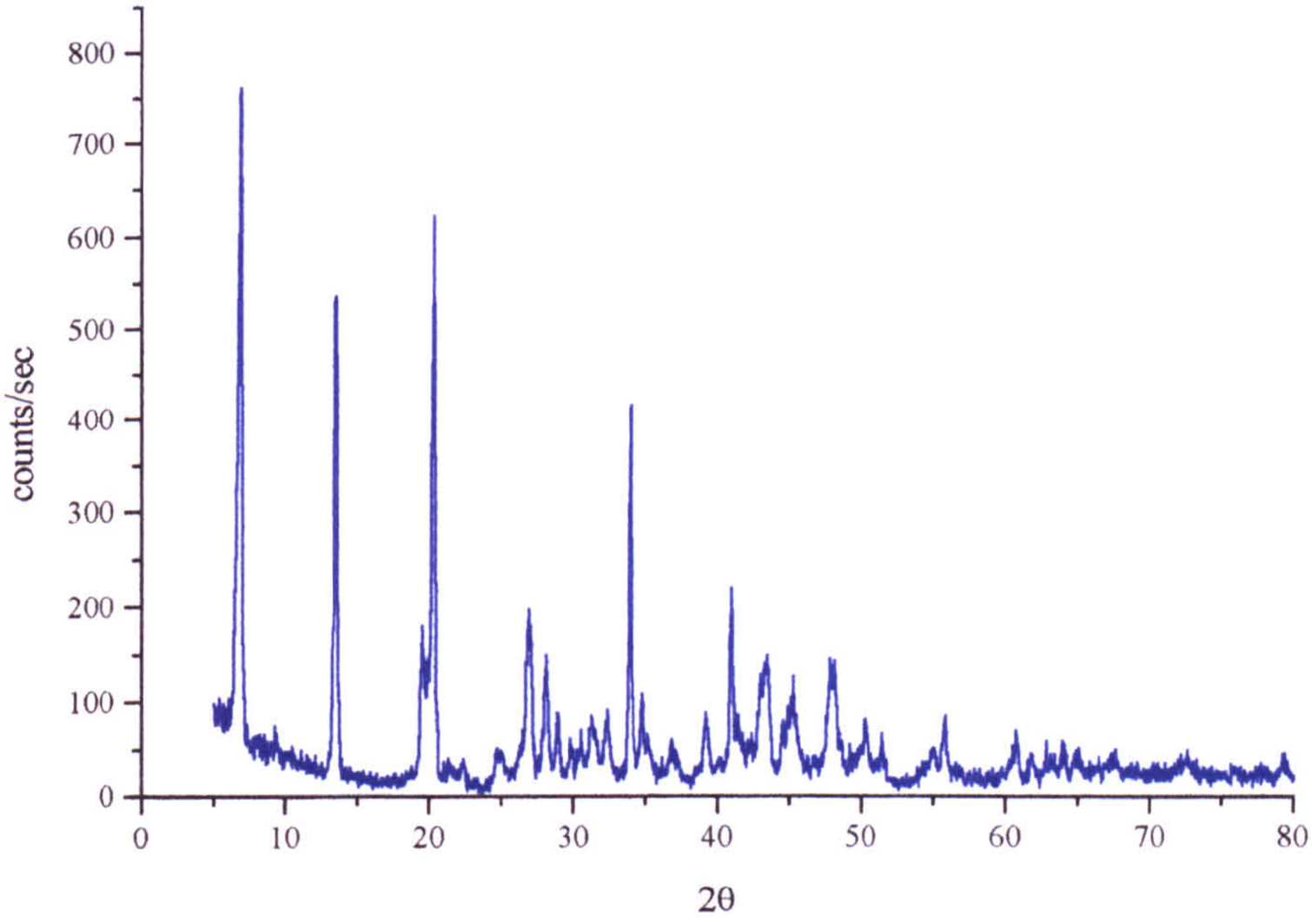

4.3 Determination of solubility products

4.3.1 Calculation of aqueous composition

The solubility product of the various lanthanide carbonate compounds synthesised are determined from the solution composition of the solution in contact with the solid phases at equilibrium. The ion concentrations were determined by analysis of the total lanthanide concentration by FIA-UV analysis and the other solution components were calculated from a knowledge of their concentrations in the starting solution and the composition the solid phase.

i.e. for $NaNd(CO_3)_2$, which forms from the reaction (equation 4.2)

$$NdCl_3(aq) + Na_2CO_3(aq) \longrightarrow NaNd(CO_3)_2(s) + 3Na^+(aq) + Cl^-(aq) \quad (4.2)$$

Cl^- remains in solution and not directly involved in the reaction (equation 4.2) and is therefore assumed unchanged from the starting solution.

The total inorganic carbonate (TIC) is removed in a ratio of 2TIC:Nd, and Na^+ removed in equal amounts to the Nd. The amount of Nd removed from solution was calculated from the difference between the initial concentration and the final concentration determined from FIA-UV analysis after the solid phase was filtered off. The aqueous equilibrium (eqm) concentrations of TIC and Na^+ can therefore be calculated from equations 4.3 and 4.4 respectively

$$[TIC]_{eqm} = [TIC]_{start} - 2([Nd]_{start} - [Nd]_{eqm}) \quad (4.3)$$
$$[Na^+]_{eqm} = [Na^+]_{start} - ([Nd]_{start} - [Nd]_{eqm}) \quad (4.4)$$

4.3.2 Solubility products (Ksp)

The solubility product (Ksp) is the reaction constant for the dissociation reaction of a solid phase into its component ions in aqueous solution. The solubility product is the sum of the stoichiometric activities of the component ions in the solution that is in equilibrium with a solid phase. i.e. when $Nd_2(CO_3)_3$ dissolves into an aqueous solution the reaction can be written as equation 4.5.

$$Nd_2(CO_3)_3(s) \longrightarrow 2Nd^{3+}(aq) + 3CO_3^{2-}(aq) \quad (4.5)$$

The reaction constant (Ksp) for the above reaction can be expressed as equation 4.6, if the solution is in equilibrium with the solid phase

$$Ksp = \frac{a^2_{Nd^{3+}} . a^3_{CO_3^{2-}}}{a_{Nd_2(CO_3)_3}} \quad (4.6)$$

where a is the activity in solution
and a = 1 for a pure solid and H_2O

When hydroxide species are involved in solubility reactions i.e. the dissolution of $Nd(OH)_3$ can be expressed in two ways, the dissociation into the component ions (equation 4.7) and the solubility product (equation 4.8),

$$Nd(OH)_3 \longrightarrow Nd^{3+} + 3OH^- \quad (4.7)$$

$$Ksp = \frac{a_{Nd^{3+}} . a^3_{OH^-}}{a_{Nd(OH)_3}} = a_{Nd^{3+}} . a^3_{OH^-} \qquad (4.8)$$

or as the hydrolysis reaction with H^+ and H_2O (equation 4.9), and the reaction constant, K, (equation 4.10)

$$Nd(OH)_3 + 3H^+ \longrightarrow Nd^{3+} + 3H_2O \qquad (4.9)$$

$$K = \frac{a_{Nd^{3+}} . a^3_{H_2O}}{a_{Nd(OH)_3} . a^3_{H^+}} = \frac{a_{Nd^{3+}}}{a^3_{H^+}} = a_{Nd^{3+}} . a^{-3}_{H^+} \qquad (4.10)$$

When the reaction constant (equation 4.10) is expressed as a log function (equation 4.11) the reaction is described in terms of pH

$$\log K = \log(a_{Nd^{3+}}) - 3\log(a_{H^+}) = \log(a_{Nd^{3+}}) + 3pH \qquad (4.11)$$

A complete set of dissociation reactions for all the solid phases investigated is given in Table 4.1. (equations 4.12 to 4.32)

The precipitation of CeO_2 is a redox sensitive reaction (equation 4.30) with the transfer of an electron in the solution reaction, the pe ($-\log a[e^-]$) of the solution can be calculated from the Eh of the solution from the equation (4.33) to allow the reaction constant of CeO_2 solubility to be expressed without the inclusion of other reduced species.

$$Eh = \frac{2.303RT}{F} . pe \qquad \therefore pe = 16.9Eh \qquad (4.33)$$

Where R = gas constant ($8.314 JK^{-1}mol^{-1}$), T = thermodynamic temperature(K) and F = Faraday constant (96.48KJ/V), Eh = redox potential (Volts) (Parkhurst, 1995)

Table 4.1 Dissociation reactions for solubility determinations

$NaLn(CO_3)_2 \longrightarrow Ln^{3+} + Na^{+} + 2CO_3^{2-}$	(4.12)
$Ksp = a_{Na^+}.a_{Ln^{3+}}.a^2_{CO_3^{2-}}$	(4.13)
$\log Ksp = \log(a_{Na^+}) + \log(a_{Ln^{3+}}) + 2\log(a_{CO_3^{2-}})$	(4.14)
$Ln_2(CO_3)_3 \longrightarrow 2Ln^{3+} + 3CO_3^{2-}$	(4.15)
$Ksp = a^2_{Ln^{3+}}.a^3_{CO_3^{2-}}$	(4.16)
$\log Ksp = 2\log(a_{Ln^{3+}}) + 3\log(a_{CO_3^{2-}})$	(4.17)
$LnCO_3OH \longrightarrow Ln^{3+} + CO_3^{2-} + OH^-$	(4.18)
$Ksp = a_{Ln^{3+}}.a_{CO_3^{2-}}a_{OH^-}$	(4.19)
$\log Ksp = \log(a_{Ln^{3+}}) + \log(a_{CO_3^{2-}}) + \log(a_{OH^-})$	(4.20)
$LnCO_3OH + H^+ \longrightarrow Ln^{3+} + CO_3^{2-} + H_2O$	(4.21)
$K = \frac{a_{Ln^{3+}}.a_{H_2O}.a_{CO_3^{2-}}}{a_{H^+}} = a_{Ln^{3+}}.a_{CO_3^{2-}}.a^{-1}_{H^+}$	(4.22)
$\log K = \log(a_{Ln^{3+}}) + \log(a_{CO_3^{2-}}) + pH$	(4.23)
$Ln(OH)_3 \longrightarrow Ln^{3+} + 3OH^-$	(4.24)
$Ksp = a_{Ln^{3+}}a^3_{OH^-}$	(4.25)
$\log Ksp = \log(a_{Ln^{3+}}) + 3\log(a_{OH^-})$	(4.26)
$Ln(OH)_3 + 3H^+ \longrightarrow Ln^{3+} + 3H_2O$	(4.27)
$K = \frac{a_{Ln^{3+}}}{a^3_{H^+}} = a_{Ln^{3+}}.a^{-3}_{H^+}$	(4.28)
$\log K = \log(a_{Ln^{3+}}) + 3pH$	(4.29)
$CeO_2 + e^- + 4H^+ \longrightarrow Ce^{3+} + 2H_2O$	(4.30)
$K = \frac{a_{Ce^{3+}}.a^2_{H_2O}}{a_{CeO_2}.a_{e^-}.a^4_{H^+}} = a_{Ce^{3+}}.a^{-1}_{e^-}.a^{-4}_{H^+}$	(4.31)
$\log K = \log(a_{Ce^{3+}}) + pe + 4pH$	(4.32)

4.3.3 Calculating solubility products

The solubility relations depend on the actual activity of each of the free ion Ln^{3+}, CO_3^{2-}, OH^-, Na^+ ions and the pH of the solutions and not the total concentrations of each element . The actual proportion of these ions compared with the total concentration does vary significantly with the composition of the solution. The

Nd^{3+} ion only exists as the free *aquo* ion at low pH and carbonate activities. Lee & Byrne (1992, 1993) have calculated a consistent set of association constants for REE hydroxy and carbonate species in seawater by linear free energy calculations (Table 4.2 and 4.3).

Table 4.2 Association aqueous reactions for the constants given in Table 4.3 after Lee & Byrne (1992, 1993)

$Ln^{3+} + H_2O \longrightarrow LnOH^{2+}$	(4.34)
$Ln^{3+} + 2H_2O \longrightarrow Ln(OH)_2^{+} + 2H^{+}$	(4.35)
$Ln^{3+} + 3H_2O \longrightarrow Ln(OH)_3^{0} + 3H^{-}$	(4.36)
$Ln^{3+} + CO_3^{2-} \longrightarrow LnCO_3^{+}$	(4.37)
$Ln^{3+} + 2CO_3^{2-} \longrightarrow Ln(CO_3)_2^{-}$	(4.38)

Table 4.3 Aqueous Species association constants after Lee & Byrne (1992, 1993)

Ln	$LnOH^{2+}$	$Ln(OH)_2^{+}$	$Ln(OH)_3^{0}$	$LnCO_3^{+}$	$Ln(CO_3)_2^{-}$
Ce	-8.41	-17.60	-27.23	7.40	12.63
Nd	-8.16	-17.04	-26.40	7.67	13.09
Eu	-7.90	-16.37	-25.41	7.95	13.40

In very dilute or ideal solutions, the charged ions in solution are assumed to be too dilute to interact with each other and therefore have a uniform distribution throughout the solution. The activity of a species is equal to the aqueous concentration of that species as the aqueous ions are assumed not to interact. In non-ideal solutions the aqueous species are charged, and therefore they can significantly interact with each other, the extent of the interactions will increase with the ionic strength of the solution. The activity coefficient (γ) is used to calculate the actual activity of a component from the expression

$$a_M = \gamma[M] \qquad (4.34)$$

where a = the activity of species M, γ = the activity coefficient and [M] is the concentration of component M.

The activity coefficient can be calculated from the Debye-Hückel expression and will be described further in Chapter 7.

A number of geochemical models (e.g. PHREEQC, Parkhurst, 1995) have been developed to calculate the speciation and activities of ions in complex solutions from a series of association constants (Table 4.3) and the Debye-Hückel expression. PHREEQC calculates the speciation in solution as the molality of each ion, from a series of association reaction constants (i.e. for lanthanides from Table 4.3) presented in a database containing all possible aqueous reactions for each element involved (Appendix 7.1, PHREEQC Database). The activity coefficient of each species is then calculated from the Debye-Hückel expression and hence the activity of each species can be derived and used to calculate the actual solubility product of a phase in equilibrium with the `solved ` solution. The model then calculates an ion activity product (IAP), as the sum of the component ions for the dissociation reaction of each solid phase that is included in the database with aqueous reactions, i.e. for the lanthanides the reactions shown in Table 4.1. The IAP is calculated for the same reaction equation as the solubility product and used to predict the saturation of a solution with any possible solid phases. The IAP is therefore equal to the solubility product when the solution is in equilibrium with a solid phase.

The solubility product for the solid phases formed from Section 4.2 were calculated for each individual solution analysis (Appendix 4.1 to 4.12), from the species activities calculated by PHREEQC using the Lee & Byrne (1992 & 1993) aqueous reaction constants.

An average composition for each solid phase could not be used in the PHREEQC model as some phases were determined from more than one set of conditions (precipitation and dissolution) that varied in ionic strength and element composition. The free ion activity of each component is also pH dependent. Each solution was therefore solved individually and an average value taken for each solubility product from all the relevant experimental data

4.3.4 Calculation of a typical solubility product (e.g. $NaNd(CO_3)_2$)

A typical example of a solubility product calculation is shown in full below, for the dissociation of $NaNd(CO_3)_2$ (equation 4.12), using the solution activities (Table 4.4) calculated by PHREEQC from the whole solution composition (Table 4.5) for an equilibrium solution.

$$NaLn(CO_3)_2 \longrightarrow Ln^{3+} + Na^{+} + 2CO_3^{2-} \qquad (4.12)$$

Table 4.4 Calculation of $NaNd(CO_3)_2$ solubility product from PHREEQC calculations (Table 4.9) from solution data (Appendix 4.2)

Element	Nd	Na	TIC
total conc^n/M	3.1×10^{-7}	0.0325	0.015
Species	Nd^{3+}	Na^{+}	CO_3^{2-}
log molality	-11.579	-1.491	-3.284
log γ	-0.820	-0.091	-0.365
log activity	-12.399	-1.582	-3.649

The solubility product is calculated from the solution activities shown above (Table 4.4) by equation 4.14 as:

$$\log Ksp = \log(a_{Na^+}) + \log(a_{Ln^{3+}}) + 2\log(a_{CO_3^{2-}}) \qquad (4.14)$$

$$= (-12.399) + (-1.582) + 2(-3.649)$$

log Ksp = -21.28, average log Ksp = -21.25±0.95 (all data, Appendix 4.2)

Similar calculations can be performed for all other solid phases prepared in Chapter 4 from the relevant equations in Table 4.1 and the solution data with activities in Appendix 4.1 to 4.12. The solubility products are summarised in Table 4.6

Table 4.5 PHREEQC output for a typical solution in equilibrium with $NaNd(CO_3)_2$

```
TITLE KSp Calc   Nd82 B1    NaNd(CO3)2
        pH  8.62
        pe  0.00
      units mol/l
        Nd  3.1E-7
        Na  0.0325
        C   0.015
        Cl  0.015
----------------------------Solution composition----------------------------
      Elements            Molality        Moles
      C                1.503e-02    1.503e-02
      Cl               1.503e-02    1.503e-02
      Na               3.256e-02    3.256e-02
      Nd               3.106e-07    3.106e-07
----------------------------Description of solution----------------------------
                                pH  =   8.622
                                pe  =   0.000
                  Activity of water  =   0.999
                     Ionic strength  =   3.183e-02
                    Mass of water (kg)  =   1.000e+00
                   Temperature (deg C)  =  25.000
                Electrical balance (eq)  =   1.906e-03
----------------------------Distribution of species----------------------------
                                                  Log          Log          Log
      Species            Molality    Activity  Molality    Activity        Gamma
      OH-              5.160e-06    4.183e-06    -5.287      -5.378       -0.091
      H+               2.739e-09    2.388e-09    -8.562      -8.622       -0.060
      H2O              5.551e+01    9.989e-01     0.000       0.000        0.000
C(-4)                  0.000e+00
      CH4              0.000e+00    0.000e+00   -51.667     -51.667        0.000
C(4)                   1.503e-02
      HCO3-            1.414e-02    1.147e-02    -1.849      -1.941       -0.091
      CO3-2            5.200e-04    2.246e-04    -3.284      -3.649       -0.365
      NaHCO3           1.686e-04    1.686e-04    -3.773      -3.773        0.000
      NaCO3-           1.349e-04    1.094e-04    -3.870      -3.961       -0.091
      H2CO3            6.129e-05    6.129e-05    -4.213      -4.213        0.000
      Nd(CO3)2-        3.054e-07    2.476e-07    -6.515      -6.606       -0.091
      NdCO3+           5.170e-09    4.191e-09    -8.287      -8.378       -0.091
Cl                     1.503e-02
      Cl-              1.503e-02    1.218e-02    -1.823      -1.914       -0.091
H(0)                   8.073e-21
      H2               4.036e-21    4.036e-21   -20.394     -20.394        0.000
Na                     3.256e-02
      Na+              3.226e-02    2.615e-02    -1.491      -1.582       -0.091
      NaHCO3           1.686e-04    1.686e-04    -3.773      -3.773        0.000
      NaCO3-           1.349e-04    1.094e-04    -3.870      -3.961       -0.091
Nd                     3.106e-07
      Nd(CO3)2-        3.054e-07    2.476e-07    -6.515      -6.606       -0.091
      NdCO3+           5.170e-09    4.191e-09    -8.287      -8.378       -0.091
      NdOH+2           2.673e-12    1.155e-12   -11.573     -11.938       -0.365
      Nd+3             2.637e-12    3.989e-13   -11.579     -12.399       -0.820
      Nd(OH)2+         7.855e-13    6.368e-13   -12.105     -12.196       -0.091
      Nd(OH)3          1.163e-13    1.163e-13   -12.934     -12.934        0.000
```

Table 4.6 Summary of the calculated solubility products (Ksp) and hydrolysis reaction constants (K) for the reactions in Table 4.1 (This work)

Phase	log Ksp	log K	Solution data and activities
$NaCe(CO_3)_2$	-22.62±2.2		Appendix 4.1
$NaNd(CO_3)_2$	-21.25±0.95		Appendix 4.2
$NaEu(CO_3)_2$	-20.48±0.69		Appendix 4.3
$Ce_2(CO)_3$	-36.04±0.75		Appendix 4.4
$Nd(CO_3)_3$	-34.43±0.35		Appendix 4.5
$Eu_2(CO_3)_3$	-32.99±1.09		Appendix 4.6
$NdCO_3OH$	-19.87±1.75	-5.87±1.75	Appendix 4.7
$EuCO_3OH$	-18.62±0.15	-4.62±0.15	Appendix 4.8
$Nd(OH)_3$	-21.41±0.67	20.59±0.67	Appendix 4.9
$Eu(OH)_3$	-22.79±0.23	19.21±0.23	Appendix 4.10
CeO_2		30.66±0.60	Appendix 4.11
$KNd(CO_3)_2$	-19.17±0.01		Appendix 4.12

The $NaCe(CO_3)_2$ equilibrium solutions have a very high ionic strength and therefore the activity coefficient has a significant impact on the solubility product, compared with the more dilute Nd and Eu double carbonates. The Debye-Hückel expression used to calculate the activity coefficients can only be used for dilute solutions, therefore any calculations involving the $NaCe(CO_3)_2$ solubility product must be considered as unreliable due to the high Na and TIC concentrations used.

4.4 Comparison of calculated solubility products with Literature Data

A summary of the lanthanide carbonate and hydroxide solubility data derived is presented in Table 4.7. The data obtained is also compared to those obtained in the literature.

Table 4.7 Comparison of the solubility products calculated in this work with this work with literature values

Phase	log K_{sp}	log K	Ref.
$NaCe(CO_3)_2.xH_2O$	-22.62±2.2		This work
	-17.5±0.1		Ferri *et al.*, (1983)
$NaNd(CO_2)_2.xH_2O$	-21.25±0.95		This work
	-21.39		Rao *et al.*, (1996a)
$NaEu(CO_3)_2.xH_2O$	-20.48±0.69		This work
$Ce_2(CO_3)_3.xH_2O$	-36.04±0.75		This work
	-37.65		Meinrath and Kim (1991a)
$Nd_2(CO_3)_3.xH_2O$	-34.43±0.35		This work
	-34.10±0.48		Firsching & Mohammadzadel (1986)
	-31.35±0.12		Runde *et al.*, (1992)
	-31.35±0.13		Meinrath and Kim (1991a)
$Eu_2(CO_3)_3.xH_2O$	-32.99±1.09		This work
	-35.03±0.25		Firsching & Mohammadzadel (1986)
	-31.78±0.22		Runde *et al.*, (1992)
$NdCO_3OH$	-19.87±1.75	-5.87±1.75	This work
	-19.94±0.16	-5.54±0.16	Runde *et al.*, (1992)
	-19.19±0.08	-5.19±0.08	Meinrath and Kim (1991a)
$EuCO_3OH$	-18.62±0.15	-4.62±0.15	This work
	-20.18±0.09	-6.18±0.09	Runde *et al.*, (1992)
$Nd(OH)_3$	-21.41±0.67	20.59±0.67	This work
	-22.3±0.7	19.7±0.7	Morss *et al.*, (1989)
	-27.04	14.96	Rao *et al.*, (1996b)
	-25.98±0.37	16.02±0.37	Diakonov *et al.*, (1998a) aged & fresh crystals
	-23.32	18.68	
$Eu(OH)_3$	-22.79±0.23	19.21±0.23	This work
	-26.5	15.5	Morss *et al.*, (1994)
	-26.54	15.46	Diakonov *et al.*, (1998b) aged & fresh crystals
	-24.40	17.6	
CeO_2		30.66±0.60	This work
$KNd(CO_3)_2$	-19.17±0.01		This work

The solubility products from this study indicate an increase in solubility of the carbonate phases with a decrease in ionic radii (Table 4.8), i.e. a relative increase in the solubility of the HREE compared with the LREE. This trend is often seen in geochemical systems and found in carbonate bearing lakes (Johannesson *et al.*,, 1994) and seawater (Elderfield & Greaves, 1982).

Table 4.8 The variation in the solubility product of lanthanide carbonate phases

Ln^{3+}	ionic radii	log Ksp $NaLn(CO_3)_2$	log Ksp $Ln_2(CO_3)_3$	log Ksp $LnCO_3OH$
Ce^{3+}	103.2pm	-22.62	-36.04	
Nd^{3+}	98.3pm	-21.25	-34.43	-19.87
Eu^{3+}	94.7pm	-20.48	-32.99	-18.62

There has not been a previous comprehensive study on a series of lanthanides, which includes all the solid phases identified in the Na^{+}-Ln^{3+}-CO_3^{2-}-OH^{-} system from this study. Previous studies have focused on direct comparisons of an Am solid phase with Nd and or Eu. Alternatively the solubility of all the lanthanides has been considered for a single solid phase, either $Ln_2(CO_3)_3$ (Firsching & Mohammadzadel, 1986) or the $Ln(OH)_3$ phase (Diakonov, 1998b). When a single solid phase has been considered for a pair of lanthanides , e.g. Nd and Eu, then the difference between the solubility products of each type of phase, for the pair of lanthanides is usually less than the difference between the solubility product of that phase for a single lanthanide in separate studies (Table 4.7).

There are no literature values for the solubility of $NaEu(CO_3)_2$ and only a single value for $NaNd(CO_3)_2$ which agrees with this study (Table 4.7). The solubility products for $NaCe(CO_3)_2$ are probably unreliable due to the high ionic strength's of the equilibrium solutions (above 2M total dissolved salts) and the Debye-Hückel equation is designed to predict aqueous species activities in dilute solutions and buffer solutions (i.e. 0.1M $NaClO_4$) are usually used to keep a constant ionic strength in solution. However the calculated solubility of $NaCe(CO_3)_2$ is similar to Nd and Eu and does follow the trend of increasing lanthanide solubility, with decreasing ionic radii for the lanthanides.

There is a wide range in the solubility products determined for lanthanide hydroxides that cluster around the extremes of the range from log Ksp -21.4 (this work) , -22.3 (Morss *et al.*, 1989) to -27.4 (this work, Rao *et al.*, 1986b) reflecting the experimental technique and the crystallinity of the sample. The lowest solubilities were derived from the partial dissolution of thermally aged

crystals formed in a 2M to 5M NaOH solution (Rao *et al.*, 1996b). In this study, the solid $Ln(OH)_3$ phases were formed by precipitation in low ionic strength solutions at less than 0.1M total inorganic carbonate or hydroxide, and allowed to stand for at least 2 months. This type of study is invaluable in determining how much of each lanthanide could be removed from solution immediately, to mimic the effects of secondary precipitation after the dissolution of an initial host mineral phase, before the lanthanide can be transported out of the system assuming no other method of removal i.e. adsorption to mineral surfaces.

The lanthanide hydroxide phases formed in this study therefore infer the initial solubility limit at 25°C from low ionic strength solutions, rather than the dissolution of highly crystalline slowly forming aged crystals. Vitorge (1992) notes that $Am(OH)_3$ forms initially as an amorphous solid which slowly transforms into a more stable and less soluble crystalline phase. The lanthanide hydroxide phases would therefore be expected to crystallise in a similar manner, however the time required for solid phase equilibration is unknown. Conversely, Silva *et al.*, (1995) indicate that $Cm(OH)_3$ crystals will show lattice defects in less than a week and $Am(OH)_3$ crystals in months from the α-particle emissions. A good crystal structure is unlikely to form after the constant disruption to the crystal lattice indicating that the less crystalline hydroxide phases (or other carbonate phases) with the higher solubility are more likely to form.

4.5 Calculation of the Gibbs Free Energy of Formation (ΔG_f^o)

The solubility product of a solid/mineral phase can be used to calculate the Standard Gibbs free energy of reaction (ΔG_{Rn}^o) for the dissociation of a solid phase from equation 4.39

$$\Delta G_{Rn}^o = -RT\ln K \qquad (4.39)$$

where K = Solubility product, T = absolute temperature (K) and R = Gas constant ($8.314 JK^{-1}mol^{-1}$).

The Gibbs free energy of reaction is the difference between the Gibbs free energy of formation of the reactants and products for any reaction (equation 4.40)

$$\Delta G_{Rn}^{\circ} = \Delta G_f^{\circ}(\text{products}) - \Delta G_f^{\circ}(\text{reactants})$$

$$\Delta G_f^{\circ}(\text{reactants}) = \Delta G_f^{\circ}(\text{products}) - \Delta G_{Rn}^{\circ} \qquad (4.40)$$

For the solubility reactions ΔG_f°(products) are the component aqueous ions on dissolution and ΔG_f°(reactants) are the solid phase and H^+ when applicable. The Gibbs free energy of formation of the lanthanide carbonate and hydroxy carbonates can be calculated from the solubility products and the aqueous thermodynamic data (Table 4.9).

Table 4.9 Selected thermodynamic data for aqueous species (Lide, 1998)

species	ΔG_f°/KJmol^{-1}	species	ΔG_f°/KJmol^{-1}
Ce^{3+}	-672.0	OH^-	-157.22
Nd^{3+}	-671.6	CO_3^{2-}	-527.90
Eu^{3+}	-574.1	CO_2	-394.37
Na^+	-261.95	H^+	0.00
H_2O	-237.14	e-	0.00

The Gibbs free energy of formation for the sodium lanthanide double carbonates can be calculated from the solubility product measured for the dissociation reaction of the solid phase into the free component ions (equation 4.12)

$$NaLn(CO_3)_2 \longrightarrow Ln^{3+} + Na^+ + 2CO_3^{2-} \qquad (4.12)$$

The component ions (from equation 4.24) can be substituted for the ΔG_f°(products) in equation 4.40 and the solid phase for the ΔG_f°(reactants) as equation 4.41. The thermodynamic data for the free ions (Table 4.9) is then substituted into equation 4.41 with the Gibbs free energy of reaction (calculated from the solubility product)

$$\Delta G_f^{\circ}(\text{reactants}) = \Delta G_f^{\circ}(\text{products}) - \Delta G_{Rn}^{\circ} \quad (4.40)$$

$$\Delta G_f^{\circ}[NaNd(CO_3)_2] = [\Delta G_f^{\circ}(Na^+) + \Delta G_f^{\circ}(Ln^{3+}) + 2\Delta G_f^{\circ}(CO_3^{2-})] - \Delta G_{Rn}^{\circ} \quad (4.41)$$

$$= [(-261.95) + (-671.6) + 2(-527.9)] - [121.3]$$

$$= -2110.7 \text{ KJmol}^{-1}$$

The Standard Gibbs free energy of formation of all the other solid carbonate and hydroxy phases prepared can be calculated for from the equations in Table 4.10 and the results summarised in Table 4.11

Table 4.10 Equations for the calculation of the Standard Gibbs free energy of formation from solubility products

$\Delta G_f^{\circ}(\text{reactants}) = \Delta G_f^{\circ}(\text{products}) - \Delta G_{Rn}^{\circ}$	(4.40)
$NaLn(CO_3)_2 \longrightarrow Ln^{3+} + Na^+ + 2CO_3^{2-}$	(4.12)
$\Delta G_f^{\circ}[NaLn(CO_3)_2] = [\Delta G_f^{\circ}(Na^+) + \Delta G_f^{\circ}(Ln^{3+}) + 2\Delta G_f^{\circ}(CO_3^{2-})] - \Delta G_{Rn}^{\circ}$	(4.41)
$Ln_2(CO_3)_3 \longrightarrow 2Ln^{3+} + 3CO_3^{2-}$	(4.15)
$\Delta G_f^{\circ}[Ln_2(CO_3)_3] = [2\Delta G_f^{\circ}(Ln^{3+}) + 3\Delta G_f^{\circ}(CO_3^{2-})] - \Delta G_{Rn}^{\circ}$	(4.42)
$LnCO_3OH \longrightarrow Ln^{3+} + CO_3^{2-} + OH^-$	(4.18)
$\Delta G_f^{\circ}[LnCO_3OH] = [\Delta G_f^{\circ}(Ln^{3+}) + \Delta G_f^{\circ}(CO_3^{2-}) + \Delta G_f^{\circ}(OH^-)] - \Delta G_{Rn}^{\circ}$	(4.43)
$LnCO_3OH + H^+ = Ln^{3+} + CO_3^{2-} + H_2O$	(4.21)
$\Delta G_f^{\circ}[LnCO_3OH] + \Delta G_f^{\circ}[H^+] = [\Delta G_f^{\circ}(Ln^{3+}) + \Delta G_f^{\circ}(CO_3^{2-}) + \Delta G_f^{\circ}(H_2O)] - \Delta G_{Rn}^{\circ}$	(4.44)
$Ln(OH)_3 \longrightarrow Ln^{3+} + 3OH^-$	(4.24)
$\Delta G_f^{\circ}[Ln(OH)_3] = [\Delta G_f^{\circ}(Ln^{3+}) + 3\Delta G_f^{\circ}(OH^-)] - \Delta G_{Rn}^{\circ}$	(4.45)
$Ln(OH)_3 + 3H^+ = Ln^{3+} + 3H_2O$	(4.27)
$\Delta G_f^{\circ}[Ln(OH)_3] + \Delta G_f^{\circ}[H^+] = [\Delta G_f^{\circ}(Ln^{3+}) + 3\Delta G_f^{\circ}(H_2O)] - \Delta G_{Rn}^{\circ}$	(4.46)
$CeO_2 + 4H^+ + e^- \longrightarrow Ce^{3+} + 2H_2O$	(4.30)
$\Delta G_f^{\circ}[CeO_2] = [\Delta G_f^{\circ}(Ce^{3+}) + 2\Delta G_f^{\circ}(H_2O)] - \Delta G_{Rn}^{\circ}$	(4.47)
$KNd(CO_3)_2 \longrightarrow K^+ + Nd^{3+} + 2CO_3^{2-}$	(4.48)
$\Delta G_f^{\circ}(KNd(CO_3)_2) = [\Delta G_f^{\circ}(K^+) + \Delta G_f^{\circ}(Nd^{3+}) + 2CO_3^{2-})] - \Delta G_{Rn}^{\circ}$	(4.49)

Table 4.11 Summary of ΔG_f° calculations for lanthanide carbonate and hydroxy phases (this work)

Phase	log Ksp	logK	ΔG_f° /KJmol^{-1}
$NaCe(CO_3)_2$	-22.62		-2118.9
$NaNd(CO_3)_2$	-21.25±0.95		-2110.7
$NaEu(CO_3)_2$	-20.48±0.69		-2008.8
$Ce_2(CO_3)_3$	-36.04±0.75		-3133.4
$Nd_2(CO_3)_3$	-34.43±0.35		-3123.4
$Eu_2(CO_3)_3$	-32.99±1.09		-2920.2
$NdCO_3OH$	-19.87±1.75	-5.87±1.75	-1470.2
$EuCO_3OH$	-18.62±0.15	-4.62±0.15	-1365.5
$Nd(OH)_3$	-21.41±0.67	20.59±0.67	-1265.5
$Eu(OH)_3$	-22.79±0.23	19.21±0.23	-1175.9
CeO_2		30.66±0.60	-971.3
$KNd(CO_3)_2$	-19.17±0.02		-2119.3

4.6 Phase Relations

The Gibbs free energy of reaction (ΔG_{Rn}°) can be calculated for any two phases in equilibrium (equation 4.40), then used to calculate the reaction constant of the equilibrium reaction between those phases from equation 4.39

$$\Delta G_{Rn}^\circ = \Delta G_f^\circ(\text{products}) - \Delta G_f^\circ(\text{reactants}) \qquad (4.40)$$

$$\Delta G_{Rn}^\circ = -RT\ln K \qquad (4.39)$$

then the reaction constant (K) can be derived as equation 4.50

$$\ln K = -\frac{\Delta G^\circ}{RT} \quad \therefore \quad K = \exp^{\frac{-\Delta G^\circ}{RT}} \qquad (4.50)$$

The reaction constant is also dependent on the activities of the aqueous components (equation 4.51)

$$K = \frac{\prod[\text{products}]}{\prod[\text{reactants}]} \qquad (4.51)$$

A phase boundary can therefore be calculated for the equilibrium between two phases if their respective Gibbs free energy of formation (ΔG_f°) are known (Tables 4.9 & 4.11).

4.6.1 $Ln_2(CO_3)_3$-$LnCO_3OH$ equilibrium

The equilibrium reaction between $Ln_2(CO_3)_3$ and $LnCO_3OH$ is usually described in terms of pH and CO_3^{2-} activity for the equilibrium reaction, equation 4.52

$$Ln_2CO_3 + 2H_2O = 2LnCO_3OH + 2H^+ + CO_3^{2-} \qquad (4.52)$$

The Gibbs free energy of reaction (ΔG_{Rn}°) can be calculated from equation 4.53, using the ΔG_f° values from Tables 4.9 and 4.11 and shown in Table 4.12

$$\Delta G_{Rn}^\circ = [2\Delta G_f^\circ(LnCO_3OH) + 2\Delta G_f^\circ(H^+) + \Delta G_f^\circ(CO_3^{2-})] - [\Delta G_f^\circ(Ln_2(CO_3)_3) + 2\Delta G_f^\circ(H_2O)] \qquad (4.53)$$

Table 4.12 Calculation of the Ln_2CO_3-$LnCO_3OH$ equilibrium reaction constant

equilibrium phase	log Ksp	ΔG_f°/KJmol^{-1} (products)	ΔG_f°/KJmol^{-1} (reactants)	ΔG_{Rn}°/ KJmol^{-1}	logK (equilibrium)
$Nd_2(CO_3)_3$ -$NdCO_3OH$	-34.43 -19.87	-3468.2	-3597.67	129.47	-22.68
$Eu_2(CO_3)_3$ -$EuCO_3OH$	-32.99 -18.62	-3258.84	-3394.45	135.61	-23.76

The reaction constant can also be expressed in terms of the activities in aqueous solution (equation 4.54)

$$K = \frac{a_{Ln_2(CO_3)_3} . a_{CO_3^{2-}} . a_{H^+}^2}{a_{LnCO_3OH} . a_{H_2O}^2} \qquad (4.54)$$

H_2O has an activity of 1, and at equilibrium the activities of Ln_2CO_3 and $LnCO_3OH$ are equal and have an activity of 1 as solid phases therefore equation 4.54 can be simplified as equation 4.55

$$K = a_{H^+}^2 . a_{CO_3^{2-}} \qquad (4.55)$$

by taking -log of equation 4.55 to convert the activity of H^+ into pH, the equilibrium phase boundary can be written in terms of the carbonate activity of the solution (equation 4.56) and the reaction constant calculated in Table 4.37

$$\log a_{CO_3^{2-}} = 2pH + \log K \qquad (4.56)$$

4.6.2 $LnCO_3OH$-$Ln(OH)_3$ equilibrium

The equilibrium reaction between the hydroxycarbonate and the hydroxide is also expressed in terms of H^+ and CO_3^{2-} activities (equation 4.57)

$$LnCO_3OH + 2H_2O = Ln(OH)_3 + 2H^+ + CO_3^{2-} \qquad (4.57)$$

and the Gibbs free energy of reaction calculated from equation 4.58

$$\Delta G_{Rn}^{\circ} = [\Delta G_f^{\circ}(Ln(OH)_3) + 2\Delta G_f^{\circ}(H^+) + \Delta G_f^{\circ}(CO_3^{2-})] - [\Delta G_f^{\circ}(LnCO_3OH) + 2\Delta G_f^{\circ}(H_2O)] \qquad (4.58)$$

The reaction constant can be derived from the ΔG_{Rn}° (Table 4.13)

Table 4.13 Calculation of the $LnCO_3OH$-$Ln(OH)_3$ equilibrium reaction constant

equilibrium phase	log Ksp	ΔG_f°/KJmol^{-1} (products)	ΔG_f°/KJmol^{-1} (reactants).	ΔG_{Rn}°/ KJmol^{-1}	logK (equilibrium)
$NdCO_3OH$ -$Nd(OH)_3$	-19.87 -21.41	-1793.36	-1944.43	151.07	-26.47
$EuCO_3OH$ -$Eu(OH)_3$	-18.62 -22.79	-1703.76	-1839.75	135.99	-23.83

The equilibrium constant can be expressed as solution activities (equation 4.59)

$$K = a_{H^+}^2 . a_{CO_3^{2-}} \qquad (4.59)$$

and by taking –log of equation 4.59 and rearranging , the carbonate activity in solution can be calculated in terms of pH and the reaction constant (equation 4.60)

$$\log a_{CO_3^{2-}} = 2pH + \log K \qquad (4.60)$$

Equations 4.56 and 4.60 indicate that the Ln_2CO_3-$LnCO_3OH$ and $LnCO_3OH$-$Ln(OH)_3$ phase boundaries have a linear relationship which are dependant on the pH and CO_3^{2-} activities in solution but displaced by the reaction constants (Tables 4.12 and 4.13). The Nd phase boundaries are separated by 4 log units, whilst the Eu phase boundaries are almost continuous with a separation of less than 1 log unit.

4.6.3 $NaLn(CO_3)_2$-$Ln_2(CO_3)_3$ equilibrium

The $NaLn(CO_3)_2$ and Ln_2CO_3 equilibrium can be described by equation 4.61

$$2NaLn(CO_3)_2 = Ln_2CO_3 + 2Na^+ + CO_3^{2-} \qquad (4.61)$$

The Gibbs free energy for the reaction can be calculated by equation 4.62 from the ΔG_f° values in Tables 4.9 and 4.11 and shown in Table 4.14

$$\Delta G_{Rn}^\circ = [\Delta G_f^\circ(Ln_2CO_3) + 2\Delta G_f^\circ(Na^+) + \Delta G_f^\circ(CO_3^{2-})] - [2\Delta G_f^\circ(NaLn(CO_3)_2)] \qquad (4.62)$$

Table 4.39 Calculation of the $NaLn(CO_3)_2$-Ln_2CO_3 equilibrium reaction constant

equilibrium phase	log Ksp	ΔG_f°/KJmol^{-1} (products)	ΔG_f°/KJmol^{-1} (reactants)	ΔG_{Rn}°/ KJmol^{-1}	logK (equilibrium)
$NaCe(CO_3)_2$ -$Ce_2(CO_3)_3$	-22.62 -36.04	-4185.18	-4237.8	52.62	-9.2
$NaNd(CO_3)_2$ -$Nd_2(CO_3)_3$	-21.25 -34.43	-4175.19	-4221.4	46.21	-8.1
$NaEu(CO_3)_2$ -$Eu_2(CO_3)_3$	-20.48 -32.99	-3971.97	-4017.52	45.55	-7.98

When the reaction constant is expressed as the aqueous components, the reaction is independent of the pH but dependant on CO_3^{2-} activity, Na^+ activity and the reaction constant (equations 4.63)

$$K = a^2_{Na^+} \cdot a_{CO_3^{2-}} \qquad (4.63)$$

and when expressed in terms of the CO_3^{2-} activity (equation 4.64)

$$\log a_{CO_3^{2-}} = \log K - 2\log a_{Na^+} \qquad (4.64)$$

the carbonate activity can be seen to be constant at a constant Na^+ activity.

4.6.4 $NaLn(CO_3)_2$-$LnCO_3OH$ equilibrium

The reaction between $NaLn(CO_3)_2$ and $LnCO_3OH$ (equation 4.65) is dependant on pH, CO_3^{2-} and Na^+ activities.

$$NaLn(CO_3)_2 + H_2O = LnCO_3OH + Na^+ + H^+ + CO_3^{2-} \qquad (4.65)$$

The Gibbs free energy of the reaction can therefore be calculated from equation 4.66

$$\Delta G_{Rn}^\circ = [\Delta G_f^\circ(LnCO_3OH) + \Delta G_f^\circ(Na^+) + \Delta G_f^\circ(H^+) + \Delta G_f^\circ(CO_3^{2-})] - [\Delta G_f^\circ(NaLn(CO_3)_2) + \Delta G_f^\circ(H_2O)] \qquad (4.66)$$

and the reaction constant calculated in Table 4.15

Table 4.15 Calculation of the $NaLn(CO_3)_2$-$LnCO_3OH$ equilibrium reaction constant

equilibrium phase	log Ksp	ΔG_f°/KJmol^{-1} (products)	ΔG_f°/KJmol^{-1} (reactants)	ΔG_{Rn}°/ KJmol^{-1}	logK (equilibrium)
$NaNd(CO_3)_2$ -$NdCO_3OH$	-21.25 -19.87	-2260.00	-2374.84	87.84	-15.40
$NaEu(CO_3)_2$ -$EuCO_3OH$	-20.48 -18.62	-2155.32	-2245.9	90.58	-15.87

The reaction constant can be calculated from equation 4.67 in terms of the aqueous components

$$K = a_{Na^+}.a_{H^+}.a_{CO_3^{2-}} \quad (4.67)$$

$$\therefore \log a_{CO_3^{2-}} = pH - \log a_{Na^+} + \log K \quad (4.68)$$

4.6.5 $NaLn(CO_3)_2$-$Ln(OH)_3$ equilibrium

At high pH $NaLn(CO_3)_2$ may form in equilibrium with the hydroxide phase, especially at high Na^+ activities in carbonate solutions from the reaction (equation 4.69)

$$NaLn(CO_3)_2 + 3H_2O = Ln(OH)_3 + Na^+ + 2CO_3^{2-} + 3H^+ \quad (4.69)$$

and the Gibbs free energy of reaction calculated from equation 4.70 in Table 4.16

$$\Delta G_{Rn}^\circ = [\Delta G_f^\circ(Ln(OH)_3) + \Delta G_f^\circ(Na^+) + 2\Delta G_f^\circ(CO_3^{2-}) + 3\Delta G_f^\circ(H^+)] - [\Delta G_f^\circ(NaLn(CO_3)_2) + 3\Delta G_f^\circ(H_2O)] \quad (4.70)$$

Table 4.16 Calculation of the $NaLn(CO_3)_2$-$Ln(OH)_3$ equilibrium reaction constant

equilibrium phase	log Ksp	ΔG_f°/KJmol^{-1} (products)	ΔG_f°/KJmol^{-1} (reactants)	ΔG_{Rn}°/ KJmol^{-1}	logK (equilibrium)
$NaNd(CO_3)_2$ -$Nd(OH)_3$	-21.25 -21.41	-2583.21	-2820.44	239.02	-41.70
$NaEu(CO_3)_2$ -$Eu(OH)_3$	-20.48 -22.79	-2493.61	-2720.18	226.57	-39.70

The reaction constant for equation 4.69 can be expressed as equation 4.71 in terms of the aqueous components

$$K = a_{CO_3^{2-}}^2.a_{H^+}^3.a_{Na^+} \quad (4.71)$$

and can be written in terms of the aqueous carbonate activity as equation 4.72

$$\log a_{CO_3^{2-}} = \tfrac{1}{2}[3pH - \log a_{Na^+} + \log K] \quad (4.72)$$

4.6.6 $Ce_2(CO_3)_3$-CeO_2 phase boundary

The $Ce_2(CO_3)_3$-CeO_2 phase boundary differs from the other lanthanide carbonate phase boundaries in that a redox reaction must take place during the phase change (equation 4.73)

$$Ce_2(CO_3)_3 + 4H_2O = 2CeO_2 + 2e^- + 8H_2O + 3CO_3^{2-} \quad (4.73)$$

The Gibbs free energy of reaction is therefore calculated from equation 4.74 as shown in Table 4.17

$$\Delta G_{Rn}^o = [2\Delta G_f^o(CeO_2) + 2\Delta G_f^o(e^-) + 8\Delta G_f^o(H^+) + 3\Delta G_f^o(CO_3^{2-})] - [\Delta G_f^o(Ce_2(CO_3)_3) + 4\Delta G_f^o(H_2O)] \quad (4.74)$$

Table 4.17 Calculation of the $Ce_2(CO_3)_3$-CeO_2 equilibrium reaction constant

equilibrium phase	log Ksp/ logK	ΔG_f^o/KJmol^{-1} (products)	ΔG_f^o/KJmol^{-1} (reactants)	ΔG_{Rn}^o/ KJmol^{-1}	logK (equilibrium)
$Ce_2(CO_3)_3$ -CeO_2	-21.25 -21.41	-3256.24	-4081.94	555.7	-97.36

The reaction constant can be determined from the aqueous composition as

$$K = a_{e^-}^2 . a_{CO_3^{2-}}^3 . a_{H^+}^8 \quad (4.75)$$

The phase boundary can therefore be described in terms of the CO_3^{2-} activity or the pe in solution with a variable pH from equations 4.76 and 4.77

$$\log a_{CO_3^{2-}} = \tfrac{1}{3}(2pe + 8pH + logK) \quad (4.76)$$

$$pe = \tfrac{1}{2}(3\log a_{CO_3^{2-}} + 8pH + logK) \quad (4.77)$$

4.7 Nd and Eu Phase Diagrams

A pH vs carbonate concentration diagram can be constructed for each of the lanthanides showing the stability region of each phase found from the titration experiments using the equations in Table 4.18. The diagrams are constructed assuming the solutions are ideal and therefore the concentration of each species is equal to the species activities in solution, at a temperature of 298.15K. The diagrams can be plotted in two dimensions therefore, the Na^+ activity will be considered at specific concentrations.

Table 4.18 Summary of solid phase equilibrium reactions and reaction constants with aqueous carbonate solutions (this work)

Equilibrium Phases	Equilibrium Reaction	logK Ce	logK Nd	logK Eu
$Ln_2(CO_3)_3$ – $LnCO_3OH$	$\log[CO_3^{2-}] = 2pH + logK$	N/A	-22.68	-23.76
$LnCO_3OH$ - $Ln(OH)_3$	$\log[CO_3^{2-}] = 2pH + logK$	N/A	-26.47	-23.83
$NaLn(CO_3)_2$ – $Ln_2(CO_3)_3$	$\log[CO_3^{2-}] =$ $logK - 2\log[Na^+]$	-9.20	-8.10	-7.98
$NaLn(CO_3)_2$ – $LnCO_3OH$	$\log[CO_3^{2-}] =$ $pH - \log[Na^+] + logK$	N/A	-15.40	-15.87
$NaLn(CO_3)_2$ – $Ln(OH)_3$	$\log[CO_3^{2-}] =$ $(3pH - \log[Na^+] + logK)/2$	N/A	-41.90	-39.70
$NaCe(CO_3)_2$ -CeO_2	$pe = 2\log[CO_3^{2-}] - 4pH$ $+ \log[Na^+] - logK$ $\log[CO_3^{2-}] = (4pH + pe$ $+ \log[Na^+] + logK)/2$	-49.93	N/A	N/A
$Ce_2(CO_3)_3$ -CeO_2	$pe = (3\log[CO_3^{2-}] - 8pH$ $- logK)/2$ $\log[CO_3^{2-}] = (2pe + 8pH$ $+ logK)/3$	-97.36	N/A	N/A

4.7.1 pH vs $\log[CO_3^{2-}]$ stability field diagrams

The interactions between the $Ln_2(CO_3)_3$, $LnCO_3OH$ and $Ln(OH)_3$ phases are directly related by the pH and CO_3^{2-} activities of the solution (equations 4.52 and 4.57)

$$Ln_2(CO_3)_3 + 2H_2O = LnCO_3OH + 2H^+ + CO_3^{2-} \qquad (4.52)$$

$$LnCO_3OH + 2H_2O = Ln(OH)_3 + \ 2H^+ + CO_3^{2-} \qquad (4.57)$$

The phase change from $Ln_2(CO_3)_3$, to $LnCO_3OH$ then to $Ln(OH)_3$ with pH, reflects the increase in hydroxide activity in solution. Similarly increasing the $[CO_3^{2-}]$ at a constant pH displaces hydroxide to form more carbonate dominant phases.

The stability field for each of these phases can be conveniently plotted on a pH vs $[CO_3^{2-}]$ diagram, to determine the most stable phase, (and therefore the solubility limiting phase), over a range of solution conditions. The stability field boundaries between $Ln_2(CO_3)_3$ with $LnCO_3OH$ and $LnCO_3OH$ with $Ln(OH)_3$, have the same relationship between CO_3^{2-} and pH (equation 4.78), therefore the stability field boundaries between these three phases will be parallel, but displaced by the constant for each equilibrium reaction.

$$K = [CO_3^{2-}][H^+]^2 \qquad (4.78)$$

$$\therefore \log[CO_3^{2-}] = 2pH + \log K \qquad (4.79)$$

In Na^+ free solutions the pH vs $\log[CO_3^{2-}]$ diagram for Nd (Figure 4.2a) shows that the Nd system has three distinct phases however, the almost identical reaction constants for the Eu phases, results in the $Eu_2(CO_3)_3$-$EuCO_3OH$-$Eu(OH)_3$ phase boundaries (Figure 4.3a) almost being superimposed. A less soluble $EuCO_3OH$ phase would push the phase boundaries apart.

The $NaLn(CO_3)_2$ stability field boundary intersects the $Ln_2(CO_3)_3$ and $LnCO_3OH$ phases at high CO_3^{2-} activities (Figures 4.2b and 4.3b). This can be seen when the addition of excess Na_2CO_3 converts $Ln_2(CO_3)_3$ to $NaLn(CO_3)_2$ according to the reaction below (equation 4.80)

$$Ln_2(CO_3)_3 + Na_2CO_3 = 2NaLn(CO_3)_2 \qquad (4.80)$$

The $NaLn(CO_3)_2$-$Ln_2(CO_3)_3$ stability field boundary is independent of pH and has an inverse relation between Na^+ and CO_3^{2-} activity i.e. increasing the Na^+ activity decreases the CO_3^{2-} activity required to form $NaLn(CO_3)_2$.

The $NaLn(CO_3)_2$-$LnCO_3OH$ stability field boundary is dependent on pH, CO_3^{2-} and Na^+ activities, increasing pH favours the formation of the hydroxycarbonate at constant CO_3^{2-} activity. The $NaLn(CO_3)_2$-$Ln(OH)_3$ stability field boundary is even more strongly dependent on pH than the $NaLn(CO_3)_2$-$LnCO_3OH$ stability field boundary, and consequently there is a further increase in the inclination of this stability field boundary.

The $NaLn(CO_3)_2$,$Ln_2(CO_3)_3$ and $LnCO_3OH$ phases form a triple point that can be experimentally verified, where all three phases are in equilibrium, the position of which depends on the Na^+ activity in the pH vs $[CO_3^{2-}]$ diagram (Figure 4.2b). The $NaLn(CO_3)_2$-$LnCO_3OH$-$Ln(OH)_3$ triple point forms at high carbonate activities, above 1M total inorganic carbonate is required to form $NaLn(CO_3)_2$, if there is less than 0.1M Na^+ in solution. The required $[CO_3^{2-}]$ then decreases with increasing $[Na^+]$.

The Nd and Eu stability field diagrams do not give any indication to the actual solubilities of the lanthanides, but do indicate the relative differences in the stability of each phase on the phase diagram, i.e. an increase in the solubility product of the $LnCO_3OH$ phase will increase the area of the $LnCO_3OH$ stability field.

Figure 4.2a Stability field diagram for the Nd-CO_3^{2-}-OH^- system at 298.15K and 1 atm pressure

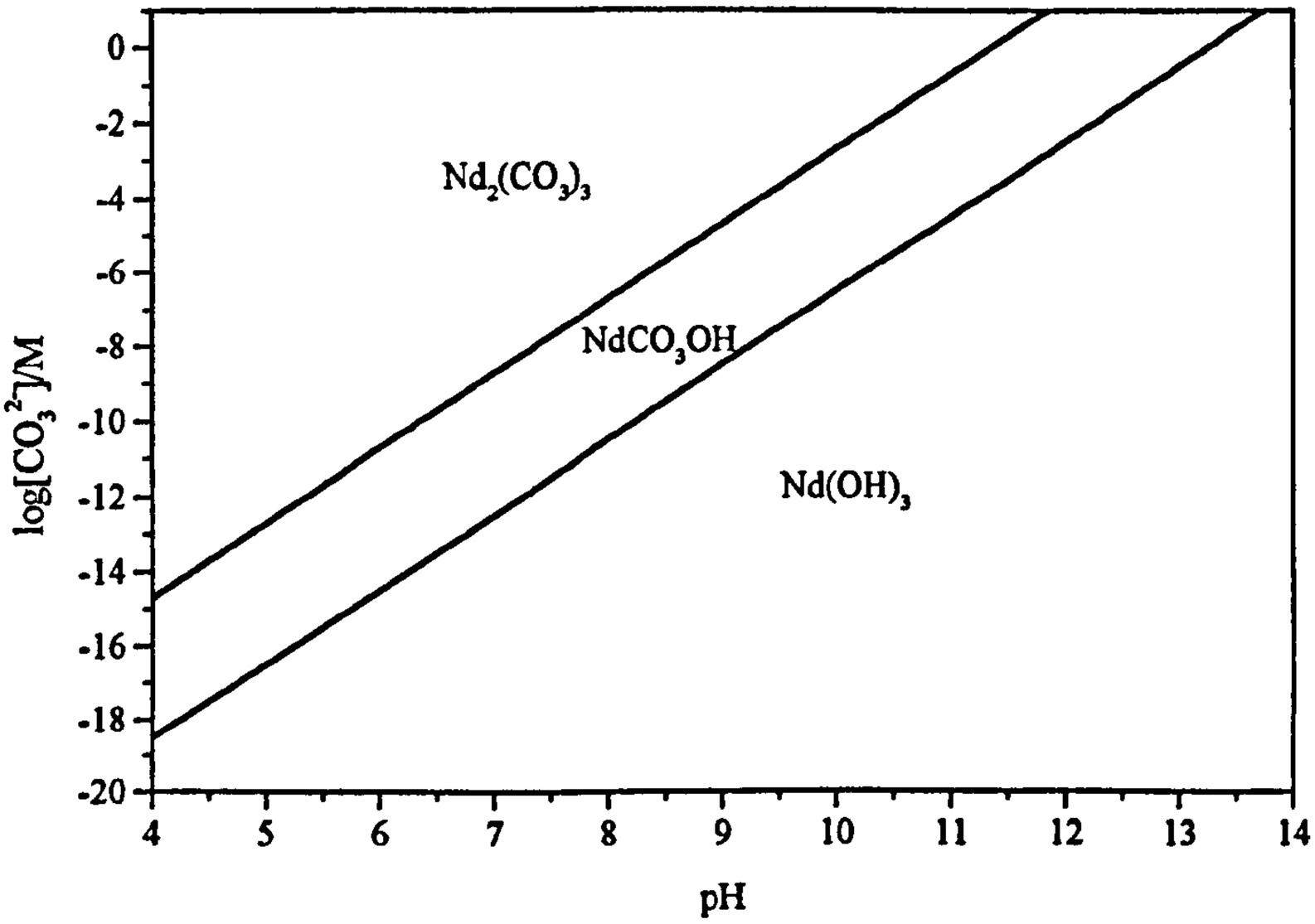

Figure 4.2b Stability field diagram for the Na-Nd-CO_3^{2-}-OH^- system at 298.15K and 1 atm pressure $[Na^+]$ = 10mM

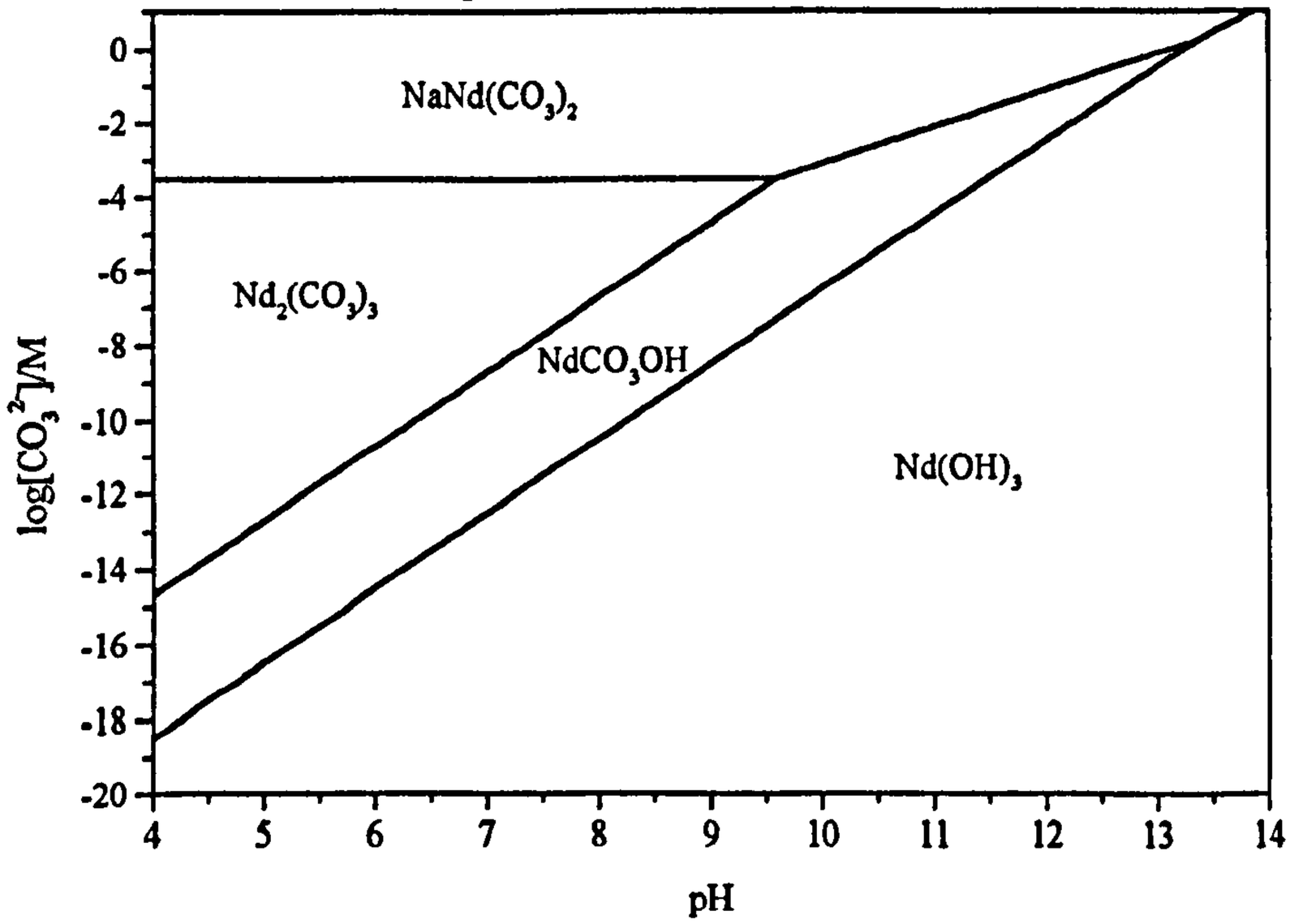

Figure 4.3a Stability field diagram for the Eu-CO_3^{2-}-OH^- system at 298.15K and 1 atm pressure

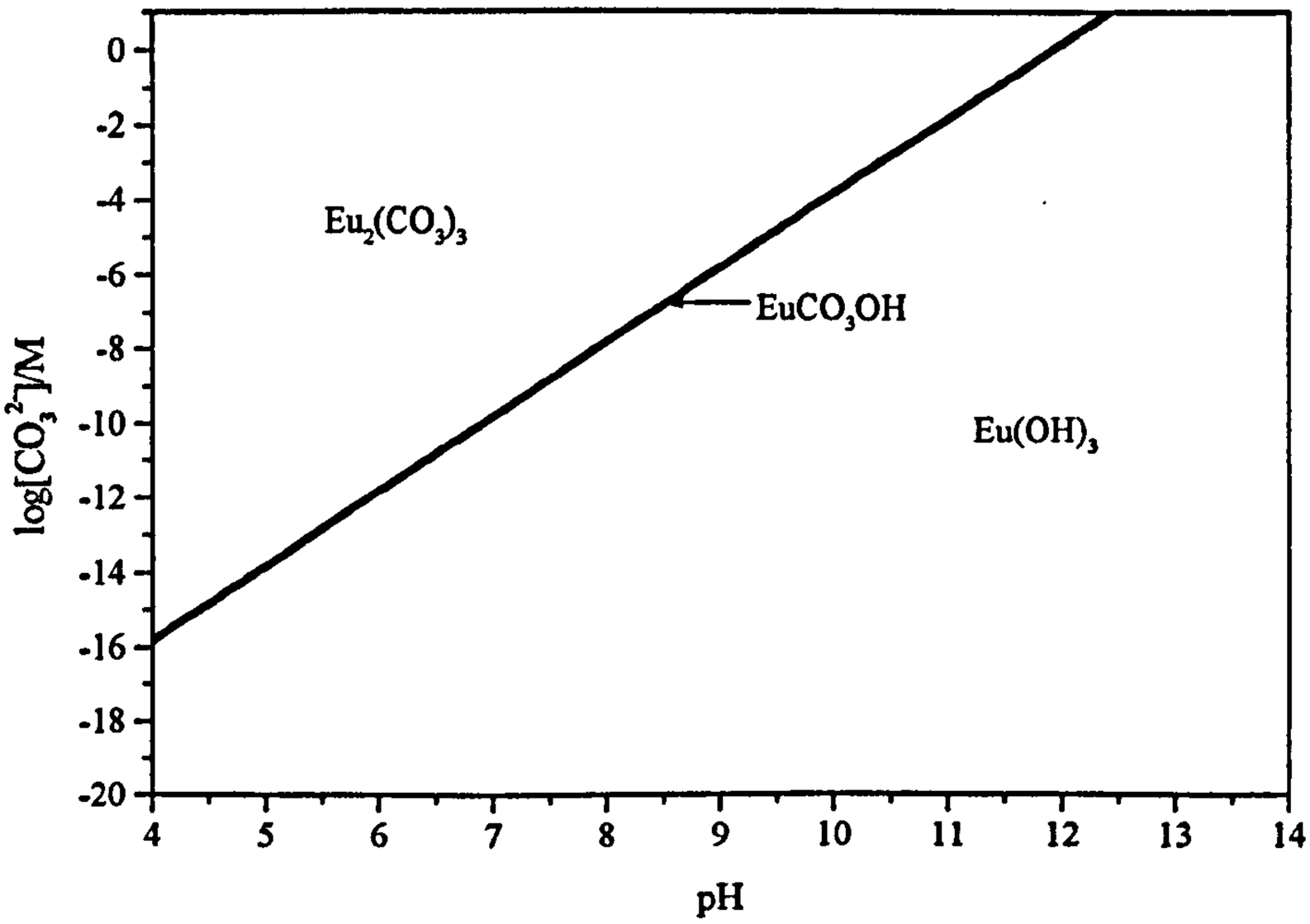

Figure 4.3b Stability field diagram for the Na-Eu-CO_3^{2-}-OH^- system at 298.15K and 1 atm pressure $[Na^+]$ = 10mM

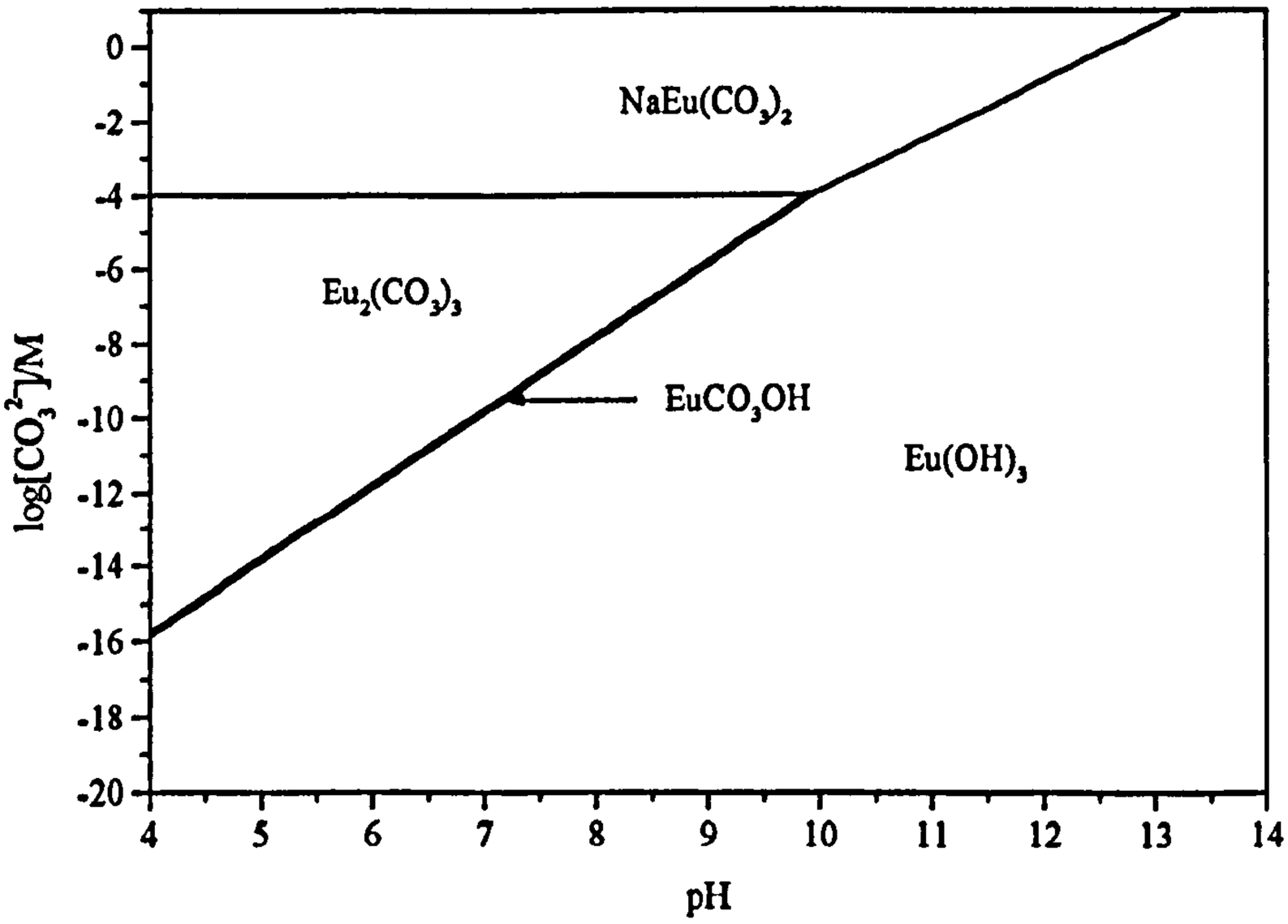

4.7.2 pH vs Total Inorganic Carbonate (TIC)

In addition to the accepted method of stability field diagram presentation, that is using the log[CO_3^{2-}], an alternative method of presenting the relationship between one phase and the next is to include the total inorganic carbonate (TIC) that will be in equilibrium with the system as pH increases.

The pH vs log[CO_3^{2-}] stability field diagrams show the direct relationship between phases and the specific component ions required for each phase, however the actual free CO_3^{2-} concentration is only equal to the total inorganic carbonate concentration [TIC] above pH 10.5. Below pH 10.5 HCO_3^- and H_2CO_3 aqueous species are the dominant aqueous species and CO_3^{2-} exists only at trace quantities (Figure 4.4). Carbonate complexes further with other cations in solution such as the Na^+ or K^+ which also alter the pH reducing further the amount of free carbonate in solution.

Figure 4.4 Carbonate speciation in 10^{-3}M Total Inorganic Carbonate (TIC) solution at 298.15K and 1 atm pressure

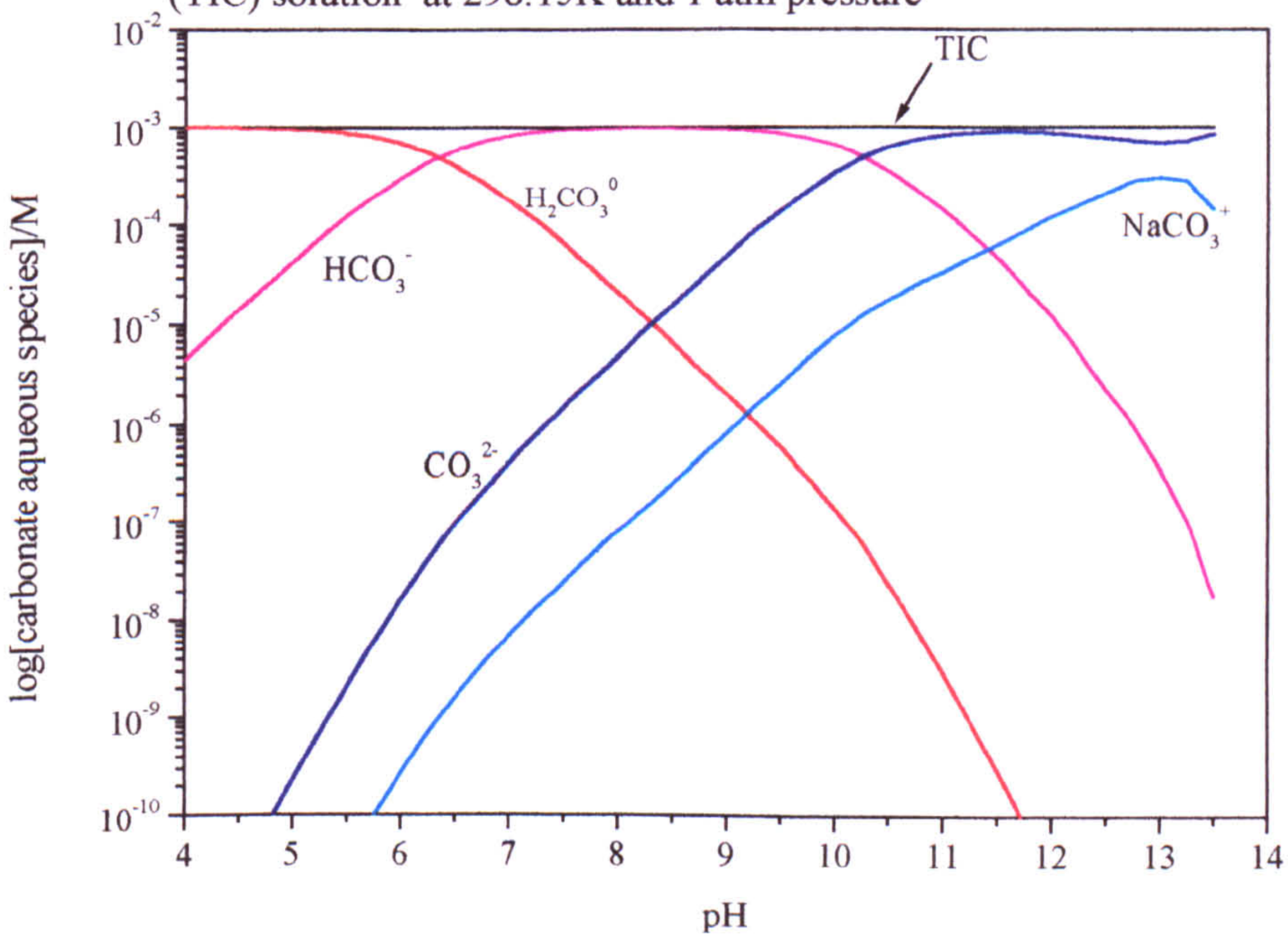

The [CO_3^{2-}] can be converted to [TIC] (from equation 4.81, Firsching and Mohammadzadel, 1986) to determine the actual total amount of aqueous carbonate required for each phase to form below pH 10.

$$[TIC] = [CO_3^{2-}]\frac{([H^+]^2 + K_1[H^+] + K_1K_2)}{K_1K_2} \qquad (4.81)$$

$K_1 = 4.16x10^{-7}$

$K_2 = 4.84x10^{-11}$

When the $[CO_3^{2-}]$ has been converted to [TIC], there is a significant effect on the appearance of the lanthanide stability field diagrams below pH 10 (Figures 4.5 and 4.6). Above pH 10 the CO_3^{2-} species is the dominant carbonate species in solution, and reflects that $[CO_3^{2-}]$ is effectively [TIC].

In the Nd system (Figure 4.5), $Nd_2(CO_3)_3$ is dominant at low pH and above 10^{-6}M TIC. $Ln(OH)_3$ is stable at high pH and in low TIC solutions (below $2x10^{-10}$M TIC). $NdCO_3OH$ forms between these two phases. $NaNd(CO_3)_2$ is the stable phase in the mid-pH range above 10^{-3}M TIC. Reducing or increasing the pH from pH 9, increases the amount of carbonate required to form $NaNd(CO_3)_2$.

Eu forms a similar stability field diagram (Figure 4.6) to the Nd system, except the $EuCO_3OH$ phase has a narrow stability field. $Eu_2(CO_3)_3$ is stable above 10^{-7}M TIC at pH 4 to 6, whilst $Eu(OH)_3$ is stable below $8x10^{-8}$M TIC between pH 4 and 6.

The $NaLn(CO_3)_2$-$Ln_2(CO_3)_3$ stability field boundary is independent of pH in pH vs $\log[CO_3^{2-}]$ stability field diagrams (Figures 4.2b and 4.3b). This phase equilibrium is controlled by pH when total inorganic carbonate is considered, as CO_3^{2-} is actually present only as trace quantities in solution. Below pH 6, $NaLn(CO_3)_2$ is unlikely to form as a [TIC] above 1M would be required (Figures 4.5 and 4.6).

The $Ln_2(CO_3)_3$-$LnCO_3OH$ and $LnCO_3OH$-$Ln(OH)_3$ phase boundaries remain parallel, however there is a minimum amount of TIC required for each phase. The $[CO_3^{2-}]$ is present at trace quantities below pH 6. Above pH 6 the proportion of aqueous CO_3^{2-} increases steadily until pH10, where CO_3^{2-} becomes the dominant species and $[CO_3^{2-}]$ is approximately equal to [TIC]

$NaLn(CO_3)_2$ forms at a minimum [TIC] of approximately pH 9 for $NaNd(CO_3)_2$ and pH 9.5 for $NaEu(CO_3)_2$. The shape of the $NaLn(CO_3)_2$ stability field results from the interaction between the increasing effects of $[CO_3^{2-}]$ in solution lowering the [TIC] required to form $NaLn(CO_3)_2$, and the increasing hydroxy activity with pH favours the formation of $LnCO_3OH$ then $Ln(OH)_3$.

The pH vs [TIC] stability field diagrams show a realistic interpretation of the Na-Ln-TIC-OH system below pH 10, compared with traditional pH vs $[CO_3^{2-}]$ diagrams. These stability field diagrams clearly indicate the solid lanthanide phase that will form in equilibrium with a solution of known composition. The lanthanide solubility can therefore be predicted over a range of solution conditions.

Figure 4.5 Stability field diagram for the Na-Nd-TIC-OH^- system at 298.15K and 1 atm pressure $[Na^+] = 10mM$

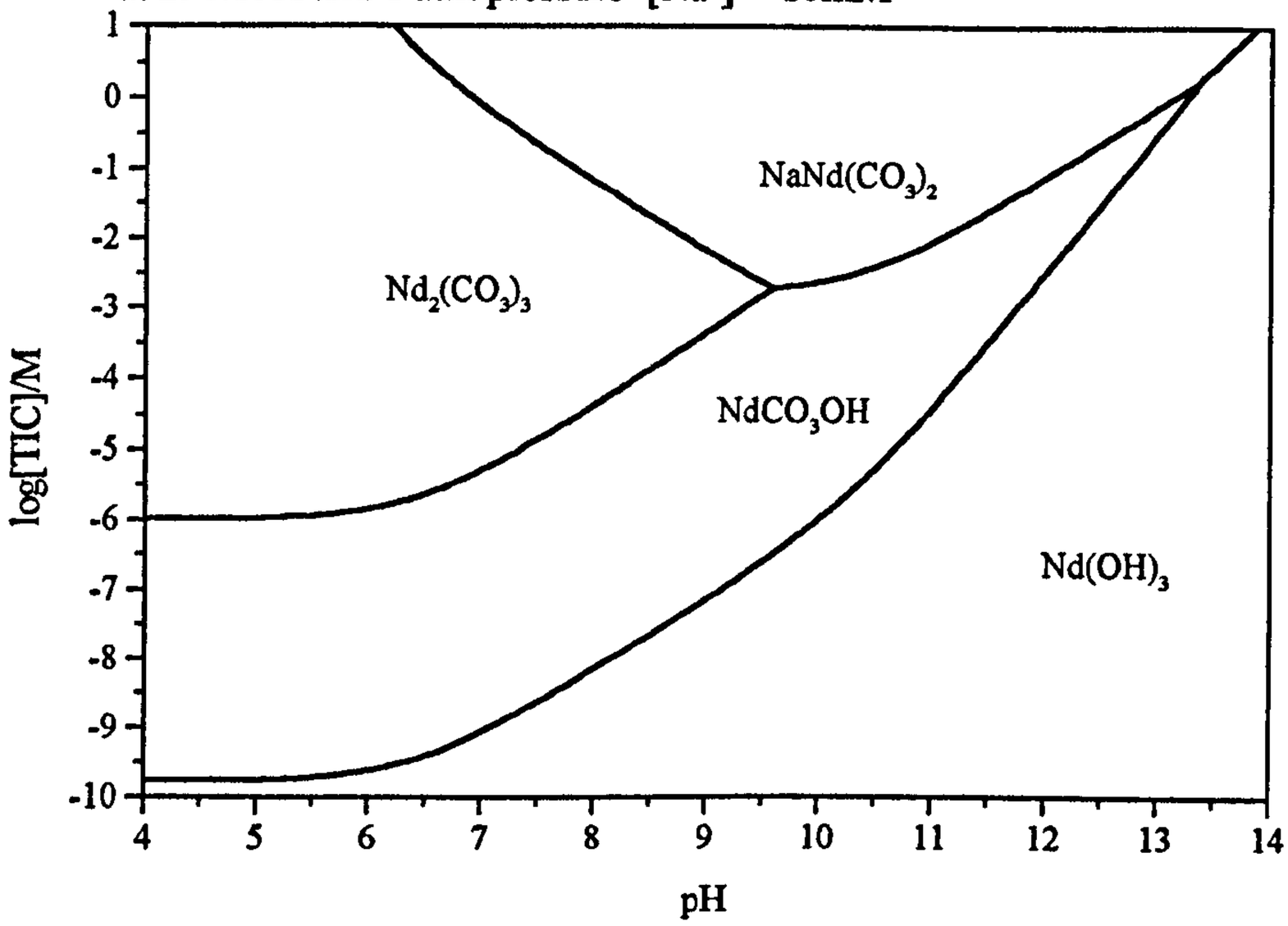

Figure 4.6 Stability field diagram for the Na-Eu-TIC-OH^- system at 298.15K and 1 am pressure $[Na^+] = 10mM$

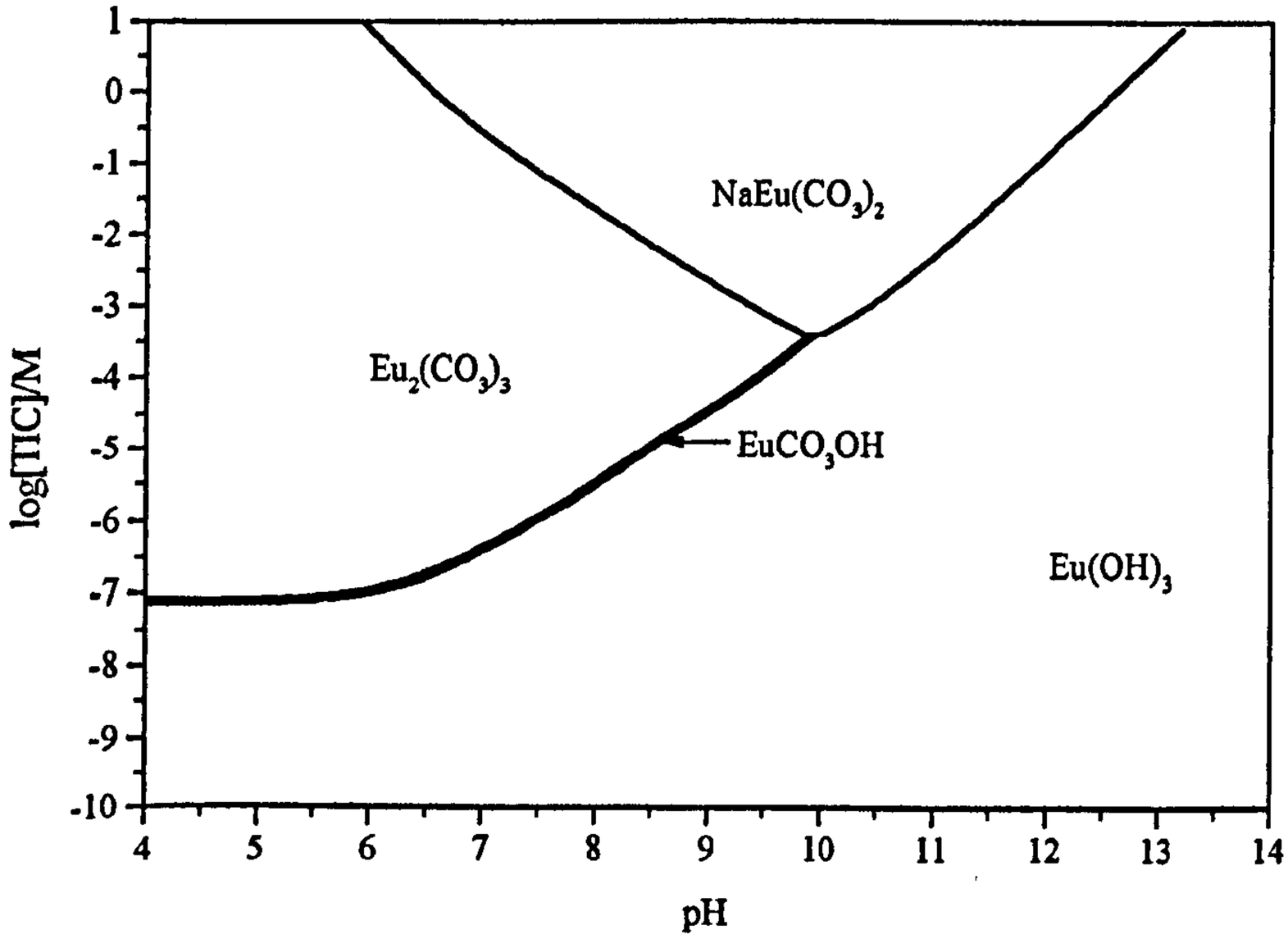

4.7.3 Solid-aqueous phase relations

The solid phase stability field diagrams only indicate the solubility limiting phases over the pH range pH 4 to14 and [TIC] from $1x10^{-10}$M to 1M solutions, they do not indicate the actual solubility of each lanthanide phase over the carbonate-pH range. The $[Ln^{3+}]$ can be calculated from the pH and the $[CO_3^{2-}]$ from the solubility product. However the actual aqueous lanthanide speciation is also dependent on the pH and CO_3^{2-} activity of the solution. Ln^{3+} is only the dominant aqueous species below pH 8.9, and a series of aqueous lanthanide hydroxy phases exist at higher pH.

Increasing the pH of a solution favours the formation of the lanthanide hydroxy species, from Ln^{3+}, through $LnOH^{2+}$ and $Ln(OH_2)^+$ to $Ln(OH)_3^0$ (Figure 4.7). Lanthanide carbonate species are also important at elevated TIC concentrations the carbonate species $LnCO_3^+$ and $Ln(CO_3)_2^-$ are the dominant aqueous lanthanide species in the mid-pH range with Nd^{3+} and $Nd(OH)_3^0$ dominant at the low and high pH extremes respectively (Figure 4.8). There is a transition region around 10^{-5}M TIC where all the aqueous species have an approximate equal activity between pH 8 and 10 (Appendix 4.13). The Ln^{3+} aqueous species is present in all solution compositions, but above pH 6, Ln^{3+} will only be present at trace quantities, i.e. between 3 to 5 orders of magnitude lower than the total lanthanide concentration.

Figure 4.7 The aqueous speciation of 10^{-7}M Nd in 10^{-7}M TIC after Lee & Byrne (1992 & 1993)

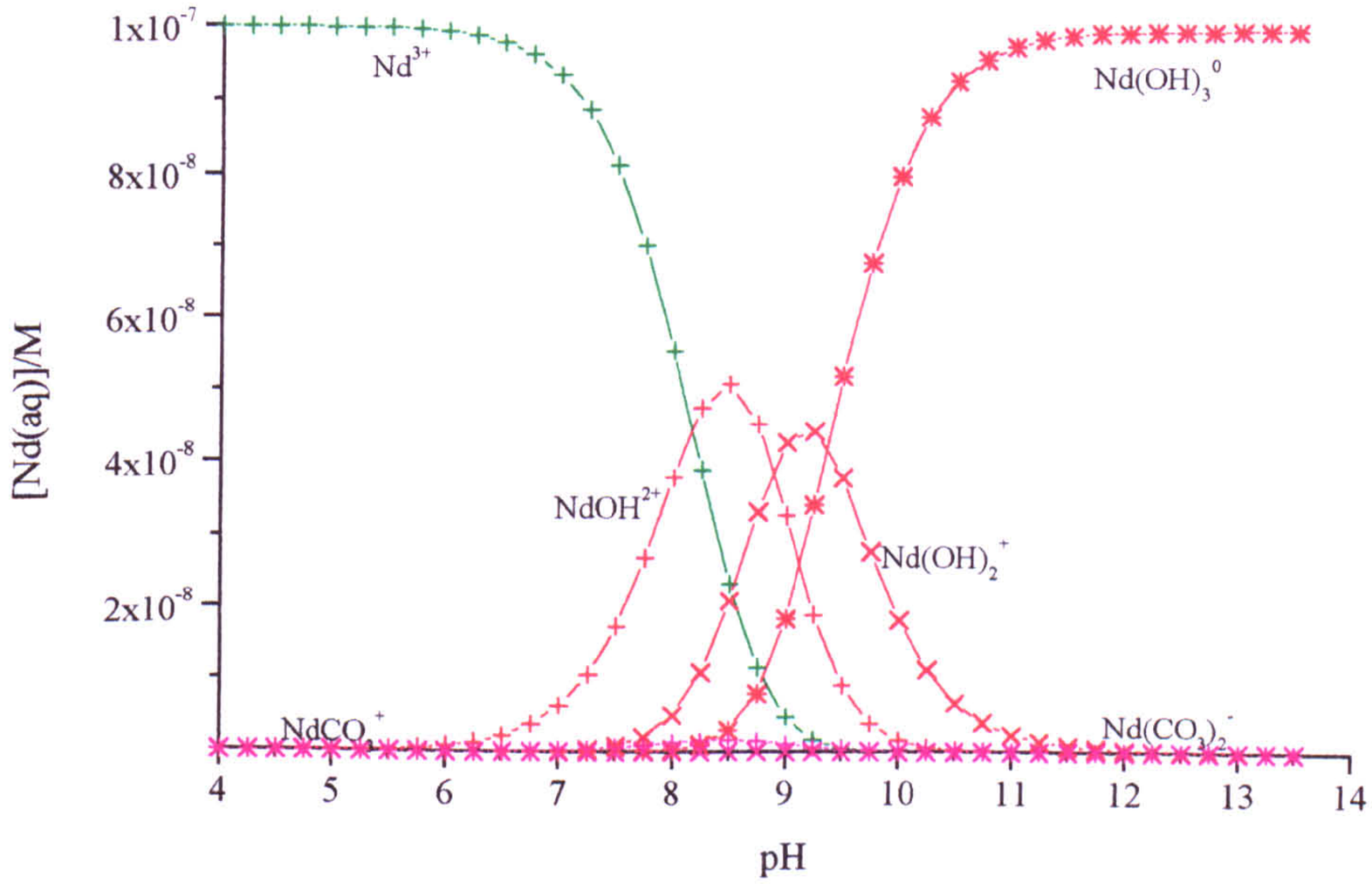

Figure 4.8 The aqueous speciation of 10^{-7}M Nd in 10^{-2}M TIC after Lee & Byrne (1992 & 1993)

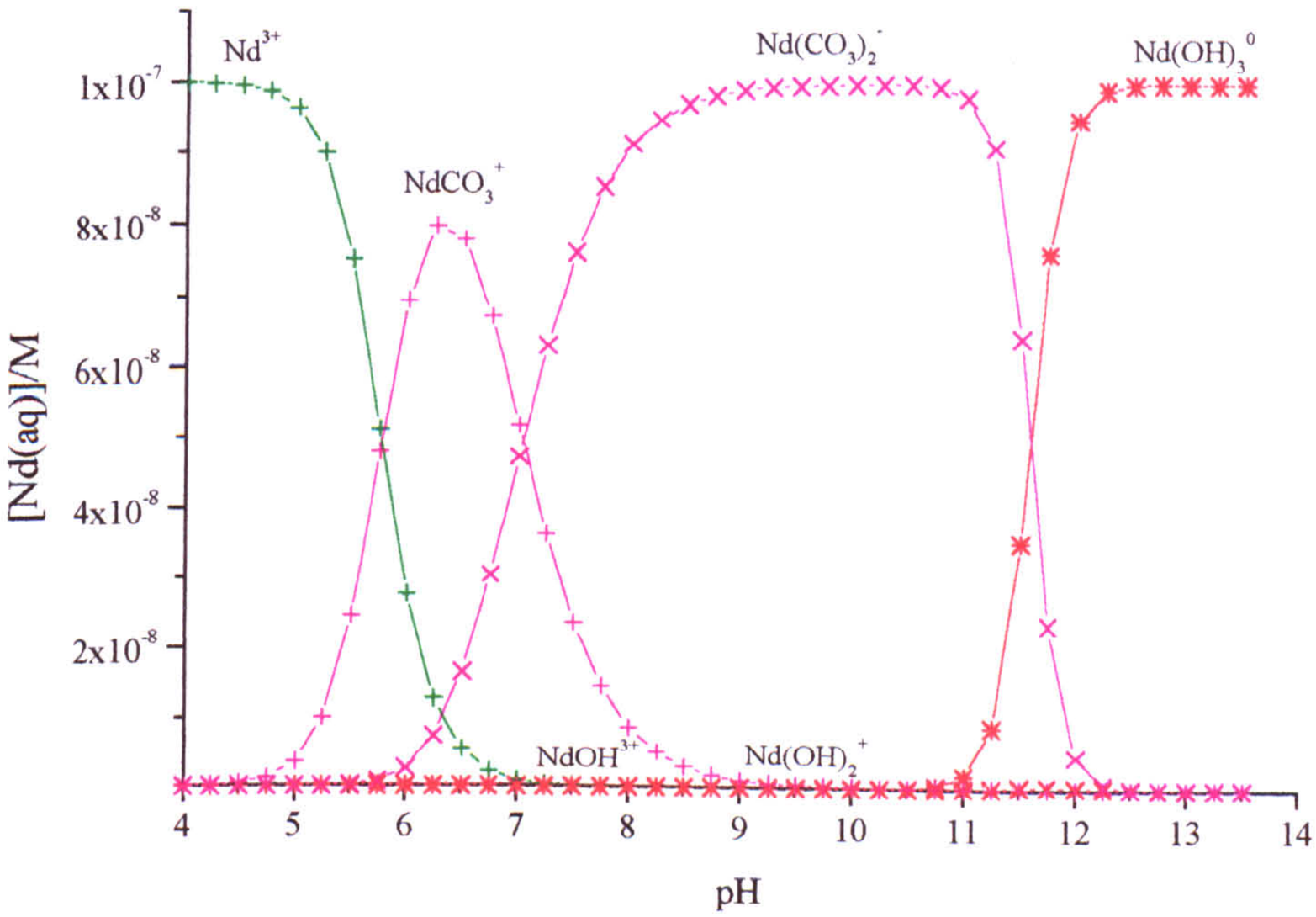

The pH vs aqueous lanthanide species diagrams (Figures 4.7 and 4.8) indicate that under most conditions there is only a single dominant aqueous lanthanide species. This dominant aqueous species can be superimposed on the pH vs [CO_3^{2-}] (Figure 4.9) and pH vs [TIC] (Figure 4.10) stability field diagrams. The aqueous-aqueous phase relationships are calculated in the same way as the solid-solid phase relationships and are shown in Appendix 4.14 for the Lee & Byrne (1992 & 1993) aqueous lanthanide stability constants.

The aqueous stability field diagrams are originally calculated as pH vs [CO_3^{2-}] (Figure 4.9), which are then converted into a pH vs [TIC] diagram (Figure 4.10). They indicate that Ln^{3+} will be the dominant aqueous phase at low pH under all TIC activities. Similarly $Ln(OH)_3^0(aq)$ will be the dominant lanthanide aqueous phase at high pH. There is a minimum amount of total carbonate (10^{-6}M TIC) required for an aqueous lanthanide carbonate species ($LnCO_3^+$) to be the dominant aqueous species. Increasing the [TIC] further will then convert the $LnCO_3^+(aq)$ to $Ln(CO_3)_2^-(aq)$. When the pH decreases below pH 8, a steady increase in the [TIC] is required to form the aqueous lanthanide carbonate species.

Figure 4.9 Stability field diagram for the solid phase and dominant aqueous lanthanide species in the Na-Nd-CO_3^{2-}-OH system at 298.15K and 1 atm pressure, $[Na^+]$ = 10mM (Lee & Byrne, 1992 and 1993 aqueous constants)

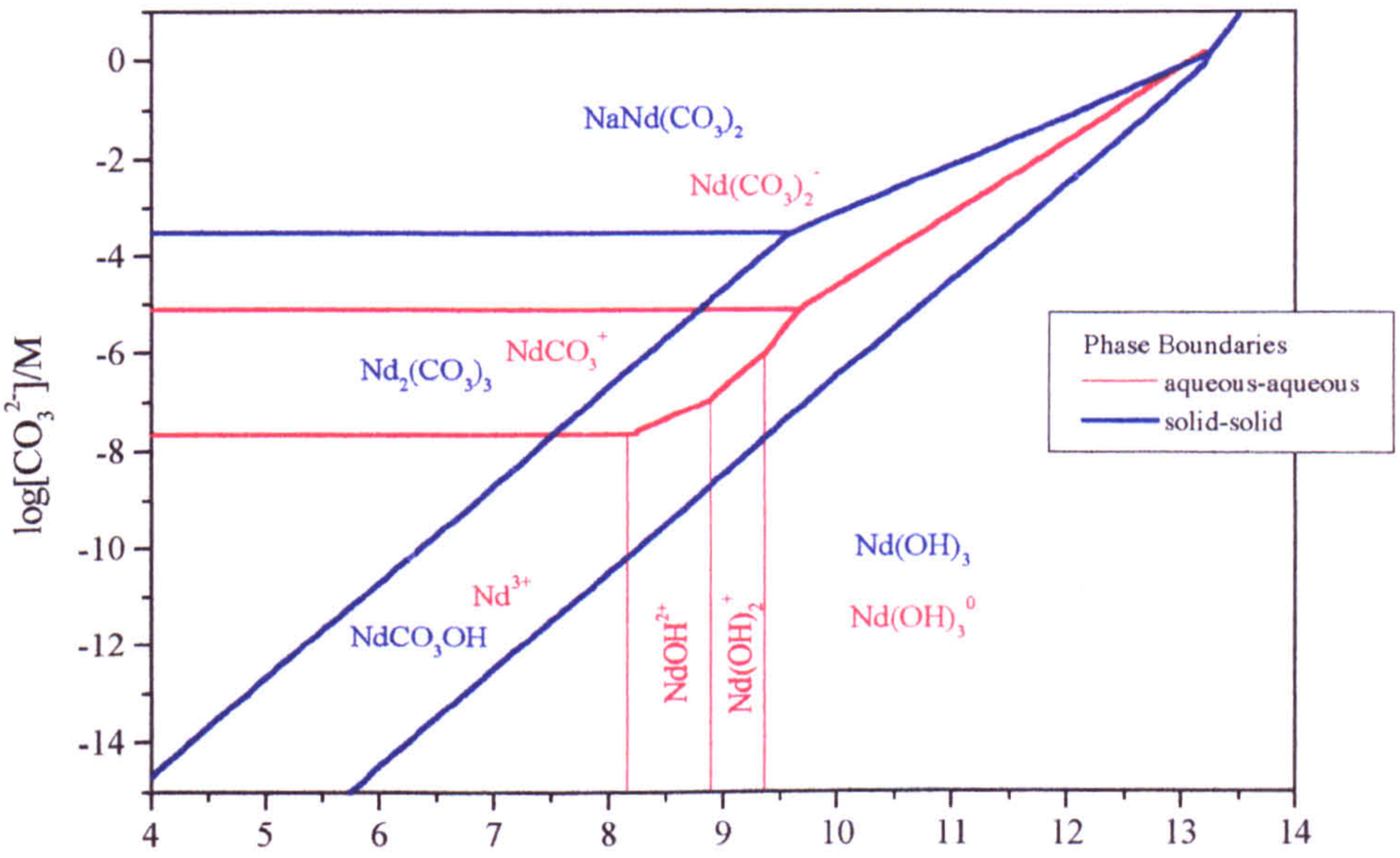

Figure 4.10 Stability field diagram for the solid phase and dominant aqueous lanthanide species in the Na-Nd-TIC-OH system at 298.15K and 1 atm pressure, $[Na^+]$ = 10mM (Lee & Byrne, 1992 and 1993 aqueous constants)

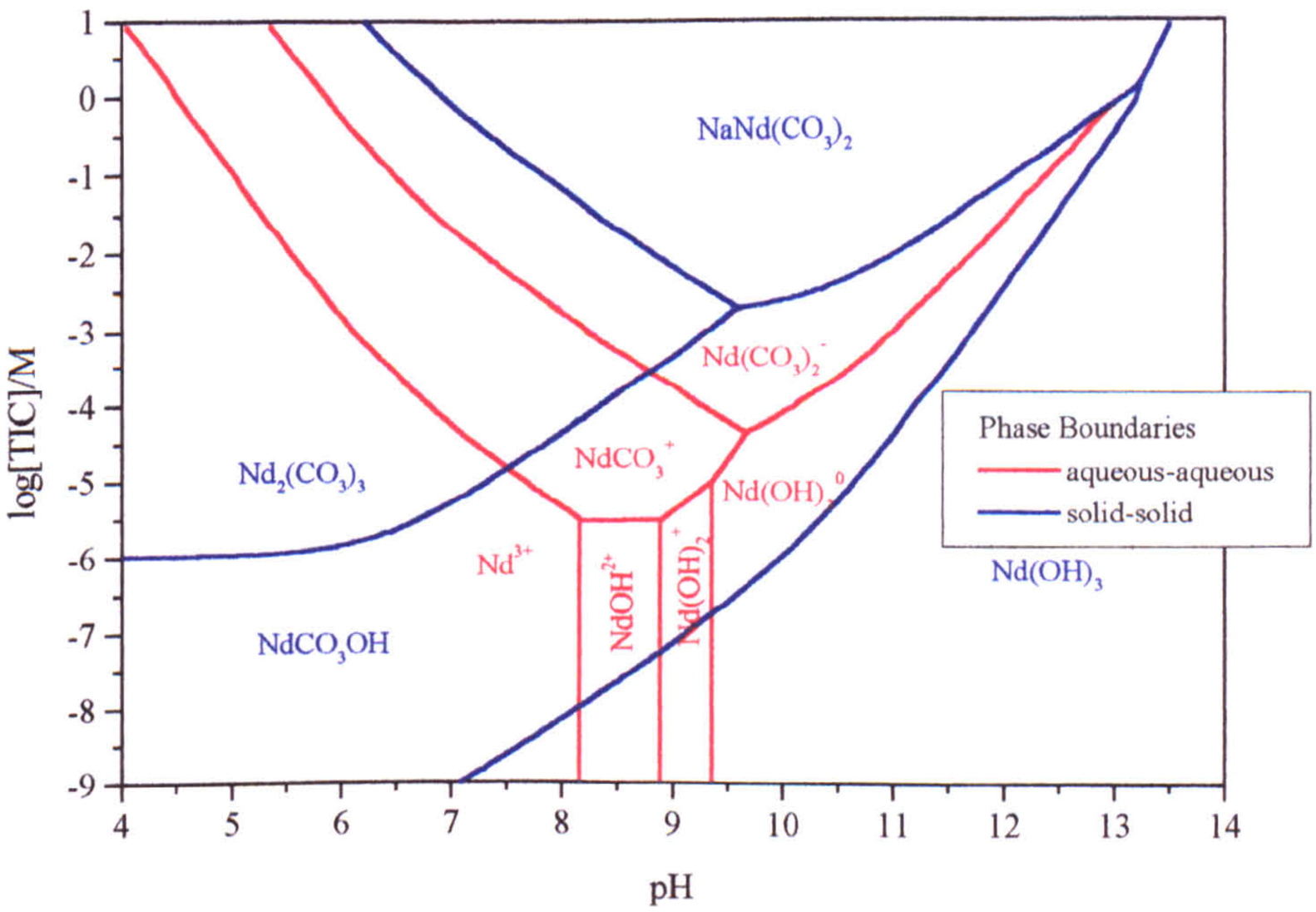

If each solid phase is assumed to be in equilibrium with the dominant aqueous species under any specific conditions then an estimation can be made of the total lanthanide solubility of each solid phase under all the pH and TIC conditions modelled. An estimation of the lanthanide solubility can be calculated from the difference between the Gibbs free energy of formation of each solid phase and the dominant aqueous phase (utilising Lee & Byrne, 1992 &1993 aqueous phase stability constants).

Figure 4.11 Contoured Nd solubility diagram, superimposed upon the solid-solid and aqueous-aqueous phase in the Na-Nd-TIC-OH system at 298.15K and 1 atm pressure

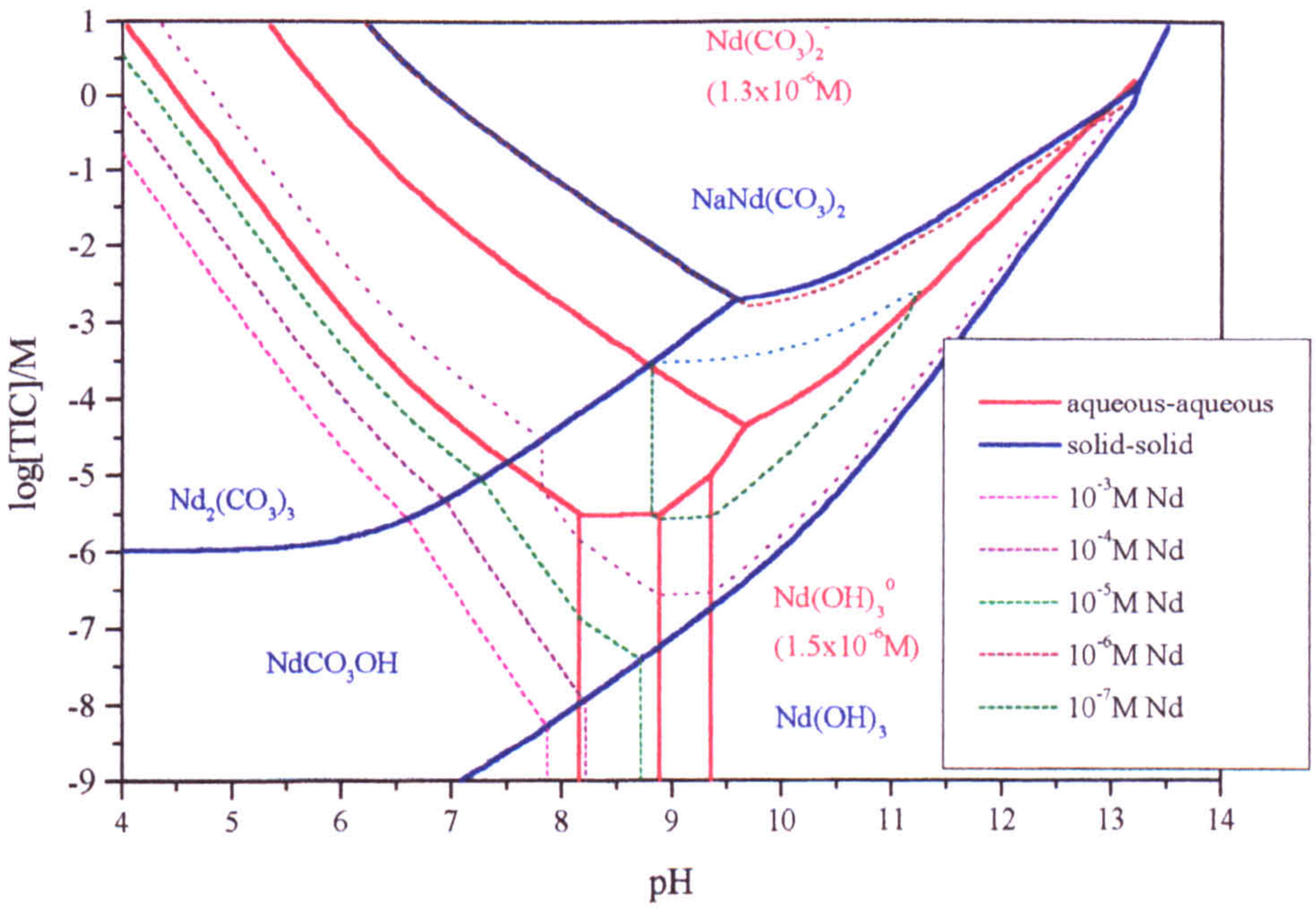

The contoured lanthanide solubility diagram (Figure 4.11, calculated from Appendix 4.15) indicates that the lanthanide solubility increases for all phases as the pH decreases below pH 8, especially if the TIC concentration also decreases. There is a solubility minimum of less than 10^{-7}M total aqueous lanthanide at the centre of the diagram. The solubility minimum forms where the aqueous $Ln(OH)_3^0$-$LnCO_3^+$-$Ln(CO_3)_2^-$ and the $Ln(OH)_2^+$-$Ln(OH)_3^0$-$LnCO_3^+$ species intersect, at approximately $2x10^{-8}$M Nd in a $8x10^{-5}$M TIC and pH 9.6.

The aqueous lanthanide solubility increases with increasing pH into the region controlled by $Nd(OH)_3$ (solid and aqueous). The lanthanide solubility decreases

until $Nd(OH)_3(s)$ is in equilibrium with $Nd(OH)_3(aq)$. The Nd solubility is then dependent on the reaction between these two phases and gives an equilibrium Nd concentration of $1.5x10^{-6}$ M.

When the TIC concentration is increased above that of the solubility minimum there is also an increase in Nd solubility. When solid $Nd_2(CO_3)_3$ and $NdCO_3OH$ convert to $NaNd(CO_3)_2$ the dominant aqueous species is $Nd(CO_3)_2^-$. The Nd solubility is therefore dependant on the equilibrium reaction constant and Na^+ activity. The Nd concentration in the contoured solubility diagram is therefore independent of pH and the TIC concentration, as $NaNd(CO_3)_2$ is in equilibrium with $Nd(CO_3)_2^-$ (equation 4.82) but is dependant on the sodium activity and reaction constant. In a 10mM Na^+ solution the total aqueous Nd in equilibrium with $NaNd(CO_3)_2$ will be approximately $1.3x10^{-6}$ M.

$$NaNd(CO_3)_2 = Na^+ + Nd(CO_3)_2^- \qquad (4.82)$$

If the Na^+ activity was increased so that the $NaNd(CO_3)_2$ phase was in equilibrium with $NdCO_3^+$ or $Nd(OH)_3^0(aq)$, then the $NaNd(CO_3)_2$ in these regions would be dependent on the carbonate activity and pH of the system, however the minimum $NaNd(CO_3)_2$ solubility would also decrease when in equilibrium with $Nd(CO_3)_2^-$.

Nd phases are extremely soluble at low total carbonate concentrations. In solutions with less than 10^{-8}M TIC, Nd solubility becomes independent of the TIC content of the solution and total aqueous Nd concentrations above 1mM will be found below pH 8.

4.7.4 Lanthanide solubility vs pH

The contoured solubility diagrams give a good estimation of the lanthanide solubility over the entire range of the stability field diagram (Figure 4.11) and can therefore be used to identify the areas of minimum or maximum lanthanide solubility. These diagrams do indicate that the total lanthanide solubility will change sharply at solid and aqueous phase boundaries and under specific

conditions the lanthanide solubility may be broadly independent, or solely dependent on the pH or TIC activity of the system. However, the method used to calculate the lanthanide solubility (by considering a single aqueous species in equilibrium with the solid phase) does not consider any of the other aqueous interactions in complex solutions. These include the interactions between aqueous carbonate with the lanthanide ions themselves, other lanthanide species or multiple cations which may be in solution.

The solubility of the lanthanides can also be calculated with PHREEQC for any solution composition. The lanthanide solubility can than be presented as a series of $[Ln]_{total}$ vs pH or other parameter (e.g. Na or TIC activities) for any solid phases that are to be considered. PHREEQC was developed to model the stability of any series of minerals under geochemical conditions, i.e. to determine the solubility of mineral phases in equilibrium with complex but known (or predicted) groundwater compositions. The model overcomes the difficulties of multiple aqueous species for each element and the interactions between ions in a multi-component system, which cannot easily be introduced into a pH vs $[CO_3^{2-}]$ stability field diagram.

A profile of $[Ln]_{total}$ vs pH for each of the solid phases to be considered can be constructed by considering each phase in equilibrium with a solution at variable pH from pH 4 to 14. The pH can be varied by adding elements to the system which are known to have minimal interactions to the system studied, e.g. KOH to increase the solution pH or HCl to reduce the pH. The model will then calculate the total lanthanide solubility and the concentration of each aqueous species that can form in that system. Then a saturation index is calculated for any solid phase that could form from the calculated equilibrium solution. The saturation index will only indicate whether other solid phases are more or less soluble than the target phase under those conditions, but will not be considered in the calculation

When the $[Ln]_{total}$ vs pH of all the solid phases are plotted on the same diagram (for the same bulk solution composition, i.e. equilibrium [TIC]), then the least soluble phase will be the solubility limiting phase. In a real solution, the more soluble phases would dissolve with the concurrent precipitation of the solubility

limiting phase. The $[Ln]_{total}$ vs pH profile is effectively a cross-section at constant TIC of the pH vs [TIC] contoured solubility diagram.

If the Nd carbonate and hydroxide phases are placed in equilibrium with 50mM Na and TIC, (Figure 4.12), all four phases will be solubility limiting at different pH ranges. $Nd_2(CO_3)_3$ below pH 7, $NaNd(CO_3)_2$ from pH 7 to 11.5, $NdCO_3OH$ from pH 11.5 to 12.5 and $Nd(OH)_3$ above pH 12.5. The minimum Nd solubility of $2x10^{-7}M$, forms in equilibrium $NaNd(CO_3)_2$, the Nd solubility in this region is broadly independent of pH. The $Nd_2(CO_3)_3$ solubility increases sharply with decreasing pH below pH 6, the Nd solubility increases to $5x10^{-3}M$ Nd by pH 4.5. The solubility of $Nd(OH)_3$ is independent of pH above pH 12.5 at $10^{-6}M$.

Reducing the Na and TIC concentrations to 1mM, (Figure 4.13), changes the solubility limiting phases. $NaNd(CO_3)_2$ will not become the solubility limiting. $Nd_2(CO_3)_3$ is the solubility limiting phase up to pH 9.5, but the total Nd solubility increases from a minimum ($3x10^{-7}M$ Nd) at pH 8 to $1x10^{-6}M$ as pH increases towards pH 9.5. The $NdCO_3OH$ solubility then decreases to $2x10^{-7}M$ at pH 11, before rising to $1x10^{-6}M$ at pH 11.5, when $Nd(OH)_3$ becomes the solubility limiting phase.

The Nd solubility profiles (Figures 4.12 and 4.13), are in good agreement with the contoured solubility diagram (Figure 4.11). In general there is a sharp increase in Nd solubility at low pH, $NaNd(CO_3)_2$ is the solubility limiting phase over the mid pH range at high Na^+ activities, $NdCO_3OH$ will not form under these conditions. Similarly $NaNd(CO_3)_2$ does not form in low TIC and Na systems. $Nd(OH)_3$ is the stable high pH phase, and the Nd solubility is independent of pH, above pH 12. There are only slight differences between the two types of diagrams, at low TIC concentrations the contoured solubility diagram are restricted to the contour interval and do not include the interactions of multiple aqueous lanthanide species, therefore small discrepancies become apparent.

The solubility of Eu in a 50mM Na and TIC solution (Figure 4.14), is similar to the Nd solubility diagram (Figure 4.12), however the Eu solubility ($2x10^{-6}$ M at

pH 8) is slightly greater than the Nd solubility ($2x10^{-7}M$ at pH 8) under the same conditions. $Eu_2(CO_3)_3$ is the solubility limiting phase below pH 7, $NaEu(CO_3)_2$ from pH 7 to 11.5, then $Eu(OH)_3$ above pH 11.5. $EuCO_3OH$ is significantly more soluble than the other phases and will not become solubility limiting. $Eu(OH)_3$ is significantly less soluble than the other Eu phases. $Eu(OH)_3$ solubility decreases sharply from pH 10 to pH 12, in the pH region expected for the aqueous speciation change from $Eu(CO_3)_2^-$ or $EuCO_3^+$ to $Eu(OH)_3^0$.

When the Na and TIC concentrations are reduced to 1mM (Figure 4.15), $NaEu(CO_3)_2$ will not form as a solubility limiting phase. $Eu_2(CO_3)_3$ solubility follows a similar profile to $Nd_2(CO_3)_3$ (Figure 4.13), of a solubility minimum at pH 7, then an increase in Eu solubility until intersecting the $EuCO_3OH$ solubility profile. Between pH 10 and 10.5, $EuCO_3OH$ is the solubility limiting phase within a narrow pH region, confirming the narrow stability field indicated in Figure 4.6, which appears to be almost a triple point. $Eu(OH)_3$ then becomes the solubility limiting phase pH 10.5. The Eu solubility decreases to a minimum at pH 11.5, and is then unaffected by increasing the solution pH.

Figure 4.12 The solubility of various Nd solid phases in
[Na] = 50mM and [TIC] = 50mM at 298.15K and 1 atm pressure
(This work, Lee & Byrne 1992 & 1993)

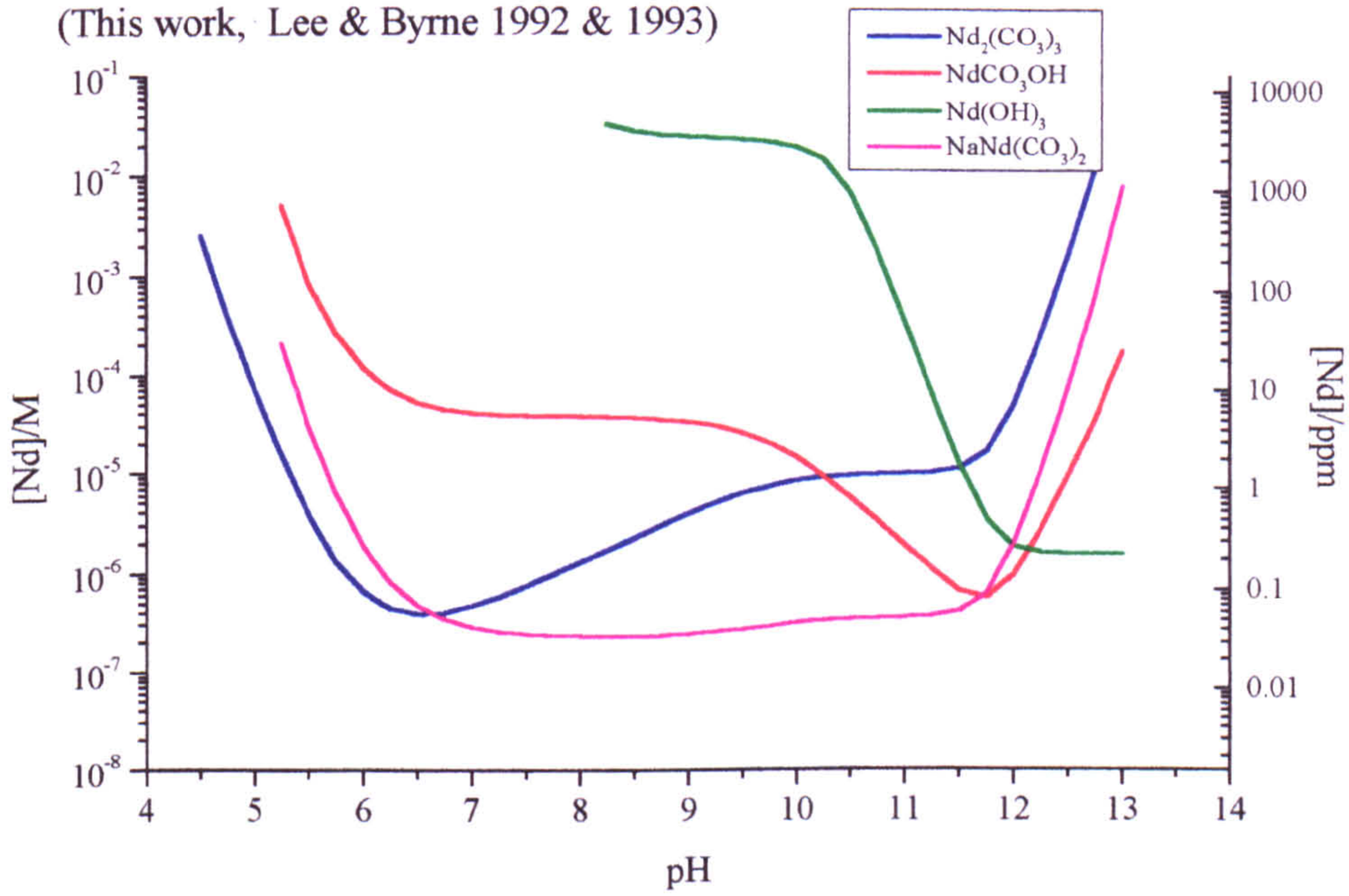

Figure 4.13 The solubility of various Nd solid phases in
[Na] = 1mM and [TIC] = 1mM at 298.15K and 1 atm pressure
(This work, Lee & Byrne 1992 & 1993)

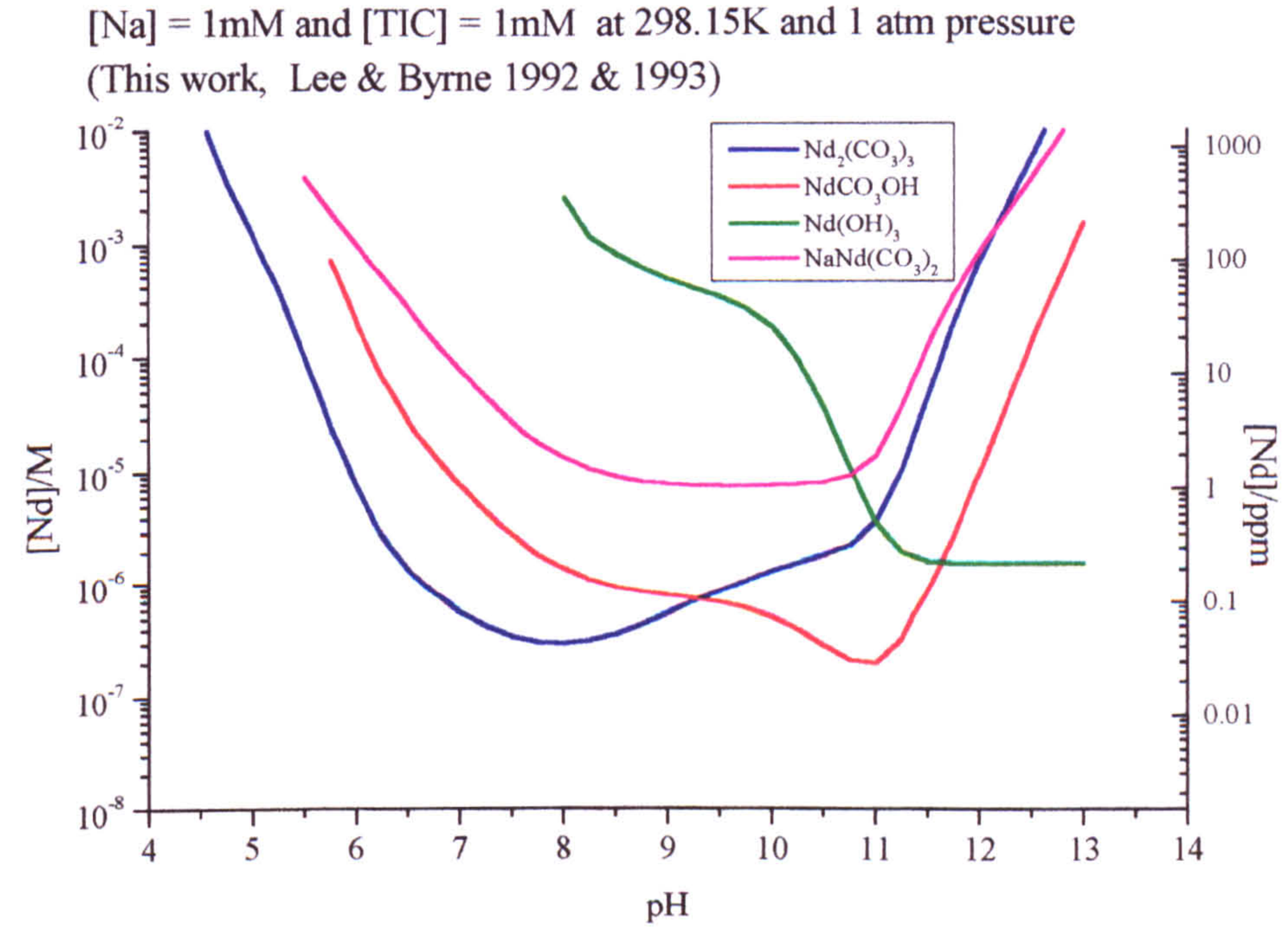

Figure 4.14 The solubility of various Eu solid phases in
[Na] = 50mM and [TIC] = 50mM at 298.15K and 1 atm pressure
(This work, Lee & Byrne 1992 & 1993)

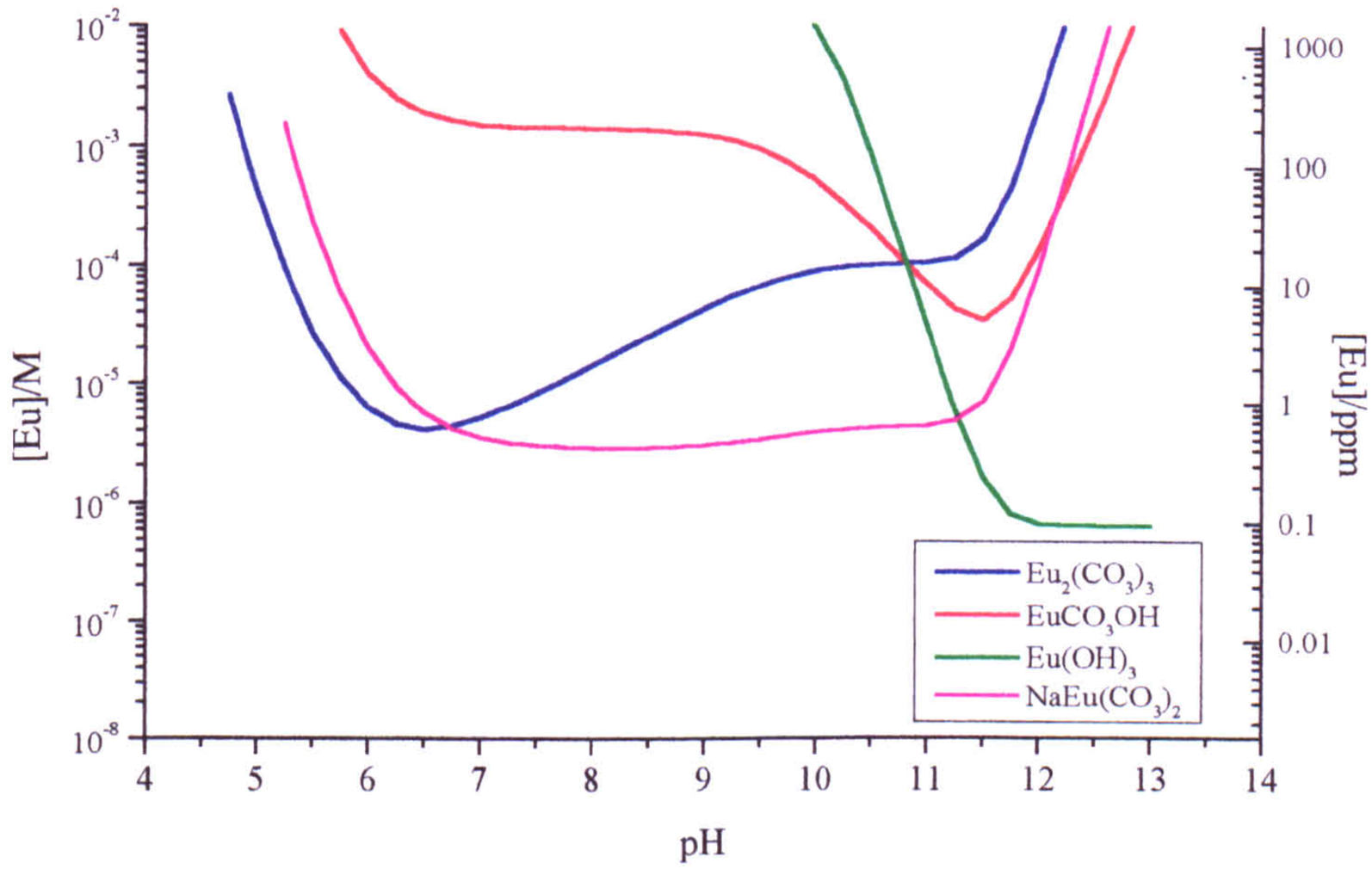

Figure 4.15 The solubility of various Eu solid phases in
[Na] = 1mM and [TIC] = 1mM at 298.15K and 1 atm pressure
(This work, Lee & Byrne 1992 & 1993)

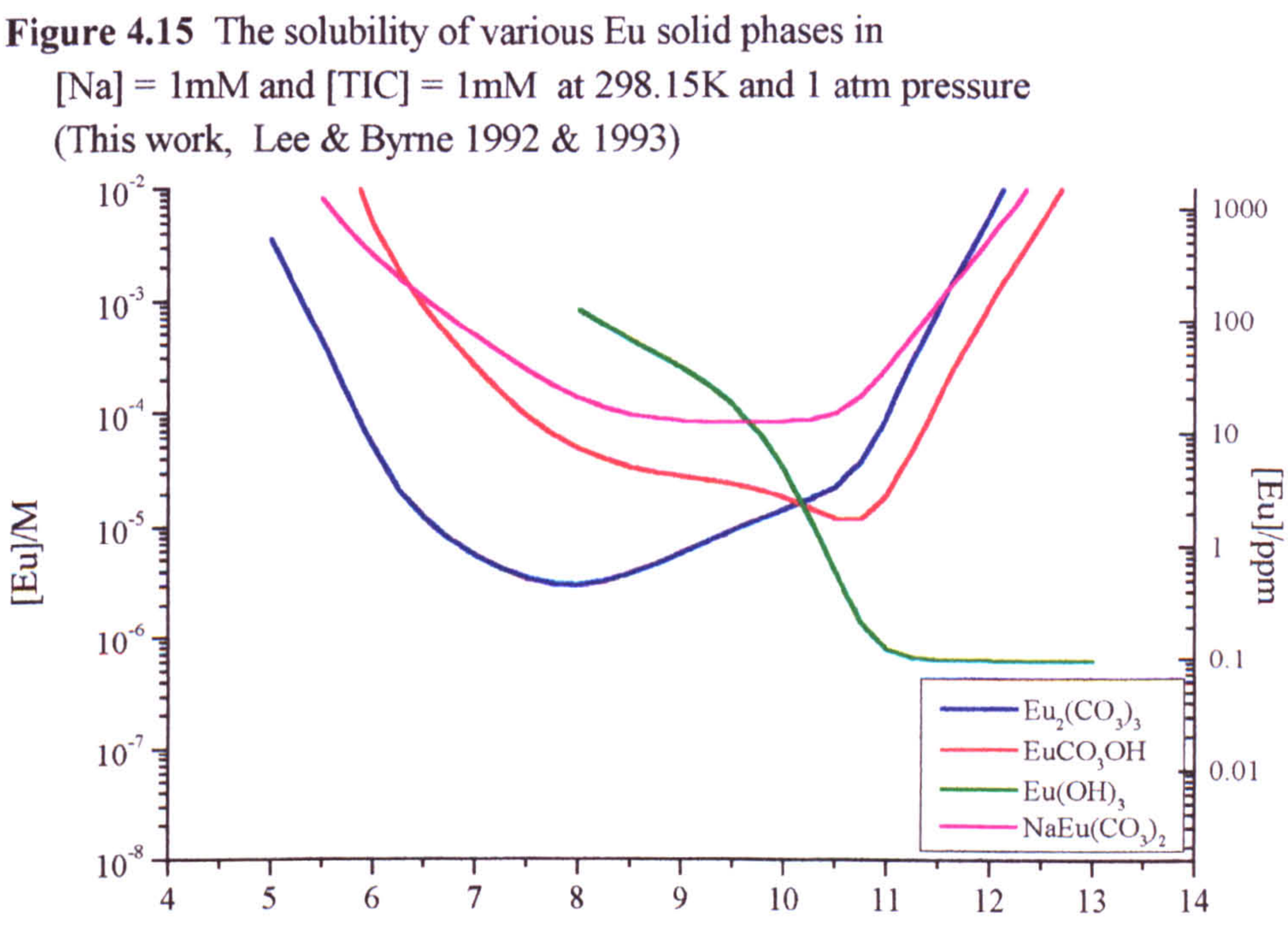

4.7.5 The effects of aqueous speciation on solubility

A series of cross-sections over the pH vs [TIC] contoured stability field diagram (Figure 4.11) indicates that the solubility minimum will vary in total aqueous lanthanide concentration, pH and [TIC]. The interactions between the solid phase and the predicted aqueous composition, even when a phase is not solubility limiting, will explain why each phase is only solubility limiting under specific bulk solution compositions. Each of the aqueous lanthanide species can be plotted on a lanthanide versus pH diagram in a similar manner to the total lanthanide versus pH diagrams in Section 4.7.4. The aqueous speciation will be shown for a single solid phase per diagram for clarity.

The contoured solubility diagram (Figure 4.11) and the $[Nd]_{total}$ vs pH plots (Figure 4.13 and 4.14) indicate that there is not a simple relationship between the lanthanide concentration and the bulk solution composition. For example, the solubility of Nd, in equilibrium with a $NdCO_3OH$ solid phase would be expected to have an inverse relationship with the carbonate activity at constant pH from the solubility reaction (equation 4.83) i.e. as carbonate increases, Nd^{3+} should decrease.

$$LnCO_3OH = Ln^{3+} + CO_3^{2-} + OH^- \qquad (4.83)$$

Increasing the TIC activity actually increases the lanthanide solubility (Figure 4.16), and $NdCO_3OH$ is less soluble in 0.1mM TIC than in 100mM TIC as shown in the contoured solubility diagram (Figure 4.11)

From pH 5 to 7 there is a sharp decrease in $NdCO_3OH$ solubility with increasing pH. At high [TIC] the solubility of $NdCO_3OH$ is independent of pH between pH 7 and 10, this region extends with an increasing [TIC]. Above pH 10 there is a sharp reduction in $NdCO_3OH$ solubility to a minimum at pH 12, followed by a sharp increase in $NdCO_3OH$ solubility. In lower [TIC] solutions, $NdCO_3OH$ solubility continues to decrease with increasing pH, to a minimum at pH 9 to 10. Above pH 10 there is then a sharp increase in $NdCO_3OH$ solubility. The solubility minimum is significantly lower in low [TIC] solutions than high [TIC] solutions.

Figure 4.16 The solubility of $NdCO_3OH$ in carbonate solution at 298.15K and 1 atm pressure, (this work, Lee & Byrne 1992 and 1993)

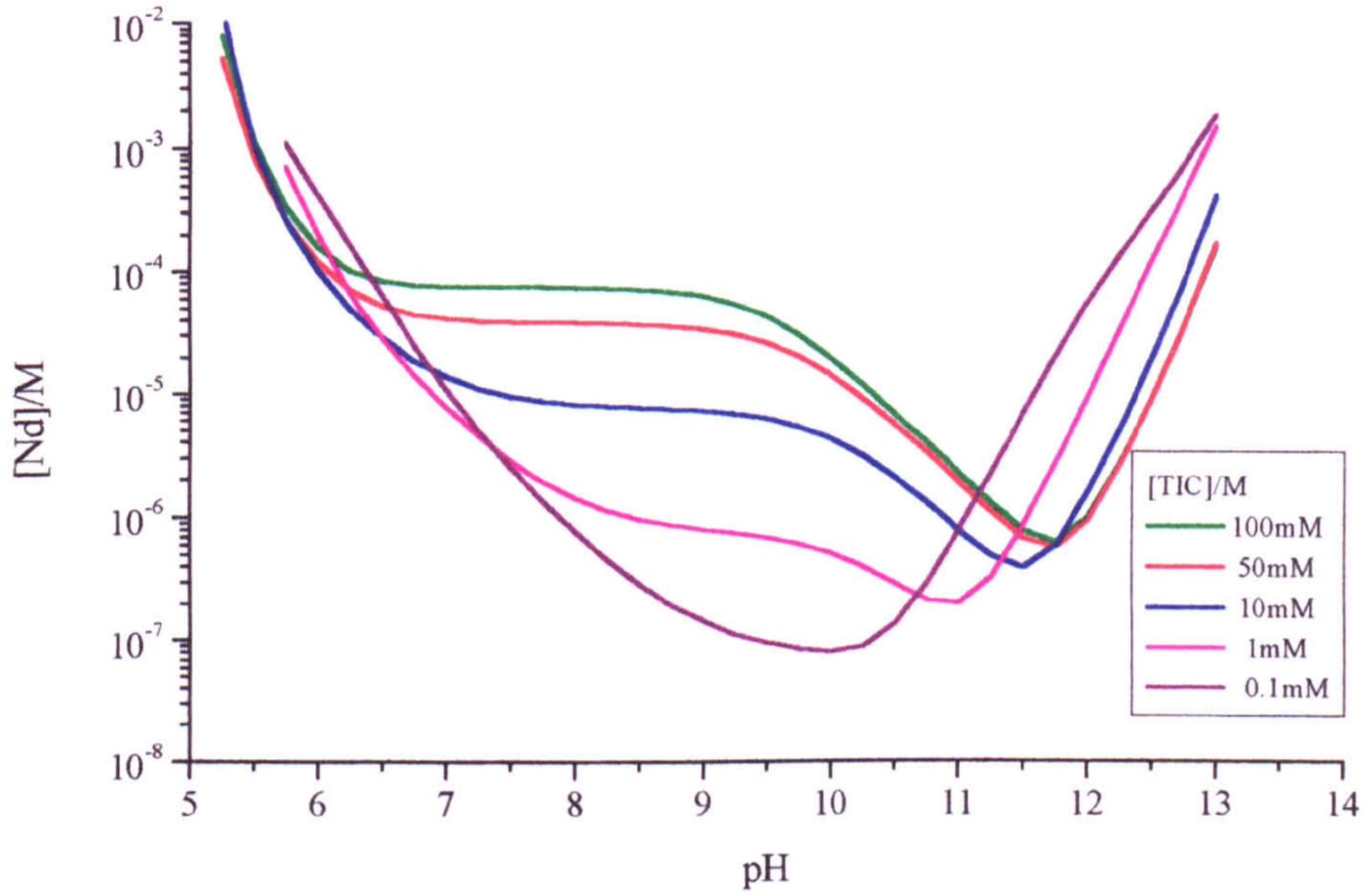

When $NdCO_3OH$ becomes the solubility limiting phase there is initially almost a constant Nd solubility with increasing pH then a sharp drop in Nd solubility (shown in Figure 4.16 and the 10^{-7}M Nd contour in Figure 4.11 contoured solubility diagram). The increase in Nd solubility, from the effects of the $Nd(CO_3)_2^-$ complex, are countered by the increasing OH^- in solution to give a constant aqueous $[Nd]_{total}$ with increasing pH.

The dominant aqueous phase between pH 7 and 11 is $Nd(CO_3)_2^-$ therefore the equilibrium formed as CO_3^{2-} increases (equation 4.84)

$$NdCO_3OH + CO_3^{2-} = Nd(CO_3)_2^- + OH^- \qquad (4.84)$$

The solubility of $NdCO_3OH$ decreases to a minimum at pH 12 (Figure 4.17) as the proportion of $Nd(OH)_3^0$ (aq) increases in solution and $Nd(CO_3)_2^-$(aq) decreases. $NdCO_3OH$ solubility increases above pH 12 when aqueous and solid hydroxy phases control lanthanide solubility and $Nd(OH)_3$(s) becomes the solubility-limiting phase.

The solubility of $NdCO_3OH$ in 0.1M $NaHCO_3$ solutions (Figure 4.18) does not plateau as severely as in higher carbonate solutions as $Nd(CO_3)_2^-$ has a limited

effect on the aqueous speciation, however the minimum solubility occurs in the small area when $Nd(CO_3)_2^-$ is the dominant aqueous species.

Figure 4.17 $NdCO_3OH$ solubility and aqueous species concentrations in [TIC] = 50mM at 298.15K and 1 atm pressure (this work, Lee & Byrne 1992/3)

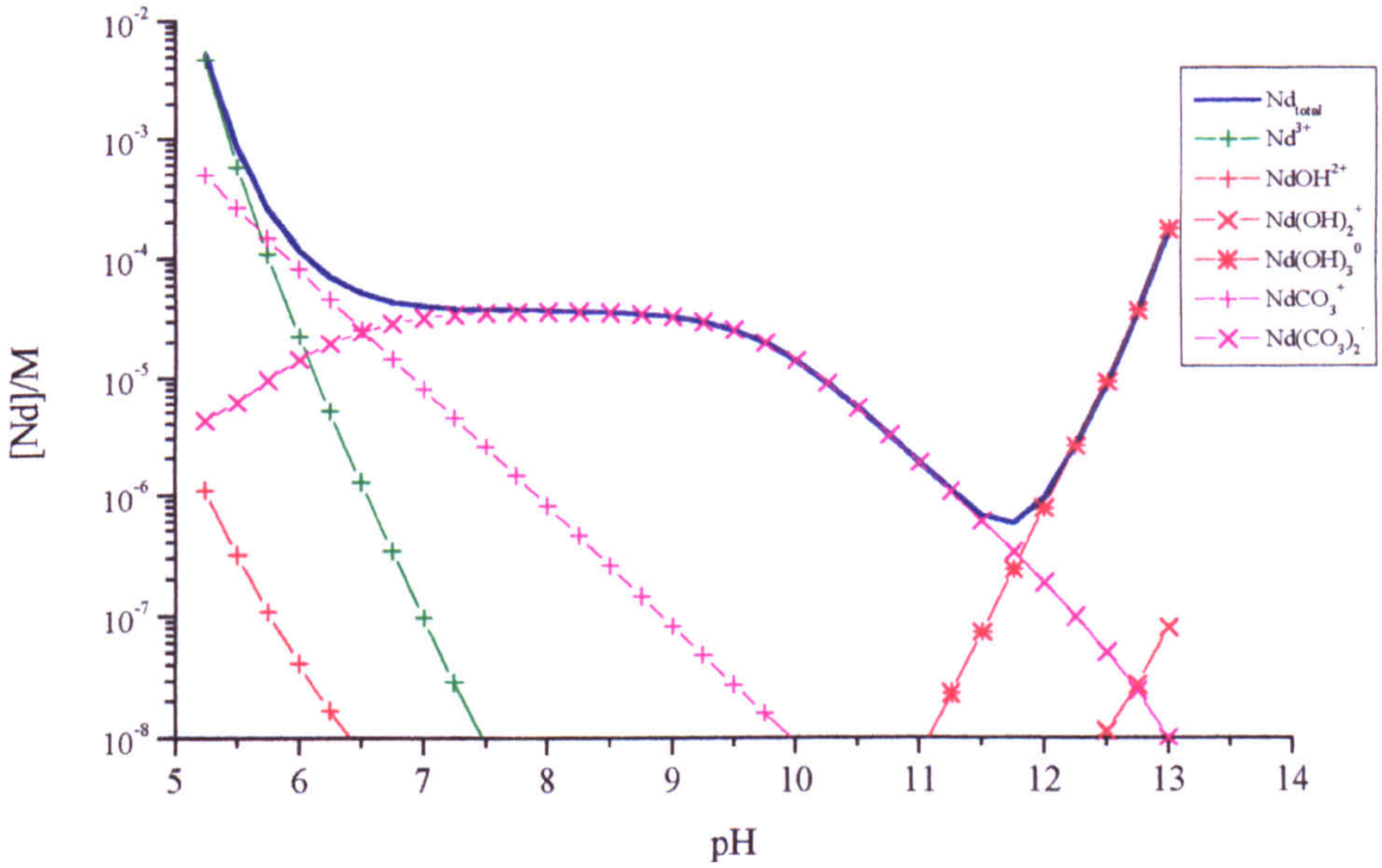

Figure 4.18 $NdCO_3OH$ solubility and aqueous species concentrations in in [TIC] = 0.1mM at 298.15K and 1 atm pressure (this work, Lee & Byrne 1992/3)

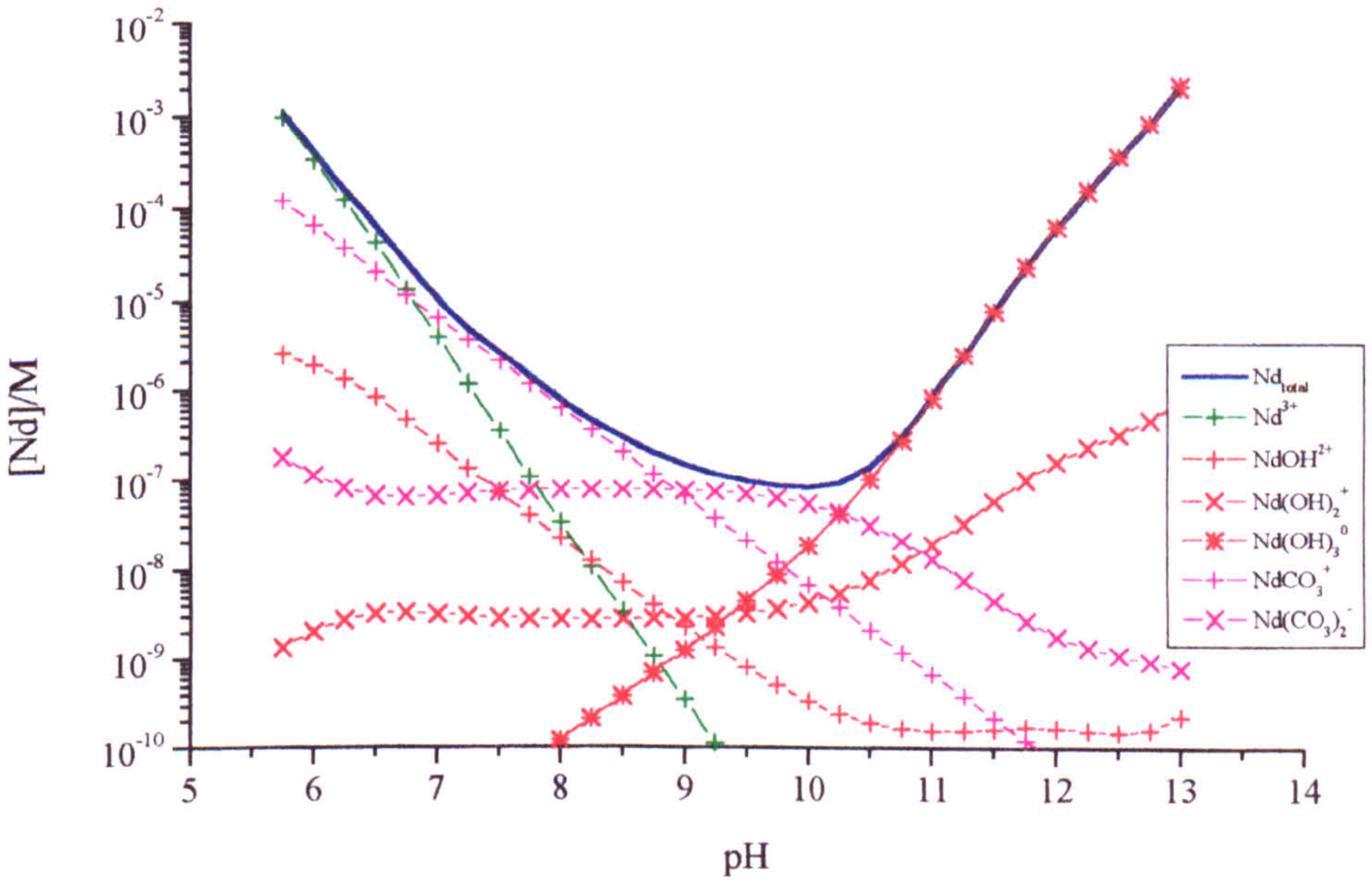

In Na^+ free systems, where $NaNd(CO_3)_2$ will not form , $NdCO_3OH$ is in equilibrium with $Nd^{3+}(aq)$ at low pH, i.e. below pH 6, Figures 4.17 and 4.18).

An increase in the carbonate activity or pH of the solution will decrease the solubility of $NdCO_3OH$, (equation 4.85)

$$NdCO_3OH(s) \longrightarrow Nd^{3+}(aq) + CO_3^{2-}(aq) + OH^-(aq) \qquad (4.85)$$

As the pH of the solution increases further aqueous lanthanide carbonate species become dominant, however when $NdCO_3^+$ is the dominant aqueous species, the solubility of $NdCO_3OH$ will still decrease with increasing pH (equation 4.86)

$$NdCO_3OH(s) \longrightarrow LnCO_3^+(aq) + OH^-(aq) \qquad (4.86)$$

When $Nd(CO_3)_2^-$ becomes the dominant aqueous species, then an increase in CO_3^{2-} activity actually increases the solubility of $NdCO_3OH$ (equation 4.87)

$$NdCO_3OH(s) + CO_3^{2-}(aq) \longrightarrow Nd(CO_3)_2^-(aq) + OH^-(aq) \quad (4.87)$$

The solubility of $NdCO_3OH$ appears to be constant as pH increases (Figure 4.17) when $Nd(CO_3)_2^-$ is the only significant aqueous species, as any expected decrease in the $NdCO_3OH$ solubility is offset by the increasing $CO_3^{2-}(aq)$ activity (at constant $[TIC]_{total}$) as pH increases. Below 10^{-4}M TIC, $Nd(CO_3)_2^-$ is not the only significant aqueous lanthanide species, therefore this plateau effect is eliminated (Figure 4.18) and the $NdCO_3OH$ solubility continues to fall to a minimum.

The solubility of $NdCO_3OH$ in high [TIC] solutions will only decrease from this plateau, when the proportion of $Nd(CO_3)_2^-$ in solution decreases at high pH. A minimum $NdCO_3OH$ solubility then occurs at the aqueous phase equilibrium between $Nd(OH)_3^0(aq)$ and $Nd(CO_3)_2^-$. A further increase in pH when $Nd(OH)_3^0(aq)$ is the only significant aqueous lanthanide species, will decrease the solubility of $NdCO_3OH$ (equation 4.88).

$$NdCO_3OH(aq) + 2OH^- \longrightarrow Nd(OH)_3^0(aq) + CO_3^{2-}(aq) \qquad (4.88)$$

However increasing the CO_3^{2-} activity in this situation will also increase the amount of aqueous $Ln(CO_3)_2^-$ in solution and the solubility minimum is pushed to a higher pH.

In solutions where the CO_3^{2-} activity is too low to form even $NdCO_3^+$ (below $1x10^{-6}$M TIC), then $NdOH^{2+}$ and $Nd(OH)_2^+$ will be the dominant lanthanide aqueous phases between pH 8 and 9.5. The solubility of $NdCO_3OH$ will increase slightly in this region above the minimum $NdCO_3OH$ solubility as CO_3^{2-} is released into the solution, (equations 4.89 and 4.90)

$$NdCO_3OH(s) \longrightarrow NdOH^{2+}(aq) + CO_3^{2-} \quad (4.89)$$
$$NdCO_3OH(s) + OH^- \longrightarrow Nd(OH)_2^+(aq) + CO_3^{2-}(aq) \quad (4.90)$$

Increasing the pH when the $Nd(OH)_2^+$ species is dominant, will increase the solubility of $NdCO_3OH$. The minimum $NdCO_3OH$ solubility will therefore be close to the equilibrium transition between the aqueous $NdCO_3^+$ and $NdOH^{2+}$ phases.

At high pH and at all carbonate concentrations, $NdCO_3OH$ is highly soluble, and $Nd(OH)_3(s)$ becomes the solubility limiting phase. Above pH 12 $Nd(OH)_3(aq)$ is the only significant aqueous phase, the total aqueous Nd will be independent of pH (equation 4.91) and depend on the reaction constant between these two phase.

$$Nd(OH)_3(s) \longrightarrow Nd(OH)_3(aq) \quad (4.91)$$

$Nd(OH)_3$ solubility will increase significantly as pH is reduced and $Nd(OH)_3^0(aq)$ is no longer the dominant aqueous species, either from the equilibrium with the aqueous carbonate species $LnCO_3^+$and $Ln(CO_3)_2^-$ or with the aqueous hydroxy species $Nd(OH)_2^+$(equations 4.92 to 4.94)

$$Nd(OH)_3(s) + 2CO_3^{2-} \longrightarrow Nd(CO_3)_2^-(aq) + 3OH^-(aq) \quad (4.92)$$
$$Nd(OH)_3(s) + CO_3^{2-} \longrightarrow NdCO_3^+(aq) + 3OH^-(aq) \quad (4.93)$$
$$Nd(OH)_3(s) \longrightarrow Nd(OH)_2^+(aq) + OH^-(aq) \quad (4.94)$$

When $Nd(OH)_3(s)$ is in equilibrium with $Nd(CO_3)_2^-(aq)$ there is an abrupt increase in solubility over a small pH range (Appendix 4.16 and Figure 4.12). The increase in $Nd(OH)_3$ solubility as pH decreases is more gradual in lower [TIC] solutions, when either $LnCO_3^+$ or $Ln(OH)_2^+$ are the dominant aqueous phases. Therefore $Nd(OH)_3(s)$ will only be the solubility limiting phase from pH 10 in solutions above 10^{-6}M TIC.

$Nd_2(CO_3)_3$ solubility which initially follows a pattern of increasing the aqueous carbonate concentration, will decrease Nd solubility. A pH transverse across a pH vs $[Ln]_{total}$ plot at constant TIC shows $Nd_2(CO_3)_3$ solubility decreases as pH increases, when in equilibrium with Nd^{3+}(equation 4.95) to a minimum when in equilibrium with $LnCO_3^+$(equation 4.96), due to the relative increase in aqueous CO_3^{2-} in the solution at constant [TIC]. The total Nd solubility then increases slightly when $Nd(CO_3)_2^-$ (equation 4.97)is the dominant aqueous species (Appendix 4.16). The increase in Nd solubility is not immediately apparent on the contoured solubility diagram (Figure 4.11).

$$Nd_2(CO_3)_3(s) \longrightarrow 2Nd^{3+}(aq) + 3CO_3^{2-}(aq) \qquad (4.95)$$
$$Nd_2(CO_3)_3(s) \longrightarrow 2NdCO_3^{+}(aq) + CO_3^{2-}(aq) \qquad (4.96)$$
$$Nd_2(CO_3)_3(s) + CO_3^{2-}(aq) \longrightarrow 2Nd(CO_3)_2^{-}(aq) \qquad (4.97)$$

When the increase in $Nd_2(CO_3)_3$ solubility intersects with the decrease in $NdCO_3OH$ solubility, then the solubility limiting phase will change. However even below pH 6, at extremely low carbonate concentrations (e.g. below 10^{-6}M TIC), $Nd_2(CO_3)_3$ will alter to $NdCO_3OH$, but only in equilibrium with extremely high total lanthanide activities.

$NaNd(CO_3)_2$ solubility (Appendix 4.18) decreases to a minimum between pH 7 and 11 with the formation of aqueous $Ln(CO_3)_2^-$ from the relationship (equation 4.98)

$$NaLn(CO_3)_2 = Ln(CO_3)_2^- + Na^+ \qquad (4.98)$$

$NaLn(CO_3)_2$ solubility increases sharply at the high and low ends of the pH scale. Below pH 6 when $NdCO_3^+$ is the dominant aqueous phase and CO_3^{2-} activity decreases in solution, or at high pH when $Nd(OH)_3^0$ becomes the dominant aqueous species above pH 11. If the Na^+ activity is also increased, then the $NaNd(CO_3)_2$ stability field will expand to lower TIC activities between pH 7 and 11, and the minimum Nd solubility in equilibrium will decrease. There will however be a similar sharp increase in the total Nd solubility across the aqueous phase boundaries, as seen at each of the pH extremes.

4.8 Ce Stability field diagrams

Cerium solubility is controlled by three factors, the carbonate activity, pH and pe in solution. The Na^+ activity is not a controlling factor. $Ce_2(CO_3)_3$ forms below pH 7, but then any Ce hydroxy phases which may form oxidise immediately to CeO_2 above pH 9 in mildly oxidising conditions. The direct oxidation to CeO_2 even in 0.1M Na^+ and TIC solutions suggests that the cerium double carbonate will not form in any natural solutions, which typically have carbonate and sodium concentrations below 10mM. $NaCe(CO_3)_2$ has been considered however it will only form at TIC concentrations above the level shown in the following diagrams, and therefore is not considered in the following stability field diagrams.

.

The standard form to present a stability field diagram, which includes a redox reaction is by a pH vs pe diagram. A pH vs pe stability field diagram for Ce in a carbonate solution (Figure 4.19), indicates that $Ce_2(CO_3)_3$ will form at a lower pe than CeO_2 (at constant pH). As the pH of a solution increases, the pe required to oxidise $Ce_2(CO_3)_3$ to CeO_2 decreases. Increasing the carbonate activity of the solution has the opposite effect of increasing the pH or the pe required for the phase change.

The Ce stability field diagrams can also be presented on a typical pH vs $[CO_3^{2-}]$ stability field diagram (Figure 4.20), then plotting the stability field over a pe range. The $Ce_2(CO_3)_3$-CeO_2 stability fields in a pH vs $\log[CO_3^{2-}]$ diagram indicates there is a linear stability field boundary between the two phases, indicating that an increase in pH is required to convert $Ce_2(CO_3)_3$ to CeO_2. The CeO_2 stability field will also increase with an increasing pe, i.e. as the solution becomes more oxidising.

If the $\log[CO_3^{2-}]$ is converted to log[TIC], (section 4.7.2), $Ce_2(CO_3)_3$ will be the stable phase above 10^{-9}M TIC (Figure 4.21), at pH 5 (even in solutions at pe 5). The oxidation of Ce^{3+} to Ce^{4+} will occur above pH 9 in 10^{-6}M TIC at pe 0.

Figure 4.19 Stability field diagram for the Ce-pH-pe system at various TIC concentrations, 298.15K and 1 atm pressure

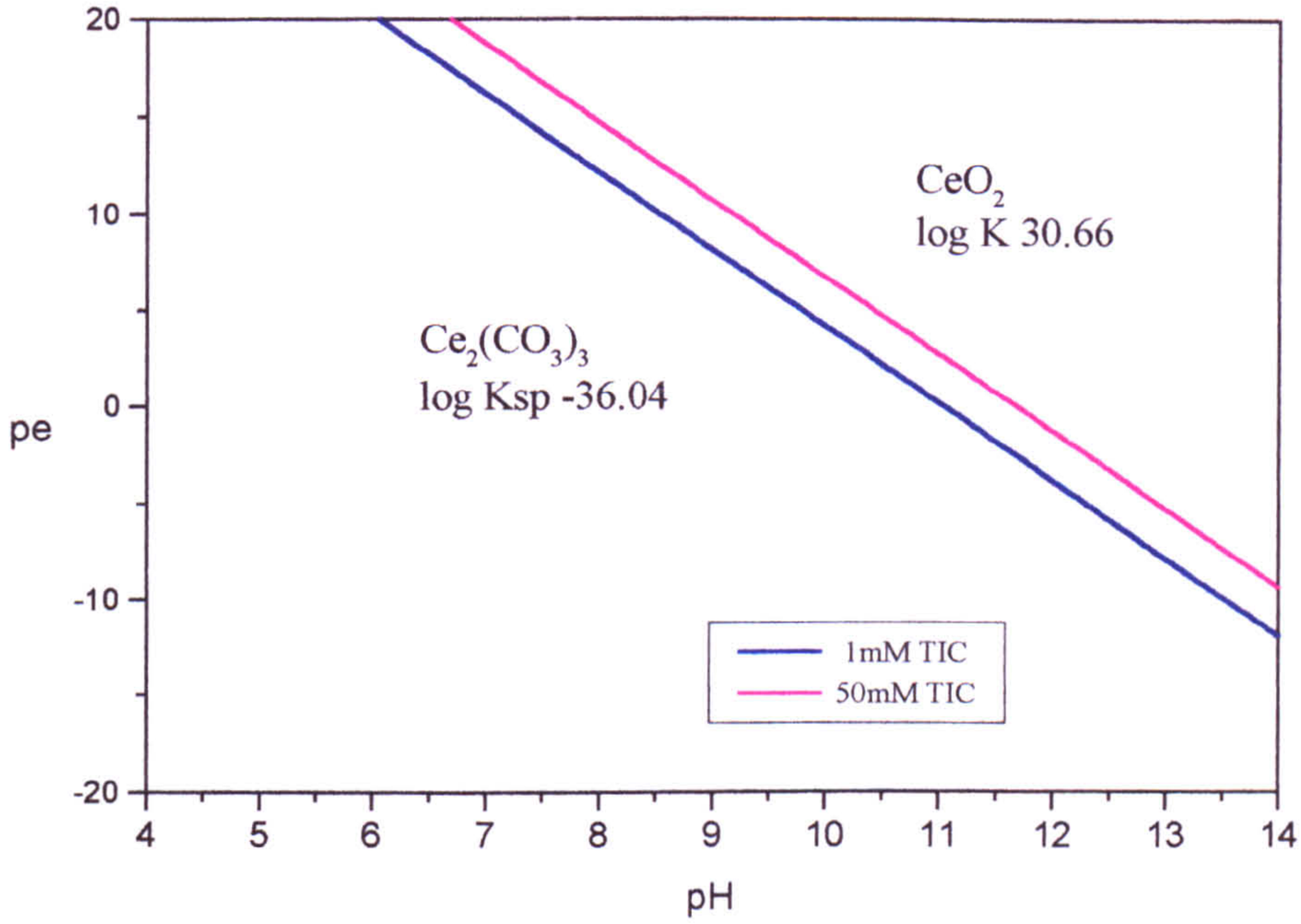

Figure 4.20 Stability field diagram for the Ce-CO_3^{2-}-OH system at varied pe at 298.15K and 1 atm pressure

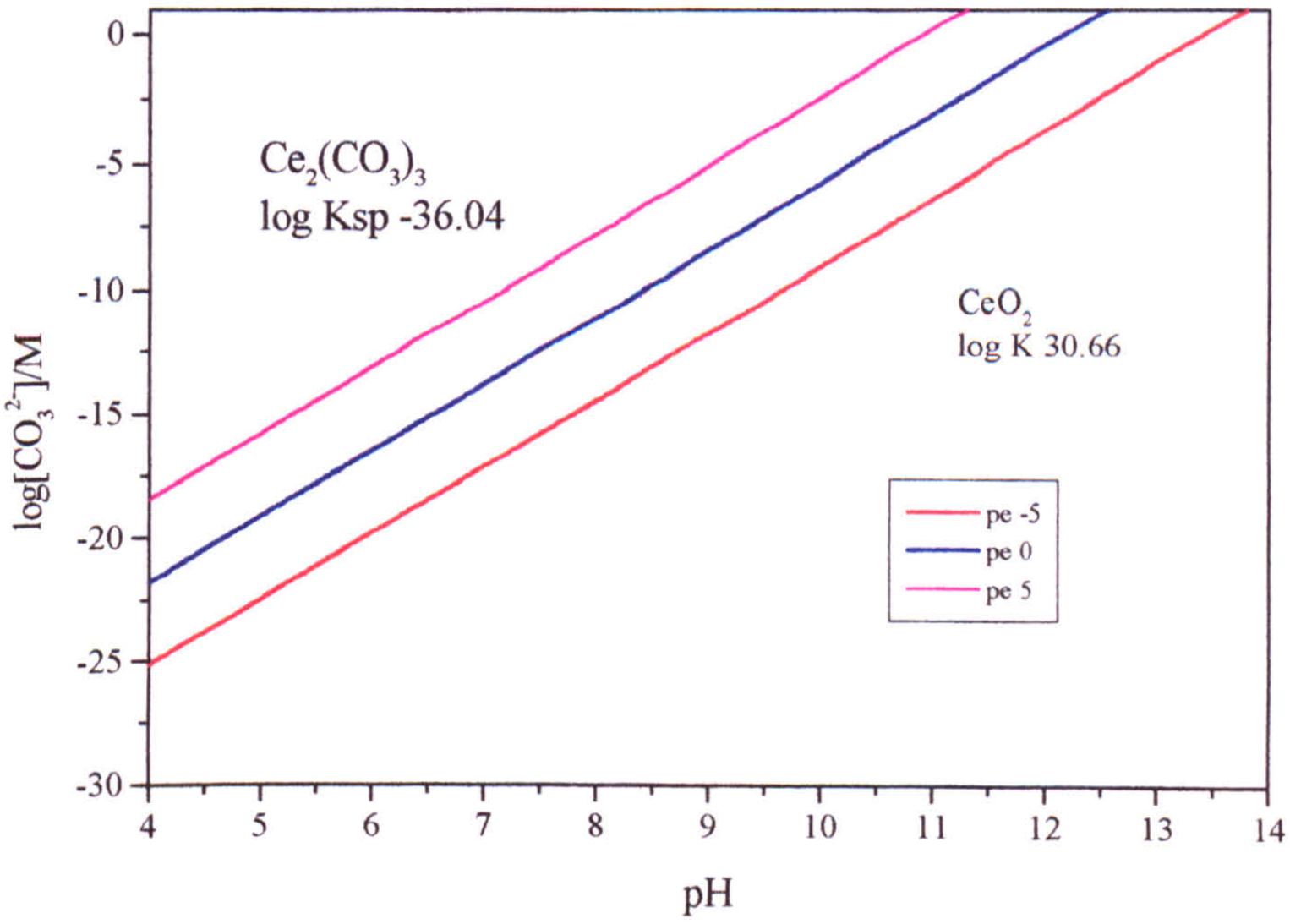

Figure 4.21 Stability field diagram for the Ce-TIC-OH system at varied pe at 298.15K and 1 atm pressure

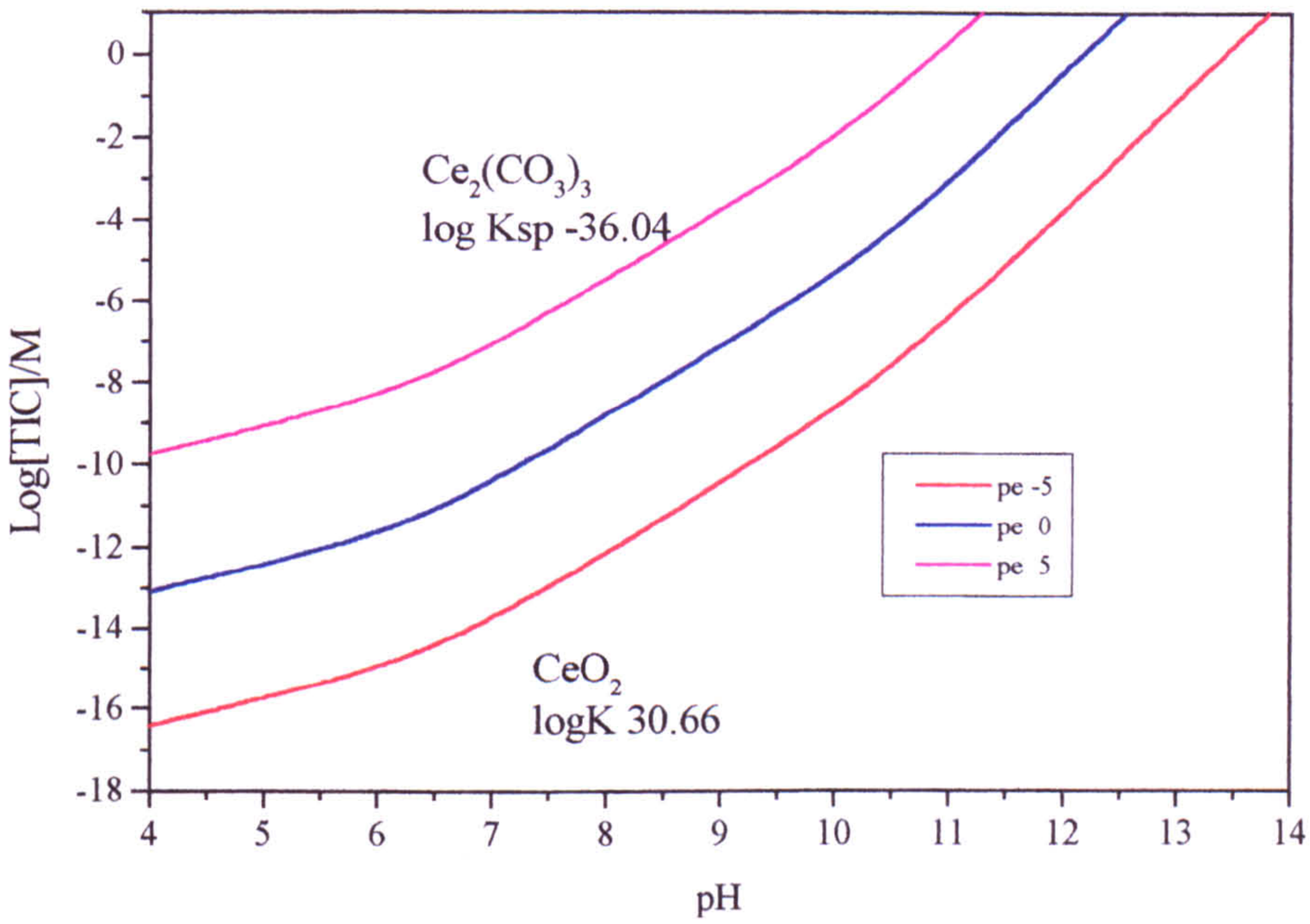

A pH vs log$[Ce]_{total}$ plot for $Ce_2(CO_3)_3$ and CeO_2 (Figures 4.22 and 4.23), indicates that $Ce_2(CO_3)_3$ will be the solubility limiting phase at low pH. In 1mM and 50mM TIC solutions, $Ce_2(CO_3)_3$ has a similar solubility with a solubility minimum of approximately $[Ce]_{total}$ 10^{-8}M at pH 6.5 to 7. The $Ce_2(CO_3)_3$ solubility is at least an order of magnitude lower than the equivalent Nd and Eu solubility minima's. $Ce_2(CO_3)_3$ solubility increases slightly above pH 7.

CeO_2 solubility is dependent on the pe of the solution. An increase in the solution pe from pe 0 to 5, will decrease the pH of the solid phase transition from pH 11.5 to 9.5. Baes & Mesmer (1986) have proposed a solubility of $Ce(OH)_3$ (from free-energy calculations and interpolations) of log K 19.9, assuming the oxidation from Ce^{3+} to Ce^{4+}. If the pe of the solution is reduced to below pe 0, then $Ce(OH)_3$ could become the solubility limiting phase above pH 11.5. The minimum solubility of CeO_2 (in solutions above pe 0) is considerably less than $Nd(OH)_3$ or $Eu(OH)_3$ and continues to decrease as pH increases.

$NaCe(CO_3)_2$ is significantly more soluble than $Ce_2(CO_3)_3$ and CeO_2 in a 50mM Na and TIC solution, and therefore will not become the solubility limiting phase, unless the Na^+ and TIC activities are significantly increased.

Figure 4.22 The solubility of various Ce phases in [Na] = 50mM, [TIC] = 50mM at 298.15K and 1 atm pressure

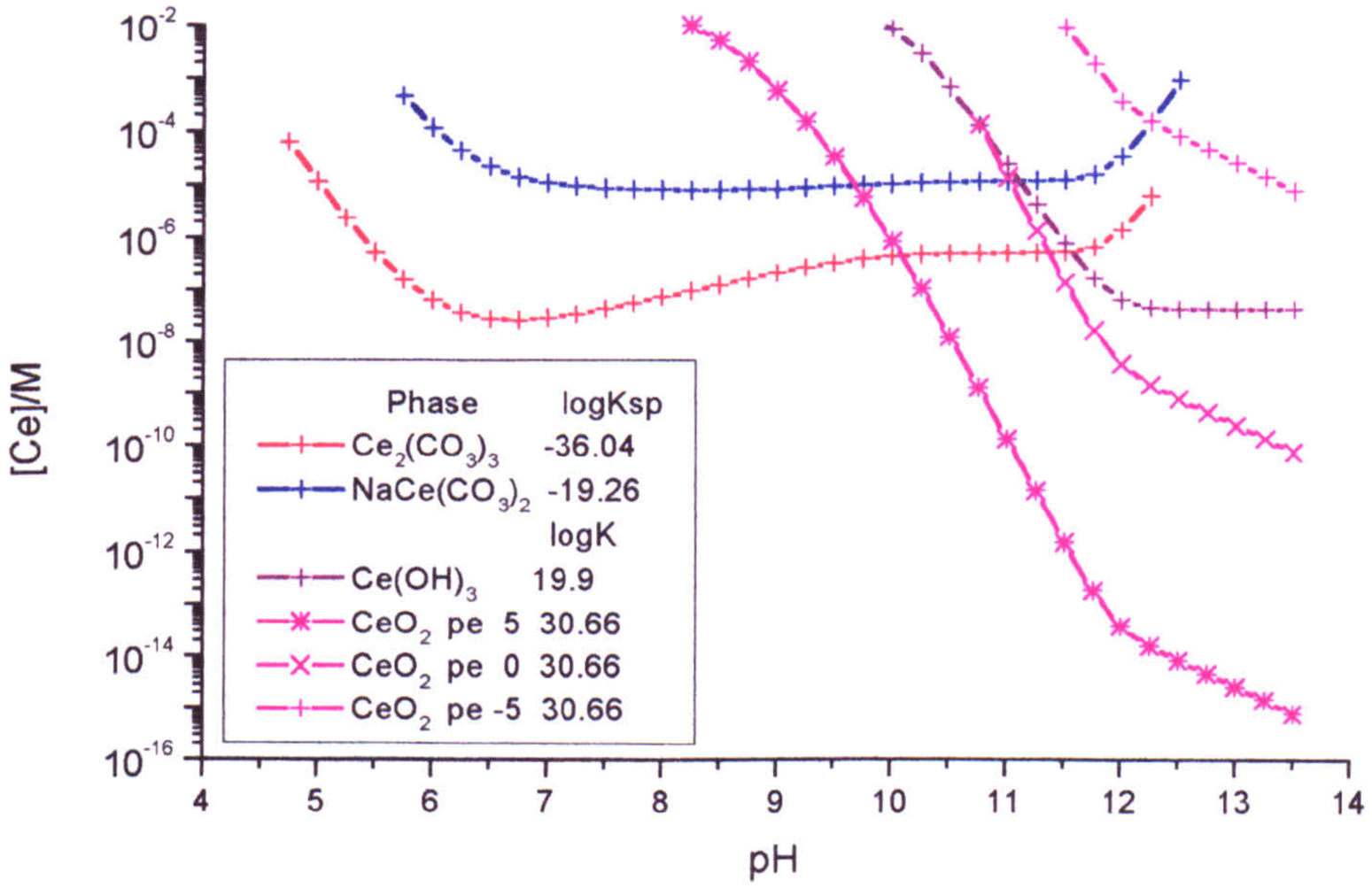

Figure 4.23 The solubility of various Ce phases in [Na] = 50mM, [TIC] = 50mM at 298.15K and 1 atm pressure

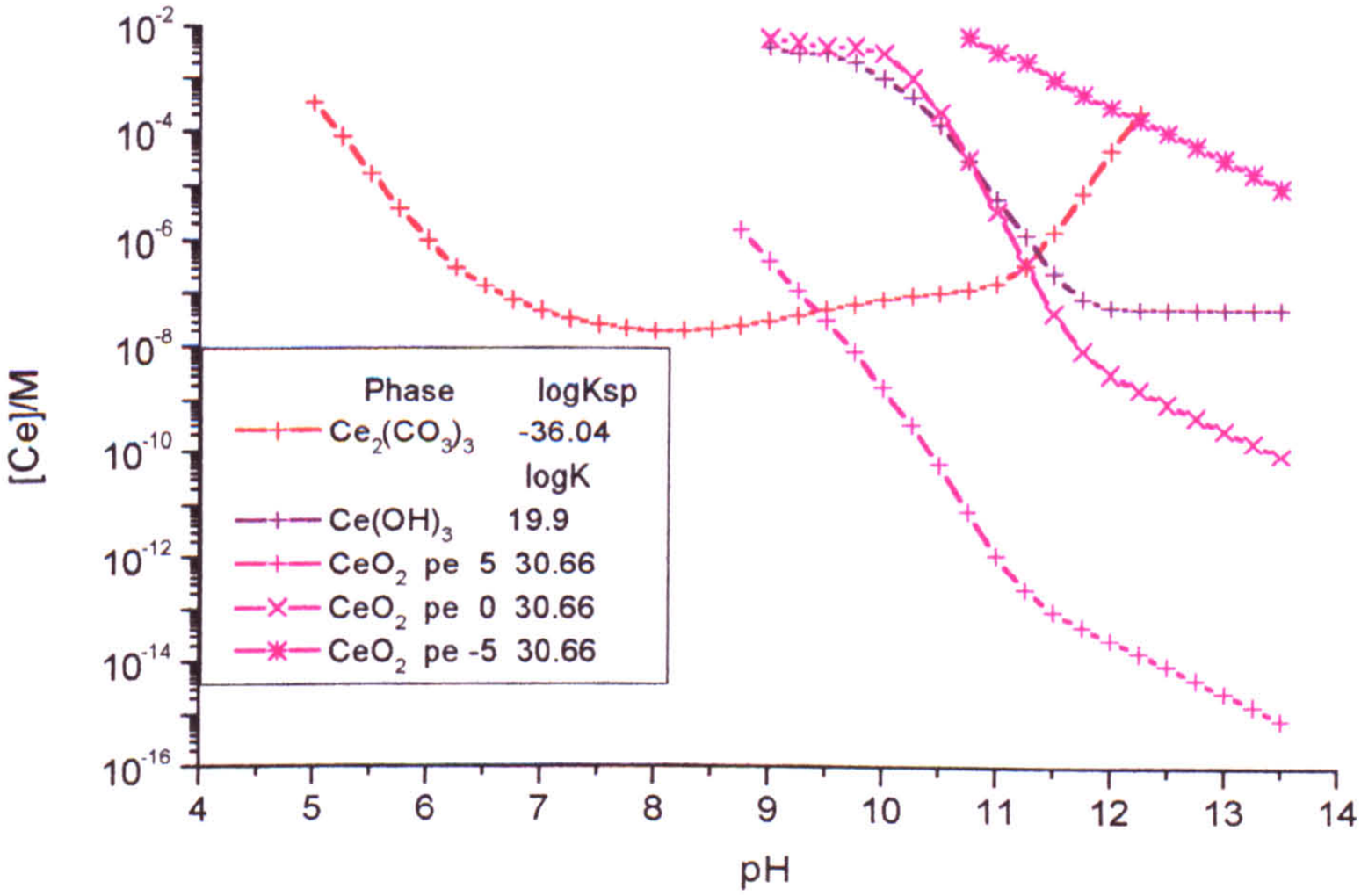

The $Ce_2(CO_3)_3$ solubility minima occurs in the same pH region as the $Nd_2(CO_3)_3$ solubility minima i.e. when in equilibrium with $CeCO_3^+$ (Figure 4.24, equation 4.99). As the activity of CO_3^{2-} increases steadily with pH at a constant TIC concentration (Figure 4.4), the dominant aqueous $CeCO_3^+$ species converts to $Ce(CO_3)_2^-$, which becomes dominant above pH 7. The increase in $Ce_2(CO_3)_3$ solubility as pH increases above pH 7 is due to the formation of the aqueous cerium dicarbonate, $Ce(CO_3)_2^-$ species (equation 4.100).

$$Ce_2(CO_3)_3(s) \longrightarrow 2CeCO_3^+(aq) + CO_3^{2-}(aq) \qquad (4.99)$$

$$Ce_2(CO_3)_3 + CO_3^{2-} \longrightarrow 2Ce(CO_3)_2^-(aq) \qquad (4.100)$$

The CeO_2 solubility profile is similar to that of $Nd(OH)_3$ when in equilibrium with aqueous Ce carbonate species. There is a sharp decrease in solubility the aqueous phase change from $Ce(CO_3)_2^-$ to $Ce(OH)_3^0$ (Figure 4.25) with increasing pH. When $Ce(OH)_3^0(aq)$ becomes the dominant aqueous phase, there is still a decrease in solubility with pH (equation 4.101), but at a slower rate of change than when in equilibrium with $Ce(CO_3)_2^-$. Ce^{4+} does not appear to be a significant aqueous species even at high pH.

$$CeO_2(s) + e^- + 2H_2O = Ce(OH)_3^0(aq) + OH^-(aq) \qquad (4.101)$$

Figure 4.25 $Ce_2(CO_3)_3$ (log Ksp -36.04) solubility and aqueous speciation in 10mM $NaHCO_3$ (this work, Lee & Byrne 1992/3)

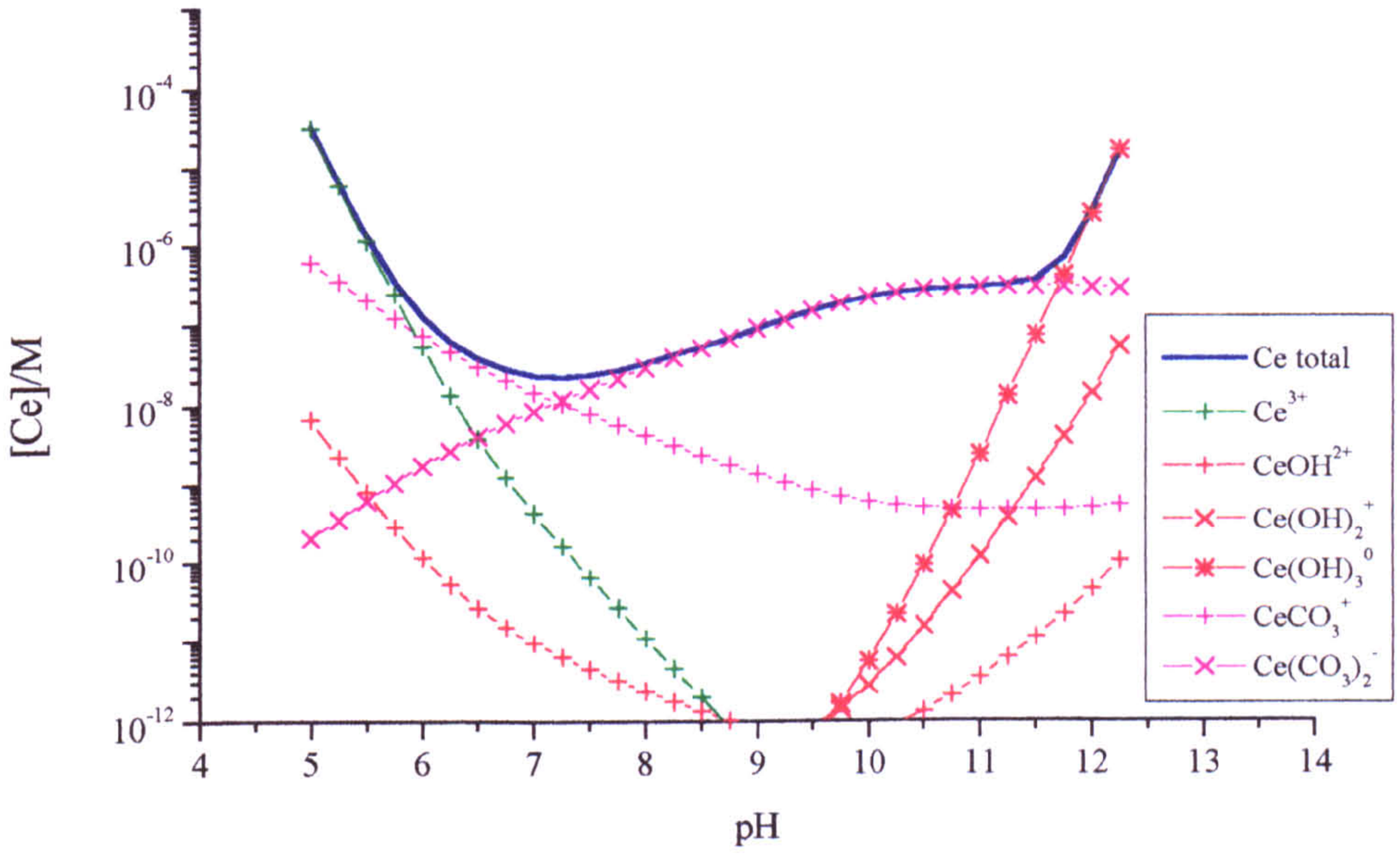

Figure 4.26 CeO_2 (log K 30.66) solubility and aqueous speciation in 1mM $NaHCO_3$ (this work, Lee & Byrne 1992/30

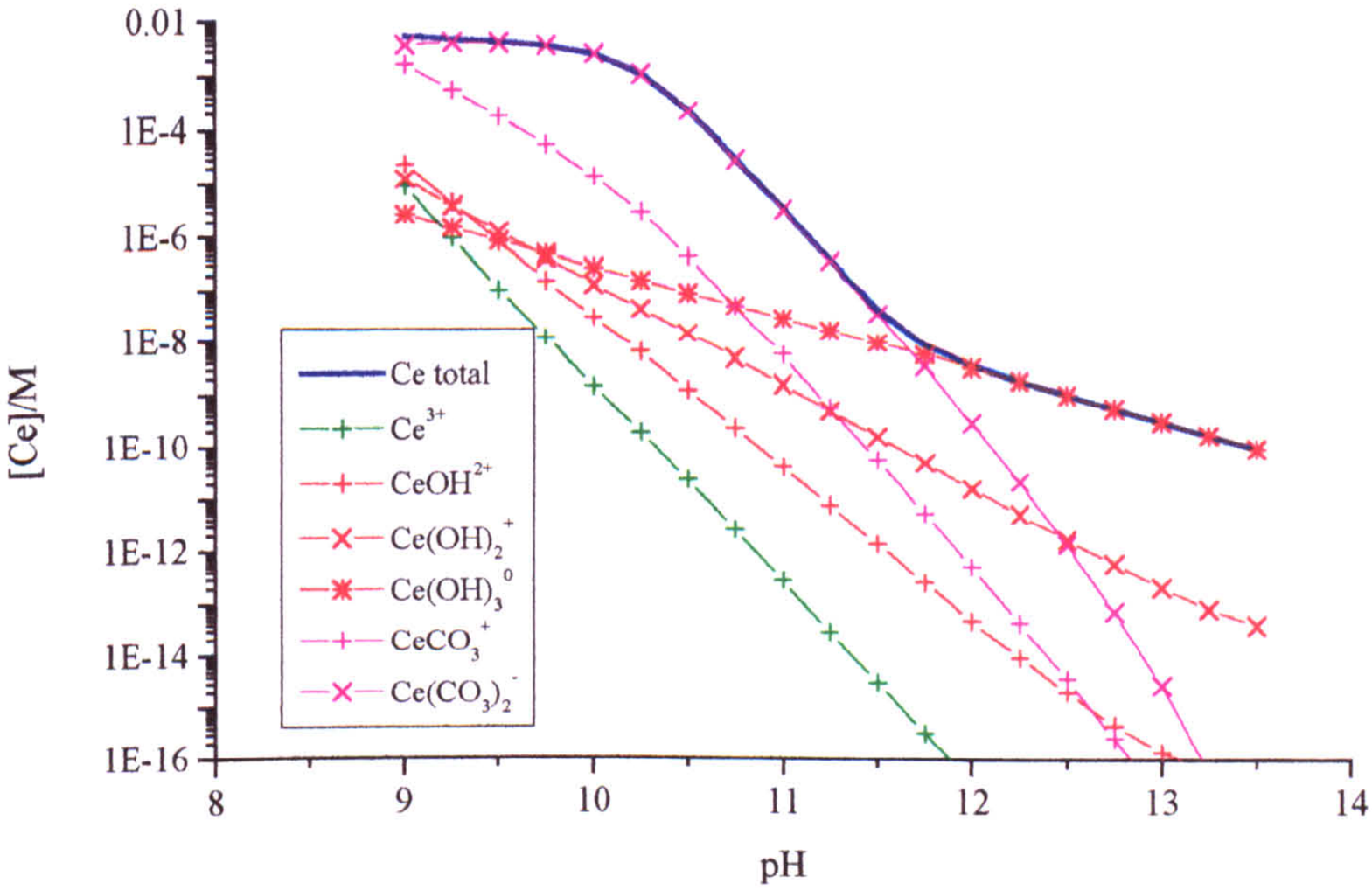

4.9 Discussion

4.9.1 Summary of the stability field diagrams

The Stability field diagrams prepared from the ΔG_f °calculations indicate the solubility limiting phases over the main controlling components in solution (i.e. carbonate activity and pH), and can predict lanthanide solubility assuming ideal solutions. Other ions can only be added at specific activities. PHREEQC was used to predict the effects of aqueous ion interactions and to predict the solubility of each phase in non-ideal and complex solutions, but is restricted to calculations at specific solution conditions, rather than the variations possible from changing environments. The aqueous speciation predicted from PHREEQC does indicate that within phase boundaries a single aqueous species is dominant which can give a reliable indication of the lanthanide solubility (Figure 4.11). The solubility of the lanthanides are controlled by the interactions between each of the possible aqueous species and the solid phases.

The Nd and Eu stability field diagrams indicate that there are three phases, $Ln_2(CO_3)_3$, $LnCO_3OH$ and $Ln(OH)_3$, that form a series of solubility limiting phases, dependent on the pH and carbonate activity of the system. These three phases are all acid soluble, with a sharp solubility edge below pH 8. An increase in the carbonate activity of the system, initially decreases the lanthanide solubility until $Ln(CO_3)_2^-$ becomes the dominant aqueous lanthanide species. The solubility of the solid $Ln_2(CO_3)_3$, $LnCO_3OH$ and $Ln(OH)_3$ phases all increase when in equilibrium with aqueous $Ln(CO_3)_2^-$, (Table 4.19).

A neodymium solubility minimum forms within the pH range pH 9 and 10.5 and total carbonate concentrations between $5x10^{-6}$ M and $5x10^{-4}$M. A similar $EuCO_3OH$ solubility minimum does not occur as $EuCO_3OH$ has a narrow stability field. The minimum Eu solubility therefore occurs when $Eu(OH)_3$(s) is in equilibrium with $Eu(OH)_3$(aq).

Table 4.19 Solid phase reactions with $Ln(CO_3)_2^-$

$Ln_2(CO_3)_{3(s)} + CO_3^{2-}{}_{(aq)}$	=	$2Ln(CO_3)_2^-{}_{(aq)}$	(4.97)
$LnCO_3OH(s) + CO_3^{2-}{}_{(aq)}$	=	$Ln(CO_3)_2^-{}_{(aq)} + OH^-{}_{(aq)}$	(4.87)
$Ln(OH)_{3(s)} + 2CO_3^{2-}{}_{(aq)}$	=	$Ln(CO_3)_2^-{}_{(aq)} + 3OH^-{}_{(aq)}$	(4.92)
$NaLn(CO_3)_{2(s)}$	=	$Ln(CO_3)_2^-{}_{(aq)} + Na^+{}_{(aq)}$	(4.98)

The $NaLn(CO_3)_2$ phase intersects each of the three phases, $Ln_2(CO_3)_3$, $LnCO_3OH$ and $Ln(OH)_3$ at high TIC activities if sufficient Na is present in solution. When $NaLn(CO_3)_2$ is in equilibrium with $Ln(CO_3)_2^-$ the lanthanide solubility is independent of the carbonate activity and pH, even though this species is dependent on both of these factors. $NaLn(CO_3)_2$ solubility increases sharply when aqueous $Ln(CO_3)_2^-$ is converted to any other phases.

$Ce_2(CO_3)_3$ has a lower solubility than the other lanthanides examined. Cerium cannot completely be part of a regular member of the group trend across the lanthanides, as many of the lanthanide hydroxy phases cannot easily be formed for Ce. There is a single phase change from $Ce_2(CO_3)_3$ to CeO_2, with a possible $Ce(OH)_4$ intermediate as pH increases. The very low solubility of $Ce_2(CO_3)_3$ inhibits the formation of $NaCe(CO_3)_2$, within the intermediate pH range, which converts directly to CeO_2, in solutions with less than 0.1M sodium.

A reducing environment will affect the solubility of CeO_2, possibly resulting in $Ce(OH)_3$ and $CeCO_3OH$ as the solubility limiting phase. These Ce^{3+} phases would limit the solubility of Ce at high pH, to similar magnitudes as Nd and Eu, compared to a CeO_2 precipitate.

4.9.2 Comparisons between the stability field diagrams and titration experiments

The reactions and phase changes identified in the Nd titration experiments (Chapter 3), can be explained by the stability field diagram (Figure 4.11). The contoured solubility diagrams indicate that as pH increases the free Nd^{3+} aquo-

ion changes to aqueous hydroxy phases at low carbonate activities, instead of precipitation. $Nd(OH)_3(s)$ would not precipitate from a 1mM Nd solution until pH was above pH ~ 7.8 in a carbonate free system, i.e. at the end of the titration buffer zone. Nd then precipitates until pH 9.4 when aqueous $Nd(OH)_3$ is in equilibrium with solid $Nd(OH)_3$.

The stability field diagrams show that $Nd_2(CO_3)_3$ would be the initial precipitate for titrations in carbonate activities above 10^{-6}M TIC solutions. Precipitation would start by pH 6.5 with $Nd_2(CO_3)_3$ as the initial precipitate at the start of the buffer zone. The initial K_2CO_3 solutions have TIC concentrations of approximately $2x10^{-5}$M TIC when precipitation starts, therefore $Nd_2(CO_3)_3$ would be the initial precipitate. Alteration to $NdCO_3OH$ only occurs above pH 8.5 in solutions with more than 1mM TIC as found at the end of the K_2CO_3 titrations. $NdCO_3OH$ did not form the initial precipitating phase as the initial addition of $NaHCO_3$ or K_2CO_3, immediately increased the amount of carbonate in solution to the concentration required for $Nd_2(CO_3)_3$ to become the equilibrium phase

The initial precipitate for Na_2CO_3 titrations was $Nd_2(CO_3)_3$, Nd rapidly precipitates to leave approximately 10^{-6}M Nd in solution. The solid phase then alters to $NaNd(CO_3)_2$, dependant on a sufficient Na^+ activity in solution. $Nd(CO_3)_2^-$ is the dominant aqueous species from pH 8-11, which generally increases the lanthanide solubility within this pH range from the reactions shown in Table 4.19. $NaNd(CO_3)_2$ is the only solid phase exception as the solid-aqueous equilibrium is dependant on the Na^+ activity and not pH or CO_3^{2-} activity.

4.9.3 Lanthanide double carbonates in experimental solutions

$NaNd(CO_3)_2$ has been excluded from many published studies as the $pCO_{2(g)}$ has been the dominant method of controlling carbonate activity at intermediate pH rather than $NaHCO_3$. Consideration of Na^+ phases were therefore not possible in Na free systems, however the introduction of $NaClO_4$ buffer solutions to regulate a constant ionic strength can have an effect on the reaction especially above pH

7. Rao *et al.*, (1996a) suggest that $NaNd(CO_3)_2$ will be an important phase for controlling Nd solubility in carbonate solutions above 0.5M Na^+, however this study has shown that $NaNd(CO_3)_2$ will form as a solubility limiting phase in 10mM Na^+ and down to 3mM TIC solutions.

One potential host rock for nuclear waste repositories are salt domes. If these are to be considered, then any groundwater flow would be saturated with NaCl. $NaNd(CO_3)_2$ could therefore be a solubility-limiting phase if there is also a source of CO_3^{2-} (e.g. from a concrete constructed repository).

Hydrated $KNd(CO_3)_2$ was prepared from an appropriate mixture of $LnCl_3$ (10mM) and excess K_2CO_3 (0.1M) solution. The XRD spectra of the resulting precipitate was similar to the $NaNd(CO_3)_2.6H_2O$ spectra (JCPDS file 30-1223), however there was no Na^+ in the system and elemental analysis indicated a 1:1 K^+/Nd^{3+} ratio in the solid phase. It was not possible to isolate a pure $KEu(CO_3)_2$ phase, Only mixed $EuCO_3OH$-$KEu(CO_3)_2$ phases with a 3:1 Eu/K ratio could be isolated. Higher K^+ and CO_3^{2-} activities (above 0.2M K_2CO_3) are therefore required to form pure $KEu(CO_3)_2$. Na^+ free 0.2M K_2CO_3 solutions are unlikely to form even in artificial groundwater conditions and therefore $KLn(CO_3)_2$ would not control lanthanide solubility in any environment. However K^+ cannot easily be used in buffer solutions, as an alternative to Na^+, to regulate the ionic strength as potassium lanthanide double carbonates may form.

4.9.4 Solubility product calculations

The narrow stability field of the $EuCO_3OH$ phase indicates the difficulty in forming $EuCO_3OH$ from the addition of $NaHCO_3$ and K_2CO_3 solutions. The amorphous phase usually formed in attempted $EuCO_3OH$ precipitation experiments indicates that $EuCO_3OH$ and $Eu(OH)_3$ do not form as mixed phases at or near the equilibrium point.

A commonly used alternative method for regulating the carbonate content of the solution is by precisely controlling the $pCO_{2(g)}$ in an otherwise inert atmosphere

(Runde *et al.*, 1992). The addition of excess K_2CO_3 to a $EuCl_3$ solution so that the precise CO_3^{2-} activity is present in solution at a pH too low for the precipitation of $Eu(OH)_3$, and carbonate activity high enough to form $Eu_2(CO_3)_3$ was difficult to obtain. If the carbonate was added as $pCO_{2(g)}$, then the carbonate activity required to form $EuCO_3OH$ may be easier to identify, however if Na^+ solutions were not used in the original preparations, then the double carbonates $NaEu(CO_3)_2$, $NaNd(CO_3)_2$ and $KNd(CO_3)_2$ phases would not have been identified.

The solubility products determined in this study are dependent on the database used to calculate the activities of the component ions (which will be discussed further in Chapter 7). Differences in the aqueous speciation constants may account for the slight differences in the range of solubility products of the carbonate phases (Table 4.7) between studies. There is however, a significant difference in the solubility products of the hydroxide phases, determined here and in other studies, which range for $Nd(OH)_3$ from log Ksp -21 to -27. The initial hydroxide phase precipitates as an amorphous phase, which then crystallises slowly at ambient temperatures in less than 0.1M solutions. The lowest solubilities can only be obtained by ageing the precipitates at high temperatures and concentrated NaOH (above 3M) solutions. These conditions are unlikely to form outside a laboratory experiment, therefore the lowest proposed $Ln(OH)_3$ solubility products are unlikely to occur.

4.10 References

BAES, C. F., and MESMER, R. E., (1986) The hydrolysis of cations. Robert E *Krieger Pub Co* Malaber Florida

DIAKONOV, I. I., TAGIROV, B. R., and RAGNARSDOTTIR, K. V., (1998a) Standard thermodynamic properties and heat capacity equations of rare earth hydroxides: I. $La(OH)_3(s)$ and $Nd(OH)_3(s)$. Comparison of thermochemical and solubility data. *Radiochim. Acta* **81** 107-116

DIAKONOV, I. I., RAGNARSDOTTIR, K. V., and TAGIROV, B. R., (1998b) Standard thermodynamic properties and heat capacity equations of rare

earth hydroxides: II. Ce(III)-, Pr-, Sm-, Eu(III)-, Gd-, Tb-, Dy-, Ho-, Er-, Tm-, Yb-, and Y-hydroxides. Comparison of thermochemical and solubility data. *Chem. Geol.* **151** 327-347

ELDERFIELD, H., and GREAVES, M. J., (1982) The REE in seawater. *Nature* **296** 214-217

FERRI, D., GRENTHE, I., HEITANEN, S., and SALVATORE, F., (1983) Studies on metal carbonate equilibria, 5. The cerium(III) carbonate complexes in aqueous perchlorate media. *Acta Chem. Scand.* **A37** 359-365

FIRSCHING, F. H., and MOHAMMADZADEL, J., (1986) Solubility products of rare-earth carbonates. *J. Chem. Eng. Data* **31** 40-42

JOHANNESSON, K. H., and LYONS, W. B., (1995) REE geochemistry of Colour Lake, an acidic freshwater lake on Axel Heiberg Island NW Territories Canada. *Chem. Geol.* **119** 209-223

LEE, J. H., and BYRNE, R. H., (1993) Complexation of trivalent REE (Ce, Eu, Gd, Tb, Yb) by carbonate ions. *Geochim. Cosmochim. Acta* **57** 295-302

LEE, J. H., and BYRNE, R. H., (1992) Examinations of comparative REE complexation behaviour using linear free-energy relationships. *Geochim. Cosmochim. Acta* **56** 1127-1137

LIDE, D. R., (1998) Handbook of chemistry and physics 79th Edition (1998-1999) *Pub. CRC*

MEINRATH, G., and KIM, J. L., (1991a) Solubility products of different Am(III) and Nd(III) carbonates. *J. Inorg. Solid State Chem.* **28** 383-388

MEINRATH, G., and KIM J. L., (1991b) The carbonate complexation of the Am(III) ion. *Radiochim. Acta* **52/53** 29-34

MOCHIZUKI, A., NAGASHIMA, K., and WAIKITA, H., (1974) The synthesis of crystalline hydrated double carbonates of rare-earth elements and sodium. *Bull. Chem. Soc. Jpn* **47** 755-756

MORSS, L. R., and WILLIAMS, C. W., (1994) Synthesis of crystalline $Am(OH)_3$ and determination of its enthalpy of formation of the solubility-product constants of actinide(III) hydroxides. *Radiochim. Acta* **66/67** 89-93

MORSS, L. R., HAAR, C. H., and MROCZKOWSKI, S., (1989) Standard molar enthalpy of formation of neodymium hydroxide. *J. Chem. Thermodyn.* **21** 1079-1083

NAGASHIMA, K., WAIKITA, H., and MOCHIZUKI, A., (1973) The synthesis of crystalline rare earth carbonates. *Bull. Chem. Soc. Japan* **46** 152-156

PARKHURST, D. L., (1995) User's guide to PHREEQC–A computer program for speciation, reaction-path, advective-transport, and inverse geochemical calculations. . *U.S. Geol. Surv., Water Resour. Inv.* 95-4227, 143pp

RAO, L. F., RAI, D. P., FELMY, A. R., FULTON, R. W., and NOVAK, C. F., (1996a) Solubility of $NaNd(CO_3)_2.6H_2O$ in concentrated Na_2CO_3 and $NaHCO_3$ solutions. *Radiochim. Acta* **75** 141-147

RAO, L. F., RAI, D. P., FELMY, A. R., FULTON, R. W., and NOVAK, C. F., (1996b) Solubility of $Nd(OH)_3$ in 0.1M NaCl aqueous solution at 25°C and 90°C. *Radiochim. Acta* **72** 151-155

RUNDE, W., MENRATH, G., and KIM, J. L., (1992) A study of solid-liquid phase-equilibria of trivalent lanthanide and actinide ions in carbonate systems. *Radiochim. Acta* **58/59** 93-100

SILVA, R. J., BIDOGOLIO, G., RAND, M. H., ROBOUCH, P. B., WANNER, H., and PUIGDOMENCH I. (1995) Chemical Thermodynamics Volume 2. Chemical thermodynamics of americium. Elsevier (Amsterdam).

VITORGE, P., (1992) $Am(OH)_3(s)$, $AmOHCO_3(s)$, $Am_2(CO_3)_3(s)$ Stabilities in environmental conditions. *Radiochim. Acta* **58/59** 105-108

Chapter 5

The Alteration of $NaLn(CO_3)_2.6H_2O$ from dehydration during the drying process

5.1 Introduction

The actinide elements are powerful X-ray emitters therefore their solid phases are often difficult to characterise from standard techniques such as X-ray Diffraction. The lanthanide elements especially Nd and Eu have almost identical ionic radii (98.3pm and 95.7pm respectively) to the actinide elements Am and Cm (97.5pm and 97pm respectively) in the M^{3+} oxidation state, resulting in the use of lanthanides as non-radioactive analogues for the characterisation of Am and Cm.

Three phases are usually considered to control solubility in the americium carbonate system across the pH range 6-13. The carbonate phase $Am_2(CO_3)_3$ alters to the hydroxycarbonate ($AmCO_3OH$) then the hydroxide, $Am(OH)_3$, with increasing pH or decreasing carbonate activity (Vitorge, 1992). The solubility product of each of these phases is normally determined in two stages, firstly the preparation of each carbonate and hydroxy phase for Am, Nd and Eu followed by solution analysis for all three metals followed by the solid phase characterisation of Nd and Eu, but not Am. The Am solid phase is then assumed to be the same as the Nd and Eu phases (Runde *et al.*, 1992).

The solutions used to determine the solubility product of each of these phases can contain $NaHCO_3$ or Na_2CO_3 to control the carbonate activity or $NaClO_4$ as a buffer to maintain a constant ionic strength in solution. The presence of Na^+ ions in solution can promote the formation of a fourth phase, namely a sodium lanthanide double-carbonate (This study , Chapter 4, Rao *et al.*, 1996). This phase has previously not been considered for Am.

The sodium lanthanide double-carbonate, $NaLn(CO_3)_2.6H_2O$, where Ln = any lanthanide element, differs significantly from the other lanthanide carbonates and hydroxy phases in that during the drying process the double carbonate decomposes. The $Ln_2(CO_3)_3.xH_2O$, $LnCO_3OH$ and $Ln(OH)_3$ are all stable when dried in the usual way, namely drying in a vacuum dessicator or oven drying at 60°C; oven drying of $Ln_2(CO_3)_3.8H_2O$ at 100°C-120°C does cause dehydration, but not decomposition. Previously Mochizuki *et al.*, (1974) have noted that even the mildest condition such as exposure to dry air was sufficient to alter the crystal

structure of a series of lanthanide (La to Dy) double carbonates, although the alteration products were not identified. Dehydrated $NaLn(CO_3)_2$ and $KLn(CO_3)_2$ have been prepared but the dehydrated crystal structure was only isolated at high CO_2 pressures (above 3000bars) Scheer and Seidel (1981), although their infra-red patterns are similar to those found as the alteration product in this study.

A series of experiments have been performed to determine the effects of varied drying conditions with time on the stability of $NaLn(CO_3)_2.6H_2O$ (Ln = Nd or Eu), and then characterise the alteration products. The drying conditions ranged from oven drying to storage in a water saturated atmosphere.

5.2 Experimental

A sample of $NaNd(CO_3)_2.6H_2O$ was prepared by adding $NdCl_3$ (0.2M, $10cm^3$) to Na_2CO_3 ($50cm^3$, 0.2M) and diluting to $200cm^3$ with distilled water. The solution was left for at least 2 months at 25°C in Nalgene HDPE bottles to ensure crystalline $NaNd(CO_3)_2.6H_2O$ formed.

A freshly prepared sample of crystalline $NaLn(CO_3)_2.6H_2O$, where Ln = Nd or Eu, was filtered under vacuum using a Whatman N°4 sintered glass crucible, then washed with $50cm^3$ of distilled water through the sintered glass crucible. The $NaLn(CO_3)_2.6H_2O$ sample was analysed immediately by FTIR and XRD spectroscopy, using minimum sample preparation and also by elemental analysis. It was then divided into four samples to examine the effects of various drying conditions:

1. oven drying at 120°C
2. drying in a vacuum dessicator over silica gel
3. air drying under an open atmosphere
4. storage in a water saturated atmosphere

The water saturated atmosphere was formed by placing an upturned $50cm^3$ beaker inside a larger $250cm^3$ beaker that was partly filled with distilled water. The water level was kept no more than half-way up the $50cm^3$ beaker. A sample of

$NaLn(CO_3)_2.6H_2O$ (0.05g) was placed on a silica plate (used for XRD sample mountings) ontop of the $50cm^3$ beaker. The $250cm^3$ beaker was covered with parafilm so any evaporating water formed a moist atmosphere within the beaker at room temperature(~ 20°C).

All samples were analysed daily by FTIR and XRD spectroscopy for the initial three weeks, then weekly until the end of the study (20 weeks), to identify any phase transformations.

5.3 Characterisation of the altered samples

The freshly prepared sample of $NaLn(CO_3)_2.6H_2O$ was characterised by elemental analysis to give a Ln^{3+}/Na^+ ratio between 0.9 and 1.1 and the XRD pattern was in agreement with the original preparation by Mochizuki *et al.*, (1974) (Figure 5.1, Table 5.1) to be the sodium double carbonate and not the $Nd_2(CO_3)_3.8H_2O$ structure. No reference pattern has been proposed for Eu but $NaEu(CO_3)_2.6H_2O$ has an identical pattern to Nd but offset to a higher 2θ between that of Sm and Gd. These lanthanide elements have larger and smaller ionic radii respectively than Eu.

The initial infrared spectrum indicates that a hydrated lanthanide carbonate is present but cannot differentiate the exact type of carbonate (Figure 5.2), although this can be used as a "fingerprint" for the hydrated $NaLn(CO_3)_2.6H_2O$.

The decomposition of $NaLn(CO_3)_2.6H_2O$ was followed using FTIR and XRD analysis. The first stage in the alteration process can be detected from the infra-red spectrum. The characteristic ν_3 doublet of the lanthanide carbonates at approximately $1500cm^{-1}$ and $1400cm^{-1}$ alters to a triplet (Table 5.1 and Figure 5.3)

Figure 5.1 Comparison of the powder XRD patterns of $NaNd(CO_3)_2.6H_2O$ and $Nd_2(CO_3)_3.8H_2O$

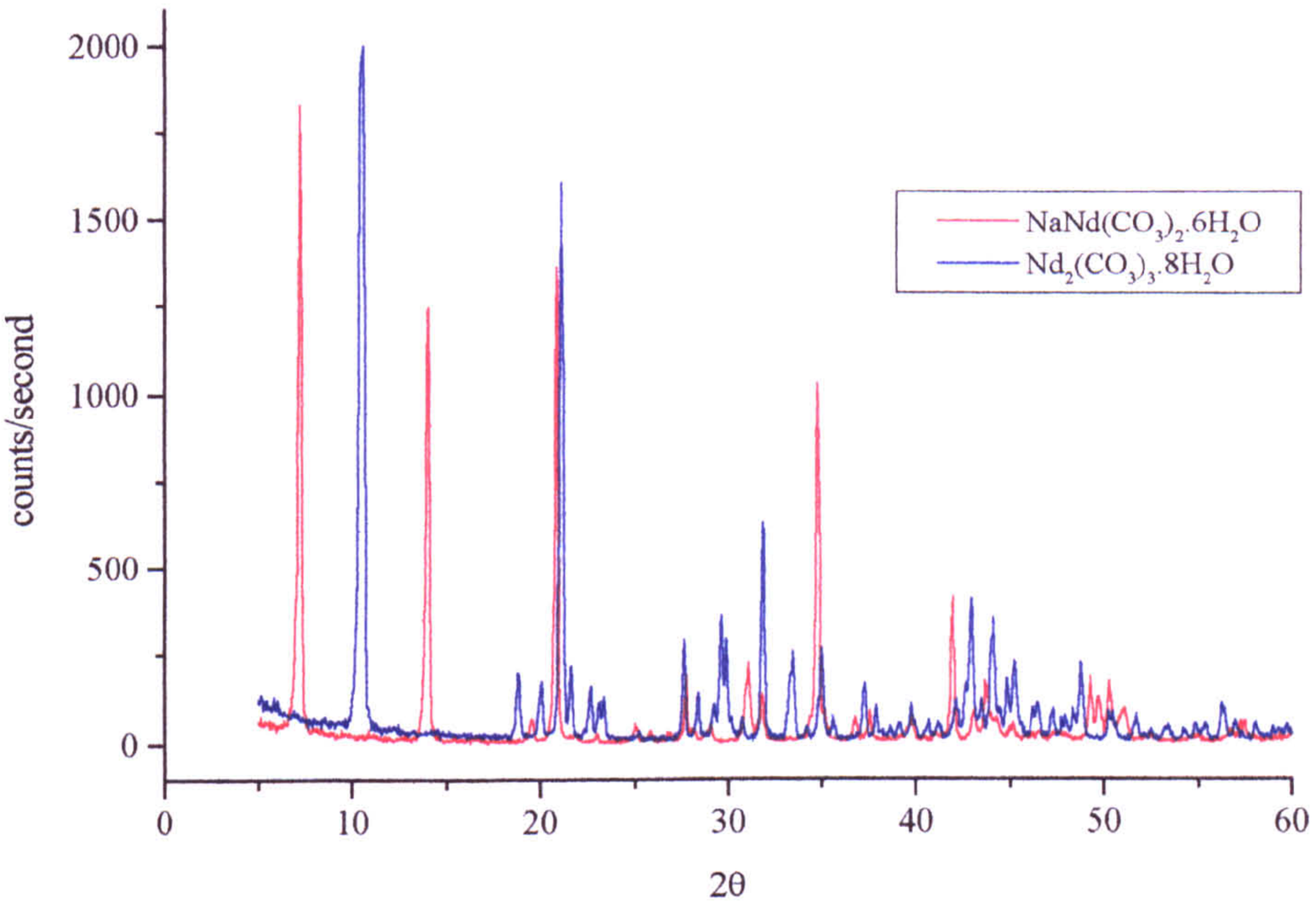

Table 5.1 XRD peaks of the initial $NaNd(CO_3)_2.6H_2O$ and $NaEu(CO_3)_2.6H_2O$ samples

[1]$NaNd(CO_3)_2.6H_2O$	Nd sample		Eu sample	
d(Å)	2θ	d(Å)	2θ	d(Å)
13.30	6.370	13.864	6.500	13.587
6.610	13.055	6.776	13.250	6.677
4.370	20.250	4.382	20.090	4.416
3.280	26.876	3.315	27.010	3.299
2.620	33.895	2.643	34.035	2.632
2.180	41.045	2.197	41.185	2.190
1.870	48.910	1.861	48.490	1.876

[1]JCPDS reference pattern after Mochizuki *et al.*, (1974)

Figure 5.2 FTIR spectrum of freshly prepared $NaNd(CO_3)_2.6H_2O$

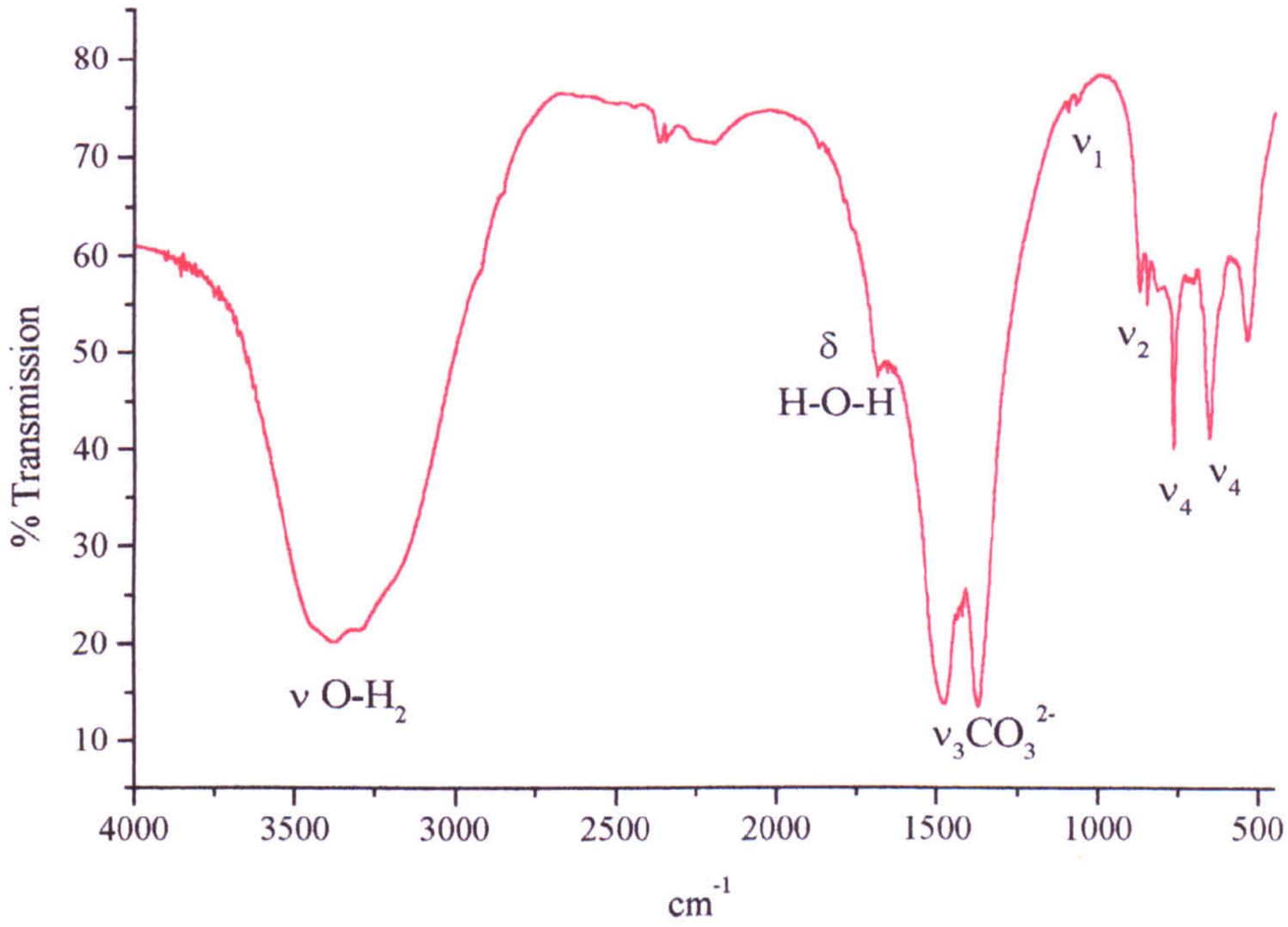

Figure 5.3 FTIR spectrum of the intermediate and end product from the alteration of $NaNd(CO_3)_2.6H_2O$

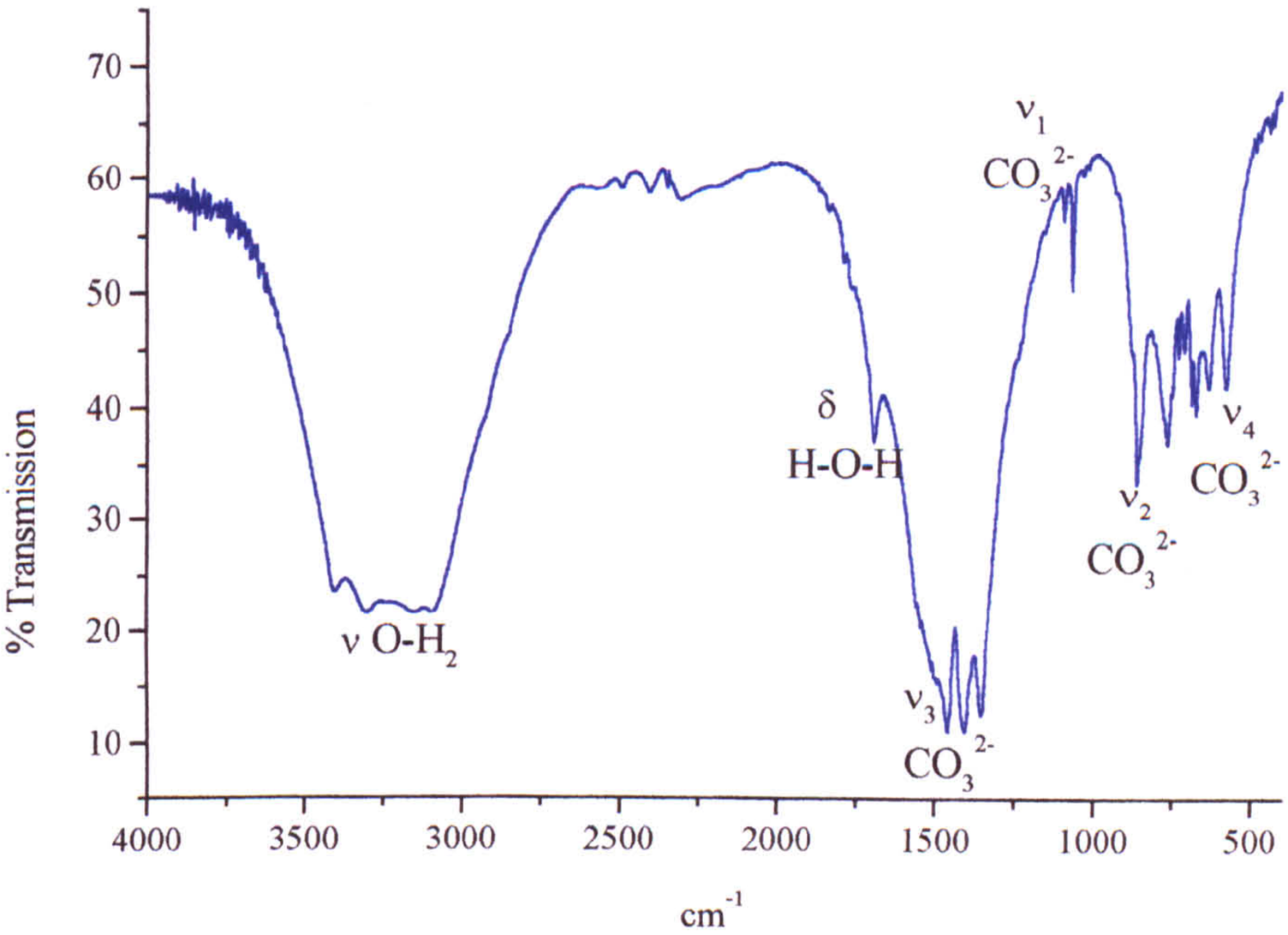

The FTIR spectra of the altered product cannot be unambiguously assigned as the ν_3 doublet characteristic of lanthanide carbonates phases $NaLn(CO_3)_2.6H_2O$, $Nd_2(CO_3)_3.xH_2O$ or Na_2CO_3 (Table 5.2), but indicates a mixture was present. A ν_3 triplet has been reported by Scheweer and Seidel (1981) for the dehydrated $NaLn(CO_3)_2$ formed under a $pCO_{2(g)}$ atmosphere of 3Kbar. All the CO_3^{2-} singlet and doublet stretches are each further split into doublets, indicating that there are at least two carbonate phases present. The presence of the ν_3 triplet immediately indicates that the onset of alteration has occurred from $NaNd(CO_3)_2.6H_2O$.

Table 5.2 Comparison of lanthanide-carbonate infra-red stretches (cm^{-1})

Stretch	[1]Nd dried product	[1]$NaNd(CO_3)_2.6H_2O$ (starting material)	[2]$Nd_2(CO_3)_3.8H_2O$	[3]Na_2CO_3
ν_1	1060.3	1072	1088	
ν_2	857.1	875/850	848	878.9
ν_3	1458.3 1404.1 1351.8	1477 1374	1491 1377	1438.7
ν_4	760.8 672.2	763 653	750 680	702.1

[1] This work, [2]Runde *et al.*, (1992), [3]Nakamoto (1986)

As a result of alteration there is a decrease in the relative X-ray background signal between the freshly prepared and altered samples due to the severe reduction in the XRD peak height (Figure 5.4) from the loss in crystallinity. However the intermediate alteration product (Figure 5.5) can be clearly seen with peaks characteristic to both $NaLn(CO_3)_2.6H_2O$ and $Nd_2(CO_3)_3.8H_2O$ (Table 5.3). The decomposition in all cases was marked by the formation of a peak at 2θ ~10° characteristic of $Nd_2(CO_3)_3.8H_2O$ (Appendix 5.1), and a reduction in all the XRD peaks which was most severe for the air-dried samples, (Figure 5.4 shows that the maximum peak height of 24,000 counts per second was reduced to 500 counts per second).

Table 5.3 JCPDS XRD Reference patterns and the intermediate alteration product

Solid Phase	[1]Intermediate Mixed Phase	$NaNd(CO_3)_2.6H_20$	$Nd_2(CO_3)_3.8H_2O$	$Nd_2(CO_3)_3.8H_2O$
[2]Ref Pattern		30-1223	29-918	31-877
d spacing (Å)	12.2593	13.30		
	8.461		8.410	8.590
	6.593	6.610		
	4.705		4.710	4.750
	4.631		4.430	4.480
	4.366	4.370		
	4.311			4.250
	4.193		4.150	4.130
	3.920			3.950
	3.913			3.880
	3.845			3.830
	3.278	3.280	3.230	3.240
	3.016		3.020	3.020
	2.985		2.979	
	2.586	2.620	2.565	
	2.220	2.180		
	2.165		2.055	
		1.870		
			1.374	

[1] Figure 5.4
[2]JCPDS Reference pattern

Figure 5.4 Initial and intermediate alteration XRD patterns of the air dried dehydration of $NaNd(CO_3)_2.6H_2O$

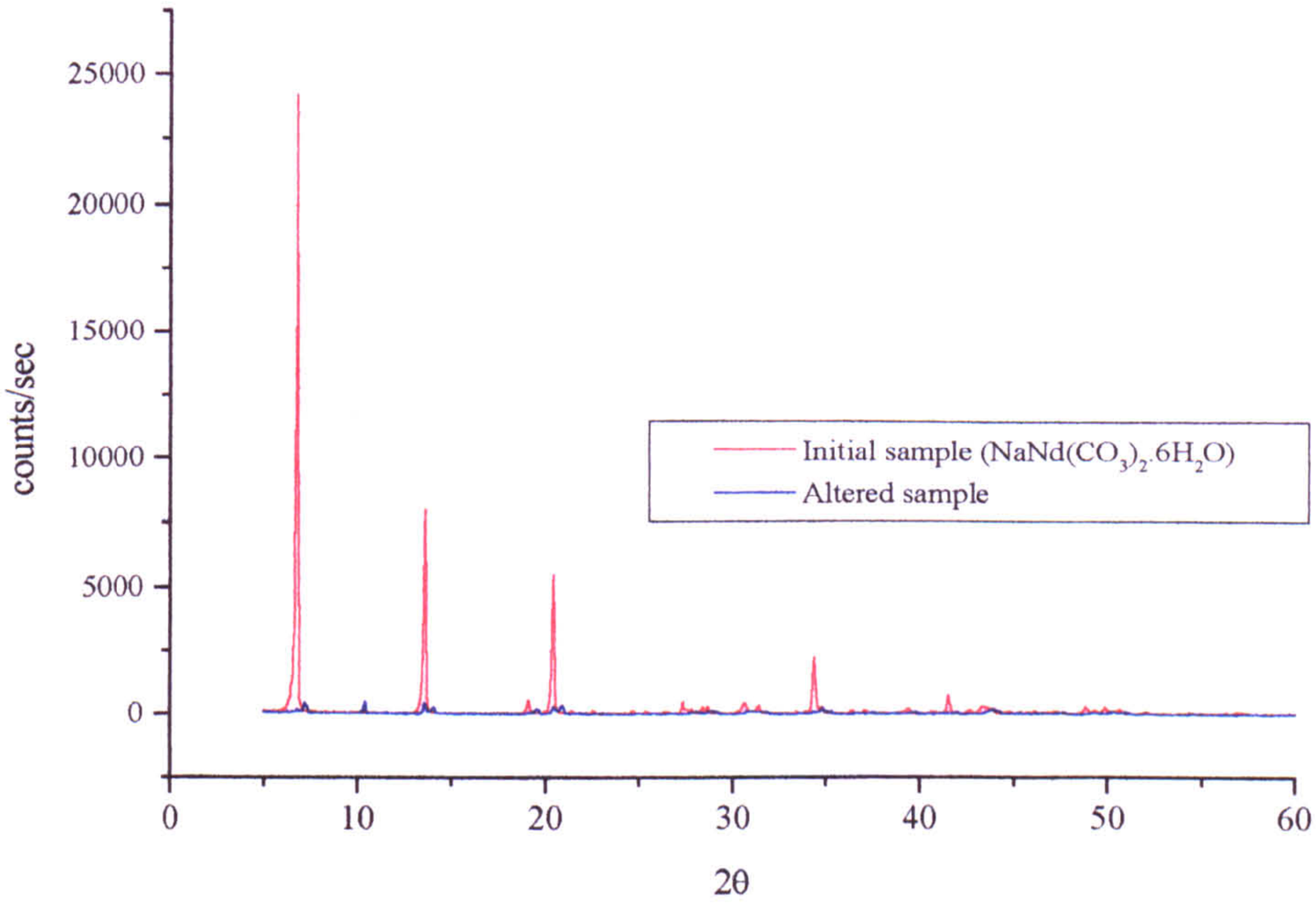

Figure 5.5 XRD pattern showing the intermediate alteration stage from $NaNd(CO_3)_2.6H_2O$ to $Nd_2(CO_3)_3.8H_2O$ shown in Figure 5.4

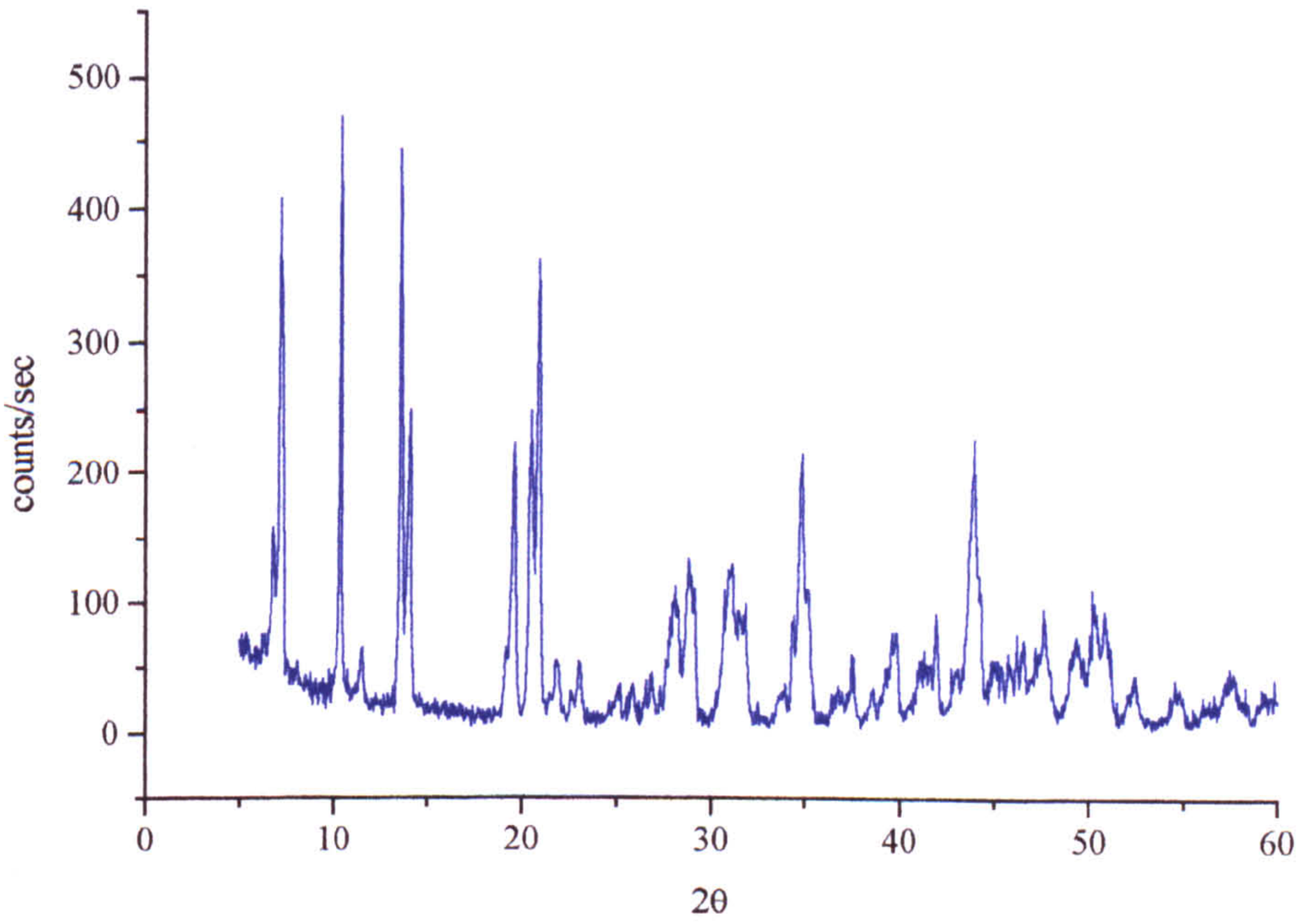

The final stage in the alteration was the complete disappearance of all peaks from $NaLn(CO_3)_2.6H_2O$, leaving peaks characteristic of either $Ln_2(CO_3)_3.8H_2O$ for dessicator dried samples (Figure 5.6) and air dried samples(Figure 5.5), or $Ln_2(CO_3)_3$ from the oven dried samples. The $Nd_2(CO_3)_3.8H_2O$ XRD spectra is more complex than that of $NaNd(CO_3)_2.6H_2O$ but because the alteration product was not often as crystalline as the original samples it consequently had smaller XRD peaks reflecting the slow crystal growth of solid-phase alteration. The FTIR spectrum remains unchanged from the intermediate spectrum dominated by a triplet ν_3 stretch.

There was no evidence of any sodium carbonate in the altered phases from the XRD analysis, however if these are amorphous then no evidence would be present as XRD analysis depends upon X-ray diffraction from crystal planes.

5.4 Alteration rate

The four drying conditions have a significant effect upon the solid phase stability of $NaNd(CO_3)_2.6H_2O$ and $NaEu(CO_3)_2.6H_2O$ (Table 5.4, Appendix 5.1). The oven dried samples can be clearly be seen to have altered immediately (in less than 5 minutes) to a dehydrated $Nd_2(CO_3)_3$ or $Eu_2(CO_3)_3$, from XRD analysis (Appendix 5.2 and 5.3). The XRD analysis of the dehydrated product did not indicate a crystalline sodium phase was present.

The rate at which the $NaLn(CO_3)_2.6H_2O$ phase altered by dessicator drying was a slower process than oven drying. An intermediate altered phase showing characteristic XRD peaks for $NaLn(CO_3)_2.6H_2O$ and $Ln_2(CO_3)_3.8H_2O$ could be seen after 24 hours, with complete alteration from $NaLn(CO_3)_2.6H_2O$ after drying for 3 days (Figure 5.6). Figure 5.6 clearly shows the complete disappearance of the sodium neodymium double carbonate, which has decomposed to form crystalline $Nd_2(CO_3)_3.8H_2O$. The XRD analysis has indicated that the dried product was a single phase of hydrated crystalline $Ln_2(CO_3)_3.8H_2O$, with no apparent evidence of a sodium phase, unless elemental and FTIR analysis are

also used to indicate that other phases must be present.

Figure 5.6 XRD pattern of the alteration of $NaNd(CO_3)_2$ in a vaccuum dessicator over silica gel

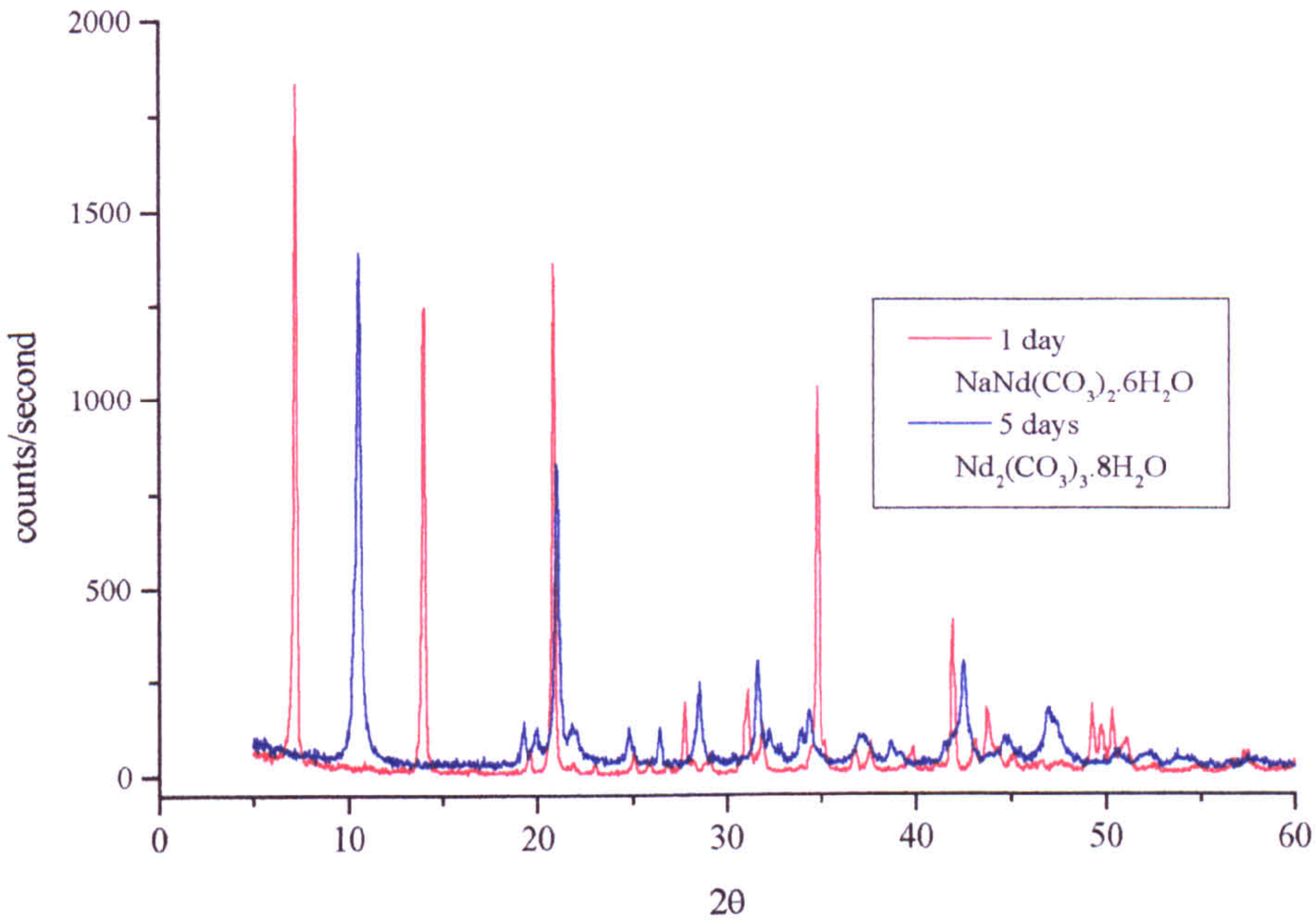

Table 5.4 Summary of alteration rate by varied drying conditions

Drying process	Alteration time	Comments
Oven 120°C	5 minutes	complete alteration to dehydrated $Ln_2(CO_3)_3$
Vacuum dessicator over silica gel	3-4 days	complete alteration
Air drying	6-10 days	initial alteration
	20 weeks	mixed system
Moist Environment	20 weeks	no alteration

Alteration under an atmosphere open to the air was a much slower process than oven drying or dessicator drying. Initial alteration products were apparent for Nd after 7 days and Eu after 10 days, indicated by infra-red analysis, and a mixture could be seen after 3 weeks. The mixtures stable for at least 20 weeks.

$NaLn(CO_3)_2.6H_2O$ crystals for Nd and Eu were stable under a water saturated

atmosphere for at least 20 weeks, with no apparent evidence of alteration.

A comparison of the ν_3 stretches of the dehydrated oven dried samples and the hydrated air dried samples for Nd and Eu (Table 5.5), indicates that the same altered carbonate phase(s) were forming during the air drying and oven dried processes, though Eu alteration was slightly slower than for Nd

Table 5.5 Comparison of the ν_3 (cm^{-1}) stretch for the alteration of hydrated $NaLn(CO_3)_2$

Neodymium			Europium			
initial ppt	dried 6 days (air)	dried 10mins oven 120°C	initial ppt	dried 6 days (air)	dried 10 days (air)	dried 10 mins oven 120°C
1476.6	1458.7	1457.6	1521.6	1521.3	1459.5	1460.1
1373.5	1403.9	1404.5	1375.8	1376.0	1413.1	1412.3
	1356.0	1352.5			1355.7	1356.3

5.5 calculation of the partial vapour pressure (pH_2O) required for the solid state reaction during dehydration

The water vapour partial pressure required for the equilibrium phase reaction between $NaNd(CO_3)_2.6H_2O$ and $Nd_2(CO_3)_3.8H_2O$ (equation 5.1) can be calculated in a similar manner as the equilibrium reactions in Chapter 4.

The Gibbs free energy of reaction (ΔG_{Rn}^{o}, equation 5.2) can be calculated for the equilibrium reaction (equation 5.1) using the Standard Gibbs free energy of formation for each phase (calculated in Appendix 5.4, using thermodynamic data from Table 4.30)

$$2NaNd(CO_3)_2.6H_2O(cr) = Nd_2(CO_3)_3.8H_2O(cr) + Na_2CO_3(am) + 4H_2O(g)$$
(log Ksp -21.39) (log Ksp -31.35) (5.1)

$$\Delta G_{Rn}^{o} = \Delta G_{f\,(Products)}^{o} - \Delta G_{f\,(Reactants)}^{o} \quad (5.2)$$

$$\therefore \Delta G_{Rn}^{o} = [(-5001.56) + (-1051.6) + 4(-228.57)] - [2(-3533.58)] \quad (5.3)$$

$$= [-6967.44 KJmol^{-1}] - [-7067.16 KJmol^{-1}] = 99.72 KJmol^{-1} \quad (5.4)$$

and the reaction constant for equation 5.1, can then be calculated from equation 5.5

$$\ln K = \frac{-\Delta G_{Rn}^{o}}{RT} \quad (5.5)$$

$$\ln K = -40.22 \quad \therefore \log K = -17.47$$

however as log K can also be expressed in terms of partial vapour pressure then

$$K = [pH_2O]^4 \quad \therefore \log K = 4\log(pH_2O) \quad (5.6)$$

$$\therefore \log(pH_2O) = \frac{\log K}{4} = \frac{-17.47}{4} = -4.4 \quad (5.7)$$

Assuming $NaLn(CO_3)_2.6H_2O$ dehydrates to $Nd_2(CO_3)_3.8H_2O$ the water vapour partial vapour pressure required for the solid state equilibrium reaction is

$$pH_2O = 4.3x10^{-5} \text{ (from } \log(pH_2O) = -4.4 \quad (5.8)$$

The actual vapour pressure calculated will however depend on the relative stability of the actual solid phases used and an increase in $Nd_2(CO_3)_3.8H_2O$ will increase the vapour required for the solid state reaction. Solid state reactions are slow compared to equilibrium between solid-aqueous systems therefore the vapour pressure required for the phase change was calculated from a relatively low value for the $Nd_2(CO_3)_3.8H_2O$, and would be expected as the initial crystalline $Nd_2(CO_3)_3$ form.

5.6 Discussion

Titration experiments (Chapter 3) have shown that $Ln_2(CO_3)_3.xH_2O$ alters to $LnCO_3OH$ when in equilibrium in a sodium ion free aqueous carbonate system (i.e. with K_2CO_3) from a solution above pH 9 which are stable upon drying.

Analysis of the dried product from the titrations containing sodium indicate that $Ln_2(CO_3)_3$ was the apparent equilibrium phase, however, $Ln_2(CO_3)_3$ cannot be the equilibrium phase in a high pH (above pH 9) in a solution containing Na_2CO_3 as the hydroxycarbonate forms as the equilibrium phase above pH 9. Alteration to the $Ln_2(CO_3)_3.xH_2O$ during the drying stages must have occurred from the initial $NaLn(CO_3)_2$ which was formed as the equilibrium phase.

Exposure to any drying processes causes the decomposition of $NaLn(CO_3)_2.6H_2O$. Decomposition occurs by the growth of $Nd_2(CO_3)_3.8H_2O$ with the removal of water from the crystalline structure $NaNd(CO_3)_2.6H_2O$, i.e. a reduction in water content from 6:1 to 4:1of H_2O/Ln^{3+}. Na_2CO_3 is not usually formed as a hydrated phase and is probably the altered Na^+ phase.

$$2NaNd(CO_3)_2.6H_2O_{(cr)} \xrightarrow{\text{Dehydration}} Nd_2(CO_3)_3.8H_2O_{(cr)} + Na_2CO_{3(am)} + 4H_2O_{(g)} \quad (5.1)$$

Mochizuki *et al.*, (1974) prepared hydrated $NaNd(CO_3)_2$ in equilibrium with solutions at temperatures from 20°C to 80°C, therefore alteration must be a dehydration effect as the phase is thermally stable under aqueous conditions. Alteration of $NaLn(CO_3)_2.6H_2O$ can only occur from the dehydration of a solid phase or changes in the bulk solution composition.

Neodymium is often used as an analogue for the identification of solid americium phases. In general solubility experiments are carried out in duplicate for Nd, Eu and Am and solution data can be obtained for all three phases, but the solid is usually only characterised for Nd and Eu as americium decay products are hazardous (from X-ray and alpha particle emission), i.e. Runde *et al.*, (1992). If Nd and Eu can alter from the initial $NaLn(CO_3)_2.6H_2O$ phases then Am could reasonably be assumed to alter in a similar manner. Care must therefore be taken in the identification of solid equilibrium phases, preferably using freshly prepared samples before any drying processes can be initiated. However the identification of wet samples can be difficult as water peaks tend to occlude the infra red spectra, and XRD peaks may be severely reduced from the amorphous nature of excess water in a sample.

The identification of the correct phase is important when calculating the solubility product as the reaction constant depends upon the component ions in solution and their formula ratio; if $Nd_2(CO_3)_3$ is misidentified instead of $NaNd(CO_3)_2$ then the solubility products (Ksp) calculated from the following reactions (equations 5.9 & 5.10) and solubility determinations (equations 5.11 & 5.12)

$$NaNd(CO_3)_2 = Na^+ + Nd^{3+} + 2CO_3^{2-} \quad (5.9)$$

$$Nd_2(CO_3)_3 = 2Nd^{3+} + 3CO_3^{2-} \quad (5.10)$$

$$\log Ksp[NaNd(CO_3)_2] = \log a_{Na^+} + \log a_{Nd^{3+}} + 2\log a_{CO_3^{2-}} \quad (5.11)$$

$$\log Ksp[Nd_2(CO_3)_3] = 2\log a_{Nd^{3+}} + 3\log a_{CO_3^{2-}} \quad (5.12)$$

where a is the species activity

will clearly be different for each solid phase when calculated from the same solution composition. The $Nd_2(CO_3)_3$ value will also be in error as the solution will not be in equilibrium with this phase.

Determination of the solubility product of radioactive materials is important because this is used to determine their solubility and ultimately used to predict the amount and possible rate of transport from a nuclear waste repository. There is the possibility in misinterpreting the equilibrium phase as an estimation of the solubility limiting phase or as an indication to the possible solution composition in equilibrium with the solid phase if the hydrated $NaLn(CO_3)_2$ has completely altered to hydrated $Ln_2(CO_3)_3$. The system can be further confused at the $NaLn(CO_3)_2$-$LnCO_3OH$ phase boundary when the two phases are in equilibrium. Drying could (partially or completely) alter the $NaLn(CO_3)_2$ to $Ln_2(CO_3)_3$ indicating either a $NaLn(CO_3)_2$-$Ln_2(CO_3)_3$-$LnCO_3OH$ triple point or a $Ln_2(CO_3)_3$-$LnCO_3OH$ equilibria under the sample conditions.

In the moist environment the $NaLn(CO_3)_2.6H_2O$ remained unaltered, therefore the phase will remain stable in the aqueous environment if precipitates from. If the precipitation environment dries to the extent that alteration occurs in a disposal regime then aqueous transport cannot occur without any fluid flow and

effectively trapping the lanthanide (or Americium analogue) crystals in the host matrix.

5.7 References

MOCHIZUKI, A., NAGASHIMA, K., and WAIKITA, H., (1974) The synthesis of crystalline hydrated double carbonates of rare-earth elements and sodium. *Bull. Chem. Soc. Jpn* **47** 755-756

NAKAMOTO, K., (1986) Infrared and ramen spectra of inorganic and coordination compounds. *Wiley* New York

RAO, L. F., RAI, D. P., FELMY, A. R., FULTON, R. W., and NOVAK, C. F., (1996) Solubility of $NaNd(CO_3)_2.6H_2O$ in concentrated Na_2CO_3 and $NaHCO_3$ solutions. *Radiochim. Acta* **75** 141-147

RUNDE, W., MEINRATH, G., and KIM, J. L., (1992) A study of solid-liquid phase-equilibria of trivalent lanthanide and actinide ions in carbonate systems. *Radiochim. Acta* **58/59** 93-100

SCHEER, VON H. and SEIDEL, H., (1981) High pressure synthesis of carbonates. VI. Sodium lanthanoid carbonates. *Z. Anorg. Allg. Chem.* **477** 196-204

VITORGE, P., (1992) $Am(OH)_3$, $AmOHCO_3$ and $Am_2(CO)_3$ stabilities in environmental conditions. *Radiochim. Acta* **58/59** 105-107

Chapter 6

Lanthanide Solubility in Sulphate bearing Solutions

6.1 Introduction

The aqueous chemistry of the lanthanide sulphate system was investigated to determine the effects of different sulphate activities over a pH range, and compare the results with those found in the carbonate and the carbonate free system. The sulphate ion (SO_4^{2-}) is present in many natural solutions as the second most abundant anion to carbonate, and may form similar phases to those found in the carbonate system. The free sulphate ion (SO_4^{2-}) is dominant at lower pH than the free carbonate ion (CO_3^{2-}), therefore the SO_4^{2-} ion may be expected to have greater effects upon lanthanide phases formed at lower pH than the comparable carbonate phases.

The sulphate system was examined following a method similar for that of the lanthanide carbonate system (Chapters 3 and 4). However it was not possible to use a sodium sulphate solution to increase the pH of the initial lanthanide chloride solutions during titrations. Therefore to study the Ln^{3+}-SO_4^{2-} system over a pH range, mixed solutions of sulphate and lanthanide were titrated against NaOH or KOH.

A number of different lanthanide sulphate compounds have been previously reported. In 1960, double salts of $NaLn(SO_4).xH_2O$ were synthesised by Tulinova *et al.*, (1960) and Zaitseva *et al.*, (1964). A series of hydroxy sulphates have also been proposed by Margulis *et al.*, (1970), with the formulae $Ln_2(OH)_4SO_4$ and $Ln(OH)SO_4$. These studies have focused on determining conditions for the synthesis and then characterising any compounds formed using XRD, IR, TGA and elemental analysis. To date no studies have been reported to determine the solubility products of the lanthanide sulphate phases.

Solubility is dependant upon the Na^+, OH^-, Ln^{3+} and SO_4^{2-} activities, therefore precipitates could form at an acidic to intermediate pH with H_2SO_4 and Na_2SO_4 or high pH from OH^-/SO_4^{2-} solutions instead of the limited intermediate to high pH solutions found for the carbonate system; as $CO_2(g)$ is evolved under acidic

conditions. A complete series of solid phase lanthanide sulphates are possible from low pH sulphates to high pH hydroxide (or carbonate) phases.

6.2 Titrations of lanthanide chlorides in sodium sulphate solutions

All solutions were prepared by dissolving an appropriate quantity of the reagent in distilled degassed water as shown in Table 6.1. The distilled water was degassed by boiling, then bubbling $N_2(g)$ through the water whilst cooling to remove any dissolved carbonate.

Table 6.1 Chemicals and dilutions of the stock solutions used in the titrations and solubility determinations

	F.W. ($gmol^{-1}$)	Dilution	conc^{n} (M)
$CeCl_3.7H_2O$ (99+%)	372.59	18.6295g in 250 cm^3	0.2M
$NdCl_3.6H_2O$ (99.9%)	358.69	17.9345g in 250 cm^3	0.2M
$SmCl_3.6H_2O$ (99.9%)	364.80	18.240g in 250 cm^3	0.2M
$EuCl_3.6H_2O$ (99.9%)	366.41	18.3205g in 250 cm^3	0.2M
NaOH (Analar)	40.00	2.00g in 500 cm^3	0.1M
KOH (Analar)	56.11	2.8055g in 500 cm^3	0.1M
Na_2SO_4 (Analar)	142.04	7.102g in 500 cm^3	0.1M
K_2SO_4 (Analar)	174.25	8.7125g in 500 cm^3	0.1M

6.2.1 Experimental

Solutions of $LnCl_3$ ($5cm^3$, 0.2M), where Ln = Ce, Nd or Eu were mixed with different volumes of Na_2SO_4 (0.2M), to give starting solutions of different ratios of lanthanide to sulphate ions as indicated in Table 6.2. The solutions were then diluted to 160 cm^3 with degassed distilled water.

Table 6.2 Lanthanide-Sulphate starting solution ratios

Solution number	volume of Na_2SO_4 added	mol ratio of Ln^{3+}/SO_4^{2-}
1	SO_4^{2-} free	1:0
2	$2.5cm^3$ Na_2SO_4	1:0.5
3	$5cm^3$ Na_2SO_4	1:1
4	$25cm^3$ Na_2SO_4	1:5
5	$50cm^3$ Na_2SO_4	1:10
6	$100cm^3$ Na_2SO_4	1:20

The mixed Ln^{3+}/SO_4^{2-} solution was placed in a $250cm^3$ three-necked round bottomed flask, which had previously been degassed with $N_2(g)$ to ensure an inert atmosphere. Nitrogen was continuously bubbled into the vessel through one side-neck to ensure a positive N_2 atmosphere. A pH electrode was fitted securely to the second side-neck. A burette was placed in the centre neck. The solution was stirred with a magnetic stirrer.

The mixed solution was titrated with a solution of NaOH (0.1M, $40cm^3$), which was added dropwise using a burette. After each addition, the solution was allowed to equilibrate, indicated by a stable pH reading. The pH value was then recorded prior to further addition. Each titration was repeated three times.

At the end of the titration experiment, the contents of the flask were transferred to $250cm^3$ HDPE Nalgene bottles under an atmosphere of N_2. The precipitate formed during the reaction was then filtered through a Whatman N°4 sintered glass crucible washed with water and then dried over silica gel in a vacuum dessicator. Additionally a set of precipitates from replicate titrations were

allowed to equilibrate in a waterbath (25°C) for at least 2 months to ensure the system had achieved equilibrium. The identity of the initial and equilibrated phases were compared by XRD, FTIR and elemental analysis.

6.2.2 Titration Results

There are no significant differences between the titration curves of each lanthanide (Ce, Nd or Eu) examined in the Na_2SO_4 bearing starting solutions. The results of a typical titration are shown in Figure 6.1. The starting solutions of Nd and Eu (lilac Nd and yellow tinge for Eu) are clear. For Ce, the solution is clear and colourless, but where a Na_2SO_4 concentration was present a slight precipitate was evident. Initial NaOH additions of $0.1cm^3$ show a rapid rise in pH from pH~4.3 to pH 7 occurs which stabilises in 5-10mins after each addition for the first $0.5cm^3$ of NaOH titrated. There was no further significant increase in pH with continued addition of a further $20cm^3$ of NaOH.

After the initial rapid rise in pH, the pH stabilises rapidly (in 20-30 seconds) after each successive addition of NaOH, and a precipitate (white Ce and Eu, pale lilac for Nd) is formed. An initial precipitate can be seen after approximately $1.0cm^3$ to $2.5cm^3$ of NaOH. The solution becomes increasingly opaque as precipitation increases.

Precipitation continues until a 2:1 OH^-:Ln^{3+} ratio is obtained (after approximately $20cm^3$ of NaOH). The pH then rises sharply from pH 8.5 to pH 10 after $23cm^3$ of NaOH was added. The rate of pH increase then slows to 0.05 pH units per $5cm^3$ of titre. The titration was stopped at 40ml NaOH and pH 11.5 and a 4:1 ratio of NaOH to $LnCl_3$ had been titrated, i.e. in excess of that expected for $Ln(OH)_3$ formation.

The Nd and Eu precipitates did not show any obvious changes after the rise to pH10, however Ce alters to a yellow precipitate.

Figure 6.1 Typical titration curve for $EuCl_3 + xNa_2SO_4$ with 4NaOH

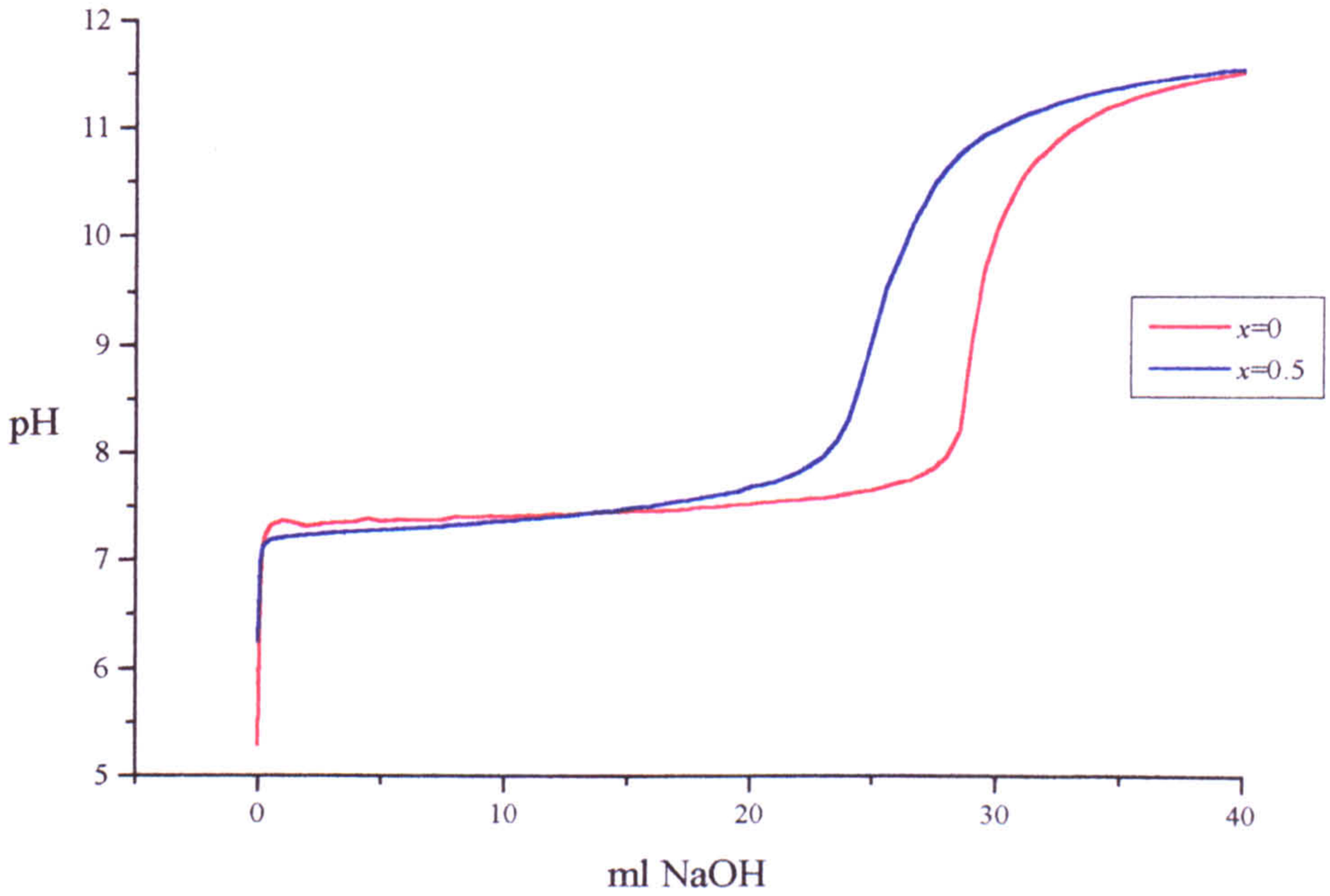

For sulphate free titrations addition of sodium hydroxide titre caused an initial sharp increase in pH, followed by a stable pH without precipitation. Precipitation occured after 26cm^3 of NaOH had added, the pH then increased sharply from pH 7 to pH 12 with further precipitation. The pH of the sulphate and sulphate free solutions remained the same after the final sharp rise in pH.

6.2.3 Characterisation of precipitates

The initial and final precipitates formed at different pH conditions from the titration of the lanthanide ion in sulphate and sulphate free systems were isolated and characterised. The precipitate formed between pH 7-8.5 for the Nd and Eu sulphate containing systems were isolated and analysed. The solid phase formed from starting solutions containing up to 30mM Na_2SO_4 had a distinctive IR pattern with sharp hydroxy stretches and a distinct sulphate triplet (Figure 6.2). This indicates the presence of a lanthanide hydroxy sulphate phase, which was confirmed as $Ln_2(OH)_4SO_4$ by powder XRD (Figure 6.3). The splitting of the sulphate into a triplet at 1130cm^{-1} (Table 6.3) is typical of a bridging sulphate

group between two metal ions within the crystalline structure, (Margulis *et al.*,, 1970).

The X-ray diffraction pattern of the solid phase precipitated at the mid point of the titration is often weak, but forms a distinctive XRD pattern that can be matched with the JCPDS reference pattern (Table 6.4), however the most crystalline samples have two extra peaks at 2θ of 10.6° and 17.6° which do not appear on the reference pattern. These peaks were not included in the original reference pattern, which was not run below a 2θ of 20°.

When the Na_2SO_4 concentration is increased to above 70mM, the phase isolated at pH6-7 is a mixture of $Ln_2(OH)_4SO_4.xH_2O$ and $NaLn(SO_4)_2$. $NaLn(SO_4)_2$ was found only as a mixture in the titration experiments and could not be isolated as a pure phase from the buffer region of the titration curve.

Table 6.3. Infra-red stretches of hydrated $Ln_2(OH)_4SO_4$ and $NaCe(SO_4)_2$, titration precipitate pH 7-8.5

	$Nd_2(OH)_4SO_4$ $.2H_2O$[1]	Nd precipitate	Eu precipitate	Ce precipitate
OH^-	3567 3440	3602 3474	3608 3475	
H_2O	3210	3227	3209	3557 3509
H_2O	1635	1638	1653	1617
H_2O	783	785	809	
SO_4^{2-}	1160 1116 1073	1183 1122 1082	1182 1128 1082	1109
SO_4^{2-}	585	617 587 538	592.1	651 596 496

[1]Margulis *et al.*, (1970)

Figure 6.2 FTIR spectra of $Ln_2(OH)_4SO_4.xH_2O$; Initial Nd and Eu precipitates between pH 7 and 8

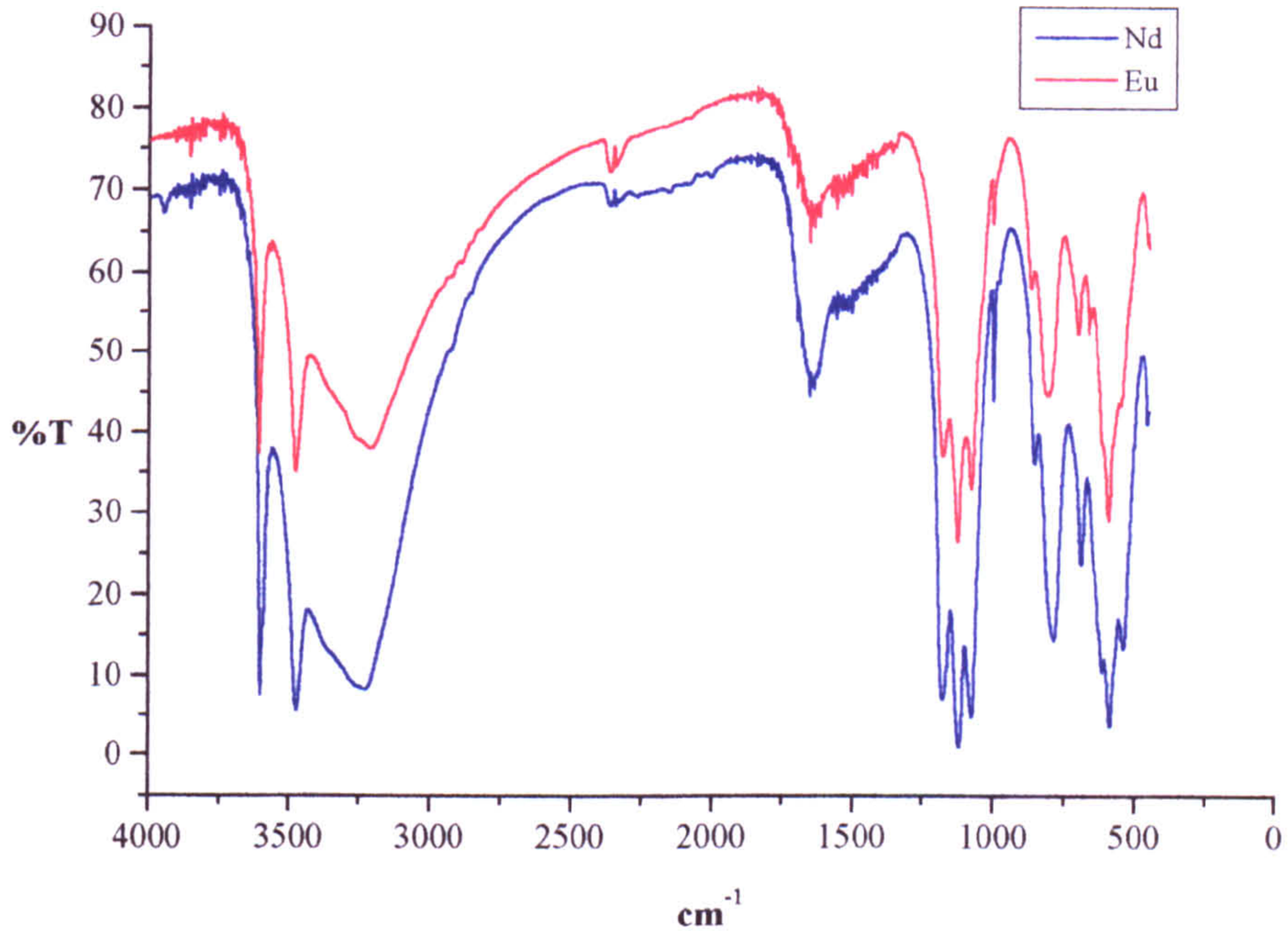

Figure 6.3 XRD pattern of $Ln_2(OH)_4SO_4.xH_2O$: Initial Nd and Eu precipitates between pH 7 and 8

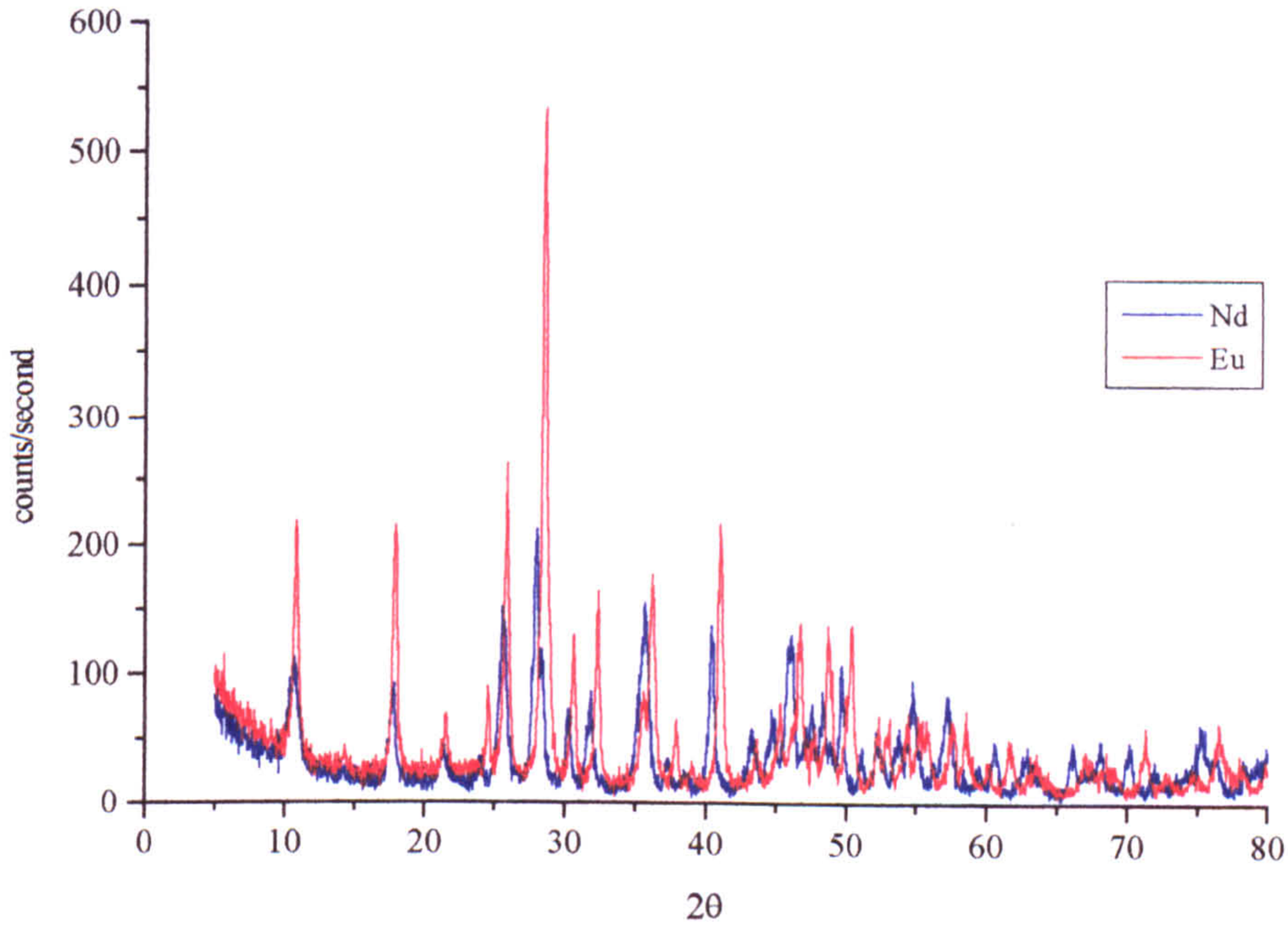

Table 6.4 XRD peaks of $Nd_2(OH)_4SO_4$ and $Eu_2(OH)_4SO_4$

Reference pattern[1]	$Nd_2(OH)_4SO_4$		$Eu_2(OH)_4SO_4$	
d(Å)	2θ	d(Å)	2θ	d(Å)
	10.635	8.3119	11.015	8.0260
	17.620	5.0294	18.000	4.9241
	21.210	4.1856	21.610	4.1090
	23.965	3.7103	24.615	3.6137
3.500	25.560	3.4822	25.915	3.4353
3.230	27.805	3.2060		
	28.215	3.1603	28.520	3.1272
3.030	30.270	2.9503	30.690	2.9109
2.830	31.670	2.8230		
	35.175	2.5493	32.510	2.7519
2.520	35.755	2.5093	35.675	2.5147
	37.280	2.4100	36.460	2.4623
	38.390	2.3429	38.095	2.3603
2.250	40.465	2.2274	39.200	2.2963
	43.245	2.0904	43.800	2.0652
1.990	44.820	2.0206	45.550	1.9899
	46.155	1.9652	46.965	1.9331
	47.095	1.9281	47.875	1.8985
	48.270	1.8839	48.935	1.8598
1.840	49.615	1.8359	50.630	1.8015
			52.275	1.7486
1.690	53.720	1.7049	53.075	1.7421
	54.770	1.6747	54.490	1.6826
			55.310	1.6596
			55.910	1.6432
1.610	57.055	1.6129	57.715	1.5960

[1]JCPDS file 23-1114

Ce on the other hand does not form a hydroxy-sulphate at intermediate pH but precipitates as the double sulphate $NaCe(SO_4)_2.xH_2O$. This is formed in all solutions containing sulphate from the titrations studied phase, a Ce hydroxy-sulphate phase was not obtained. Infra red analysis of the $NaCe(SO_4)_2$ shows a characteristic strong single sulphate stretch at $1100cm^{-1}$ (Table 6.3, Figure 6.4) and indicates that a bridging sulphate group is not present, implying that the compound is a double salt. There is no published infra red data for $NaCe(SO_4)_2.xH_2O$, although confirmation of the compound was performed by XRD and elemental analysis (Figure 6.5) which compares well with the data obtained by Tulinova *et al.*, (1960) and Zaitseva *et al.*, (1964). $NaCe(SO_4)_2$ forms a significantly stronger X-ray diffraction pattern than obtained for the hydroxy-sulphate phases.

Figure 6.4 FTIR spectrum of $NaCe(SO_4)_2$: Initial Ce precipitate

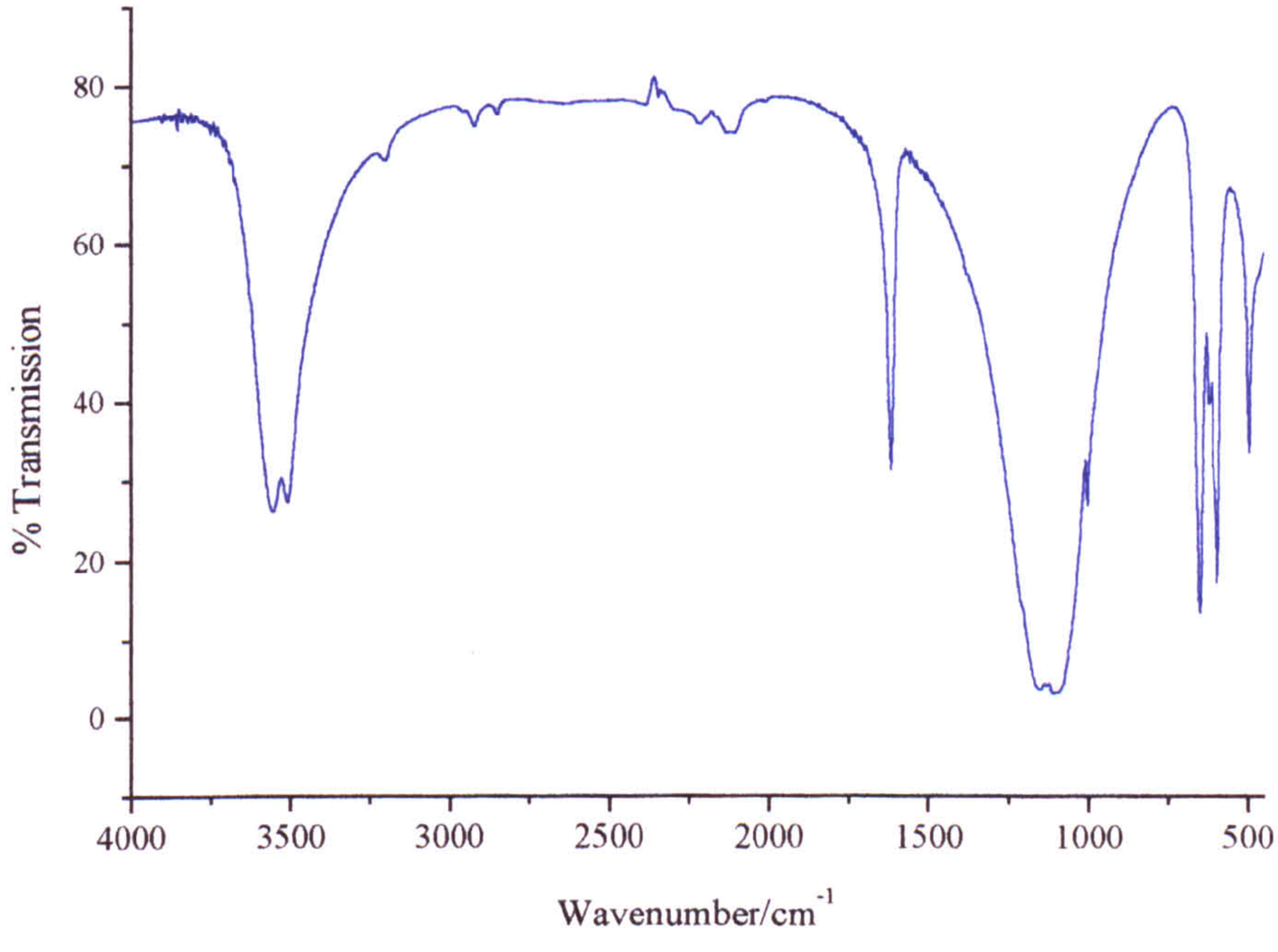

Table 6.5 $NaCe(SO_4)_2$ XRD data JCPDS File 40-481 $NaNd(SO_4)_2$ (after Zaitseva *et al.*, 1964)

Reference	Ce precipitate		Reference	Ce precipitate	
d(Å)	2θ	d(Å)	d(Å)	2θ	d(Å)
6.048	15.050	5.882	1.572	57.030	1.614
5.472	16.580	5.343	1.563	59.465	1.553
3.501	25.895	3.438	1.494	62.170	1.492
3.034	29.925	2.984	1.468	63.540	1.463
2.859	30.755	2.9048	1.452	64.830	1.437
2.483	36.735	2.445	1.386		
2.376	38.190	2.355	1.375	68.165	1.375
2.167	41.270	2.186	1.364	68.965	1.361
1.936	45.905	1.975	1.322	71.805	1.314
1.876	49.220	1.850	1.287	73.490	1.288
1.757	52.755	1.734	1.264	74.805	1.268
1.716	53.345	1.716	1.227	78.630	1.216
1.687	53.970	1.698	1.189		
1.591	55.085	1.666			

Figure 6.5 XRD pattern of $NaCe(SO_4)_2.2H_2O$
Initial precipitate from Ce/SO_4^{2-} titrations

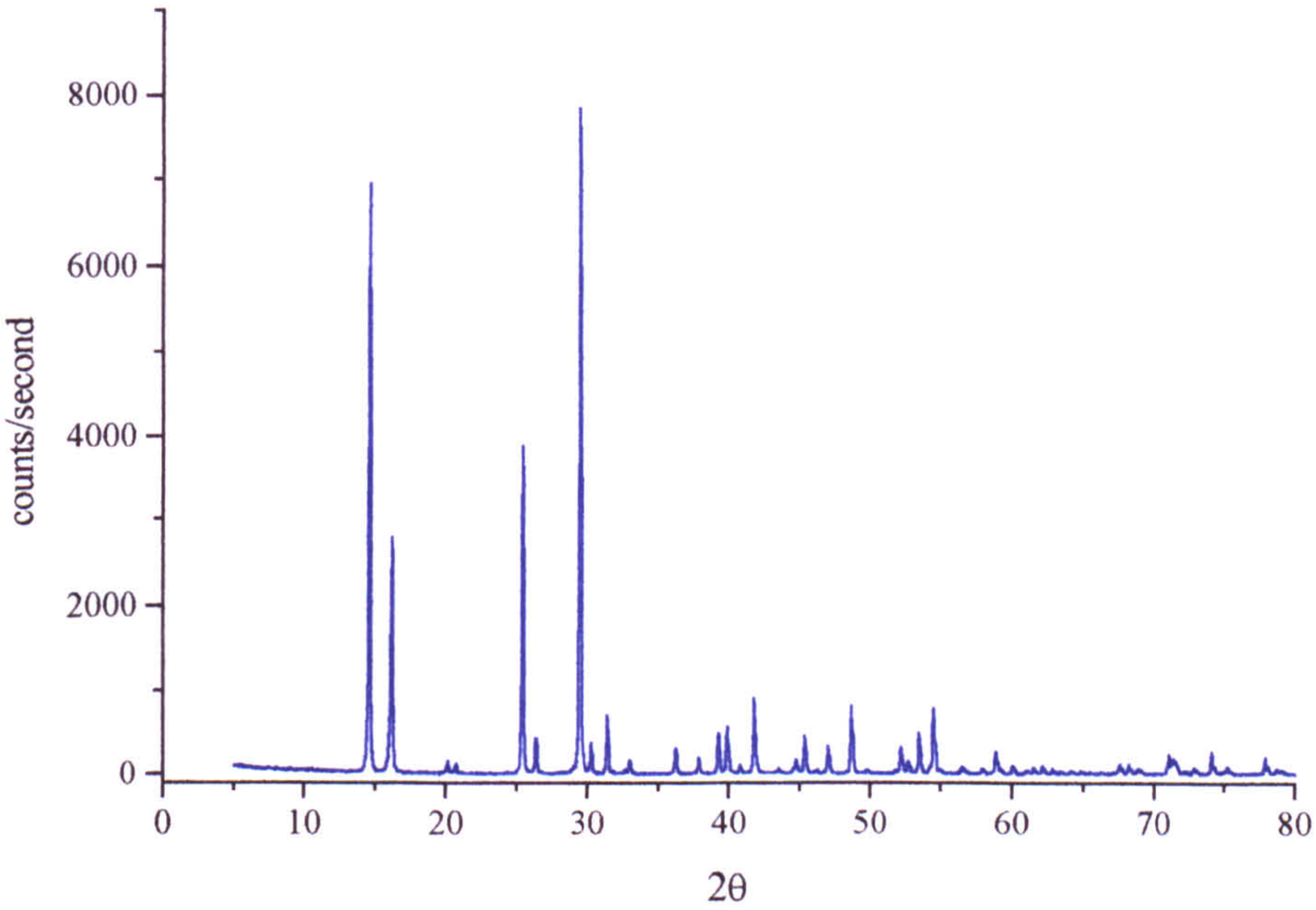

When the titrations for all rare earth element solutions are continued above pH 10, the $Nd_2(OH)_4SO_4$ and $Eu_2(OH)_4SO_4$ precipitates alter to $Nd(OH)_3$ and $Eu(OH)_3$ respectively, whilst Ce oxidises to the yellow coloured CeO_2. The nature of these compounds are the same as found in the sulphate free titrations. FTIR analysis indicates residual SO_4^{2-} at $1120cm^{-1}$ in the end products, although there was no trace of a sulphate phase from XRD analysis. The sulphate was not present in the infra red spectrum after 2 months equilibration (Figure 6.6, Table 6.6).

Occasionally there is slight evidence of a ν_3 carbonate doublet at $1500cm^{-1}$ in the infra-red spectrum, especially if the sample was formed above pH 8 (Figure 6.6). This is due to carbonate contamination caused during the drying and isolation process and usually forms as a surface layer only detectable from infra-red analysis (Diakonov *et al.*, 1998). XRD analysis of the end product shows an almost amorphous (XRD maximum peak height <150 counts) $Ln(OH)_3$ for Nd and Eu. Ce is oxidised to the yellow CeO_2 (fully characterised in Section 3.3.3).

Table 6.6 FTIR stretches of $CeO_2/Ln(OH)_3$ from the end precipitate of the sulphate and sulphate free NaOH titrations

stretch	Ce ppt	Nd ppt	Eu ppt
OH^-		3608	3608
H_2O	3340	3423	3422
H_2O	1624	1636	1638
OH^-		668	701

Figure 6.6 FTIR Spectra of CeO_2 and $Ln(OH)_3$: End precipitate of the sulphate and sulphate free NaOH titrations

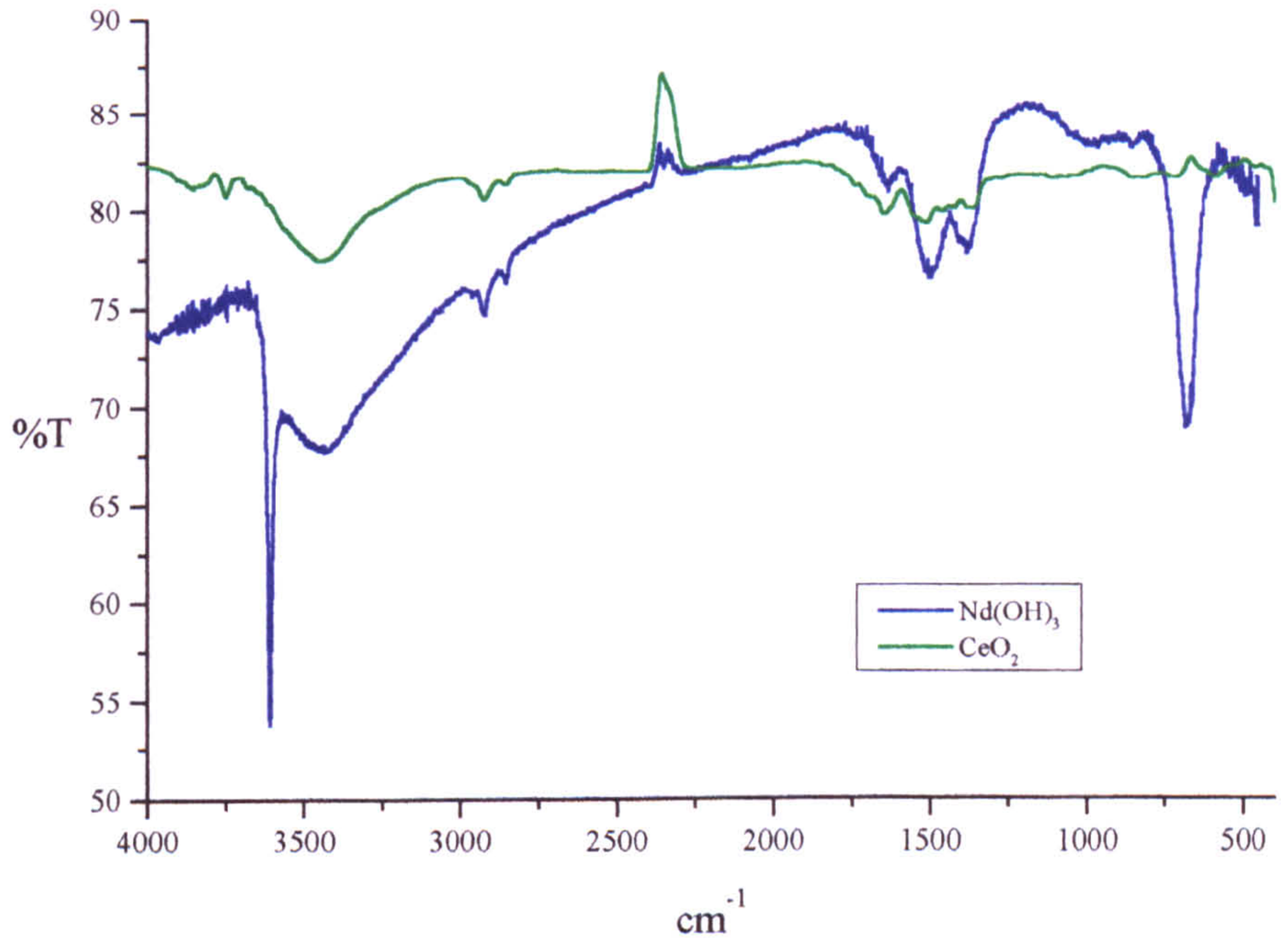

6.2.4 Titration Discussion

Four phases precipitate in the lanthanide-sulphate-sodium-hydroxide system examined in the titration experiments. Ce initially precipitates as the sodium cerium double sulphate, $NaCe(SO_4)_2.xH_2O$ from pH 5, which is then oxidised to CeO_2 above pH 11. Cerium hydroxy phases were not isolated. Nd and Eu initially precipitate above pH 7.5 as the hydroxy-sulphates $Nd_2(OH)_4SO_4$ and $Eu_2(OH)_4SO_4$, even if Nd and Eu are in excess of the sulphate concentration. Nd and Eu will form the double salt $NaLn(SO_4)_2.xH_2O$, at the Na^+ and SO_4^{2-}

activities used in the titrations, but only as mixtures with the hydroxy-sulphates, $Nd_2(OH)_4SO_4$ and $Eu_2(OH)_4SO_4$. The $Nd_2(OH)_4SO_4$ and $Eu_2(OH)_4SO_4$ precipitates alter to the hydroxide phases $Nd(OH)_3$ and $Eu(OH)_3$ respectively above pH 11.

Figure 6.7 Typical titration curves for $NdCl_3 + xNa_2SO_4$ with 4NaOH

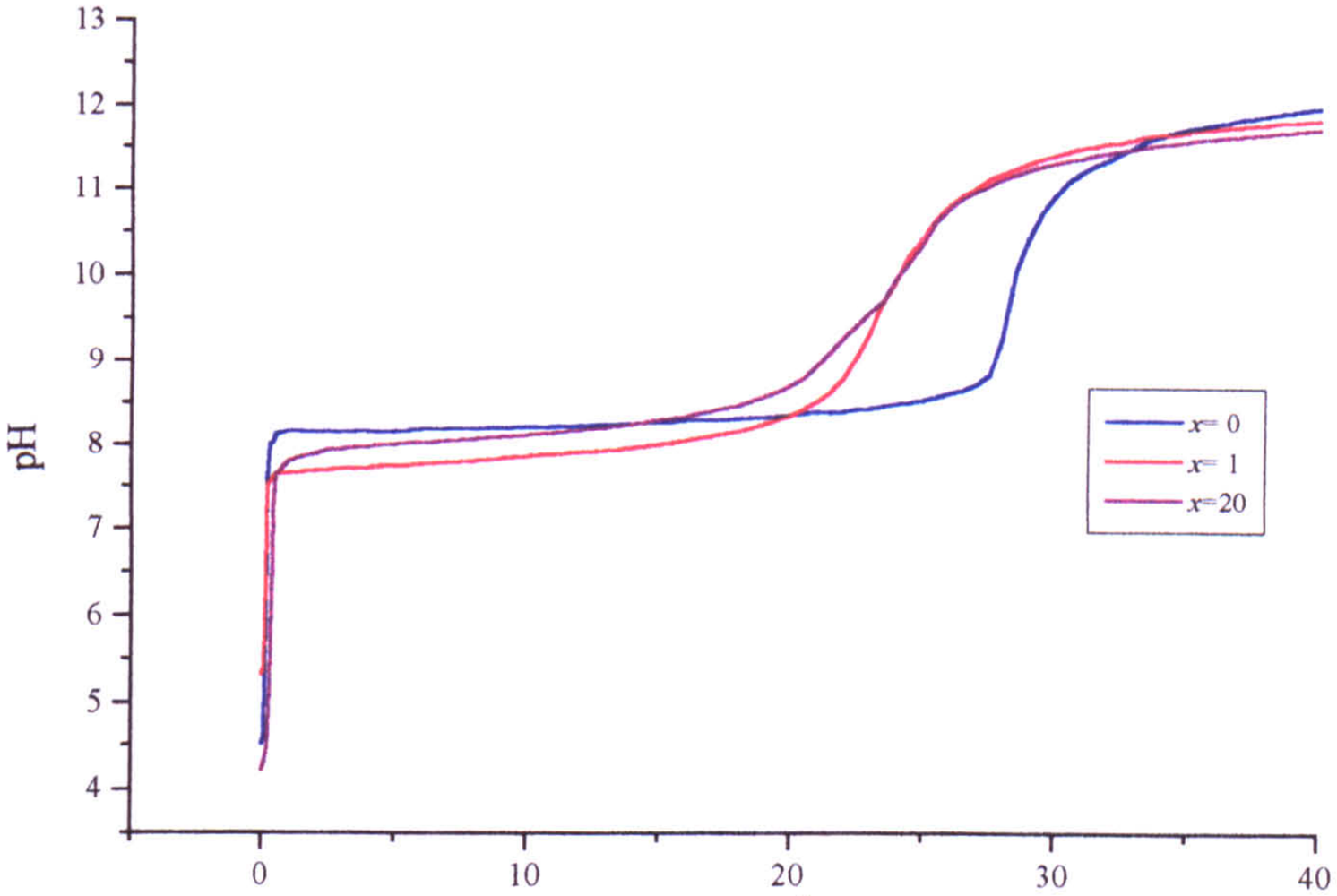

There were no significant observable differences in the titration curves for increasing the sulphate concentration in solution from a starting solution of excess Ln^{3+} to SO_4^{2-} (Figure 6.1) to an initial solution of excess SO_4^{2-} to Ln^{3+} (Figure 6.7), and for the three lanthanides examined, even though the Ce precipitates were significantly different to the Nd and Eu precipitates. In all cases, the initial rise in pH from pH5 to pH 7.5 was followed by precipitation, the pH was then buffered by continuous precipitation during the addition of NaOH(aq) until a 2:1 ratio of NaOH to Ln^{3+} had been added to the solution.

In the Nd and Eu systems the $Ln_2(OH)_4SO_4$ precipitate forms according to equation 6.1 and indicates that all of the Nd or Eu has precipitated by this point.

$$LnCl_3 + \tfrac{1}{2}Na_2SO_4 + 2NaOH \longrightarrow \tfrac{1}{2}Ln_2(OH)_4SO_4(s) + 3NaCl(aq) \quad (6.1)$$

An excess of Na_2SO_4 in the initial solution will therefore not have an effect upon the titration curve as the precipitation rate is controlled by the addition of OH^- to the solution. The initial $Ln_2(OH)_4SO_4$ phase does not appear to form below pH 7 due to the low hydroxide activity of the solution.

After a 2:1 NaOH to Ln^{3+} has been added to the solution all the aqueous Ln^{3+} has precipitated and the pH cannot be buffered further. The pH then rises sharply to pH 12 and a further reaction between the solid phase and aqueous hydroxide (equation 6.2) causes the $Ln_2(OH)_4SO_4$ to alter to $Ln(OH)_3$ for Nd and Eu.

$$\tfrac{1}{2}Ln_2(OH)_4SO_4(s) + OH^-(aq) \longrightarrow Ln(OH)_3(s) + \tfrac{1}{2}SO_4^{2-}(aq) \qquad (6.2)$$

Nd and Eu require higher Na^+ and SO_4^{2-} activities to form the sodium double sulphate than Ce.

The carbonate titrations (Chapter 3), indicated that cerium does not form stable hydroxy phases, as indicated by the direct conversion of $Ce_2(CO_3)_3$ to CeO_2, without an intermediate hydroxycarbonate phase, therefore a stable $Ce_2(OH)_4SO_4$ is unlikely to form. The CO_3^{2-} ion is the dominant carbonate species only above pH 10 (Figure 4.4), whilst the SO_4^{2-} ion is the dominant aqueous sulphate species above pH 2 (Figure 6.8), therefore the sodium cerium double sulphate can form at a lower pH than the equivalent sodium lanthanide carbonates (Chapter 4) which form above pH 8.

Figure 6.8 Aqueous speciation of 1mM sulphate from pH 2-10

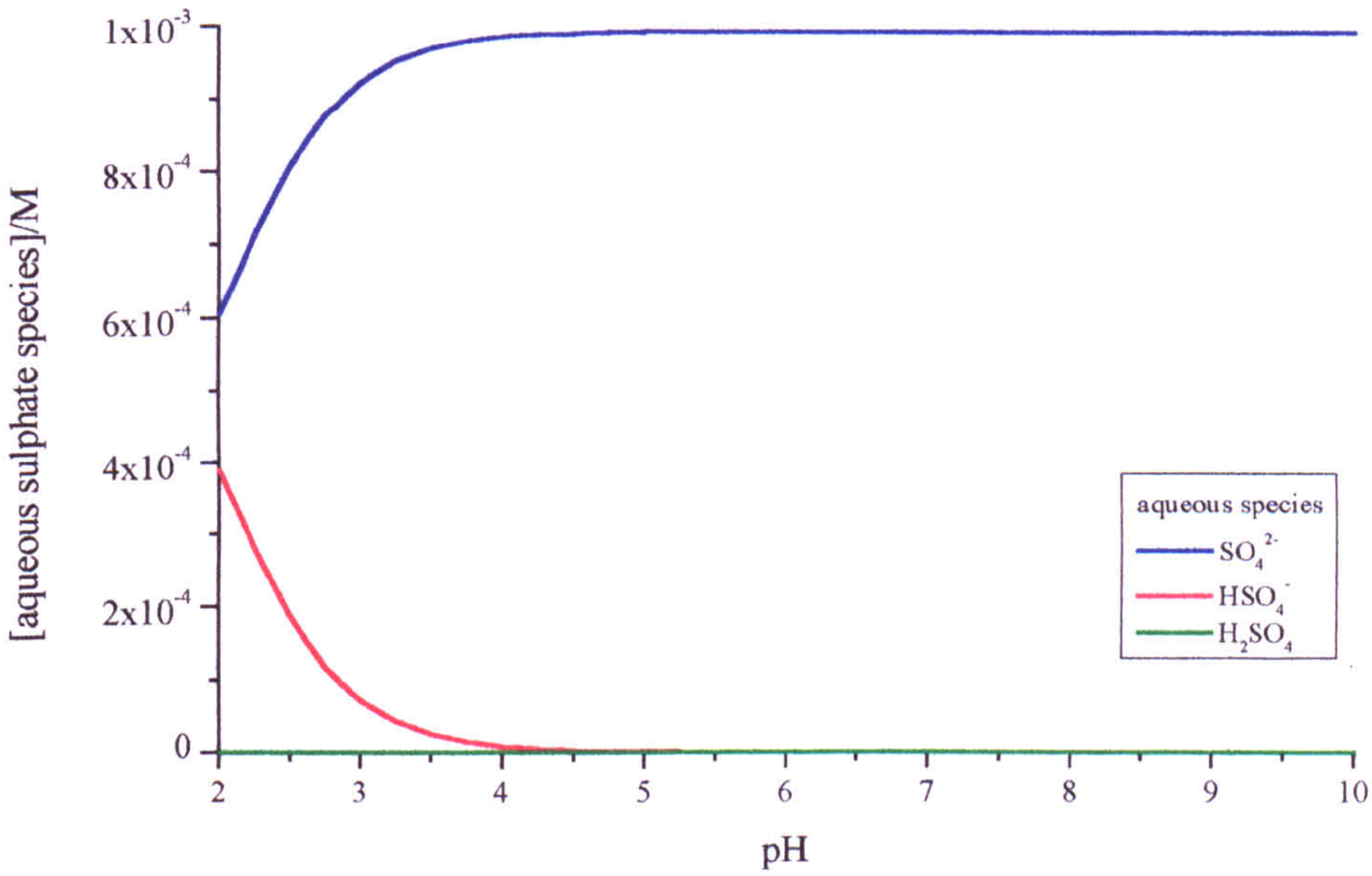

A 2:1 ratio of SO_4^{2-} to Ce^{3+} is required to form $NaCe(SO_4)_2$ (equation 6.3)

$$CeCl_3(aq) + 2Na_2SO_4 \longrightarrow NaCe(SO_4)_2(s) + 3NaCl(aq) \qquad (6.3)$$

If sufficient Na_2SO_4 is introduced to the $CeCl_3$ solution then precipitation may take place immediately at pH 4.5. A Ce hydroxy phase was not isolated but may have formed as an intermediate phase in equilibrium with the aqueous sulphate solution. It is possible that the weak hydroxy-sulphate and CeO_2 X-ray patterns may be occluded by the much stronger $NaCe(SO_4)_2$ XRD pattern.

At high pH, the $NaCe(SO_4)_2$ (s) phase also alters, but is oxidised to CeO_2 instead of forming $Ce(OH)_3$ (equation 6.4)

$$NaCe(SO_4)_2(s) + 2OH^- \longrightarrow CeO_2(s) + e^- + 2H^+ + 2SO_4^{2-} + Na^+ \qquad (6.4)$$

$$\longrightarrow CeO_2(s) + \tfrac{1}{2}H_2 + H^+ + 2SO_4^{2-} + Na^+$$

In the sulphate free titrations where NaOH is added directly to the aqueous $LnCl_3$, no precipitate was seen below pH 8. The only phases to form in these titrations was $Nd(OH)_3$, $Eu(OH)_3$ and CeO_2 and below pH 8 the Ln^{3+} is soluble. The pH increases from pH 4.5 to pH 7 from the first addition of NaOH. Further additions of NaOH do not increase the solution pH or form a precipitate. This implies the

formation of aqueous lanthanide hydroxy species indicated by the buffered pH region. Figure 6.9 shows that $NdOH^{2+}(aq)$ forms as a significant aqueous species above pH 7. The formation of two further species, $Ln(OH)_2^{+}$ and $Ln(OH)_3^{0}(aq)$ can also buffer the solution pH.

When sufficient NaOH has been added to convert all the aqueous lanthanide to $Ln(OH)_3^{0}$ (equation 6.5), the solution pH then rises sharply and precipitation of $Ln(OH)_3(s)$ occurs at this point.

$$LnCl_3(aq) + 3NaOH(aq) \longrightarrow Ln(OH)_3^{0}(aq) + 3NaCl(aq) \quad (6.5)$$

In comparing the carbonate and sulphate systems, it is apparent that the $Ln_2(SO_4)_3$ is more soluble than the equivalent $Ln_2(CO_3)_3$ phase which precipitates almost immediately from $NaHCO_3$ titrations.

Figure 6.9 Aqueous hydroxy speciation of 10^{-7}M Nd from pH 2 to 10 (After Lee & Byrne, 1992)

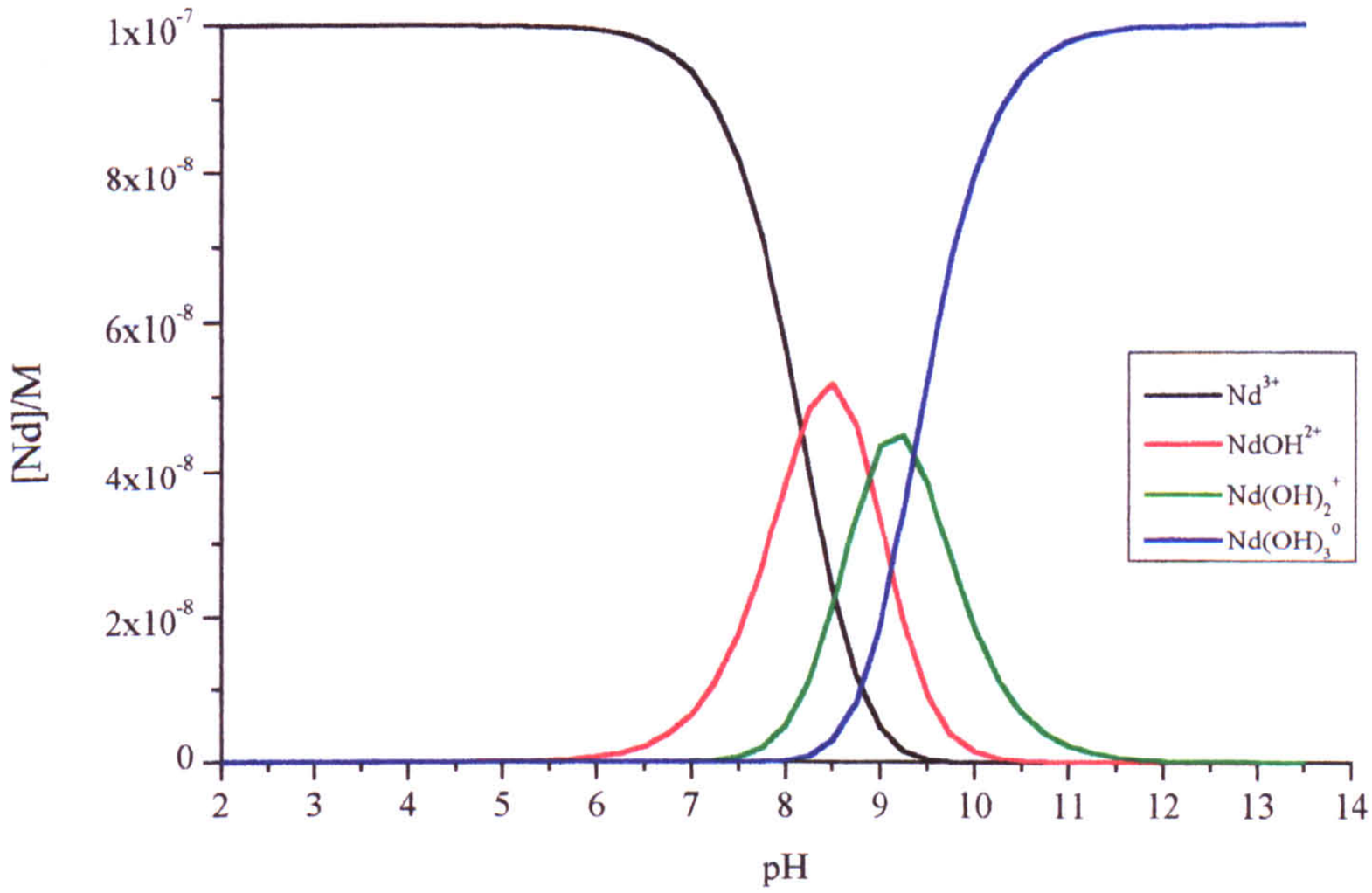

6.3 Solubility Determination of lanthanide sulphate phases

The solubility product of the sulphate phases can be used to calculate the solubility limit of lanthanides under a variety of conditions and therefore determine the important lanthanide-sulphate solubility limiting phases. The Gibbs free energy of formation of each phase can be calculated from the solubility product, which can be subsequently used to derive the exact phase relations between the $NaLn(SO_4)_2$ or $Ln_2(OH)_4SO_4$ phases and the relevant carbonate phases (Chapter 4).

Preliminary batch experiments were conducted to identify the phases formed over specific zones of the titration curve. Preliminary experiments showed that the phases formed often occurred as mixtures. Namely the $NaLn(SO_4)_2$ and $Ln_2(OH)_4SO_4$ phases occur at high sulphate activities (i.e. >50mM), at lower sulphate activities below pH 9, mixtures of $Ln(OH)_3$ and $Ln_2(OH)_4SO_4$ form.

However pure phases of $NaLn(SO_4)_2.xH_2O$ could be isolated at pH~0 by controlling pH and SO_4^{2-} activity with H_2SO_4, and by carefully controlling solution pH between pH 5 and 8, $Ln_2(OH)_4SO_4.xH_2O$ could be isolated from solution. At high pH the hydroxide phase $Ln(OH)_3$ forms. Full details of the preparations are given below.

The K analogue $KLn(SO_4)_2$ could not be prepared for Ce, Nd or Eu, but the Ce analogue $K_{10}Ce_2(SO_4)_8$ was formed using K_2SO_4 instead of Na_2SO_4. This was found to revert to CeO_2 at intermediate pH. The $K_{10}Ce_2(SO_4)_8$ phase was not examined in greater detail, as the phase altered to $NaCe(SO_4)_2$ if Na^+ was present in solution. The Nd and Eu analogues could not be prepared. $Ln_2(SO_4)_3$ phases could not be formed under any of the conditions studied in either titration or batch experiments, and are not considered further.

6.3.1 Preparation of $Ln_2(OH)_4SO_4.xH_2O$

$Ln_2(OH)_4SO_4.xH_2O$ (Ln = Nd or Eu) was prepared by precipitation in a CO_2-free environment. All vessels were degassed with N_2 and all solutions prepared with degassed distilled water.

A mixture of $LnCl_3$ (0.2M, $5cm^3$), Na_2SO_4 (0.2M, $25cm^3$) and NaOH (0.2M, $10cm^3$) was diluted to $100cm^3$ with degassed distilled water in $125cm^3$ HDPE Nalgene bottles. The reaction mixture was kept under N_2 in a waterbath at 25°C for 2 months to ensure complete reaction and equilibration before being filtered. The precipitates were filtered through Whatman N°4 sintered glass crucibles then washed with degassed distilled water to remove any remaining aqueous ions before drying in a vacuum dessicator. The identity and purity of the solid precipitates was determined by FTIR and XRD spectroscopy as previously described in section 6.2.3. The pH of the filtrate was determined immediately prior to filtering and the filtrate analysed for Nd and Eu by FIA-UV. Other components were calculated from a knowledge of the starting materials and the amount removed by precipitation of the pure phase. Any mixed or amorphous precipitates were discarded from solubility calculations.

6.3.2.1 Preparation of $NaLn(SO_4)_2.xH_2O$

Ce, Nd and Eu all form $NaLn(SO_4)_2$ in solutions with high sulphate and sodium activities.

The $NaLn(SO_4).xH_2O$ phases were prepared at low pH by mixing $LnCl_3$ (0.1M, $100cm^3$) with H_2SO_4 (conc, 10ml) and Na_2SO_4 (1M, $100cm^3$) and then diluted to $250cm^3$ in $250cm^3$ HDPE Nalgene bottles and kept at 60°C for 2 months. The crystalline phases were filtered through Whatman N°4 sintered glass crucibles then washed with $200cm^3$ of degassed distilled water to remove any remaining aqueous ions before drying in a vacuum dessicator. The solubility product was not determined, as the compounds were not formed at 25°C. The dried crystals

were characterised by FTIR and XRD before being used in dissolution experiments.

6.3.2.2 Dissolution of $NaLn(SO_4)_2$

$NaLn(SO_4)_2$ (approximately 0.3g) was added to a solution of Na_2SO_4 (0.1M, 190cm^3) and H_2SO_4 (conc, 10cm^3) in a 250ml HDPE Nalgene bottle and allowed to equilibrate for 5 months in a waterbath (25°C) under a atmosphere of N_2. The pH of the final solution was measured before filtering the precipitate through Whatman N°4 sintered glass crucibles. The precipitate was then dried and analysed by XRD and FTIR. The filtrate was analysed for total lanthanide content by FIA-UV and Ce by spectrofluorimetry. Other components were calculated from a knowledge of the starting materials and the amount removed from solution by precipitation of the pure phase.

6.3.2.3 Precipitation of Nd and Eu $NaLn(SO_4)_2.xH_2O$

$NaNd(SO_4)_2$ and $NaEu(SO_4)_2$ were also prepared from a more dilute solution and at a lower temperature than the original preparation (Section 6.3.2.1)

$LnCl_3$ (0.2M, 10ml) was added to Na_2SO_4 (0.5M, 100ml) with NaCl (1m, 20cm^3) H_2SO_4(conc, 5cm^3) in a 125cm^3 HDPE Nalgene bottle (actual vol ~137ml). The solution and precipitate formed was kept in a thermostated waterbath at 25°C for 2 months. The pH of the solution was measured before filtering through a Whatman N°4 sintered glass crucible. Precipitation of the $NaEu(SO_4)_2$ was slow and excess NaCl (20g) was added to facilitate precipitation.

To determine the solubility of the $NaLn(SO_4)_2$ phase, the filtrate was analysed for Nd and Eu by FIA-UV and other components were calculated from a knowledge of the starting materials and the amount removed by precipitation of the pure phase.

6.3.2.4 Precipitation of $NaCe(SO_4)_2.xH_2O$

$NaCe(SO_4)_2.xH_2O$ was precipitated from $CeCl_3$ (0.5M, 12ml) with 50ml(0.2M) Na_2SO_4 (0.2M, $50cm^3$), NaCl (10g) and H_2SO_4 (conc, $10cm^3$) and then diluted to $120cm^3$ with degassed distilled water in a $125cm^3$ HDPE Nalgene bottle. NaCl was added to promote precipitation between pH 6-8 (i.e. without H_2SO_4). After the solid phase formed, the solutions were kept in a waterbath (25°C) for at least 2 months. After this time the solution pH was measured immediately prior to filtering through Whatman N°4 sintered glass crucibles and the precipitate was analysed by FTIR and XRD. The Ce^{3+} and total aqueous Ce (Ce^{3+} and Ce^{4+}) concentrations in the filtrate were analysed by spectrofluorimetry and FIA-UV respectively. Other components were calculated from a knowledge of the starting materials and the amount removed by precipitation of the pure phase.

6.4 Calculation of Solubility Products

To determine the solubility products, and hence the free energies of formation of the $NaLn(SO_4)_2$ and $Ln_2(OH)_4SO_4$ phases, the total lanthanide concentration and the pH of the equilibrated solutions were measured and the total solution composition calculated. All experimental data for the dissolution experiments are shown in Appendix 6.1 - 6.5.

The total sulphate and sodium removed from solution was calculated from a knowledge of the starting solution composition and the amount removed from solution by precipitation of the lanthanide phase. For example $NaLn(SO_4)_2$: sulphate is precipitated in a 2:1 ratio of SO_4^{2-} to Ln^{3+} (equation 6.6) and sodium in a 1:1 ratio of Na^+ to Ln^{3+} (equation 6.7). For $Ln_2(OH)_4SO_4$: SO_4^{2-} is removed from solution in a 2:1 ratio of Ln^{3+} to SO_4^{2-} (equation 6.8).

$NaLn(SO_4)_2$

$$[SO_4^{2-}]_{eq} = [SO_4^{2-}]_{start} - 2([Ln^{3+}]_{start} - [Ln^{3+}]_{eq}]) \qquad (6.6)$$

$$[Na^+]_{eq} = [Na^+]_{start} - ([Ln^{3+}]_{start} - [Ln^{3+}]_{eq}]) \qquad (6.7)$$

$Ln_2(OH)_4SO_4$

$$[SO_4^{2-}]_{eq} = [SO_4^{2-}]_{start} - ½([Ln^{3+}]_{start} - [Ln^{3+}]_{eq}]) \qquad (6.8)$$

The hydroxide activity was calculated from the pH and the chloride concentration is assumed unchanged from the initial solution.

The solubility product was calculated for the dissociation reactions of the $NaLn(SO_4)_2$ and $Ln_2(OH)_4SO_4$ from the free ion activities derived using the computer speciation programmes PHREEQC and PHREEQE and using the lanthanide sulphate association constants shown in Table 6.7, for the aqueous speciation reactions 6.9 to 6.13.

Table 6.7 Log of the lanthanide sulphate and hydroxy aqueous association constants for reactions 6.9 to 6.13

Ln	$LnSO_4^+$	$Ln(SO_4)_2^-$	$LnOH^{2+}$	$Ln(OH)_2^+$	$Ln(OH)_3^0$
Ce	3.62[1]	5.20[2]	-8.41[5]	-17.60[5]	-27.23[5]
Nd	3.55[3]	5.20[3]	-8.16[5]	-17.04[5]	-26.40[5]
Eu	3.67[4]	5.41[2]	-7.90[5]	-16.37[5]	-25.41[5]

[1]Martell & Smith (1989) Critical stability constants Volume 6: Second supplement *Plenium Press* New York
[2] Martell & Smith (1989) Critical stability constants Volume 4: Inorganic complexes *Plenium Press* New York
[3]Izatt *et al.*, (1969) *J. Chem. Soc.* 47-53
[4]Hale, C. F., & Spedding, F. H., (1972) *J. Phys. Chem.* **76** 1887
[5]Lee & Byrne (1992)

The aqueous association reactions used in the determination of the free ions in solution are:

$$Ln^{3+} + SO_4^{2-} \longrightarrow LnSO_4^+ \qquad (6.9)$$

$$Ln^{3+} + 2SO_4^{2-} \longrightarrow Ln(SO_4)_2^- \qquad (6.10)$$

$$Ln^{3+} + H_2O \longrightarrow LnOH^{2+} + H^+ \qquad (6.11)$$

$$Ln^{3+} + 2H_2O \longrightarrow Ln(OH)_2^+ + 2H^+ \qquad (6.12)$$

$$Ln^{3+} + 3H_2O \longrightarrow Ln(OH)_3^0 + 3H^+ \qquad (6.13)$$

The solubility products for the solid phases formed in Section 6.3, were calculated for each individual equilibrium solution (Solution data Appendix 6.1-6.5), and an average of the solubility products for each phase was then taken for the solubility product.

Calculation of a typical solubility product ($Nd_2(OH)_4SO_4$)

A typical example of a solubility calculation is shown in full below, for the dissociation of $Nd_2(OH)_4SO_4$ (equation 6.14), using the solution activities (Table 6.8) calculated by PHREEQC from the whole solution composition (Table 6.9) for an equilibrium solution

$$Ln_2(OH)_4SO_4 \longrightarrow 2Ln^{3+} + 4OH^- + SO_4^{2-} \qquad (6.14)$$

$$Ksp = a^2_{Ln^{3+}} . a^4_{OH^-} . a_{SO_4^{2-}} \qquad (6.15)$$

$$\log Ksp = 2\log(a_{Ln^{3+}}) + 4\log(a_{OH^-}) + \log(a_{SO_4^{2-}}) \qquad (6.16)$$

$$\log Ksp = 2(-5.596) + 4(-7.011) + (-2.198) = -41.15$$

The solubility can also be calculated for the hydrolysis reaction (equation 6.17) to give a hydrolysis constant (equations 6.18 and 6.19)

$$Ln_2(OH)_4SO_4 + 4H^+ \longrightarrow 2Ln^{3+} + 4H_2O + SO_4^{2-} \qquad (6.17)$$

$$K = \frac{a^2_{Ln^{3+}} . a^4_{H_2O} . a_{SO_4^{2-}}}{a^4_{H^+}} \qquad (6.18)$$

$$\log K = 2\log(a_{Ln^{3+}}) + \log(a_{SO_4^{2-}}) + 4pH \qquad (6.19)$$

$$= 2(-5.596) + (-2.198) + 4(6.99) = 14.55$$

Table 6.8 Data required for a typical calculation of the $Nd_2(OH)_4SO_4$ solubility constant from PHREEQC calculations (Table 6.9)

	Nd	SO_4^{2-}	pH 6.99	
total conc/M	$2.9x10^{-4}$	0.045		
species	Nd^{3+}	SO_4^{2-}	H^+	OH^-
log molality	-3.759	-1.382	-6.896	-6.807
log γ	-1.836	-0.816	-0.094	-0.204
log activity	-5.596	-2.198	-6.990	-7.011

The sodium lanthanide double sulphates can be similarly calculated for the dissociation reaction (equation 6.20) from equation 6.22 and the experimental data in Appendix 6.1 to 6.5 and are summarised in Table 6.10 for all lanthanide sulphate phases prepared.

$$NaLn(SO_4)_2 \longrightarrow Na^+ + Ln^{3+} + 2SO_4^{2-} \qquad (6.20)$$

$$Ksp = a_{Na^+}.a_{Ln^{3+}}.a^2_{SO_4^{2-}} \qquad (6.21)$$

$$\log Ksp = \log(a_{Na^+}) + \log(a_{Ln^{3+}}) + 2\log(a_{SO_4^{2-}}) \qquad (6.22)$$

The solubility product for $NaCe(SO_4)_2$ fell within two regions, dependent upon the ionic strength of the solution. The first with a log Ksp -10.68±0.5, from a solution of pH 4.5±0.5 and total ionic strength less than 0.1M. And a second set of samples formed at pH 0, with greater than 1M total ionic strength from the addition of H_2SO_4 and Na_2SO_4 which gave a log Ksp -23±5. The Debye-Hückel expression used to calculate the species activities within dilute solutions cannot be used at the high ionic strength's of the latter, consequently these high ionic strength experiments were disregarded.

Table 6.9 PHREEQC output for a typical solution in equilibrium with $Nd_2(OH)_4SO_4$

```
TITLE KSp Calc   NdS 18d  Nd2(OH)4SO4
SOLUTION 1
        pH  6.99
        pe  0.00
      units mol/l
        Nd  2.9E-4
        Na  0.12
        S   0.045
        Cl  0.030
----------------------------Solution composition----------------------------
Elements            Molality       Moles
Cl                  3.025e-02   3.025e-02
Na                  1.210e-01   1.210e-01
Nd                  2.924e-04   2.924e-04
S                   4.537e-02   4.537e-02
----------------------------Description of solution----------------------------
                            pH  =   6.990
                            pe  =   0.000
                  Activity of water  =   0.997
                     Ionic strength  =   1.595e-01
                    Mass of water (kg)  =   1.000e+00
                Temperature (deg C)  =  25.000
----------------------------Distribution of species----------------------------
                                                  Log         Log         Log
Species                Molality    Activity    Molality    Activity      Gamma
OH-                 1.558e-07   9.740e-08     -6.807      -7.011      -0.204
H+                  1.269e-07   1.023e-07     -6.896      -6.990      -0.094
H2O                 5.551e+01   9.967e-01     -0.001      -0.001       0.000
Cl                  3.025e-02
   Cl-              3.025e-02   1.891e-02     -1.519      -1.723      -0.204
Na                  1.210e-01
   Na+              1.173e-01   7.331e-02     -0.931      -1.135      -0.204
   NaSO4-           3.726e-03   2.329e-03     -2.429      -2.633      -0.204
Nd                  2.924e-04
   Nd+3             1.741e-04   2.539e-06     -3.759      -5.595      -1.836
   NdSO4+           9.135e-05   5.711e-05     -4.039      -4.243      -0.204
   Nd(SO4)2-        2.587e-05   1.617e-05     -4.587      -4.791      -0.204
   NdOH+2           1.120e-06   1.711e-07     -5.951      -6.767      -0.816
   Nd(OH)2+         3.514e-09   2.197e-09     -8.454      -8.658      -0.204
   Nd(OH)3          9.340e-12   9.340e-12    -11.030     -11.030       0.000
O(0)                0.000e+00
   O2               0.000e+00   0.000e+00    -58.123     -58.123       0.000
S(-2)               5.646e-32
   HS-              5.646e-32   3.530e-32    -31.248     -31.452      -0.204
S(6)                4.537e-02
   SO4-2            4.150e-02   6.339e-03     -1.382      -2.198      -0.816
   NaSO4-           3.726e-03   2.329e-03     -2.429      -2.633      -0.204
   NdSO4+           9.135e-05   5.711e-05     -4.039      -4.243      -0.204
   Nd(SO4)2-        2.587e-05   1.617e-05     -4.587      -4.791      -0.204
   HSO4-            1.014e-07   6.339e-08     -6.994      -7.198      -0.204
```

Table 6.10 Summary of lanthanide-sulphate solubility products

Phase	log Ksp	log K	Solution data and activities
$Nd_2(OH)_4SO_4$	-42.22±1.38	13.77±1.35	Appendix 6.1
$Eu_2(OH)_4SO_4$	-42.50±0.68	13.50±0.68	Appendix 6.2
$NaCe(SO_4)_2$	-10.68±0.5	N/A	Appendix 6.3
$NaNd(SO_4)_2$	-19.86±0.12	N/A	Appendix 6.4
$NaEu(SO_4)_2$	-27.05±1.29	N/A	Appendix 6.5

There is no published solubility data for sodium lanthanide sulphate or lanthanide hydroxy sulphate solubility. The sodium lanthanide double sulphates appear to be very soluble with lanthanide concentrations of approximately 1mM below pH 7. The Nd and Eu sodium double sulphates alter to the hydroxy sulphate at pH above 7 in less than 0.05M sulphate solution, therefore the double sulphate will not control lanthanide solubility in natural solutions. $NaCe(SO_4)_2$ also appears to have an approximate 1mM solubility limit in sulphate solutions between pH 7 and 8, however as a Ce hydroxy sulphate does not form, then $NaCe(SO_4)_2$ will probably alter to a carbonate phase even at very low carbonate activities.

The buffering of pH by the precipitation of solid $Nd_2(OH)_4SO_4$ and $Eu_2(OH)_4SO_4$ phases during the titrations showed that the aqueous lanthanide concentration does decrease in equilibrium from the addition of NaOH. The lanthanide hydroxy sulphate may therefore have a significant influence on the lanthanide solubility limit in aqueous carbonate bearing sulphate solutions.

The Debye-Hückel expression used for the calculation of aqueous activity coefficients was designed for use in dilute solutions. Nevertheless, because the formation of $NaNd(SO_4)_2$ and $NaEu(SO_4)_2$ phases require very high concentrations of supporting electrolytes, the Debye-Hückel expression was used for the solubility product calculations. Further ΔG_f° phase relationship calculations and phase diagrams must therefore be used with caution when these values are used.

6.5 Standard Gibbs Free Energy Calculations

The Standard Gibbs free energy of a reaction (ΔG_{Rn}°) can be derived from the solubility product from equation 6.23, which in turn can be used to calculate the Standard Gibbs free energy of formation of each solid phase from equation 6.24 and the thermodynamic data in Table 6.19;

$$\Delta G_{Rn}^{\circ} = -RT\ln K \qquad (6.23)$$

where R is the gas constant ($8.314 JK^{-1}mol^{-1}$), T is the thermodynamic temperature (298.15K for all reactions) and K is the solubility product.

$$\Delta G_{Rn}^{\circ} = \Delta G_f^{\circ}(\text{products}) - \Delta G_f^{\circ}(\text{reactants}) \qquad (6.24)$$

$$\Delta G_f^{\circ}(\text{reactants}) = \Delta G_f^{\circ}(\text{products}) - \Delta G_{Rn}^{\circ} \qquad (6.25)$$

where ΔG_f°(products) are the free component ions in the Ksp dissociation reaction and ΔG_f°(reactant) is the solid phase.

Table 6.11 Selected aqueous species thermodynamic data (Lide, 1998)

species	$\Delta G_f^{\circ}/KJmol^{-1}$	species	$\Delta G_f^{\circ}/KJmol^{-1}$
Ce^{3+}	-672.0	OH^-	-157.22
Nd^{3+}	-671.6	SO_4^{2-}	-744.0
Eu^{3+}	-574.1	CO_3^{2-}	-527.9
Na^+	-261.95	H^+	0.00
H_2O	-237.14	e-	0.00

6.5.1 ΔG_f° $Ln_2(OH)_4SO_4$

The Gibbs free energy of formation for the lanthanide hydroxy sulphates can be calculated for the reaction (equation 6.14), using the thermodynamic data from Table 6.11 and the ΔG_{Rn}° calculated from the solubility product as shown below

$$Ln_2(OH)_4SO_4 \longrightarrow 2Ln^{3+} + 4OH^- + SO_4^{2-} \qquad (6.14)$$

$$\Delta G_f^{\circ}(Ln_2(OH)_4SO_4) = [2\Delta G_f^{\circ}(Ln^{3+}) + 4\Delta G_f^{\circ}(OH^-) + \Delta G_f^{\circ}(SO_4^{2-})] - \Delta G_{Rn}^{\circ} \qquad (6.26)$$

$$\Delta G_f^{\circ}(Nd_2(OH)_4SO_4) = [2(-671.6) + 4(-157.22) + (-744.0)] - [241.0]$$
$$= -2957.1 KJmol^{-1}$$

Similarly the ΔG_f° for the dissociation of the sodium double sulphates (equation 6.20) can be calculated from equation 6.27

$$NaCe(SO_4)_2 \longrightarrow Na^+ + Ce^{3+} + 2SO_4^{2-} \qquad (6.20)$$

$$\Delta G_f^\circ(\text{reactants}) = \Delta G_f^\circ(\text{products}) - \Delta G_{Rn}^\circ \qquad (6.25)$$

$$\Delta G_f^\circ(Ln_2(OH)_4SO_4) = [\Delta G_f^\circ(Na^+) + \Delta G_f^\circ(Ln^{3+}) + 2\Delta G_f^\circ(SO_4^{2-})] - \Delta G_{Rn}^\circ \qquad (6.27)$$

The Gibbs free energy of formation (ΔG_f°)for each solid phase studied is summarised in (Table 6.12).

Table 6.12 Summary of the ΔG_f° calculated from the solubility products (this work, Table 6.18)

Phase	log Ksp	log K	ΔG_f°/KJmol^{-1}
$Nd_2(OH)_4SO_4$	-42.22± .38	13.77±1.35	-2957.07
$Eu_2(OH)_4SO_4$	-42.50±0.68	13.50±0.68	-2763.66
$NaCe(SO_4)_2$	-10.68±0.5	N/A	-2481.0
$NaNd(SO_4)_2$	-19.86±0.12	N/A	-2534.9
$NaEu(SO_4)_2$	-27.05±1.29	N/A	-2478.45
[1]CeO_2	N/A	30.66±0.32	-10265.5
[1]$Nd(OH)_3$	-21.41±0.67	20.08±0.62	-1265.5
[1]$Eu(OH)_3$	-22.79±0.23	19.17±0.23	-1175.9

[1]This work Chapter 4

6.6 Phase Relations

The Gibbs free energy of formation can then be used to calculate the position of the stability field boundary between each two solid phases by calculating the Gibbs free energy for each equilibrium reaction, which in turn is used to calculate an equilibrium reaction constant, K

6.6.1 $Ln_2(OH)_4SO_4$-$Ln(OH)_3$ equilibrium

The equilibrium reaction between $Ln_2(OH)_4SO_4$ and $Ln(OH)_3$ can be described in terms of the pH and sulphate activity of the solution as indicated by equation 6.29. The Gibbs free energy of reaction can be calculated from equation 6.30 and the results are presented in Table 6.13, using the thermodynamic data in Tables 6.11 and 6.12

$$Ln_2(OH)_4SO_4 + 2H_2O = 2Ln(OH)_3 + SO_4^{2-} + 2H^+ \quad (6.29)$$

$$\Delta G_{Rn}^{\circ} = [2\Delta G_f^{\circ}(Ln(OH)_3) + \Delta G_f^{\circ}(SO_4^{2-}) + 2\Delta G_f^{\circ}(H^+)] - [\Delta G_f^{\circ}(Ln_2(OH)_4SO_4) + 2\Delta G_f^{\circ}(H_2O)] \quad (6.30)$$

Table 6.13 Calculation of the $Ln_2(OH)_4SO_4$-$Ln(OH)_3$ equilibrium reaction constant

equilibrium phase	log Ksp	ΔG_f°/KJmol^{-1} (products)	ΔG_f°/KJmol^{-1} (reactants)	ΔG_{Rn}°/ KJmol^{-1}	logK (equilibrium)
$Nd_2(OH)_4SO_4$ -$Nd(OH)_3$	-42.22 -21.41	-3275.0	-3431.4	156.4	-27.4
$Eu_2(OH)_4SO_4$ -$Eu(OH)_3$	-42.50 -22.83	-3095.8	-3237.9	142.1	-24.9

The reaction constant can be expressed in terms of the activities of the component ions in solution (equation 6.31), when the solid phases have an equal activity when at equilibrium (of 1) and H_2O also has an activity of 1.

$$K = a_{SO_4^{2-}} . a_{H^+}^2 \quad (6.31)$$

Equation 6.31 can be rewritten in terms of pH and sulphate activity (equation 6.32) by taking -log of equation 6.31

$$\log a_{SO_4^{2-}} = 2pH + \log K \quad (6.32)$$

6.6.2 $NaCe(SO_4)_2$-CeO_2 equilibrium

The $NaCe(SO_4)_2$ and CeO_2 phase boundary includes a change in the oxidation state of the Ce and is dependent upon the pH, pE, Na^+ and SO_4^{2-} activities of the solution (equation 6.33)

$$NaCe(SO_4)_2 + 2H_2O = CeO_2 + e^- + Na^+ + 4H^+ \quad (6.33)$$

The Gibbs free energy of reaction is therefore described by equation 6.34;

$$\Delta G_{Rn}^\circ = [\Delta G_f^\circ(CeO_2) + \Delta G_f^\circ(e^-) + \Delta G_f^\circ(Na^+) + 2\Delta G_f^\circ(SO_4^{2-}) + 4\Delta G_f^\circ(H^+)] - [\Delta G_f^\circ(NaCe(SO_4)_2) + 2\Delta G_f^\circ(H_2O)] \quad (6.34)$$

The Gibbs free energy of reaction can be calculated from the thermodynamic data in Tables 6.11 and 6.12, and converted into a reaction constant from equation 6.23, as shown in Table 6.14

Table 6.14 Calculation of the $NaCe(SO_4)_2$-CeO_2 equilibrium reaction constant

Equilibrium phases	log Ksp /log K	ΔG_f°/KJmol^{-1} (products)	ΔG_f°/KJmol^{-1} (reactants)	ΔG_{Rn}°/ KJmol^{-1}	logK (equilibrium)
$NaCe(SO_4)_2$ -CeO_2	-10.68 30.66	-2721.3	-2955.3	234.0	-41.0

The reaction constant can be expressed in terms of the equilibrium components (equation 6.35)

$$K = a_{Na^+}.a^2_{SO_4^{2-}}.a_{e^-}.a^4_{H^+} \quad (6.35)$$

by taking -log of equation 6.35, the equilibrium reaction can be written in terms of pe (equation 6.36) or SO_4^{2-} activity (equation 6.37).

$$pe = -(4pH - \log a_{Na^+} - 2\log a_{SO_4^{2-}} + \log K) \quad (6.36)$$

$$\log a_{SO_4^{2-}} = \tfrac{1}{2}(4pH + pe - \log a_{Na^+} + \log K) \quad (6.37)$$

6.6.3 $NaLn(SO_4)_2$-$Ln_2(OH)_4SO_4$ equilibrium

The $NaNd(SO_4)_2$ and $NaEu(SO_4)_2$ solubility products calculated in Section 6.4.2 are unreliable due to the high ionic strength of the equilibrium solutions. However if the solubility product of $NaNd(SO_4)_2$ and $NaEu(SO_4)_2$ is assumed to be the same as the $NaCe(SO_4)_2$ then an estimation of the $NaLn(SO_4)_2$-$Ln_2(OH)_4SO_4$ phase boundary could be made, which may be important at low

hydroxide activities. The reaction constant for the phase boundary can be calculated for equation 6.38, by equation 6.39.

$$2NaLn(SO_4)_2 + 4H_2O = Ln_2(OH)_4SO_4 + 4H^+ + 2Na^+ + 3SO_4^{2-} \quad (6.38)$$

$$\Delta G_{Rn}^\circ = [\Delta G_f^\circ(Ln_2(OH)_4SO_4) + 4\Delta G_f^\circ(H^+) + 2\Delta G_f^\circ(Na^+) + 3\Delta G_f^\circ(SO_4^{2-}) - [\Delta G_f^\circ(NaLn(SO_4)_2) + 4\Delta G_f^\circ(H_2O)] \quad (6.39)$$

The reaction constant can be calculated from the thermodynamic data in Tables 6.11 and 6.12, and shown in Table 6.15

Table 6.15 Equilibrium reaction constants between the sodium lanthanide double sulphates ($NaLn(SO_4)_2$) and lanthanide hydroxy-sulphates ($Ln_2(OH)_4SO_4$)

equilibrium phase	log Ksp /log K	ΔG_f°/KJmol^{-1} (products)	ΔG_f°/KJmol^{-1} (reactants)	ΔG_{Rn}°/ KJmol^{-1}	logK (equilibrium)
$NaLn(SO_4)_2$ -$Nd_2(OH)_4SO_4$	-10.68 -42.22	-5713.0	-5910.6	197.6	-34.6
$NaLn(SO_4)_2$ -$Eu_2(OH)_4SO_4$	-10.68 -42.50	-5519.6	-5718.6	199.0	-34.9
$NaNd(SO_4)_2$ -$Nd_2(OH)_4SO_4$	-19.86 -42.22	-5713.0	-6018.4	305.4	-53.5
$NaEu(SO_4)_2$ -$Eu_2(OH)_4SO_4$	-27.05 -42.50	-5519.6	-5905.5	385.9	-67.6

The phase boundary can be expressed in terms of the aqueous components (equation 6.40), and the aqueous sulphate activity (equation 6.41)

$$K = a_{H^+}^4 . a_{Na^+}^2 . a_{SO_4^{2-}}^3 \quad (6.40)$$

$$\log a_{SO_4^{2-}} = \tfrac{1}{3}(4pH - 2\log a_{Na^+} + \log K) \quad (6.41)$$

6.7 Phase equilibria

The phase boundaries between the lanthanide sulphate and hydroxy phases can be seen to be dependant upon pH and the sulphate activity in solution and are summarised in Table 6.16. A series of pH vs sulphate concentration diagrams can be plotted for each lanthanide, assuming the solutions are ideal and therefore the species concentration has been used instead of activities in solution.

Table 6.16. Summary of the lanthanide sulphate solid phase equilibrium reactions and constants (Data from Tables 6.13 -6.15)

Equilibrium Phases	Equilibrium Reaction	logK Ce	logK Nd	logK Eu
$Ln_2(OH)_4SO_4$ -$Ln(OH)_3$	$\log[SO_4^{2-}] = 2pH + logK$	N/A	-27.4	-24.9
$NaLn(SO_4)_2$ -CeO_2	$-pe = (4pH - \log[Na^+] - 2\log[SO_4^{2-}] + logK)$	-41.0	N/A	N/A
$NaCe(SO_4)_2$ -$Ln_2(OH)_4SO_4$	$\log[SO_4^{2-}] = {}^1/_3(4pH-2\log[Na^+]+logK)$	N/A	-34.6	-34.9
$NaLn(SO_4)_2$ -$Ln_2(OH)_4SO_4$	$\log[SO_4^{2-}] = {}^1/_3(4pH-2\log[Na^+]+logK)$	N/A	-53.5	-67.6

6.7.1 Nd and Eu phase equilibria

Using the estimated data for $NaNd(SO_4)_2$ and $NaEu(SO_4)_2$, a plot of pH with $\log[SO_4^{2-}]$ (Figure 6.10) shows that there is a phase transition with an increase in OH^- activity from $NaNd(SO_4)_2$ to $Nd_2(OH)_4SO_4$ to $Nd(OH)_3$ at a constant sulphate activity. $Nd(OH)_3$ forms at high hydroxide activities and low sulphate activities. $NaNd(SO_4)_2$ is the equilibrium phase at high sulphate activities, below pH 8, but only in the presence of aqueous sodium ions. The hydroxy-sulphate, $Nd_2(OH)_4SO_4$, forms an intermediate equilibrium phase between $NaNd(SO_4)_2$ and $Nd(OH)_3$, i.e. at a lower pH and higher sulphate activity than $Nd(OH)_3$, not at higher pH and lower sulphate activity than $NaNd(SO_4)_2$.

The experimentally determined log Ksp value of -19.86 for $NaNd(SO_4)_2$ predicts a phase transition from the double sulphate to the hydroxy sulphate, $Nd_2(OH)_4SO_4$, at pH 9 in 1mM SO_4^{2-} and Na^+ solution. If the $NaNd(SO_4)_2$ has a log Ksp of -10.68 (i.e. if the $NaNd(SO_4)_2$ solubility product is similar to the $NaCe(SO_4)_2$ solubility product) then a reasonable estimation can be made of this phase boundary at pH 5 in a 1mM SO_4^{2-} and Na^+ solution. Preliminary solubility experiments at pH 6 in 10mM SO_4^{2-} solution indicated that a mixture of $NaNd(SO_4)_2$ and $Nd_2(OH)_4SO_4$ forms as predicted by a log Ksp of -10.68 for $NaNd(SO_4)_2$. An increase in the Na^+ activity increases the pH required to form the $NaNd(SO_4)_2$-$Nd_2(OH)_4SO_4$ phase transition.

The stability field diagram predicts $Nd_2(OH)_4SO_4$ would be the initial precipitate above pH 6.5 in the titration experiments, followed by alteration to $Nd(OH)_3$ at high pH. The $Nd_2(OH)_4SO_4$ - $Nd(OH)_3$ phase boundary forms at pH 11 in 0.1mM SO_4^{2-} solution and pH 12 in 10mM SO_4^{2-}, and therefore indicates the solid phase transition occurs after the sharp rise in pH at the end of the buffer zone, in agreement with the titrations.

The Eu pH vs sulphate stability field diagram (Figure 6.11) is similar to the equivalent Nd diagram, but the $Eu_2(OH)_4SO_4$ - $Eu(OH)_3$ phase boundary forms at one pH unit lower than the equivalent phase boundary, probably as a result of a relatively less soluble hydroxide phase. The experimentally derived $NaEu(SO_4)_2$ - $Eu_2(OH)_4SO_4$ phase boundary (formed in concentrated H_2SO_4) does not agree with the experimental results, and forms at a higher pH than the $Eu_2(OH)_4SO_4$ - $Eu(OH)_3$ phase boundary. When the $NaCe(SO_4)_2$ log Ksp (-10.68) is substituted for $NaEu(SO_4)_2$, the phase boundary shows a good comparison with the Nd phase boundary, and is in the region experimentally verified to form a $NaEu(SO_4)_2$ - $Eu_2(OH)_4SO_4$ mixture.

Figure 6.10 Stability field diagram of the Na^{+}-Nd^{3+}-SO_4^{2-}-OH^{-} system [Na^{+}] = 1mM at 298.15K and 1 atm pressure (This work)

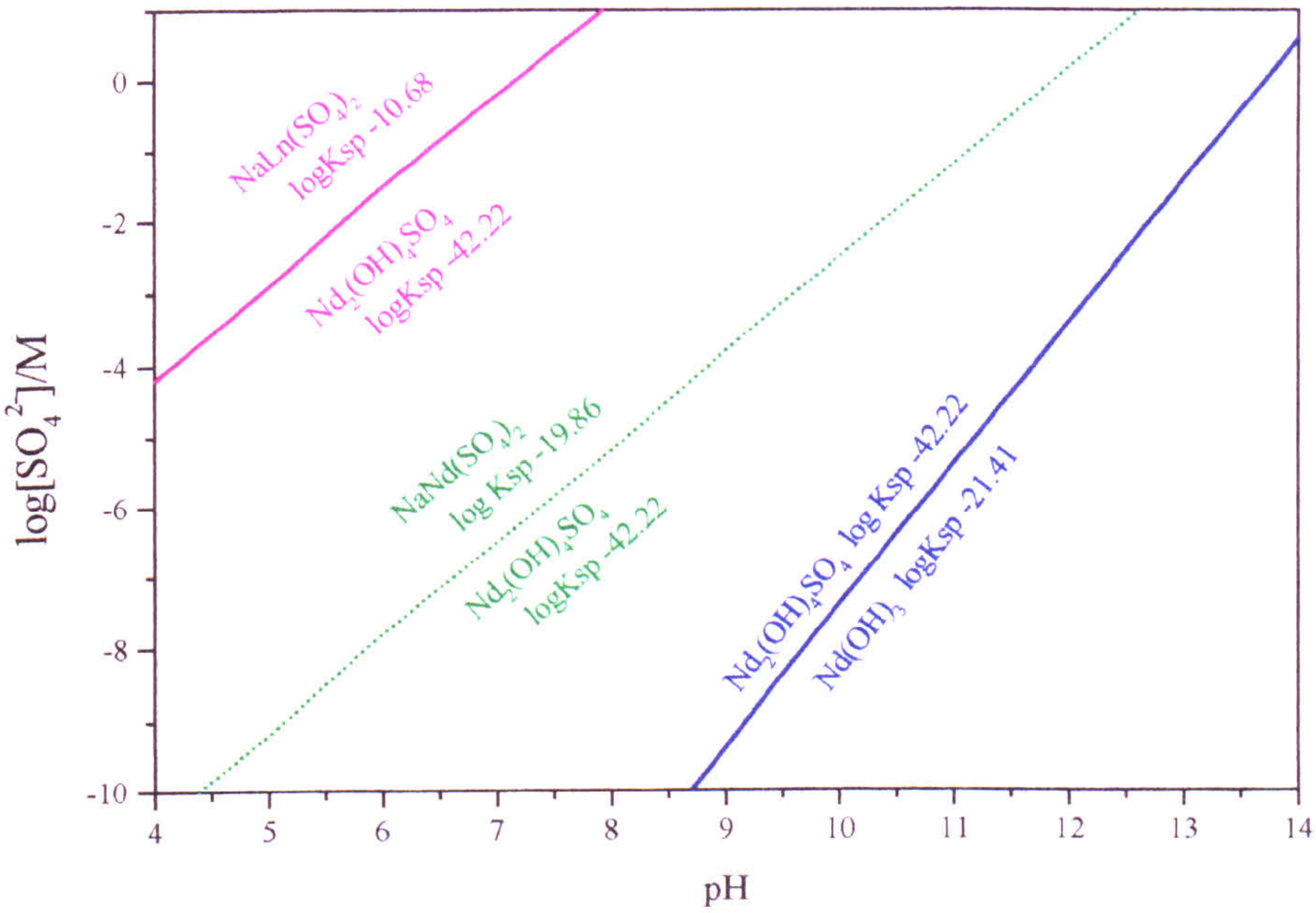

Figure 6.11 Stability field diagram of the Na^{+}-Eu^{3+}-SO_4^{2-}-OH^{-} system [Na^{+}] = 1mM at 298.15K and 1 atm pressure (This work)

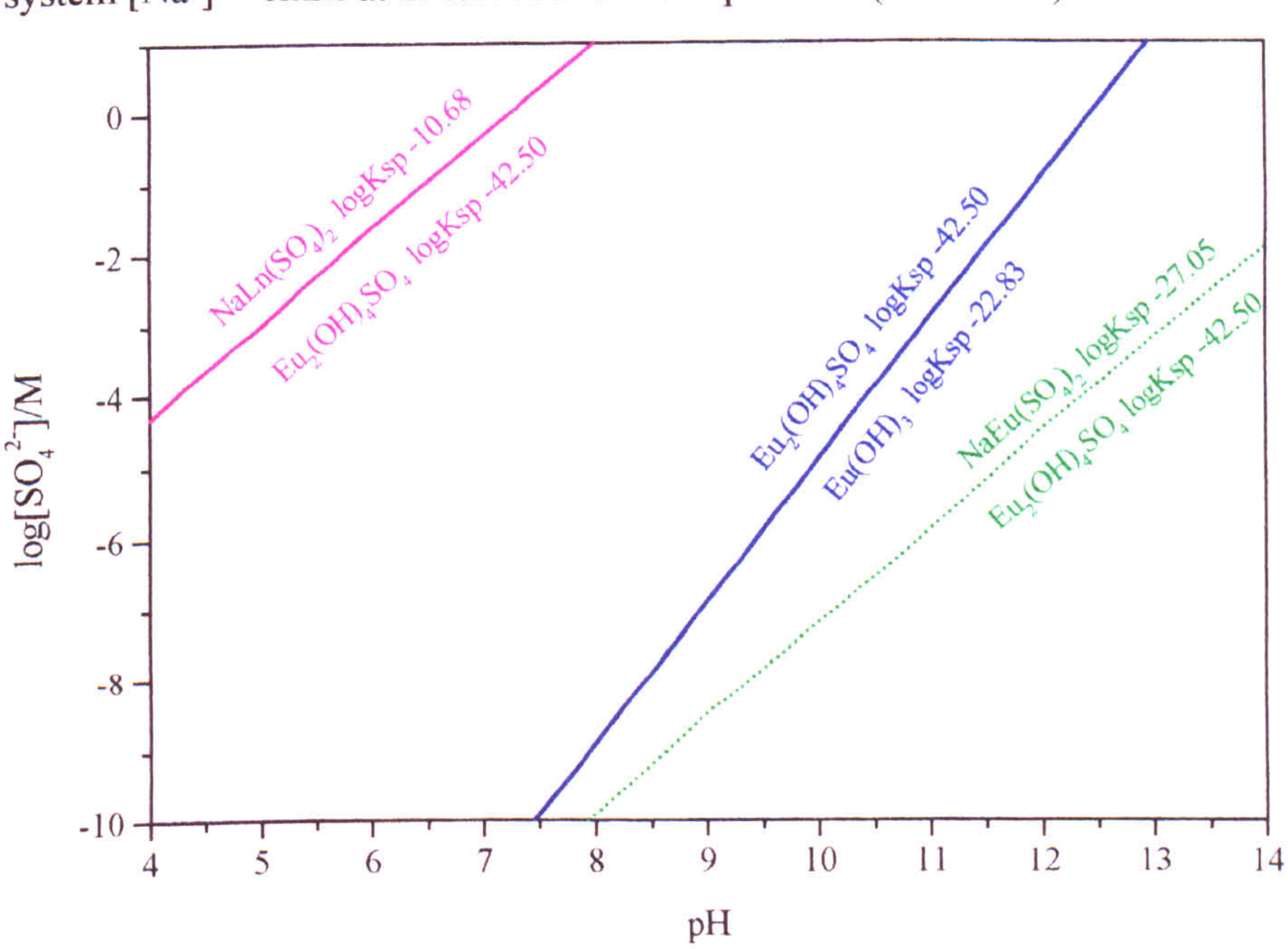

6.7.2 Nd and Eu solubility in sulphate solutions

The relationship between solid and aqueous phases can also be examined from pH vs lanthanide concentration diagrams under set solution conditions, e.g. SO_4^{2-} and Na^+ concentrations, calculated using PHREEQC. When the predicted solubility of a series of phases are plotted on a pH vs aqueous lanthanide concentration diagram, then the least soluble phase at each pH value will be the solubility limiting phase, under those conditions (Figure 6.12). The variation in solubility of each phase with pH can also be examined with the relative effects of all the aqueous species in equilibrium with that phase (Figure 6.13). The plots predict the solubility of an aqueous phase with a solution at equilibrium and the interaction of all aqueous species. From this an explanation can be derived for the relative changes in solubility across the entire pH range for any solution composition, to identify why a phase becomes the solubility limiting phase only under specific conditions.

Solid lanthanide sulphates are very soluble at low pH. Below pH 6.5 mixed $NaLn(SO_4)_2/Ln_2(OH)_4SO_4$ phases or the $NaLn(SO_4)_2$ would be expected to form. The solubility of $NaLn(SO_4)_2$ is independent of pH between pH 5 and 8 (Figure 6.12), but decreases below pH 4.5, when aqueous sulphate alters from SO_4^{2-} to HSO_4^-. Even though $NaLn(SO_4)_2$ has a relatively high solubility compared to other lanthanide hydroxy sulphate, carbonate or hydroxide phases, $NaLn(SO_4)_2$ may still form the significant solubility limiting phase under some acidic conditions. However below pH 4.5, aqueous SO_4^{2-} converts to HSO_4^- (Figure 6.8), therefore the aqueous SO_4^{2-} activity is reduced and $NaLn(SO_4)_2$ solubility consequently increases (Figure 6.12).

Nd and Eu have similar $Ln_2(OH)_4SO_4$ solubilities (solubility diagrams are shown for Nd, Figures 6.12 and 6.13), which are strongly dependant upon the solution pH. There is a sharp solubility minimum of approximately 10^{-8}M aqueous lanthanide between pH 9 and 9.5 in a 0.01M sulphate solution. The higher solubility of 10^{-4}-10^{-3}M for $Ln_2(OH)_4SO_4$ below pH 7 found in the batch experiments (Section 6.3) was due to the very low aqueous hydroxide activity in acidic solutions. The $Ln_2(OH)_4SO_4$ solubility decreases with an increase in pH

from pH 4 to pH 8.5, when Ln^{3+} and $LnSO_4^+$ are the dominant aqueous species (Figure 6.13) then forms a solubility minima when the dominant aqueous lanthanide species is $Ln(OH)_2^+$, the $Ln_2(OH)_4SO_4$ dissolution reaction is then independent of pH (equation 6.41);

$$Ln_2(OH)_4SO_4(s) = 2Ln(OH)_2^+(aq) + SO_4^{2-}(aq) \qquad (6.41)$$

The region dominated by the $Ln(OH)_2^+$ aqueous species is however pH dependent, which restricts the pH range of this equilibrium reaction to between pH 9 and pH 10. The total Nd or Eu concentration at the solubility minima will also be dependent upon the aqueous SO_4^{2-} activity, and will decrease with increasing SO_4^{2-} activity.

Lanthanide solubility then increases with pH when the $Ln(OH)_3^0(aq)$ species forms the dominant aqueous species. Equation 6.42, shows that an increase in the OH^- activity will increase the solubility of $Ln_2(OH)_4SO_4(s)$, $Ln(OH)_3(s)$ will then become the solubility limiting phase at high pH.

$$Ln_2(OH)_4SO_4(s) + 2OH^-(aq) \longrightarrow 2Ln(OH)_3^0(aq) + SO_4^{2-}(aq) \qquad (6.42)$$

The $Nd_2(OH)_4SO_4$ solubility minimum falls below the minimum solubility predicted by literature values for the $Nd(OH)_3$ solubility product (Figure 6.12), but not below the solubility of well formed thermally aged $Nd(OH)_3$ crystals (i.e. Rao *et al.*, 1996). When the $Ln(OH)_3$ phase only becomes the solubility limiting phase at pH > 11, reflecting the fact that an initial amorphous $Ln(OH)_3$ phase will form at the end stage of the titrations when excess OH^- had been added to the solution. The $Ln(OH)_3$ may then slowly increase in crystallinity over time. Crystalline $Ln(OH)_3$ must be kinetically slow to form, otherwise the $Ln_2(OH)_4SO_4$ phase would not form.

Figure 6.12 Lanthanide solubility in 0.01M Na_2SO_4

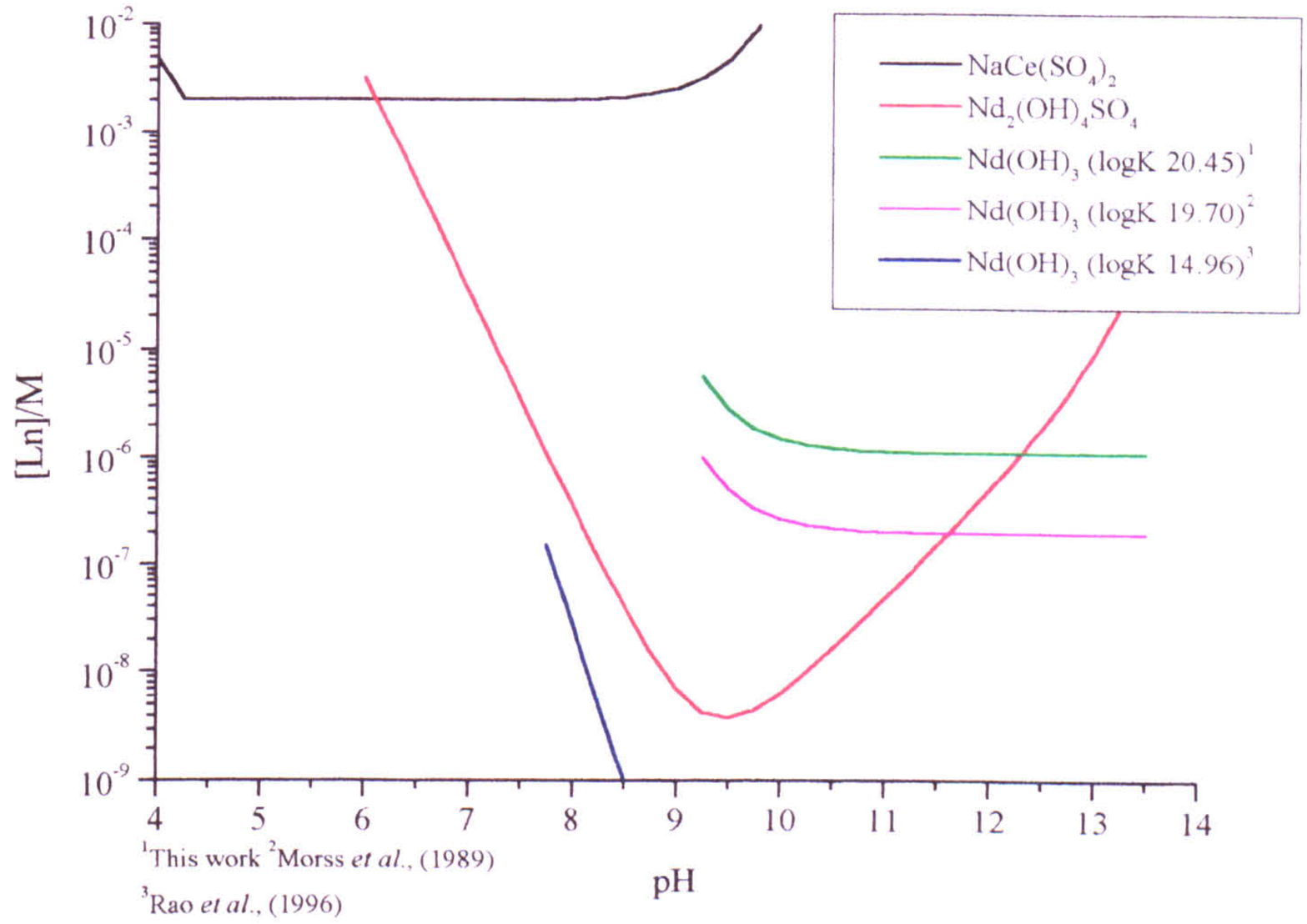

Figure 6.13 $Nd_2(OH)_4SO_4$ solubility and aqueous speciation in 1mM SO_4^{2-}

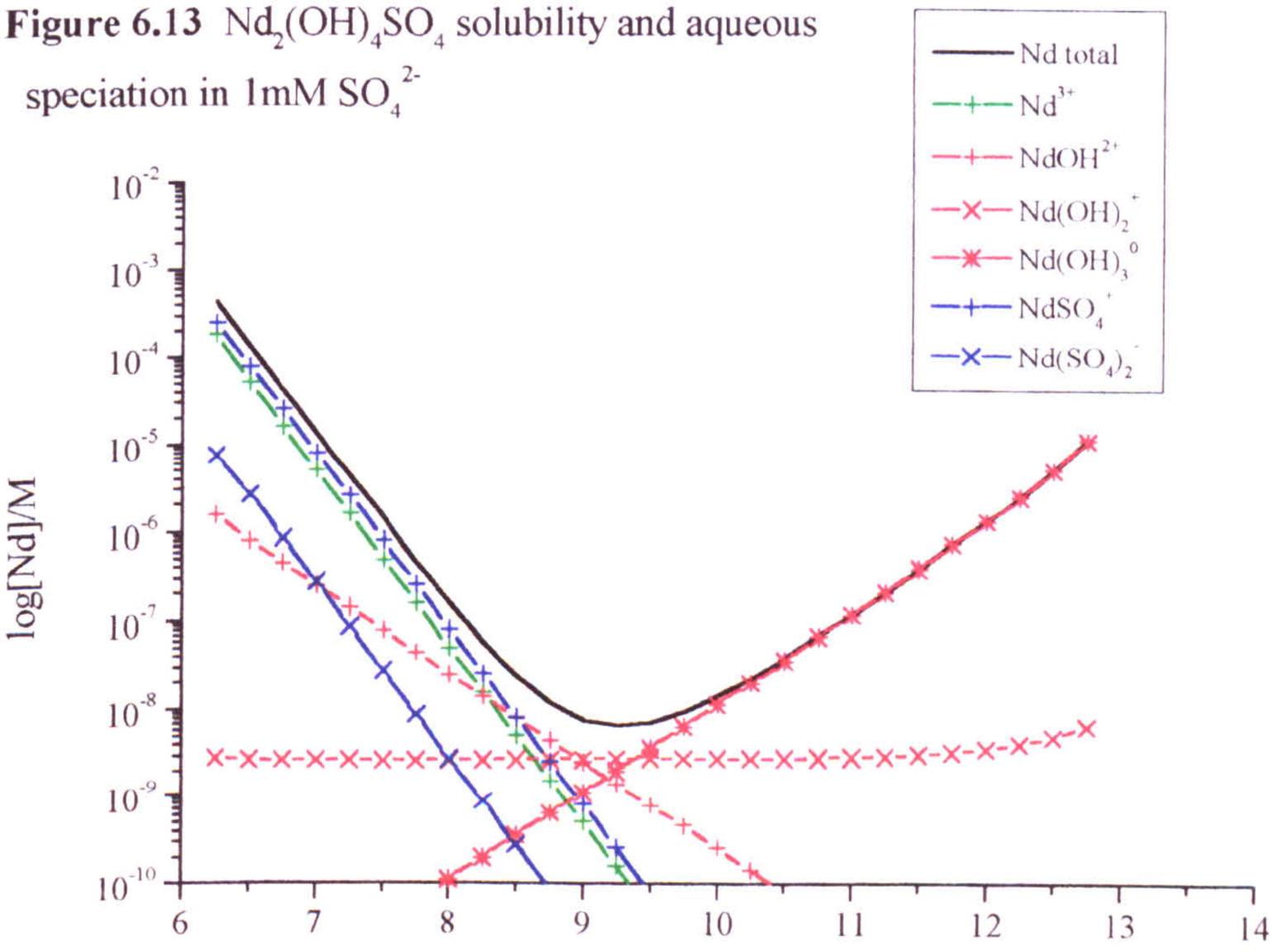

6.7.3 Ce phase equilibria

The conditions for the formation of cerium solid phases are dependent upon the redox potential of the system. The $NaCe(SO_4)_2$-CeO_2 phase boundary is pushed to a lower pH by increasing the pe of the solution (Figure 6.14) and to a higher pH by increasing Na^+ and SO_4^{2-} activities (Figure 6.15). The solubility of CeO_2 (Figure 6.16) is also controlled by the pe of the solution. Under reducing conditions, if Ce^{3+} is not oxidised to Ce^{4+}, then $Ce(OH)_3$ would become the solubility limiting phase, at pe 0 and up to pH 10.5, above which Ce would be oxidised to CeO_2. Under reducing conditions (e.g. pe -5) The predicted CeO_2 solubility is significantly higher than $Ce(OH)_3$, therefore $Ce(OH)_3$ will be the equilibrium phase even above pH 11.

The solubility of $Ln(OH)_3$, where Ln = Ce, Nd or Eu, is approximately constant from pH 9.5-14 when $Ln(OH)_3^0$ (aq) is the dominant aqueous species. The solubility of CeO_2 is not similarly controlled (Figure 6.16) and the solubility continues to decrease with increasing pH. Below pH 8 CeO_2 (and $Ce(OH)_3$) solubility increases sharply until $NaCe(SO_4)_2$ becomes the solubility limiting phase.

The redox potential of the system will also control the SO_4^{2-} activity in solution as the sulphate can be reduced to form sulphide (S^{2-}) ions in solution, which would affect the stability field of $NaCe(SO_4)_2$ and CeO_2 at low pe, but not indicated in the diagrams (Figures 6.14 to 6.16)

Figure 6.14 Stability field diagram for the Ce-pH-pe system and various SO_4^{2-} activities $[Na^+]$ = 1mM at 298.15K and 1 atm pressure

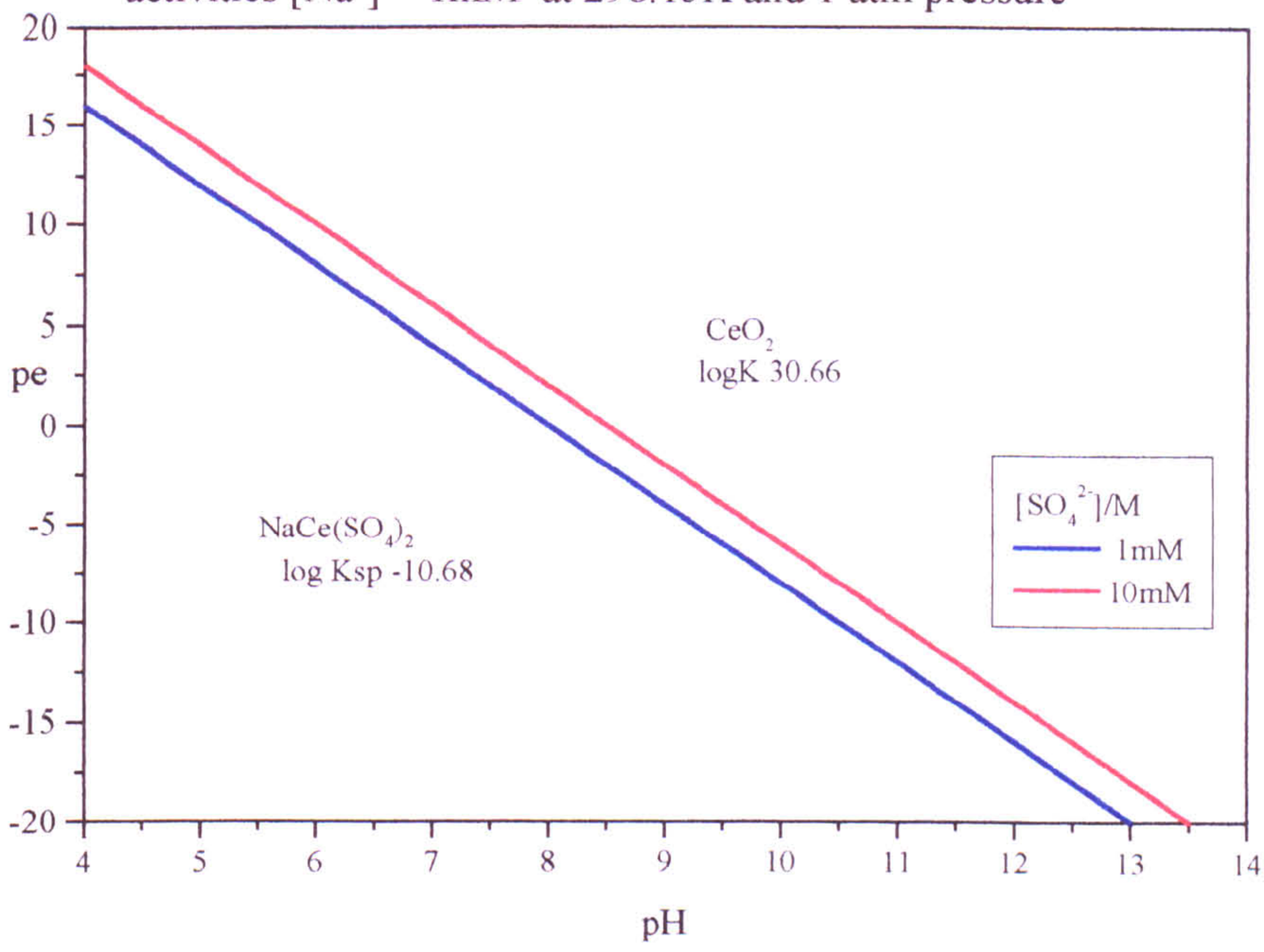

Figure 6.15 Stability field diagram for the Ce-Na^+-SO_4^{2-}-pH system at 1mM Na^+ and varied pe (assuming SO_4^{2-} is not reduced to S^{2-})

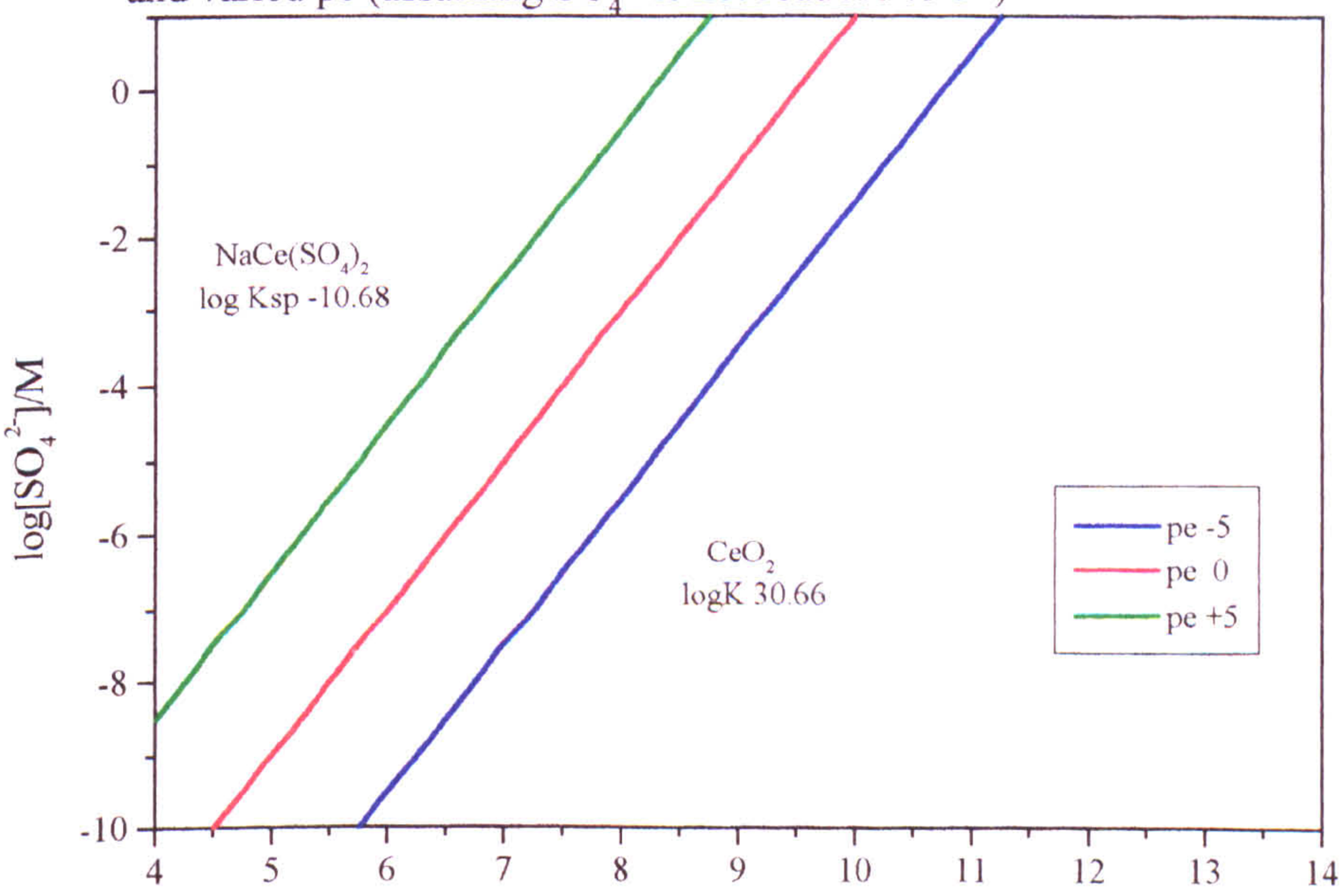

Figure 6.16 The solubility of various Ce phases with pH in 10^{-2}M Na_2SO_4 solution (assuming SO_4^{2-} is not reduced to S^{2-})

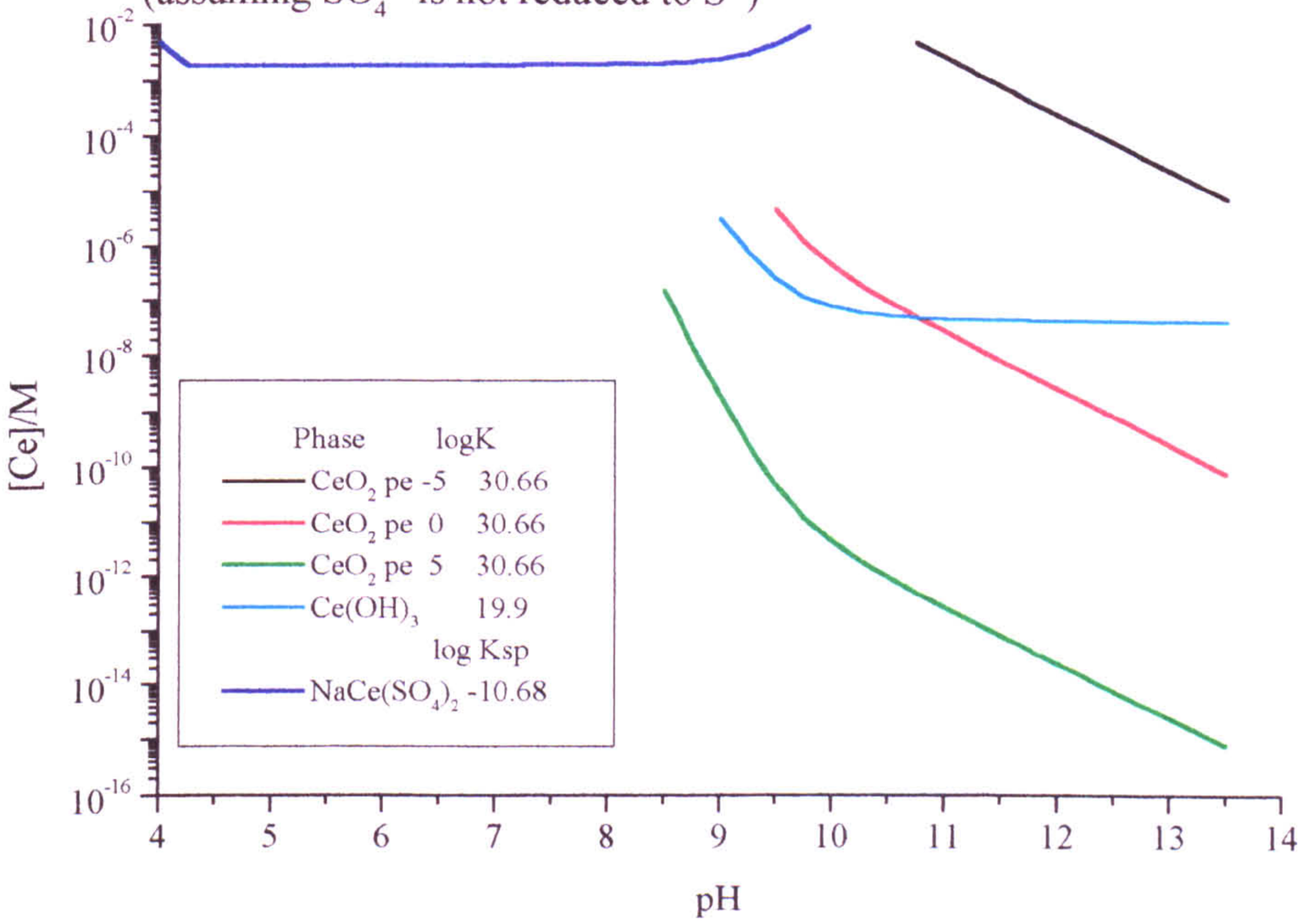

6.8 Nd and Eu phase relations in sulphate-carbonate solutions

Most natural solutions (above pH 5) are likely to include carbonate ions through the dissolution of $CO_2(g)$ or carbonate bearing minerals. The solubility of solid sulphate phases must therefore be considered from a mixed carbonate-sulphate bearing solution. The solid phases within the CO_3^{2-}-SO_4^{2-}-Na^+-pH system can be examined in a similar manner to the individual carbonate and sulphate systems by calculating a reaction constant between each pair of phases (Table 6.17) from Gibbs Free Energy calculations.

When the sulphate phases are included in a pH vs log[TIC] diagram for Nd (Figure 6.17, derived from a pH vs log[CO_3^{2-}] diagram, appendix 6.6) at constant Na^+ and SO_4^{2-} activities, the sulphate phases form the stable equilibrium phases at low carbonate activities. Similarly solid carbonate phases form the equilibrium phase at low sulphate activities as indicated in a pH vs [SO_4^{2-}] plot, (Appendix 6.7). The phase boundaries between $NaNd(SO_4)_2$, $Nd_2(OH)_4SO_4$ and $Nd(OH)_3$ are dependent upon pH at constant Na^+ and SO_4^{2-} activities and independent of the carbonate concentration. The phase boundaries between solid

carbonate and sulphate phases are dependent upon the pH and carbonate activity at constant Na^+ and SO_4^{2-} activities.

In a 1mM Na^+ and 0.1mM SO_4^{2-} solution, $NaNd(SO_4)_2$ will convert to $Nd_2(OH)_4SO_4$ above pH 4.2. The hydroxy-sulphate, $Nd_2(OH)_4SO_4$, will then convert to $Nd(OH)_3$ above pH 12. In this sulphate solution (Figure 6.17), the phase boundaries between sulphate and carbonate solid phases are predicted to form between 0.05mM and 1mM TIC from pH 4 to 11.5. The carbonate and sulphate phases will then alter to $Ln(OH)_3$ above pH 11.5

If the sulphate concentration is increased to 10mM (Figure 6.18), the $Nd_2(OH)_4SO_4$ stability field increases to a higher pH at the expense of the $Nd(OH)_3$ stability field, and to higher TIC concentrations at the expense of $NdCO_3OH$. $Nd_2(OH)_4SO_4$ is predicted to be stable up to pH 12.5 and 10^{-2}M TIC in a 10mM SO_4^{2-} solution. If the Na^+ activity is also increased to 10mM, then the $NaNd(SO_4)_2$ phase will become significant below pH 6, by restricting the stability fields of $Nd_2(CO_3)_3$ and $Nd_2(OH)_4SO_4$. The Na^+ and SO_4^{2-} activities would have to increase to above 20mM, before a sulphate phase (i.e. $Nd_2(OH)_4SO_4$) could interact directly with $NaNd(CO_3)_2$.

Table 6.17 Carbonate-Sulphate solid phase reactions, (This work, Lide 1998)

Solid phases	logKsp	Equilibrium reaction	
$NaNd(SO_4)_2$ $-Nd_2(OH)_4SO_4$	-10.68 -42.22	$2NaNd(SO_4)_2 + 4H_2O = Nd_2(OH)_4SO_4 + 3SO_4^{2-} + 4H^+ + 2Na^+$	$pH = (3\log[SO_4^{2-}] + 2\log[Na^+] - (-34.32))/4$ $\log[SO_4^{2-}] = (4pH - 2\log[Na^+] + (-34.32))/3$
$Nd_2(OH)_4SO_4$ $-Nd(OH)_3$	-42.22 -21.41	$Nd_2(OH)_4SO_4 + 2H_2O = 2Nd(OH)_3 + SO_4^{2-} + 2H^+$	$pH = (\log[SO_4^{2-}] - (-27.4))/2$ $\log[SO_4^{2-}] = 2pH + (-27.40)$
$NaNd(SO_4)_2$ $-Nd_2(CO_3)_3$	-10.68 -34.43	$2NaNd(SO_4)_2 + CO_3^{2-} = Nd_2(CO_3)_3 + 4SO_4^{2-} + 2Na^+$	$\log[CO_3^{2-}] = (4\log[SO_4^{2-}] + 2\log[Na^+] - (13.60))/3$ $\log[SO_4^{2-}] = (3\log[CO_3^{2-}] - 2\log[Na^+] + (13.60))/4$
$Nd_2(OH)_4SO_4$ $-Nd_2(CO_3)_3$	-42.22 -34.43	$Nd_2(OH)_4SO_4 + 4H^+ + 3CO_3^{2-} = Nd_2(CO_3)_3 + 4H_2O + SO_4^{2-}$	$\log[CO_3^{2-}] = (\log[SO_4^{2-}] + 4pH - (48.21))/3$ $\log[SO_4^{2-}] = 3\log[CO_3^{2-}] - 4pH + (48.21)$
$Nd_2(OH)_4SO_4$ $-NdCO_3OH$	-42.22 -19.87	$Nd_2(OH)_4SO_4 + 2CO_3^{2-} + 2H^+ = 2NdCO_3OH + SO_4^{2-} + 2H_2O$	$\log[CO_3^{2-}] = (\log[SO_4^{2-}] + 2pH - (25.54))/2$ $\log[SO_4^{2-}] = 2\log[CO_3^{2-}] - 2pH + (25.54)$
$Nd_2(CO_3)_3$ $-NdCO_3OH$	-34.43 -19.87	$Nd_2(CO_3)_3 + 2H_2O = 2NdCO_3OH + 2H^+ + CO_3^{2-}$	$\log[CO_3^{2-}] = 2pH + (-22.68)$
$NdCO_3OH$ $-Nd(OH)_3$	-19.87 -21.41	$NdCO_3OH + 2H_2O = Nd(OH)_3 + 2H^+ + CO_3^{2-}$	$\log[CO_3^{2-}] = 2pH + (-26.47)$
$NaNd(CO_3)_2$ $-Nd_2(CO_3)_3$	-21.25 -34.43	$2NaNd(CO_3)_2 = Nd_2(CO_3)_3 + 2Na^+ + CO_3^{2-}$	$\log[CO_3^{2-}] = -2\log[Na^+] + (-8.10)$
$NaNd(CO_3)_2$ $-NdCO_3OH$	-21.25 -19.87	$NaNd(CO_3)_2 + H_2O = NdCO_3OH + Na^+ + CO_3^{2-}$	$\log[CO_3^{2-}] = (pH - \log[Na^+] + (-15.40))/2$
$NaNd(CO_3)_2$ $-Nd(OH)_3$	-21.25 -21.41	$NaNd(CO_3)_2 + 3H_2O = Nd(OH)_3 + Na^+ + 2CO_3^{2-} + 3H^+$	$\log[CO_3^{2-}] = (3pH - \log[Na^+] + (-42.01))/2$

Figure 6.17 Stability field diagram for the Na-Nd-TIC-OH system

$[Na^+]$ = 1mM, $[SO_4^{2-}]$ = 0.1mM at 298.15K and 1 atm pressure

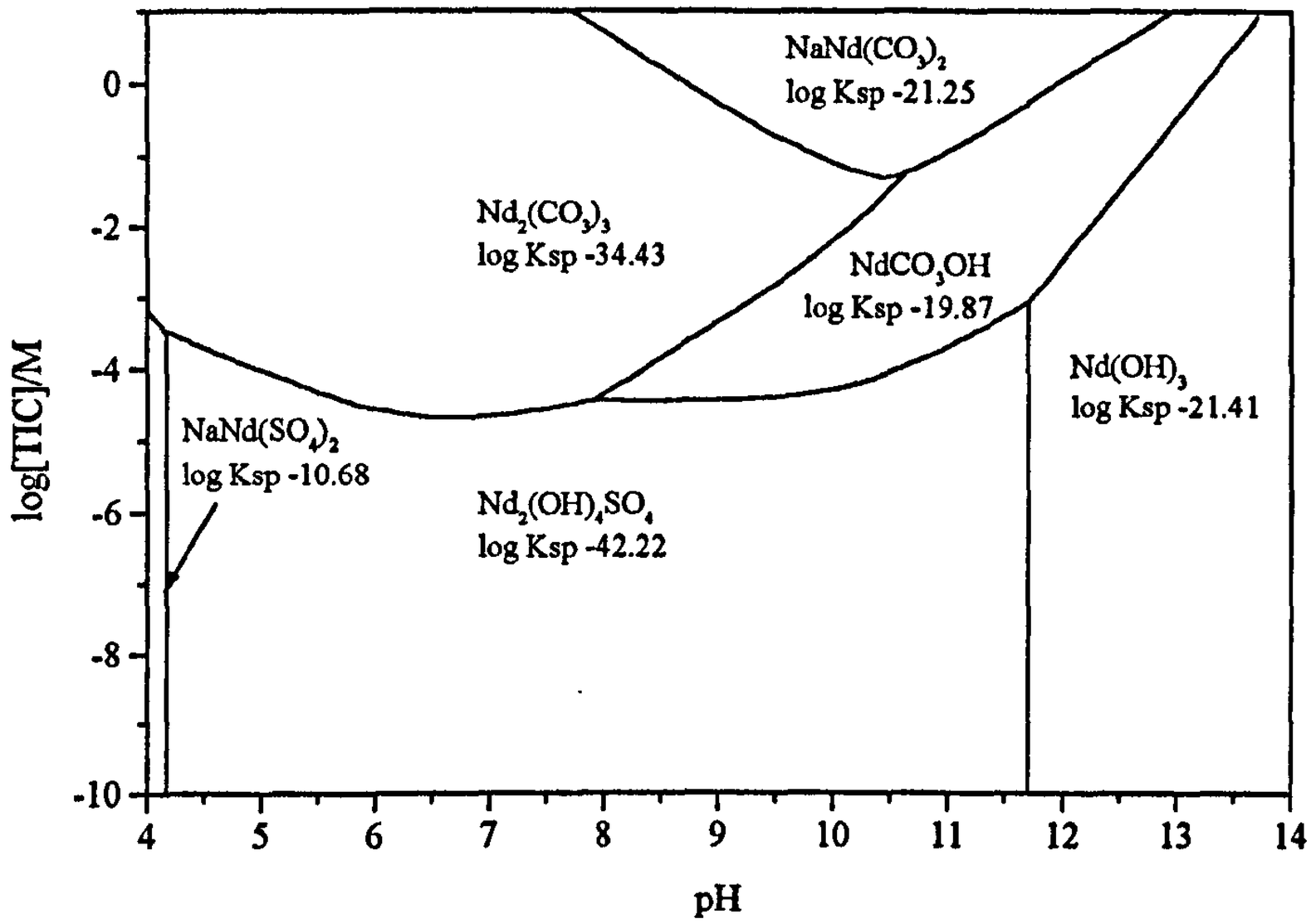

Figure 6.18 Stability field diagram for the Na-Nd-TIC-OH system

in $[Na^+]$ = 10mM, $[SO_4^{2-}]$ = 10mM at 298.15K and 1 atm pressure

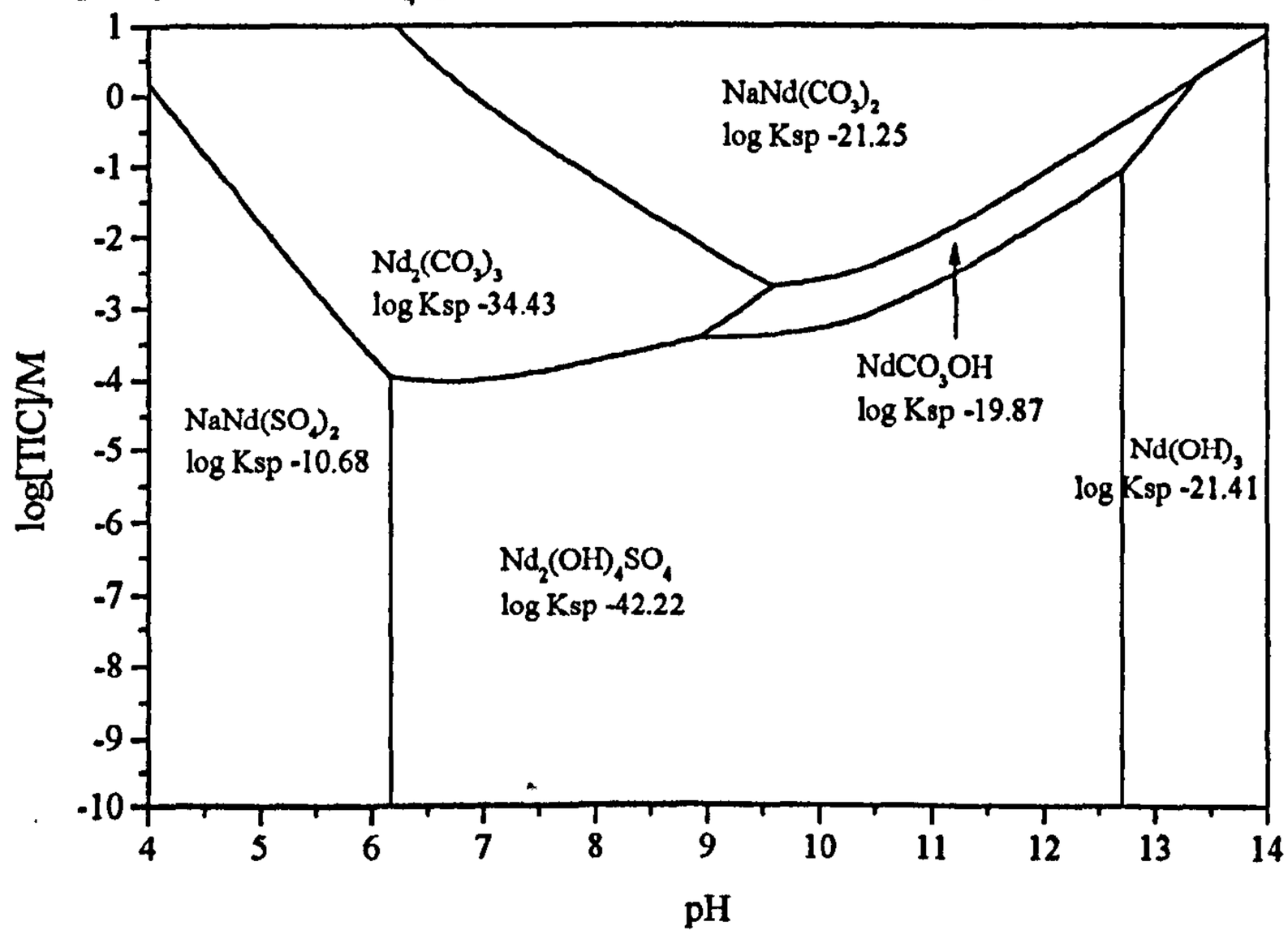

6.8.1 Nd and Eu solubility in sulphate-carbonate solutions

$NaLn(SO_4)_2$ is very soluble and if it forms with a similar solubility product as $NaCe(SO_4)_2$ then the total aqueous Nd or Eu concentration will be at least 10^{-4}M in a 10mM Na and SO_4 solution. Decreasing the Na^+ or SO_4^{2-} activity in solution will further increase Nd or Eu solubility.

In carbonate free systems, $Nd_2(OH)_4SO_4$ and $Eu_2(OH)_4SO_4$, are in equilibrium with aqueous lanthanide hydroxy phases above pH 7. $Ln_2(OH)_4SO_4$ shows a decrease in solubility from pH 4 to a minimum at pH 9.5 (Figures 6.12 and 6.13), then the $Ln_2(OH)_4SO_4$ solubility increases above pH 9.5, resulting in $Ln(OH)_3$ becoming the solubility limiting phase. When carbonate is added to the system the solubility of $Ln_2(OH)_4SO_4$ is increased (Figures 6.19 to 6.21), and the profile of the $Ln_2(OH)_4SO_4$ solubility from pH 4 to 14 changes significantly.

In a 0.1mM sulphate solution, the solubility of $Ln_2(OH)_4SO_4$ is relatively unaffected by 0.01mM TIC (Figure 6.19) $LnCO_3OH$, will have a similar shaped solubility profile, but will not become the solubility limiting phase. Below pH 7, the low hydroxide activity of the solution results in a phase change from $Ln_2(OH)_4SO_4$ to the carbonate $Ln_2(CO_3)_3$. The carbonate will then alter to the double sulphate, $NaLn(SO_4)_2$, below pH 5, if sufficient Na^+ is present in solution.

When the TIC and SO_4^{2-} activities are increased to 1mM, the solubility of $Ln_2(OH)_4SO_4$ increases significantly (Figure 6.20). The entire solubility profile of $Ln_2(OH)_4SO_4$ as plotted on a pH vs aqueous lanthanide diagram, changes significantly to a profile similar to that of $LnCO_3OH$ in high carbonate bearing solutions (Figure 4.17 and Figure 6.21). The solubility of $Ln_2(OH)_4SO_4$ flattens at a higher concentrations than in the carbonate free system between pH 7 and pH 9.5, then falls to a solubility minimum between pH 11 to 11.5. $LnCO_3OH$ has a similar solubility profile, but is slightly less soluble than $Ln_2(OH)_4SO_4$ in the region below pH 11. The solubility minima's at pH 11 to 11.5 are however of similar magnitudes, therefore $Ln_2(OH)_4SO_4$ may become the solubility limiting phase, before conversion to $Ln(OH)_3$ at a higher pH. Under these aqueous

conditions (Figures 6.20), the $Ln_2(OH)_4SO_4$ solubility minimum has not only been displaced from pH 9.5 to pH 11.5, there is also an associated increase in aqueous lanthanide concentration from $5x10^{-9}$M to 10^{-7}M.

If the aqueous TIC is increased to 10mM (Figure 6.21) and sulphate concentration remains at 1mM, then the predicted $Ln_2(OH)_4SO_4$ solubility increases to the extent that it is unlikely to become the solubility limiting phase. When the aqueous sulphate concentration is also increased to 10mM, $Ln_2(OH)_4SO_4$ will not become a solubility limiting phase (Appendix 6.8).

Figure 6.19 The solubility of various Nd phases in 0.1mM Na^+, 0.1mM SO_4^{2-} and 0.01mM TIC solution (This work, Lee & Byrne 1992)

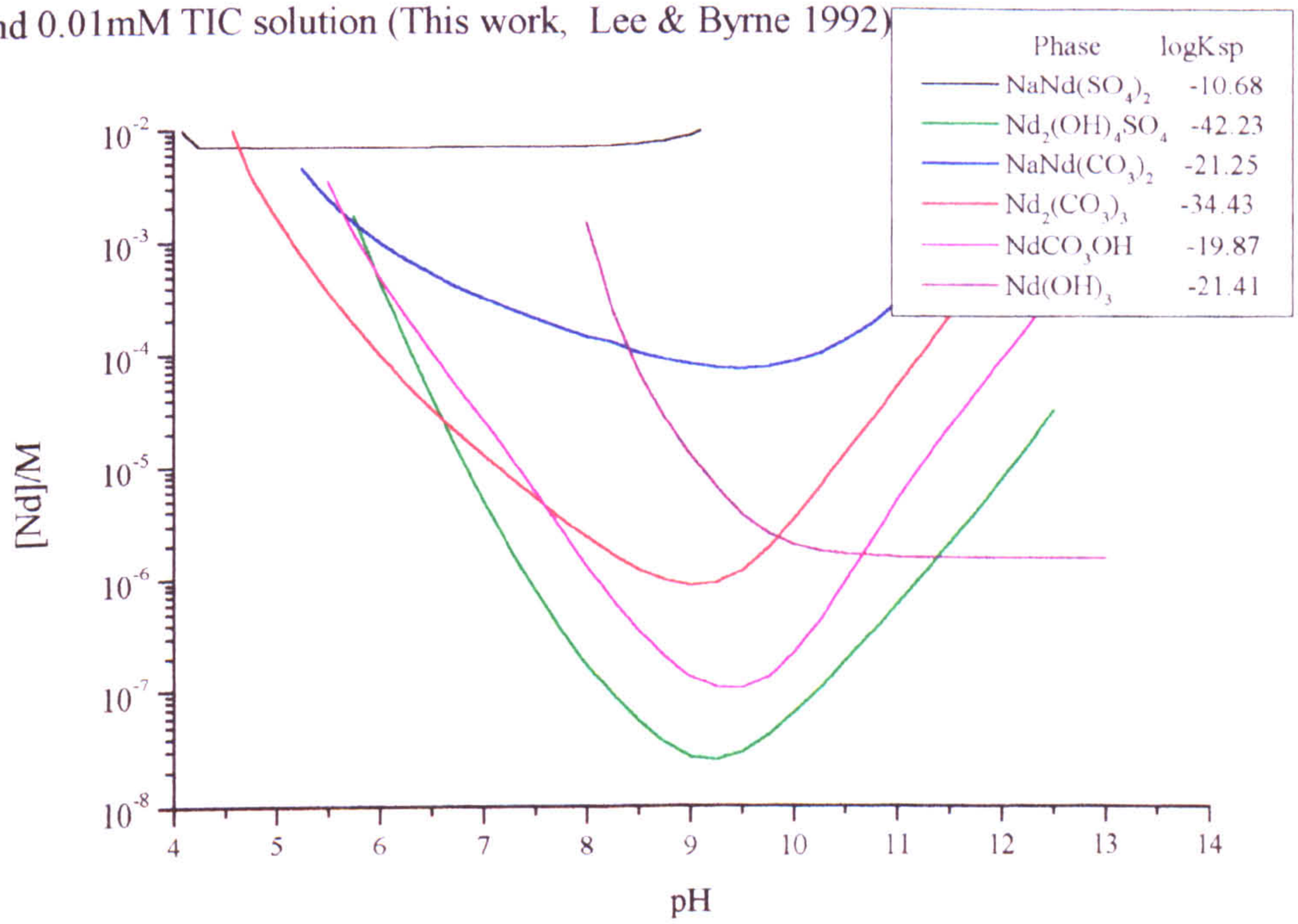

Figure 6.20 The solubility of various Nd phases in 1mM Na^+, 1mM TIC and 1mM SO_4^{2-} Lee & Byrne (1992/3) aqueous data

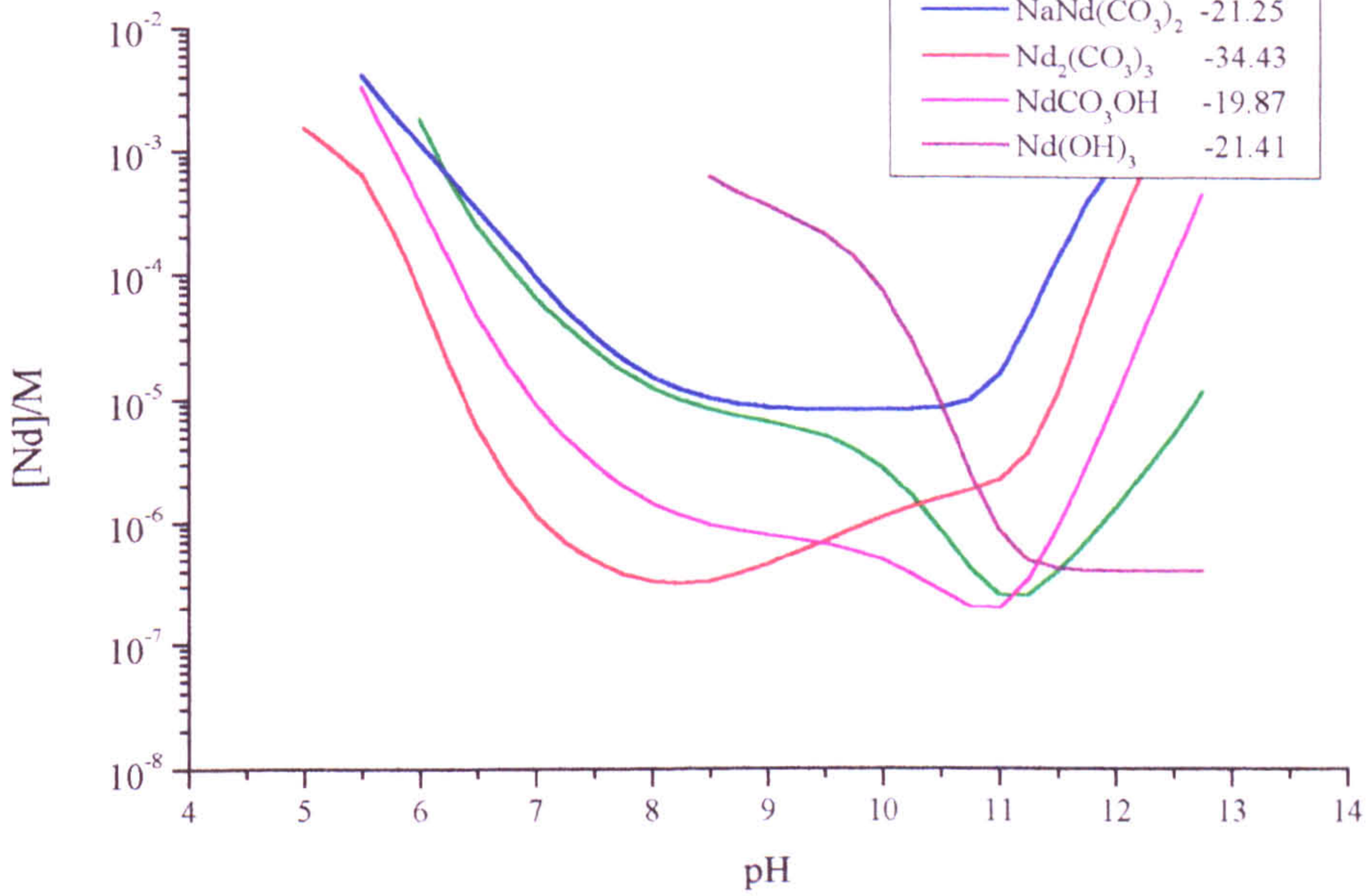

Figure 6.21 The solubility of various Nd phases in 10mM Na^+, 10mM TIC and 1mM SO_4^{2-} Lee & Byrne (1992/3) aqueous data

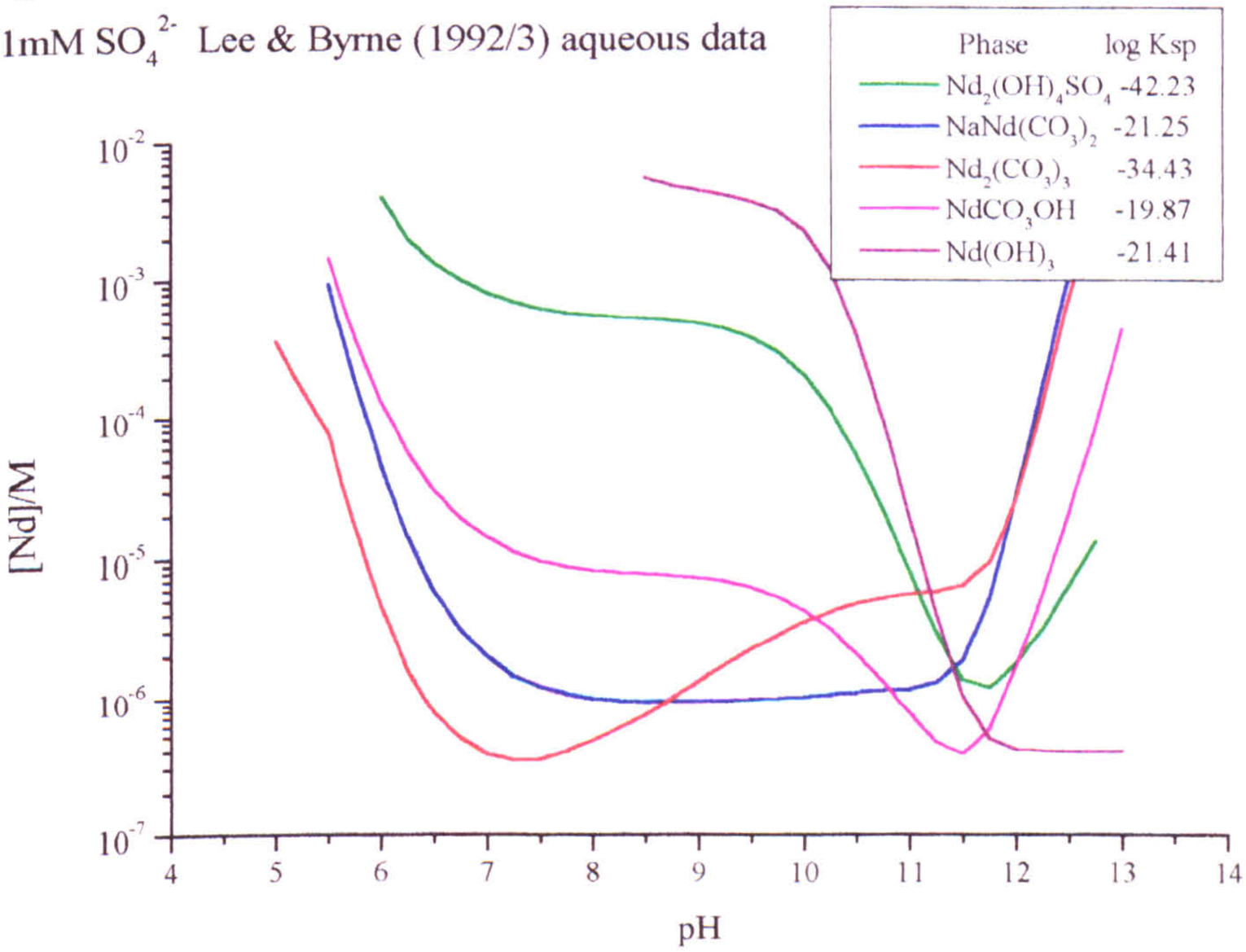

6.8.2 The effects of aqueous species on $Ln_2(OH)_4SO_4$ solubility

The significant increase in solubility of $Ln_2(OH)_4SO_4$ can be explained by the influence of aqueous lanthanide carbonate species in solution and shown by a pH vs $[Ln]_{total}$ plot indicating the variation in the amounts of each aqueous lanthanide species in solution with pH. The TIC concentration must be less than 10^{-5}M to have a negligible affect upon $Ln_2(OH)_4SO_4$ solubility (Figures 6.19 and 6.22), however even in sulphate free solutions. Aqueous carbonate species only make a minor contribution to the aqueous speciation at 10^{-5}M.

The presence of aqueous carbonate concentrations above 0.01mM does however have a considerable effect on the solubility of $Ln_2(OH)_4SO_4$. In a 0.01mM TIC and 0.1mM SO_4^{2-} solution, the solubility of $Ln_2(OH)_4SO_4$ is increased but the profile of the solubility curve still indicates a solubility minimum at pH 9.5. If the proportion of TIC to SO_4^{2-} remains the same, but increased to 0.1mM TIC and 1mM SO_4^{2-} (Figure 6.23), then the carbonate aqueous species, $LnCO_3^+$ between pH 7.5 and 8.5, and $Ln(CO_3)_2^-$ between pH 8.5 and 10.5 are the dominant aqueous species.

In carbonate containing solutions the solubility minimum that forms at the aqueous phase boundary between the aqueous species $LnSO_4^+$, $Ln(OH)_2^+$ and $Ln(OH)_3^0$ in carbonate free systems can no longer form, as the lanthanide solubility increases due to the presence of $Ln(CO_3)_2^-$. Therefore in carbonate solutions the solubility minimum forms as the proportion of aqueous $Ln(CO_3)_2^-$ reduces and $Ln(OH)_3^0$(aq) increases. This solubility minima also becomes shifted to pH 10.5, the phase boundary between $Ln(CO_3)_2^-$(aq) and $Ln(OH)_3^0$(aq).

When the TIC concentration is increased to the same level as the SO_4^{2-} concentration at 1mM (Figure 6.24), the solubility of $Ln_2(OH)_4SO_4$ increases significantly between pH 8 and pH 11.5, due to interactions of $Ln(CO_3)_2^-$(aq). The solubility minimum still forms at the aqueous transition between $Ln(CO_3)_2^-$ and $Ln(OH)_3^0$.

Figure 6.22 $Nd_2(OH)_4SO_4$ solubility and aqueous speciation in 0.01mM TIC and 0.1mM SO_4^{2-}

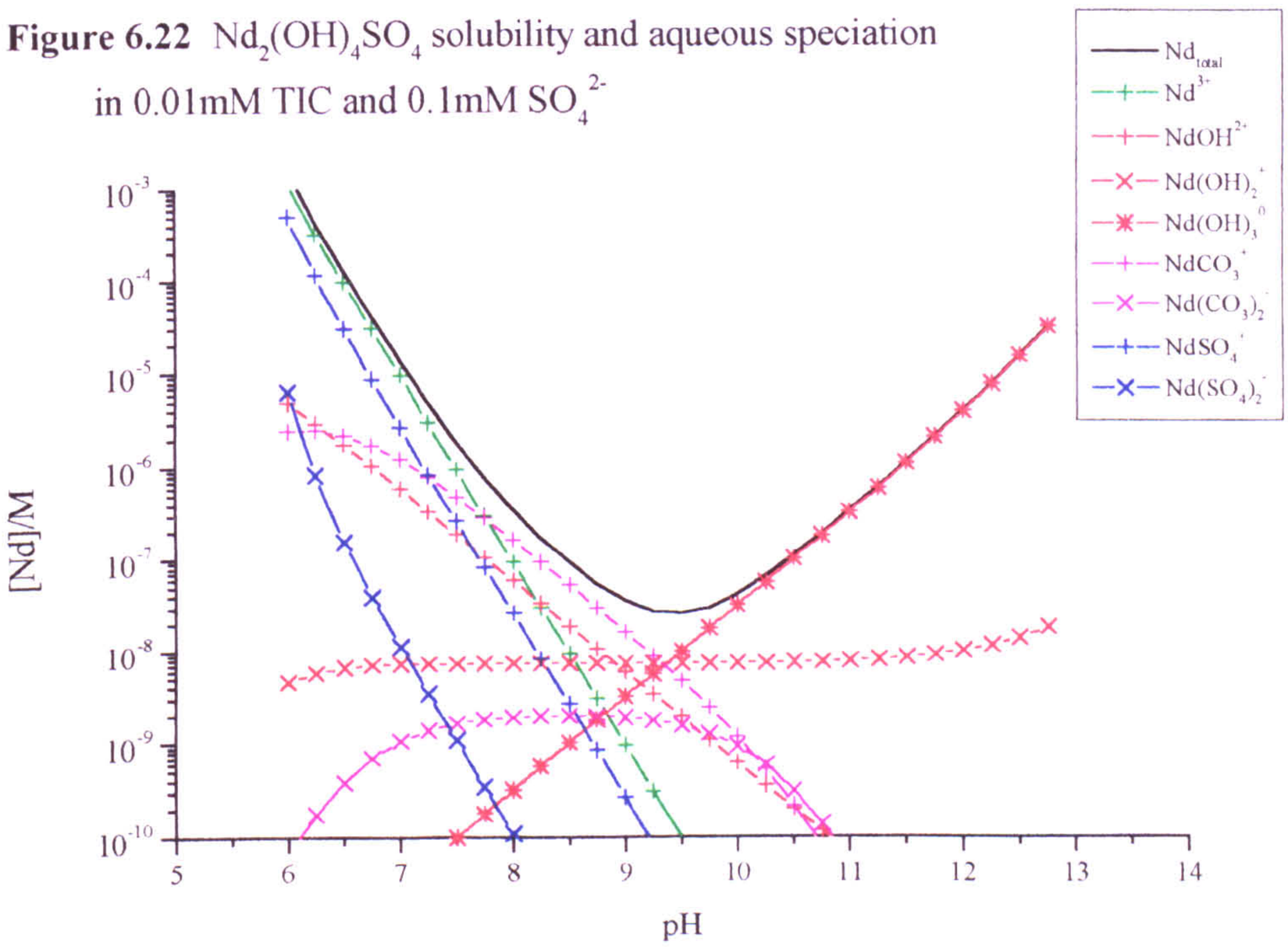

Figure 6.23 $Nd_2(OH)_4SO_4$ solubility and aqueous speciation in 0.1mM TIC and 1mM SO_4^{2-}

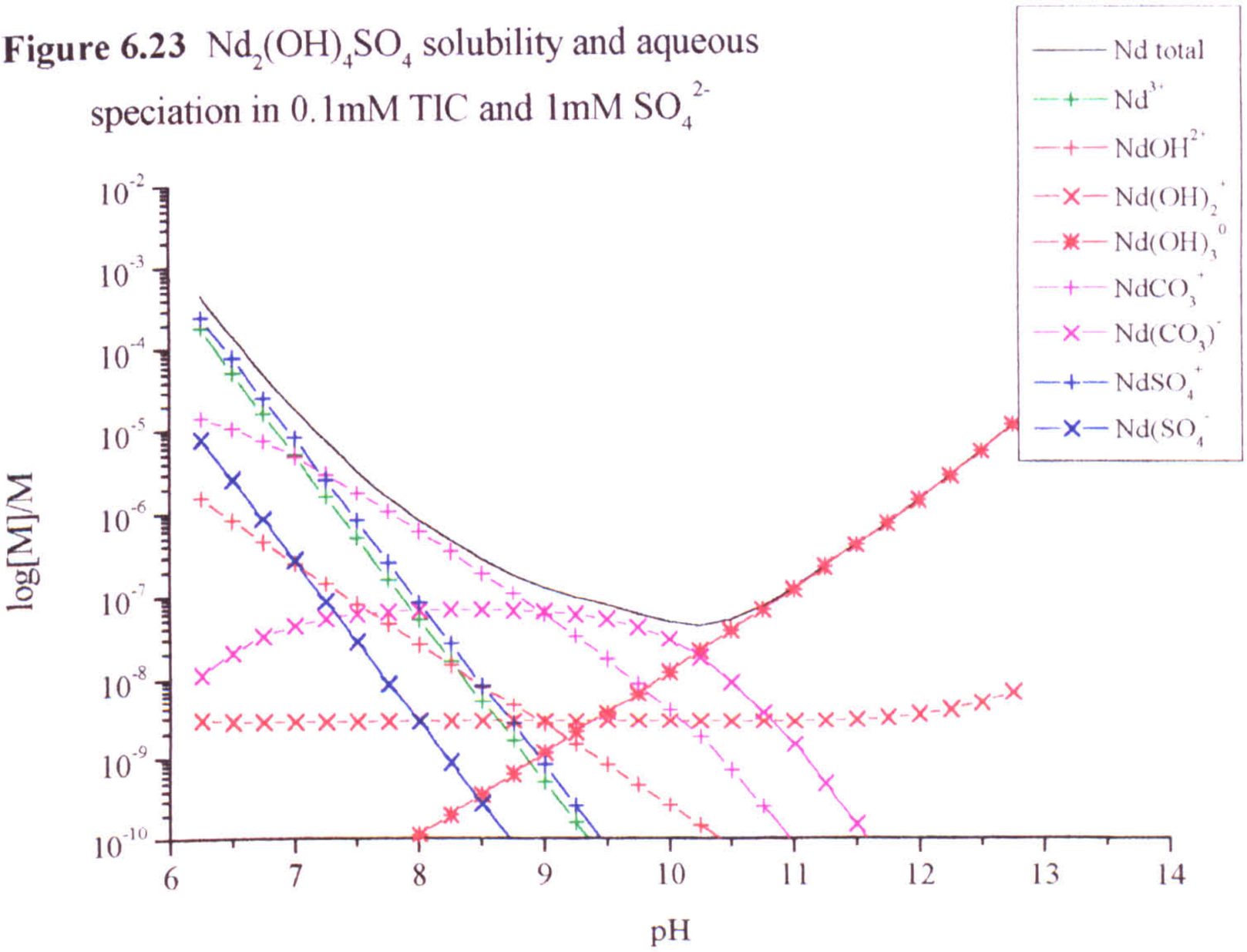

Figure 6.24 $Nd_2(OH)_4SO_4$ solubility and aqueous speciation in 1mM CO_3^{2-} and 1mM SO_4^{2-}

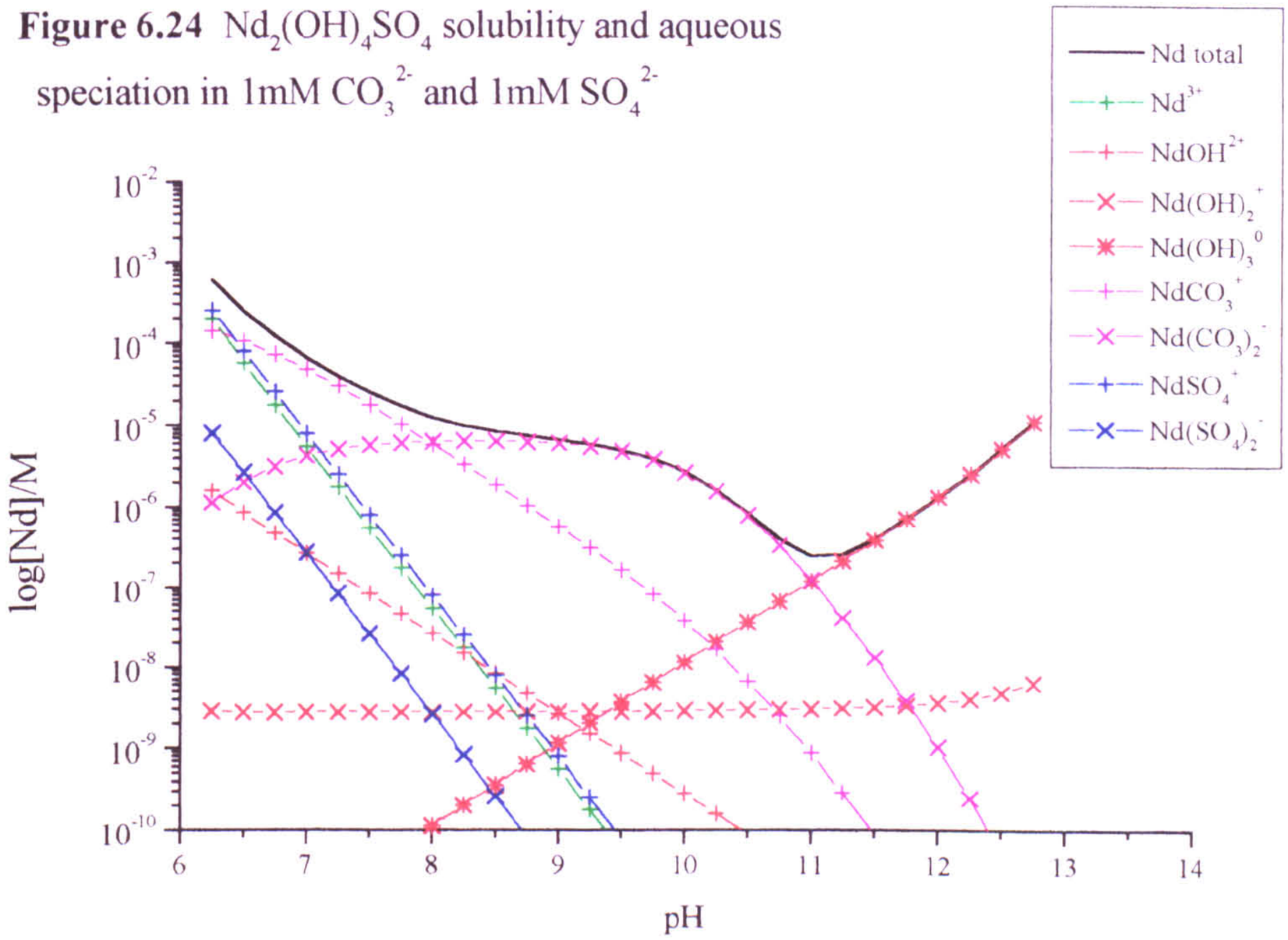

6.9 Discussion

The sulphate system was studied as a comparison with the carbonate system, as the sulphate ion will be the second most abundant anion in many solutions compared to carbonate, therefore its relative influence upon solubility must be examined. The SO_4^{2-} ion has the same charge as the CO_3^{2-} ion and therefore may be expected to have similar properties, but the SO_4^{2-} ion is the dominant sulphate species at a lower pH range than the CO_3^{2-} ion.

The solubilities and stability of three lanthanide sulphate phases, $NaCe(SO_4)_2$, $Nd_2(OH)_4SO_4$ and $Eu_2(OH)_4SO_4$ have been determined. The lanthanide sulphates form a series of phases from $NaLn(SO_4)_2$, $Ln_2(OH)_4SO_4$ and $Ln(OH)_3$ as pH increases. The equivalent $Ln_2(CO_3)_3$ and $LnCO_3OH$ phases found in the carbonate system did not form in any of the sulphate systems studied. The hydroxy sulphate $Ln_2(OH)_4SO_4$, is a very insoluble phase, with a potential solubility minima less than that of $Ln_2(CO_3)_3$ and $LnCO_3OH$ within the region between pH 7 and 12. The solubility of $Ln_2(OH)_4SO_4$ does however increase

with the addition of carbonate to the system. The $Ln_2(OH)_4SO_4$ solubility minimum is similar to $LnCO_3OH$ in a 1mM TIC and 1mM SO_4^{2-} solution at pH 11. Carbonate phases will then control the lanthanide solubility above 1mM TIC

The carbonate and hydroxy ions form stronger aqueous complexes with lanthanide ions than the equivalent sulphate complexes. Aqueous lanthanide sulphate complexes ($LnSO_4^+$ and $Ln(SO_4)_2^-$) mirror the effects of the free lanthanide ion (Ln^{3+}) in solution, which is the dominant aqueous species only below pH 7. At low TIC concentrations (below 10^{-5}M), the aqueous lanthanide concentration in sulphate bearing solutions is likely to be controlled by the equilibrium between solid lanthanide sulphates and aqueous lanthanide hydroxy species, rather than with lanthanide carbonate phases. The aqueous lanthanide carbonate phases, $LnCO_3^+$ and $Ln(CO_3)_2^-$, become significant above 10^{-4}M TIC between pH 6 and 11, (i.e. a different pH region from the lanthanide sulphate aqueous phases), even when the total sulphate concentration is an order of magnitude higher than the TIC concentration.

The formation of pure $NaNd(SO_4)_2$ and $NaEu(SO_4)_2$ will be difficult in low ionic strength solutions as the mixed phases form with $Ln_2(OH)_4SO_4$ in less than 100mM Na_2SO_4 solutions at pH 6, with total lanthanide solubilities of approximately 1mM. The sodium lanthanide double sulphate may be a solubility limiting phase under extreme conditions of acidic pH, such as in a a sodium sulphate bearing brine. However, as the total aqueous lanthanide concentration will typically be between 0.1mM and 1mM if in equilibrium with $NaLn(SO_4)_2$, then even when trace amounts of aqueous carbonate (i.e. on exposure to the atmosphere) are added to a system then $Ln_2(CO_3)_3$ may become the solubility limiting phase above pH 5.

In natural systems, aqueous sulphate ions are only found in near surface oxidising systems, especially associated with the oxidation of sulphide minerals to form aqueous sulphates. Lanthanide sulphates are therefore probably restricted to precipitation in near surface (oxidised) environments, which may later alter to a sulphide phase when buried. The oxidation process that forms the SO_4^{2-} may

also have the dual purpose of oxidising Ce^{3+} to CeO_2, provided the correct pH conditions are present.

The examination of solid lanthanide sulphides would therefore be a logical extension of this work on lanthanide sulphates, to fully model the effects of lanthanides especially in enclosed reducing environments (e.g. bacteriological reducing regimes) where carbonate may also be restricted.

6.10 References

DIAKONOV, I. I., TAGIROV, B. R., and RAGNARSDOTTIR, K. V., (1998) Standard thermodynamic properties and heat capacity equations of rare earth hydroxides: I. $La(OH)_3(s)$ and $Nd(OH)_3(s)$. Comparison of thermochemical and solubility data. *Radiochim. Acta* **81** 107-116

HALE, C. F., and SPEDDING, F. H., (1972) *J. Phys. Chem.* **76** 1887

Izatt *et al.*, (1969) *J. Chem. Soc.* 47-53

LEE, J. H., and BYRNE, R. H., (1992) Examinations of comparative REE complexation behaviour using linear free-energy relationships. *Geochim. Cosmochim. Acta* **56** 1127-1137

LIDE, D. R., (1998) Handbook of chemistry and physics 79th edition 1998-1999. *pub. CRC*

MARGULIS, E. V., SHOKAREV, M. M., NOVOSELOVA, V. N., and VERSHININA, F. I., (1970) Thermolysis of neodymium hydroxide and hydroxide sulphates. *Russ. J. Inorg. Chem.* **15** 745-749

MARTELL and SMITH (1989a) Critical stability constants Volume 4: Inorganic complexes *Plenium Press* New York

MARTELL and SMITH (1989b) Critical stability constants Volume 6: Second supplement *Plenium Press* New York

MORSS, L. R., HAAR, C. H., and MROCZKOWSKI, S., (1989) Standard molar enthalpy of formation of neodymium hydroxide. *J. Chem. Thermodyn.* **21** 1079-1083

RAO, L. F., RAI, D. P., FELMY, A. R., FULTON, R. W., and NOVAK, C. F., (1996) Solubility of $Nd(OH)_3$ in 0.1M NaCl aqueous solution at 25°C and 90°C. *Radiochim. Acta* **72** 151-155

TULINOVA, V. B., PLYUSCHEHEV, I. V., LUKOVA, S. N., and SAMAUSEVA, R. G., (1960) Joint solubility of lanthanum and sodium sulphate. *Russ. J. Inorg. Chem.* **5** 335-337

ZAITSEVA, L. L., KONAREV, M. I., KRUGLOV, A. A., and CHERSTVENKOVA, E. P., (1964) Double sulphates of sodium and rare-earth elements. *Russ. J. Inorg. Chem.* **9** 1380-1382

ZAITSEVA, L. L., KONAREV, M. I., KRUGLOV, A. A., CHERSTVENKOVA, E. P., and YAROSHINSKII, V. I. (1965) Thermal properties of double sulphates of sodium and rare-earth elements of the cerium subgroup. *Russ. J. Inorg. Chem.* **10** 783-787

Chapter 7

Predicting REE reactions and solubility in aqueous carbonate and sulphate solutions

7.1 Introduction

The reaction constant for the dissolution of a solid phase into aqueous solution is usually considered in terms of the dissociation reaction. For example, $Nd_2(CO_3)_3$ dissociates into Nd^{3+} and CO_3^{2-} and at equilibrium, can be written as equation 7.1

$$Nd_2(CO_3)_3(s) = 2Nd^{3+}(aq) + 3CO_3^{2-}(aq) \qquad (7.1)$$

There are two methods used to calculate the solubility product from experimental data. The first method is by measuring the heat change (ΔH°) when a pure solid phase dissolves in water to calculate the Gibbs free energy (ΔG°) for the reaction from equation 7.2.

$$\Delta G^\circ = \Delta H^\circ + T\Delta S^\circ \qquad (7.2)$$

where T is the thermodynamic temperature and ΔS^0 is the entropy change for the reaction.

The Gibbs free energy change is directly related to the reaction constant for the dissolution reaction by equation 7.3

$$\Delta G^\circ = -RT\ln K \qquad (7.3)$$

where R = gas constant (8.314 $JK^{-1}mol^{-1}$), T the temperature (K) and K the reaction constant.

The alternative is to calculate the solubility from the analysis of a solution in equilibrium with a pure solid phase. The solid phase may be precipitated directly from the solution, or have been partially dissolved. The solubility product is calculated from the sum of the stoichiometric amounts of the free ion concentrations in equilibrium with the solid phase. The solubility product for the reaction in equation 7.1 is shown in equation 7.4

$$Ksp = [Nd^{3+}]^2.[CO_3^{2-}]^3 \qquad (7.4)$$

The solubility product cannot be calculated directly from the aqueous composition as aqueous association reactions do occur i.e. carbonate forms three different aqueous species (H_2CO_3, HCO_3^-- and CO_3^{2-}) as well as aqueous metal carbonate species in solution. The total concentration of an element will therefore not be equal to the concentration of the free ion required for the solubility calculation. There is a further complication from the attraction of opposing charged ions in solution preventing a uniform distribution of each ion in solution.

At low ionic strengths the activity of each component can be approximated to the concentration. However in non-ideal solutions the actual concentration of each species must be calculated from a series of aqueous association reactions for each species, then corrected for the ionic strength of the solution and the charged ion distribution in solution, from the calculation of an ion activity coefficient for each ion to correct for the non-ideal nature of the solution. A series of geochemical models (i.e. PHREEQE) have been derived to calculate the actual species distribution for each element and their activities in real solutions. The models are designed to predict the solubility of mineral phases in a variety of solutions, and therefore will calculate the solubility product directly from the chemical analysis of a solution in equilibrium with a solid phase.

7.2 PHREEQE and PHREEQC

PHREEQE (pH, REdox, EQuilibrium Equations) is a computer program developed by the U.S. Geological Survey (Pankhurst *et al.*, 1980) to determine aqueous species equilibrium in natural geochemical solutions. (i.e. the outflow from mine leachates and subsequent mixing with groundwaters and river systems). The following section is an introduction to the use and capabilities of PHREEQE and the upgrade from Fortran to C, PHREEQC (Parkhurst, 1995) in this project and is not intended as a complete description of the calculations involved in each model.

PHREEQC calculates a number of parameters in an aqueous system namely

i, pH

ii, pe

iii, total element concentration

iv, distribution of aqueous species

v, the saturation of solid or gaseous phases in equilibrium with the solution

vi, phase transport in and out of the system

PHREEQC calculates the speciation of each aqueous species from the reaction constant as association reactions i.e. for the formation of $Ln(CO_3)_2^-$ (equation 7.5)

$$Ln^{3+} + 2CO_3^{2-} = Ln(CO_3)_2^- \qquad (7.5)$$

The reaction constant (K) for equation 7.5 can be expressed as equation 7.6

$$K=\frac{[Ln(CO_3)_2^-]}{[Ln^{3+}][CO_3^{2-}]^2} \qquad (7.6)$$

Solubility reactions are expressed as the aqueous dissociation of a solid phase, if hydroxide is involved the reaction is expressed as the acid dissolution

i.e. the dissolution of $LnCO_3OH$ can be written as equations 7.7 and 7.8

$$LnCO_3OH(s) + H^+ = Ln^{3+}(aq) + CO_3^{2-}(aq) + H_2O \qquad (7.7)$$

$$K=\frac{[Ln^{3+}][CO_3^{2-}][H_2O]}{[H^+]} \qquad (7.8)$$

However the thermodynamic activity is only equal to concentration in ideal solutions therefore, PHREEQC calculates the activity for each species from the Debye-Hückel or the Davis expressions (equations 7.9 and 7.10 respectively) for the activity coefficients in non-ideal solutions.

Debye-Hückel expression for activity coefficient (γ)

$$\log\gamma_i=\frac{Az_i^2\sqrt{\mu}}{1+Ba_i^o\sqrt{\mu}}+b_i\mu \qquad (7.9)$$

Davis expression

$$\log\gamma_i = -Az_i^2\left(\frac{\sqrt{\mu}}{1+\sqrt{\mu}} - 0.3\mu\right) \qquad (7.10)$$

A and B are temperature dependant constants, a_i^o and b_i are ion-specific parameters fitted from mean-salt activity–coefficients data, z_i is the ionic charge of aqueous species i and chemical potential μ. PHREEQC calculates the activity of each species from the sum of the concentration of each species multiplied by its activity coefficient.

Many solution reactions and changes in geochemical conditions include reduction-oxidation (redox) changes in some species
i.e. the oxidation of aqueous Ce^{3+} to $Ce^{(IV)}O_2$ (equation 7.11)

$$CeO_2 + 4H^+ + e^- = Ce^{3+} + 4H_2O \qquad (7.11)$$

The redox state of the system must be included in the model to conserve solution neutrality of the bulk system. Conservation of electrons is obtained from the introduction of term pe for the log of e^- activity (a_{e^-}), similar to the pH term for H^+ ion activity (equation 7.12)

$$pe = -\log_{10} a_{e^-} \qquad (7.12)$$

The equilibrium equation for CeO_2 dissolution can be written as equation 7.13,

$$K = \frac{a_{Ce^{3+}} a_{H_2O}^4}{a_{CeO_2} a_{H^+} a_{e^-}} \qquad (7.13)$$

as the activity of a solid phase and water are unity in an ideal system, equation 7.13 can be simplified as equation 7.14,

$$\begin{aligned} \log K &= \log a_{(Ce^{3+})} - \log a_{(H^+)} - \log a_{(e^-)} \\ &= \log a_{(Ce^{3+})} + pH + pe \end{aligned} \qquad (7.14)$$

7.2.1 Using PHREEQC

PHREEQC requires at least three files, a database of all reaction constants of all solid phases, gaseous phases and aqueous species for each element to be considered in the model. An input file defining the initial solution conditions and any reactions to be modelled. PHREEQC then creates an output file of all the equilibrium solution conditions with saturation indexes of any other phases. A second selected output file of the specific data required can also be created. Each element i.e. (Na, Nd and C) are introduced as the total concentration of that element at a specified pH, pe and temperature. A series of possible reactions are then defined for the initial solution.

The model initially defines the initial solution. The speciation of each element is calculated from association reactions based on a series of master species (defined in the required database i.e. Nd^{3+}) for each element in the input solution. The speciation of each element is presented as concentration, activity coefficients and activities. The saturation index (SI) for all solid and gaseous phases in the database included are calculated from the difference between the ion activity product (IAP), calculated from a combination of the ions that compose each solid phase, and the solubility reaction constant of that solid phase (KT) at temperature T, (equation 7.15).

$$\log SI = \log IAP - \log KT \qquad (7.15)$$

Positive log saturation indexes indicate that the solid (or gaseous phase) is saturated in solution and would precipitate, whilst negative saturation indexes indicate that the solution is under-saturated in the required components and further dissolution would occur.

When PHREEQC has solved the original solution a series of reactions are possible.

i, mixing with other solutions as a single addition or as stepwise additions (similar to titration experiments)

ii, equilibrium with a solid phase

iii, equilibrium with a gaseous phase

iv, surface complexation reactions

v, equilibrium at varied pH, pe or temperature conditions

vi, a combination of the above reactions

The equilibrium solution can be saved for further reactions or the initial solution can be reused for a series of reactions modelling changes in equilibrium conditions, i.e. the effects of altering pH on the solubility of a solid phase.

PHREEQC presents the results as an output file composed of the original input data, the initial solution speciation and saturation indexes for all possible solid phases that involve the specified master species. Each reaction solution is then presented as a series of bulk solution parameters, aqueous speciation and saturation indexes. A second output can be created of the specific data required, which can be extracted to a graphics file for presentation as a set of variables, e.g. Nd solubility vs pH when the solution is in equilibrium with $NaNd(CO_3)_2$, $Nd_2(CO_3)_3$, $NdCO_3OH$ or $Nd(OH)_3$ at a series of TIC activities, or the variation of Nd aqueous species with pH and carbonate concentration.

An unknown solubility product can be calculated for a solid phase from the ion activation product (IAP) of a known solution. If the solution composition is known to be experimentally in equilibrium with a solid phase then the activity of each component species is automatically calculated. The solubility product is then derived from the sum of the activities of all the species in the solid phase. The sum of all the activities is the IAP and therefore the experimentally derived solubility product.

The IAP calculated from PHREEQC for hydroxide species for the acid dissolution reaction i.e. equation 7.16

$$Nd(OH)_3(s) + 3H^+(aq) = Nd^{3+}(aq) + 3H_2O(aq) \qquad (7.16)$$

therefore

$$K=\frac{a_{Nd^{3+}}}{a_{H^+}{}^3} \qquad (7.17)$$

$$\therefore \log K = \log a_{Nd^{3+}} + 3pH$$

rather than as the solubility product (equation 7.18)

$$Nd(OH)_3(s) = Nd^{3+}(aq) + 3OH^-(aq) \qquad (7.18)$$

when the solubility expression is shown as equation 7.19

$$Ksp=a_{Nd^{3+}}.a_{OH^-}{}^3 \qquad (7.19)$$

$$\therefore \log Ksp = \log a_{Nd^{3+}} + 3\log a_{OH^-}$$

When all the association constants of the possible aqueous species are known and the equilibrium phase has been determined then the model will calculate the solid-aqueous equilibrium between the solution and required solid phase, i.e. if $NdCO_3OH$ is put in equilibrium with a Nd free, carbonate bearing solution, then PHREEQC will calculate the amount of Nd that would dissolve to obtain equilibrium at the specified pH and total inorganic carbonate concentration.

Various solutions can be modelled i.e. pure water, seawater, simulated repository solutions or native groundwater solutions. For example, the fate and maximum solubility of each lanthanide (and Am or Cm) can be predicted within the repository through the changing geochemical conditions that would be found as radionuclides are dispersed over time. This includes predicting the solubility of secondary precipitates that may form in equilibrium with evolving solutions as the primary host matrix is breached, then the further changes in solubility that may occur during the aqueous transport away from the near field system out through the far field host rock groundwater system, then ultimately to the solubility in a lakewater or seawater type environment.

Surface complexation reactions are possible below the aqueous solubility limit and are an important mechanism of removing toxic and radioactive species from

solution. Modelling surface complexation reactions requires the appropriate equation and constant for each reaction. Surface complexation reaction constants can be derived from experimental data from FITEQL (Section 7.3). The surface must also be characterised and PHREEQC requires the surface area and number of sites per unit area for each surface available for reaction. The surface effectively becomes a separate phase available for the removal of species from solution.

An example of selected PHREEQC input, database and output files can be found in Appendix 7.1

7.3 FITEQL v32

FITEQL is a computer program designed by Herbelin and Westall (1996) to calculate equilibrium constants from experimental data. The model is capable of determining

i, stability constants of complexes

ii, total concentrations of components

iii, solubility products of solids

iv, double layer adsorption at charged surfaces

In the work presented here, the model will be exclusively used for the calculation of lanthanide-goethite adsorption equilibrium constants. The program requires each possible species reaction with equilibrium constants for all elements present, solubility product data is not required as the adsorption experiments were carried out below the lanthanide solubility limits. The solid surface phase (goethite) was assumed to be insoluble for the experimental equilibrium reactions.

The amount of the surface (g/litre) and the specific surface area (m^2/g) available for reaction are required to characterise the surface. PHREEQC also requires the number of sites in mols/g for predictions involving surface complexation.

FITEQL v.32 optimises the unknown (goethite-lanthanide) adsorption equilibrium constant from an initial estimate and a series of pH vs adsorbed lanthanide concentration isotherms from experimental data.
The other components are assumed unchanged in solution i.e. Na^+ and K^+, carbonate, chloride and sulphate remain in solution although aqueous Ln complexes are considered in the model.

7.4 Aqueous databases

The PHREEQE, PHREEQC and FITEQL models are entirely dependant on the choice and quality of aqueous species and solubility databases available. PHREEQE and PHREEQC contain a database (containing two sections, aqueous species and potential solid phases) generated for the general requirements of geochemical problems that contains the bulk elements in groundwater solutions and the typical heavy metals found from mine leachate solutions. The database does not include lanthanide elements or actinide elements, however some other nuclear fission products (i.e. Pb may be included as a toxic heavy metal). The databases involved can be adapted to include literature and experimental data. Two additional databases have been proposed for the predication of the solubility of nuclear waste (Tables 7.1 and 7.2) and will be considered here, NEA Version 9 (NEA, 1996) and CHEMVAL Version 6 (Atkins, 1996)

These databases have been comprehensively constructed for U, Pu and Am, as the major radioactive elements to be considered in nuclear waste disposal. However lanthanides have not been considered as thoroughly as the actinides elements. Experimental work over the last ten years using first Eu to represent all the lanthanides and as a chemical analogue for Am, then Nd as a specific analogue for Am as the lanthanide with closet 3^+ ionic radii of 98.3pm and 97.8pm for Nd and Am respectively, has not resulted in the inclusion of equivalent lanthanide and Am phases, probably mirroring the limited importance of lanthanides to radioactive waste disposal compared with U, Pu and Am.

Table 7.1 Comparison of the aqueous species association constants in the NEA Version 9 (NEA, 1996) and CHEMVAL Version 6 (Atkins, 1996) databases

Database	NEA version 9 (NEA, 1996)				CHEMVAL Version 6 (Atkins, 1996)				Lee & Byrne (1992/3)[11/12]		
Species	Am	Ce[2]	Nd[1]	Eu	Am	Ce	Nd	Eu	Ce	Nd	Eu
MOH^{2+}	-6.40[1]	-8.30[2]	-7.60[4]	-7.80[6]	-8.01[8]	-5.59[11]	-5.84[11]	-6.10[11]	-8.41	-8.16	-7.90
$M(OH)_2^{+}$	-14.10[1]		-14.30[4]		-16.92[8]	-10.40[11]	-10.96[11]	-11.63[11]	-17.60	-17.04	-16.37
$M(OH)_3^{0}$	-25.70[1]		-24.90[4]		-26.53[8]	-14.77[11]	-15.60[11]	-16.59[11]	-27.23	-26.40	-25.41
$M(OH)_4^{-}$											
MCO_3^{+}	7.80[1]	7.94[3]	7.50[5]	7.11[7]	6.53[9]	6.86[12]	7.67[12]	7.41[12]	7.40	7.67	7.95
$M(CO_3)_2^{-}$	12.30[1]	13.30[3]	12.53[5]	10.60[7]	14.04[9]	11.10[12]	12.29[12]	11.87[12]	12.63	13.09	13.40
$M(CO_3)_3^{3-}$	15.20[1]	14.20[3]				14.20[13]					
$M(CO_3)_4^{5-}$		13.70[3]				13.70[13]	15.35[14]	15.55[14]			
M^{4+}	-44.20[1]				-39.57[10]	-29.58[10]		-106.49[10]			

[1]Silva *et a.,l* (1995) Chemical thermodynamics vol2: The chemical thermodynamics of americium. *Elsevier Amsterdam*

[2]Baes, C. F., and Mesmer, R. E., (1989) The hydrolysis of cations. *Robert E. Krieger Pub. Co. Malaber Florida.*

[3]Martell, A. E., and Smith, R. M., (1989) Critical stability constants vol 6: Second supplement. *Plenum Press, New York.*

[4]Makino *et al.*, (1993) Nd(III) hydrolysis constants and solubilities of Nd(III) hydroxide. *J. Chem. Soc. Japan.* 5 445-450

[5]Shibutani, S. (1996) Solubility measurement of trivalent lanthanide for performance assessment of geological disposal of high level radioactive waste. *PNC Technical Review N° 97*

[6]Baes, C. F., and Mesmer, R. E., (1976) The hydrolysis of cations. *Wiley.*

[7] Martell, A. E., and Smith, R. M., (1982) Critical stability constants vol 5. *Plenum Press, New York.*

[8]Edelstein, N., *et al.*, (1982) Rep. ONWI/LBL-14325.

[9]Lundquist, R., (1982) *Acta Chem. Scand.* **36** 741

[10]Nugent, L.J., *et al.*, (1971) *J. Inorg. Nucl. Chem.* **33** 2503

[11]adapted from Lee, J. H., and Byrne, R. H., (1992) *Geochim. et Cosmochim. Acta* **56** 1127-1137

[12] adapted from Lee, J. H., and Byrne, R. H., (1993) *Geochim. et Cosmochim. Acta* **57** 295-302

[13]Ferri, D. *et al.*, (1983) *Acta Chem. Scand.* **A37** 359-365

[14]Dumonceau, J. (1979) *Rev. Chem. Miner.* **16** 583-592

Table 7.2 Comparison of the solid phase dissociation constants from the CHEMVAL 6 (Atkins 1996) and NEA 9 (NEA 1996) databases (including their source references)

	NEA 9				CHEMVAL 6			
Phase	Am	Ce	Nd	Eu	Am	Ce	Nd	Eu
MO_2	34.84[1]				34.84[1]	21.21[12]		
$M(OH)_3$	15.40[2]	19.90[3]	16.00[5]	17.50[7]	16.56[9]	19.90[13]	18.90[13]	15.50[13]
MCO_3OH	-5.70[3]		-7.89[6]		-8.52[10]			
$M_2(CO_3)_3$	-33.40[1]	-35.11[4]		-32.30[8]	-37.65[11]		-33.00[14]	-36.86[15]

[1]Silva *et al.*, (1995) Chemical thermodynamics Vol 2: The chemical thermodynamics of americium

[2]Cross *et al.*, (1995) Thermodynamic modelling of radioactive waste disposal . NSSR/311

[3]Baes, C. F., and Mesmer, R. E., (1986) The Hydrolysis of cations. *Robert E. Krieger Pub. Co. Malabar Florida*

[4]Martell, A. E., and Smith, R. M., (1989) Critical stability constants Vol 6: Second supplement. *Plenum Press new York*

[5]Makino *et al.*, (1993) Nd(III) hydrolysis constants and solubilities of Nd(III) hydroxide. *J. Chem. Soc. Japan* **5** 445-450

[6]Shibutani, S. (1996) Solubility measurements of trivalent lanthanide for performance assessment of geological disposal of high level radioactive waste. *PNC Technical Review N°97*

[7]Baes, C. F., and Mesmer, R. E., (1976) The hydrolysis of cations. *J. Wiley & Sons New York.*

[8]Martell, A. E., and Smith, R. M., (1982) Critical stability constants Vol 5: Sirst supplement. *Plenum Press New York.*

[9]Silva, R. (1982) *Lawerence Berkeley Laboratory Report*, LBL-15055

[10]Silva, R., and Nitsche., (1984) *U.S. Nucl. Reg. Comm. Rep.* NUREG/CP-0052

[11]Shiloh *et al.*, (1969) *J. Inorg. Nucl. Chem.* **31** 1807

[12]Baker *et al.*, (1971) *J. Chem. Thermodynamics* **3** 77-83

[13]Morss, L. R., and Williams, C. W., (1992) *Mat. Res. Soc. Symp. Proc.* **257** 283-288

[14]Jordanav, N., and Havezov, I., (1966) *Z. Anorg. Allg. Chem.* **347** 101-106

[15]Rard, J. A., (1987) Update of the europium database, Oct. 1987, LLNL Internal Memo.

7.4.1 CHEMVAL Version 6

Aqueous species

Four Am solid phases in the Na^+ CO_3^{2-} OH^- system, $Am_2(CO_3)_3$, $AmCO_3OH$ and $Am(OH)_3$ and the oxidised AmO_2 are formed based on pH and CO_3^{2-} activities of a solution. The equivalent lanthanide system includes the $Ln_2(CO_3)_3$ and $Ln(OH)_3$ forms but not the $LnCO_3OH$ for either Nd and Eu. Ce is the only lanthanide that can be relatively easily oxidised to Ln^{4+} and CeO_2 forms in preference to the hydroxycarbonate and hydroxide unless under strongly reducing conditions.

The lanthanide aqueous carbonate and hydroxy phases in CHEMVAL 6 were based on linear free energy interpolation from Lee and Byrne (1992 & 1993), however these values differ by up to 10 log units for the aqueous $Ln(OH)_3$ species between the actual reference and the database. The lanthanide in the original reference are similar to the Am aqueous species data (which has been derived from multiple sources, Table 7.1), especially for Nd. There is no published equivalent aqueous lanthanide $Ln(CO_3)_3^{3-}$ phase, possibly due to Lee & Byrne estimating their aqueous speciation from seawater where the TIC activity was predicted to be too low to form a $Ln(CO_3)_3^{3-}$ species. Rao *et al.*, (1996a) have calculated Nd solid phase stability constants "from Am data assuming that the value of the equilibrium constant for the formation of a given species is identical to the equilibrium constant for the corresponding Nd reaction". Their species constants were presented as chemical potentials (as μ°/RT) and not as association reaction constants. This is in contrast to other authors (e.g. Runde *et al.*, 1992) who characterise Nd and Eu phases then assume that Am will have formed the same phase under the same experimental conditions.

When each of the actual data sets are examined, the CHEMVAL 6 aqueous constants predict only two dominant aqueous lanthanide species (Appendix 7.2 indicates the dominant Ce and Nd species), Ln^{3+} (below pH 5) and $Ln(OH)_3^0$

(above pH 5), in 10^{-3}M and 10^{-5}M TIC solutions. All the other predicted species form a minor component of the total aqueous lanthanide.

The actual reference data from Lee and Byrne (1992 & 1993) predict that $LnCO_3^+$ and $Ln(CO_3)_2^-$ will be dominant species in a 10^{-3}M TIC solution. The lanthanides have almost identical aqueous constants and are shown for Nd in Appendix 7.3. In a 10^{-3}M TIC solution, Nd^{3+} is the dominant aqueous lanthanide species at low pH (below pH 6), then $NdCO_3^+$ from pH 6 to 8, followed by $Nd(CO_3)_2^-$ from pH 8 to 11, then $Nd(OH)_3^0$ above pH 11. If the [TIC] is reduced to 10^{-5}M, then $Nd(CO_3)_2^-$ will not be a dominant species. Nd^{3+} is dominant to a higher pH (pH 8), $NdCO_3^+$ is restricted by hydroxy species to between pH 8 and 9.5, $NdOH^{2+}$ at pH 9.5, then $Nd(OH)_3^0$ above pH 9.5.

The Am aqueous speciation is significantly different to the lanthanide CHEMVAL 6 datasets, but similar to the Lee and Byrne (1992 & 1993) data. In 10^{-3}M TIC solutions (Appendix 7.4a) Am^{3+} is dominant below pH 6.5, $Am(CO_3)_2^-$ between pH 6.5 and 11.5, followed by $Am(OH)_3^0$ from pH 11.5 to 13.5. There is an additional $Am(OH)_4^-$ aqueous species, which is not present in any aqueous lanthanide dataset, which is dominant above pH 13.5. $AmCO_3^+$ and $Am(CO_3)_3^{3-}$ are only present as trace amounts. If the [TIC] is reduced to 10^{-5}M (Appendix 7.4b), Am^{3+} is still the dominant low pH aqueous species (up to pH 8), between pH 8 and 10, there are three important species, $AmOH^{2+}$, $Am(CO_3)_2^-$ and $Am(OH)_2^+$. $Am(OH)_3^0$ is the dominant aqueous species above pH 10, then $Am(OH)_4^-$ above pH 13.5.

Solid phase solubility products

There is a complete set of Am solubility products for the Am^{3+}-CO_3^{2-}-pH-pe system (Table 7.2), which include the phases AmO_2, $Am_2(CO_3)_3$, $AmCO_3OH$ and $Am(OH)_3$. However, there is not an equivalent set of lanthanide solubility products. There are only two Ce solid phases, CeO_2 and $Ce(OH)_3$. Cerium(III) phases easily oxidise to CeO_2 at high pH, therefore $Ce(OH)_3$ is unlikely to form.

$Ce_2(CO_3)_3$ is not present at all. There are also only two Nd and Eu solid phases, the carbonate, $Ln_2(CO_3)_3$ and the hydroxide, $Ln(OH)_3$.

The Eu solubility products are closest to Am in the CHEMVAL 6 database, but they do suggest that the solid phases are less soluble than those found in this study (Chapter 4). The inconsistencies within the CHEMVAL 6 database mean that comparisons between the lanthanides and Am cannot be made without substantial revision of the database.

7.4.2 NEA version 9 (NEA 9) database (NEA, 1996)

The NEA 9 database for Am was produced using the recommended Am species and solid phase data recommended in the review of published Am thermodynamic data by Silva *et al.*, (1995), then revised to include enthalpy data. Am^{3+}, $AmOH^{2+}$, $Am(OH)_2^+$, $Am(OH)_3^0$, $AmCO_3^+$, $Am(CO_3)_2^-$ and $Am(CO_3)_3^-$ are all represented. There are major discrepancies between the hydroxy species of the four elements examined. There is a complete set of Am and Nd hydroxy aqueous species, but there are no equivalent Ce and Eu $Ln(OH)_2^+$ and $Ln(OH)_3^0$ aqueous species. Ce is the only lanthanide with an equivalent set of carbonate species to Am, but there is an additional Ce carbonate aqueous species, $Ce^{(III)}(CO_3)_4^{5-}$, which does not have an Am analogue. There are Nd and Eu $LnCO_3^+$ and $Ln(CO_3)_2^-$ aqueous species, but there is not a Nd and Eu aqueous tricarbonate species ($Ln(CO_3)_3^{3-}$). The Nd aqueous association reaction constants are within 0.3 log units of the equivalent Am constants (Table 7.1), therefore a neodymium tricarbonate species could possibly be extrapolated, but there are no distinct trends from Ce-Nd-Am-Eu based on ionic radii to predict all the required species.

Aqueous association reaction constants

The Am and Nd species from the NEA database are dominated by the hydroxy species $M(OH)_2^+$ and $M(OH)_3^0$ (Appendix 7.5 and 7.6) which are the dominant aqueous speciation above pH 7 and have a stronger influence on the aqueous species than the Lee & Byrne (1992 & 1993) hydrolysis constants suggest (Appendix 7.3).

In 10^{-5}M TIC solutions aqueous Am and Nd species do not influence the aqueous speciation. There are four dominant Am species across the pH range. The dominant species are; Am^{3+} below pH 6.5, $AmOH^{2+}$, from pH 6.5 to 8, $Am(OH)_2^+$, from pH 6.5 to 11, then $Am(OH)_3^0$ above pH 11.5. The $Am(OH)_4^-$ species is not included in the database. When the [TIC] is increased to 1mM, $AmOH^{2+}$ is replaced by $AmCO_3^+$ in the mid pH range between pH 6 and 9. The proportion of aqueous $Am(OH)_2^+$ above pH 9 is also reduced by an aqueous $Am(CO_3)_2^-$ component. $Am(CO_3)_3^{3-}$ has a limited influence in 10^{-3}M TIC solutions, however in 10^{-2}M TIC solutions, all the americium carbonate species are dominant between pH 6 and 12. Am^{3+} remains dominant at low pH, below pH 6. $AmCO_3^+$ is dominant from pH 6 to 8, $Am(CO_3)_2^-$ from pH 8 to 9.5, then $Am(CO_3)_3^{3-}$ between pH 9.5 and 11.5. At pH 11.5 to 12, there are equal proportions of the three aqueous species $Am(CO_3)_3^{3-}$, $Am(OH)_2^+$ and $Am(OH)_3^0$. Above pH 12 aqueous $Am(OH)_3^0$ is the dominant species.

There are only three dominant Nd species in 10^{-5}M TIC solution. The Hydrolysis constants in the NEA 9 database (calculated by Maskino *et al.*, 1993) predict that $NdOH^{2+}$(aq) will not be a dominant species, and is replaced by $Nd(OH)_2^+$(aq). Nd^{3+} is dominant below pH 7.5 and $Nd(OH)_3^0$ above pH 11, with $Nd(OH)_2^+$ dominant between these two extremes. If the [TIC] is increased to 10^{-3}M, aqueous neodymium carbonate species are dominant between pH 6.5 and 9.5. $NdCO_3^+$ is dominant up to pH 8.5, then two species $Nd(CO_3)_2^-$ and $Nd(OH)_2^+$ are the dominant aqueous species up to pH 11.

Similar diagrams (as Appendix 7.5 diagrams) cannot be constructed for Ce and Eu as the $Ln(OH)_2^+$ and $Ln(OH)_3^0$ aqueous species are not present in the NEA 9 database. The lanthanide hydrolysis constants were originally calculated by Baes & Mesmer (1976), who only calculated the first hydrolysis constants for all the lanthanides, but data for each of the three hydrolysis reaction constants was only presented for selected lanthanides (including Nd, but not Ce and Eu). Group trends could be extrapolated for the further Ce or Eu hydrolysis constants, but the Nd hydrolysis constants in NEA 9, have been replaced by the revised Nd hydrolysis constants calculated by Makino *et al.*, (1993) (as an analogue for Am). The first hydrolysis constant for Nd is lower than both Ce and Eu, making inferences between the lanthanides difficult and tenuous at best.

Lanthanide carbonate species formation constants increase from Ce to Eu ($LnCO_3^+$ 7.41 to 7.95, $Ln(CO_3)_2^-$ 12.63 to 13.40 respectively) in Lee & Byrne 1993, however the group trend within the NEA 9 database for the carbonate formation constants have the opposite trend of decreasing from Ce to Eu ($LnCO_3^+$ 7.94 to 7.11, $Ln(CO_3)_2^-$ 13.30 to 10.60 respectively). The constants are of similar magnitude in both data for Ce, but the equivalent Eu constants differ by up to 3 log units. The NEA 9 data set for the three lanthanides examined comes from three separate sources over 11 years and are not consistent. An increase in the aqueous lanthanide-carbonate association constants from Ce to Eu, follows the general trend seen in natural systems in which the HREE are more soluble than the LREE in carbonate solutions (Chapter 1), the trend calculated by Lee & Byrne (1993), and not the trend in the NEA 9 data set. The Lee & Byrne (1992/3) formation constants were therefore chosen to calculate the solubility products in this study as they form the most consistent set of formation constants for Ce, Nd and Eu.

Solid phase dissociation constants

The Am solubility data for $Am_2(CO_3)_3$ and $Am(OH)_3$ was originally taken from the review by Silva *et al.*, (1995) though the hydroxide is intermediate between Silva *et al.*, *'s* amorphous and crystalline extremes. The sodium double carbonate was acknowledged but there was insufficient experimental data for Silva *et al.*, (1995) to recommend a solubility product. However the reappraisal to include thermal data for $AmCO_3OH$ has had a significant effect on phase solubility within the database. The solubility product for the $AmCO_3OH$ hydrolysis reaction (equation 7.20) has been altered from log K= -7.2 (Silva *et al.*, 1995) to log K= -5.7).

$$AmCO_3OH + H^+ = Am^{3+} + CO_3^{2-} + H_2O \qquad (7.20)$$

This reappraisal was designed to incorporate thermal data (ΔH), to calculate Am solubility over a temperature range, which may be required for elevated temperature in a nuclear waste repository. The new association constant has had the effect of eliminating $AmCO_3OH$ as a stable phase (Figure 7.1) to be replaced by an $Am_2(CO_3)_3$-$Am(OH)_3$ equilibrium with a direct effect on Am solubility. The $Am_2(CO_3)_3$-$AmCO_3OH$ equilibrium has the effect of increasing Am solubility in the region that the $AmCO_3OH$ phase recommended by Silva *et al.*,(1995), log K -7.2, was the solubility limiting phase (Figure 7.2)

Figure 7.1 Stability field diagram for the Am^{3+}-TIC-OH^- system

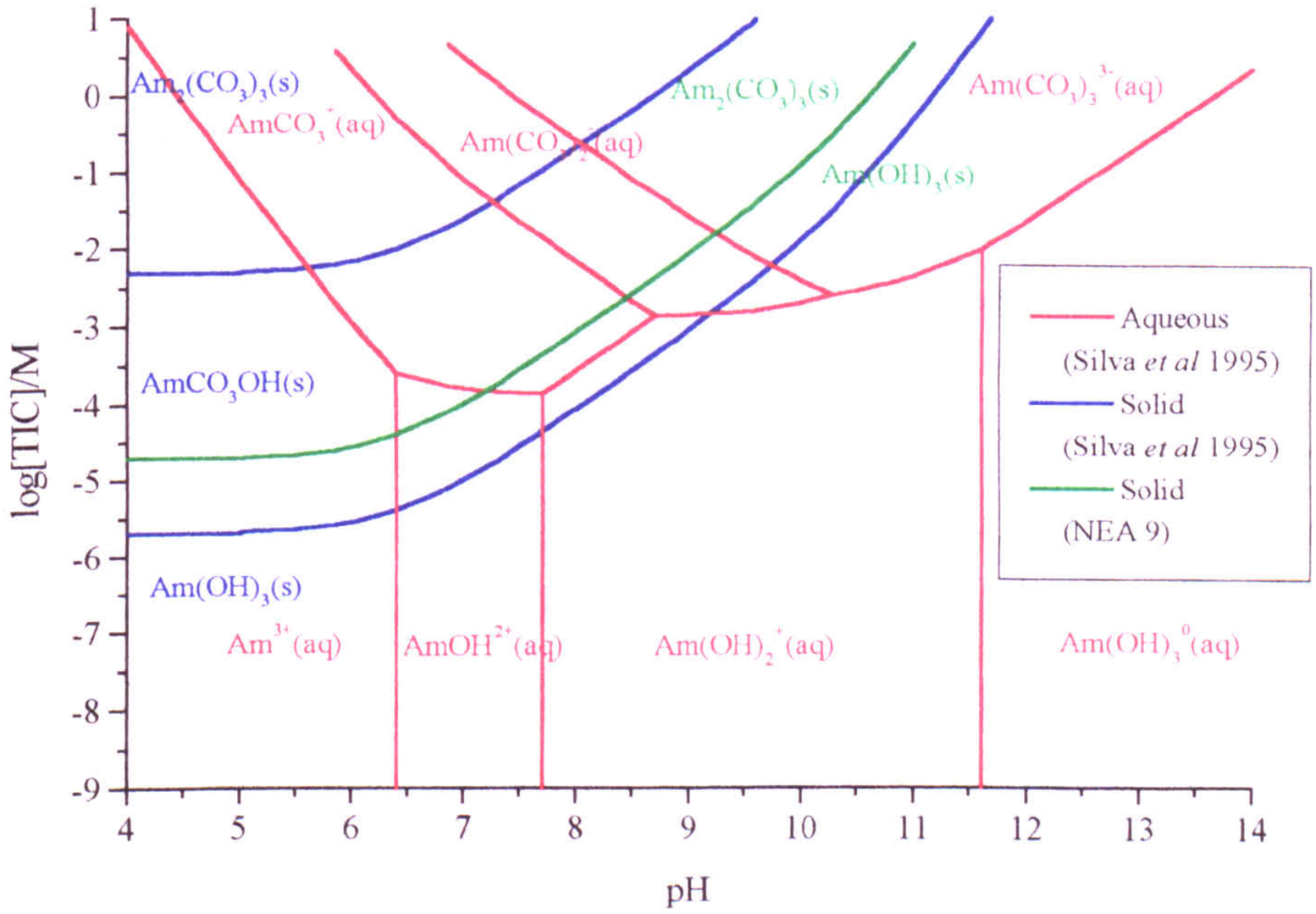

Experiments at varied $pCO_{2(g)}$ have clearly shown that $AmCO_3OH$ (implied from the formation of $NdCO_3OH$ and $EuCO_3OH$, e.g. Runde *et al.*, 1992) is stable under intermediate pH conditions and a stability field diagram based on the Silva *et al.*, (1995) data predicts that $AmCO_3OH$ will be the solubility limiting phase under most environmental conditions (e.g. pH 6 to 8 and 0.01mM to 5mM TIC). The revised association constant (log K -5.7) suggests that the hydroxycarbonate, found under experimental conditions is a kinetically formed metastable phase, which later alters either to the carbonate or the hydroxide.

Lanthanide solid phases in the NEA 9 database have a few peculiarities. The $Ln_2(CO_3)_3$ phase is not present for Nd but is for Ce and Eu, whilst $NdCO_3OH$ is present but $EuCO_3OH$ is not. All three lanthanides have hydroxide phases, but $Ce(OH)_3$ is unknown unless under very reducing conditions at high pH. If $Ce(OH)_3$ could be expected to form, then $CeCO_3OH$ must also be considered. An amorphous (purple) metastable $Ce(OH)_4$ has been postulated to form which alters to (yellow) CeO_2 within a few hours. CeO_2 has also been removed from the NEA database, even though Ce is easily oxidised to CeO_2 instead of forming hydroxy phases (Chapter 3).

A direct comparison of the stability fields between the lanthanides and Am (and even between individual lanthanides) cannot be made from the NEA 9 database. Ce and Eu hydrolysis constants must all be evaluated into a consistent dataset with Nd. The equivalent aqueous carbonate species (specifically $Ln(CO_3)_3^{3-}$) must be determined for all the lanthanides before solubility predictions and stability field diagrams can be produced for the lanthanides using the NEA 9 database.

Neodymium solubility calculations

Nd is the only lanthanide that can be successfully compared between the databases. If the Nd solubility is calculated using log Ksp from this work (Chapters 4 & 5), and associated Lee and Byrne (1992 & 1993) data, then compared with the predicted solubility using the same solubility products with NEA aqueous species (e.g. Makino *et al.*, 1993) significant differences can be seen in the shape of the solubility curves of each of the hydroxy phases. Nd solubility profiles (Appendix 7.7), calculated using the NEA 9 aqueous species data and the solubility products from this work (Chapters 4 and 6), predict that the minimum total Nd solubility remains between $2x10^{-7}M$ to $10^{-6}M$ for all the solubility limiting phases, except for $Nd(OH)_3$ which increases in solubility to $[Nd]_{total} \approx 10^{-5}M$. $Nd_2(CO_3)_3$ becomes the minimum solubility limiting phase rather than $NdCO_3OH$ from the Lee & Byrne (1992/3) data.

When the $NdCO_3OH$ or $Nd_2(OH)_4SO_4$ solubility is calculated in 1mM TIC and SO_4^{2-} solutions using the Lee and Byrne (1992 & 1993) aqueous constants, there is a slight plateau effect between pH 8 and 10, in which the Nd solubility is approximately constant as pH increases due to the equilibrium reaction between the solid phase and aqueous $Nd(CO_3)_2^-$. Above pH 10, $NdCO_3OH$ and $Nd_2(OH)_4SO_4$ solubility falls to a minimum before rising sharply as $Nd(CO_3)_2^-$ alters to aqueous $Nd(OH)_3$. The plateau effect is not apparent if the solubility of each is calculated using the NEA 9 database.

The $NdCO_3OH$ and $Nd_2(OH)_4SO_4$ solubility minimum, when $Nd(CO_3)_2^-(aq)$ converts to $Nd(OH)_3(aq)$ does not occur. These effects are due to the dominance of the $Nd(OH)_2^+$ species rather than $Nd(CO_3)_2^-$ in the mid-pH range, between pH 7.5-10 (Appendix 7.7). There is also a slight increase in the solubility of Nd, when calculated using the NEA 9 aqueous constants, compared to that when calculated with the Lee and Byrne (1992 & 1993) aqueous constants.

The Nd solid phases in the NEA 9 database (Table 7.3) are considerably less soluble than the equivalent phases found from this study. The NEA 9 database predicts that the minimum $NdCO_3OH$ solubility is approximately $5x10^{-9}M$ in a 1mM TIC solution. The $NdCO_3OH$ solubility increases slightly in 10mM TIC, as found from this study (Chapter 4). $Nd(OH)_3$ is independent of the carbonate concentration above pH 11.5, and is predicted to have a minimum solubility of $10^{-9}M$. The solubility of $Nd(OH)_3$ and $NdCO_3OH$ are considerably lower than found in this study (Chapter 4, Appendix 7.7). NEA 9 predicts that $Nd(OH)_3$ is more soluble than $Am(OH)_3$ and $NdCO_3OH$ is less soluble than $AmCO_3OH$ (Figures 7.2 & 7.3). Further comparisons between the lanthanides (Nd and Eu) and the determination of group trends that may include Am cannot be made as the NEA 9 lanthanide datasets are incomplete.

Table 7.3 Comparison of the Nd solubility products (log K) between the NEA 9 database and this work

Solid Phase	NEA 9	This work
$Nd_2(CO_3)_3$		-34.43
$NdCO_3OH$	-21.89	-19.87
$Nd(OH)_3$	-26	-21.9
$NaNd(CO_3)_2$		-21.25
$Nd_2(OH)_4SO_4$		-42.23

Aqueous $[Nd]_{total}$ vs pH diagrams show that $Nd(CO_3)_3^{3-}$ would have a significant effect in increasing solubility between pH 8 to 10.5 in 10mM TIC solutions for all

phases. $Nd(CO_3)_3^{3-}$ had a limited and almost unobservable affect in 1mM TIC solutions (Appendix 7.6, Figure 7.4)

Figure 7.2 Am solubility in 1mM TIC after NEA 9 and Silva *et al* (1995) at 298.15K and 1 atm pressure

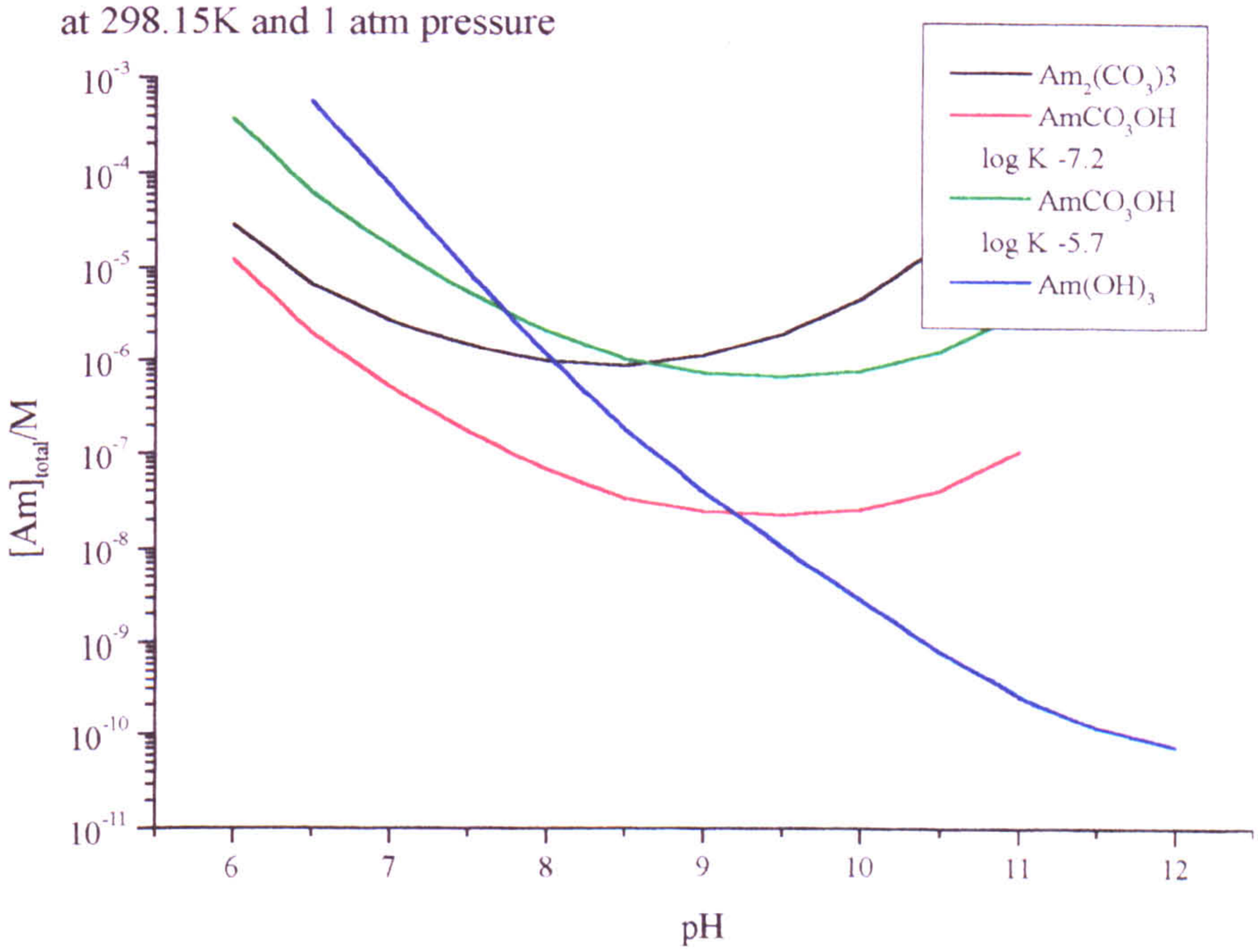

Figure 7.3 Nd Solubility in 10mM and 1mM TIC NEA Solid and aqueous data (Tables 7.1 & 7.2) at 298.15K and 1 atm pressure

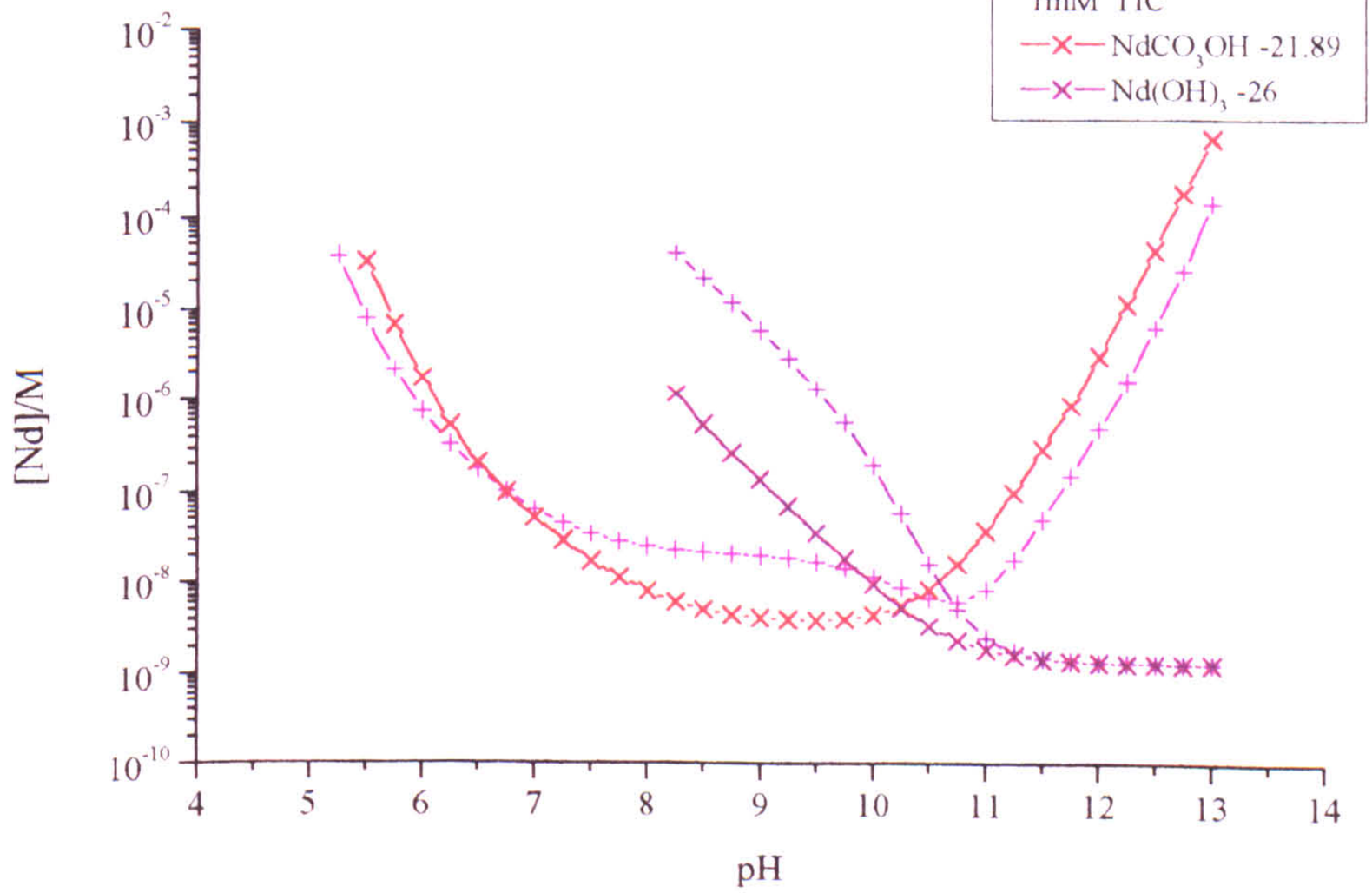

7.4.3 The effects of aqueous speciation on calculating solubility products

There are no proposed literature values for the aqueous $Ln(CO_3)_3^{3-}$ tricarbonate species. If the lanthanides are to be considered as true analogues for Am (and heavier actinides including Cm), then data for the actinide speciation must be revised, or a $Ln(CO_3)_3^{3-}$ species considered for the lanthanides. Rao *et al.*, (1996b) suggested that as Nd was the analogue for Am then Am speciation could be used for calculating the $NaNd(CO_3)_2$ solubility product with $Nd(CO_3)_3^{3-}$ as the dominant aqueous species in a 0.1M sodium carbonate solution.

Lee & Byrne (1993) predicted their lanthanide carbonate species from linear free energy calculations of 0.1mM TIC solutions and therefore $Ln(CO_3)_3^{3-}$ was not considered. If $Ln(CO_3)_3^{3-}$ exists then the solubility products of $LnCO_3OH$ and $NaLn(CO_3)_2$ phases formed at approximately pH 10 must be re-evaluated. Assuming the $Nd(CO_3)_3^{3-}$ formation constant is as the NEA 9 $Am(CO_3)_3^{3-}$ constant and approximately 2.5 log units greater than for the equivalent $Ln(CO_3)_2^-$ species then:

$Nd(CO_3)_3^{3-}$ log K 15.2
$Eu(CO_3)_3^{3-}$ log K > 15.6

Recalculating the solubility products of the Nd and Eu solid phases derived in Chapter 4 to include the $Ln(CO_3)_3^{3-}$ species above (with the NEA constants for Nd and Lee & Byrne for Eu) increases the solubility products of the phases which were found to exist in equilibrium with either the $Nd(OH)_2^+$, $Nd(CO_3)_3^{3-}$ and $Eu(CO_3)_3^{3-}$ aqueous phases (Table 7.4) i.e. $NaNd(CO_3)_2$, $NdCO_3OH$ and $NaEu(CO_3)_2$.

Table 7.4 Recalculated solubility products (from this work, Chapter 4) using the NEA 9 database including the $Ln(CO_3)_3^{3-}$ aqueous species

	adjusted log Ksp	log Ksp (Chapter 4)
$NaNd(CO_3)_2$	-21.95	-21.25
$NaEu(CO_3)_2$	-21.46	-20.48
$NdCO_3OH$	-22.96	-19.87

When the experimental data (Chapter 4) is re-appraised with solubility products calculated using NEA aqueous data including a $Ln(CO_3)_3^{3-}$ aqueous species, $Ln(CO_3)_3^{3-}$ becomes the dominant aqueous phase in equilibrium with $NaLn(CO_3)_2$. The amount of aqueous Ln^{3+} decreases compared with that calculated using the Lee & Byrne (1993) aqueous carbonate constants, therefore the solubility product also decreases. The total lanthanide solubility is independent of the CO_3^{2-} activity in solution (equation 7.21), when $NaLn(CO_3)_2$ is in equilibrium with $Ln(CO_3)_2^-$. If $Ln(CO_3)_3^{3-}$ forms, then the $NaLn(CO_3)_2$ solubility will increase in equilibrium with this aqueous phase (equation 7.22)

$$NaLn(CO_3)_2 = Na^+ + Ln(CO_3)_2^- \qquad (7.21)$$

$$NaLn(CO_3)_2 + CO_3^{2-} = Na^+ + Ln(CO_3)_3^{3-} \qquad (7.22)$$

The most significant effect of the reappraisal using the NEA 9 database is on $NdCO_3OH$. The $NdCO_3OH$ stability field increases significantly to the exclusion of the $Nd_2(CO_3)_3$ and $NaNd(CO_3)_2$ phases (Figure 7.3). The exclusion of the $NaNd(CO_3)_2$ and the $Nd_2(CO_3)_3$ phases from the stability field diagram is a direct result of a calculated significant increase in the stability of the $NdCO_3OH$ phase. The increase in the proportion of aqueous carbonate phases (i.e. $Nd(CO_3)_3^{3-}$), decreases the activity of Nd^{3+} in the high pH regime that was in equilibrium with $NdCO_3OH$. When the tricarbonate aqueous species (i.e. $Nd(CO_3)_3^{3-}$) is dominant there is also a relative increase in the solubility of the Nd phase $NdCO_3OH$, from the reaction shown in equation 7.23, compared to that if $Nd(CO_3)_2^-$ was the dominant aqueous phase.

$$NdCO_3OH + 2CO_3^{2-} = Nd(CO_3)_3^{3-} + OH^- \qquad (7.23)$$

The solubility of $NdCO_3OH$ is also increased by the stability of the $Nd(OH)_2^+$ aqueous species (equation 7.24), resulting in the complete exclusion of $NdOH^{2+}$ as a major aqueous species.

$$NdCO_3OH + OH^- = Nd(OH)_2^+ + CO_3^{2-} \qquad (7.24)$$

The value of the $EuCO_3OH$ solubility product does not change as $EuCO_3OH$ was experimentally formed in less than 10mM TIC solutions. The Lee & Byrne

(1992) hydrolysis constants were used to calculate the $EuCO_3OH$ solubility product in both databases. The $EuCO_3OH$ stability field can only expand in two ways to: either the $EuCO_3OH$ must have a lower solubility product than suggested from this work, or the $Eu_2(CO_3)_3$ and $Eu(OH)_3$ phases are less stable than predicted from this study (e.g. by decreasing the $Eu_2(CO_3)_3$ solubility product as shown in Figure 7.4).

$Nd_2(CO_3)_3$ and $Eu_2(CO_3)_3$ form in equilibrium with Ln^{3+}, $LnCO_3^+$ and $Ln(CO_3)_2^-$ which are largely unaffected between the databases. The values of the $Ln(OH)_3^0(aq)$ formation constant is also similar throughout all the aqueous databases examined, therefore the $Ln(OH)_3(s)$ stability field is largely unchanged between each set of stability constants for Nd and Eu.

The stability field diagrams (Figures 7.3 and 7.4) clearly indicate inconsistencies between the experimental data and the solubility products calculated using the NEA 9 database, including a $Ln(CO_3)_3^{3-}$ aqueous species. The $NdCO_3OH$ stability field calculated from a log Ksp -22.96, eliminates all other carbonate phases even though the recalculated $NaNd(CO_3)_2$ solubility product would indicate a larger stability field.

Figure 7.4 Nd solid-solid and aqueous-aqueous stability field diagram.
Solubility products recalculated to include $Nd(CO_3)_3^{3-}(aq)$ from this work (solution data, Appendix 4) and NEA 9 aqueous association constants $[Na^+]$ = 1mM at 298.15K and 1 atm pressure

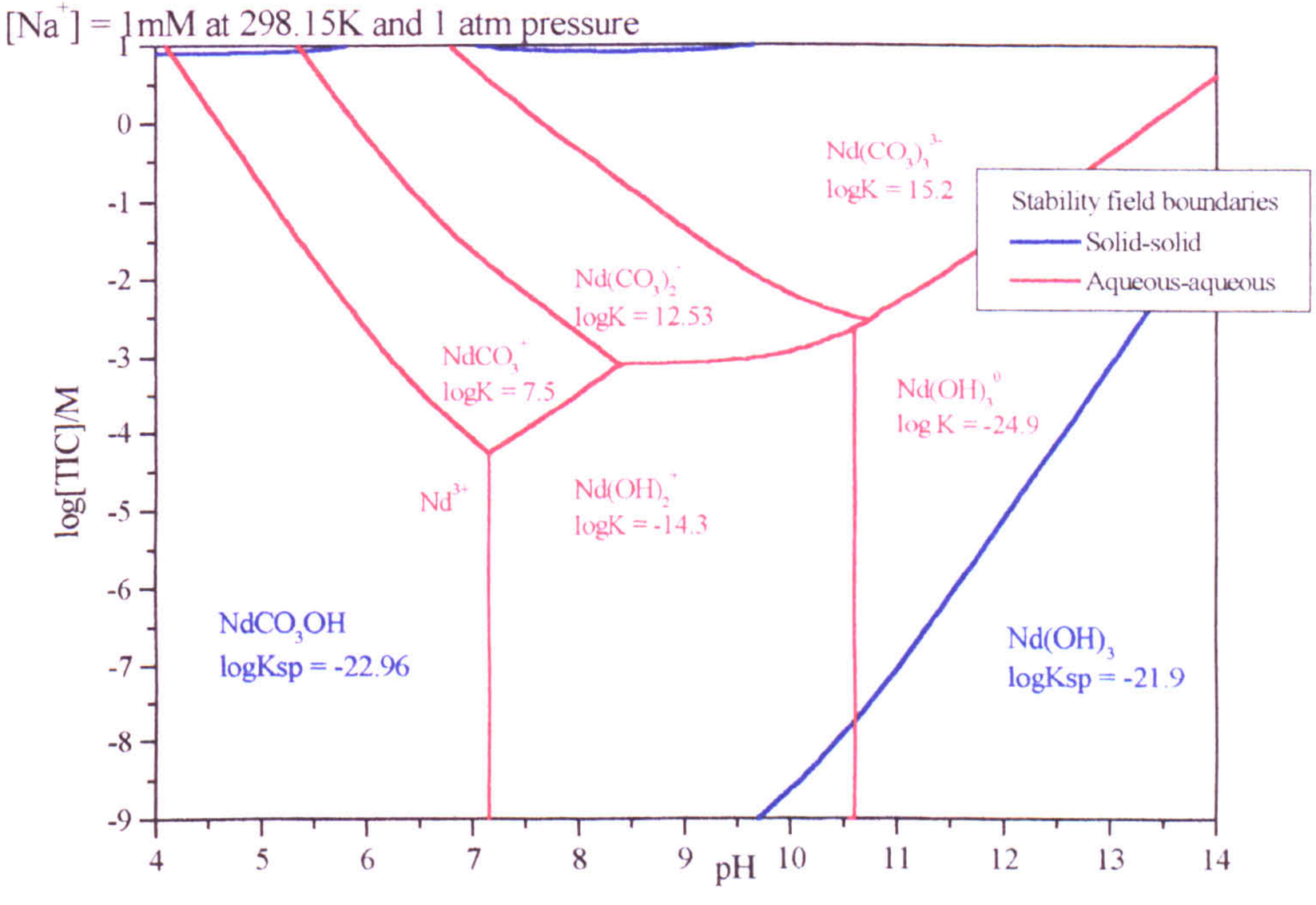

Figure 7.5 Eu solid-solid and aqueous-aqueous stability field diagram.
Solubility products recalculated to include $Eu(CO_3)_3^{3-}(aq)$ from this work (solution data, Appendix 4) and Lee and Byrne (1992 & 1993) aqueous association constants $[Na^+]$ = 1mM at 298.15K and 1 atm pressure

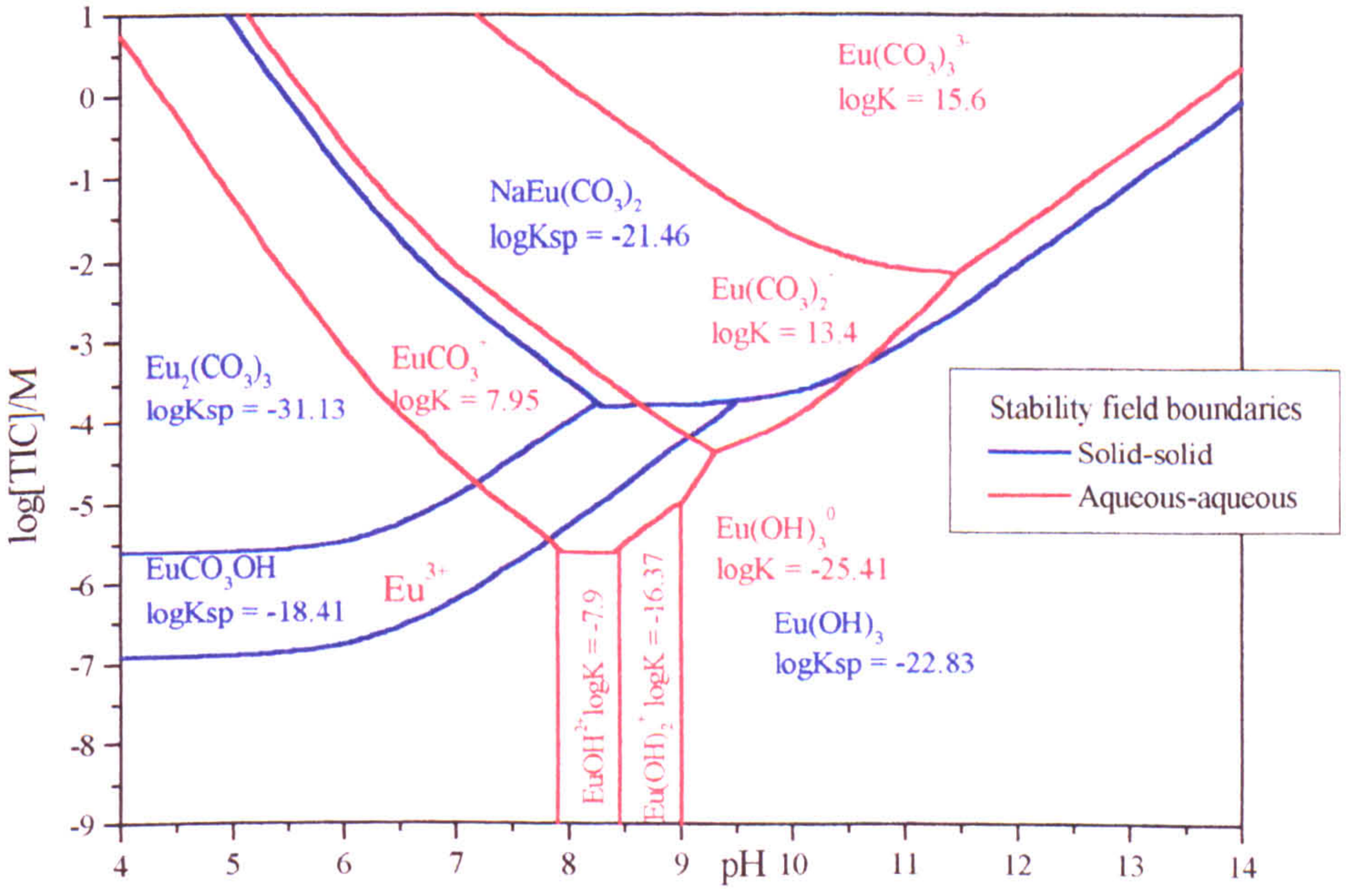

7.5 The variations in lanthanide stability fields and solubility from the range of solubility products in the literature

The main variation between the literature solubility products (Table 4.7) is the stability of the $Ln(OH)_3$ solid phase, which has a log Ksp range from -21.41 to -27.04 in this work and Rao *et al.*, (1996a) respectively for Nd. The range in the $Eu(OH)_3$ solubility products has a similar magnitude of between -22.79 and -26.54 in this work and Diakonov *et al.*, (1998b) respectively. $Ln(OH)_3$ may originally crystallise as an amorphous phase, which crystallises over time. The carbonate and hydroxy carbonate phases have a much smaller range of solubility products and a set of "modal" solubility data from this study and literature sources as shown in Table 4.7 is given in Table 7.5

Table 7.5 Summary of "modal" solubility products derived from Table 4.7

Solid phase	Nd		Eu	
	log Ksp	ΔG_f^o/KJmol^{-1}	log Ksp	ΔG_f^o/KJmol^{-1}
$NaLn(CO_3)_2$	-21.35	-2111.21	-20.48	-2008.74
$Ln_2(CO_3)_3$	-33.7	-3119.25	-33.0	-2920.25
$LnCO_3OH$	-19.9	-1470.30	-20.1	-1373.94
$Ln(OH)_3$	-21.9	-1268.26	-22.8	-1175.33
$Ln(OH)_3$(cr)	-27.04	-1297.37	-26.54	-1196.68

Stability field diagrams can be constructed using the data from Table 7.5, to directly compare the effects of $Ln(OH)_3$ crystallinity and any variation between other stability constants (Table 4.7)

The stability field diagrams shown in Sections 7.4 and 7.5 indicate that the area of each stability field on a pH vs log [TIC] diagram and the actual solubility limiting phase depends on the relative differences between the solubility products for each phase. The stability region that each phase controls does not however determine the actual total lanthanide solubility. Predictions for the solubility of the Nd and Eu carbonate and hydroxide phases in 1mM to 10mM TIC solutions

can be between 10^{-4}M to 10^{-8}M at pH 6 and up to 10^{-6}M to 10^{-12}M total aqueous lanthanide at pH 12 depending on the chosen solubility products.

Nd solubility and stability field diagrams (Figures 7.6 - 7.9 & Appendix 7.8 - 7.10)

The variation in solubility products presented in Tables 4.7, 7.4 and 7.5 has a significant effect on the stability fields of the four types of phase examined in the Na-Nd-TIC-pH system when compared with the stability fields found in this work, (Chapter 4 and Appendix 7.8-7.9). The $NaNd(CO_3)_2$ stability field is least effected and only increases slightly at the expense of $Nd_2(CO_3)_3$ and $NdCO_3OH$ (Figure 7.6). The amount of carbonate required for the $Nd_2(CO_3)_3$-$NdCO_3OH$ stability field boundary also increases, effectively reducing the area of the $Nd_2(CO_3)_3$ stability field and extending the $NdCO_3OH$ stability field. The main effect is however the size of the $Nd(OH)_3$ stability field.

When stability field diagrams are constructed directly from the data in Table 7.5, two stability field systems are immediately apparent (Figures 7.6 and 7.7). When $Nd(OH)_3$ is relatively amorphous (this work, log Ksp -21.9), even after equilibrium for 3 months, there are four solid phases in the system (Figure 7.6). $Nd_2(CO_3)_3$ alters to $NdCO_3OH$ then $Nd(OH)_3$ as the hydroxide activity in solution increases. $NaNd(CO_3)_2$ is the stable phase at high carbonate activities and intermediate pH. If there is a significant increase in $Nd(OH)_3$ crystallinity (Rao *et al.*, 1996b, log Ksp -27.04, Figure 7.7), then $NdCO_3OH$ is eliminated from the stability field diagram. The $Nd_2(CO_3)_3$-$NdCO_3OH$ stability field boundary is at a higher carbonate activity than the $NdCO_3OH$ boundary. The crystalline $Nd(OH)_3$ phase also restricts the $NaNd(CO_3)_2$ stability field at high pH.

If all the proposed Nd solubility products are taken at face value and the solubility calculated using the Lee and Byrne (1992 & 1993) aqueous species constants then even though there is a smaller range in solubility products proposed between the $Nd_2(CO_3)_3$, $NdCO_3OH$ and $NaNd(CO_3)_2$ phases than for $Nd(OH)_3$ there is still a large difference in the predicted Nd solubilities between the solubilities of the

modal solubility products (Figure 7.8) and the extreme values (Figure 7.9, Appendix 7.10). The most soluble Nd phases found in the literature predict that in 1mM Na^+ and TIC solutions (Figure 7.9), $NaNd(CO_3)_2$ will not form as a solubility limiting phase. $Nd_2(CO_3)_3$ converts directly to $NdCO_3OH$ at pH 7 and a total aqueous Nd concentration of approximately $3x10^{-4}$M. $NdCO_3OH$ is the solubility limiting phase between pH 9 and 12, with a solubility minimum ([Nd] = $3x10^{-6}$ M) at pH 11.5. $Nd(OH)_3$ forms the solubility limiting phase above pH 12. The least soluble solubility products (Figure 7.9) predict that $NdCO_3OH$ would be the solubility limiting phase between pH 5 and pH 9.5, followed by $Nd(OH)_3$ above pH 9.5. The $Nd(OH)_3$ solubility is predicted to be as low as 10^{-11}M Nd. $Nd_2(CO_3)_3$ would not be expected to form.

If the aqueous Na^+ and TIC concentrations are increased to 10mM (Appendix 7.10), then $NaNd(CO_3)_2$ will become a solubility limiting phase ([Nd] = $2x10^{-6}$ M) only if the most stable $NdCO_3OH$ phase cannot form. However the solubility of $NdCO_3OH$ and $Nd(OH)_3$ will increase from that of 1mM TIC solutions when aqueous Nd carbonate species are dominant. There is a range of 3 log units in the $Nd_2(CO_3)_3$ solubility product, which increases the Nd solubility minimum by approximately one and half orders of magnitude(from $[Nd]_{total} \approx 5x10^{-7}$ M to $1x10^{-5}$M) which does not vary significantly if the aqueous TIC concentration is increased from 1mM to 10mM.

The range in the solubility products that can be found in the literature may be due to the experimental method of the solubility determination. Solubility products calculated from phases that have precipitated directly from solution, may reflect either the kinetic phase or a less crystalline form, whilst phases formed under extreme conditions may reflect the thermodynamically stable phase. However the $Nd(OH)_3$ phase calculated from this study (Chapter 4, log Ksp -21.9), was calculated after an equilibrium period of greater than 3 months, the time period usually required to ensure the system is in chemical equilibrium. The most extreme crystal forms of $Nd(OH)_3$ (e.g. Rao *et al.*, 1996, Diakonov *et al.*, 1998a) may not be able to form in dilute solutions either by direct precipitation of an

initially amorphous $Nd(OH)_3$ phase or the solid state reaction from another kinetically favourable phase, e.g. $NdCO_3OH$. The titration experiments (Chapter 3 and 6), indicate that in carbonate solutions the solid phase changes with an evolving solution composition initially from an amorphous $Nd_2(CO_3)_3$ phase, which will start to crystallise in less than two hours if allowed to stand, to either the solid $NaNd(CO_3)_2$ or $NdCO_3OH$ phases (but not $Nd(OH)_3$) almost immediately if pH increases to above pH 9. A direct phase change to $Nd(OH)_3$ could only be observed in sulphate bearing, carbonate free solutions. The low to intermediate pH phase, $Nd_2(OH)_4SO_4$, can be seen to alter to a relatively amorphous solid $Nd(OH)_3$ phase above pH 10. The initial solid phase reaction in equilibrium with a solution is therefore rapid, however complete crystallisation to the most thermodynamically stable phase, especially for the hydroxide phase may not actually occur in relatively dilute (i.e. less than 0.1M) solutions.

Figure 7.6 Stability field diagram for the Na-Nd-TIC-pH system at 298.15K and 1 atm pressure $[Na^+] = 1mM$

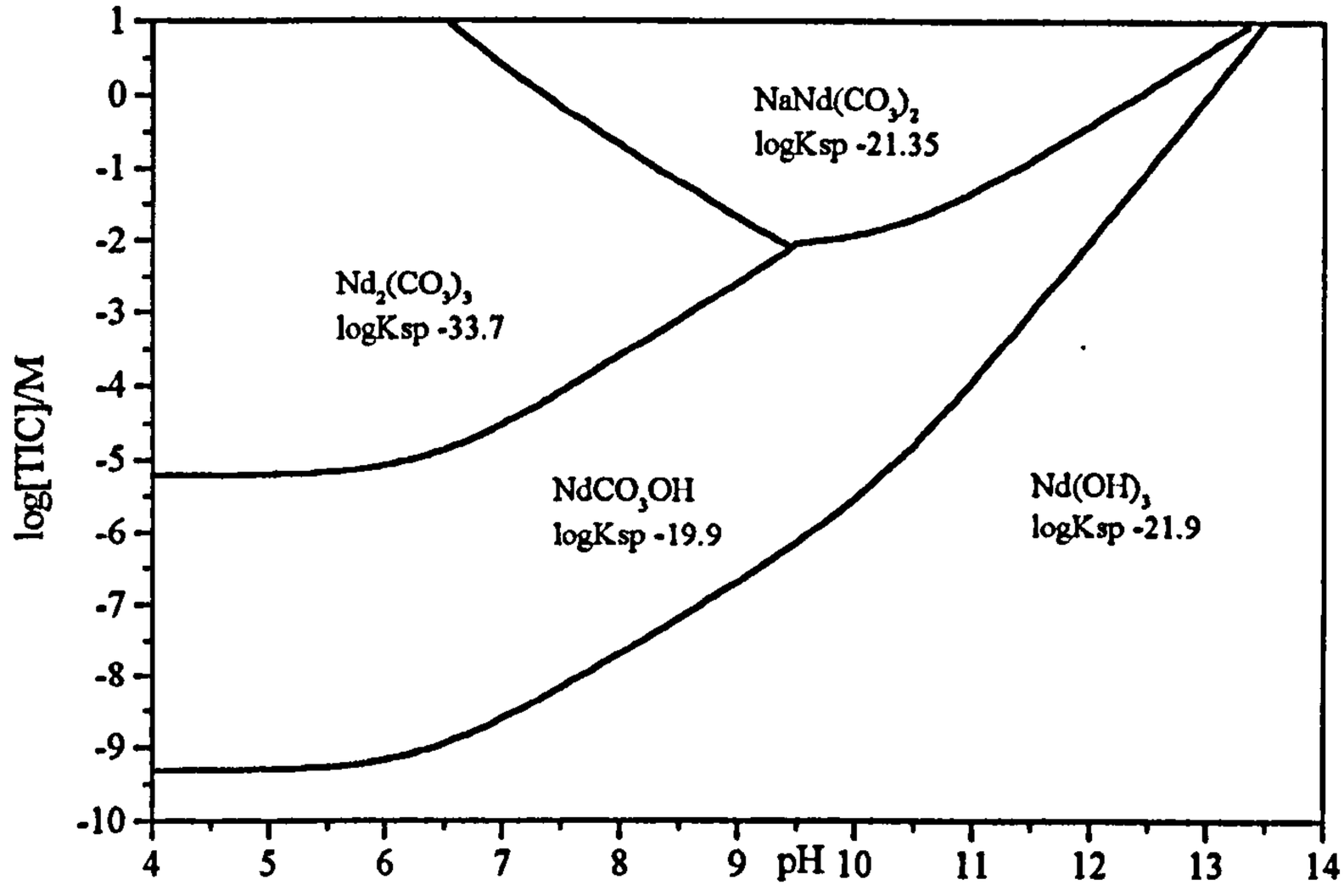

Figure 7.7 Stability field diagram for the Na-Nd-TIC-pH system assuming crystalline $Nd(OH)_3$ at 298.15K and 1 atm pressure $[Na^+] = 1mM$

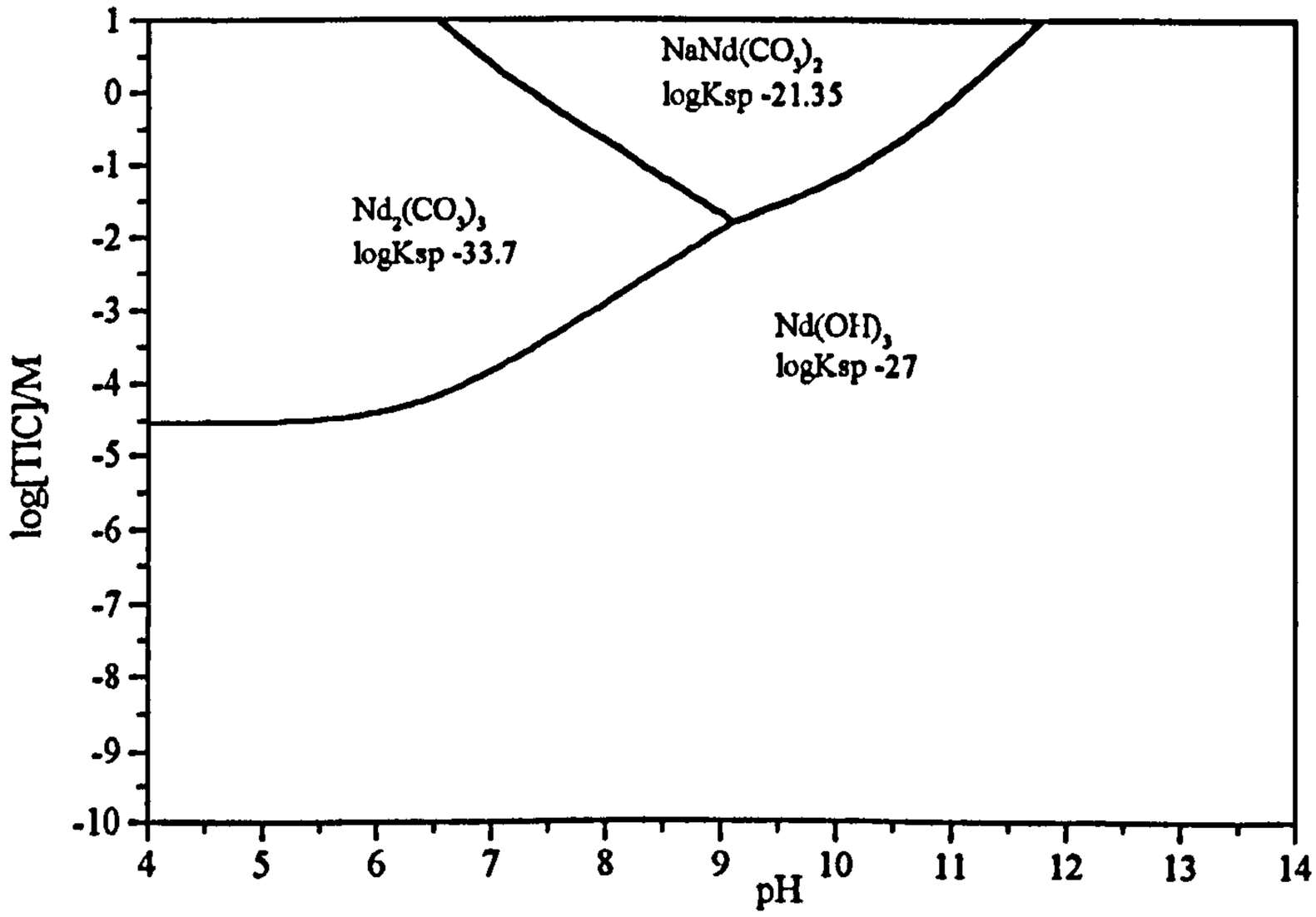

Figure 7.8 Nd solubility in 1mM Na^+ and 1mM TIC solution calculated from modal solubility products (Table 7.6) using aqueous data from Lee & Byrne (1992 & 1993) at 298.15K and 1 atm pressure

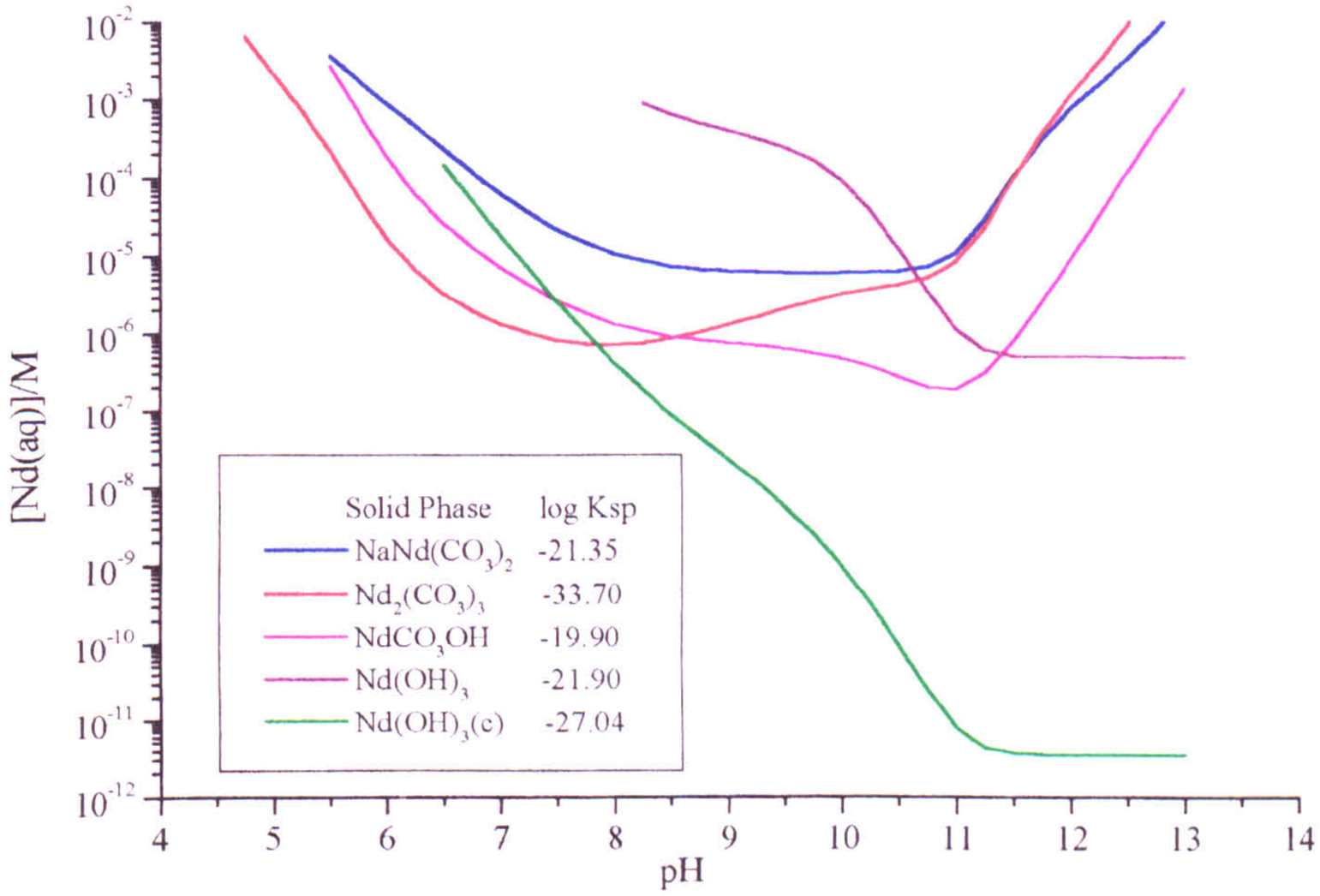

Figure 7.9 Nd solubility in 1mM Na^+ and 1mM TIC with various solubility products (Table 4.7) aqueous data from Lee & Byrne (1992 & 1993)

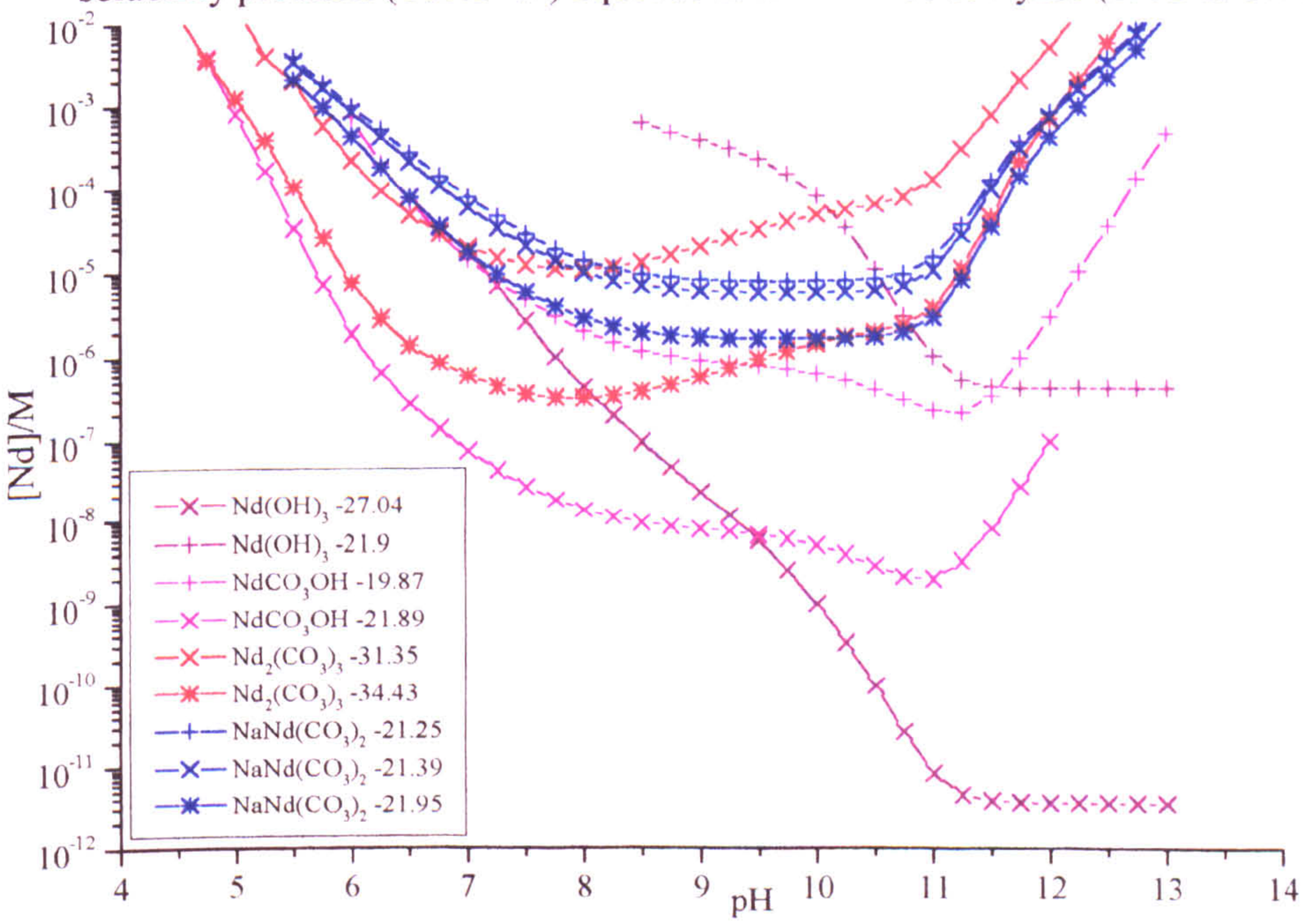

Eu solubility and stability field diagrams (Figures 7.10 – 7.13 & Appendix 7.11 – 7.13)

The variation in the stability of $EuCO_3OH$ and $Eu(OH)_3$ (Table 7.5) has a comparable effect on the europium stability field diagrams as reported for the Nd system. The $EuCO_3OH$ solubility product found in this work (log Ksp -18.62), results in a very narrow stability range even when $Eu(OH)_3$ is formed by precipitation from a dilute solution (this work, log Ksp -22.8) and consequently is only slightly crystalline (Appendix 7.11). Increases in the $Eu(OH)_3$ crystallinity (Diakonov *et al.*, 1998b, log Ksp -26.54) eliminate $EuCO_3OH$ as a solubility limiting phase. This study predicts $EuCO_3OH$ to have a similar solubility as $AmCO_3OH$ (NEA 9, log K -5.70) and $AmCO_3OH$ is not predicted to be a solubility limiting phase under any conditions in the NEA 9 database (Figure 7.1). If the solubility of $Eu_2(CO_3)_3$ is increased to the most soluble literature value (after Runde *et al.*, 1992, log Ksp -31.78) then the $EuCO_3OH$ stability field will increase (Appendix 7.12), although the highly soluble $EuCO_3OH$ phase (This work, log Ksp -18.62) will still be eliminated as a solubility limiting phase by the most crystalline $Eu(OH)_3$ phase.

Increasing the $EuCO_3OH$ solubility product to log Ksp -20.1 (Runde *et al.*, 1992), predicts that $EuCO_3OH$ will be a major phase in equilibrium with amorphous $Eu(OH)_3$ (Figure 7.10) and will even form with a narrow stability field when $Eu(OH)_3$ is crystalline (Figure 7.11). $NaEu(CO_3)_2$ is the stable phase at slightly higher carbonate activities than the equivalent $NaNd(CO_3)_2$ analogue, and can form in equilibrium with 1mM Na^+ solutions which have a carbonate concentration above 0.1M TIC.

The solubility of the modal Eu phases can vary significantly from the most soluble and least soluble extremes (Figures 7.12 & 7.13). The Eu solubility, predicted by the most soluble solubility products (Figure 7.13), predicts that there will be three solubility limiting phases between pH 4 and 14. In 1mM Na^+ and TIC solutions, $Eu_2(CO_3)_3$ is the solubility limiting phase below pH 9, $EuCO_3OH$

between pH 9 and 11.5 and total aqueous Eu concentrations of approximately $1x10^{-5}$M, followed by $Eu(OH)_3$ above pH 10.5, with [Eu] at $1x10^{-6}$M. If the Na^+ and TIC concentrations are increased to 10mM (Appendix 7.13) then $NaEu(CO_3)_2$ is predicted to be the solubility limiting phase in the mid-pH region from pH 7.5 to 11 ([Eu] $1x10^{-5}$M) as the solubility of $EuCO_3OH$ increases with increasing carbonate activities, and $NaEu(CO_3)_2$ solubility decreases with increasing Na^+ activity. The other extreme, calculated from the least soluble solubility products, indicates that there are only two solubility limiting phases in 10mM and 1mM TIC and Na^+ solutions. $Eu_2(CO_3)_3$ alters to $Eu(OH)_3$ at pH 9 in 1mM TIC solutions and pH 9.5 in 10mM TIC solutions.

There is a similar range in $Eu_2(CO_3)_3$ solubility products as for Nd (Table 7.6, Appendix 7.14 & 7.15). Increasing the TIC concentration from 1mM to 10mM, does increase the $EuCO_3OH$ solubility, but does not significantly change the $Eu_2(CO_3)_3$ solubility, although there is an increasingly prominent Eu solubility minimum in equilibrium with $Eu_2(CO_3)_3$ at pH 6.5 - 7 as TIC increases.

The most significant difference in Eu solubility products is as for Nd, between the various $Eu(OH)_3$ solubility products. Above pH 11.5, $Eu(OH)_3$(s) solubility is independent of the carbonate concentration and pH. The total aqueous Eu ranges from 10^{-6}M to 10^{-10}M (log Ksp -22.79 this work and -26.54 Diakonov *et al.*, 1998b respectively). If $Eu(OH)_3$ initially precipitates as amorphous, then the three phases $NaEu(CO_3)_2$, $EuCO_3OH$ and $Eu_2(CO_3)_3$ are likely to form below pH 10 in the appropriate Na^+ and CO_3^{2-} solution conditions. The intermediate pH phases $EuCO_3OH$ and $NaEu(CO_3)_2$ may however be replaced as $Eu(OH)_3$ crystallises further.

The wide range in the predicted solubility of Eu, is similarly controlled as Nd, by the wide range in the proposed solubility products that is available in the literature. A definite prediction of the solubility limiting phase under specific conditions cannot be made from a review of all the literature data alone, which

can be seen to be contradictory, if all the relevant solid phases and aqueous species are to be considered together.

Figure 7.10 Stability field diagram for the Na-Eu-TIC-pH system at 298.15K and 1 atm pressure $[Na^+]$ = 1mM

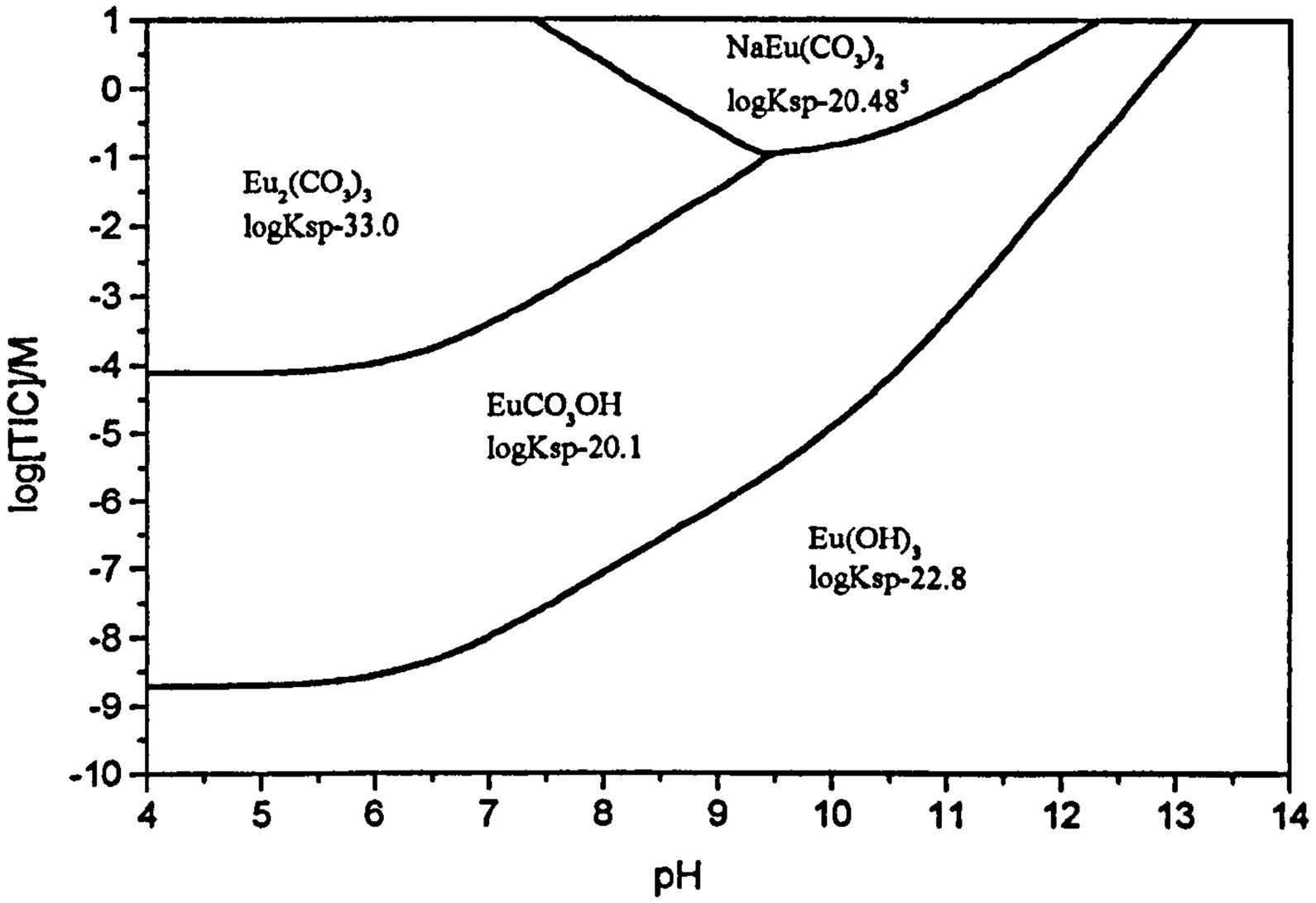

Figure 7.11 Stability field diagram for the Na-Eu-TIC-pH system assuming crystalline $Eu(OH)_3$ at 298.15K and 1 atm presure $[Na^+]$ = 1mM

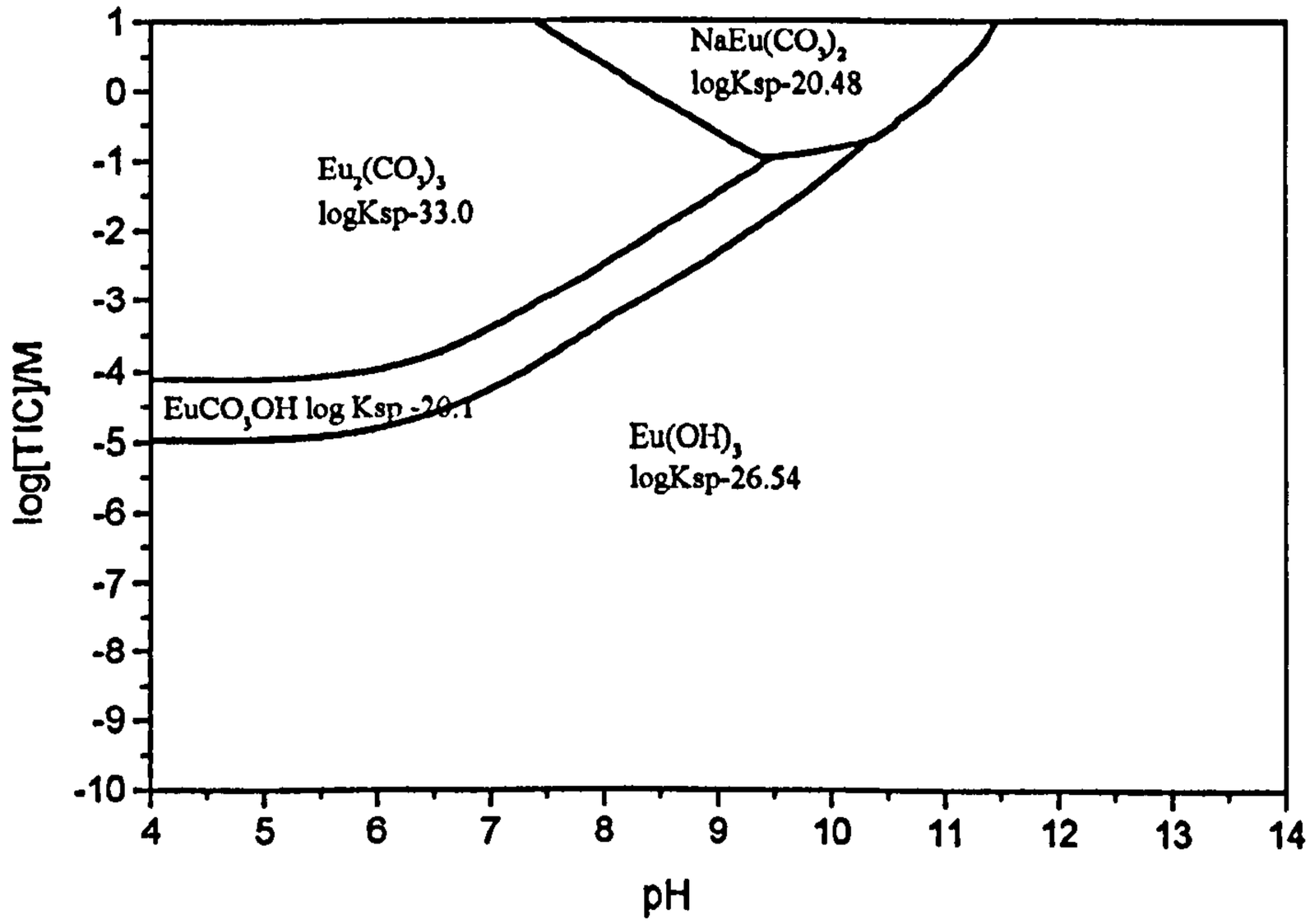

Figure 7.12 Eu solubility in 1mM Na^+ and 1mM TIC solution calculated from modal solubility products (Table 7.6) using aqueous data from Lee & Byrne (1992 & 1993) at 298.15K and 1 atm pressure

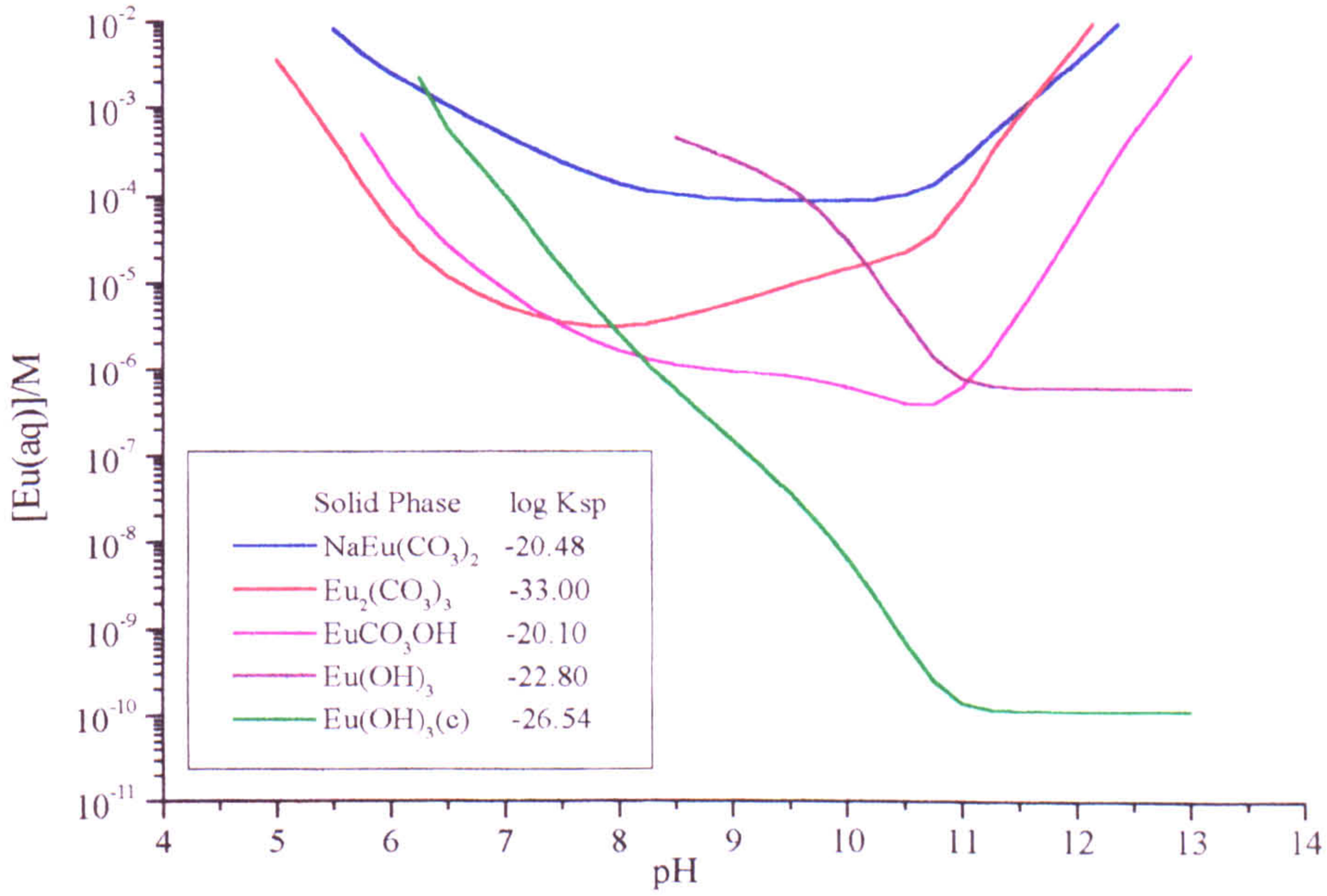

Figure 7.13 Eu solubility in 1mM Na^+ and 1mM TIC solution with various solubility products (Table 4.7) Lee & Byrne (1992 & 1993) aqueous data

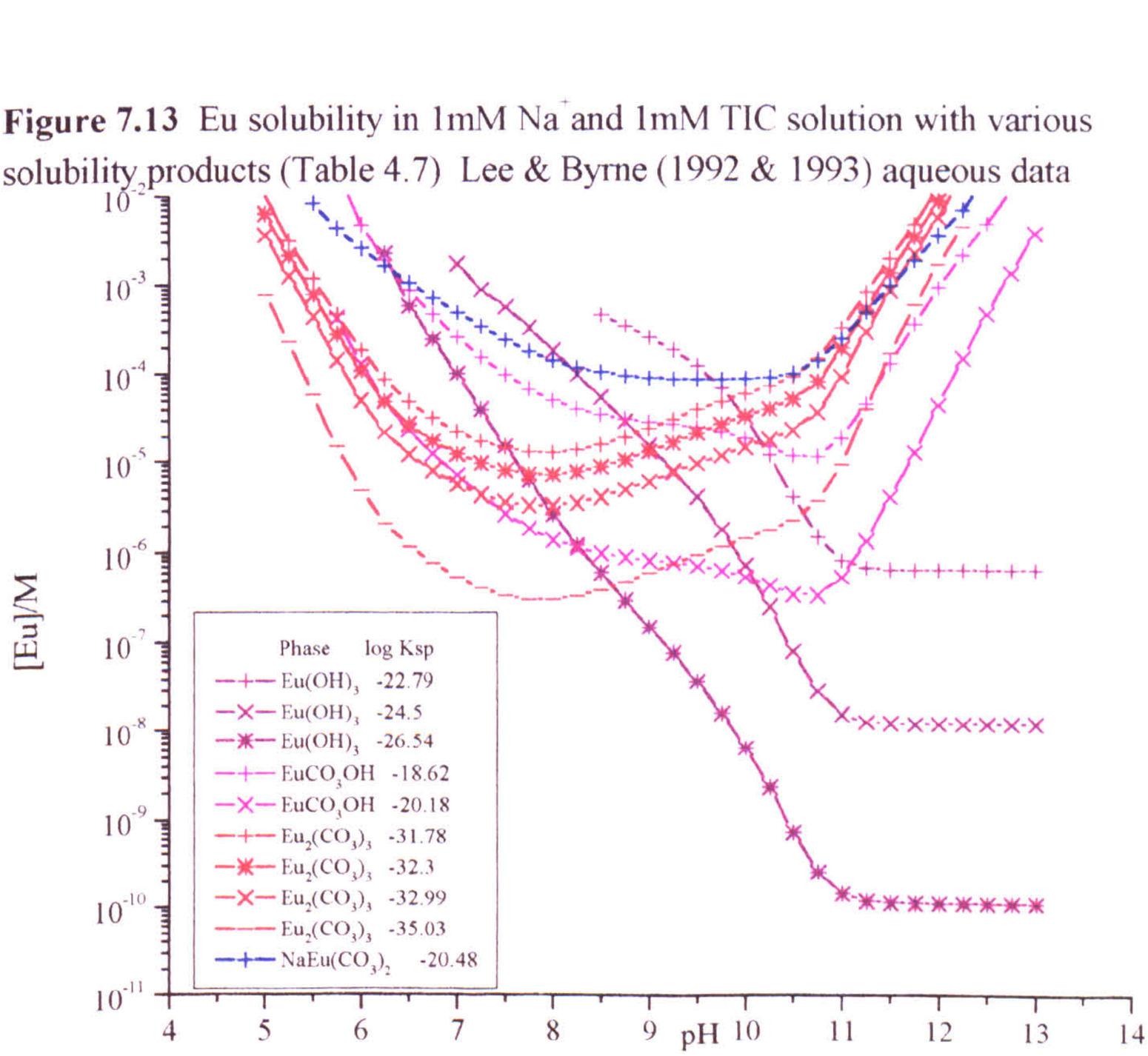

Ce solubility and stability field diagrams (Figures 7.14 - 7.15 & Appendix 7.14 - 7.15)

There is a similar discrepancy in calculating the CeO_2 solubility as the predictions of $Nd(OH)_3$ and $Eu(OH)_3$ solubility. The CeO_2 hydrolysis constant in this study (log K 30.66), is significantly more soluble than other published values (e.g. Baker *et al.*, 1971, log K 21.12). This could suggest that CeO_2 also precipitates initially as an amorphous phase then slowly crystallises. The more amorphous CeO_2 phases were produced by measuring the solution conditions that the CeO_2 precipitated under after 2 to 3 months, whilst the most crystalline examples were formed from more rigorously aged crystals in concentrated solutions, before measuring the heat capacity of the resulting aged crystals.

Figure 7.14 Stability field diagram for the Ce-pH-pe system
[TIC] = 1mM 298.15K and 1 atm pressure

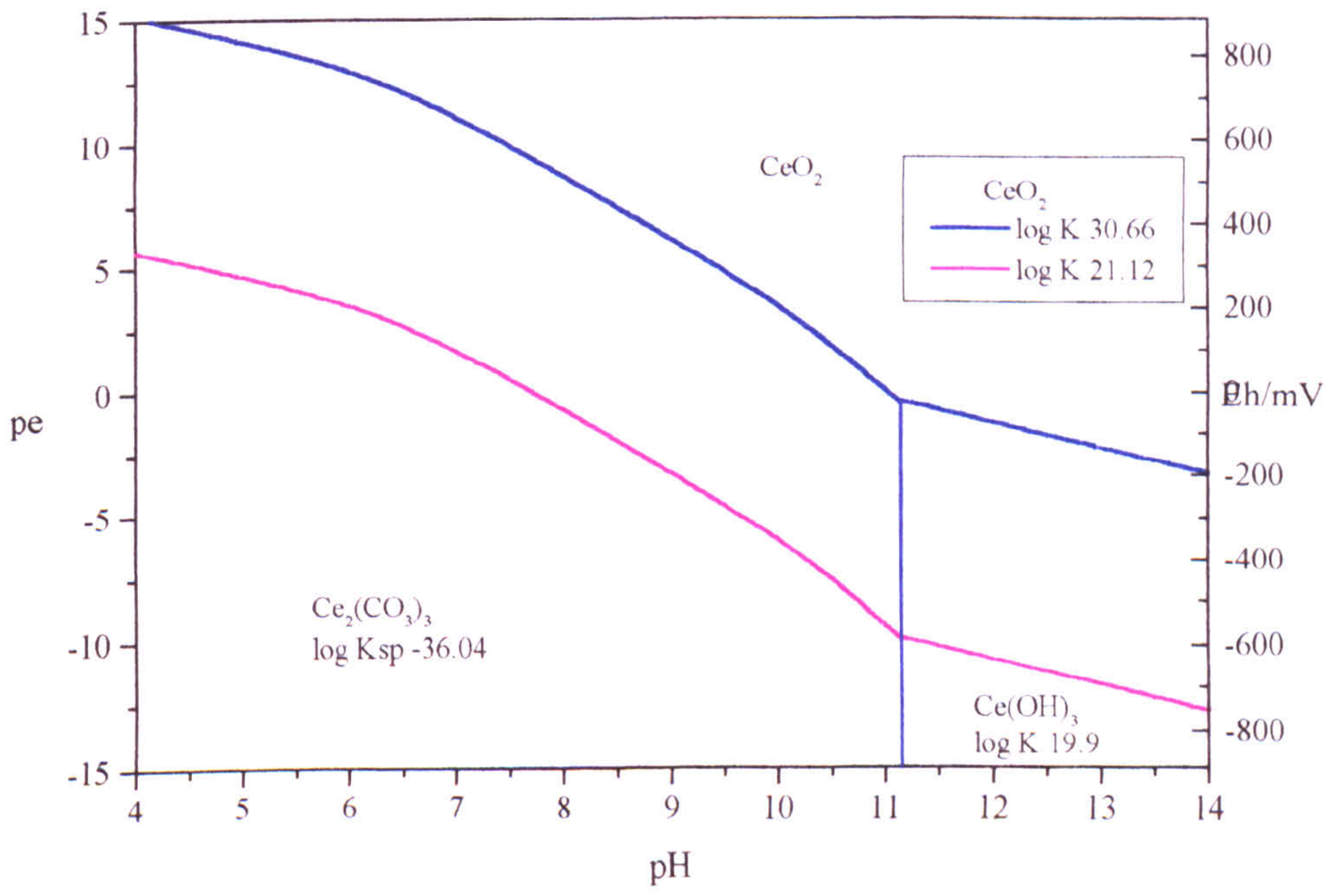

A pe vs pH diagram (Figure 7.14) predicts that by altering the CeO_2 solubility constant from log K 30.66 to 21.12, could decrease the pe required for the phase change from $Ce_2(CO_3)_3$ to CeO_2 by 10pe units. At high pH $Ce_2(CO_3)_3$ would also alter to $Ce(OH)_3$ in sufficiently reducing conditions (to inhibit Ce^{3+} oxidation to Ce^{4+}). The $Ce(OH)_3$-CeO_2 stability field boundary is independent of the

carbonate concentration and could be as low as pe -10, when in equilibrium with crystalline CeO_2. However the $Ce(OH)_3$ solubility product is also likely to be dependent on crystallinity, therefore the $Ce(OH)_3$ solubility would decrease with time, which will have an effect on the CeO_2-$Ce(OH)_3$ stability field boundary.

If $Ce(OH)_3$ has a log K of 19.9, then $Ce(OH)_3$ is likely to form under low carbonate conditions in equilibrium with an amorphous CeO_2 phase, under most environmental pe conditions i.e. between pe ±1. $Ce(OH)_3$ could form at up to pH 11.75, and 10^{-2}M TIC solutions (Appendix 7.12). However if CeO_2 is more crystalline (log K 21.12), then $Ce(OH)_3$ would not form above pH 4 (Appendix 7.13). The CeO_2-$Ce(OH)_3$ stability field boundary between pe±1 would be between pH 2 and 3. The total Ce solubility under these low pH conditions would be very high i.e. above 0.1M.

Figure 7.15 Ce solubility in 1mM Na^+ and TIC
using Lee and Byrne (1992 & 1993) aqueous speciation constants
at 298.15K and 1 atm pressure

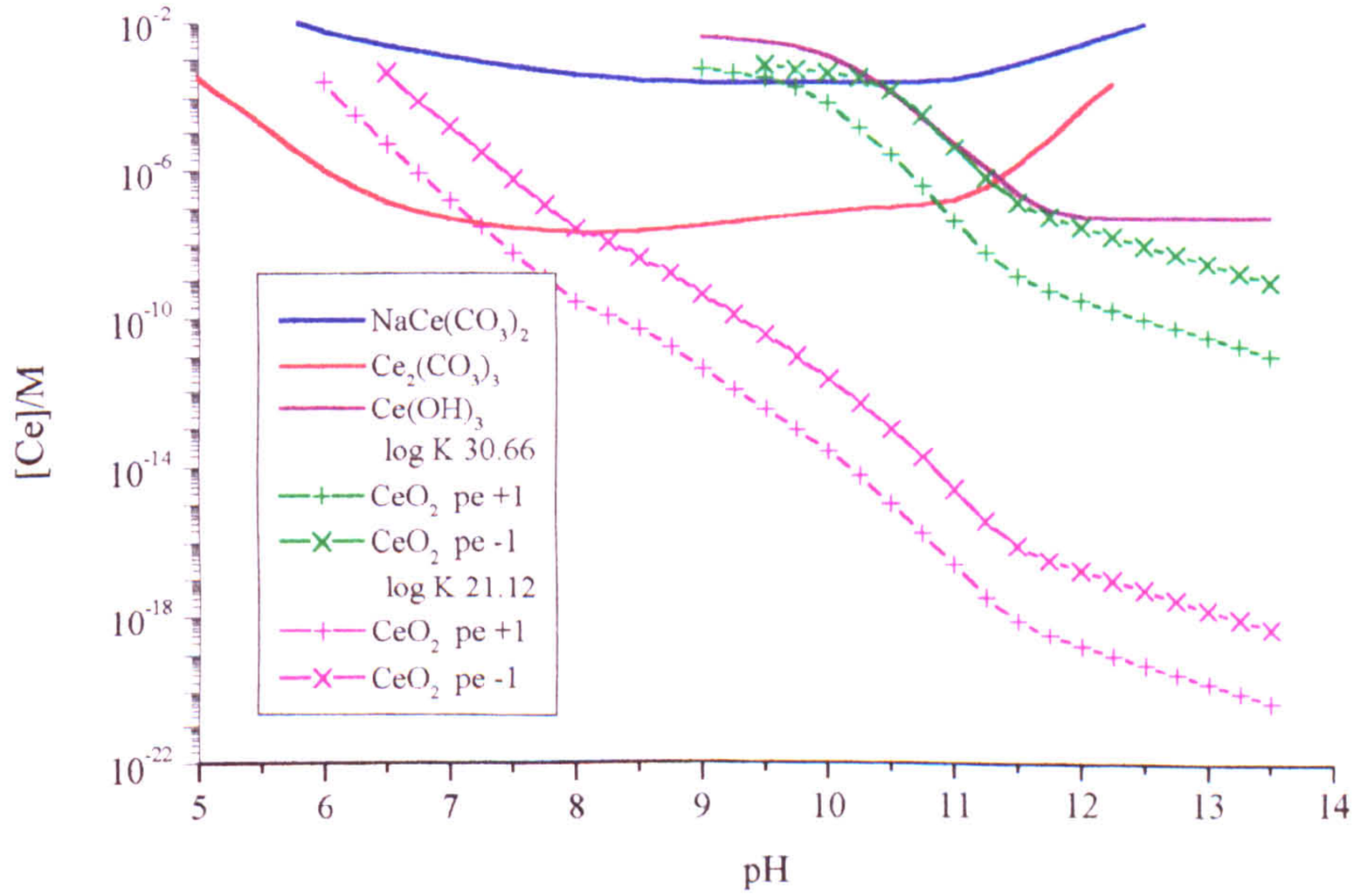

In 1mM Na^+ and TIC solutions between pe ±1, the minimum $Ce_2(CO_3)_3$ solubility is between 10^{-7}M and 10^{-8}M Ce in 1mM TIC, between pH 6 and 11. At high pH the solubility of CeO_2(s) continues to fall (even when in equilibrium

with $Ce(OH)_3^0(aq)$) down to 10^{-20}M Ce at pH 12. These concentrations are substantially below those predicted by the most crystalline Nd, Eu and Am hydroxides, and lower than most analytical detection levels.

Baker *et al.*, (1971) calculated their CeO_2 solubility constant from heat capacity measurements of aged crystals, rather than solubility measurements in relatively dilute solutions.

7.6 Lanthanide solubility in geochemical solutions

The modelling process can be used to predict the lanthanide and americium solubility under specific conditions in more complex real solutions. Groundwater solutions typically contain carbonate, sulphate, phosphate, nitrate, chloride and fluoride anions, each of which may influence the solubility of lanthanides or actinides. The major cations will not directly control the lanthanide solubility but will affect the activity of the anions in solution.

Wood (1990a) suggested four anionic groundwater compositions that would include the composition range found in most geochemical regimes (Table 7.6, which include a modal groundwater, high phosphate/low sulphate, high fluoride/low sulphate and high carbonate/low sulphate solutions), which would determine the aqueous lanthanide speciation over the entire pH range. The nitrate and chloride composition does not control the formation of any of the solubility limiting phases, however the CO_3^{2-}, SO_4^{2-}, PO_4^{3-}, and F^- activities all influence the solubility limiting phase between pH 4 and 14. In groundwater systems the two anions F^- and PO_4^{3-}, will influence lanthanide solubility especially at low pH, when carbonate and hydroxy phases are highly soluble. The F^- and PO_4^{3-} ions are however dependent on the solubility and quantity of specific trace minerals (e.g. apatite) in the host rock and may not be present in significant quantities to influence the bulk aqueous groundwater composition.

When each of the Nd phases are put in equilibrium with Wood's (1990a) modal groundwater and include the solubility products for NdF_3 and $NdPO_4$ (after Ménard *et al.*, 1998), predict $NdPO_4$ as the solubility limiting phase over the pH range 4 to 9.5, if a very crystalline $Nd(OH)_3$ phase forms, or from pH 4 to 11.5, if a less crystalline $Nd(OH)_3$ phase occurs (Figure 7.16a). The NdF_3 phase is also less soluble than the solid carbonate ($Nd_2(CO_3)_3$) phase below pH 7.5. All three other groundwater compositions also predict $NdF_3/NdPO_4/Nd(OH)_3$ as the only solubility limiting phases (Appendix 7.16).

Table 7.6 Groundwater compositions after Wood (1990a)

Anion	Modal	high phosphate low sulphate	high fluoride low sulphate	high carbonate low sulphate
carbonate	10^{-4}M	10^{-4}M	10^{-4}M	10^{-3}M
sulphate	10^{-4}M	10^{-6}M	10^{-6}M	10^{-6}M
phosphate	10^{-6}M	0.01M	10^{-6}M	10^{-6}M
nitrate	10^{-4}M	10^{-4}M	10^{-4}M	10^{-4}M
chloride	$2x10^{-4}$M	$2x10^{-4}$M	$2x10^{-4}$M	$2x10^{-4}$M
fluoride	10^{-6}M	10^{-6}M	10^{-4}M	10^{-6}M

If F^- and PO_4^{3-} ions are not present in solution, there are four initial solubility limiting phases $Nd_2(CO_3)_3$, $NdCO_3OH$, $Nd_2(OH)_4SO_4$ and $Nd(OH)_3$ between pH 4 and 14. The initial precipitates indicate that there is a decrease in Nd solubility from pH 4 to a solubility minimum at pH 10 (10^{-7}M total aqueous Nd), then a slight increase in Nd solubility from pH 10 to 11.5, above which Nd solubility is independent of pH (Figure 7.16b). The less crystalline $Nd(OH)_3$ phase represents the initial amount of Nd that can be removed from solution within 3 months. Any slight decrease in the sulphate/carbonate ratio either by increasing the carbonate activity or decreasing the sulphate will eliminate $Nd_2(OH)_4SO_4$ as a solubility limiting phase. If $Nd(OH)_3$ can form as a very crystalline phase, then $Nd_2(CO_3)_3$ is predicted to convert directly to $Nd(OH)_3$ above pH 7, and there will be a Nd solubility minima above pH 10.5 of between 10^{-11}M to 10^{-12}M total aqueous Nd. An increase in the carbonate concentration from 10^{-4}M to 10^{-3}M will increase the

pH of the $NdCO_3OH$ solubility minima from pH 10 to pH 11, or increase the pH of the $Nd_2(CO_3)_3$-crystalline $Nd(OH)_3$ equilibrium from pH 7 to pH 8.

Cerium converts directly from $Ce_2(CO_3)_3$ to CeO_2 under the same solution conditions (Appendix 7.17), however the solubility minimum is significantly lower at high pH. In a solution of pe 0, the initial CeO_2 precipitate is in equilibrium with 10^{-9}M Ce at pH 12, but this may decrease to 10^{-18}M aqueous cerium if the most crystalline CeO_2 solubility products are correct. Increasing the carbonate concentration from 10^{-4}M to 10^{-3}M also increases the $Ce_2(CO_3)_3$-CeO_2 equilibria by half a pH unit.

Figure 7.16a Nd Solubility in modal groundwater (after Wood, 1990a)

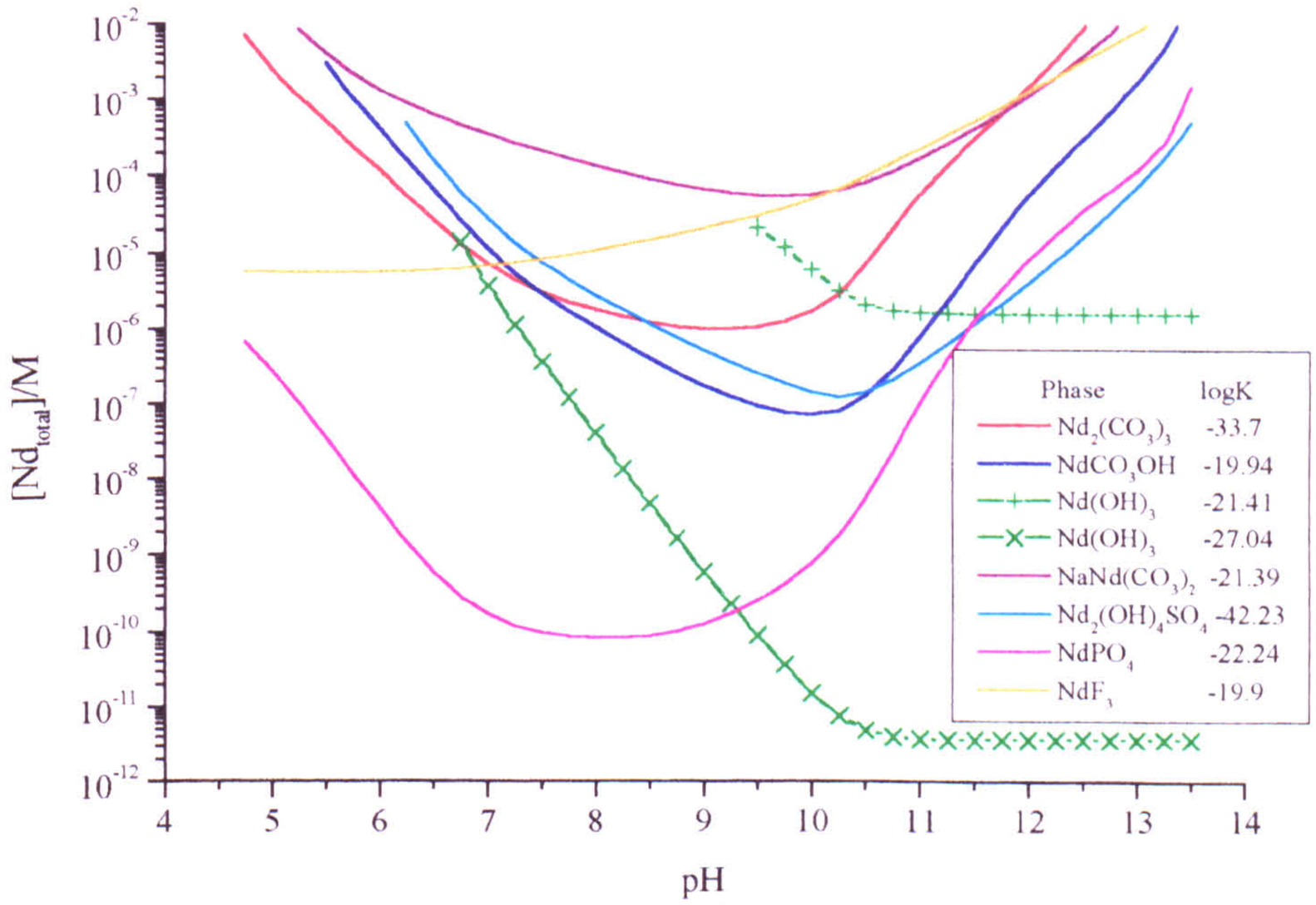

Figure 7.16b Nd Solubility in modal groundwater (after Wood, 1990a)

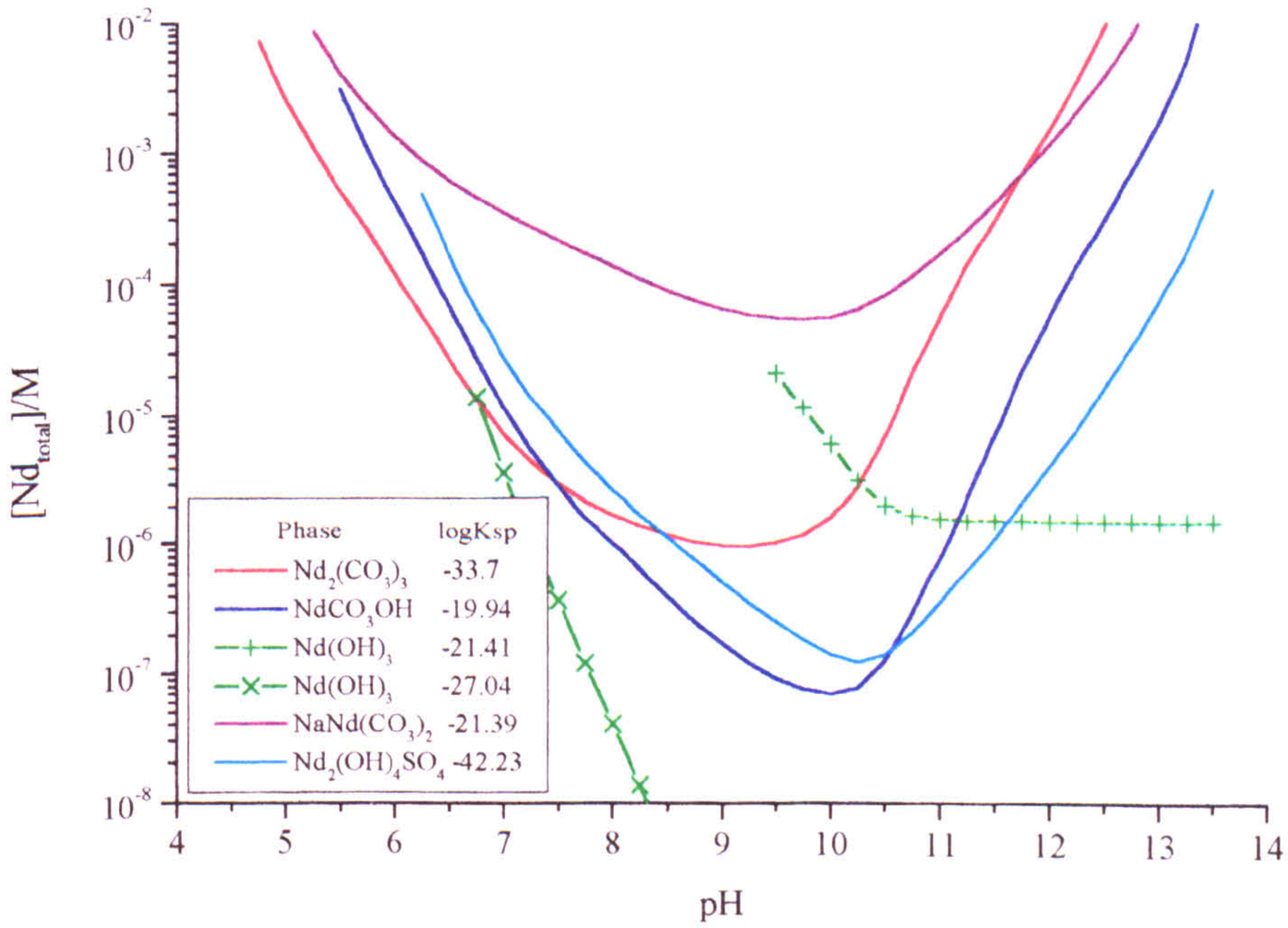

Plutonium (some of which will decay to Am) is considered as Intermediate Level Waste or as smaller quantities within Low Level Waste (Chapter 1), therefore, it will be disposed of in a concrete based grouted system, and not as a phosphate bearing glass. Solid americium and lanthanide phosphates are therefore unlikely to occur and be able to limit aqueous lanthanide transport away from the waste repository. If the elements Am, Ce, Nd and Eu are placed in equilibrium with a series of solutions (Table 7.7), their solubility limit and solubility limiting phases can be determined under these specific single composition conditions. A comparison can therefore be made between the solubility and the stable phase for each of the elements examined (Table 7.8).

Table 7.7 Solution compositions

	[1]Groundwater	[2]Vault	[2]Trench
TIC/M	$5.36x10^{-4}$	$3.27x10^{-3}$	$2.83x10^{-3}$
SO_4/M	$3.96x10^{-4}$	$3.09x10^{-4}$	1.09^{x10-4}
Cl/M	$1.34x10^{-3}$	$4.43x10^{-4}$	$5.0x10^{-3}$
Na/M	$1.36x10^{-3}$	$1.09x10^{-3}$	$3.00x10^{-3}$
K/M		$5.24x10^{-4}$	$4.68x10^{-4}$
Ca/M	$2.01x10^{-3}$	$6.04x10^{-4}$	$2.85x10^{-3}$
Mg/M	$7.94x10^{-4}$	$8.23x10^{-6}$	$6.00x10^{-4}$
Fe/M	$1.03x10^{-5}$		
H_4SiO_4/M	$1.61x10^{-4}$		
pH	7.35	11.4	7.3
pe	-0.74		

[1]Randall, M., (1998) *Personal communication*

[2]Kelly, E., (1996) *Personal communication*

Table 7.9 Lanthanide and Am solubility and solubility limiting phases in various solutions (Solution compositions Table 7.7), indicating the differences in the solubility limiting phases for proposed variations in crystallisation occur. (calculated using Lee & Byrne 1992 and 1993 aqueous constants for Ce, Nd and Eu NEA9 aqueous constants for Am).

Solution	M	Am	Ce	Nd	Eu
Groundwater *i*	Phase	$Am_2(CO_3)_3$	$Ce_2(CO_3)_3$	$Nd_2(CO_3)_3$	$Eu_2(CO_3)_3$
	log Ksp	-33.4	-36.04	-33.7	-32.99
	$[M(aq)]_{total}$	$8.1x10^{-7}$	$2.3x10^{-8}$	$7.7x10^{-7}$	$3.4x10^{-6}$
ii	Phase	$AmCO_3OH$			
	log Ksp	-21.20			
	[M(aq)]/M	$2.4x10^{-7}$			
Trench *i*	Phase	$Am_2(CO_3)_3$	$Ce_2(CO_3)_3$	$Nd_2(CO_3)_3$	$Eu_2(CO_3)_3$
	log Ksp	-33.4	-36.04	-33.70	-32.99
	$[M(aq)]_{total}$	$1.2x10^{-6}$	$2.8x10^{-8}$	$8.4x10^{-7}$	$3.7x10^{-6}$
	Phase	$AmCO_3OH$			
	log Ksp	-21.20			
	[M(aq)]/M	$2.8x10^{-7}$			
Vault *i*	Phase	$Am(OH)_3$	CeO_2	$Nd(OH)_3$	$Eu(OH)_3$
	log Ksp	-26.6	[1]21.12	-27.04	-26.54
	$[M(aq)]_{total}$	$1.5x10^{-10}$	$8.9x10^{-18}$	$5.7x10^{-12}$	$1.3x10^{-10}$
Vault *ii*	Phase		[1]CeO_2	$NdCO_3OH$	$Eu(OH)_3$
	log Ksp		30.66	-19.94	-22.79
	$[M(aq)]_{total}$		$2.5x10^{-8}$	$2.9x10^{-7}$	$7.1x10^{-7}$

[1]CeO_2 solubility as log K

i, solubility assuming the most extreme (thermodynamically) solubility limiting phase predicted (Nd and Eu Table 7.5, Ce Table 7.2, Am Table 7.3) forms in equilibrium with the solution

ii, solubility assuming the most extreme (kinetic) solubility limiting phase predicted (Nd and Eu Table 7.5 Ce this work, Am Table 7.3) does not form in and a kinetic solubility limiting phase forms

There is a general broad agreement between the solubility of Am, Nd and Eu, although this agreement does depend on the selection of solubility products available. The most significant difference occurs when there may be a dispute over the actual solubility limiting phase for those specific conditions (e.g. Table 7.8, rows *i* kinetic phase and *ii* thermodynamic stable phase).

Solubility calculations for Ce, Nd and Eu under the same solution conditions indicate that the smaller lanthanides are more soluble than the larger lanthanides, i.e. Eu is more soluble than Nd, which is more soluble than Ce.

In the high pH environment (pH 11.4), the maximum solubility would be limited by either a hydroxycarbonate or hydroxide phase, with Nd and Eu concentrations between $2x10^{-7}$M and $7x10^{-7}$M . If the hydroxide phase could crystallise fully, then the maximum Am, Nd and Eu solubility could be reduced to between 10^{-10}M and 10^{-12}M. There is a larger range in the Ce solubility between the most initial and most crystalline CeO_2 phases of 10^{-8}M to 10^{-18}M total aqueous cerium. The pe of the system would reduce in enclosed systems, as biodegradation produces a reducing system. The solubility of CeO_2 would therefore increase from that found in an open system even if CeO_2 does not convert to $Ce(OH)_3$.

Aqueous transport away from the repository will follow a pattern of dilution and dispersal throughout the groundwater system. The most significant factor will be a reduction of the solution pH to near neutral values. The hydroxide activity is therefore too low to form even the most crystalline hydroxide or CeO_2 phases. The carbonate phase will be the solubility limiting phase with between 10^{-6}M and 10^{-8}M aqueous Am, Ce, Nd or Eu. If the most crystalline hydroxide phases do not form, the solubility limit will remain between 10^{-6}M to 10^{-8}M between pH 7 and 12, with a solubility minimum between pH 10 and 11.5, although the actual solubility limiting phase will change with pH (Appendix 7.18).

The trench solution is a simulated solution representing the earliest disposal processes of infilled trench systems (now discontinued). The lanthanide solubility

in these systems is similar to the groundwater systems of between 10^{-8}M to 10^{-6}M aqueous lanthanide, when in equilibrium with the solid carbonate.

7.7 Summary

The solid phases determined from the titration experiments show four solid phases are present in the Na^{+}-CO_3^{2-}-OH^{-} system $NaLn(CO_3)_2$, $Ln_2(CO_3)_3$, $LnCO_3OH$ and $Ln(OH)_3$ for Nd and Eu, $Ce_2(CO_3)_3$ and CeO_2 were the only two phases identified in the Ce system below 0.1M solutions. $NaCe(CO_3)_2$, $KNd(CO_3)_2$ and $KEu(CO_3)_2$ were identified at higher concentrations. Solubility products derived from batch experiments and solution analysis relies on the actual species activities determined from PHREEQE and therefore determined by the choice of aqueous species. Investigations between aqueous speciation databases predict there is a decrease in the $NaNd(CO_3)_2$ solubility product by 0.5 log units when calculated by using the Lee & Byrne data and NEA9 databases if $Nd(CO_3)_3^{3-}$ is present and identical to the Am value (Rao *et al.*, 1996a). The CO_3^{2-} activity and pH of the system are the dominant factors which determine the solubility limiting phase and hence the actinide and lanthanide solubility limit of aqueous systems.

The crystallisation period to a significantly less soluble $Nd(OH)_3$ and $Eu(OH)_3$ phase, to replace $NaLn(CO_3)_2$ or $LnCO_3OH$ at intermediate pH, will take longer than 3 months if precipitated from a dilute solution. If the lanthanides are truly analogous to the actinides then this process is unlikely to significantly affect the long-term crystallisation of $Am(OH)_3$ and $Cm(OH)_3$. Am and Cm ions destabilise their crystal structures by α-particle emissions (Silva *et al.*, 1995), therefore the significantly low $An(OH)_3$ solubilities may not form over long time periods. Variations in hydroxide crystallinity control solubility at high pH and reflect the large variations in literature data i.e. log Ksp -27.0 to -22.0 from Rao *et al.*, (1996b) and Morss *et al.*, (1989) respectively. This decrease in $Ln(OH)_3$ solubility, would effectively eliminate the hydroxycarbonate as a solubility limiting phase between pH 8 and 11, which would be replaced by a $Ln_2(CO_3)_3$-

$Ln(OH)_3$ solid phase equilibrium, if the crystallisation process can continue to these extreme extents.

There are no published values for $Nd(CO_3)_3^{3-}$ and $Eu(CO_3)_3^{3-}$ association constants and there are major discrepancies between each data source for the other carbonate and hydrolysis association constants for each individual lanthanide. A complete series of solid phase and aqueous relationship cannot be exactly derived to compare if Am does fit into a trend from Ce-Nd-Am-Sm-Eu based on the slight variations in ionic radii between the elements. Despite these variations, the difference in the solubility of Nd and Am phases (of up to 1 log unit) is less than the variations between Ce, Nd and Eu phases (of up to 2 log units) if the appropriate aqueous databases are utilised. The solubility calculations by PHREEQC and all the phase relations are however entirely reliant on the use of a consistent set of aqueous association constants for solubility predictions and the initial calculation of any solubility products from solution compositions.

The calculated solubility limits of the lanthanides and Am, between 10^{-8}M to 10^{-6}M, especially in near-neutral pH solutions, are significantly higher than the concentrations that would cause a significant hazard to health (Chapter 1). The insolubility of the crystalline hydroxide phases cannot be relied on to inhibit aqueous transport after release by the host matrix, as the most extreme crystal phases may not form. A second mechanism i.e. sorption to solid mineral surfaces in the host matrix must also be considered, which will inhibit lanthanide and actinide mobility from any repository system.

7.8 References

ATKINS, (1996) CHEMVAL Version 6 Database. *W. S. Atkins Environment.* **European Commission Report EUR 16897 EN**

BAES, C. F., and MESMER, R. E., (1976) The hydrolysis of cations. *J. Wiley & Sons New York.*

BAES, C. F., and MESMER, R. E., (1986) The Hydrolysis of cations. *Robert E. Krieger Pub. Co. Malabar Florida*

BAES, C. F., and MESMER, R. E., (1989) The hydrolysis of cations. *Robert E. Krieger Pub. Co. Malaber Florida.*

BAKER, F. B., HUBER JR., E. J., HOLLEY JR., C. E., and KRIKORIAN, N. H., (1971) Enthalpies of formation of cerium dioxide, cerium sesquicarbide and cerium dicarbide. *J. Chem. Thermodynamics* **3** 77-83

CROSS *et al.*, (1995) Thermodynamic modelling of radioactive waste disposal . NSSR/311

DIAKONOV, I. I., TAGIROV, B. R., and RAGNARSDOTTIR, K. V., (1998a) Standard thermodynamic properties and heat capacity equations for rare earth element hydroxides. *Radiochim. Acta* **81** 107-116

DIAKONOV, I. I., RAGNARSDOTTIR, K. V., and TAGIROV, B. R., (1998b) Standard thermodynamic properties and heat capacity equations for rare earth element hydroxides. II. Ce(III)-, Pr-, Sm-, Eu(III)-, Gd-, Tb, Dy-, Ho-, Er-, Tm-, Yb-, and Y-hydroxides. Comparisons of thermochemical and solubility data. *Chem. Geol.* **151** 327-347

DUMONCEAU, J. (1979) *Rev. Chem. Miner.* **16** 583-592

EDELSTEIN, N., *et al.*, (1982) Rep. ONWI/LBL-14325.

FERRI, D., GRENTHE, I., HEITANEN, S., and SALVATORE, F., (1983) Studies on metal carbonate equilibria, 5. The cerium(III) carbonate complexes in aqueous perchlorate media. *Acta Chem. Scand.* **A37** 359-365

JORDANAV, N., AND HAVEZOV, I., (1966) *Z. Anorg. Allg. Chem.* **347** 101-106

LEE, J. H., and BYRNE, R. H., (1992) Examinations of comparative REE complexation behaviour using linear free-energy relationships. *Geochim. Cosmochim. Acta* **56** 1127-1137

LEE, J. H., and BYRNE, R. H., (1993) Complexation of trivalent REE (Ce, Eu, Gd, Tb, Yb) by carbonate ions. *Geochim. Cosmochim. Acta* **57** 295-302

LUNDQUIST, R., (1982) Hydrophilic complexes of the actinides, I. Carbonates of trivalent americium and europium. *Acta Chem. Scand.* **A36** 741-750

MARTELL, A. E., AND SMITH, R. M., (1982) Critical stability constants vol 5. *Plenum Press, New York.*

MARTELL, A. E., AND SMITH, R. M., (1989) Critical stability constants vol 6: Second supplement. *Plenum Press, New York.*

MASKINO, H., YAJIMA, T., YOSHIKAWA, H., YUI, M., and SASAKI, N., (1993) Nd(III) hydrolysis constants and solubilities of Nd(III)hydroxide. *J. Chem. Soc. Jpn.* **5** 445-450

MÉNARD, O., ADVOCAT, T., AMBROSI, J. P., and MICHARD, A., (1998) Behaviour of actinides (Th, U, Np and Pu) and rare earths (La, Ce, and Nd) during aqueous leaching of a nuclear glass under geological disposal conditions. *App. Geochem.* **13** 105-126

MORSS, L. R., AND WILLIAMS, C. W., (1992) *Mat. Res. Soc. Symp. Proc.* **257** 283-288

MORSS, L. R., and WILLIAMS, C. W., (1994) Synthesis of crystalline $Am(OH)_3$ and determination of its enthalpy of formation of the solubility-product constants of actinide(III) hydroxides. *Radiochim. Acta* **66/67** 89-93

NEA, (1996) HATCHES (Harwell/Nirex Thermodynamic Databse for Chemical Equilibrium Studies). Database published by the Nuclear Energy Agency, OCED, Paris as NEA Version 9

NUGENT, L.J., *et al* (1971) *J. Inorg. Nucl. Chem.* **33** 2503

PARKHURST, D. L., THORSTENSION, D. C., and PLUMMER, L. N., (1980) PHREEQE–A computer program for geochemical calculations. *U.S. Geol. Surv., Water Resour. Inv.* 80-96, 210pp

PARKHURST, D. L., (1995) User's guide to PHREEQC–A computer program for speciation, reaction-path, advective-transport, and inverse geochemical calculations. . *U.S. Geol. Surv., Water Resour. Inv.* 95-4227, 143pp

RAI, D., STRICKERT, R. G., MOORE, D. A., and RYAN, J. L., (1983) Am(III) hydrolysis constants and solubility of Am(III) hydroxide. *Radiochim. Acta* **33** 201-206

RAI, D., FELMY, A. R., and FULTON, R. W., (1995) Nd^{3+} and Am^{3+} ion interactions with sulfate ion and their influence on $NdPO_4$(c) solubility. *J. Soln. Chem.* **24** 875-895

RAO, L. F., RAI, D. P., FELMY, A. R., FULTON, R. W., and NOVAK, C. F., (1996a) Solubility of $NaNd(CO_3)_2.6H_2O$ in concentrated Na_2CO_3 and $NaHCO_3$ solutions. *Radiochim. Acta* **75** 141-147

RAO, L. F., RAI, D. P., FELMY, A. R., FULTON, R. W., and NOVAK, C. F., (1996b) Solubility of $Nd(OH)_3$ in 0.1M NaCl aqueous solution at 25°C and 90°C. *Radiochim. Acta* **72** 151-155

RARD, J. A., (1987) Update of the europium database, Oct. 1987, LLNL Internal Memo.

RUNDE, W., MENRATH, G., and KIM, J. L., (1992) A study of solid-liquid phase-equilibria of trivalent lanthanide and actinide ions in carbonate systems. *Radiochim. Acta* **58/59** 93-100

SHIBUTANI, S. (1996) Solubility measurement of trivalent lanthanide for performance assessment of geological disposal of high level radioactive waste. *PNC Technical Review N° 97*

SHIBUTANI, S. (1996) Solubility measurements of trivalent lanthanide for performance assessment of geological disposal of high level radioactive waste. *PNC Technical Review N°97*

SHILOH *et al.*, (1969) *J. Inorg. Nucl. Chem.* **31** 1807

SILVA, R. (1982) *Lawerence Berkeley Laboratory Report*, LBL-15055

SILVA, R. J., BIDOGOLIO, G., RAND, M. H., ROBOUCH, P. B., WANNER, H., and PUIGDOMENCH I. (1995) Chemical Thermodynamics Volume 2. Chemical thermodynamics of americium. Elsevier (Amsterdam).

SILVA, R., and NITSCHE., (1984) *U.S. Nucl. Reg. Comm. Rep.* NUREG/CP-0052

WOOD, S. A., (1990a) The aqueous geochemistry of the REE and Y. 1: Reviews of available data for inorganic complexes and the inorganic REE speciation of natural waters. *Chem. Geol.* **82** 159-186

WOOD, S. A., (1990b) The aqueous geochemistry of the REE and Y. 2: Theoretical predictions of speciation in hydrothermal solutions to 350°C. *Chem. Geol.* **88** 99-125

Chapter 8

The Removal of REE from Solution below the Solubility Limit

8.1 Introduction

The solubility limit controls the maximum amount of an ion that will remain in solution in equilibrium with a solid phase under equilibrium conditions. This is typically above 10^{-7}M for the lanthanides. However these concentrations are above the permitted levels required by radiological safety regulations (Table 1.1, ICRP 1979).

In addition to mineral precipitation reactions, metal ions can be further removed from solution by adsorption to mineral surfaces. Even though oxide, oxyhydroxide and hydroxide minerals comprise a small component of soils and sediments compared with the quartz, silicates and clay minerals, their high surface area and reactive surfaces accomplish a significant proportion of the entire sorption capacity of soils and sediments (Fendorf and Fendorf, 1997). Iron minerals form the dominant proportion of oxide and oxyhydroxide minerals though Mn and Ti oxides are also important. Iron oxy phases are efficient scavengers of metal ions including the REE and the transition metals Cd, Co and Zn from river and seawater systems. Various studies such as that by Koeppenkastrop and Decarlo (1993) have shown that uptake of lanthanides from solution onto metal oxides is rapid and almost complete (above 99%) between 20 minutes and 2 hours.

There are mechanisms, dependent on the aqueous solution composition, which may reduce the amount of aqueous lanthanide that can be removed from solution by sorption processes. Sorption processes occur from the electrostatic interactions between aqueous ions and a charged surface as three types of reaction, simple adsorption from solution onto a charged surface, ion exchange reactions between adsorbed ions and aqueous species or the complete absorption of an aqueous ion into a mineral phase. The surface of oxide minerals can be assumed to be a charged layer with replaceable H^+ ions, which varies significantly with the solution pH. At low pH the oxide surface is likely to be positively charged (e.g. for goethite, FeOOH, the surface charge may be

considered as $FeOOH_2^+$), and adsorbing anions (e.g. SO_4^{2-}, Karltun 1997), whilst at high pH, surface H^+ ions are released into solution and the surface becomes negatively charged (e.g. as FeO^-, Dzombaki & Morel, 1990) favouring cation adsorption. The precise structural and co-ordination arrangements between the mineral surface and adsorbed ions can be determined by sophisticated equipment (e.g. EXAFS analysis) but interactions are usually depend on the crystal structure of the surface (Vienema *et al.*, 1996).

Increased ionic strength will compete for surface sites or form aqueous lanthanide species, which could reduce the total lanthanide adsorbed. If other cations e.g. Ca^{2+}, are present in excess of the lanthanides, or even the number of surface sites, then a proportion of the lanthanides may be displaced from the surface by ion-exchange reactions. In addition the lanthanides are known to form a series of aqueous species, for example $LnOH^{2+}$, $LnCO_3^+$ etc (chapters 4, 5 & 7). The actual species distribution will be dependent on the total composition and pH of the reacting solution. The aqueous species reduce the charge of the lanthanide ion, which may even become neutral or negative (e.g. $Ln(OH)_3^0$ and $Ln(CO_3)_2^-$) and significantly increase the size of the aqueous species. Other mechanisms, such as the effects of organic molecules on mineral surfaces and mobile colloidal particles will also increase lanthanide mobility but will not be considered here. The dominant transport of lanthanides, Am and Cm in natural systems is actually through the mobility of particulates and not as dissolved ions (von Gunten & Benes, 1995).

A series of sorption experiments have been designed to examine the effects of solution pH and ionic strength interactions with Ce, Nd and Eu below their solubility limits onto goethite as an example of a metal oxide surface.

Goethite ($\alpha FeOOH$) has been chosen as a typical oxide mineral for examination, as the crystalline phase can be consistently prepared and characterised and easily compared with other adsorption surfaces and adsorbing metals from literature sources. Goethite is a naturally occurring Fe-oxyhydroxide found in aqueous

environments from pH 3 (as an acid mine waste precipitate, Bigham *et al.*, 1996), in seawater (Ballistrieri & Murray, 1981) and can be precipitated from solutions at pH 12 (Atkinson *et al.*, 1967). Goethite is therefore stable over a wide pH range, from the near field repository to far field environments, as a secondary mineral within soils and iron oxides and oxyhydroxides can be assumed to form as a possible alteration phase from the decomposition of the original host steel containers for nuclear waste within an engineered environment.

8.2 Experimental

The sorption experiments were carried out in 5 stages to characterise the adsorption of aqueous lanthanide ions onto goethite

1. Preparation of a goethite solid phase
2. determination of the rate of adsorption over time
3. determination of the lanthanide adsorption limit to goethite
4. the effects of pH upon adsorption
5. desorption from aqueous complexes and competitive adsorption

8.2.1 Preparation of Goethite

Goethite was prepared following the method of Atkinson *et al.*, (1967). Purple $Fe(NO_3)_3.9H_2O$ (50g) crystals were dissolved in distilled water ($800cm^3$) to form a clear rust-brown coloured solution at pH ~ 2. A solution of KOH (2.5M, $200cm^3$) was added to the $Fe(NO_3)_3$ solution and an amorphous rust-brown precipitate was formed. The solution was stirred vigorously and the pH adjusted to pH 12.0 with $NH_3(aq)$. The solution and precipitate were kept at 60°C for 24hrs in a thermostated waterbath to age the precipitate to yellow coloured crystals.

The solution was decanted and the precipitate washed by soaking the crystals in 1dm^3 of distilled water, stirring vigorously to remove any adsorbed K^+ or NO_3^- ions. The precipitate was allowed to settle and then the water was decanted. The precipitate was repeatedly washed with 10 further 1dm^3 portions.

The precipitate was filtered off and the filtrate discarded. The iron oxide was oven dried at 120°C, crushed then sieved to a particle size between 180μm-250μm, any fraction less than 180μm was discarded. The sieved material was kept in a dessicator over silica gel to prevent water absorption.

The precipitate was characterised by FTIR, XRD and TGA, and the surface area of the sieved sample determined with a NOVA-2000 BET Surface Area Analyzer.

8.2.2 Goethite Characterisation

Goethite was characterised by comparison with the XRD JCPDS powder diffraction pattern number 17-536 shown in Table 8.1 and the XRD pattern Figure 8.1. The infra-red spectra (Figure 8.2) can be assigned from Table 8.2 after Parida and Das (1996). Oven drying removes any crystalline and adsorbed water from the crystals.

Figure 8.1 Powder XRD pattern of synthetic goethite (α-FeOOH) prepared in Section 8.2.1

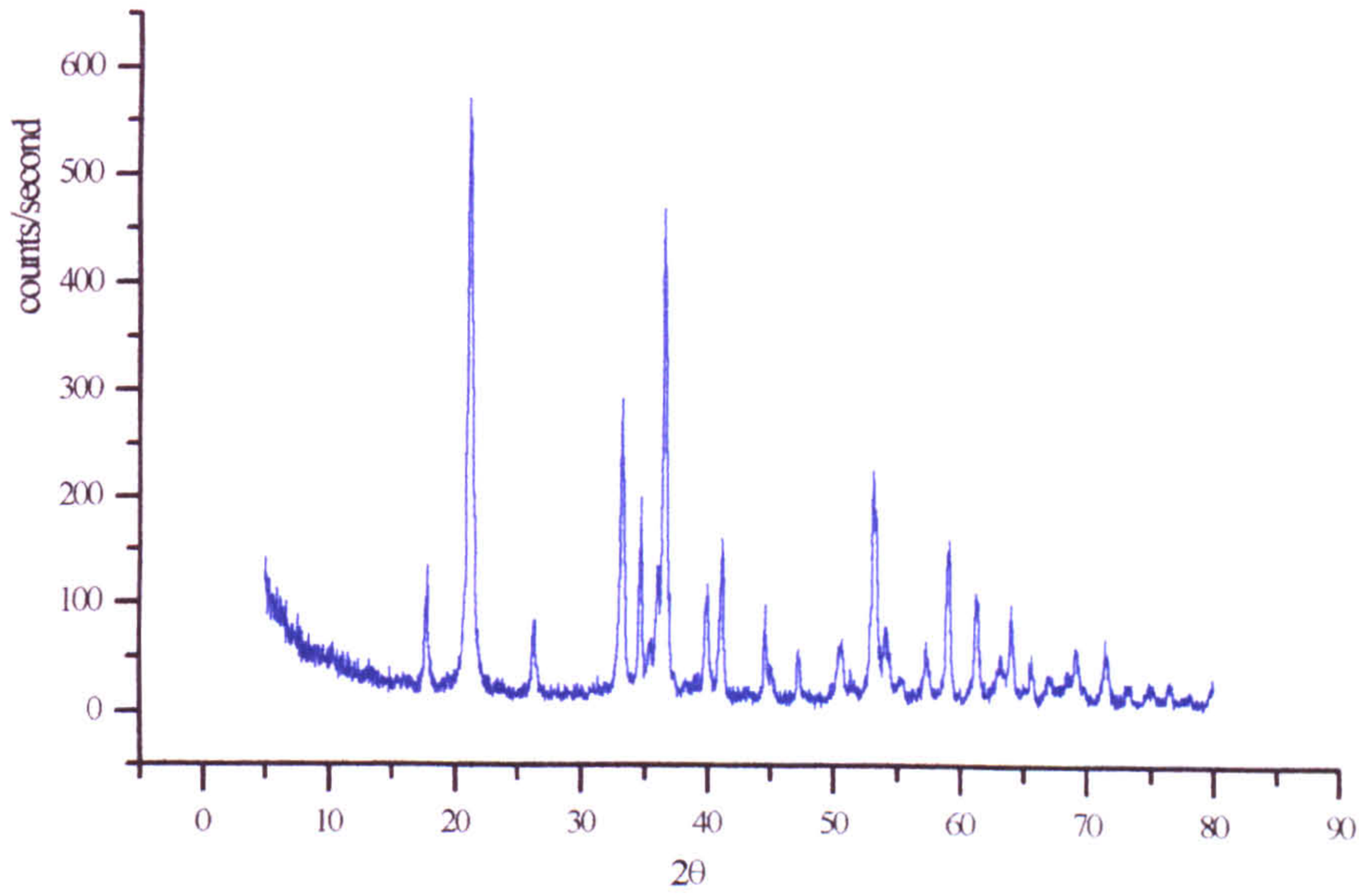

Figure 8.2 FTIR spectrum of synthetic goethite (α-FeOOH) prepared in Section 8.2.1

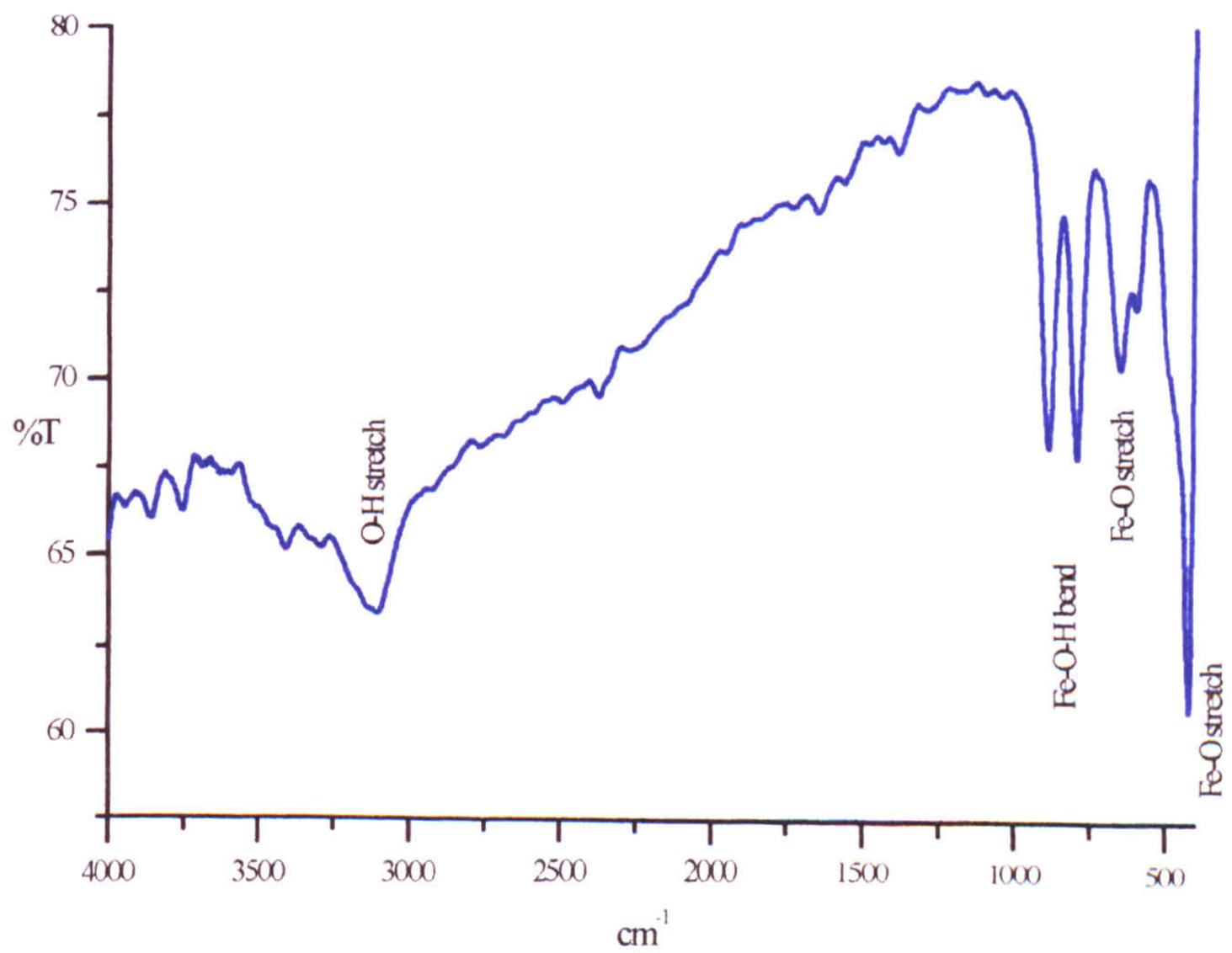

Table 8.1 XRD characterisation of goethite(α-FeOOH)

JCPDS 17-536	This work	
d(Å)	d(Å)	2θ
4.980	4.9707	17.830
4.180	4.1875	21.200
3.380	3.828	26.325
2.690	2.6927	33.245
2.580	2.5799	33.745
2.520		
2.490	2.4877	36.075
2.452	2.4484	36.675
2.252	2.2503	40.035
2.192	2.1871	41.245
2.009	2.0302	44.595
1.920	1.9223	47.245
1.799	1.7953	50.820
1.770		
1.721	1.7217	55.155
	1.7154	53.365
1.694	1.6992	54.155
1.661	1.6540	55.515
1.606	1.6048	57.370
1.564	1.5654	58.955
1.509	1.5116	61.275
1.467	1.4697	63.220
1.453	1.4543	63.965
1.418	1.4203	65.685
1.392	1.3942	67.080
1.357	1.3577	69.135
1.317	1.3199	71.410
1.264	1.2907	73.285
1.241	1.2651	75.015

Table 8.2 Goethite (α-FeOOH) IR characteristic bands

	Parida &Das (1996) (cm^{-1})	This work (cm^{-1})
Fe-O-H bend	890/790	889/796
Fe-O stretch	670/455/418	647/422
O-H stretch		3108

The surface area was measured as $70m^2/g$ for a sieved 180μm-250μm particle size fraction which gives a surface site density of 3.83μmols m^{-2} (Table 8.3) assuming there are 2.31sites per nm^2 available for adsorption reactions on the goethite surface (Dzombaki & Morel 1990).

Table 8.3 Calculation of goethite (prepared in Section 8.2.1) surface site density (after Dzombaki & Morel 1990)

Assuming 2.31 sites nm^{-2}

therefore $\frac{2.31}{(1\times10^{-9})^2} = 2.31 \times10^{18}$ sites m^{-2}

therefore the sites per surface area

$$\text{mols } m^{-2} = \frac{2.31\times10^{18}}{\text{Avogadro's N°}} = \frac{2.31\times10^{18}}{6.022\times10^{23}}$$

$$= 3.83\times10^{-6} \text{ mols } m^{-2} = 3.83\mu\text{mols } m^{-2}$$

and sites per unit mass for a surface area of $70m^2/g$

$70m^2/g \times 3.83\mu\text{mols } m^{-2} = 2.68\times10^{-4}$ mols/g
$= 0.00027$mols/g

The point of zero charge (PZC) was not determined during this study, but has been previously determined at pH 7.8 by Atkinson *et al.*, (1967) and Karltun (1997)

8.2.3 The effects of surface area on sorption

$LnCl_3$ (1×10^{-5}M, $100cm^3$) was added to a batch of samples with a range of masses of goethite from 0.05g-0.5g in $125cm^3$ HDPE Nalgene bottles. The solution and goethite was stirred with a magnetic stirrer for 3 hours, then filtered through a Whatman N° 4 sintered glass crucible. The filtrate was then analysed by FIA-UV for the total lanthanide content and spectrofluorimetry for Ce^{3+} determination.

8.2.4 Rate of adsorption

$LnCl_3$ ($1x10^{-5}M$, $100cm^3$) was added to 0.05g of goethite in a $125cm^3$ HDPE Nalgene bottle. Each sample was stirred for a specific time to give a range of samples with reaction times from 30 seconds to 20 minutes, the pH was measured and then the suspension filtered. A sample was allowed to react for 2 hours. The filtrate was analysed for the total lanthanide concentration by FIA-UV analysis.

8.2.5 The effects of solution pH on adsorption

A series of goethite (0.05g) samples were added to solutions of $LnCl_3$ ($2x10^{-7}M$, $50cm^3$) in $125cm^3$ HDPE Nalgene bottles. The Ln^{3+} was allowed to adsorb onto the goethite for two hours. After this time the pH of each solution was adjusted with either nitric acid or ammonia solution so that a series of solutions were prepared with different pH's from pH 4 to pH 11. The solution was allowed to equilibrate for at least 7 days in a thermostated waterbath at 25°C. The pH of the solution was measured and then the solution was filtered. The filtrate was analysed by FIA-UV and ICP-MS.

8.2.6 The effects of ionic strength on adsorption

A $LnCl_3$ ($5x10^{-7}M$) solution was prepared with either $KHCO_3$ (0.1mM, 1mM, or 10mM), K_2CO_3 (0.1mM, 1mM or 10mM) or $CaCl_2$ (0.1mM, 1mM or 10mM) in degassed distilled water. The $LnCl_3$ solution ($50cm^3$) was mixed with goethite (0.05g) in $125cm^3$ HDPE Nalgene bottles and the pH adjusted to give a batch of samples with a pH range of pH 4 to pH 12 for each ion at each concentration. The solution-goethite samples were allowed to equilibrate for at least 7 days at 25°C in a thermostated waterbath. The pH of the solution was measured then the

solution filtered through a Whatman N°4 sintered glass crucible. The filtrate was then analysed for the aqueous lanthanide concentration by ICP-MS.

8.3 Results

8.3.1 Uptake rate and surface saturation

Uptake rate

Preliminary results indicate that the uptake of Ce onto goethite is rapid and almost total, over 90% adsorption occurs within 60 seconds of the Ce^{3+} solution being exposed to the goethite surface (Figure 8.3). The initial uptake did not vary significantly over a 3 hour period. The determination of the uptake rate at less then 60 seconds was difficult as the time required to measure the solution pH and transfer the sample to a sintered glass crucible and filtering time was approximately 40 seconds.

Figure 8.3 Timed $CeCl_3$ ($50cm^3$, $5x10^{-6}M$) adsorption onto goethite (0.2g)

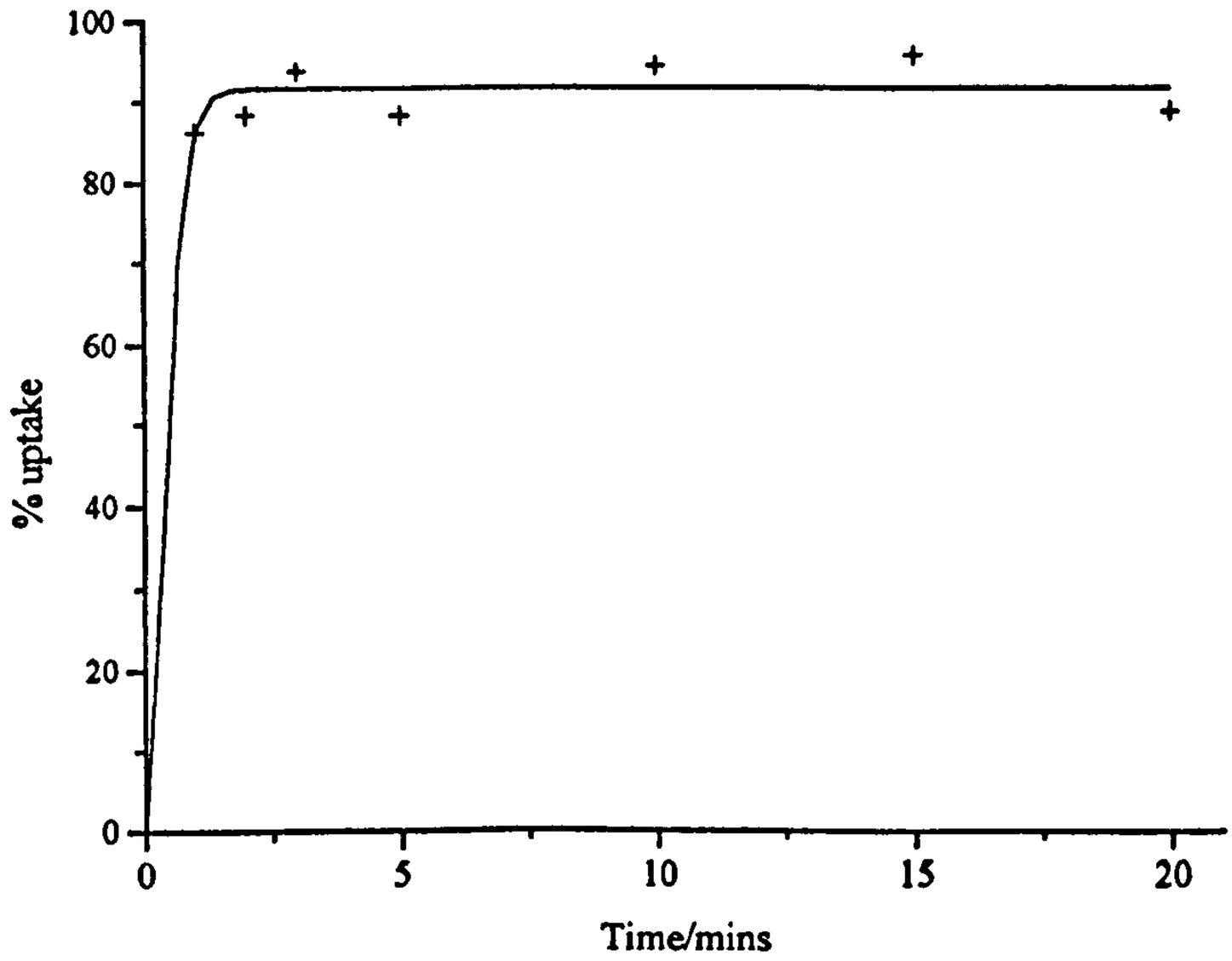

Surface saturation and distribution coefficient (K_d)

The total uptake of Ce^{3+} from a $50cm^3$, $10^{-5}M$ $CeCl_3$ solution, appears to be independent of the mass of goethite at equilibrium when there is between 0.05g and 0.5g of goethite (Figure 8.4). A total of 85% to 95% of the total aqueous Ce had been removed from the solution for samples containing between 0.05g and 0.5g of goethite.

When the distribution coefficient (K_d, equation 8.1) is calculated for the same experimental data as Figure 8.4 (Appendix 8.2, Figure 8.5), there appears to be a slight drop in the log K_d from a maximum log K_d of 5.5 to a minimum log K_d of 4.2 as the mass of goethite in the sample increases. The average log K_d is 4.88 with a standard deviation of 0.42.

$$K_d = \frac{\text{Concentration REE on solid phase (mols g}^{-1})}{\text{Concentration REE in aqueous phase (mols ml}^{-1})} = \text{ml g}^{-1} \qquad (8.1)$$

The slight decrease in the K_d is probably due to less efficient mixing of the goethite with the Ce solution, from the significant increase in the volume of the solid phase over a mass range of 0.05g-0.5g of goethite. The maximum Ce uptake onto the smaller surface volumes suggests that the surface was not saturated with respect to lanthanides.

A small volume of the solid phase (0.05g) is capable of efficiently extracting at least 90% of the aqueous REE. The small volume of solid phase ensures that there is efficient mixing of the solid phase with the aqueous phase and rapid separation of the aqueous and solid phases during filtration. The goethite surface is probably not saturated with the adsorbed lanthanide, Ce, even when only 0.05g of goethite was present.

Figure 8.4 The adsorption of Ce (10^{-5}M, 50cm^3) onto various masses of a goethite surface. Solution pH 6-7.7 log K_d 4.88±0.42

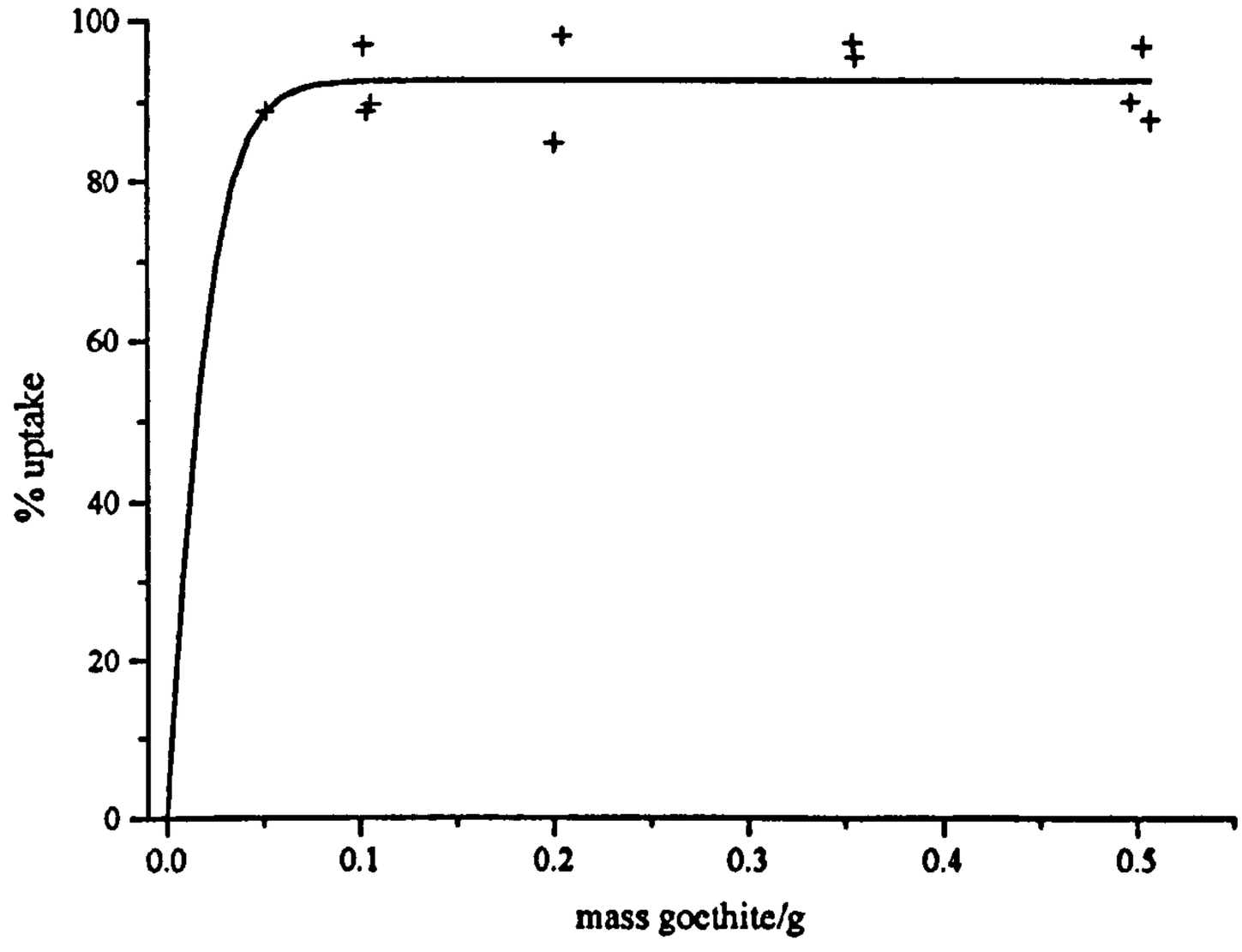

Figure 8.5 Distribution coefficient for the adsorption of Ce (10^{-5}M, 50cm^3) onto various masses of a goethite surface. Solution pH 6-7.7

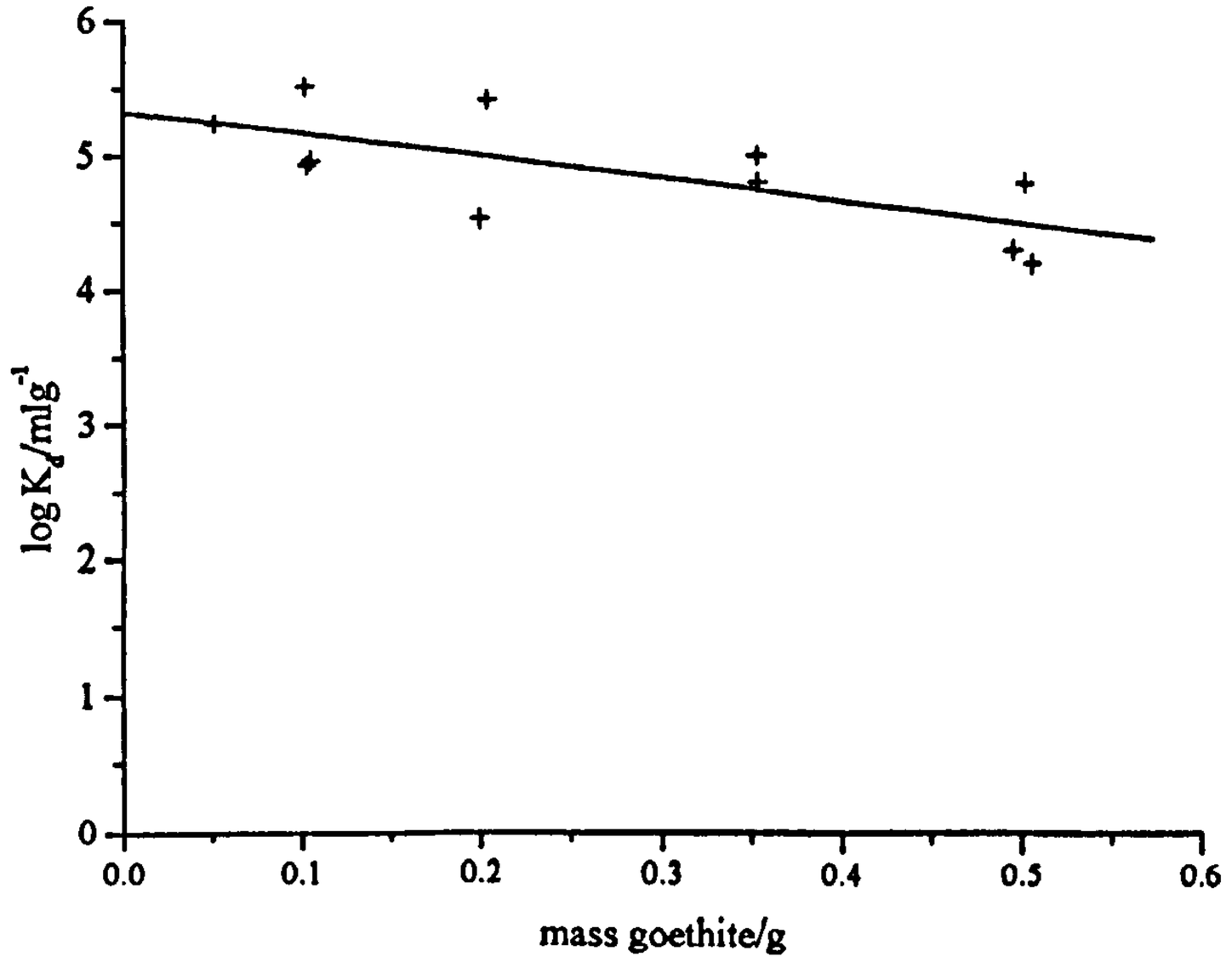

8.3.2 The effects of pH and ionic strength on Nd and Eu adsorption

The pH of each initial batch of samples was adjusted with HNO_3 or NH_3, to form a series of samples with a regular increase in pH from pH 3 to pH 12. During the surface-aqueous equilibrium reaction the pH of the solution was buffered towards two distinct areas (Figures 8.6 and 8.7) each of which was associated with above 90% adsorption of the lanthanides to the metal surface. The initial regular sample spacing was concentrated into one of these two groups either at pH 6.5 or pH 11. The uptake of Nd and Eu onto the goethite surface is pH dependent (Figure 8.6, Appendix 8.3). There is a sharp adsorption edge from pH 4.5 to pH 6, when adsorption increases from less than 10% towards 99%. After equilibrium, most samples initially set between pH 4 and 6, had increased in pH to between pH 6.5 and 8. There was therefore relatively few samples along the adsorption edge, but a concentration at the top of the adsorption edge.

Excess Ca^{2+} in solution

A similar process occurred when Ca^{2+} was added to the lanthanide solution (Figure 8.7, Appendix 8.4). A sharp adsorption edge between pH 4 and 6, was followed by two concentrations of sample groups of above 90% lanthanide uptake between pH 6.5-8 and pH 9.5 and 12. Excess Ca (up to 10mM) did not displace the lanthanides from the goethite surface.

Excess CO_3^{2-} and SO_4^{2-} in solution

Carbonate solutions cannot be easily acidified to low pH, as $CO_2(g)$ is released as the solution is acidified. The bottom of the adsorption edge could not be identified at low pH, however as Ln^{3+} is the dominant aqueous lanthanide species below pH 5 (Chapters 4 & 7) in the lanthanide-carbonate system, then carbonate is unlikely to effect absorption at low pH. The high Nd uptake (90%) of two samples from a 1mM K_2SO_4 solution at pH 4 (Figure 8.8, Appendix 8.8d), may

be the result of sulphate adsorption to the goethite surface at low pH also removing lanthanide-sulphate species from solution, or even a co-precipitation or surface alteration reaction to an iron-sulphate mineral (e.g. Jarosite or Schwertmannite). The sulphate adsorption edge would be expected to follow the opposite trend to the Nd adsorption edge, however further samples would be required for confirmation. Above pH 6, there was complete uptake of Nd onto the goethite surface. Sulphate ions are known to adsorb onto goethite surface sites (Karltun, 1997) under acidic conditions, with an adsorption edge from pH 4 (above 90% adsorption) to pH 7 (less than 5% adsorption), therefore SO_4^{2-} adsorption may affect Ln^{3+} adsorption but only below pH 5, i.e. from acid mine drainage systems but not in intermediate to high pH engineered systems.

Above pH 6, carbonate does not appear to effect Nd or Eu adsorption onto the goethite surface (Figures 8.8 & 8.9, Appendix 8.5 & 8.6 respectively), however there is a regular sample distribution from pH 6 to 12 associated with above 90% uptake onto the surface, and not the sample concentrations around pH 6.5 and 11 as indicated by Figures 8.6 and 8.7. Carbonates are most likely to affect the sorption process between pH 7 and pH 10 when aqueous $Ln(CO_3)_x^{3-2x}$ complexes are dominant in solution, however no direct evidence could be seen from this study.

Figure 8.6 The adsorption of the aqueous lanthanides Nd and Eu ($50cm^3$) onto a goethite (0.05g) surface

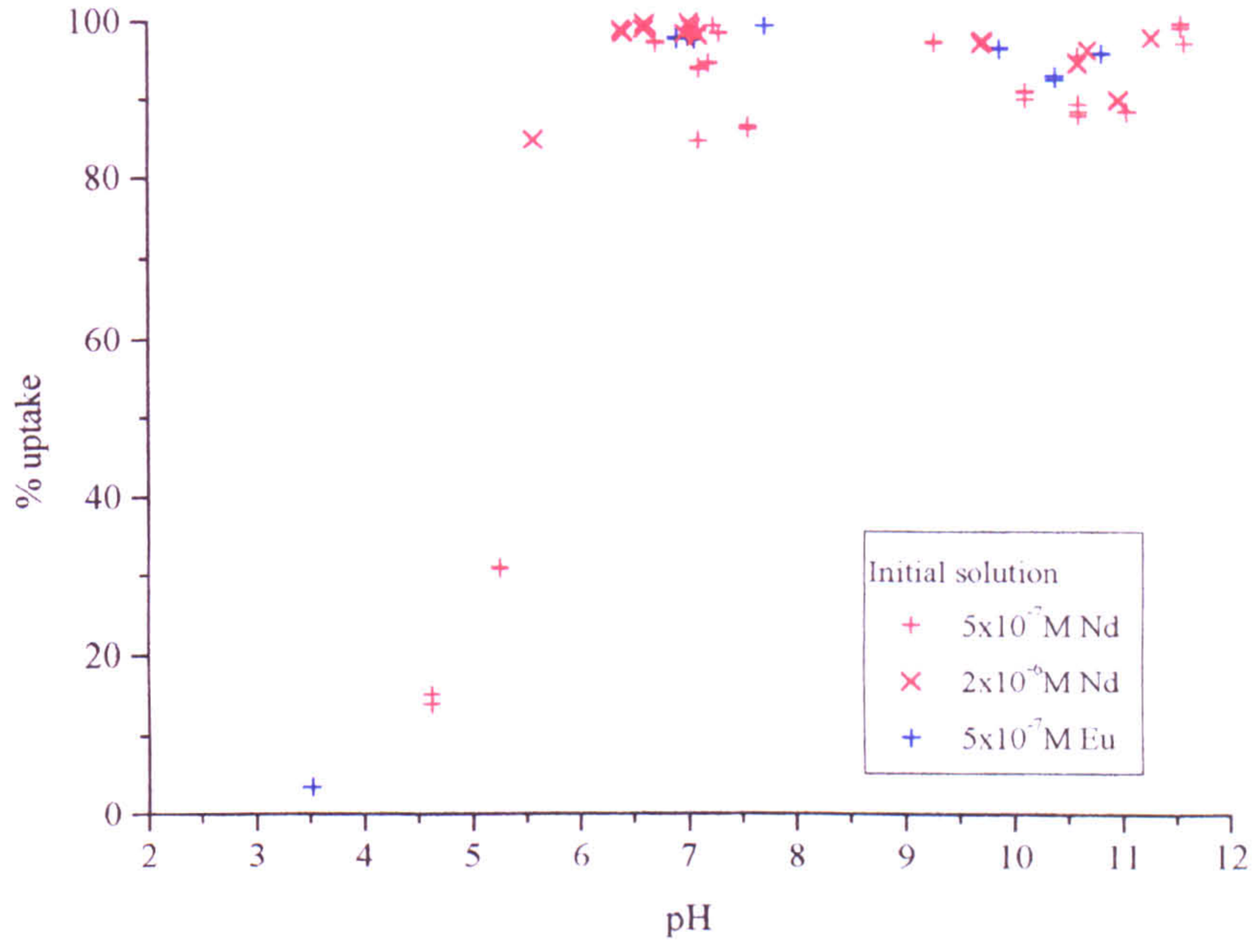

Figure 8.7 Competitive adsorption between the aqueous lanthanides, Nd and Eu, ($50\ cm^3$) and Ca^{2+} to a goethite surface (0.05g) with pH

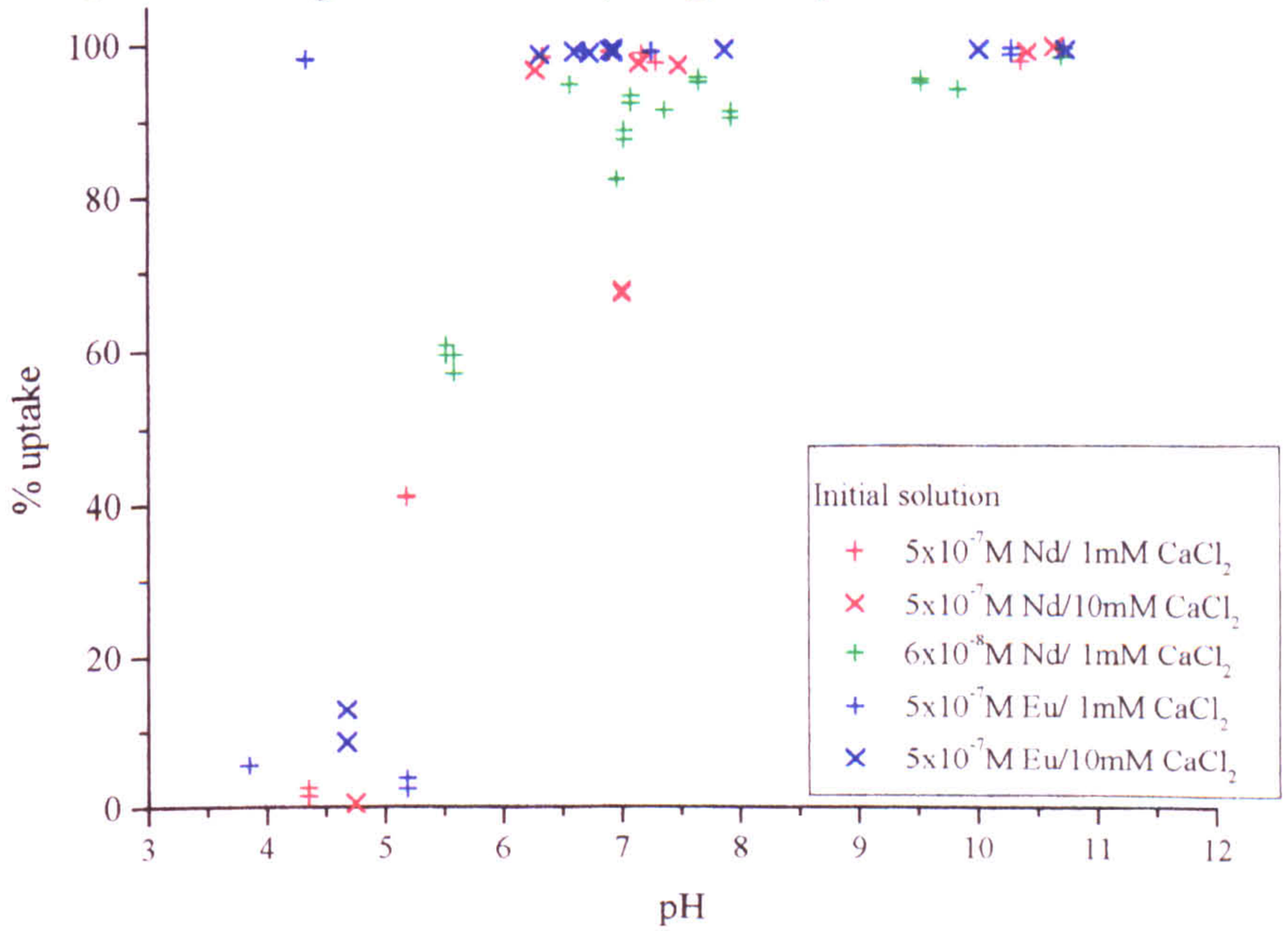

Figure 8.8 The effects of aqueous species on the uptake of Nd ($5x10^{-7}$M, 50 cm^3) onto goethite (0.05g) in carbonate and sulphate solutions

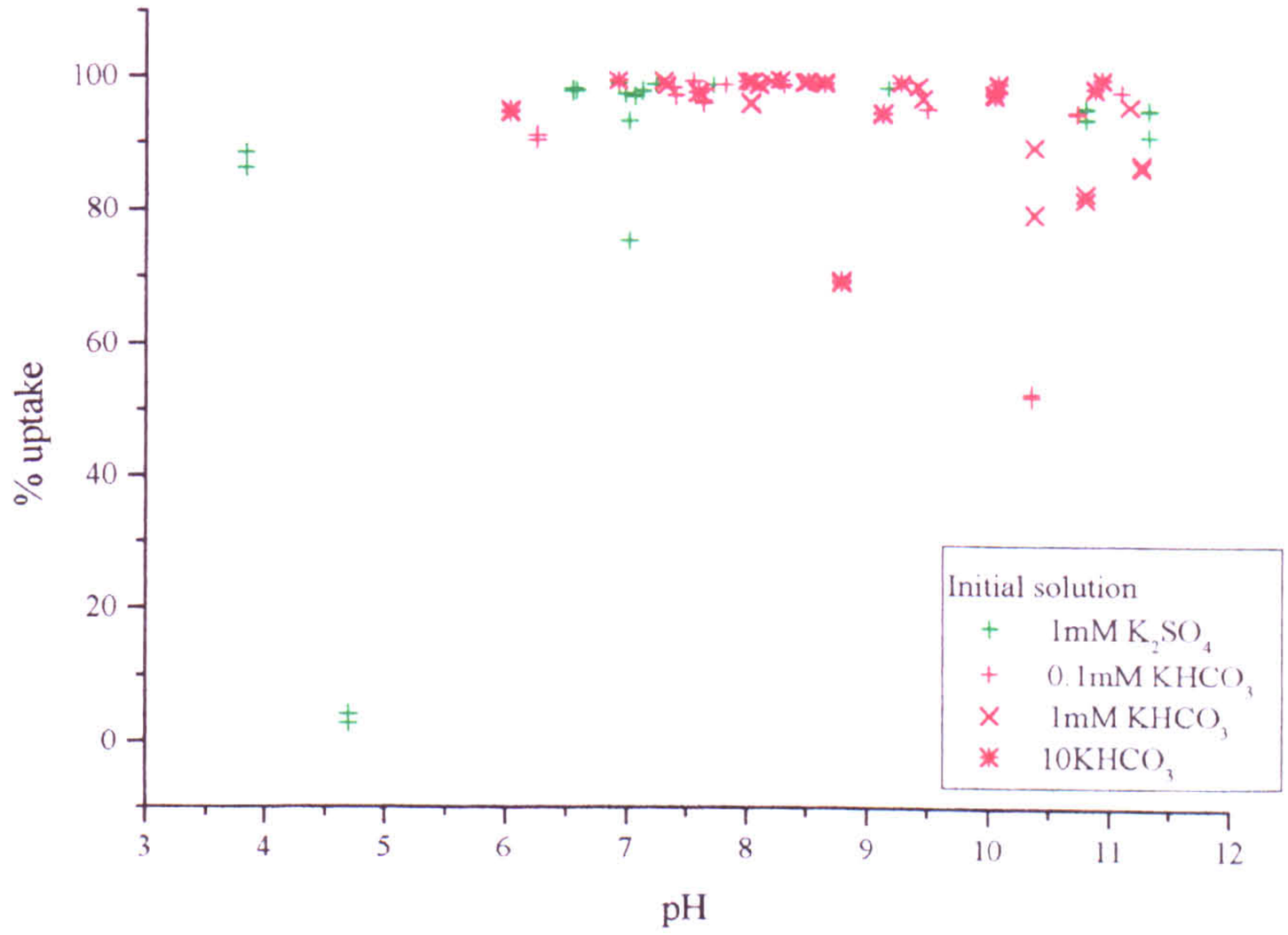

Figure 8.9 The effects of aqueous species on the uptake of Eu ($5x10^{-7}$M, 50 cm^3) onto goethite (0.05g) in carbonate solution

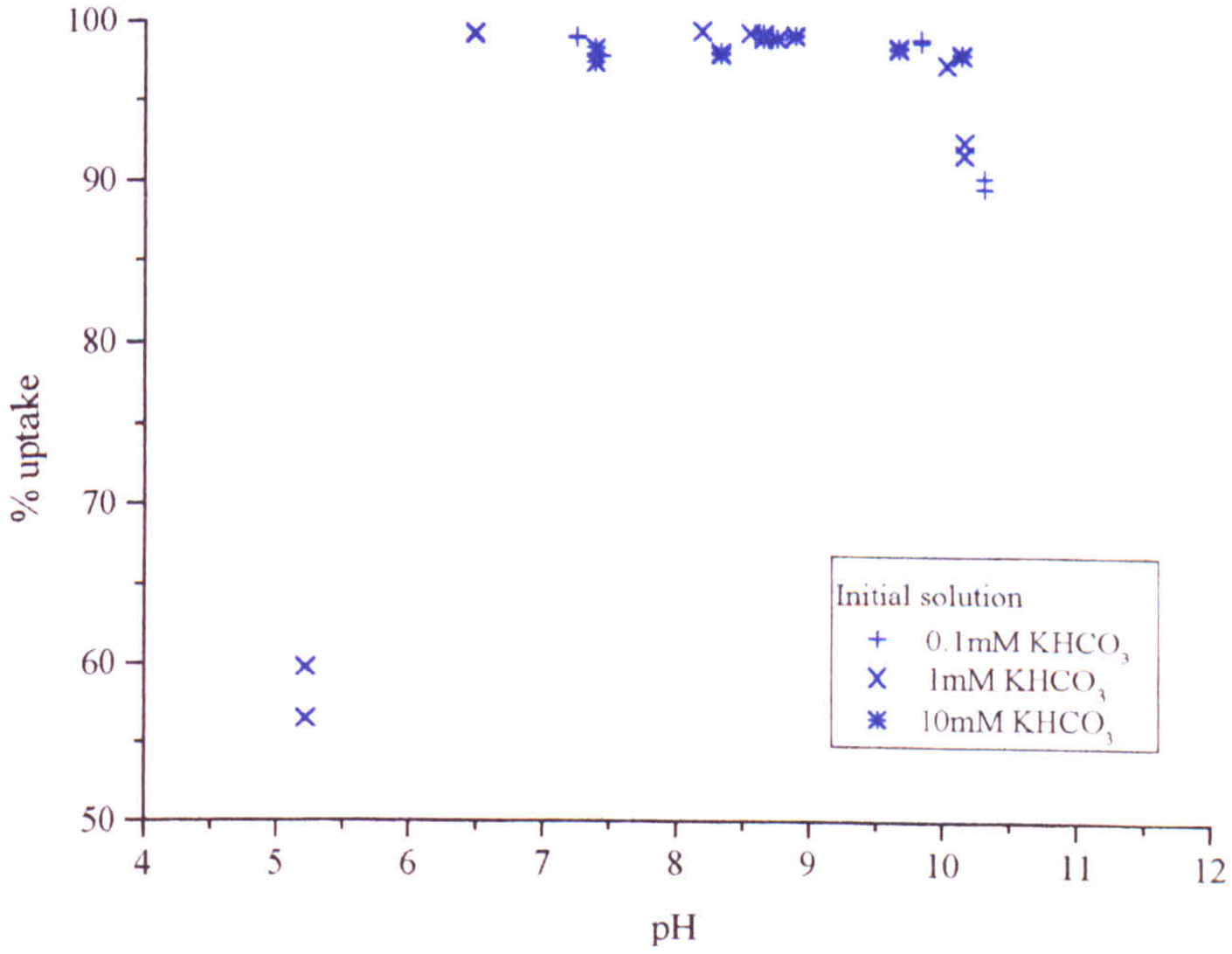

8.3.3 Surface saturation and distribution coefficients (K_d)

Surface-aqueous distribution

The distribution coefficient (K_d, equation 8.1) for the samples above pH 6 (Table 8.4) indicates a strong retention onto the goethite surface. Log K_d values between 4.4 and 5.7, indicate that there was at least a 10^4 fold concentration of the lanthanides on the goethite surface compared with the solution above pH 6.5 and after a 10 day equilibrium period.

Table 8.4 Summary of the calculated distribution coefficient (K_d) for the adsorption of Nd or Eu from a $LnCl_3$ solution ($50cm^3$) to a goethite surface (0.05g) above pH 6.5 (Figures 8.6-8.9, Appendix 8.4-8.6)

Initial solution		Nd		Eu	
$[LnCl_3]$	[bulk solution]	log K_d	std dev	log K_d	std dev
$5x10^{-7}$M		4.43	0.51	4.56	0.30
$2x10^{-6}$ M		4.75	0.38		
$5x10^{-7}$M	0.1mM $KHCO_3$	4.47	0.54	4.62	0.43
$5x10^{-7}$M	1mM $KHCO_3$	4.75	0.56	4.52	0.76
$5x10^{-7}$M	10mM $KHCO_3$	4.85	0.60	4.81	0.16
$5x10^{-7}$M	1mM K_2SO_4	5.71	0.50		
$5x10^{-7}$M	1mM $CaCl_2$	4.87	0.27	5.02	0.18
$5x10^{-7}$M	10mM $CaCl_2$	4.55	0.68	5.05	0.11

The distribution coefficient is however a simple comparison of the relative distribution of the target element (e.g. a lanthanide or Am) between the surface and solution during the adsorption reaction. The K_d is useful for the comparison of mixed or uncharacterised surfaces but does not give a direct indication of the saturation state of the surface, i.e. the number of surface sites available for

reaction compared with the actual amount of competing ions for the surface (i.e. an ion exchange reaction including H^+).

Surface saturation state

The surface site density for a $70m^2/g$ surface area at 2.31 sites nm^{-2} (Dzombaki & Morel, 1990) was $3.83\mu mols/m^{-2}$ (or 0.00027mols/g) of goethite(Table 8.2). The simplest model for the surface adsorption reaction is assumed to be a 1:1 reaction as shown in equation 8.2, (Tessier *et al.*, 1985)

$$FeOOH + Ln^{3+} = FeOO\text{-}Ln^{2+} + H^+ \qquad (8.2)$$

assuming the Ln^{3+} displaced H^+ from the goethite and that a FeOO-Ln complex forms, then there are $1.34x10^{-5}$ mols of surface sites available in a 0.05g goethite sample for reaction with the aqueous solution.

In 50 cm^3 of a $5x10^{-7}M$ $LnCl_3$ solution, there are $2.5x10^{-8}$mols of Ln^{3+} available for reaction and in $50cm^3$ of $2x10^{-6}$ M $LnCl_3$ solution there are $1x10^{-7}$ mols of Ln^{3+} available. There is therefore an excess of goethite surface sites compared to the total lanthanide in the experimental solutions, even if the Ln^{3+} is bidentate or tridentately bound to the surface.

There is an excess of Ca^{2+} in solution in the 1mM Ca^{2+} ($5x10^{-5}$ mols of Ca) and the 10mM ($5x10^{-4}$ mols of Ca) solutions compared with the number of goethite sites. The surface site saturation increases further if Ca^{2+} binds to two sites on the goethite surface. The experimental data (Appendix 8.4, Figure 8.7) indicate that an excess of Ca^{2+} did not displace the Ln^{3+} from the goethite surface. Ca^{2+}, Nd^{3+} and Eu^{3+} have similar ionic radii of 100pm, 98.3pm and 95.8pm respectively, therefore the lanthanides will have a significantly greater charge density than the Ca^{2+} ions and the Ln^{3+} ions are unlikely to be displaced from the sorption surface by the excess of Ca. The smaller Mg^{2+} ion (ionic radii 72pm) may be a competitive ion for surface sites if in sufficient abundance.

The adsorption of transition metals to goethite surfaces has been studied in more detail than for the lanthanides (Venema *et al.*, 1996). These have shown that divalent cations, for example Cd^{2+}, will be bound as a mixture of monodentate, bidentate and tridentate complexes, however the monodentate and bidentate sites are more numerous on the surface although individual reaction constants could not be determined for each of the single, doubly and triply coordinated complexes. The stronger lanthanide binding than Ca to the goethite surface cannot be simply explained by surface co-ordination number.

8.4 Predicting lanthanide adsorption to goethite

Adsorption reactions can remove above 99.9% of the aqueous lanthanides (even when below their solubility limit in carbonate solutions) if the pH is above the adsorption edge. However the trace amounts remaining in solution may still be radiologically hazardous. A reaction constant, for the adsorption reaction which is dependent upon complex solution parameters (for example aqueous species composition and solution pH) must be derived to predict the actual amount of each target element that is to be immobilised.

FITEQL v*3.2 modelling*

FITEQL (Fit equilibrium constant) is a model developed to calculate the equilibrium constant for a reaction from experimental data (Section 7.3). FITEQL v3.2 requires the association constants for any aqueous reactions that may occur and then calculates an unknown reaction constant, in this case the adsorption of lanthanides to goethite (equation 8.2), from the experimental data assuming the total lanthanide content of the system is known and the amount of lanthanide as the adsorbed FeOO-Ln complex.

$$FeOO^{-} + Ln^{3+}(aq) = FeOO\text{-}Ln^{2+} \qquad (8.2)$$

There were insufficient experimental data points across the adsorption edge (and all the data points above the adsorption edge were near the analytical detection limit) to calculate a reliable equilibrium constant. Consequently, the resulting equilibrium constant between Nd or Eu with goethite calculated using FITEQL must be treated with caution. For all the systems shown in Figures 8.6 to 8.9 suggest a value of log K between 2.4 and 10.1. The initial estimates from the Kd calculations of approximately 4.9 (Table 8.4) are therefore within the calculated range from FITEQL.

PHREEQC modelling

The sorption of lanthanides has been shown to be pH dependent and therefore the K_d (equation 8.1) will reduce with pH to a K_d of zero below pH 3 as lanthanide ions will be in the aqueous phase. A pH term must be included to predict the sorption capacity of a surface if the solution conditions are likely to change. The simplest model for lanthanide sorption to a goethite surface (equation 8.3) introduces a pH term for the sorption reaction constant (equation 8.4) which considers the actual amount of surface sites available and any other aqueous species that form.

PHREEQC can also be used to predict the adsorption of an aqueous species to a surface. The surface complexation reaction with the appropriate reaction constant must be included with the aqueous species association constants and solid phase dissociation reactions. The number of surface sites per unit mass of surface must be calculated as a molar quantity before incorporation into the PHREEQC database. The surface reaction (equation 8.3) therefore becomes a quantifiable mechanism for removing aqueous ions from solution. An initial 1:1 reaction between goethite and Nd can be expressed as equation 8.3, with reaction constant

K (equation 8.4). Similar equations (and reaction constants) can be expressed for other surface complexation reactions which may be involved.

$$FeOOH_{(surface)} + Nd^{3+}_{(aq)} = FeOO\text{-}Nd^{2+}_{(abs)} + H^{+}_{(aq)} \qquad (8.3)$$

$$K = \frac{[FeOO\text{-}Nd^{2+}]_{abs} . [H^{+}]}{[FeOOH]_{surface} . [Ln^{3+}]} \qquad (8.4)$$

Two other equilibrium reactions are required for the association and dissociation reactions of the goethite surface with H^+ ions in solution to determine the surface charge over the entire pH range for the modelling process (equations 8.5 and 8.6) after Dzombaki and Morel (1990)

$$FeOOH + H^{+} = FeOOH_2^{+} \qquad \log K\ 7.35 \qquad (8.5)$$

$$FeOOH = FeOO^{-} + H^{+} \qquad \log K\ -9.17 \qquad (8.6)$$

An estimation of the adsorption reaction constant for equation 8.3, can be made if a series of pH vs log[Nd] plots across the absorption edge, are calculated for the range of potential reaction constants and compared directly with experimental data.

If the percentage uptake from the experimental data (Figures 8.6 to 8.9, Appendix 8.3 to 8.6) for Nd and Eu are converted to an aqueous concentration assuming an initial solution contained $5x10^{-7}M$ total aqueous Ln, and 0.05g of goethite was available per $50cm^3$ of aqueous solution (i.e. 1g of goethite per $1dm^3$ of solution), then the experimental data can be compared directly with the predicted uptake of REE by goethite from PHREEQC calculations (Figure 8.10).

The predicted sorption to goethite is zero below pH 4 and 100% above pH 7. The experimental data approximately follows the logK 3.8 line, but is spread over a region from logK 2.5 to 4.5 for the reaction shown in equation 8.3. The experimental data appears to follow the predicted solubility adsorption edge at high pH but deviates slightly at the low pH end.

Figure 8.10 Predicted uptake of Nd ($50cm^3$, $5x10^{-7}M$) onto goethite (0.05g)
Composite for all experimental data of the % uptake at the adsorption edge
(assuming 100% uptake removes $5x10^{-7}M$ Nd from solution)

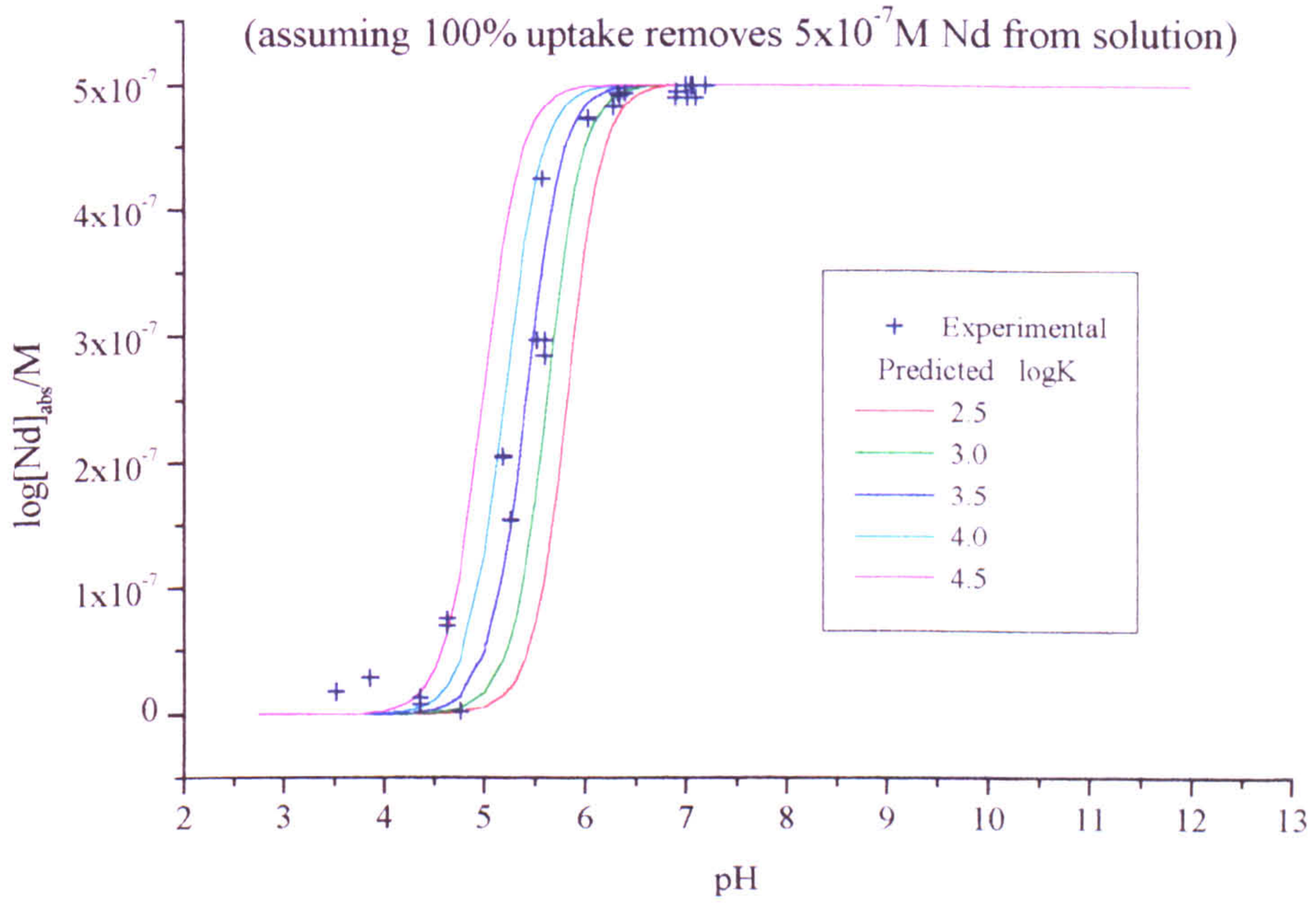

If the reaction for equation 8.3 is logK 3.8, then a pH vs [Ln]aq diagram can be drawn for each of the lanthanides. Figure 8.11, indicates that Nd^{3+} is the only significant aqueous species to form below pH 12 in carbonate free solutions. There is a sharp adsorption edge from pH 4 below which no adsorption to the surface occurs, to pH 7 above which all the Nd is immobilised on the goethite surface. However if Nd is to used as an analogue for Am, aqueous concentrations below $10^{-7}M$ must be considered. If the [Nd(aq)] axis is expanded as shown in Figure 8.12, the pH vs log[Nd] diagram indicates that the aqueous Nd concentration varies significantly with pH and as different aqueous species become dominant across the entire pH range.

Nd in the presence of goethite (Figure 8.12) is dominantly present as the Nd^{3+} species below pH 5, but sorption increases at a steady rate from pH 2.5 until pH 6.5, by which point the surface FeOO-Nd complex immobilises more than 99.9% of the Nd. The adsorption of lanthanides to the goethite surface is actually a log-log relationship between log[Nd(ads)] and pH (i.e. $\log[H^+]$) below pH 6. There is a steady increase in the proportion of aqueous Nd hydroxy species from pH 2.5

to pH 5.5, but they do not influence the adsorption edge (Figure 8.11). The total aqueous Nd concentration is predicted to reduce further as pH increases above pH 6.5, to a minimum at pH 9.5, of 10^{-16}M The proportion of aqueous Nd as Nd hydroxy species also increases. Above pH 9.5 $Nd(OH)_3^0(aq)$ forms the dominant aqueous Nd species in a carbonate free system and total Nd solubility increases, and above pH 12 the increase is at a sharper rate than found in the adsorption edge between pH 4 and 7. Above pH 13.5 the aqueous Nd concentration will exceed the adsorbed Nd, even when there are excess sorption sites available on the goethite surface compared with the total Nd. Nd solubility must therefore be controlled by precipitation of $Nd(OH)_3(s)$ above pH 13.5.

In carbonate systems (Figures 8.13 and 8.14) of 10mM TIC, the $NdCO_3^+$ species has a slight effect on the adsorption edge at pH 5.5, which is undetectable at lower TIC concentrations (Appendix 8.7 & 8.8). $NdCO_3^+$ and $Nd(CO_3)_2^-$ species are dominant between pH 7.5 to pH 10 in 10mM TIC solutions, and which increase the total aqueous Nd concentration by 2 log units and shifts the solubility minima to pH 11.5 at a [Nd(aq)] 10^{-14}M, compared with the equivalent carbonate free system (Figure 8.11). Above pH 11.5 $Nd(OH)_3^0(aq)$ forms the dominant aqueous species and the Nd solubility increases at a similar rate to the carbonate free systems.

The carbonate concentration therefore does reduce the amount of Nd adsorbed onto a goethite surface, however the aqueous concentration (between 10^{-9}M to 10^{-13}) is still likely to be significantly lower than typical analytical detection limits, i.e. from ICP-MS.

A similar reaction constant for other metals e.g. Ca, would be required to predict the actual amount of other cations in solution required to reduce the quantity of lanthanide adsorbed to the surface.

Figure 8.11 Predicted Nd Sorption to goethite with pH
inital solution $[Nd]_{total}$ $5x10^{-7}$M, surface 1g/dm^3 logK 3.8
(Lee and Byrne 1992 & 1993 aqueous data)

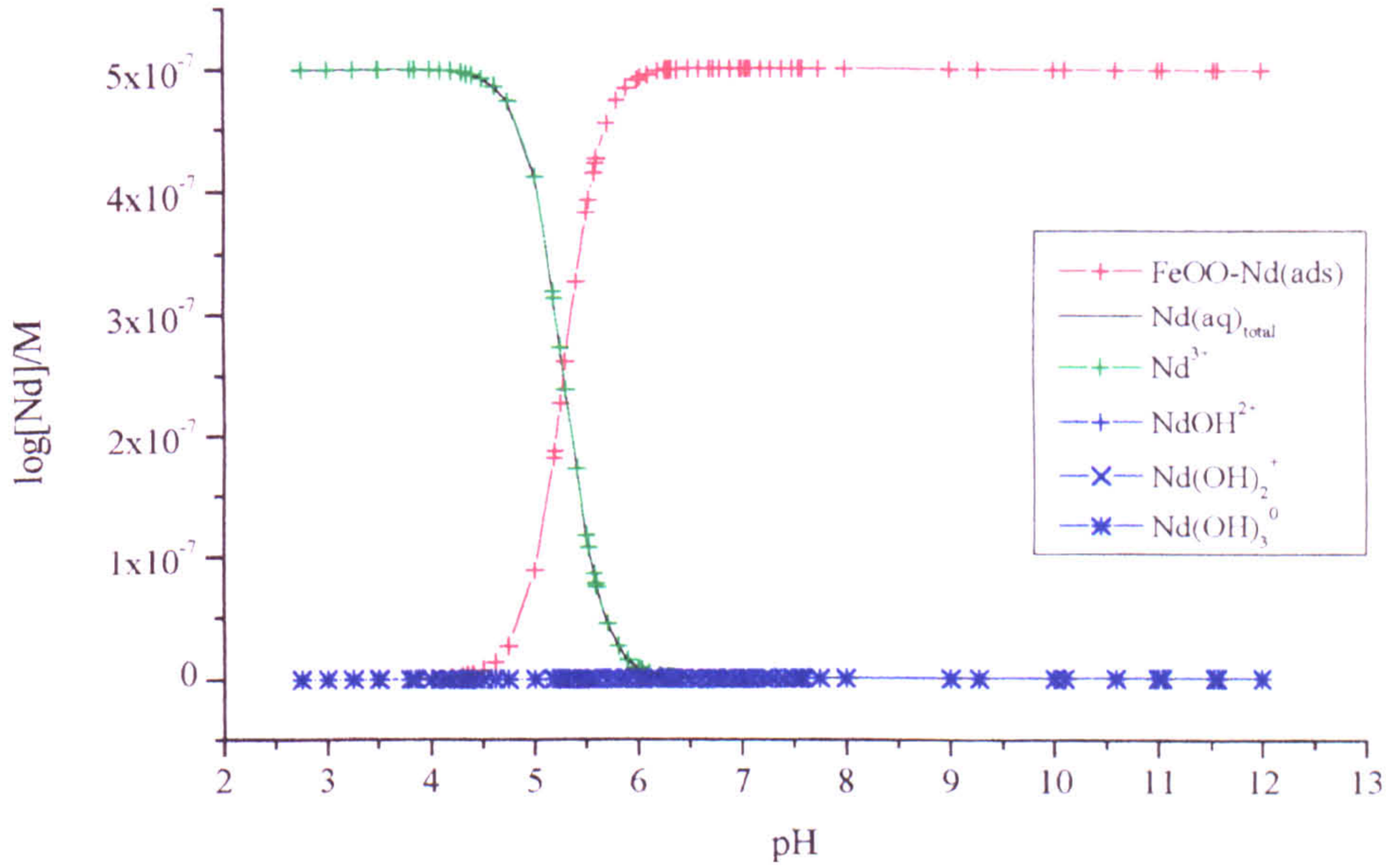

Figure 8.12 Predicted Nd solubility in equilibrium with a goethite surface
initial solution $[Nd]_{total}$ $5x10^{-7}$M, surface 1g/dm^3 logK 3.8
(Lee and Byrne 1992 & 1993 aqueous data)

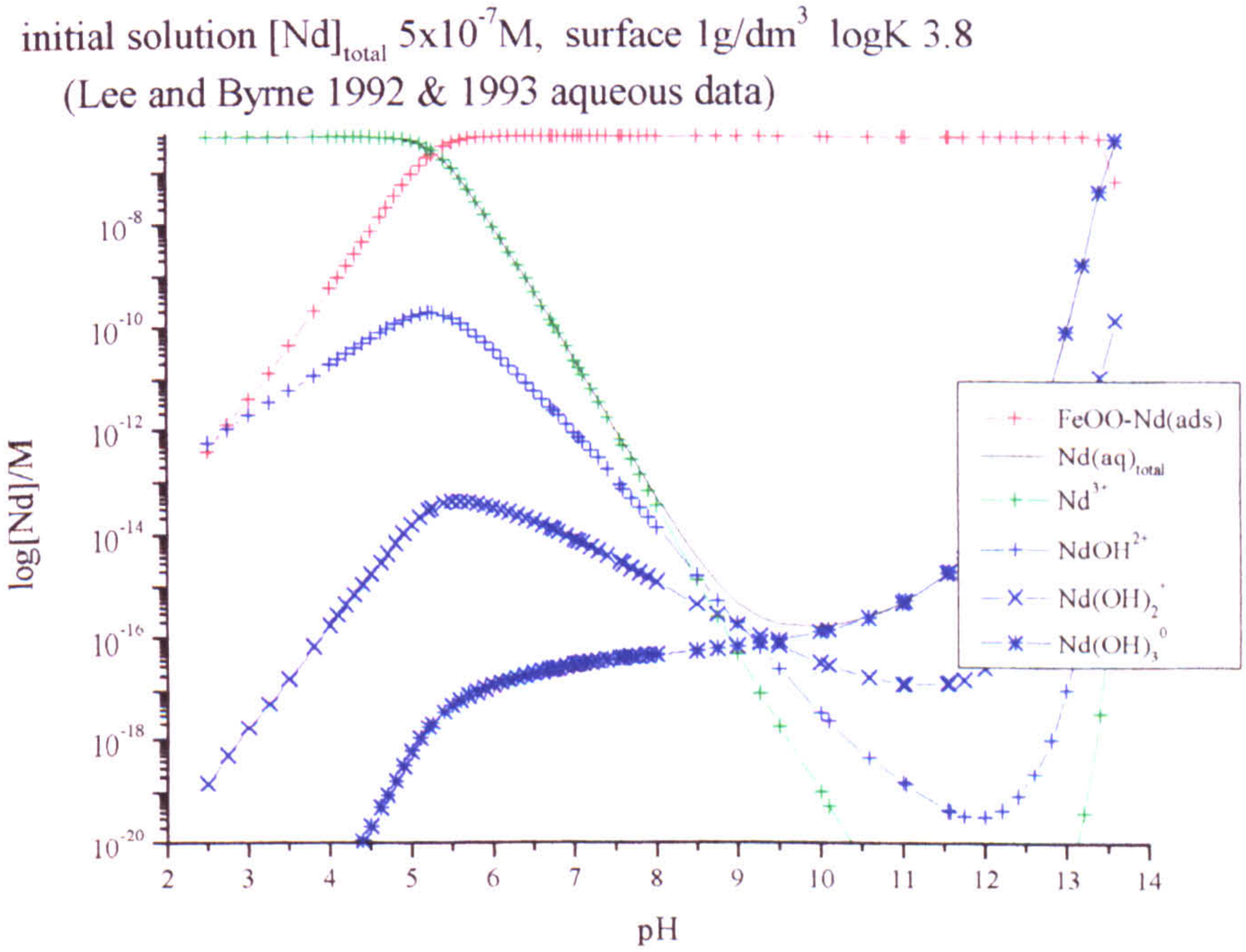

Figure 8.13 Predicted Nd sorption to goethite in 10mM TIC solution with pH initial solution $[Nd]_{total}$ $5x10^{-7}$M surface $1g/dm^3$ logK 3.8 (Lee and Byrne 1992 & 1993 aqueous data)

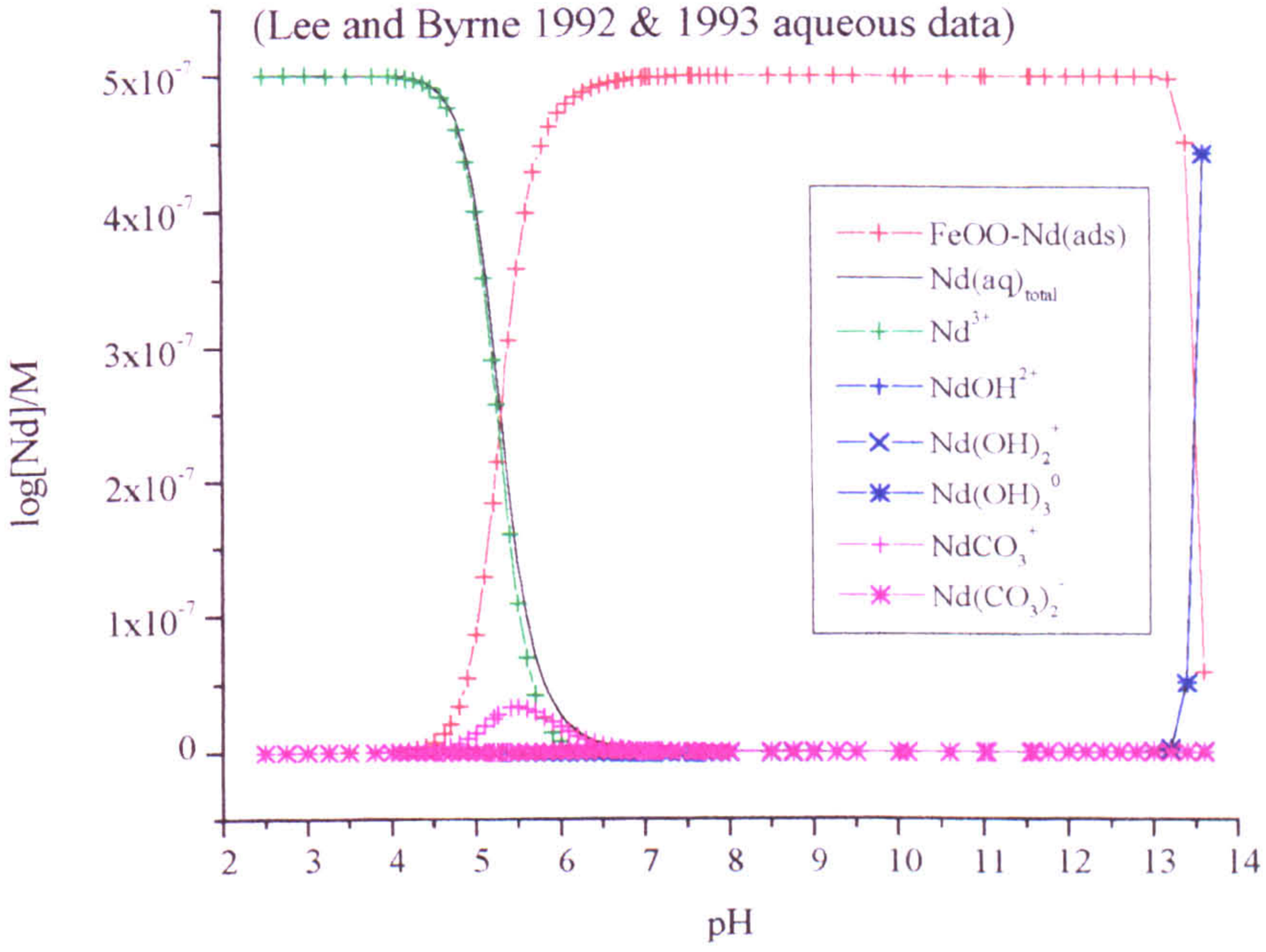

Figure 8.14 Predicted Nd solubility in equilibrium with a goethite surface ($1g/dm^3$) in 10mM TIC solution. Initial solution $[Nd]_{total}$ $5x10^{-7}$M logK 3.8 (Lee and Byrne 1992 & 1993 aqueous data)

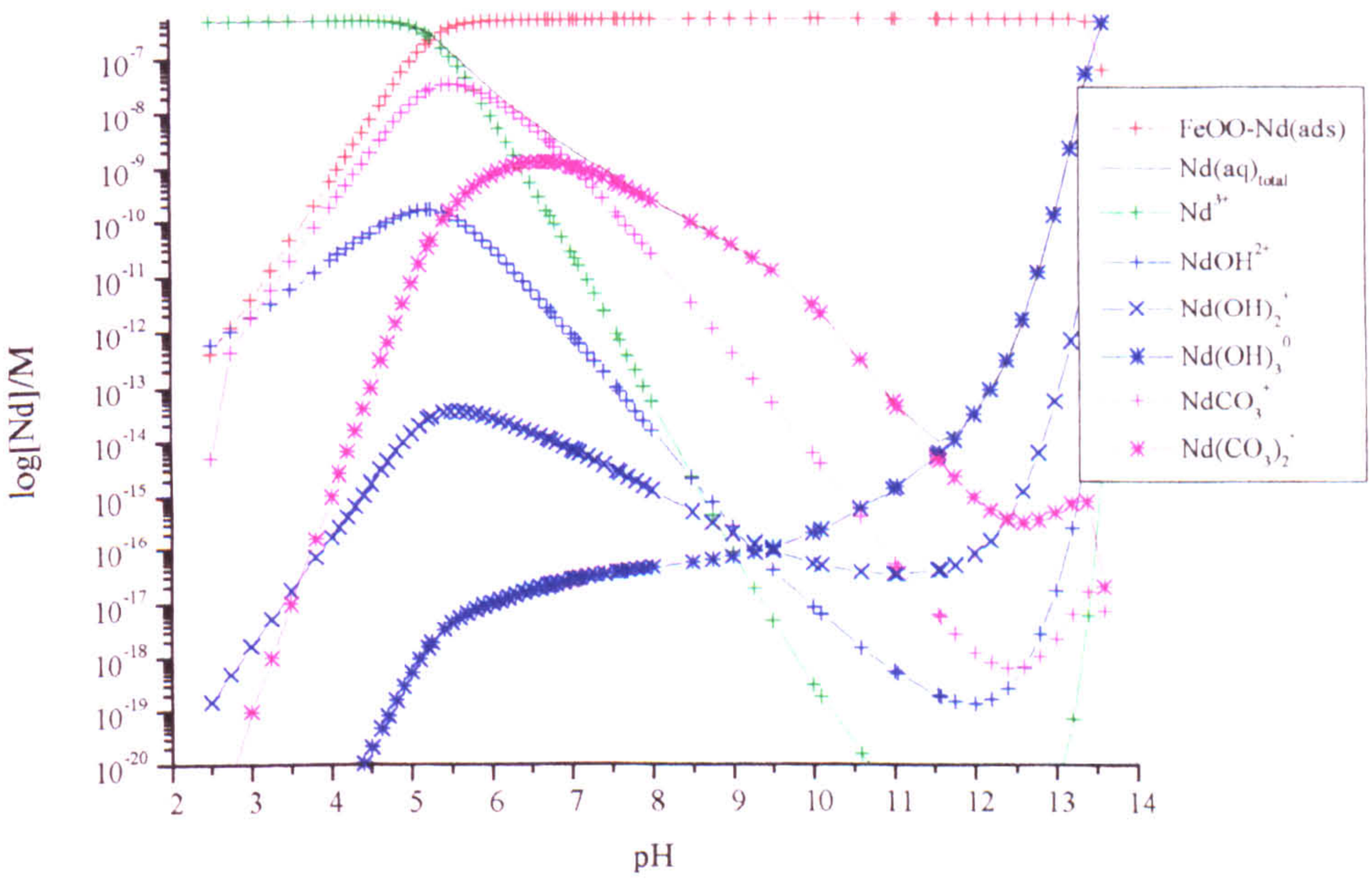

8.5 Discussion

The sorption of lanthanides to iron oxide surfaces, specifically goethite, is a rapid efficient method for the removal of lanthanides from solution and therefore inhibiting lanthanide mobility in an aqueous system. The presence of iron oxides in a solid matrix is likely to reduce aqueous lanthanide (or americium) concentrations to below that of their solubility limit in carbonate solutions. If lanthanides are released slowly into solution from an initial solid matrix; the dissolution of lanthanides from mineral phases has shown that lanthanides tend to remain in the solid phases compared to the release of other cations (Barret, 1992), therefore lanthanide concentrations are unlikely to approach their solubility limit (typically $>10^{-7}$M, Chapter 4). The adsorption to mineral surfaces (for example iron oxides, calcite, clay minerals) therefore remains the major sink for lanthanides. Sorption reactions combined with a slow release from the initial solid matrix, should effectively immobilise lanthanides ions, released either from natural minerals or synthetic phases used to encapsulate nuclear waste.

Fendorf and Fendorf (1997) note that transmission electron microscopy indicates that up to pH 8 sorption occurs as a uniform layer structure over parts of the goethite surface. The lanthanide sorption edge occurs below the goethite PZC (pH 7.8) and therefore the initial uptake must be by hydrolysed Ln^{3+} ions overcoming electrostatic repulsion from a positively charged surface. Surface precipitation of $Ln(OH)_3$ will occur if the lanthanide concentration is above the solubility limit (and typically above pH 8.5) in which $Ln(OH)_3$ aggregates into discrete particles that are not evenly distributed across the surface. The surface may therefore act as a nucleation surface for the precipitation of a solid hydroxide phase. In a similar study on Nd interactions with calcite, Caroll (1992) indicates that calcium carbonate minerals promotes the precipitation of lanthanide carbonate phases by the displacement of Ca^{2+} ions to form a solid solution series which becomes incorporated into the calcite structure.

The distribution coefficient K_d (equation 8.1, after Koeppenkastrop and De Carlo, 1992) describes the equilibrium system between the aqueous concentration and surface phase for specific solution conditions, i.e. pH and assumes the surface is not saturated. However a number of ions can be compared directly from a complex solution onto a mixed solid phase (i.e. soils or sediments Furhamann *et al.*, 1997 or Jarzemba & Manteufel, 1997) for a site specific estimation of the sorption capacity of a solid matrix, or the direct comparison of the sorption capacity of individual mineral surfaces and their proportion in the solid matrix from the K_d value. Such comparisons between the lanthanides Am and Cm are usually good, with K_d values in the order of 10^4 as confirmed by this study (Table 8.4).

The reaction constant (equation 8.4) could not be determined precisely by FITEQL due to insufficient data points across the adsorption edge, most data points were acquired for pH values above the adsorption edge, when above 98% adsorption occurred.

PHREEQC calculations for Nd from pH 2.5 to 12 predicts that there should be above 99.99% uptake of Nd onto the goethite surface above the adsorption edge and the adsorbed concentration was the same for a log K of 2.5 to 5. Variations in the log K could only be distinguished from a slight shift in the adsorption edge to a lower pH with increasing log K in the analytical range $1x10^{-9}$M to $5x10^{-7}$M available for ICP-MS determinations. Further experimental data points are therefore required to clarify the exact equilibrium constant for the sorption process.

The surface complexation model using Equation 8.3 assumes that the adsorption of Ln^{3+} occurs to a single sorption site, but does not differentiate between monodentate, bidentate and tridentate adsorption of a single Ln^{3+} ion. The reaction between aqueous $LnOH^{2+}$ or $Ln(OH)_2^+$ species would increase the adsorption capacity of the oxide surface capacity further than that suggested by

the FeOO-Ln adsorbed complex alone. The adsorption reaction constants are important as even though the percentage uptake diagrams indicate that all the lanthanide ions have been adsorbed to the goethite surface, there are still trace quantities remaining in solution (from 10^{-10}M to 10^{-16}M). These quantities are radiologically important for the actinide analogue elements Am and Cm.

The predicted increase in the lanthanide solubility above pH 12 was not identified from the experimental data which had a maximum pH of pH 11.5. The predicted solubilities of less than 10^{-9}M Ln, are also significantly lower than the detection limit using ICP-MS analysis. A preconcentration stage (requiring a larger sample volume of at least 1dm^3) or radiotracer experiments (and therefore beyond the scope of this study) are required to confirm the predicted lanthanide solubility when in equilibrium with a sorption surface.

The pH remains the controlling factor in the adsorption capacity of lanthanides to mineral surfaces. There is unlikely to be significantly high enough quantities of other equal or higher charged density ions to inhibit lanthanide sorption from the goethite surface; an excess of Ca^{2+} did not displace the lanthanide ions from the goethite surface. Organic coatings on mineral surfaces will reduce the sorption capacity of minerals by reducing the availability of surface sites and possibly altering the surface charge (Fairhurst *et al.*, 1995). The strong sorption capacity of lanthanides to particle surfaces does mean that mobilisation will be possible on inorganic colloidal particles (Sätmark *et al.*, 1996).

The maximum adsorption for the Ce solutions of approximately 90% indicates that the varied mass experiments were carried out below the pH for the top of the adsorption edge. Higher uptake rates would occur at higher pH, however above pH 8 there is also the possibility of CeO_2 precipitation or the oxidation of Ce^{3+} to Ce^{4+} by the goethite surface which would interfere with any sorption calculations. Consequently a larger proportion of Ce would be expected to be removed from solution in the presence of oxide minerals compared to other lanthanides and

accounts for Ce anomalies when Ce co-precipitates with iron oxides from seawater (Zhang *et al.*, 1994)

8.6 References

ATKINSON, R. J., POSNER, A. M., and QUIRK, J. P., (1967) Adsorption of potential-determining ions at the ferric oxide-electrolyte interface. *J. Phys. Chem.* **71** 550-558

BALISTRIERI, L. S., and MURRAY, J. W., (1981) The surface chemistry of goethite (αFeOOH) in major ion seawater. *Amer. J. Sci.* **281** 788-806

BARRET, P., (1992) Short term processes of radionuclide immobilization in cement: A chemical approach. *App. Geochem.(Supp. Issue)* **1** 109-124

BIGHAM, J. M., SCHWERTMANN, U., and PFAB, G., (1996) Influence of pH on mineral speciation in a bioreactor simulating acid mine drainage. *App. Geochem.* **11** 845-849

CARROLL, S. A., (1992) Mechanisms controlling $NdOHCO_3$-$CaCO_3$ solid solution formation. pp89-92 in *Water-Rock Interactions (eds Y. K. Kharaka & A. S. Maest)* Balkema, Amsterdam.

DZOMBAKI, D. A., and MOREL, F. M. M., (1990) Surface complexation modelling: Hydrous ferric oxide. *Wiley* New York

FAIRHURST, A. J., WARWICK, P., AND RICHARDSON, S., (1995) The effect of pH on europium-mineral interactions in the presence of humic acid. *Radiochim. Acta* **69** 103-111

FENDORF, S., and FENDORF, M., (1997) Sorption mechanisms of lanthanum on oxide minerals. *Clays and Minerals* **44** 220-227

FUHRMANN, M., ZHOU, H., NEIHEISEL, J., SCHOONEN, M. A. A., and DYER, R., (1997) Sorption/desorption of radioactive contaminants by sediment from the Kara Sea. *The Science of the Total Environment.* **202** 5-24

ICRP (1979) Limits for intakes of radionuclides by workers. *Annals of the ICRP* **Publication 30 Vol 2** *Pergammon Press Oxford*

JARZEMBA, M. S., AND MANTEUFEL, R. D., (1997) An analytically based model for the simultaneous leaching-chain decay of radionuclides from contaminated ground surface soil layers. *Health Physics* **73** 919-927

KARLTUN, E., (1997) Modelling SO_4^{2-} surface complexation on variable charge minerals: I. H^+ and SO_4^{2-} exchange under different solution conditions. *Eur. J. Soil Sci.* **48** 483-491

KOEPPENKASTROP, D., and DECARLO, E. H., (1993) Uptake of rare-earth elements from solution by metal oxides. *Environ. Sci. Tech.* **27** 1796-1802

PARIDA, K., and DAS, J., (1996) Studies on ferric oxide hydroxides II. Structural properties of goethite samples (α-FeOOH) prepared by homogenous precipitation from $Fe(NO_3)_3$ solution in the presence of sulfate ions. *J. Coll. Interface Sci.* **178** 586-593

SÄTMARK, B., ALBINSSON, Y., and LIANG, L., (1996) Chemical effects of goethite colloid on the transport of radionuclides through a quartz-packed column. *J. Contaminant Hydrology* **21** 231-241

TESSIER, A., RAPIN, F., and CARIGAN, R., (1985) Trace metals in oxic lake sediments: possible adsorption onto iron oxyhydroxides. *Geochim et Cosmochim Acta* **49** 183-194

VENEMA, P., HIEMSTRA, T., and VAN RIEMSDIJK, W. H., (1996) Multisite adsorption of cadmium on goethite. *J. Colloid and Interface Sci.* **183** 515-527

VON GUNTEN, H.R., and BENES, P., (1995) Speciation of radionuclides in the environment. *Radiochim. Acta* **69** 1-29

ZHANG, J., AMAKAWA, H., and NOZAKI, Y., (1994) The comparative behaviours of yttrium and lanthanides in the seawater of the North Pacific. *Geophys. Res. Letts.* **21** 2677-2680

Chapter 9

Conclusions

9.1 REE solubility

A number of phases have been identified in the REE-Carbonate-Sulphate-Sodium-pH-pe system (Table 9.1) all of which can control the lanthanide solubility under certain solution conditions. The aqueous lanthanide solubility is further controlled by the ageing process of the crystalline phases, although this process may not be fully achieved in dilute solutions.

Table 9.1 Lanthanide solid phases in the $Ln\text{-}CO_3^{2-}\text{-}SO_4^{2-}\text{-}Na^+\text{-}pH\text{-}pe$ system

Nd and Eu		Ce	
$NaLn(CO_3)_2$	$NaLn(SO_4)_2$	$NaCe(CO_3)_2$	$NaCe(SO_4)_2$
$Ln_2(CO_3)_3$		$Ce_2(CO_3)_3$	
$LnCO_3OH$	$Ln_2(OH)_4SO_4$	CeO_2	
$Ln(OH)_3$			

In carbonate and hydroxide containing solutions (below 0.1M), precipitation is rapid and limits the aqueous lanthanide concentration to between 10^{-8}M to 10^{-6}M. Ce, Nd and Eu precipitate rapidly when added to excess carbonate and hydroxide ions in solutions above pH 7, The solid phases precipitate initially as an amorphous phase, which crystallises into an identifiable phase in under 2 months. There are only slight decreases in the lanthanide solubility between 1 week and 2 months equilibration. The carbonate phases crystallises into a distinct identifiable phase faster than the hydroxide phases. The carbonate phases also exhibit stronger XRD patterns than the hydroxide phases two months after the initial precipitation from a dilute solution.

The lanthanide carbonates, hydroxides and sulphates are all significantly more soluble in acidic solutions than alkaline solutions. There is a sharp decrease in lanthanide solubility from pH 4 to 10 at all carbonate and sulphate concentrations. The lanthanide solubility limit then remains at an approximately constant level, relatively independent of pH and bulk solution composition.

There are two commonly used experimental techniques for measuring solubility products; precipitation from solution followed by solution analysis, as used here, or the preparation of crystals from concentrated solutions followed by dissolution or heat capacity experiments. The major difference between these two experimental techniques is the state of the crystals. Slow growing crystals (e.g. $Ln(OH)_3$) are likely to be less well defined when grown from a dilute solution, compared to force growing crystals in concentrated and probably high temperature solutions (i.e. between 3M and 5M NaOH, Rao *et al.*, 1996, Diakonov *et al.*, 1998a). These discrepancies can underestimate the solubility product of the solid phase when slow grown and overestimate the solubility products of the same force grown phase. The slow grown crystal is however more likely to predict the amount of REE initially precipitated from solution, an amount which may not increase significantly, if the solid phase does not crystallise out fully.

9.2 Comparisons between the REE and the actinide americium

Similar solid phases have been identified for Am and the REE in the carbonate-pH system. These include $Am_2(CO_3)_3$, $AmCO_3OH$ and $Am(OH)_3$, each of which have solubility products similar to the lanthanides Nd and Eu. The sodium double carbonate has also been reported, $NaAm(CO_3)_2$, but the equivalent americium sulphate phases have not. There are however significant differences in aqueous speciation and association constants for Am, which as yet have no equivalent lanthanide analogue. Therefore a direct comparison and use of Nd and Eu as analogues must be made in the full knowledge of the limitations of the comparison. Direct comparisons of the equivalent aqueous association and solid phase dissociation constants between Am, Nd and Eu indicate that variations between separate studies are often greater than variations between these three elements in the same study. A consistent set of association constants must therefore be determined.

Crystal destabilisation from α-particle release is likely to deform the crystal lattice and inhibit good crystal growth and increase Am solubility from the most thermodynamically stable form. The relatively high solubilities of the precipitated $Nd(OH)_3(s)$ and $Eu(OH)_3(s)$, compared to the force grown hydroxide crystals are therefore likely to predict the actual $Am(OH)_3(s)$ solubility.

9.3 The retardation of REE from waste repositories

If americium or other lanthanides are contained within an ILW repository, the bulk chemistry of the pore waters is likely to be controlled by the in-flowing groundwaters and the equilibrium with a calcium-carbonate-silicate host material to give initially a high pH solution, which will reduce on dilution. The hydroxy-carbonate, hydroxy-sulphate and hydroxide are likely to be the initial solubility limiting phases (and CeO_2 if under the required redox conditions). In carbonate and sulphate solutions between pH 7.5 and 12, the solubility limit of the lanthanide carbonates, hydroxy-carbonates, hydroxy-sulphates, hydroxides and CeO_2 is initially between 10^{-8}M and 10^{-6}M, for Ce, Nd and Eu. Na^+ and CO_3^{2-} activities of less than 20mM are generally too low to support the formation of double salts, such as $NaLn(CO_3)_2.6H_2O$. The solubility of the lanthanide hydroxides and CeO_2 (e.g. Rao *et al.*, 1996, Diakonov *et al.*, 1998a, Diakonov *et al.*, 1998b and Baker *et al.*, 1971), have been reported to be lower than the values determined in this study. The lower solubilities of the crystalline lanthanide hydroxides imply that the lanthanide hydroxy-carbonates are only metastable kinetically formed phases, even though the hydroxycarbonate has been consistently produced by controlling the $pCO_{2(g)}$ of the solution. The hydroxy-carbonate should therefore re-crystallise to the lanthanide hydroxide as the crystals age over time, this observation has not been reported. The lowest lanthanide hydroxide solubilities have been reported from heat capacity measurements of crystals produced in concentrated solutions, which represents the solubility of well defined crystal structures which may only be obtained in

geochemical situations over significant time periods, rather than the solubility products obtained from crystals produced by precipitation from solutions reaching the lanthanide or americium saturation point for an initial amorphous crystal. If the initial reasoning behind nuclear waste disposal of initial isolation and containment until the radioactive waste inventory is reduced, then slow dispersal and dilution throughout the far-field is achieved, therefore a very crystalline precipitate controlling lanthanide retardation is unlikely to occur.

The retardation of lanthanides (and hence americium and curium) must therefore be via other mechanisms, i.e. retention of these elements as part of the altered original host mineral phase, then the sorption of any aqueous lanthanides and actinides released onto mineral surfaces (Chapter 8). The importance of sorption in retarding lanthanide mobility can be seen from natural solutions as the aqueous lanthanide concentrations reported in the literature (reviewed in Chapter 1) are consistently below the solubility limits expected for the lanthanides, except for the concentrations reported in acidic solutions e.g. by Smedly (1991), where aqueous lanthanide concentrations are similar to the NdF_3 solubility limit. These high concentrations occur at a pH below the expected adsorption edge for lanthanides onto mineral surfaces, therefore sorption cannot impede lanthanide mobility in this situation and the aqueous lanthanide concentrations increase towards the solubility limits.

9.4 Recommendations for further study

The major uncertainty in predicting lanthanide chemistry is the aqueous data and association constants. A consistent set of aqueous association constants must be evaluated for a number of lanthanides (e.g. Nd, Sm and Eu) to determine the exact group trends before meaningful comparisons with the other dominant An^{3+} ions (e.g. Am and Cm) as all solubility predictions depend upon the exact aqueous speciation and complex stability. Solubility products calculated using

one set of association constants will give different predicted solubilities each time the database of aqueous association constant is revised.

Solubility products should be derived from heat capacity measurements, precipitation and dissolution experiments, to minimise the discrepancies found between different experimental techniques. The solubility data should be obtained for a series of precipitates and solutions to determine the rate of crystal growth from solutions after the initial precipitation to the equilibrium conditions from dilute solutions, through to the most thermodynamically stable conditions found from aged crystals formed using concentrated reagents. Metastable kinetic phases can therefore be determined to characterise initial solution conditions and the time scales required for a solid-solution reaction to a more thermodynamically stable phase (if any) to occur.

The role of other anions in solution (e.g. phosphates and sulphides) on lanthanide solubility may also be important (as indicated in Chapter 7) in controlling lanthanide mobility, especially if the carbonate activity and the redox potential of equilibrium solutions are variable.

Sorption reactions and not the relatively high solubilities of the carbonate phases may control the retardation of lanthanides and actinide elements. Analogue studies should therefore be directed towards characterising the effects of aqueous species, below their relatively high solubility limit onto mineral surfaces, particularly those found in engineered multiple barrier systems.

9.5 References

BAKER, F. B., HUBER JR., E. J., HOLLEY JR., C. E., and KRIKORIAN, N. H., (1971) Enthalpies of formation of cerium dioxide, cerium sesquicarbide and cerium dicarbide. *J. Chem. Thermodynamics* **3** 77-83

DIAKONOV, I. I., TAGIROV, B. R., and RAGNARSDOTTIR, K. V., (1998a) Standard thermodynamic properties and heat capacity equations for rare earth element hydroxides. *Radiochim. Acta* **81** 107-116

DIAKONOV, I. I., RAGNARSDOTTIR, K. V., and TAGIROV, B. R., (1998b) Standard thermodynamic properties and heat capacity equations for rare earth element hydroxides. II. Ce(III)-, Pr-, Sm-, Eu(III)-, Gd-, Tb, Dy-, Ho-, Er-, Tm-, Yb-, and Y-hydroxides. Comparisons of thermochemical and solubility data. *Chem. Geol.* **151** 327-347

RAO, L. F., RAI, D. P., FELMY, A. R., FULTON, R. W., and NOVAK, C. F., (1996) Solubility of $Nd(OH)_3$ in 0.1M NaCl aqueous solution at 25°C and 90°C. *Radiochim. Acta* **72** 151-155

SMEDLY, P. L., (1991) The geochemistry of REE in groundwater from the Carnmenellis area SW England. *Geochim. Cosmochim. Acta* **55** 2767-2779

Appendix

For Chapters 4, 5, 6, 7 & 8

Appendix 4.1 Summary of $NaCe(CO_3)_2$ sodium double carbonate solution analysis

Sample	Phase	Log Ksp	Equilibrium	pH	[Ln]/M	[Na]/ M	[TIC]/ M	[Cl⁻]/ M	Log $a_{Ce^{3+}}$	Log $a_{CO_3^{2-}}$	Log a_{Na^+}
Ce93a	$NaCe(CO_3)_2$	-24.58	7 months	8.91	$9.0x10^{-8}$	1.95	0.96	1.01	-15.98	-3.97	-0.65
Ce93b	$NaCe(CO_3)_2$	-24.12	7 months	8.72	$2.3x10^{-7}$	1.95	0.96	1.01	-15.54	-3.97	-0.65
Ce93c	$NaCe(CO_3)_2$	-24.21	7 months	8.65	$1.8x10^{-7}$	1.95	0.96	1.01	-15.64	-3.96	-0.65
Ce93d	$NaCe(CO_3)_2$	-24.29	7 months	8.67	$1.5x10^{-7}$	1.95	0.96	1.01	-15.72	-3.96	-0.65
Ce93e	$NaCe(CO_3)_2$	-24.18	7 months	8.67	$2.0x10^{-7}$	1.95	0.96	1.01	-15.60	-3.96	-0.65
Ce94a	$NaCe(CO_3)_2$	-20.92	7 months	8.64	$2.7x10^{-7}$	0.97	0.96	1.01	-13.84	-3.16	-0.76
Ce94b	$NaCe(CO_3)_2$	-20.76	7 months	8.64	$4.0x10^{-7}$	0.97	0.96	1.01	-13.68	-3.16	-0.76
Ce94c	$NaCe(CO_3)_2$	-21.05	7 months	8.60	$1.9x10^{-7}$	0.97	0.96	1.01	-14.00	-3.15	-0.75
Ce94d	$NaCe(CO_3)_2$	-21.02	7 months	8.60	$2.0x10^{-7}$	0.97	0.96	1.01	-13.97	-3.15	-0.75
Ce94e	$NaCe(CO_3)_2$	-21.36	7 months	8.67	9.6x10-8	0.97	0.96	1.01	-14.29	-3.16	-0.76

Appendix 4.2a Summary of $NaNd(CO_3)_2$ sodium double carbonate solution analysis

Sample	Phase	Log Ksp	Equilibrium	pH	[Ln]/M	[Na]/ mM	[TIC]/ mM	[Cl]/ mM	Log $a_{Nd^{3+}}$	Log $a_{CO_3^{2-}}$	Log a_{Na^+}
NdC 7a	$NaNd(CO_3)_2$	-20.20	5 weeks	10.67	$2.8x10^{-6}$	50	10	32	-13.45	-2.66	-1.44
NdC 7b	$NaNd(CO_3)_2$	-21.51	5 weeks	10.72	$1.4x10^{-7}$	50	10	32	-14.77	-2.65	-1.44
NdC 7c	$NaNd(CO_3)_2$	-21.20	5 weeks	10.63	$2.8x10^{-7}$	50	10	32	-14.44	-2.66	-1.44
NdC 7d	$NaNd(CO_3)_2$	-20.81	5 weeks	10.55	$6.8x10^{-7}$	50	10	32	-14.03	-2.67	-1.44
NdC 7e	$NaNd(CO_3)_2$	-21.94	5 weeks	10.71	$5.2x10^{-8}$	50	10	32	-15.20	-2.65	-1.44
NdC 7f	$NaNd(CO_3)_2$	-21.12	5 weeks	10.69	$3.4x10^{-7}$	50	10	32	-14.38	-2.65	-1.44
NdC 8a	$NaNd(CO_3)_2$	-19.86	5 weeks	10.82	$5.0x10^{-6}$	70	10	32	-13.67	-2.44	-1.33
NdC 8b	$NaNd(CO_3)_2$	-21.09	5 weeks	10.83	$3.0x10^{-7}$	70	10	32	-14.89	-2.44	-1.33
NdC 8c	$NaNd(CO_3)_2$	-20.56	5 weeks	10.82	$1.0x10^{-6}$	70	10	32	-14.36	-2.44	-1.33
NdC 8d	$NaNd(CO_3)_2$	-21.39	5 weeks	10.86	$1.5x10^{-7}$	70	10	32	-15.19	-2.43	-1.33
NdC 8e	$NaNd(CO_3)_2$	-20.59	5 weeks	10.83	$9.4x10^{-7}$	70	10	32	-14.39	-2.44	-1.33
NdC 8f	$NaNd(CO_3)_2$	-20.80	5 weeks	10.84	$5.8x10^{-7}$	70	10	32	-14.60	-2.44	-1.33
NdC 14a	$NaNd(CO_3)_2$	-19.45	4 months	11.33	$6.8x10^{-6}$	400	200		-14.09	-2.28	-0.81
NdC 14b	$NaNd(CO_3)_2$	-20.54	4 months	11.33	$5.6x10^{-7}$	400	200		-15.17	-2.28	-0.81
NdC 14c	$NaNd(CO_3)_2$	-20.49	4 months	11.33	$6.2x10^{-7}$	400	200		-15.13	-2.28	-0.81
NdC 14d	$NaNd(CO_3)_2$	-20.49	4 months	11.33	$6.2x10^{-7}$	400	200		-15.13	-2.28	-0.81
NdC 14e	$NaNd(CO_3)_2$	-20.45	4 months	11.33	$6.8x10^{-7}$	400	200		-15.09	-2.28	-0.81
Nd82 B1	$NaNd(CO_3)_2$	-21.28	8 months	8.62	$3.1x10^{-7}$	32.5	15	15	-12.40	-3.65	-1.58
Nd83 B2	$NaNd(CO_3)_2$	-21.30	12 months	9.62	$3.1x10^{-7}$	32.5	15	15	-14.09	-2.81	-1.60
Nd84 B3	$NaNd(CO_3)_2$	-21.55	12 months	9.58	$1.7x10^{-7}$	32.5	15	15	-14.30	-2.83	-1.60
Nd85 B4	$NaNd(CO_3)_2$	-21.41	12 months	9.66	$2.4x10^{-7}$	32.	15	15	-14.25	-2.80	-1.60
Nd86 B5	$NaNd(CO_3)_2$	-20.99	12 months	9.26	$6.1x10^{-7}$	32.5	15	15	-13.26	-3.07	-1.59

Appendix 4.2b Summary of $NaNd(CO_3)_2$ sodium double carbonate solution analysis

Sample	Phase	Log Ksp	Equilibrium	pH	[Ln]/M	[Na]/ mM	[TIC]/ mM	[Cl⁻]/ mM	Log $a_{Nd^{3+}}$	Log $a_{CO_3^{2-}}$	Log a_{Na^+}
Nd 154a	$NaNd(CO_3)_2$	-20.20	2 months	11.53	$1.6x10^{-6}$	170	62	45.8	-14.73	-2.22	-1.03
Nd 154b	$NaNd(CO_3)_2$	-20.23	2 months	11.52	$1.5x10^{-6}$	170	62	45.8	-14.76	-2.22	-1.03
Nd 154c	$NaNd(CO_3)_2$	-21.20	2 months	11.54	$2.0x10^{-6}$	170	62	45.8	-14.65	-2.22	-1.03
Nd 154d	$NaNd(CO_3)_2$	-20.21	2 months	11.52	$1.6x10^{-6}$	170	62	45.8	-14.74	-2.22	-1.03
Nd 155a	$NaNd(CO_3)_2$	-20.37	2 months	11.49	$1.3x10^{-6}$	135.5	62	11	-14.92	-2.16	-1.13
Nd 155b	$NaNd(CO_3)_2$	-20.19	2 months	11.50	$1.9x10^{-6}$	135.5	62	11	-14.74	-2.16	-1.13
Nd 155c	$NaNd(CO_3)_2$	-20.49	2 months	11.52	$9.9x10^{-7}$	135.5	62	11	-15.04	-2.16	-1.13
Nd 155d	$NaNd(CO_3)_2$	-20.24	2 months	11.52	$1.7x10^{-6}$	135.5	62	11	-14.79	-2.16	-1.13
Nd 162a	$NaNd(CO_3)_2$	-18.94	14 days	10.70	$6.5x10^{-5}$	35.1	10.1	16	-12.28	-2.54	-1.57
Nd 162b	$NaNd(CO_3)_2$	-22.17	6 weeks	11.01	$4.0x10^{-8}$	35.0	10.0	16	-12.57	-2.51	-1.57
Nd 162c	$NaNd(CO_3)_2$	-19.21	14 days	10.76	$3.5x10^{-5}$	35.0	10.1	16	-12.57	-2.54	-1.57
Nd 162d	$NaNd(CO_3)_2$	-19.58	14 days	10.78	$1.5x10^{-5}$	35.0	10.0	16	-12.94	-2.53	-1.57
Nd 163a	$NaNd(CO_3)_2$	-21.94	6 weeks	11.03	$5.0x10^{-8}$	55.0	20.0	16	-15.85	-2.34	-1.42
Nd 163b	$NaNd(CO_3)_2$	-19.22	14 days	10.69	$2.6x10^{-5}$	55.0	20.0	16	-13.08	-2.36	-1.41
Nd 163c	$NaNd(CO_3)_2$	-21.41	6 weeks	11.02	$1.7x10^{-7}$	55.0	20.0	16	-15.32	-2.34	-1.42
Nd 163d	$NaNd(CO_3)_2$	-21.79	6 weeks	11.02	$7.0x10^{-8}$	55.0	20.0	16	-15.70	-2.34	-1.42
Nd 164a	$NaNd(CO_3)_2$	-21.16	6 weeks	11.07	$2.5x10^{-7}$	75.0	30.0	16	-15.33	-2.26	-1.31
Nd 164b	$NaNd(CO_3)_2$	-21.44	6 weeks	11.11	$1.3x10^{-7}$	75.0	30.0	16	-15.62	-2.25	-1.31
Nd 164c	$NaNd(CO_3)_2$	-21.20	6 weeks	11.11	$2.3x10^{-7}$	75.0	30.0	16	-15.37	-2.25	-1.31
Nd 164d	$NaNd(CO_3)_2$	-21.14	6 weeks	11.11	$2.6x10^{-7}$	75.0	30.0	16	-15.32	-2.25	-1.31

Appendix 4.2c Summary of $NaNd(CO_3)_2$ sodium double carbonate solution analysis

Sample	Phase	Log K	Equilibrium	pH	[Ln]/M	[Na]/ mM	[K]/ mM	[TIC]/ mM	[Cl]/ mM	Log $a_{Nd^{3+}}$	Log $a_{CO_3^{2-}}$	Log a_{Na^+}
Nd 166a	$NaNd(CO_3)_2$	-20.50	2.5 months	10.98	$1.1x10^{-6}$	70		20	32	-14.42	-2.38	-1.31
Nd 166b	$NaNd(CO_3)_2$	-20.77	2.5 months	11.01	$6.0x10^{-7}$	70		20	32	-14.68	-2.38	-1.32
Nd 166c	$NaNd(CO_3)_2$	-20.15	2.5 months	11.02	$2.5x10^{-6}$	70		20	32	-14.07	-2.38	-1.32
Nd 166d	$NaNd(CO_3)_2$	-20.94	2.5 months	11.01	$4.0x10^{-7}$	70		20	32	-14.86	-2.38	-1.32

Appendix 4.3a Summary of $NaEu(CO_3)_2$ sodium double carbonate solution analysis

Sample	Phase	Log Ksp	Equilibrium	pH	[Ln]/M	[Na]/ mM	[TIC]/ mM	[Cl⁻]/ mM	Log $a_{Eu^{3+}}$	Log $a_{CO_3^{2-}}$	Log a_{Na^+}
EuC 7a	$NaEu(CO_3)_2$	-19.66	5 weeks	10.42	$2.0x10^{-5}$	50	10	32	-12.82	-2.70	-1.44
EuC 7b	$NaEu(CO_3)_2$	-19.70	5 weeks	10.45	$1.8x10^{-5}$	50	10	32	-13.80	-2.70	-1.44
EuC 7c	$NaEu(CO_3)_2$	-21.12	5 weeks	10.60	$7.0x10^{-7}$	50	10	32	-14.35	-2.67	-1.44
EuC 7d	$NaEu(CO_3)_2$	-19.78	5 weeks	10.40	$1.5x10^{-5}$	50	10	32	-12.94	-2.70	-1.44
EuC 7e	$NaEu(CO_3)_2$	-19.64	5 weeks	10.53	$2.1x10^{-5}$	50	10	32	-12.85	-2.68	-1.44
EuC 7f	$NaEu(CO_3)_2$	-19.58	5 weeks	10.50	$2.4x10^{-5}$	50	10	32	-12.78	-2.44	-1.33
EuC 8a	$NaEu(CO_3)_2$	-21.34	8 weeks	10.74	$3.4x10^{-7}$	70	20	32	-15.13	-2.44	-1.33
EuC 8b	$NaEu(CO_3)_2$	-21.34	8 weeks	10.73	$3.4x10^{-7}$	70	20	32	-15.13	-2.44	-1.33
EuC 8c	$NaEu(CO_3)_2$	-21.65	8 weeks	10.74	$1.7x10^{-7}$	70	20	32	-15.44	-2.44	-1.33
EuC 8d	$NaEu(CO_3)_2$	-20.83	8 weeks	10.74	$1.1x10^{-6}$	70	20	32	-14.62	-2.44	-1.33
EuC 8e	$NaEu(CO_3)_2$	-20.89	8 weeks	10.74	$9.6x10^{-7}$	70	20	32	-14.68	-2.44	-1.33
EuC 8f	$NaEu(CO_3)_2$	-21.51	8 weeks	10.74	$2.3x10^{-7}$	70	20	32	-15.30	-2.44	-1.33
EuC 14a	$NaEu(CO_3)_2$	-19.71	4 months	11.53	$1.4x10^{-5}$	400	200		-14.34	-2.28	-0.81
EuC 14b	$NaEu(CO_3)_2$	-19.79	4 months	11.58	$1.4x10^{-5}$	400	200		-14.42	-2.28	-0.81
EuC 14d	$NaEu(CO_3)_2$	-20.14	4 months	11.60	$6.8x10^{-6}$	400	200		-14.76	-2.28	-0.81
EuC 14e	$NaEu(CO_3)_2$	-19.75	4 months	11.56	$1.4x10^{-5}$	400	200		-14.38	-2.28	-0.81
Eu 54a	$NaEu(CO_3)_2$	-20.65	3 months	11.48	$1.9x10^{-6}$	171	62.1	45.8	-15.09	-2.26	-1.04
Eu 54b	$NaEu(CO_3)_2$	-20.53	3 months	11.48	$2.5x10^{-6}$	171	62.1	45.8	-14.97	-2.26	-1.04
Eu 54c	$NaEu(CO_3)_2$	-20.56	3 months	11.49	$2.4x10^{-6}$	171	62.1	45.8	-15.00	-2.26	-1.04
Eu 54d	$NaEu(CO_3)_2$	-20.54	3 months	11.49	2.5x10-6	171	62.1	45.8	-14.98	-2.26	-1.04

Appendix 4.3b Summary of $NaEu(CO_3)_2$ sodium double carbonate solution analysis

Sample	Phase	Log Ksp	Equilibrium	pH	[Ln]/M	[Na]/ mM	[TIC]/ mM	[Cl]/ mM	Log $a_{Eu^{3+}}$	Log $a_{CO_3^{2-}}$	Log a_{Na^+}
Eu 55a	$NaEu(CO_3)_2$	-20.63	3 months	11.50	$2.1x10^{-6}$	135.5	62.1	11	-15.16	-2.17	-1.13
Eu 55b	$NaEu(CO_3)_2$	-20.63	3 months	11.50	$2.1x10^{-6}$	135.5	62.1	11	-15.16	-2.17	-1.13
Eu 55c	$NaEu(CO_3)_2$	-20.41	3 months	11.50	$3.5x10^{-6}$	135.5	62.1	11	-14.98	-2.17	-1.13
Eu 55d	$NaEu(CO_3)_2$	-20.54	3 months	11.50	$2.6x10^{-6}$	135.5	62.1	11	-15.07	-2.17	-1.13
Eu 58a	$NaEu(CO_3)_2$	-20.73	9 days	10.80	$1.4x10^{-6}$	70.6	20	32	-14.53	-2.44	-1.33
Eu 58b	$NaEu(CO_3)_2$	-20.94	9 days	10.80	$8.7x10^{-7}$	70.6	20	32	-14.78	-2.44	-1.33
Eu 58 c	$NaEu(CO_3)_2$	-20.88	9 days	10.80	$1.0x10^{-6}$	70.6	20	32	-14.68	-2.44	-1.33
Eu 58d	$NaEu(CO_3)_2$	-20.84	9 days	10.80	$1.1x10^{-6}$	70.6	20	32	-14.64	-2.44	-1.33
Eu 59a	$NaEu(CO_3)_2$	-21.11	3 months	10.91	$6.0x10^{-7}$	70	20	32	-14.92	-2.43	-1.33
Eu 59b	$NaEu(CO_3)_2$	-21.49	3 months	10.94	$2.5x10^{-7}$	70	20	32	-15.30	-2.43	-1.33
Eu 59c	$NaEu(CO_3)_2$	-21.20	3 months	10.94	$5.0x10^{-7}$	70	20	32	-15.01	-2.43	-1.33
Eu 59d	$NaEu(CO_3)_2$	-20.94	3 months	10.94	$9.0x10^{-7}$	70	20	32	-14.76	-2.43	-1.33
Eu 64a	$NaEu(CO_3)_2$	-19.78	2.5 months	10.13	$2.5x10^{-5}$	25.0	5.05	16	-12.17	-2.96	-1.69
Eu 64b	$NaEu(CO_3)_2$	-19.04	2.5 months	10.21	$1.4x10^{-4}$	25.1	5.28	16	-11.49	-2.93	-1.69
Eu 64c	$NaEu(CO_3)_2$	-19.01	2.5 months	10.24	$1.5x10^{-4}$	25.1	5.30	16	-11.48	-2.92	-1.70
Eu 64d	$NaEu(CO_3)_2$	-20.11	2.5 months	10.36	$1.2x10^{-5}$	25.0	5.02	16	-12.66	-2.89	-1.61
Eu 65a	$NaEu(CO_3)_2$	-20.36	2.5 months	10.67	$5.4x10^{-6}$	35	10	16	-13.63	-2.58	-1.58
Eu 65b	$NaEu(CO_3)_2$	-20.18	2.5 months	10.64	$8.0x10^{-6}$	35	10	16	-13.44	-2.58	-1.58
Eu 65c	$NaEu(CO_3)_2$	-20.18	2.5 months	10.69	$8.1x10^{-6}$	35	10	16	-13.46	-2.58	-1.58
Eu 65d	$NaEu(CO_3)_2$	-20.65	2.5 months	10.86	$2.9x10^{-6}$	35	10	16	-13.96	-2.55	-1.58
Eu 66a	$NaEu(CO_3)_2$	-20.37	2.5 months	10.93	$4.0x10^{-6}$	55	20	16	-14.22	-2.36	-1.42
Eu 66b	$NaEu(CO_3)_2$	-19.66	2.5 months	10.89	$2.0x10^{-5}$	55	20	16	-13.51	-2.37	-1.42
Eu 66c	$NaEu(CO_3)_2$	-19.82	2.5 months	10.93	$1.4x10^{-5}$	55	20	16	-13.67	-2.37	-1.42
Eu 66d	$NaEu(CO_3)_2$	-19.68	2.5 months	10.89	$2.0x10^{-5}$	55	20	16	-13.52	-2.37	-1.42

Appendix 4.4 Summary of $Ce_2(CO_3)_3$ cerium carbonate solution analysis

Sample	Phase	Log Ksp	Equilibrium	pH	[Ln]/M	[Na]/ mM	[K]/ mM	[TIC]/ mM	[Cl]/ mM	Log $a_{Ce^{3+}}$	Log $a_{CO_3^{2-}}$
CeC 5a	$Ce_2(CO_3)_3$	-30.33	5 weeks	5.61	$6.4x10^{-4}$		30	16.0	32	-4.15	-7.35
CeC 5b	$Ce_2(CO_3)_3$	-30.22	5 weeks	5.64	$6.2x10^{-4}$		30	15.9	32	-4.17	-7.30
CeC 5c	$Ce_2(CO_3)_3$	-30.23	5 weeks	5.64	$6.1x10^{-4}$		30	15.9	32	-4.18	-7.30
CeC 5d	$Ce_2(CO_3)_3$	-29.83	5 weeks	5.74	$5.8x10^{-4}$		30	15.8	32	-4.23	-7.12
CeC 5e	$Ce_2(CO_3)_3$	-30.08	5 weeks	5.69	$5.6x10^{-4}$		30	15.8	32	-4.23	-7.21
CeC 5f	$Ce_2(CO_3)_3$	-30.11	5 weeks	5.70	$5.1x10^{-4}$		30	15.8	32	-4.27	-7.19
CeC 5g	$Ce_2(CO_3)_3$	-29.94	5 weeks	5.70	$6.2x10^{-4}$		30	15.9	32	-4.19	-7.19
CeC 5h	$Ce_2(CO_3)_3$	-30.03	5 weeks	5.69	$5.9x10^{-4}$		30	15.9	32	-4.21	-7.21
CeC 5i	$Ce_2(CO_3)_3$	-29.92	5 weeks	5.76	$4.7x10^{-4}$		30	15.7	32	-4.33	-7.09
CeC 5j	$Ce_2(CO_3)_3$	-30.01	5 weeks	5.70	$5.7x10^{-4}$		30	15.9	32	-4.23	-7.19
Ce 79a	$Ce_2(CO_3)_3$	-35.70	10 months	7.90	$5.3x10^{-8}$	20		14.1	12	-11.29	-4.38
Ce 79b	$Ce_2(CO_3)_3$	-37.01	10 months	8.44	$2.0x10^{-8}$	20		14.0	12	-12.74	-3.84
Ce 79c	$Ce_2(CO_3)_3$	-35.26	10 months	7.89	$8.8x10^{-8}$	20		14.1	12	-11.06	-438
Ce 79d	$Ce_2(CO_3)_3$	-36.17	10 months	8.00	$3.4x10^{-8}$	20		14.1	12	-11.67	-4.28
Ce 95a	$Ce_2(CO_3)_3$	-33.00	2 months	7.08	$8.0x10^{-7}$	20		12.5	16	-8.56	-5.30
Ce 95b	$Ce_2(CO_3)_3$	-33.00	2 months	7.11	$8.0x10^{-7}$	20		12.5	16	-8.59	-5.27
Ce 95c	$Ce_2(CO_3)_3$	-33.60	2 months	7.11	$4.0x10^{-7}$	20		12.5	16	-8.91	-5.26
Ce 95 d	$Ce_2(CO_3)_3$	-33.25	2 months	7.23	$6.0x10^{-7}$	20		12.5	16	-8.93	-5.13

Appendix 4.5 Summary of $Nd_2(CO_3)_3$ neodymium carbonate solution analysis

Sample	Phase	Log Ksp	Equilibrium	pH	[Ln]/M	[Na]/ mM	[K]/ mM	[TIC]/ mM	[Cl]/ mM	Log $a_{Nd^{3+}}$	Log $a_{CO_3^{2-}}$
Nd 77A1	$Nd_2(CO_3)_3$	-34.03	2 months	7.29	$6.6x10^{-7}$	25		17.5	15	-9.62	-4.93
Nd 78A2	$Nd_2(CO_3)_3$	-34.61	2 months	7.35	$3.5x10^{-7}$	25		17.5	15	-10.02	-4.86
Nd 79A3	$Nd_2(CO_3)_3$	-34.06	2 months	7.25	$6.2x10^{-7}$	25		17.5	15	-9.59	-4.96
Nd 80A4	$Nd_2(CO_3)_3$	-34.77	2 months	7.28	$2.8x10^{-7}$	25		17.5	15	-9.98	-4.93
Nd 81A5	$Nd_2(CO_3)_3$	-34.66	2 months	7.30	$3.2x10^{-7}$	25		17.5	15	-9.95	-4.92
NdC 5a	$Nd_2(CO_3)_3$	-32.04	5 weeks	5.51	$1.7x10^{-4}$		30	15.2	32	-4.70	-7.55
NdC 5b	$Nd_2(CO_3)_3$	-31.81	5 weeks	5.52	$2.1x10^{-4}$		30	15.3	32	-4.61	-7.53
NdC 5c	$Nd_2(CO_3)_3$	-31.95	5 weeks	5.54	$1.6x10^{-4}$		30	15.2	32	-4.73	-7.49
NdC 5d	$Nd_2(CO_3)_3$	-31.67	5 weeks	5.55	$2.1x10^{-4}$		30	15.3	32	-4.62	-7.48
NdC 6a	$Nd_2(CO_3)_3$	-32.56	5 weeks	9.73	$2.1x10^{-4}$		40.6	5.0	32	-11.50	-3.19
NdC 6b	$Nd_2(CO_3)_3$	-32.65	5 weeks	9.88	$2.1x10^{-4}$		40.6	5.0	32	-11.68	-3.10
NdC 6c	$Nd_2(CO_3)_3$	-33.70	5 weeks	9.31	$1.0x10^{-5}$		40.6	5.0	32	-11.19	-3.50
NdC 6d	$Nd_2(CO_3)_3$	-32.10	5 weeks	9.23	$2.3x10^{-5}$		40.6	5.0	32	-10.69	-3.57
NdC 6e	$Nd_2(CO_3)_3$	-32.05	5 weeks	9.22	$2.4x10^{-5}$		40.6	5.0	32	-10.66	-3.58
Nd 170a	$Nd_2(CO_3)_3$	-32.14	2 months	6.70	$5.1x10^{-6}$	20		12.5	16	-7.47	-5.74
Nd 170b	$Nd_2(CO_3)_3$	-33.43	2 months	6.65	$1.2x10^{-6}$	20		12.5	16	-8.01	-5.80
Nd 170c	$Nd_2(CO_3)_3$	-32.86	2 months	6.65	$2.3x10^{-6}$	20		12.5	16	-7.73	-5.80
Nd 170d	$Nd_2(CO_3)_3$	-33.40	2 months	6.69	$1.2x10^{-6}$	20		12.5	16	-8.08	-5.75

Appendix 4.6 Summary of $Eu_2(CO_3)_3$ europium carbonate solution analysis

Sample	Phase	Log Ksp	Equilibrium	pH	[Ln]/M	[K]/ mM	[TIC]/ mM	[Cl⁻]/ mM	Log $a_{Eu^{3+}}$	Log $a_{CO_3^{2-}}$
EuC 5a	$Eu_2(CO_3)_3$	-31.41	5 weeks	5.39	$7.9x10^{-4}$	30	16.2	32	-4.08	-7.75
EuC 5b	$Eu_2(CO_3)_3$	-31.50	5 weeks	5.37	$8.0x10^{-4}$	30	16.2	32	-4.07	-7.79
EuC 5c	$Eu_2(CO_3)_3$	-32.40	5 weeks	5.20	$7.7x10^{-4}$	30	16.2	32	-4.04	-8.11
EuC 5d	$Eu_2(CO_3)_3$	-32.16	5 weeks	5.24	$7.9x10^{-4}$	30	16.2	32	-4.04	-8.03
EuC 6a	$Eu_2(CO_3)_3$	-31.52	5 weeks	8.55	$4.6x10^{-5}$	40.6	5.0	32	-9.45	-4.21
EuC 6b	$Eu_2(CO_3)_3$	-33.38	5 weeks	8.62	$5.8x10^{-6}$	40.6	5.0	32	-10.50	-4.13
EuC 6c	$Eu_2(CO_3)_3$	-34.35	5 weeks	8.50	$1.7x10^{-6}$	40.6	5.0	32	-10.80	-4.25
EuC 6d	$Eu_2(CO_3)_3$	-34.16	5 weeks	8.67	$2.5x10^{-6}$	40.6	5.0	32	-10.96	-4.08
EuC 6e	$Eu_2(CO_3)_3$	-33.68	5 weeks	8.62	$4.1x10^{-6}$	40.6	5.0	32	-10.65	-4.13

Appendix 4.7 Summary of $NdCO_3OH$ hydroxy-carbonate solution analysis

Sample	Phase	Log Ksp	log K	Equilibrium	pH	[Ln]/M	[Na]/ mM	[K]/ mM	[TIC]/ mM	[Cl]/ mM	Log $a_{Ln^{3+}}$	Log $a_{CO_3^{2-}}$
Nd87 C1	$NdCO_3OH$	-19.55	-5.55	12 months	9.78	$2.0x10^{-6}$	15		0.002	15	-8.83	-6.50
Nd88 C2	$NdCO_3OH$	-19.33	-5.33	12 months	9.32	$2.0x10^{-6}$	15		0.002	15	-7.77	-6.87
Nd89 C3	$NdCO_3OH$	-22.03	-8.03	12 months	10.01	$1.5x10^{-7}$	15		0.00015	15	-10.56	-7.47
Nd90 C4	$NdCO_3OH$	-21.37	-7.37	12 months	10.05	$3.4x10^{-7}$	15		0.00034	15	-10.32	-7.10
Nd91 C5	$NdCO_3OH$	-21.85	-7.85	12 months	9.90	$1.6x10^{-7}$	15		0.00016	15	-10.24	-7.51
Nd 156a	$NdCO_3OH$	-20.99	-6.99	3.5 months	10.33	$9.0x10^{-7}$		78	92.5	15	-15.27	-2.05
Nd 156b	$NdCO_3OH$	-21.08	-7.08	3.5 months	10.32	$7.5x10^{-7}$		78	92.5	15	-15.35	-2.05
Nd 156c	$NdCO_3OH$	-20.74	-6.74	3.5 months	10.32	$1.7x10^{-7}$		78	92.5	15	-15.01	-2.05
Nd 156d	$NdCO_3OH$	-21.01	-7.01	3.5 months	10.32	$8.8x10^{-7}$		78	92.5	15	-15.28	-2.05
Nd 169a	$NdCO_3OH$	-17.45	-3.45	2.5 months	7.04	$2.95x0^{-3}$		30.5	2.95	32	-3.93	-6.56
Nd 169b	$NdCO_3OH$	-17.50	-3.50	2.5 months	6.96	$3.25x0^{-3}$		30.5	3.25	32	-3.87	-6.58
Nd 169c	$NdCO_3OH$	-17.66	-3.66	2.5 months	6.86	$2.95x0^{-3}$		30.5	2.95	32	-3.86	-6.67
Nd 169d	$NdCO_3OH$	-17.78	-3.78	2.5 months	6.79	2.8^{x10-3}		30.5	2.80	32	-3.84	-6.73

Appendix 4.8 Summary of $EuCO_3OH$ hydroxy-carbonate solution analysis

Sample	Phase	Log Ksp	log K	Equilibrium	pH	[Ln]/M	[Na]/ mM	[K]/ mM	[TIC]/ mM	[Cl]/ mM	Log $a_{Ln^{3+}}$	Log $a_{CO_3^{2-}}$
EuC 9a	$EuCO_3OH$	-18.77	-4.77	2 months	6.65	$9.23x10^{-4}$	30.5		0.91	32	-4.18	-7.25
EuC 9b	$EuCO_3OH$	-18.70	-4.70	2 months	6.56	$1.32x10^{-3}$	30.5		1.31	32	-4.04	-7.21
EuC 9d	$EuCO_3OH$	-18.54	-4.54	2 months	6.83	$8.90x10^{-4}$	30.5		0.88	32	-4.26	-7.11
EuC 9e	$EuCO_3OH$	-18.45	-4.45	2 months	6.81	$1.10x10^{-4}$	30.5		1.09	32	-4.20	-7.07

Appendix 4.9 Summary of $Nd(OH)_3$ neodymium hydroxide solution analysis

Sample	Phase	Log Ksp	LogK	Equilibrium	pH	[Ln]/M	[Na]/ mM	[Cl⁻]/ mM	Log $a_{Ln^{3+}}$
NdC 13a	$Nd(OH)_3$	-19.85	22.15	4 months	12.79	$5.6x10^{-5}$	100		-16.22
NdC 13b	$Nd(OH)_3$	-21.69	20.31	4 months	12.77	$8.1x10^{-7}$	100		-18.00
NdC 13c	$Nd(OH)_3$	-21.20	20.80	4 months	12.78	$2.5x10^{-6}$	100		-17.54
NdC 13d	$Nd(OH)_3$	-20.58	21.42	4 months	10.74	$1.1x10^{-5}$	0		-10.80
Nd92 D1	$Nd(OH)_3$	-21.15	20.85	12 months	11.85	$2.8x10^{-6}$	25	15	-14.70
Nd93 D2	$Nd(OH)_3$	-21.10	20.90	12 months	11.84	$3.2x10^{-6}$	25	15	-14.62
Nd94 D3	$Nd(OH)_3$	-22.01	19.99	12 months	11.87	$3.9x10^{-7}$	25	15	-15.62
Nd95 D4	$Nd(OH)_3$	-21.65	20.35	12 months	11.87	$8.9x10^{-7}$	25	15	-15.26
Nd96 D5	$Nd(OH)_3$	-21.83	20.17	12 months	11.88	$5.9x10^{-7}$	25	15	-15.50
Nd 167a	$Nd(OH)_3$	-22.00	20.00	12 months	12.25	$4.0x10^{-7}$	49.8	32	-16.75
Nd 167c	$Nd(OH)_3$	-21.90	20.05	12 months	12.27	$5.0x10^{-7}$	49.8	32	-16.71
Nd167d	$Nd(OH)_3$	-21.95	20.59	12 months	12.28	$4.5x10^{-7}$	49.8	32	-16.78

Appendix 4.10 Summary of $Eu(OH)_3$ europium hydroxide solution analysis

Sample	Phase	Log Ksp	LogK	Equilibrium	pH	[Ln]/M	[Na]/ mM	[Cl]/ mM	Log $a_{Ln^{3+}}$
Eu 60a	$Eu(OH)_3$	-23.11	18.89	3 months	12.17	$3.0x10^{-7}$	49.8	32	-17.62
Eu 60b	$Eu(OH)_3$	-23.11	18.89	3 months	12.21	$3.0x10^{-7}$	49.8	32	-17.74
Eu 60d	$Eu(OH)_3$	-22.69	19.31	3 months	12.28	$8.0x10^{-7}$	49.8	32	-17.52
EuC 13a	$Eu(OH)_3$	-22.53	19.45	4 months	13.03	$1.1x10^{-6}$	100		-19.63
EuC 13b	$Eu(OH)_3$	-22.69	19.31	4 months	13.26	$7.9x10^{-7}$	100		-20.46
EuC 13c	$Eu(OH)_3$	-22.73	19.27	4 months	13.23	$7.2x10^{-7}$	100		-20.41
EuC 13d	$Eu(OH)_3$	-22.65	19.35	4 months	13.22	$8.6x10^{-7}$	100		-20.31

Appendix 4.11 Summary of CeO_2 solution analysis

Sample	Phase	Log K	Equilibrium	pH	pe	[Ln]/M	[Na]/ mM	$[SO_4^{2-}]$/ mM	[Cl]/ mM	Log $a_{Ce^{3+}}$
CeOH 1a	CeO_2	30.93	3 months	11.43	-0.98	$1.8x10^{-7}$	50		30	-13.81
CeOH 1b	CeO_2	31.21	3 months	11.91	-1.01	$1.2x10^{-7}$	50		30	-15.42
CeOH 1c	CeO_2	30.73	3 months	11.93	-1.01	$3.8x10^{-8}$	50		30	-15.98
CeOH 1d	CeO_2	30.89	3 months	11.93	-1.01	$5.5x10^{-8}$	50		30	-15.82
CeOH 1e	CeO_2	31.05	3 months	11.95	-0.98	$7.1x10^{-8}$	50		30	-15.77
CeS6d	CeO_2	30.41	4 months	11.51	-1.18	$7.2x10^{-8}$	102	3.6	22	-14.45
CeS7d	CeO_2	29.42	4 months	11.43	-1.35	$1.3x10^{-8}$	174	7.25	22	-14.95

Appendix 4.12 Summary of $KNd(CO_3)_2$ potassium double carbonate solution analysis

Sample	Phase	Log K	Equilibrium	pH	[Ln]/M	[K]/ mM	[TIC]/ mM	[Cl]/ mM	Log $a_{Nd^{3+}}$	Log $a_{CO_3^{2-}}$	Log a_{K^+}
Nd 157a	$KNd(CO_3)_2$	-19.19	3 months	10.44	$1.4x10^{-5}$	190	96	15	-13.90	-2.15	-0.99
Nd 157b	$KNd(CO_3)_2$	-19.16	3 months	10.45	$1.5x10^{-5}$	190	96	15	-13.88	-2.15	-0.99
Nd 157c	$KNd(CO_3)_2$	-19.17	3 months	10.45	$1.5x10^{-5}$	190	96	15	-13.89	-2.15	-0.99
Nd 157d	$KNd(CO_3)_2$	-19.16	3 months	10.45	$1.5x10^{-5}$	190	96	15	-13.88	-2.15	-0.99
Nd 157e	$KNd(CO_3)_2$	-19.18	3 months	10.45	$1.5x10^{-5}$	190	96	15	-13.89	-2.15	-0.99

Appendix 4.13a The aqueous speciation of 10^{-7}M Nd in 0.01mM TIC after Lee & Byrne (1992 & 1993) at 298.15K and 1 atm pressure

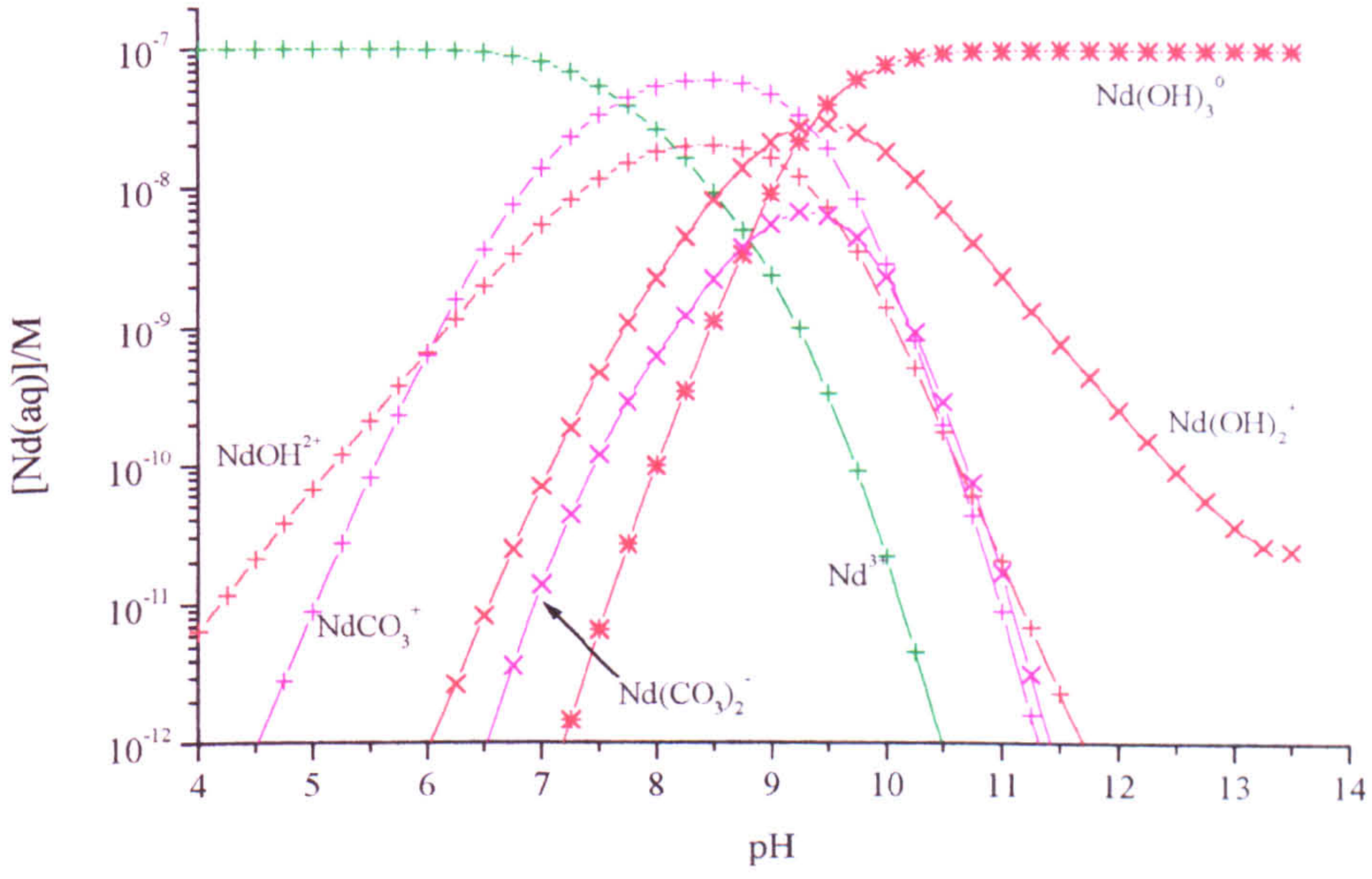

Appendix 4.13b The aqueous speciation of 10^{-7}M Nd in 0.01mM TIC after Lee & Byrne (1992 & 1993) at 298.15K and 1 atm pressure

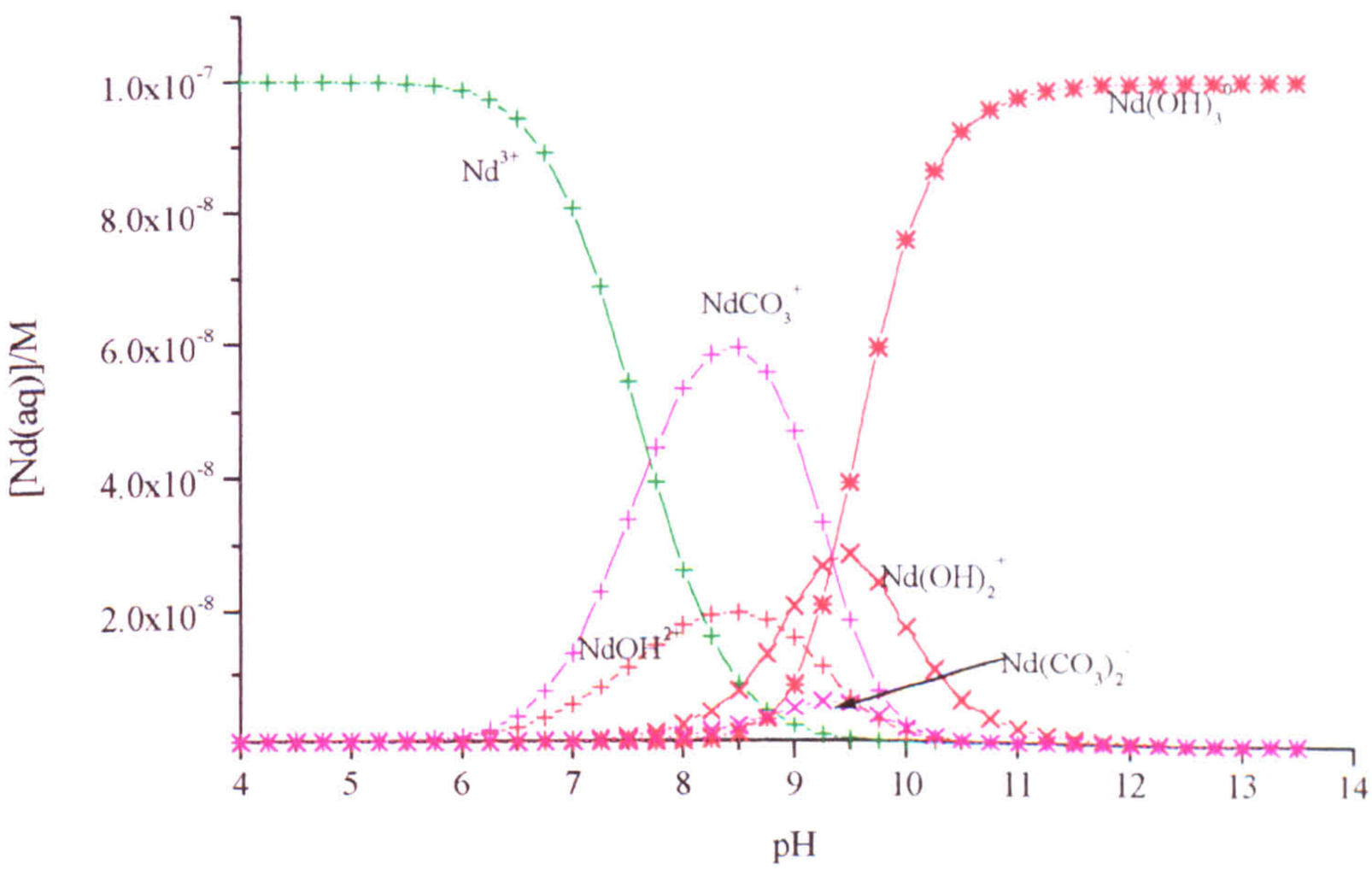

Appendix 4.14 Neodymium aqueous-aqueous phase relations
(after Lee & Byrne, 1992 and 1993)

Nd^{3+}	↔	$NdOH^{2+}$	pH 8.16
$NdOH^{2+}$	↔	$Nd(OH)_2^+$	pH 8.89
$Nd(OH)_2^+$	↔	$Nd(OH)_3^0$	pH 9.36
$NdCO_3^+$	↔	Nd^{3+}	$\log[CO_3^{2-}] = -7.67$
$NdCO_3^+$	↔	$NdOH^{2+}$	$\log[CO_3^{2-}] = pH-15.85$
$NdCO_3^+$	↔	$Nd(OH)_2^+$	$\log[CO_3^{2-}] = 2pH-24.74$
$NdCO_3^+$	↔	$Nd(OH)_3^0$	$\log[CO_3^{2-}] = 3pH-34.10$
$NdCO_3^+$	↔	$Nd(CO_3)_2^-$	$\log[CO_3^{2-}] = -5.10$
$Nd(CO_3)_2^-$	↔	$Nd(OH)_3^0$	$\log[CO_3^{2-}] = {}^1/_2(3pH-39.20)$

Appendix 4.15 Neodymium solid-aqueous phase relations
(aqueous data after Lee & Byrne, 1992 and 1993, and solid phase data, this work)

$Nd(OH)_3$	↔	Nd^{3+}	$pH = {}^1/_3(20.60 - \log[Nd^{3+}])$
	↔	$NdOH^{2+}$	$pH = {}^1/_2(12.44 - \log[NdOH^{2+}])$
	↔	$Nd(OH)_2^+$	$pH = (3.55 - \log[Nd(OH)_2^+])$
	↔	$Nd(OH)_3^0$	$\log[Nd(OH)_3^0] = -5.8$ $(1.5\times10^{-6}\ M)$
	↔	$NdCO_3^+$	$\log[CO_3^{2-}] = 3pH + \log[NdCO_3^+] - 28.29$
	↔	$Nd(CO_3)_2^-$	$\log[CO_3^{2-}] = {}^1/_2[3pH + \log[Nd(CO_3)_2^-] - 33.68]$
	↔	$Nd(CO_3)_3^{3-}$	
$NdCO_3OH$	↔	Nd^{3+}	$\log[CO_3^{2-}] = -1(pH + \log[Nd^{3+}] + 5.87)$
	↔	$NdOH^{2+}$	$\log[CO_3^{2-}] = -1(\log[NdOH^{2+}] + 14.02)$
	↔	$Nd(OH)_2^+$	$\log[CO_3^{2-}] = pH - \log[Nd(OH)_2^+] - 22.91$
	↔	$Nd(OH)_3^0$	$\log[CO_3^{2-}] = 2pH - \log[Nd(OH)_3^0] - 32.28$
	↔	$NdCO_3^+$	$pH = 1.82 - \log[NdCO_3^+]$
	↔	$Nd(CO_3)_2^-$	$\log[CO_3^{2-}] = pH + \log[Nd(CO_3)_2^-] - 7.22$
$Nd_2(CO_3)_3$	↔	Nd^{3+}	$\log[CO_3^{2-}] = {}^{-1}/_3(2\log[Nd^{3+}] + 34.43)$
	↔	$NdOH^{2+}$	$\log[CO_3^{2-}] = {}^1/_3(2pH - 2\log[NdOH^{2+}] - 50.73)$
	↔	$Nd(OH)_2^+$	$\log[CO_3^{2-}] = {}^1/_3(4pH - 2\log[Nd(OH)_2^+] - 68.51)$
	↔	$Nd(OH)_3^0$	$\log[CO_3^{2-}] = {}^1/_3(6pH - 2\log[Nd(OH)_3^0] - 87.24)$
	↔	$NdCO_3^+$	$\log[CO_3^{2-}] = -2\log[NdCO_3^+] - 19.04$
	↔	$Nd(CO_3)_2^-$	$\log[CO_3^{2-}] = 2\log[Nd(CO_3)_2^-] + 8.11$
$NaNd(CO_3)_2$	↔	Nd^{3+}	$\log[CO_3^{2-}] = {}^{-1}/_2(\log[Na^+] + \log[Nd^{3+}] + 20.97)$
	↔	$NdOH^{2+}$	$\log[CO_3^{2-}] = {}^1/_2(pH - \log[Na^+] - \log[NdOH^{2+}] - 29.07)$
	↔	$Nd(OH)_2^+$	$\log[CO_3^{2-}] = {}^1/_2(2pH - \log[Na^+] - \log[Nd(OH)_2^+] - 38.01)$
	↔	$Nd(OH)_3^0$	$\log[CO_3^{2-}] = {}^1/_2(3pH - \log[Na^+] - \log[Nd(OH)_3^0] - 47.37)$
	↔	$NdCO_3^+$	$\log[CO_3^{2-}] = -1(\log[Na^+] + \log[NdCO_3^+] + 13.28)$
	↔	$Nd(CO_3)_2^-$	$\log[Nd(CO_3)_2^-] = -1(\log[Na^+] + 7.88)$

Appendix 4.16 The aqueous speciation and solubility of Nd in equilibrium with $Nd(OH)_3$ at 298.15K and 1 atm pressure [TIC] = 50mM

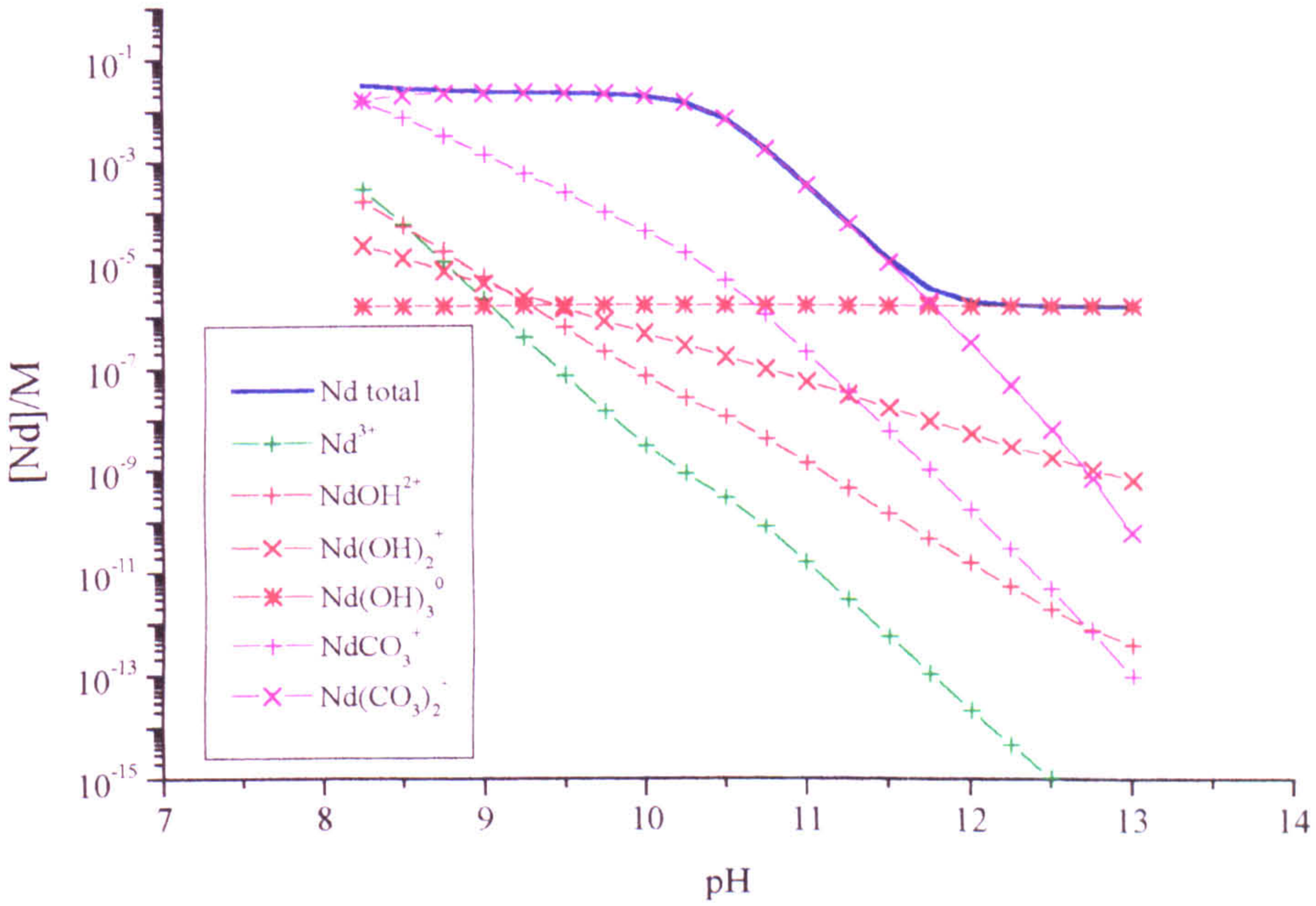

Appendix 4.17 The aqueous speciation and solubility of Nd in equilibrium with $Nd_2((CO)_3)_3$ at 298.15K and 1 atm pressure [TIC] = 50mM

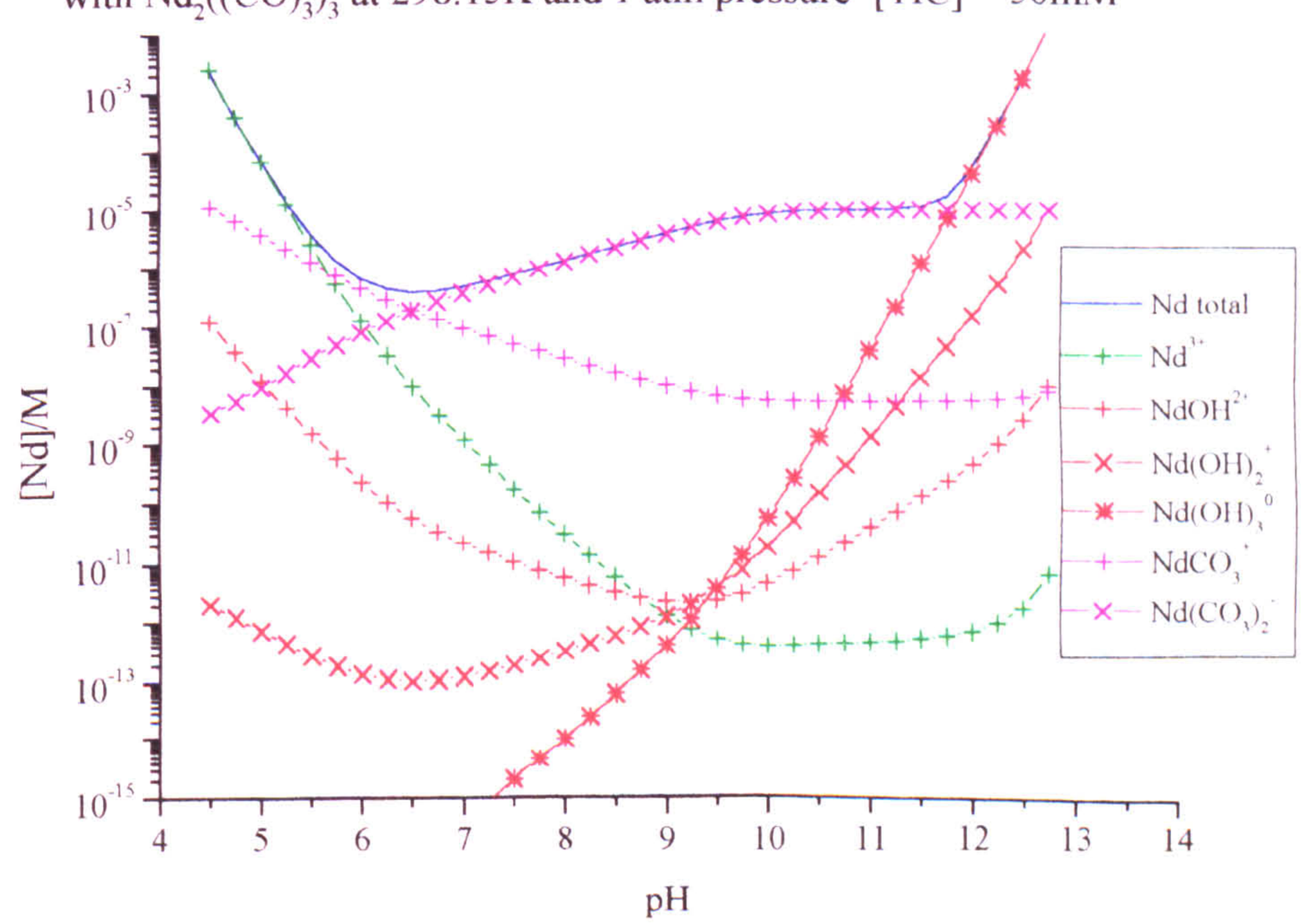

Appendix 4.18 The aqueous speciation and solubility of Nd in equilibrium with $NaNd((CO)_3)_2$ at 298.15K and 1 atm pressure [TIC] = 50mM

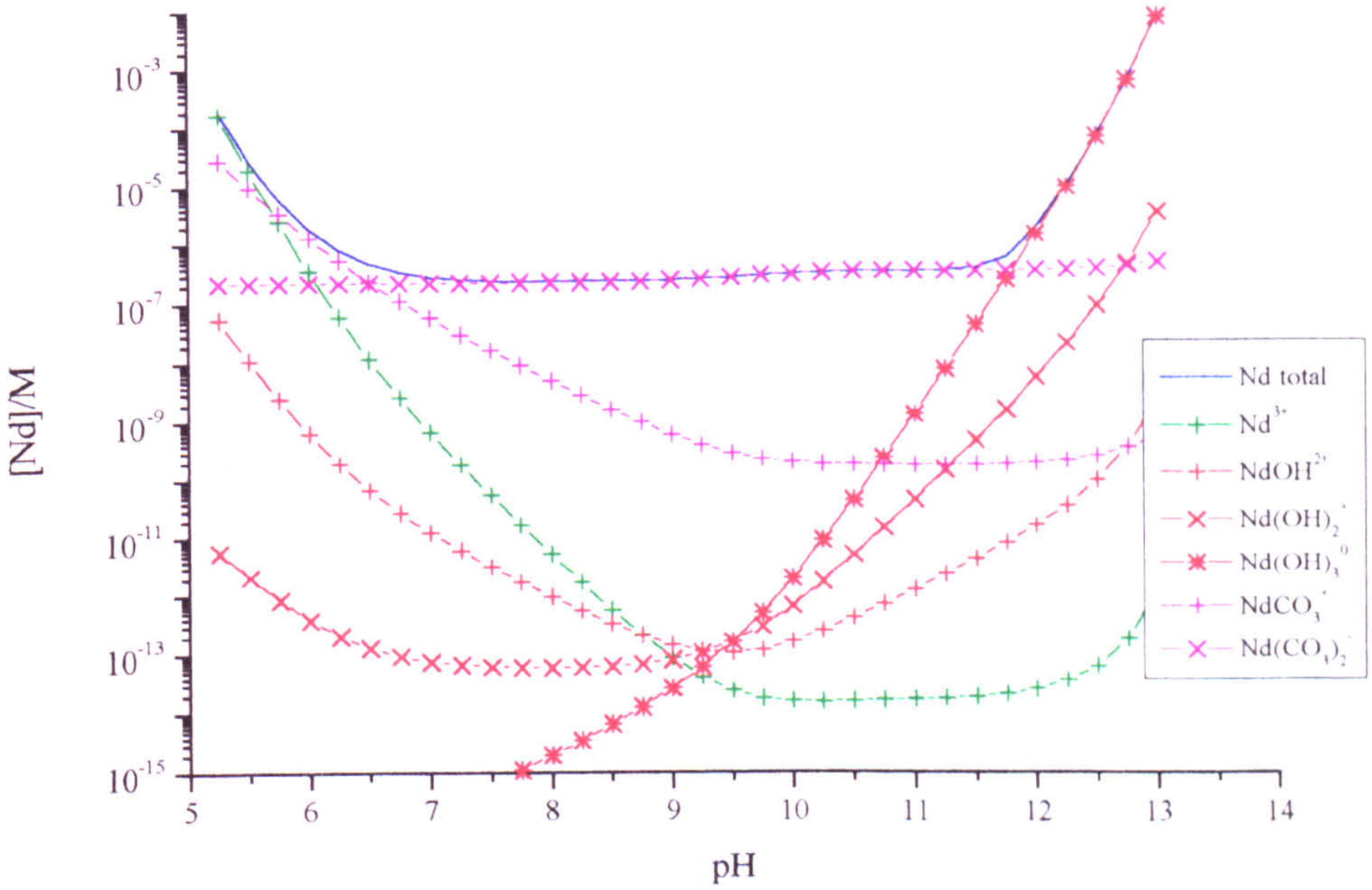

Appendix 5.1 XRD patterns for $NaLn(CO_3)_2.6H_2O$ alteration when dried under varied drying conditions

Solid Phase	$NaNd(CO_3)_2$ $.6H_2O$	$Nd_2(CO_3)_3$ $.8H_2O$	Nd moist atmosphere	Eu moist atmosphere	Nd air dried	Eu air dried	Nd dessicator	Eu dessicator	Nd oven	Eu oven
	JCPDS Ref Pattern		20 weeks	20 weeks	20 weeks	20 weeks	5 days	5 days	10 minutes	10 minutes
	30-1223	29-918								
d-spacing (Å)	13.30		13.864	13.587	12.700	12.773				
		8.410			8.407	8.632	8.355	8.277	8.670	8.674
	6.610		6.715	6.679	6.600	6.667				
						6.567				
					6.442	6.400				
		4.710					4.610	4.563		
		4.430	4.432	4.420	4.587	4.408	4.447	4.396		
	4.370		4.311	4.299	4.383					
					4.314					
		4.150			4.242	4.287	4.227	4.226	4.298	4.303
							4.049			
					3.601	3.627	3.582	3.348	3.617	3.588
	3.280	3.230	3.306	3.300	3.277	3.293			3.386	3.369
		3.020			3.242		3.128	3.110	3.135	3.127
		2.979			2.835		2.831	2.820	2.858	2.861
	2.620	2.565	2.637	2.611	2.622	2.628	2.613	2.607	2.618	2.606
					2.598	2.577		2.409	2.438	2.409
	2.180		2.193	2.174	2.168	2.187	2.126	2.122	2.140	2.143
		2.055			2.083		2.030	1.925	2.037	2.030
	1.870		1.877	1.877	1.861	1.874			1.803	1.797
		1.374			1.304	1.307	1.394	1.387	1.362	1.364

Appendix 5.2 XRD patterns of the alteration of the oven dried (120°C) alteration of $NaNd(CO_3)_2.6H_2O$ to dehydrated $Nd_2(CO_3)_3$

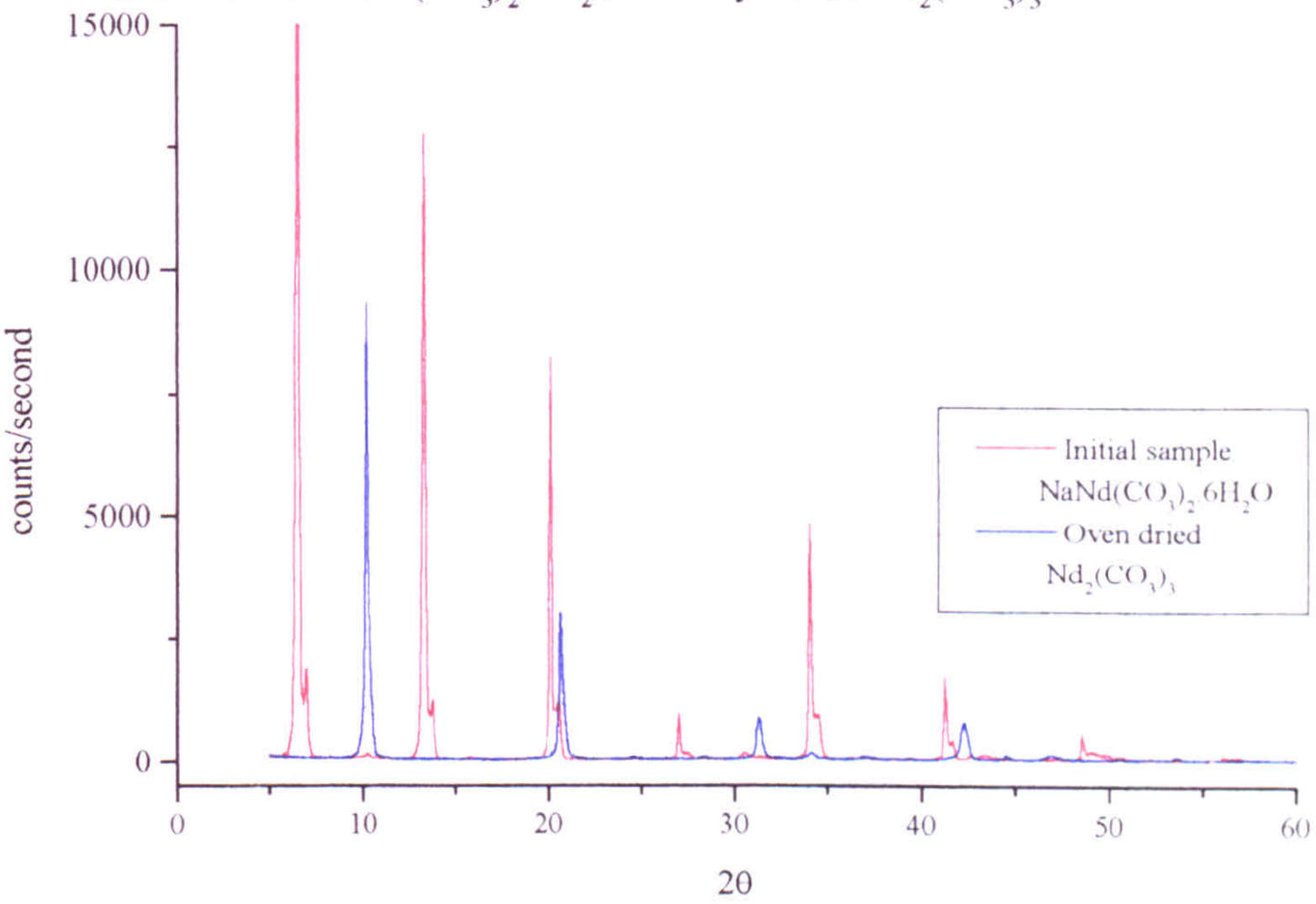

Appendix 5.3 XRD patterns of the alteration of the oven dried (120°C) alteration of $NaEu(CO_3)_2.6H_2O$ to dehydrated $Eu_2(CO_3)_3$

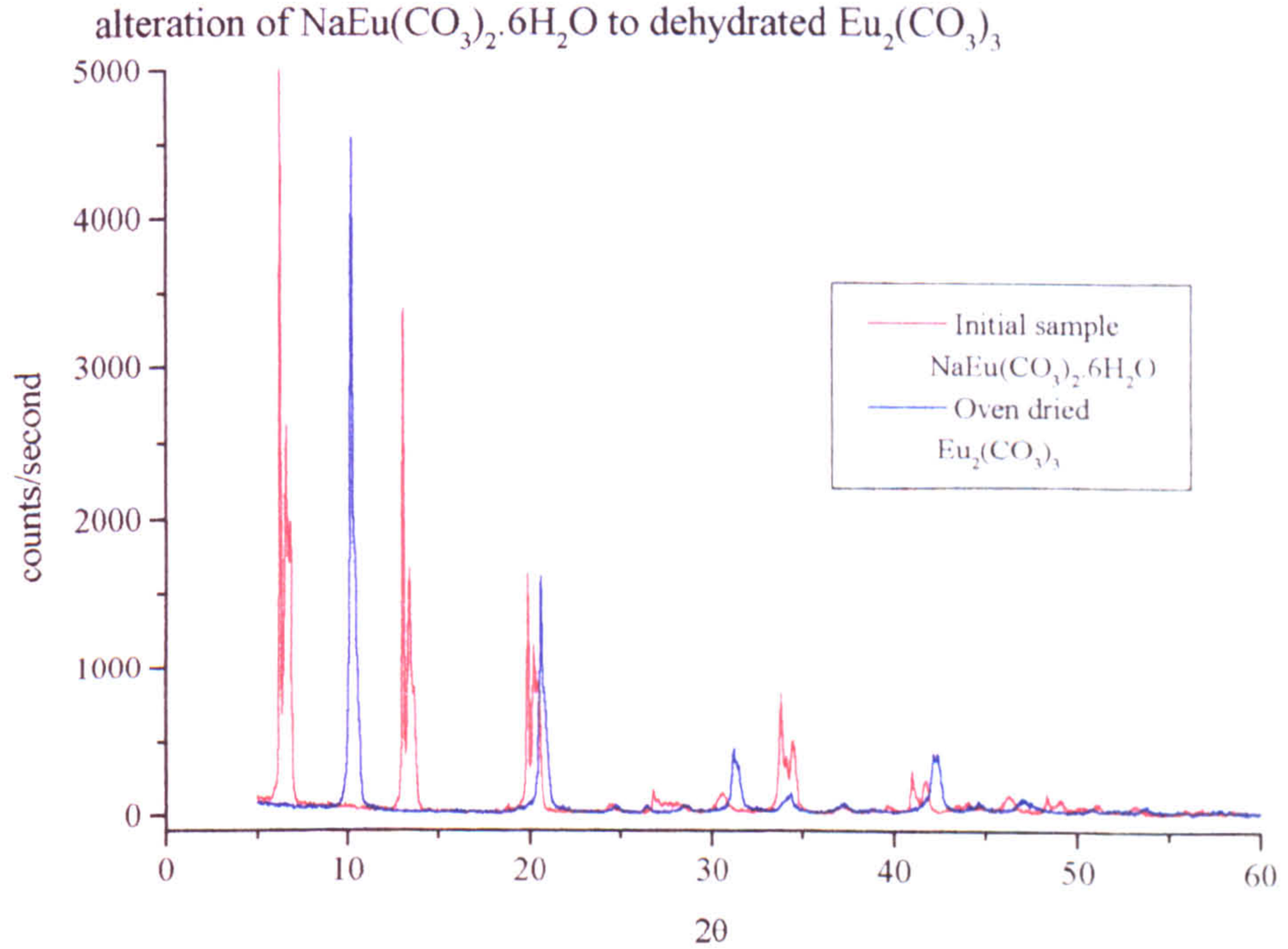

Appendix 5.4 Calculation of the Gibbs free energy of formation of $NaNd(CO_3)_2.6H_2O$ (Rao *et al*, 1996) and $Nd_2(CO_3)_3.8H_2O$ (Runde *et al*, 1992) from their solubility products

$\Delta G_f^\circ(NaNd(CO_3)_2.6H_2O)$ log Ksp -21.39, $\therefore \Delta G_{Rn}^\circ = 122.09\ KJmol^{-1}$

$$NaNd(CO_3)_2.6H_2O = Na^+ + Nd^{3+} + 2CO_3^{2-} + 6H_2O$$

$\Delta G_{Rn}^\circ = \Delta G^\circ_{(Products)} - \Delta G^\circ_{(Reactants)}$ $\therefore \Delta G^\circ_{(Reactants)} = \Delta G^\circ_{(Products)} - \Delta G_{Rn}^\circ$

$\Delta G_f^\circ(NaNd(CO_3)_2.6H_2O)$

$= [\Delta G_f^\circ(Na^+) + \Delta G_f^\circ(Nd^{3+}) + 2\Delta G_f^\circ(CO_3^{2-}) + 6\Delta G_f^\circ(H_2O)] - \Delta G_{Rn}^\circ$

$= [(-261.95) + (-670.90) + 2(-527.90) + 6(-237.14)] - [122.09]$

$= [-3411.49 KJmol^{-1}] - [122.09 KJmol^{-1}]$

$= \underline{-3533.38 KJmol^{-1}}$

$\Delta G_f^\circ(Nd_2(CO_3)_3.xH_2O)$ log Ksp -31.35 $\therefore \Delta G_{Rn}^\circ = 178.94\ KJmol^{-1}$

$$Nd_2(CO_3)_3.xH_2O = 2Nd^{3+} + 3CO_3^{2-} + xH_2O$$

$\Delta G_f^\circ(Nd_2(CO_3)_3.8H_2O) = [2\Delta G_f^\circ(Nd^{3+}) + 3\Delta G_f^\circ(CO_3^{2-}) + 8\Delta G_f^\circ(H_2O)] - \Delta G_{Rn}$

$= [2(-670.90) + 3(-527.90) + 8(-237.14)] - [178.94]$

$= [-4822.62 KJmol^{-1}] - [178.94 KJmol^{-1}]$

$= \underline{-5001.56 KJmol^{-1}}$

Appendix 6.1a Summary of $Nd_2(OH)_4SO_4$ solution analysis

Sample	Phase	Log Ksp	Log K	Equilibrium	pH	[Ln]/mM	[Na]/ mM	$[SO_4^{2-}]$/ mM	$[Cl^-]$/ mM	log $a_{Ln^{3+}}$	log $a_{SO_4^{2-}}$	log a_{OH^-}
NdS 5a	$Nd_2(OH)_4SO_4$	-41.2614	14.7386	13 month	6.08	5.0	21.8	6.2	21.8	-3.375	-2.831	-7.920
NdS 5b	$Nd_2(OH)_4SO_4$	-42.0403	13.9597	13 month	6.23	1.0	29.0	4.2	21.8	-4.090	-2.778	-7.770
NdS 6a	$Nd_2(OH)_4SO_4$	-39.9433	16.0567	13 month	6.41	6.2	79.8	6.7	21.8	-3.349	-2.881	-7.591
NdS 6b	$Nd_2(OH)_4SO_4$	-41.8164	14.1836	13 month	6.57	0.32	87.0	3.8	21.8	-4.605	-2.883	-7.431
NdS 10a	$Nd_2(OH)_4SO_4$	-45.8225	10.1775	10 month	5.08	2.9	20	1.5	30	-3.354	-3.432	-8.920
NdS 10b	$Nd_2(OH)_4SO_4$	-45.5563	10.7737	10 month	5.45	1.2	25	0.6	30	-3.661	-3.702	-8.550
NdS 11a	$Nd_2(OH)_4SO_4$	-43.9211	12.0789	10 month	5.52	3.3	25	6.7	30	-2.699	-3.650	-8.480
NdS 11b	$Nd_2(OH)_4SO_4$	-43.8840	12.1160	10 month	5.75	1.2	30	5.6	30	-4.105	-2.672	-8.250
NdS 12a	$Nd_2(OH)_4SO_4$	-42.6108	13.3892	10 month	6.24	2.7	115	96.4	30	-4.973	-1.617	-7.762
NdS 12b	$Nd_2(OH)_4SO_4$	-42.7349	13.2651	10 month	6.47	0.82	120	95.4	30	-5.497	-1.613	-7.532
NdS 13a	$Nd_2(OH)_4SO_4$	-41.8312	14.1688	10 month	6.69	2.0	257.5	246	15	-5.658	-1.260	-7.313
NdS 13b	$Nd_2(OH)_4SO_4$	-41.8764	14.1236	10 month	6.83	1.0	260	245	15	-5.962	-1.259	-7.173
NdS 15a	$Nd_2(OH)_4SO_4$	-43.3245	12.676	6 month	6.04	1.5	55	35.8	30	-4.768	-1.945	-7.981
NdS 15b	$Nd_2(OH)_4SO_4$	-42.3004	13.700	6 month	6.07	4.1	55	37.1	30	-4.305	-1.966	-7.931
NdS 15c	$Nd_2(OH)_4SO_4$	-42.5147	13.485	6 month	6.00	4.4	55	37.2	30	-4.271	-1.969	-8.001
NdS 15d	$Nd_2(OH)_4SO_4$	-42.6090	13.391	6 month	6.01	3.8	55	36.9	30	-4.343	-1.964	-7.971
NdS 16a	$Nd_2(OH)_4SO_4$	-41.0381	14.962	7 month	6.51	1.6	27.5	18.3	15	-4.459	-2.158	-7.490
NdS 16b	$Nd_2(OH)_4SO_4$	-40.9373	15.063	7 month	6.55	1.5	27.5	18.3	15	-4.490	-2.155	-7.450
NdS 16c	$Nd_2(OH)_4SO_4$	-41.1723	14.828	7 month	6.45	1.8	27.5	18.4	15	-4.405	-2.161	-7.550
NdS 16d	$Nd_2(OH)_4SO_4$	-41.4122	14.588	7 month	6.39	1.8	27.5	18.4	15	-4.405	-2.161	-7.610

Appendix 6.1b Summary of the $Nd_2(OH)_4SO_4$ solution analysis

Sample	Phase	Log Ksp	Log K	Equilibrium	pH	[Ln]/M	[Na]/ mM	$[SO_4^{2-}]$/ mM	$[Cl^-]$/ mM	log $a_{Ln^{3+}}$	log $a_{SO_4^{2-}}$	log a_{OH^-}
NdS 18a	$Nd_2(OH)_4SO_4$	-39.81	16.19	2 months	7.10	$1.2x10^{-3}$	120	46	30	-5.002	-2.201	-6.901
NdS 18b	$Nd_2(OH)_4SO_4$	-41.28	14.72	2 months	7.01	$3.2x10^{-4}$	120	45	30	-5.560	-2.198	-6.991
NdS 18c	$Nd_2(OH)_4SO_4$	-41.38	14.62	2 months	6.96	$3.6x10^{-4}$	120	45	30	-5.508	-2.199	-7.041
NdS 18d	$Nd_2(OH)_4SO_4$	-41.45	14.55	2 months	6.99	$2.9x10^{-4}$	120	45	30	-5.603	-2.198	-7.011
NdS 18e	$Nd_2(OH)_4SO_4$	-41.73	14.27	2 months	6.86	$3.8x10^{-4}$	120	45	30	-5.483	-2.199	-7.141
NdS 18f	$Nd_2(OH)_4SO_4$	-41.67	14.33	2 months	6.88	$3.7x10^{-4}$	120	45	30	-5.495	-2.199	-7.121

Appendix 6.2 Summary of the $Eu_2(OH)_4SO_4$ solution analysis

Sample	Phase	Log Ksp	Log K	Equilibrium	pH	[Ln]/M	[Na]/ mM	$[SO_4^{2-}]$/ mM	$[Cl^-]$/ mM	log $a_{Ln^{3+}}$	log $a_{SO_4^{2-}}$	log a_{OH^-}
EuS 6a	$Eu_2(OH)_4SO_4$	-43.3125	12.69	12 month	5.89	$3.5x10^{-3}$	79.8	34.4	21.8	-4.427	-2.014	-8.111
EuS 6b	$Eu_2(OH)_4SO_4$	-42.3693	13.63	12 month	6.52	$5.9x10^{-4}$	87.0	32.9	21.8	-5.225	-1.996	-7.481
EuS18b	$Eu_2(OH)_4SO_4$	-43.10	12.90	2 months	6.44	$6.25x10^{-4}$	120	45	30	-5.328	-2.200	-7.561
EuS 18c	$Eu_2(OH)_4SO_4$	-42.02	13.98	2 months	6.85	$3.29x10^{-4}$	120	45	30	-5.608	-2.197	-7.151
EuS 18d	$Eu_2(OH)_4SO_4$	-42.16	13.84	2 months	6.85	$2.80x10^{-4}$	120	45	30	-5.678	-2.196	-7.151
EuS 18e	$Eu_2(OH)_4SO_4$	-41.66	14.34	2 months	6.94	$3.29x10^{-4}$	120	45	30	-5.609	-2.197	-7.061
EuS 18f	$Eu_2(OH)_4SO_4$	-41.98	14.02	2 months	6.84	$3.62x10^{-4}$	120	45	30	-5.567	-2.197	-7.161

Appendix 6.3a Summary of the $NaCe(SO_4)_2$ solution analysis

Sample	Phase	Log Ksp	Equilibrium	pH	[Ln]/M	[Na]/ mM	$[SO_4^{2-}]$/ mM	$[Cl^-]$/ mM	$\log a_{Ln^{3+}}$	$\log a_{SO_4^{2-}}$	$\log a_{Na^+}$
CeS 5a	$NaCe(SO_4)_2$	-12.00	2 months	4.00	$5.4x10^{-3}$	20	3.55	22	-3.317	-3.440	-1.805
CeS 6b	$NaCe(SO_4)_2$	-10.16	2 months	4.04	$6.0x10^{-3}$	74	23	22	-3.883	-2.494	-1.289
CeS 6c	$NaCe(SO_4)_2$	-10.97	2 months	4.49	$5.0x10^{-4}$	80	22.5	22	-5.076	-2.315	-1.261
CeS 7a	$NaCe(SO_4)_2$	-10.73	2 months	4.25	$8.2x10^{-4}$	150	60	22	-5.322	-2.172	-1.062
CeS 7b	$NaCe(SO_4)_2$	-10.29	2 months	4.14	$2.6x10^{-3}$	160	63	22	-4.862	-2.193	-1.041
CeS 7c	$NaCe(SO_4)_2$	-11.05	2 months	4.61	$4.5x10^{-4}$	59	59	22	-5.501	-2.052	-1.446
CeS 12a	$NaCe(SO_4)_2$	-10.95	2 months	4.94	$7.9x10^{-4}$	206	82	30	-5.604	-2.189	-0.962
CeS 12b	$NaCe(SO_4)_2$	-10.95	2 months	4.94	$8.0x10^{-4}$	211	82	30	-5.606	-2.195	-0.953
CeS 12c	$NaCe(SO_4)_2$	-10.57	2 months	4.90	$2.2x10^{-3}$	217	84	30	-5.209	-2.208	-0.946
CeS 12d	$NaCe(SO_4)_2$	-10.48	2 months	4.92	$2.6x10^{-3}$	223	82	30	-5.120	-2.213	-0.932
CeS 22a	$NaCe(SO_4)_2$	-12.22	2 months	5.33	$4.1x10^{-4}$	392	169	48	-6.183	-2.309	-0.786
CeS 22b	$NaCe(SO_4)_2$	-12.14	2 months	5.34	$5.0x10^{-4}$	393	169	48	-6.730	-2.310	-0.785
CeS 22c	$NaCe(SO_4)_2$	-12.21	2 months	5.33	$4.2x10^{-4}$	393	169	48	-6.803	-2.309	-0.786
CeS 22d	$NaCe(SO_4)_2$	-12.13	2 months	5.32	$5.0x10^{-4}$	392	169	48	-6.729	-2.309	-0.786
CeS 22e	$NaCe(SO_4)_2$	-12.44	2 months	4.94	$6.8x10^{-4}$	465	209	48	-6.949	-2.372	-0.749
CeS 22f	$NaCe(SO_4)_2$	-12.19	2 months	5.31	$4.3x10^{-4}$	450	151	48	-6.767	-2.351	-0.723

Appendix 6.3b Summary of the $NaCe(SO_4)_2$ solution analysis

Sample	Phase	Log Ksp	equilibrium	pH	[Ln]/M	[Na]/ M	$[SO_4^{2-}]$/ M	$[Cl^-]$/ M	$\log a_{Ln^{3+}}$	$\log a_{SO_4^{2-}}$	$\log a_{Na^+}$
CeS 17a	$NaCe(SO_4)_2$	-18.56	5 months	0.09	$6.3x10^{-4}$	0.19	1.00		-10.451	-3.309	-1.487
CeS 17b	$NaCe(SO_4)_2$	-18.68	5 months	0.09	$4.7x10^{-4}$	0.19	1.00		-10.577	-3.308	-1.487
CeS 17c	$NaCe(SO_4)_2$	-18.07	5 months	0.07	$2.9x10^{-4}$	0.19	1.01		-9.886	-3.345	-1.497
CeS 17d	$NaCe(SO_4)_2$	-18.61	5 months	0.06	$6.9x10^{-4}$	0.19	1.00		-10.456	-3.332	-1.492
CeS 17e	$NaCe(SO_4)_2$	-18.50	5 months	0.11	$6.2x10^{-4}$	0.19	1.00		-10.432	-3.295	-1.484
CeS 20a	$NaCe(SO_4)_2$	-28.25	2 months	-0.33	$1.00x10^{-4}$	1.44	1.59	1.44	-16.519	-5.302	-1.127
CeS 20b	$NaCe(SO_4)_2$	-28.28	2 months	-0.33	$9.4x10^{-5}$	1.44	1.59	1.44	-16.546	-5.302	-1.127
CeS 20c	$NaCe(SO_4)_2$	-28.11	2 months	-0.30	$1.00x10^{-4}$	1.44	1.59	1.46	-16.449	-5.271	-1.119
CeS 20d	$NaCe(SO_4)_2$	-28.11	2 months	-0.30	$9.4x10^{-5}$	1.44	1.59	1.44	-16.460	-5.264	-1.118
CeS 20e	$NaCe(SO_4)_2$	-26.76	2 months	-0.06	$1.9x10^{-4}$	1.44	1.59	1.44	-15.634	-5.032	-1.060

Appendix 6.4 Summary of the $NaNd(SO_4)_2$ solution analysis

Sample	Phase	Log Ksp	Equilibrium	pH	[Ln]/M	[Na]/ M	$[SO_4^{2-}]$/ M	$[Cl^-]$/ M	$\log a_{Ln^{3+}}$	$\log a_{SO_4^{2-}}$	$\log a_{Na^+}$
NdS 17a	$NaNd(SO_4)_2$	-20.70	5 months	0.28	0.32	1.90	1.00		-12.277	-3.892	-0.639
NdS 17b	$NaNd(SO_4)_2$	-20.37	5 months	0.23	0.86	1.90	1.00		-11.897	-3.915	-0.644
NdS 17c	$NaNd(SO_4)_2$	-20.37	5 months	0.25	0.78	1.90	1.00		-11.920	-3.906	-0.642
NdS 17d	$NaNd(SO_4)_2$	-19.21	5 months	0.25	32.0	1.90	1.00		-10.538	-4.003	-0.666
NdS 17e	$NaNd(SO_4)_2$	-20.30	5 months	0.26	0.88	1.90	1.00		-11.859	-3.902	-0.641
NdS 19a	$NaNd(SO_4)_2$	-19.32	2 months	0.37	$6.2x10^{-4}$	0.87	1.01	0.24	-11.261	-3.577	-0.904
NdS 19b	$NaNd(SO_4)_2$	-19.55	2 months	0.37	$3.6x10^{-4}$	0.87	1.01	0.24	-11.495	-3.577	-0.904
NdS 19c	$NaNd(SO_4)_2$	-19.57	2 months	0.35	$3.7x10^{-4}$	0.87	1.01	0.24	-11.496	-3.583	-0.905
NdS 19d	$NaNd(SO_4)_2$	-19.63	2 months	0.34	$3.3x10^{-4}$	0.87	1.01	0.24	-11.552	-3.587	-0.906
NdS 19e	$NaNd(SO_4)_2$	-19.58	2 months	0.34	$3.7x10^{-4}$	0.87	1.01	0.24	-11.502	-3.587	-0.906

Appendix 6.5 Summary of the $NaEu(SO_4)_2$ solution analysis

Sample	Phase	Log Ksp	Equilibrium	pH	[Ln]/M	[Na]/ M	$[SO_4^{2-}]$ /M	$[Cl^-]$/ M	$\log a_{Ln^{3+}}$	$\log a_{SO_4^{2-}}$	$\log a_{Na^+}$
EuS 17d	$NaEu(SO_4)_2$	-17.50	5 months	0.29	$3.1x10^{-3}$	0.19	1.00		-9.605	-3.211	-1.147
EuS 19a	$NaEu(SO_4)_2$	-25.54	2 months	0.12	$9.22x10^{-4}$	2.84	1.01	2.207	-14.620	-5.096	-0.731
EuS 19b	$NaEu(SO_4)_2$	-25.75	2 months	0.12	$3.95x10^{-4}$	2.78	1.01	2.144	-14.918	-5.052	-0.731
EuS 19c	$NaEu(SO_4)_2$	-28.00	2 months	-0.04	$4.28x10^{-4}$	3.41	1.01	2.777	-16.091	-5.575	-0.757
EuS 19d	$NaEu(SO_4)_2$	-27.93	2 months	-0.06	$5.92x10^{-4}$	3.42	1.01	2.776	-15.989	-5.592	-0.760
EuS 19e	$NaEu(SO_4)_2$	-28.04	2 months	0.00	$2.96x10^{-4}$	3.41	1.01	2.775	-16.192	-5.549	-0.750

Appendix 6.6 Stability field diagram for the Na-Nd-CO_3^{2-}-OH system in $[Na^+]$ = 10mM and $[SO_4^{2-}]$ = 10mM at 298.15K and 1atm pressure

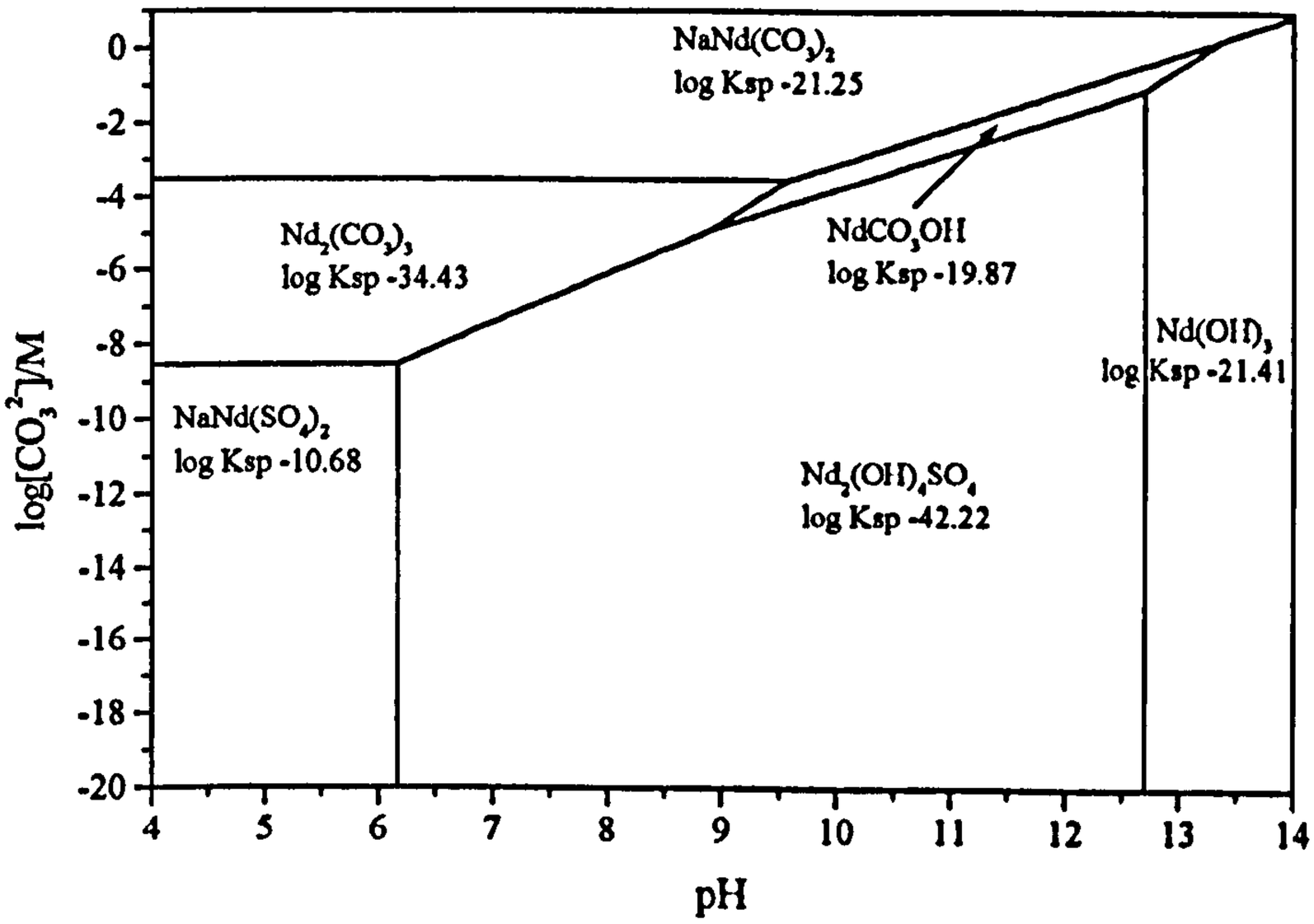

Appendix 6.7 Stability field diagram for the Na-Nd-SO_4^{2-}-OH system $[Na^+]$ = 1mM, [TIC] = 0.1mM at 298.15K and 1 atm pressure

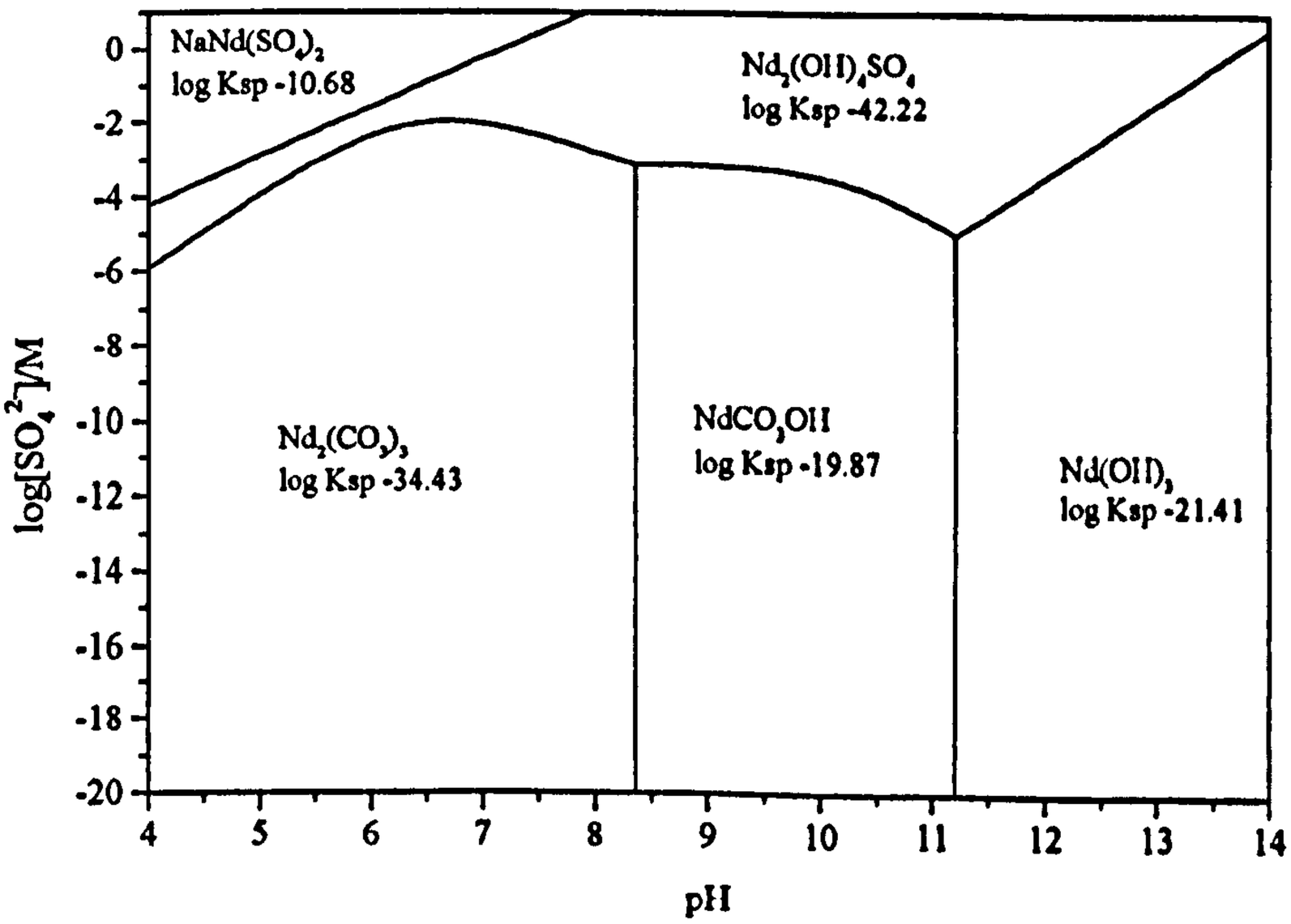

Appendix 6.8 $Nd_2(OH)_4SO_4$ solubility and aqueous speciation in 10mM TIC and 10mM SO_4^{2-}

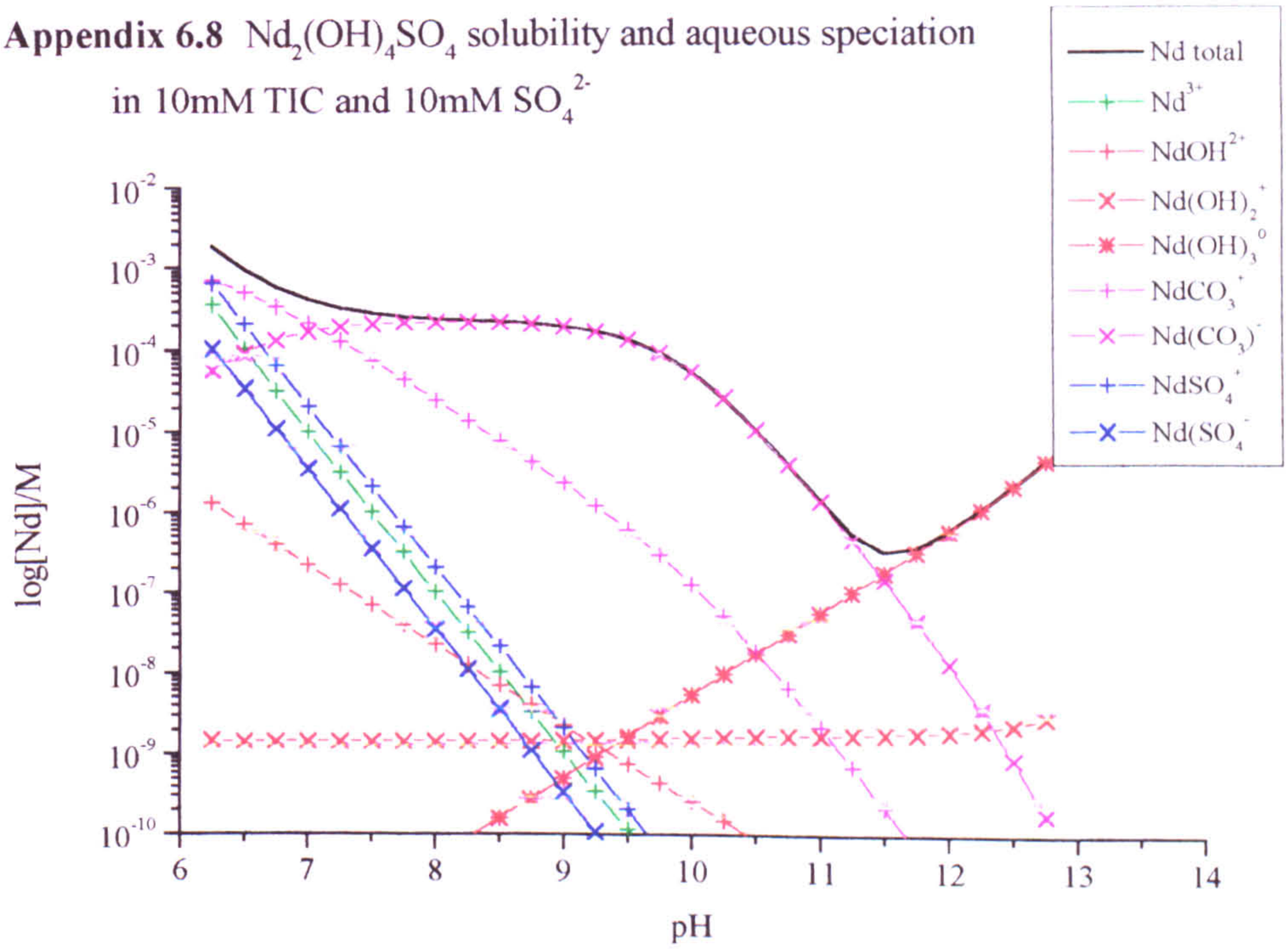

Appendix 6.9 $Nd_2(OH)_4SO_4$ solubility and aqueous speciation in 10mM SO_4^{2-}

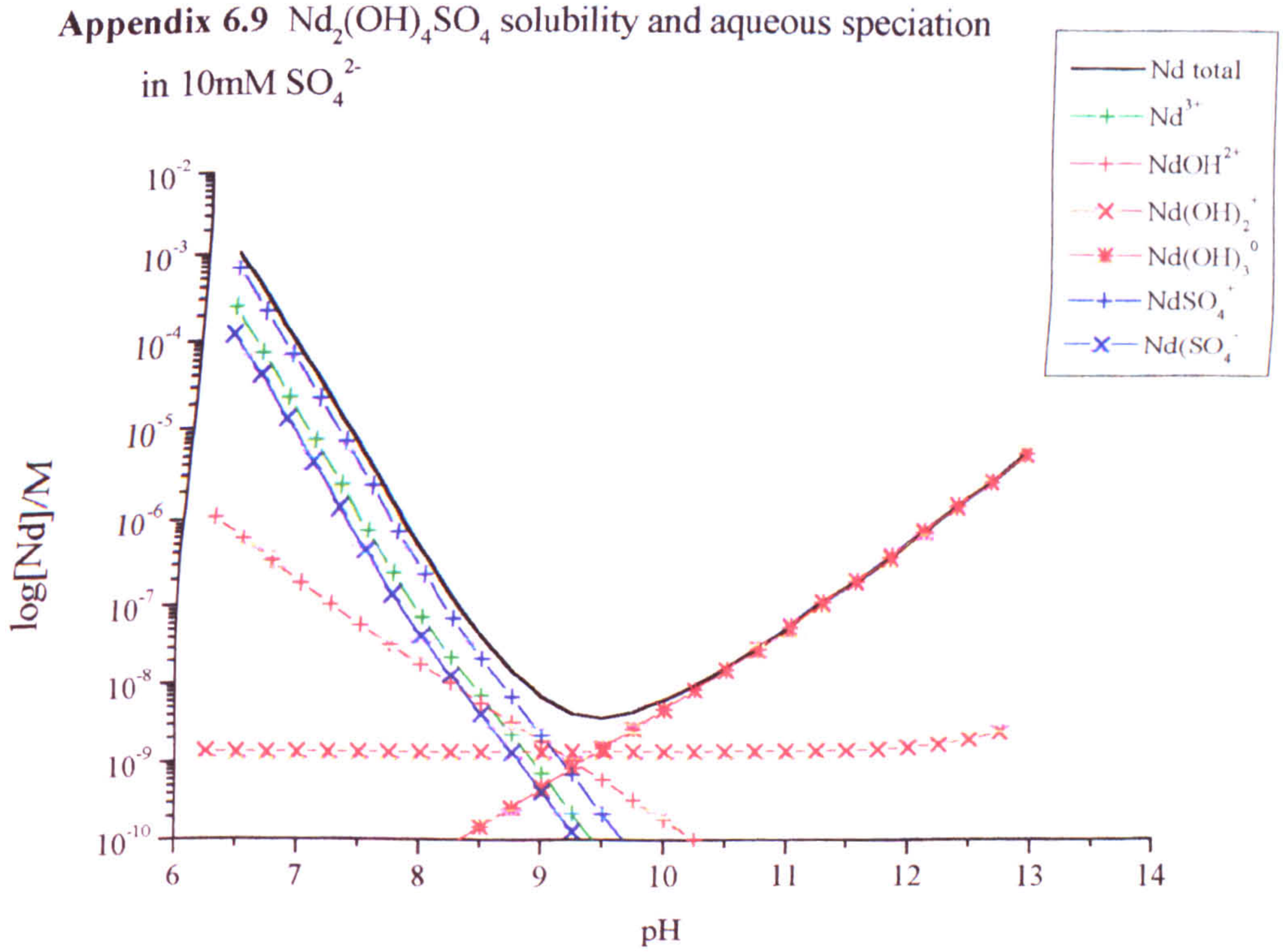

Appendix 7.1 NEA 9 database including Neodymium aqueous species and solid phases. (further Am, Ce Nd and Eu constants are summarised in Tables 7.1 and 7.2 in sections 7.3 and 7.4)

```
SOLUTION_MASTER_SPECIES
#
        E               e-              0.0     0.0
#
        H               H+              -1.0    H               1.008
        H(0)            H2              0.0     H
        H(1)            H+              -1.0    0.0
        O               H2O             0.0     O               16.
        O(-2)           H2O             0.0     0.0
        O(0)            O2              0.0     O
        Ca              Ca+2            0.0     Ca              40.08
        Na              Na+             0.0     Na              22.9898
        K               K+              0.0     K               39.0983
        Cl              Cl-             0.0     Cl              35.453
        C               CO3-2           2.0     C               44.0098
        C(4)            CO3-2           2.0     HCO3
        C(-4)           CH4             0.0     CH4
        S               SO4-2           0.0     S               96.06
        S(6)            SO4-2           0.0     SO4
        S(-2)           HS-             1.0     S
        N               NO3-            0.0     N               62.0049
        N(5)            NO3-            0.0     N
        N(3)            NO2-            0.0     N
        N(0)            N2              0.0     N
        N(-3)           NH4+            0.0     N
        Nd              Nd+3            0.0     Nd              144.2
SOLUTION_SPECIES
        H+ = H+
                log_k       0.0
                delta_h     0.0     kcal
                -analytic   0.0     0.0     0.0     0.0     0.0
                -gamma      9.0     0.0
        e- = e-
                log_k       0.0
                delta_h     0.0     kcal
                -analytic   0.0     0.0     0.0     0.0     0.0
                -gamma      0.0     0.0
        H2O = H2O
                log_k       0.0
                delta_h     0.0     kcal
                -analytic   0.0     0.0     0.0     0.0     0.0
                -gamma      0.0     0.0
Ca+2 = Ca+2
                log_k       0.0
                delta_h     0.0     kcal
                -analytic   0.0     0.0     0.0     0.0     0.0
                -gamma      0.0     0.0
Na+ = Na+
                log_k       0.0
                delta_h     0.0     kcal
                -analytic   0.0     0.0     0.0     0.0     0.0
                -gamma      0.0     0.0
K+ = K+
                log_k       0.0
                delta_h     0.0     kcal
                -analytic   0.0     0.0     0.0     0.0     0.0
                -gamma      0.0     0.0
Cl- = Cl-
                log_k       0.0
                delta_h     0.0     kcal
                -analytic   0.0     0.0     0.0     0.0     0.0
                -gamma      0.0     0.0
CO3-2 = CO3-2
                log_k       0.0
                delta_h     0.0     kcal
                -analytic   0.0     0.0     0.0     0.0     0.0
                -gamma      0.0     0.0
SO4-2 = SO4-2
                log_k       0.0
                delta_h     0.0     kcal
                -analytic   0.0     0.0     0.0     0.0     0.0
                -gamma      0.0     0.0
NO3- = NO3-
                log_k       0.0
                delta_h     0.0     kcal
                -analytic   0.0     0.0     0.0     0.0     0.0
                -gamma      3.0     0.0
Nd+3 = Nd+3
                log_k       0.0
                delta_h     0.0     kcal
                -analytic   0.0     0.0     0.0     0.0     0.0
                -gamma      0.0     0.0
```

```
H2O = OH- + H+
        log_k       -14.0
        delta_h     13.35     kcal
        -analytic    0.0       0.0       0.0       0.0       0.0
        -gamma       0.0       0.0
2H2O = O2 + 4H+ + 4e-
        log_k       -86.08
        delta_h     134.79    kcal
        -analytic    0.0       0.0       0.0       0.0       0.0
        -gamma       0.0       0.0
2H+ + 2e- = H2
        log_k       -3.15
        delta_h     -1.76     kcal
        -analytic    0.0       0.0       0.0       0.0       0.0
        -gamma       0.0       0.0
CO3-2 + H+ = HCO3-
        log_k       10.33
        delta_h     -3.5      kcal
        -analytic    0.0       0.0       0.0       0.0       0.0
        -gamma       0.0       0.0
CO3-2 + 10H+ + 8e- = CH4 + 3H2O
        log_k       38.2
        delta_h     345.5     kcal
        -analytic    0.0       0.0       0.0       0.0       0.0
        -gamma       0.0       0.0
CO3-2 + 2H+ = H2CO3
        log_k       16.68
        delta_h     -5.5      kcal
        -analytic    0.0       0.0       0.0       0.0       0.0
        -gamma       0.0       0.0
SO4-2 + H+ = HSO4-
        log_k       1.99
        delta_h     5.4       kcal
        -analytic    0.0       0.0       0.0       0.0       0.0
        -gamma       0.0       0.0
SO4-2 + 8H+ + 8e- = S-2 + 4H2O
        log_k       20.64
        delta_h     -28.04    kcal
        -analytic    0.0       0.0       0.0       0.0       0.0
        -gamma       0.0       0.0
SO4-2 + 9H+ + 8e- = HS- + 4H2O
        log_k       33.65
        delta_h     -40.14    kcal
        -analytic    0.0       0.0       0.0       0.0       0.0
        -gamma       0.0       0.0
SO4-2 + 10H+ + 8e- = H2S + 4H2O
        log_k       40.64
        delta_h     -65.44    kcal
        -analytic    0.0       0.0       0.0       0.0       0.0
        -gamma       0.0       0.0
NO3- + 2H+ + 2e- = NO2- + H2O
        log_k       28.57
        delta_h     -43.76    kcal
        -analytic    0.0       0.0       0.0       0.0       0.0
        -gamma       0.0       0.0
2NO3- + 12H+ + 10e- = N2 + 6H2O
        log_k       207.08
        delta_h     -312.13   kcal
        -analytic    0.0       0.0       0.0       0.0       0.0
        -gamma       0.0       0.0
NO3- + 9H+ + 8e- = NH3 + 3H2O
        log_k       109.83
        delta_h     -174.58   kcal
        -analytic    0.0       0.0       0.0       0.0       0.0
        -gamma       0.0       0.0
NO3- + 10H+ + 8e- = NH4+ + 3H2O
        log_k       119.08
        delta_h     -187.05   kcal
        -analytic    0.0       0.0       0.0       0.0       0.0
        -gamma       0.0       0.0
NO3- + 10H+ + 8e- + SO4-2 = NH4SO4- + 3H2O
        log_k       120.19
        delta_h     -187.46   kcal
        -analytic    0.0       0.0       0.0       0.0       0.0
        -gamma       0.0       0.0
NO3- + H+ = HNO3
        log_k       -1.43
        delta_h     -0.56     kcal
        -analytic    0.0       0.0       0.0       0.0       0.0
        -gamma       0.0       0.0
Ca+2 + H2O = CaOH+ + H+
        log_k       -12.6
        delta_h     14.53     kcal
        -analytic    0.0       0.0       0.0       0.0       0.0
        -gamma       0.0       0.0
Ca+2 + CO3-2 = CaCO3
        log_k       3.15
        delta_h     4.02      kcal
```

```
        -analytic   0.0         0.0         0.0         0.0         0.0
        -gamma      0.0         0.0
Ca+2 + CO3-2 + H+ = CaHCO3+
        log_k       11.35
        delta_h     1.81        kcal
        -analytic   0.0         0.0         0.0         0.0         0.0
        -gamma      0.0         0.0
Ca+2 + SO4-2 = CaSO4
        log_k       2.31
        delta_h     1.47        kcal
        -analytic   0.0         0.0         0.0         0.0         0.0
        -gamma      0.0         0.0
Ca+2 + NO3- = CaNO3+
        log_k       0.6
        delta_h     0.0         kcal
        -analytic   0.0         0.0         0.0         0.0         0.0
        -gamma      0.0         0.0
Ca+2 + 2NO3- = Ca(NO3)2
        log_k       0.5
        delta_h     0.0         kcal
        -analytic   0.0         0.0         0.0         0.0         0.0
        -gamma      0.0         0.0
Na+ + CO3-2 = NaCO3-
        log_k       1.27
        delta_h     8.91        kcal
        -analytic   0.0         0.0         0.0         0.0         0.0
        -gamma      0.0         0.0
Na+ + H+ + CO3-2 = NaHCO3
        log_k       10.08
        delta_h     -3.6        kcal
        -analytic   0.0         0.0         0.0         0.0         0.0
        -gamma      0.0         0.0
Na+ + SO4-2 = NaSO4-
        log_k       0.7
        delta_h     1.12        kcal
        -analytic   0.0         0.0         0.0         0.0         0.0
        -gamma      0.0         0.0
Na+ + NO3- = NaNO3
        log_k       -0.55
        delta_h     0.0         kcal
        -analytic   0.0         0.0         0.0         0.0         0.0
        -gamma      0.0         0.0
K+ + SO4-2 = KSO4-
        log_k       0.85
        delta_h     2.25        kcal
        -analytic   0.0         0.0         0.0         0.0         0.0
        -gamma      0.0         0.0
K+ + NO3- = KNO3
        log_k       -0.19
        delta_h     0.0         kcal
        -analytic   0.0         0.0         0.0         0.0         0.0
        -gamma      0.0         0.0
2SO4-2 + 16H+ + 14e- = S2-2 + 8H2O
        log_k       57.6
        delta_h     -104.7      kcal
        -analytic   0.0         0.0         0.0         0.0         0.0
        -gamma      0.0         0.0
3SO4-2 + 24H+ + 20e- = S3-2 + 12H2O
        log_k       94.4
        delta_h     -174.0      kcal
        -analytic   0.0         0.0         0.0         0.0         0.0
        -gamma      0.0         0.0
4SO4-2 + 32H+ + 26e- = S4-2 + 16H2O
        log_k       130.9
        delta_h     -218.3      kcal
        -analytic   0.0         0.0         0.0         0.0         0.0
        -gamma      0.0         0.0
5SO4-2 + 40H+ + 32e- = S5-2 + 20H2O
        log_k       167.3
        delta_h     -274.6      kcal
        -analytic   0.0         0.0         0.0         0.0         0.0
        -gamma      0.0         0.0
SO4-2 + 4H+ + 2e- = O2S + 2H2O
        log_k       5.33
        delta_h     3.5         kcal
        -analytic   0.0         0.0         0.0         0.0         0.0
        -gamma      0.0         0.0
SO4-2 + 2H+ + 2e- = O3S-2 + H2O
        log_k       -3.65
        delta_h     -2.64       kcal
        -analytic   0.0         0.0         0.0         0.0         0.0
        -gamma      0.0         0.0
2SO4-2 + 10H+ + 8e- = O3S2-2 + 5H2O
        log_k       37.7
        delta_h     -62.8       kcal
        -analytic   0.0         0.0         0.0         0.0         0.0
        -gamma      0.0         0.0
2SO4-2 + 8H+ + 6e- = SO4S-2 + 4H2O
```

```
        log_k       10.49
        delta_h     -18.7       kcal
        -analytic    0.0         0.0         0.0         0.0         0.0
        -gamma       0.0         0.0
2SO4-2 + 6H+ + 4e- = OSO4S-2 + 3H2O
        log_k       2.33
        delta_h     -2.9        kcal
        -analytic    0.0         0.0         0.0         0.0         0.0
        -gamma       0.0         0.0
2SO4-2 + 4H+ + 2e- = O2SO4S-2 + 2H2O
        log_k       -8.57
        delta_h     11.6        kcal
        -analytic    0.0         0.0         0.0         0.0         0.0
        -gamma       0.0         0.0
2SO4-2 = (SO4)2-2 + 2e-
        log_k       -66.4
        delta_h     114.6       kcal
        -analytic    0.0         0.0         0.0         0.0         0.0
        -gamma       0.0         0.0
3SO4-2 + 12H+ + 8e- = O2SO4S2-2 + 6H2O
        log_k       25.8
        delta_h     -44.6       kcal
        -analytic    0.0         0.0         0.0         0.0         0.0
        -gamma       0.0         0.0
4SO4-2 + 20H+ + 14e- = O2SO4S3-2 + 10H2O
        log_k       72.79
        delta_h     -106.5      kcal
        -analytic    0.0         0.0         0.0         0.0         0.0
        -gamma       0.0         0.0
5SO4-2 + 28H+ + 20e- = O2SO4S4-2 + 14H2O
        log_k       97.0
        delta_h     -165.3      kcal
        -analytic    0.0         0.0         0.0         0.0         0.0
        -gamma       0.0         0.0
SO4-2 + 3H+ + 2e- = O2SOH- + H2O
        log_k       3.57
        delta_h     -1.38       kcal
        -analytic    0.0         0.0         0.0         0.0         0.0
        -gamma       0.0         0.0
2SO4-2 + 9H+ + 6e- = HSO4S- + 4H2O
        log_k       12.98
        delta_h     0.0         kcal
        -analytic    0.0         0.0         0.0         0.0         0.0
        -gamma       0.0         0.0
SO4-2 + 4H+ + 2e- = OS(OH)2 + H2O
        log_k       5.33
        delta_h     3.5         kcal
        -analytic    0.0         0.0         0.0         0.0         0.0
        -gamma       0.0         0.0
SO4-2 + 2H+ = H2SO4
        log_k       -99.0
        delta_h     0.0         kcal
        -analytic    0.0         0.0         0.0         0.0         0.0
        -gamma       0.0         0.0
2SO4-2 + 10H+ + 6e- = H2SO4S + 4H2O
        log_k       13.34
        delta_h     0.0         kcal
        -analytic    0.0         0.0         0.0         0.0         0.0
        -gamma       0.0         0.0
2SO4-2 + 2H+ = H2(SO4)2 + 2e-
        log_k       -99.0
        delta_h     0.0         kcal
        -analytic    0.0         0.0         0.0         0.0         0.0
        -gamma       0.0         0.0
2SO4-2 + 11H+ + 8e- = O2S2OH- + 5H2O
        log_k       39.3
        delta_h     0.0         kcal
        -analytic    0.0         0.0         0.0         0.0         0.0
        -gamma       0.0         0.0
2SO4-2 + 12H+ + 8e- = OS2(OH)2 + 5H2O
        log_k       39.9
        delta_h     0.0         kcal
        -analytic    0.0         0.0         0.0         0.0         0.0
        -gamma       0.0         0.0
NO3- + 10H+ + 8e- + Cl- = NH4Cl + 3H2O
        log_k       120.6
        delta_h     0.0         kcal
        -analytic    0.0         0.0         0.0         0.0         0.0
        -gamma       0.0         0.0
NO3- + 9H+ + 8e- = NH4OH + 2H2O
        log_k       109.84
        delta_h     0.0         kcal
        -analytic    0.0         0.0         0.0         0.0         0.0
        -gamma       0.0         0.0
Nd+3 + H2O = NdOH+2 + H+
        log_k       -8.16
        delta_h     0.0         kcal
        -analytic    0.0         0.0         0.0         0.0         0.0
```

```
        -gamma      0.0       0.0
Nd+3 + 2H2O = Nd(OH)2+ + 2H+
        log_k      -17.04
        delta_h    0.0       kcal
        -analytic   0.0       0.0       0.0       0.0       0.0
        -gamma      0.0       0.0
Nd+3 + 3H2O = Nd(OH)3 + 3H+
        log_k      -26.40
        delta_h    0.0       kcal
        -analytic   0.0       0.0       0.0       0.0       0.0
        -gamma      0.0       0.0
Nd+3 + CO3-2 = NdCO3+
        log_k      7.67
        delta_h    0.0       kcal
        -analytic   0.0       0.0       0.0       0.0       0.0
        -gamma      0.0       0.0
Nd+3 + 2CO3-2 = Nd(CO3)2-
        log_k      13.09
        delta_h    0.0       kcal
        -analytic   0.0       0.0       0.0       0.0       0.0
        -gamma      0.0       0.0
Nd+3 + SO4-2 = NdSO4+
        log_k      3.55
        delta_h    5.0       kcal
        -analytic   0.0       0.0       0.0       0.0       0.0
        -gamma      0.0       0.0
Nd+3 + 2SO4-2 = Nd(SO4)2-
        log_k      5.2
        delta_h    10.6      kcal
        -analytic   0.0       0.0       0.0       0.0       0.0
        -gamma      0.0       0.0
PHASES
Nd(OH)3
        Nd(OH)3 + 3H+ = Nd+3 + 3H2O
        log_k      20.59
        delta_h    0.0       k_cal
        -analytic   0.0       0.0       0.0       0.0       0.0
NdOHCO3
        NdOHCO3 + H+ = Nd+3 + H2O + CO3-2
        log_k      -5.87
        delta_h    0.0       k_cal
        -analytic   0.0       0.0       0.0       0.0       0.0
Nd2(CO3)3
        Nd2(CO3)3 = 2Nd+3 + 3CO3-2
        log_k      -34.43
        delta_h    0.0       k_cal
        -analytic   0.0       0.0       0.0       0.0       0.0
NaNd(CO3)2
        NaNd(CO3)2 = Nd+3 + 2CO3-2 + Na+
        log_k      -21.25
        delta_h    0.0       k_cal
        -analytic   0.0       0.0       0.0       0.0       0.0
KNdCO3
        KNd(CO3)2 = Nd+3 + 2CO3-2 + K+
        log_k      -19.17
        delta_h    0.0       k_cal
        -analytic   0.0       0.0       0.0       0.0       0.0
NaNd(SO4)2
        NaNd(SO4)2 = Nd+3 + 2SO4-2 + Na+
        log_k      -10.68
        delta_h    0.0       k_cal
        -analytic   0.0       0.0       0.0       0.0       0.0
Nd2SO4(OH)4
        Nd2SO4(OH)4 + 4H+ = 2Nd+3 + 4H2O + SO4-2
        log_k      13.77
        delta_h    0.0       k_cal
        -analytic   0.0       0.0       0.0       0.0       0.0
ANHYDRIT
        CaSO4 = Ca+2 + SO4-2
        log_k      -4.27
        delta_h    -4.3      k_cal
        -analytic   0.0       0.0       0.0       0.0       0.0
ANTARCTI
        CaCl2(H2O)6 = Ca+2 + 2Cl- + 6H2O
        log_k      4.13
        delta_h    3.92      k_cal
        -analytic   0.0       0.0       0.0       0.0       0.0
ARAGONIT
        CaCO3 = Ca+2 + CO3-2
        log_k      -8.34
        delta_h    -2.86     k_cal
        -analytic   0.0       0.0       0.0       0.0       0.0
ARCANITE
        K2SO4 = 2K+ + SO4-2
        log_k      -1.69
        delta_h    6.24      k_cal
        -analytic   0.0       0.0       0.0       0.0       0.0
CA(OH)2
```

```
        Ca(OH)2 + 2H+ = Ca+2 + 2H2O
        log_k       22.81
        delta_h     -30.69     k_cal
        -analytic    0.0        0.0        0.0        0.0        0.0
CALCITE
        CaCO3 = CO3-2 + Ca+2
        log_k       -8.47
        delta_h     -2.58      k_cal
        -analytic    0.0        0.0        0.0        0.0        0.0
CALCIUM
        CaCl2(H2O)4 = Ca+2 + 2Cl- + 4H2O
        log_k       4.9
        delta_h     0.0        k_cal
        -analytic    0.0        0.0        0.0        0.0        0.0
CASO4.HY
        CaSO4(H2O).5 = Ca+2 + SO4-2 + .5H2O
        log_k       -3.47
        delta_h     -4.62      k_cal
        -analytic    0.0        0.0        0.0        0.0        0.0
GYPSUM
        CaSO4(H2O)2 = Ca+2 + SO4-2 + 2H2O
        log_k       -4.6
        delta_h     -0.03      k_cal
        -analytic    0.0        0.0        0.0        0.0        0.0
K2CO3.3/
        K2CO3(H2O)1.5 = 2K+ + CO3-2 + 1.5H2O
        log_k       3.14
        delta_h     0.2        k_cal
        -analytic    0.0        0.0        0.0        0.0        0.0
LAB.SALT
        Na4Ca(SO4)3(H2O)2 = 4Na+ + Ca+2 + 3SO4-2 + 2H2O
        log_k       -5.73
        delta_h     0.0        k_cal
        -analytic    0.0        0.0        0.0        0.0        0.0
MERCALLI
        KHSO4 = K+ + H+ + SO4-2
        log_k       -1.38
        delta_h     0.0        k_cal
        -analytic    0.0        0.0        0.0        0.0        0.0
MIRABILI
        Na2SO4(H2O)10 = 2Na+ + SO4-2 + 10H2O
        log_k       -1.07
        delta_h     19.0       k_cal
        -analytic    0.0        0.0        0.0        0.0        0.0
MISENITE
        K8H6(SO4)7 = 8K+ + 6H+ + 7SO4-2
        log_k       -10.58
        delta_h     0.0        k_cal
        -analytic    0.0        0.0        0.0        0.0        0.0
MONOHYDR
        CaCO3H2O = Ca+2 + CO3-2 + H2O
        log_k       -7.62
        delta_h     -1.6       k_cal
        -analytic    0.0        0.0        0.0        0.0        0.0
NA2CO3
        Na2CO3 = 2Na+ + CO3-2
        log_k       0.67
        delta_h     -5.95      k_cal
        -analytic    0.0        0.0        0.0        0.0        0.0
OXYCH-CA
        Ca4(OH)6Cl2(H2O)13 + 6H+ = 4Ca+2 + 2Cl- + 19H2O
        log_k       1222.97
        delta_h     0.0        k_cal
        -analytic    0.0        0.0        0.0        0.0        0.0
PIRSSONI
        Na2Ca(CO3)2(H2O)2 = 2Na+ + Ca+2 + 2CO3-2 + 2H2O
        log_k       -9.26
        delta_h     7.0        k_cal
        -analytic    0.0        0.0        0.0        0.0        0.0
S(C)
        S + 4H2O = SO4-2 + 6e- + 8H+
        log_k       -35.76
        delta_h     55.9       k_cal
        -analytic    0.0        0.0        0.0        0.0        0.0
SYLVITE
        KCl = K+ + Cl-
        log_k       0.96
        delta_h     4.5        k_cal
        -analytic    0.0        0.0        0.0        0.0        0.0
SYNGENIT
        K2Ca(SO4)2H2O = 2K+ + Ca+2 + 2SO4-2 + H2O
        log_k       -7.45
        delta_h     4.3        k_cal
        -analytic    0.0        0.0        0.0        0.0        0.0
THENARDI
        Na2SO4 = 2Na+ + SO4-2
        log_k       -0.24
        delta_h     -0.17      k_cal
```

```
        -analytic   0.0         0.0         0.0         0.0         0.0
THERMONA
        Na2CO3H2O = 2Na+ + CO3-2 + H2O
        log_k       0.66
        delta_h     -3.1        k_cal
        -analytic   0.0         0.0         0.0         0.0         0.0
VATERITE
        CaCO3 = Ca+2 + CO3-2
        log_k       -7.91
        delta_h     0.0         k_cal
        -analytic   0.0         0.0         0.0         0.0         0.0
ZZ-CH4(G
        CH4 + 3H2O = 10H+ + 8e- + CO3-2
        log_k       -41.08
        delta_h     61.2        k_cal
        -analytic   0.0         0.0         0.0         0.0         0.0
ZZ-H2(g)
        H2 = 2H+ + 2e-
        log_k       0.0
        delta_h     0.0         k_cal
        -analytic   0.0         0.0         0.0         0.0         0.0
ZZ-H2S(G
        H2S + 4H2O = SO4-2 + 10H+ + 8e-
        log_k       -41.63
        delta_h     60.9        k_cal
        -analytic   0.0         0.0         0.0         0.0         0.0
O2(g)
        O2 + 4H+ + 4e- = 2H2O
        log_k       83.12
        delta_h     -136.63     k_cal
        -analytic   0.0         0.0         0.0         0.0         0.0
ZZ-PCO2
        CO2 + H2O = CO3-2 + 2H+
        log_k       -18.15
        delta_h     0.79        k_cal
        -analytic   0.0         0.0         0.0         0.0         0.0
ZZ-SO2(G
        O2S + 2H2O = SO4-2 + 4H+ + 2e-
        log_k       -5.24
        delta_h     -9.75       k_cal
        -analytic   0.0         0.0         0.0         0.0         0.0
END
```

Appendix 7.1b PHREEQC input file for $Nd_2(CO_3)_3$ in equilibrium with an aqueous solution at fixed pH and pe.

```
Trench water
□
TITLE Nd
□
SOLUTION 1
□
        pH 7.3
□
        pe  0.0
□
        units mol/l
□
        Ca  2.85E-3
□
        Mg  6.0E-4
□
        Na  3.0E-3
□
        Cl  5.0E-3
□
        C   2.83E-3
□
        S   1.09E-3
□
PHASES
□
         FIX_H+
□
         H+ = H+
         log_K 0.0
        FIX_e-
        e- = e-
         log_K 0.0
END
TITLE   Nd in trench solution
USE Solution 1
EQUILIBRIUM_PHASES 1
        Nd2(CO3)3
        FIX_H+  -7.3    HCl     10.0
        FIX_e-   0.742    O2(g)     10.0
END
TITLE   Eu in trench solution
USE Solution 1
EQUILIBRIUM_PHASES 1
        Eu2(CO3)3
        FIX_H+  -7.3    HCl     10.0
        FIX_e-   0.742    O2(g)     10.0
END
```

Appendix 7.1c PHREEQC output file $Nd_2(CO_3)_3$ in equilibrium with aqueous solution defined in Appendix 7.1b, using the database shown in Appendix 7.1a

```
------------------
Reading data base.
------------------

        SOLUTION_MASTER_SPECIES
        SOLUTION_SPECIES
        PHASES
        END
-----------------------------------
Reading input data for simulation 1.
-----------------------------------

                                Trench water
        TITLE Nd
        SOLUTION 1
                pH 7.3
                pe  0.0
                units mol/l
                Ca  2.85E-3
                Mg  6.0E-4
                Na  3.0E-3
                Cl  5.0E-3
                C   2.83E-3
                S   1.09E-3
        PHASES
                FIX_H+
                H+ = H+
                log_K 0.0
                FIX_e-
                e- = e-
                log_K 0.0
        END
-----
TITLE
-----

 Nd

-------------------------------------------
Beginning of initial solution calculations.
-------------------------------------------

Initial solution 1.

-----------------------------Solution composition------------------------------

        Elements           Molality        Moles

        C                2.832e-03   2.832e-03
        Ca               2.852e-03   2.852e-03
        Cl               5.003e-03   5.003e-03
        Mg               6.004e-04   6.004e-04
        Na               3.002e-03   3.002e-03
        S                1.091e-03   1.091e-03

----------------------------Description of solution----------------------------

                                pH  =   7.300
                                pe  =   0.000
                  Activity of water =   1.000
                     Ionic strength =   1.345e-02
                    Mass of water (kg) =   1.000e+00
          Total alkalinity (eq/kg) =   2.594e-03
             Total CO2 (mol/kg) =   2.832e-03
                Temperature (deg C) =  25.000
          Electrical balance (eq) =   1.279e-04
                       Iterations =   6
                          Total H = 1.110155e+02
                          Total O = 5.551907e+01

----------------------------Distribution of species----------------------------

                                                  Log         Log         Log
            Species          Molality    Activity Molality  Activity    Gamma

            OH-            2.286e-07   1.995e-07   -6.641     -6.700    -0.059
            H+             5.548e-08   5.012e-08   -7.256     -7.300    -0.044
            H2O            5.551e+01   9.997e-01    0.000      0.000     0.000
C(-4)       0.000e+00
            CH4            0.000e+00   0.000e+00  -40.487    -40.487     0.000
C(4)        2.832e-03
            HCO3-          2.522e-03   2.201e-03   -2.598     -2.657    -0.059
            H2CO3          2.469e-04   2.469e-04   -3.607     -3.607     0.000
```

	CaHCO3+		4.051e-05	3.534e-05	-4.392	-4.452	-0.059
	MgHCO3+		1.014e-05	9.014e-06	-4.994	-5.045	-0.051
	CaCO3		4.449e-06	4.449e-06	-5.352	-5.352	0.000
	CO3-2		3.544e-06	2.054e-06	-5.451	-5.687	-0.237
	NaHCO3		3.229e-06	3.229e-06	-5.491	-5.491	0.000
	MgCO3		6.857e-07	6.878e-07	-6.164	-6.163	0.001
	NaCO3-		1.144e-07	9.979e-08	-6.942	-7.001	-0.059
Ca		2.852e-03					
	Ca+2		2.647e-03	1.534e-03	-2.577	-2.814	-0.237
	CaSO4		1.599e-04	1.599e-04	-3.796	-3.796	0.000
	CaHCO3+		4.051e-05	3.534e-05	-4.392	-4.452	-0.059
	CaCO3		4.449e-06	4.449e-06	-5.352	-5.352	0.000
	CaOH+		8.808e-09	7.685e-09	-8.055	-8.114	-0.059
Cl		5.003e-03					
	Cl-		5.003e-03	4.365e-03	-2.301	-2.360	-0.059
H(0)		3.557e-18					
	H2		1.778e-18	1.778e-18	-17.750	-17.750	0.000
Mg		6.004e-04					
	Mg+2		5.477e-04	3.510e-04	-3.261	-3.455	-0.193
	MgSO4		4.189e-05	4.202e-05	-4.378	-4.377	0.001
	MgHCO3+		1.014e-05	9.014e-06	-4.994	-5.045	-0.051
	MgCO3		6.857e-07	6.878e-07	-6.164	-6.163	0.001
Na		3.002e-03					
	Na+		2.991e-03	2.609e-03	-2.524	-2.583	-0.059
	NaSO4-		7.654e-06	6.678e-06	-5.116	-5.175	-0.059
	NaHCO3		3.229e-06	3.229e-06	-5.491	-5.491	0.000
	NaCO3-		1.144e-07	9.979e-08	-6.942	-7.001	-0.059
O(0)		0.000e+00					
	O2		0.000e+00	0.000e+00	-56.880	-56.880	0.000
S(-2)		5.222e-36					
	HS-		5.222e-36	4.556e-36	-35.282	-35.341	-0.059
S(6)		1.091e-03					
	SO4-2		8.812e-04	5.106e-04	-3.055	-3.292	-0.237
	CaSO4		1.599e-04	1.599e-04	-3.796	-3.796	0.000
	MgSO4		4.189e-05	4.202e-05	-4.378	-4.377	0.001
	NaSO4-		7.654e-06	6.678e-06	-5.116	-5.175	-0.059
	HSO4-		2.867e-09	2.501e-09	-8.543	-8.602	-0.059
	H2SO4		1.253e-18	1.253e-18	-17.902	-17.902	0.000
	O2S		6.892e-28	6.892e-28	-27.162	-27.162	0.000
	H2S		2.231e-36	2.231e-36	-35.651	-35.651	0.000
	S-2		0.000e+00	0.000e+00	-40.814	-41.051	-0.237
	S2-2		0.000e+00	0.000e+00	-65.546	-65.783	-0.237
	S3-2		0.000e+00	0.000e+00	-90.437	-90.674	-0.237
	S4-2		0.000e+00	0.000e+00	-115.629	-115.866	-0.237
	S5-2		0.000e+00	0.000e+00	-140.920	-141.157	-0.237

-----------------------------Saturation indices-------------------------------

Phase	SI	log IAP	log KT	
ANHYDRIT	-1.84	-6.11	-4.27	CaSO4
ANTARCTI	-11.66	-7.53	4.13	CaCl2(H2O)6
ARAGONIT	-0.16	-8.50	-8.34	CaCO3
CA(OH)2	-11.02	11.79	22.81	Ca(OH)2
CALCITE	-0.03	-8.50	-8.47	CaCO3
CALCIUM	-12.43	-7.53	4.90	CaCl2(H2O)4
CASO4.HY	-2.64	-6.11	-3.47	CaSO4(H2O).5
FIX_e-	0.00	0.00	0.00	e-
FIX_H+	-7.30	-7.30	0.00	H+
GYPSUM	-1.51	-6.11	-4.60	CaSO4(H2O)2
LAB.SALT	-17.29	-23.02	-5.73	Na4Ca(SO4)3(H2O)2
MIRABILI	-7.39	-8.46	-1.07	Na2SO4(H2O)10
MONOHYDR	-0.88	-8.50	-7.62	CaCO3H2O
NA2CO3	-11.52	-10.85	0.67	Na2CO3
O2(g)	-53.92	29.20	83.12	O2
OXYCH-CA	-1195.15	27.82	1222.97	Ca4(OH)6Cl2(H2O)13
PIRSSONI	-10.10	-19.36	-9.26	Na2Ca(CO3)2(H2O)2
S(C)	-25.93	-61.69	-35.76	S
THENARDI	-8.22	-8.46	-0.24	Na2SO4
THERMONA	-11.51	-10.85	0.66	Na2CO3H2O
VATERITE	-0.59	-8.50	-7.91	CaCO3
ZZ-CH4(G	-37.61	-78.69	-41.08	CH4
ZZ-H2(g)	-14.60	-14.60	0.00	H2
ZZ-H2S(G	-34.66	-76.29	-41.63	H2S
ZZ-PCO2	-2.14	-20.29	-18.15	CO2
ZZ-SO2(G	-27.25	-32.49	-5.24	O2S

```
------------------
End of simulation.
------------------------------------
Reading input data for simulation 2.
------------------------------------

        TITLE   Nd in trench solution
        USE Solution 1
        EQUILIBRIUM_PHASES 1
                Nd2(CO3)3
                FIX_H+  -7.3    HCl     10.0
```

```
                FIX_e-   0.742    O2(g)      10.0
        END
-----
TITLE
-----

   Nd in trench solution

-----------------------------------
Beginning of reaction calculations.
-----------------------------------

Reaction step 1.

Using solution 1.

Using pure phase assemblage 1.

-------------------------------Phase assemblage--------------------------------

                                                    Moles in assemblage
Phase                SI log IAP  log KT    Initial       Final       Delta

FIX_e-             0.74    0.74    0.00
        O2                 is reactant     1.000e+01   1.000e+01 -1.768e-15
FIX_H+            -7.30   -7.30    0.00
        HCl                is reactant     1.000e+01   1.000e+01 -1.750e-07
Nd2(CO3)3          0.00  -33.70  -33.70    1.000e+01   1.000e+01 -4.208e-07

-----------------------------Solution composition------------------------------

Elements            Molality        Moles

C                   2.833e-03   2.833e-03
Ca                  2.852e-03   2.852e-03
Cl                  5.003e-03   5.003e-03
Mg                  6.004e-04   6.004e-04
Na                  3.002e-03   3.002e-03
Nd                  8.416e-07   8.416e-07
S                   1.091e-03   1.091e-03

----------------------------Description of solution----------------------------

                                pH  =   7.300      Charge balance
                                pe  =  -0.742      Adjusted to redox equilibrium
                   Activity of water  =   1.000
                      Ionic strength  =   1.345e-02
                   Mass of water (kg)  =   1.000e+00
               Total alkalinity (eq/kg)  =   2.596e-03
                     Total CO2 (mol/kg)  =   2.833e-03
                   Temperature (deg C)  =  25.000
                Electrical balance (eq)  =   1.279e-04
                          Iterations  =  11
                             Total H  = 1.110155e+02
                             Total O  = 5.551908e+01

----------------------------Distribution of species----------------------------

                                                  Log         Log         Log
            Species          Molality    Activity Molality    Activity    Gamma

            OH-              2.286e-07   1.995e-07   -6.641      -6.700   -0.059
            H+               5.548e-08   5.012e-08   -7.256      -7.300   -0.044
            H2O              5.551e+01   9.997e-01    0.000       0.000    0.000
C(-4)                2.811e-35
            CH4              2.811e-35   2.811e-35  -34.551     -34.551    0.000
C(4)                 2.833e-03
            HCO3-            2.522e-03   2.201e-03   -2.598      -2.657   -0.059
            H2CO3            2.469e-04   2.469e-04   -3.607      -3.607    0.000
            CaHCO3+          4.051e-05   3.534e-05   -4.392      -4.452   -0.059
            MgHCO3+          1.014e-05   9.014e-06   -4.994      -5.045   -0.051
            CaCO3            4.450e-06   4.450e-06   -5.352      -5.352    0.000
            CO3-2            3.544e-06   2.054e-06   -5.450      -5.687   -0.237
            NaHCO3           3.229e-06   3.229e-06   -5.491      -5.491    0.000
            MgCO3            6.858e-07   6.879e-07   -6.164      -6.162    0.001
            NdCO3+           5.284e-07   4.610e-07   -6.277      -6.336   -0.059
            Nd(CO3)2-        2.854e-07   2.490e-07   -6.544      -6.604   -0.059
            NaCO3-           1.144e-07   9.979e-08   -6.942      -7.001   -0.059
Ca                   2.852e-03
            Ca+2             2.647e-03   1.534e-03   -2.577      -2.814   -0.237
            CaSO4            1.599e-04   1.599e-04   -3.796      -3.796    0.000
            CaHCO3+          4.051e-05   3.534e-05   -4.392      -4.452   -0.059
            CaCO3            4.450e-06   4.450e-06   -5.352      -5.352    0.000
            CaOH+            8.808e-09   7.685e-09   -8.055      -8.114   -0.059
Cl                   5.003e-03
            Cl-              5.003e-03   4.365e-03   -2.301      -2.360   -0.059
H(0)                 1.084e-16
            H2               5.420e-17   5.420e-17  -16.266     -16.266    0.000
```

Mg		6.004e-04				
	Mg+2		5.477e-04	3.510e-04	-3.261	-3.455	-0.193
	MgSO4		4.189e-05	4.202e-05	-4.378	-4.377	0.001
	MgHCO3+		1.014e-05	9.014e-06	-4.994	-5.045	-0.051
	MgCO3		6.858e-07	6.879e-07	-6.164	-6.162	0.001
Na		3.002e-03				
	Na+		2.991e-03	2.609e-03	-2.524	-2.583	-0.059
	NaSO4-		7.654e-06	6.678e-06	-5.116	-5.175	-0.059
	NaHCO3		3.229e-06	3.229e-06	-5.491	-5.491	0.000
	NaCO3-		1.144e-07	9.979e-08	-6.942	-7.001	-0.059
Nd		8.416e-07				
	NdCO3+		5.284e-07	4.610e-07	-6.277	-6.336	-0.059
	Nd(CO3)2-		2.854e-07	2.490e-07	-6.544	-6.604	-0.059
	Nd+3		1.638e-08	4.799e-09	-7.786	-8.319	-0.533
	NdSO4+		9.966e-09	8.695e-09	-8.001	-8.061	-0.059
	NdOH+2		1.143e-09	6.623e-10	-8.942	-9.179	-0.237
	Nd(SO4)2-		2.273e-10	1.983e-10	-9.643	-9.703	-0.059
	Nd(OH)2+		1.996e-11	1.742e-11	-10.700	-10.759	-0.059
	Nd(OH)3		1.516e-13	1.516e-13	-12.819	-12.819	0.000
O(0)		0.000e+00				
	O2		0.000e+00	0.000e+00	-59.848	-59.848	0.000
S(-2)		4.506e-30				
	HS-		4.506e-30	3.932e-30	-29.346	-29.405	-0.059
S(6)		1.091e-03				
	SO4-2		8.812e-04	5.106e-04	-3.055	-3.292	-0.237
	CaSO4		1.599e-04	1.599e-04	-3.796	-3.796	0.000
	MgSO4		4.189e-05	4.202e-05	-4.378	-4.377	0.001
	NaSO4-		7.654e-06	6.678e-06	-5.116	-5.175	-0.059
	NdSO4+		9.966e-09	8.695e-09	-8.001	-8.061	-0.059
	HSO4-		2.867e-09	2.501e-09	-8.543	-8.602	-0.059
	Nd(SO4)2-		2.273e-10	1.983e-10	-9.643	-9.703	-0.059
	H2SO4		1.253e-18	1.253e-18	-17.902	-17.902	0.000
	O2S		2.101e-26	2.101e-26	-25.678	-25.678	0.000
	H2S		1.926e-30	1.926e-30	-29.715	-29.715	0.000
	S-2		1.323e-35	7.666e-36	-34.878	-35.115	-0.237

----------Saturation indices----------

Phase	SI	log IAP	log KT	
ANHYDRIT	-1.84	-6.11	-4.27	CaSO4
ANTARCTI	-11.66	-7.53	4.13	CaCl2(H2O)6
ARAGONIT	-0.16	-8.50	-8.34	CaCO3
CA(OH)2	-11.02	11.79	22.81	Ca(OH)2
CALCITE	-0.03	-8.50	-8.47	CaCO3
CALCIUM	-12.43	-7.53	4.90	CaCl2(H2O)4
CASO4.HY	-2.64	-6.11	-3.47	CaSO4(H2O).5
FIX_e-	0.74	0.74	0.00	e-
FIX_H+	-7.30	-7.30	0.00	H+
GYPSUM	-1.51	-6.11	-4.60	CaSO4(H2O)2
LAB.SALT	-17.29	-23.02	-5.73	Na4Ca(SO4)3(H2O)2
MIRABILI	-7.39	-8.46	-1.07	Na2SO4(H2O)10
MONOHYDR	-0.88	-8.50	-7.62	CaCO3H2O
NA2CO3	-11.52	-10.85	0.67	Na2CO3
NaNd(CO3)2	-0.89	-22.28	-21.39	NaNd(CO3)2
NaNd(SO4)2	-6.81	-17.49	-10.68	NaNd(SO4)2
Nd(OH)3	-7.01	13.58	20.59	Nd(OH)3
Nd(OH)3(c)	-1.38	13.58	14.96	Nd(OH)3
Nd2(CO3)3	0.00	-33.70	-33.70	Nd2(CO3)3
Nd2SO4(OH)4	-4.50	9.27	13.77	Nd2SO4(OH)4
NdOHCO3	-0.77	-6.71	-5.94	NdOHCO3
O2(g)	-56.89	26.23	83.12	O2
OXYCH-CA	-1195.15	27.82	1222.97	Ca4(OH)6Cl2(H2O)13
PIRSSONI	-10.10	-19.36	-9.26	Na2Ca(CO3)2(H2O)2
S(C)	-21.48	-57.24	-35.76	S
THENARDI	-8.22	-8.46	-0.24	Na2SO4
THERMONA	-11.51	-10.85	0.66	Na2CO3H2O
VATERITE	-0.59	-8.50	-7.91	CaCO3
ZZ-CH4(G	-31.67	-72.75	-41.08	CH4
ZZ-H2(g)	-13.12	-13.12	0.00	H2
ZZ-H2S(G	-28.73	-70.36	-41.63	H2S
ZZ-PCO2	-2.14	-20.29	-18.15	CO2
ZZ-SO2(G	-25.77	-31.01	-5.24	O2S

End of simulation.

Appendix 7.2a The aqueous speciation of 10^{-7}M Ce in 1mM TIC (after CHEMVAL 6)

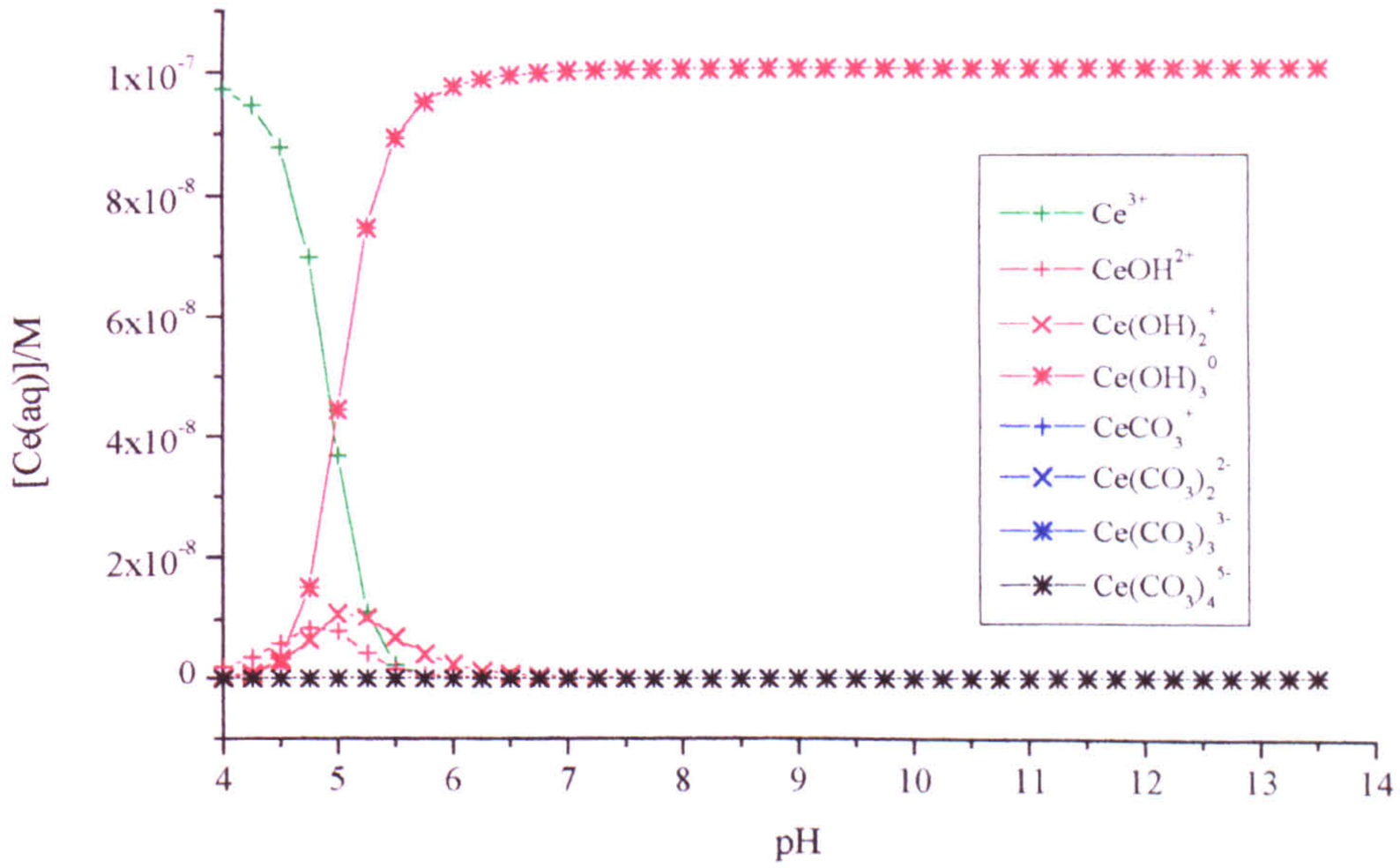

Appendix 7.2b Aqueous speciation of 10^{-7}M Ce in 0.01mM TIC (after CHEMVAL 6)

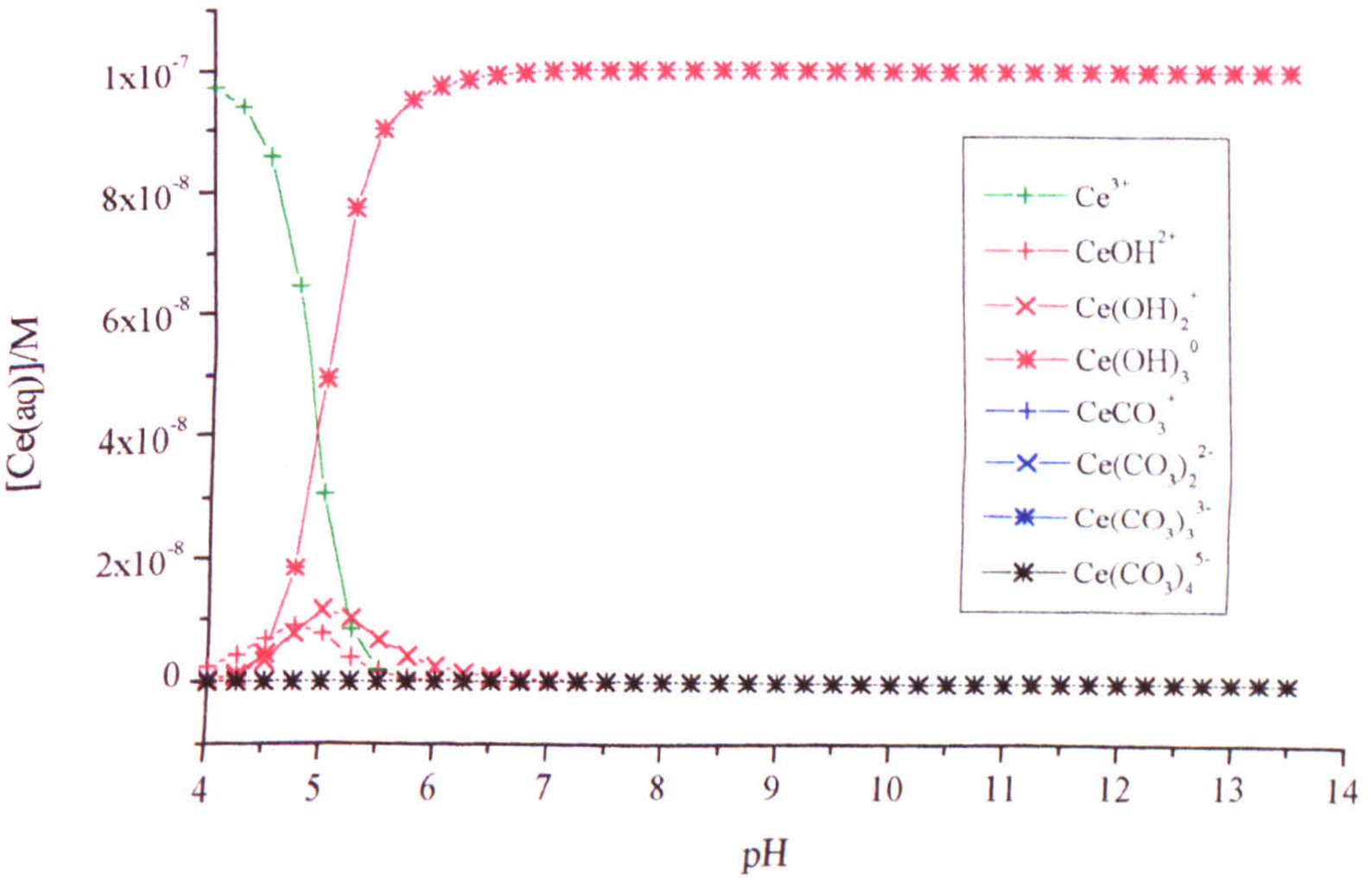

Appendix 7.2c The aqueous speciation of 10^{-7}M Nd in 1mM TIC (after CHEMVAL 6)

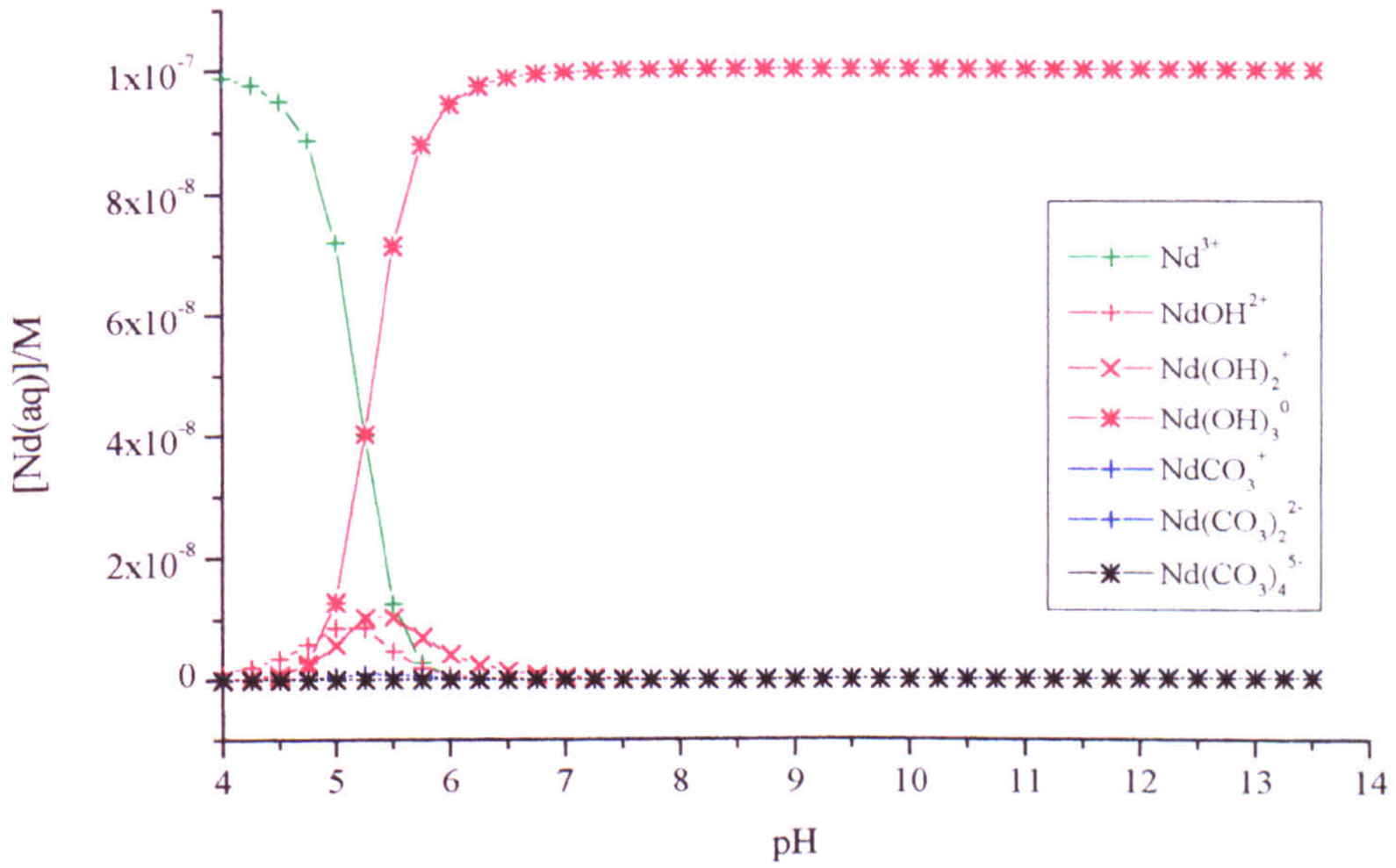

Appendix 7.2d The aqueous speciation of 10^{-7}M Nd in 0.01mM TIC (after CHEMVAL 6)

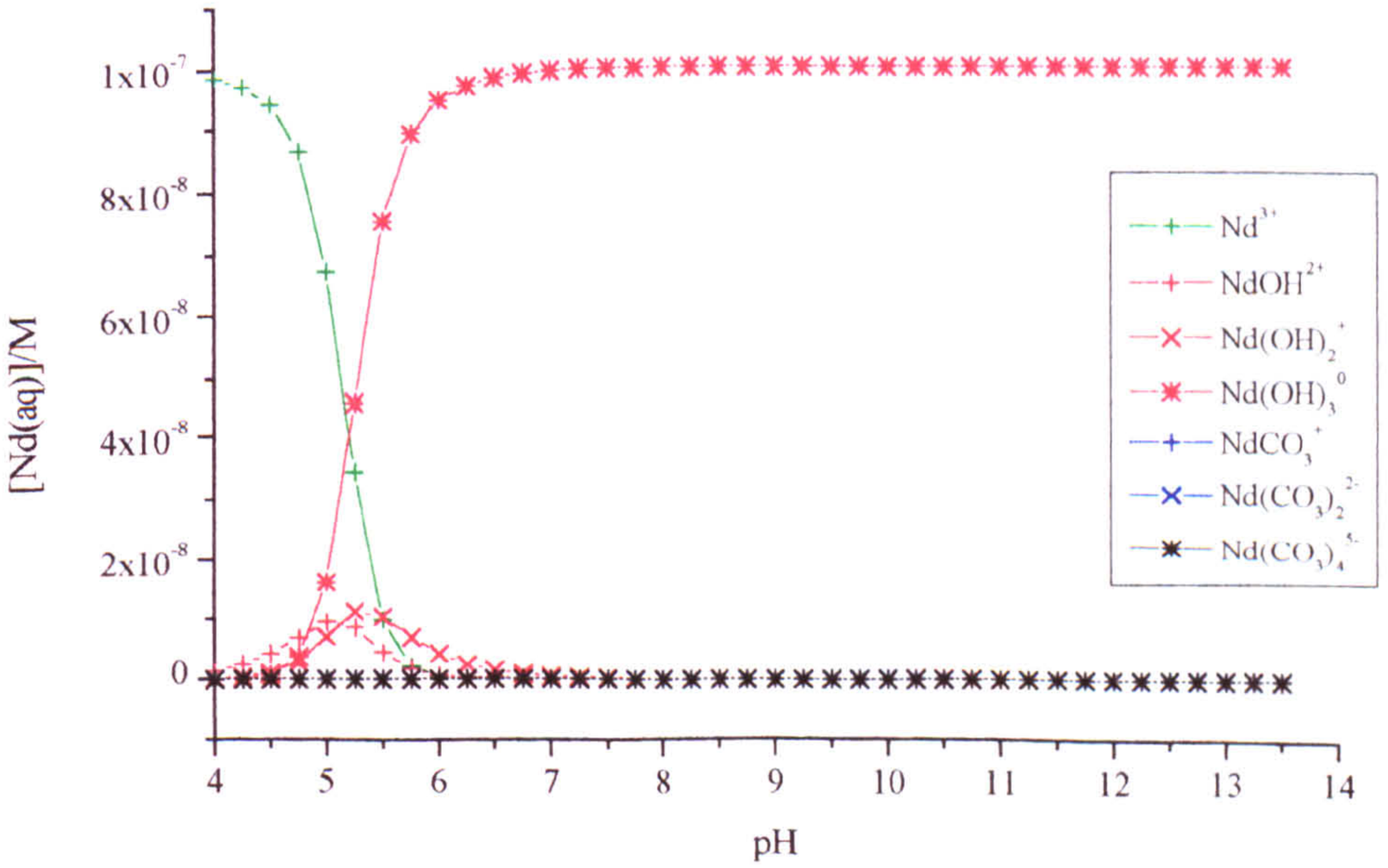

Appendix 7.3a The aqueous speciation of 10^{-7}M Nd in 10^{-3}M TIC (after Lee & Byrne 1992/1993)

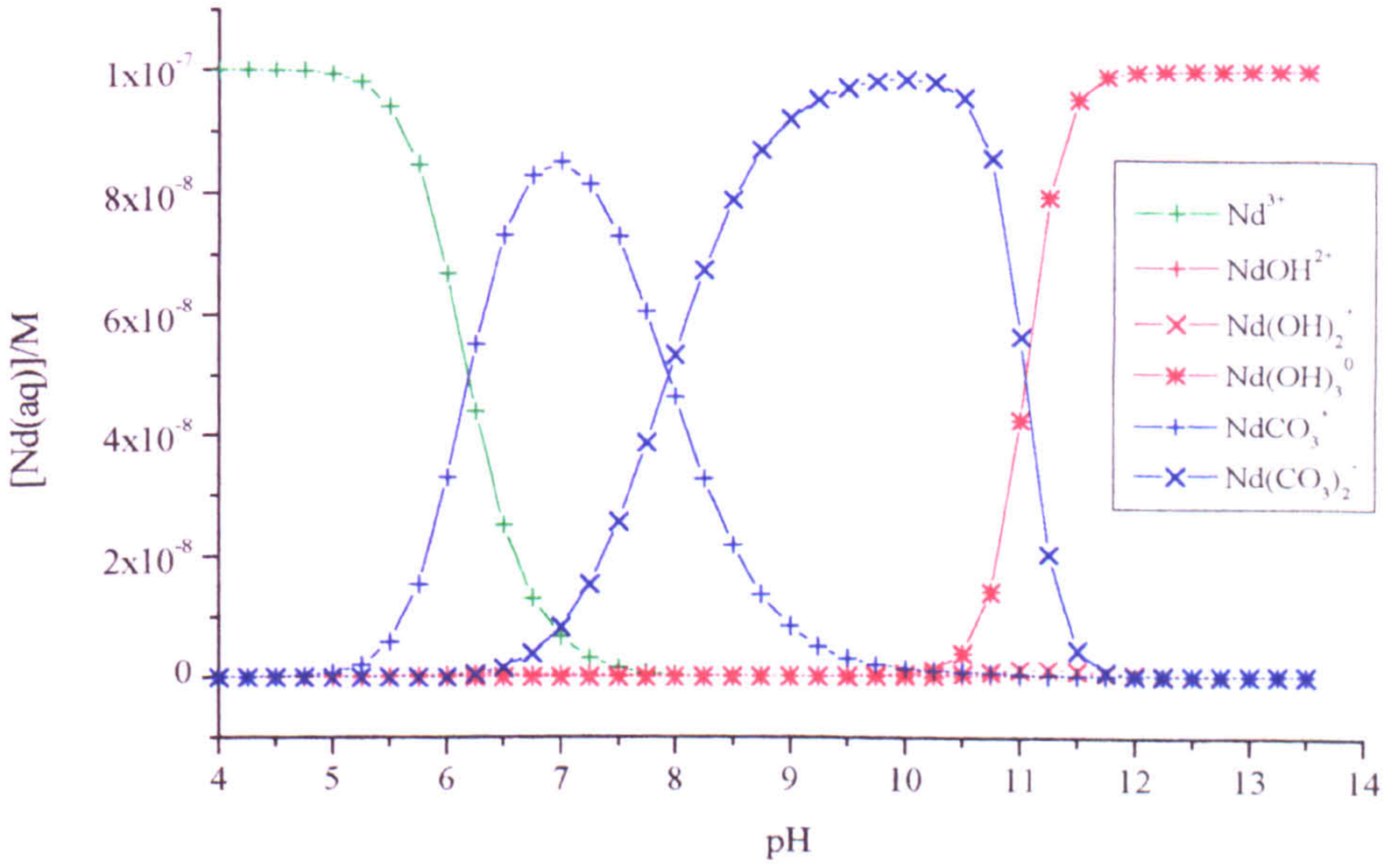

Appendix 7.3b The aqueous speciation of 10^{-7}M Nd in 10^{-5}M TIC (after Lee & Byrne database)

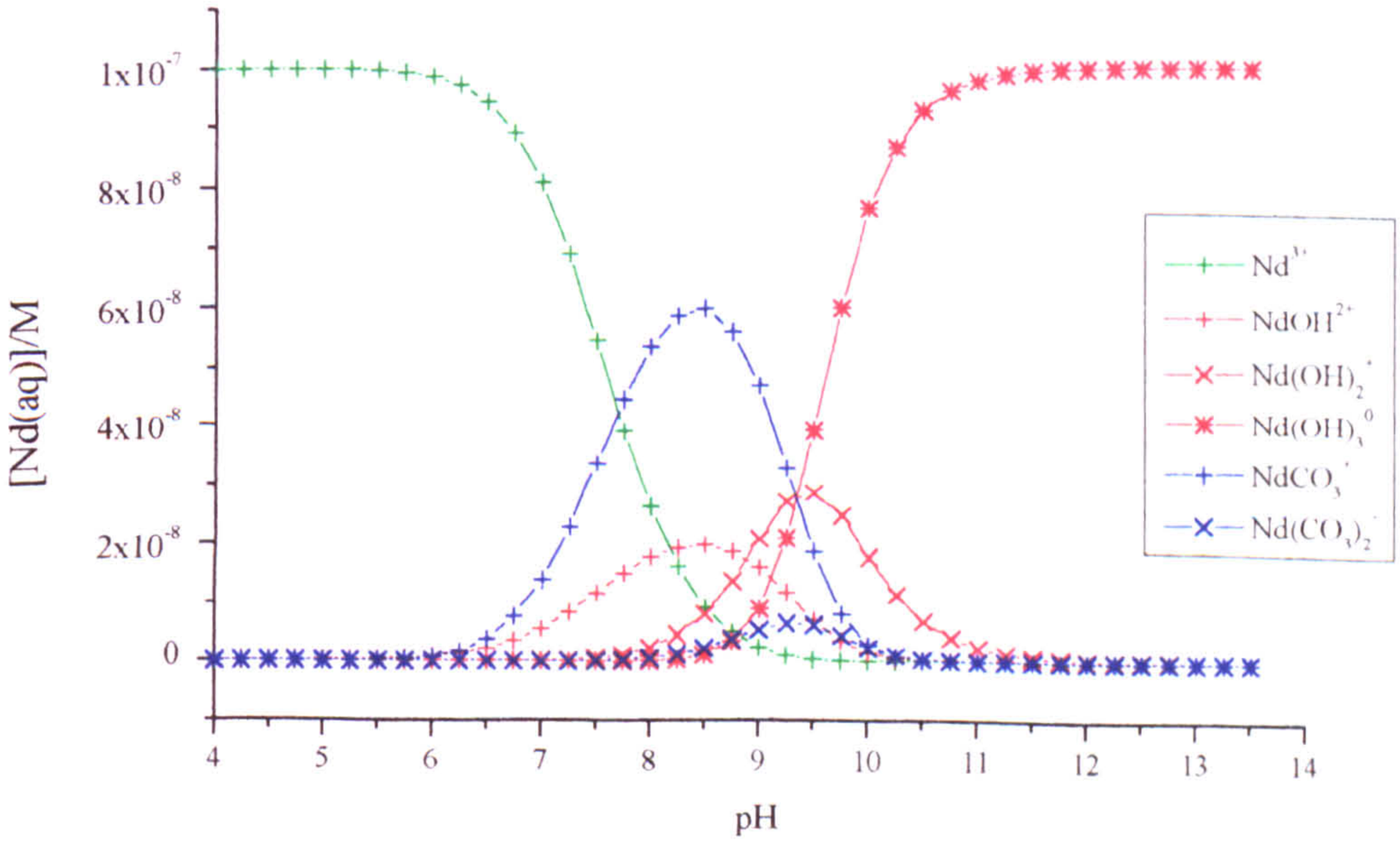

Appendix 7.3c The aqueous speciation of 10^{-7}M Nd in 10^{-3}M TIC
(after Lee & Byrne 1992/1993)

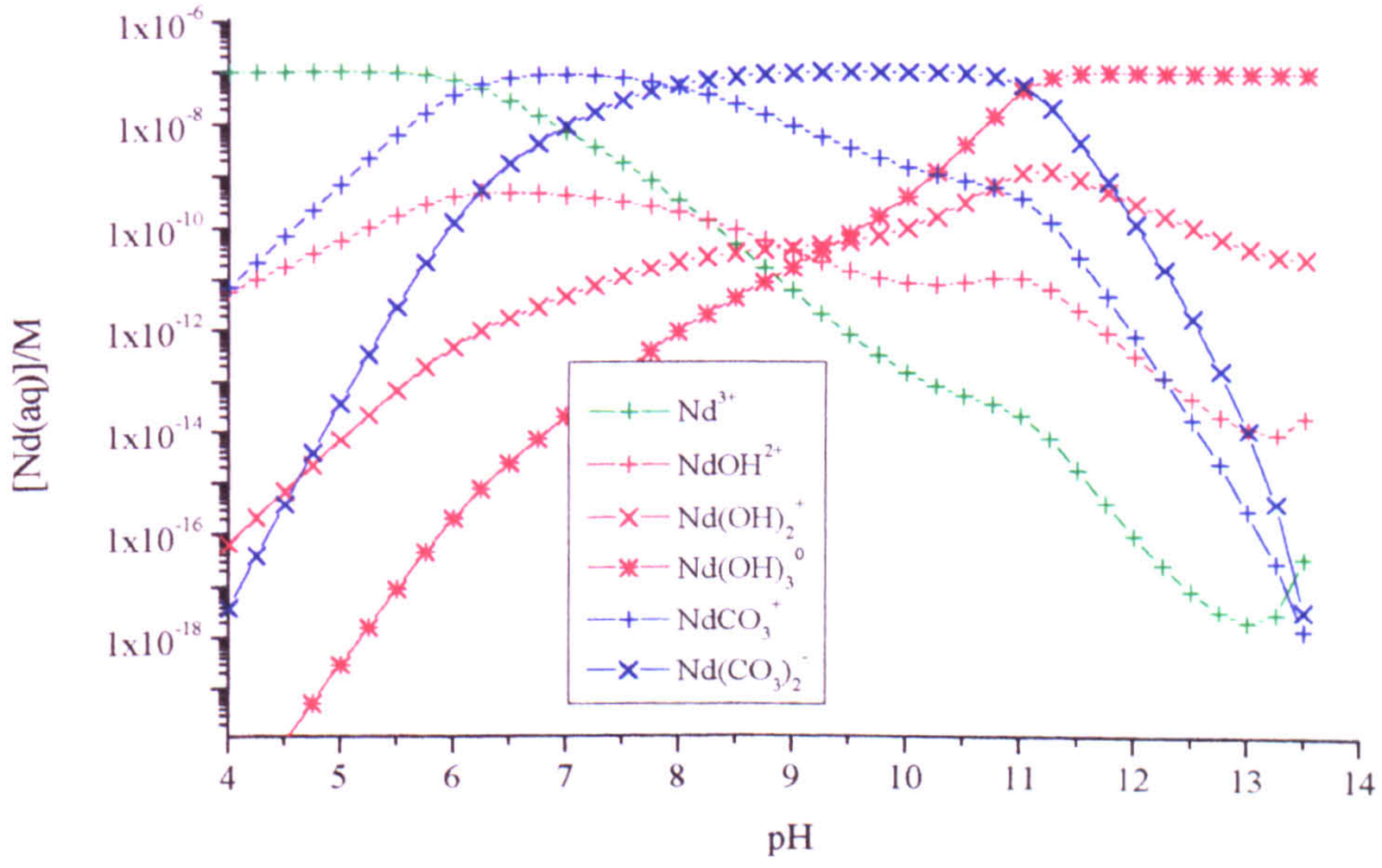

Appendix 7.3d The aqueous speciation of 10^{-7}M Nd in 10^{-5}M TIC
(after Lee & Byrne database)

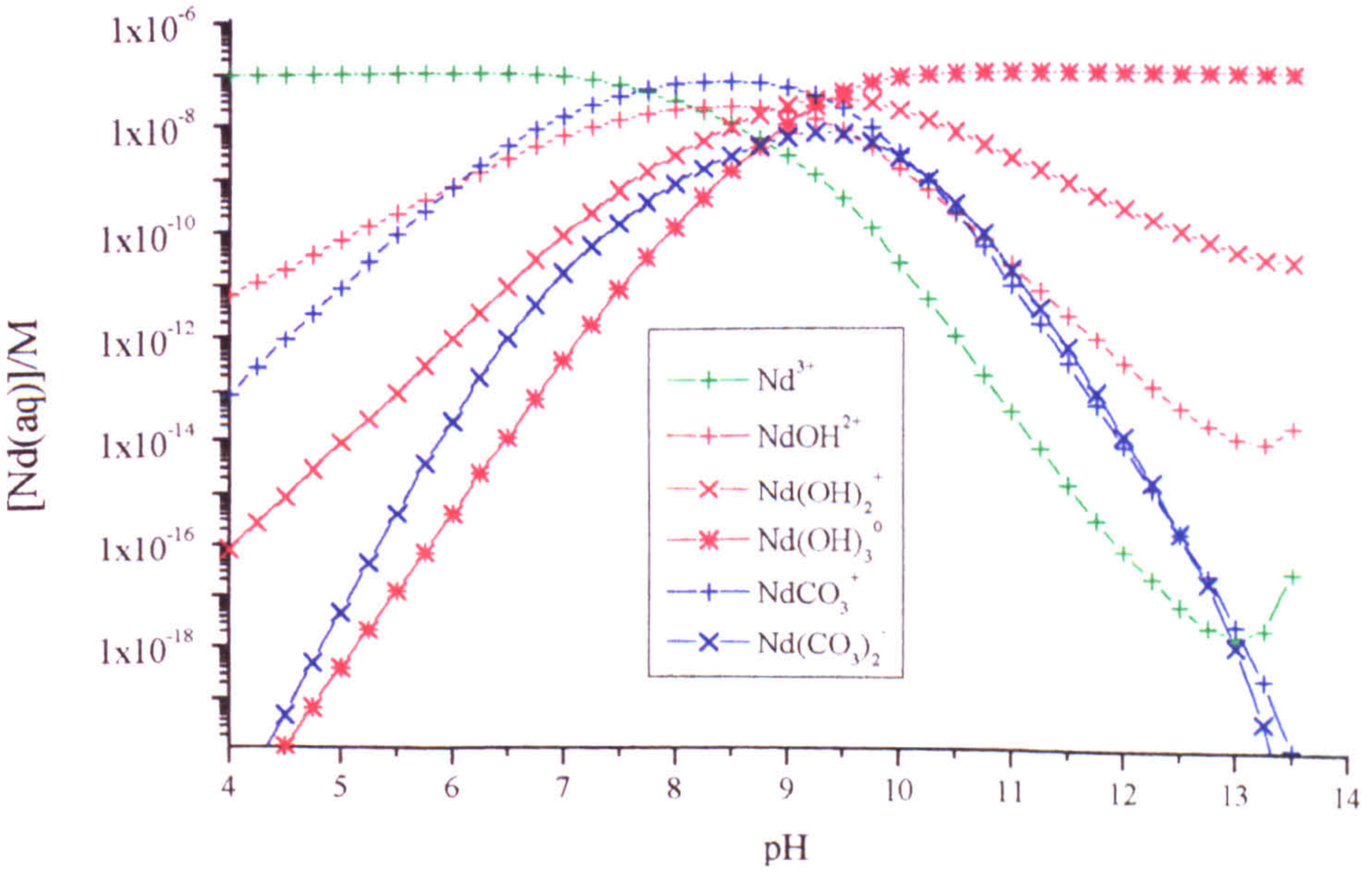

Appendix 7.4a The speciation of aqueous 10^{-7}M Am in 10^{-3}M TIC (after CHEMVAL 6)

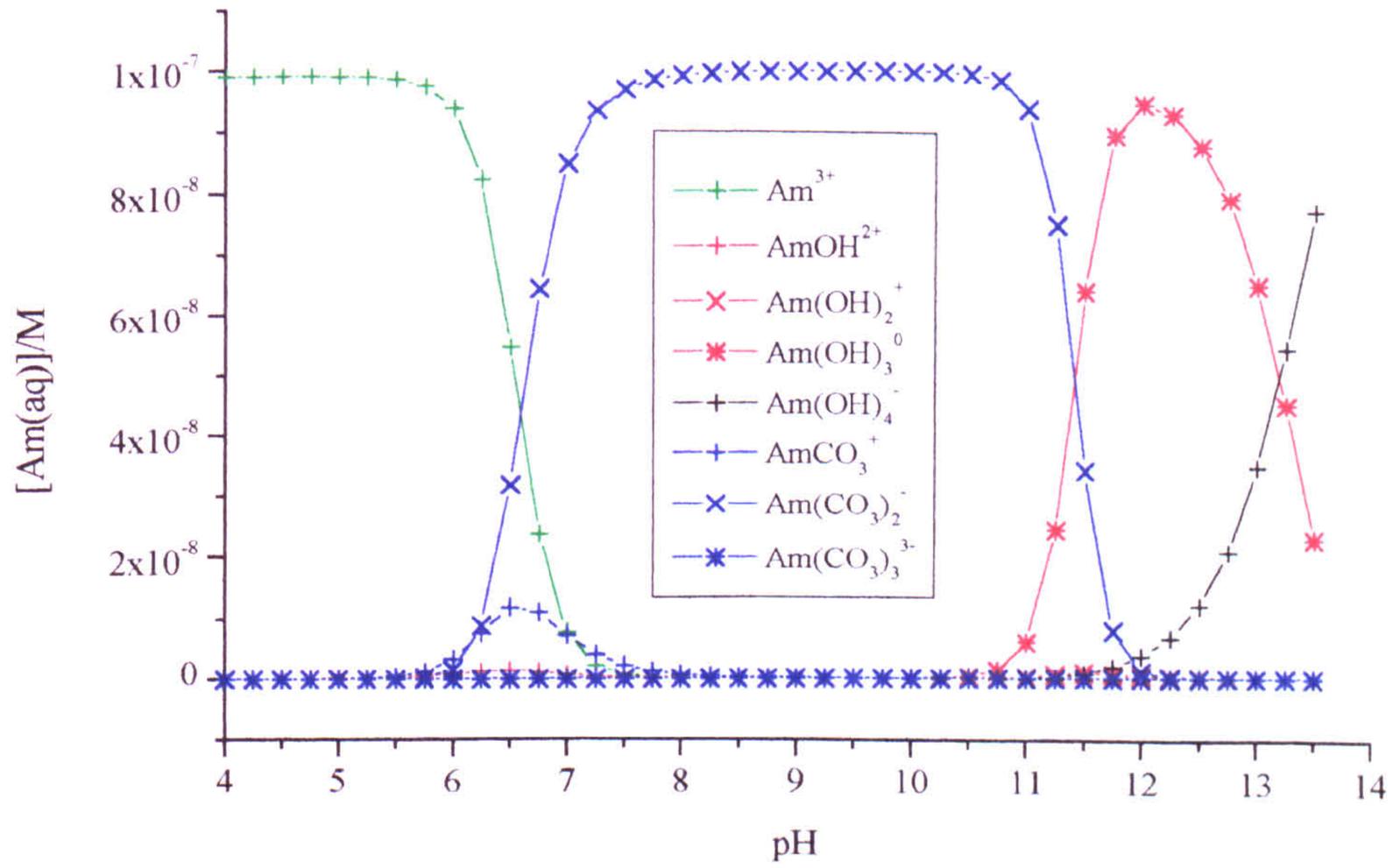

Appendix 7.4b The speciation of 10^{-7}M Am in 10^{-5}M TIC (after CHEMVAL 6)

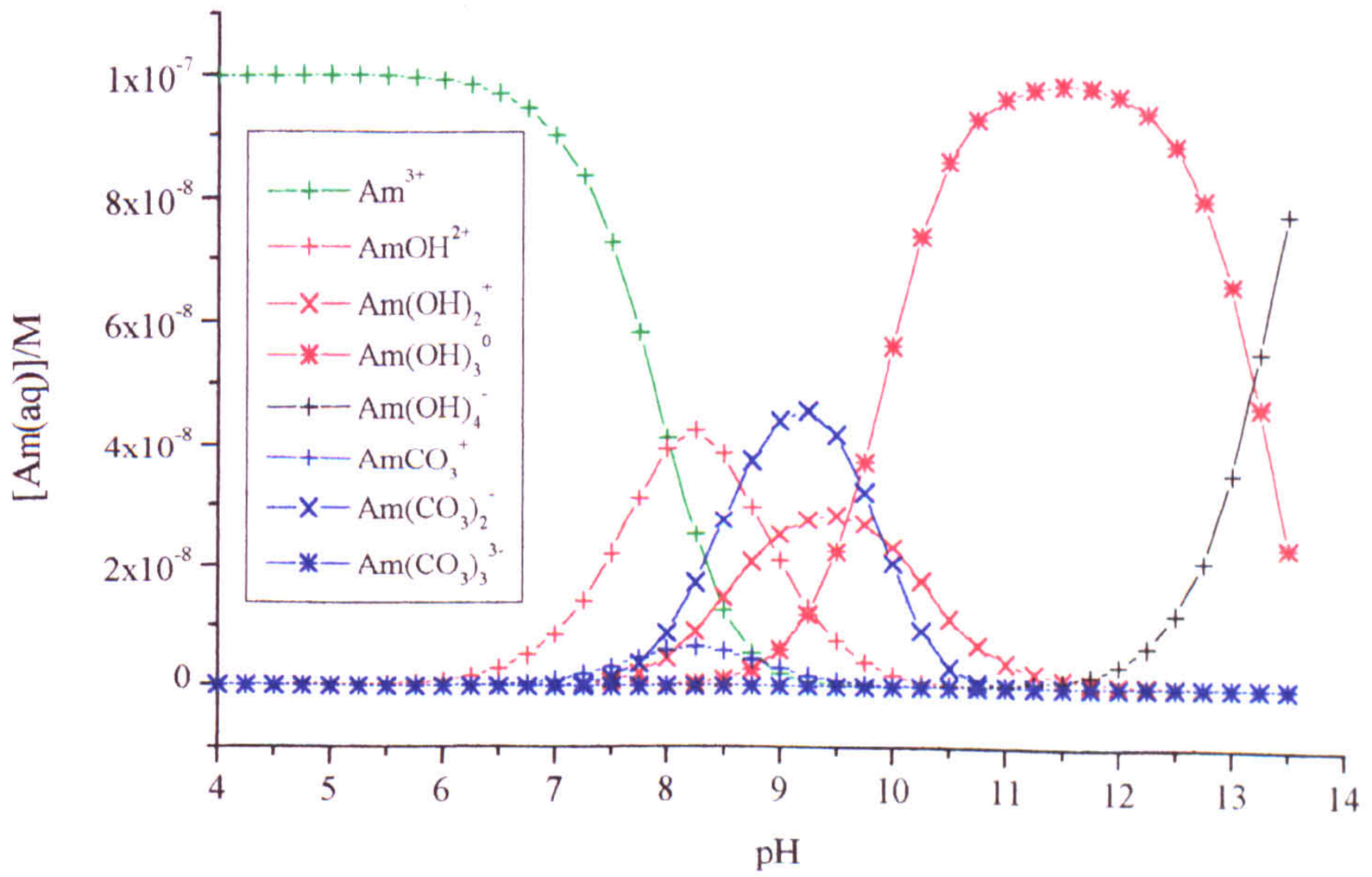

Appendix 7.5a The speciation of 10^{-7}M Am in 10mM TIC solution (after Silva *et al.*, (1995)/NEA 9)

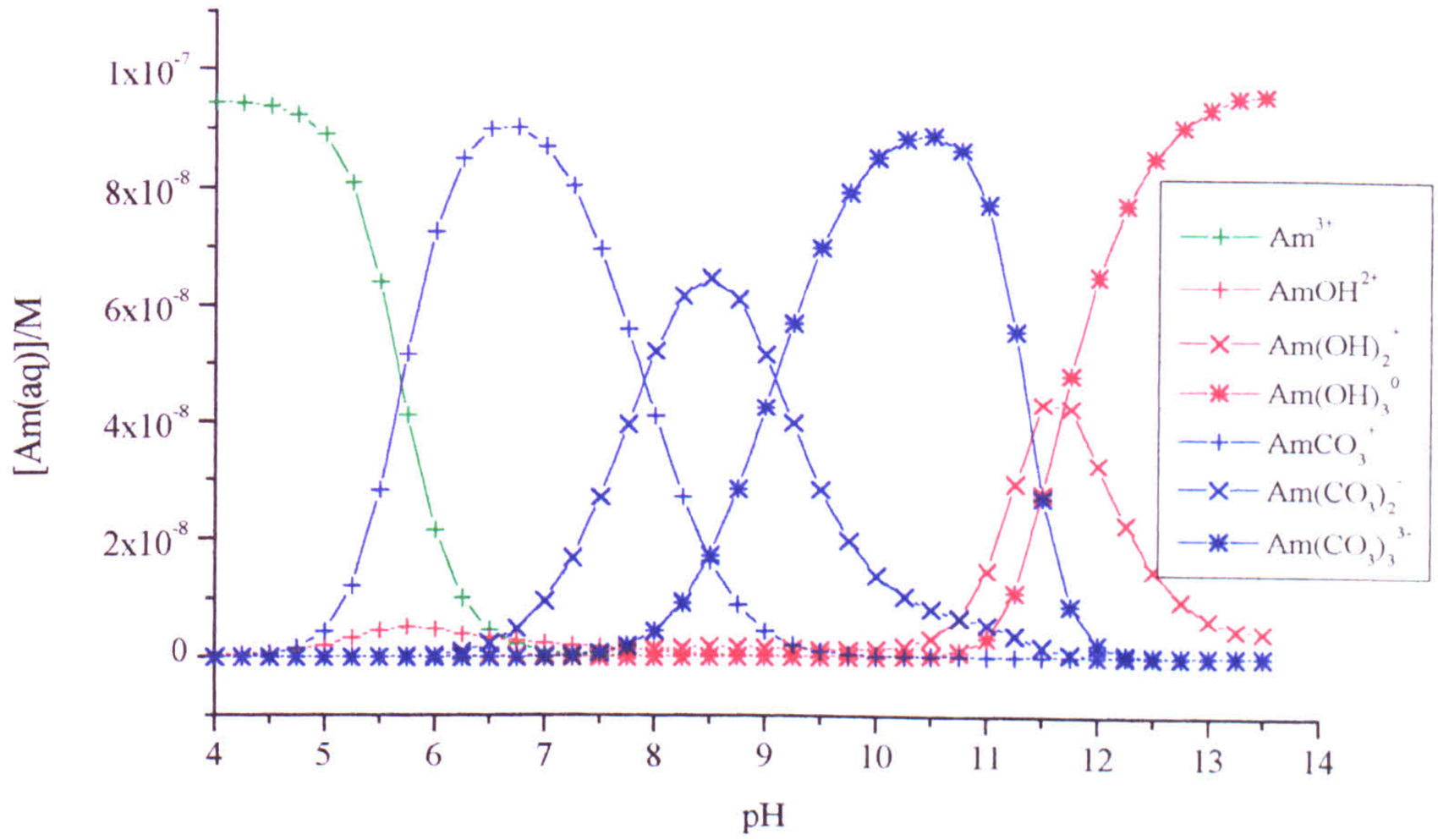

Appendix 7.5b The speciation of 10^{-7}M Am in 1mM TIC solution (after Silva *et al.*, (1995)/NEA 9)

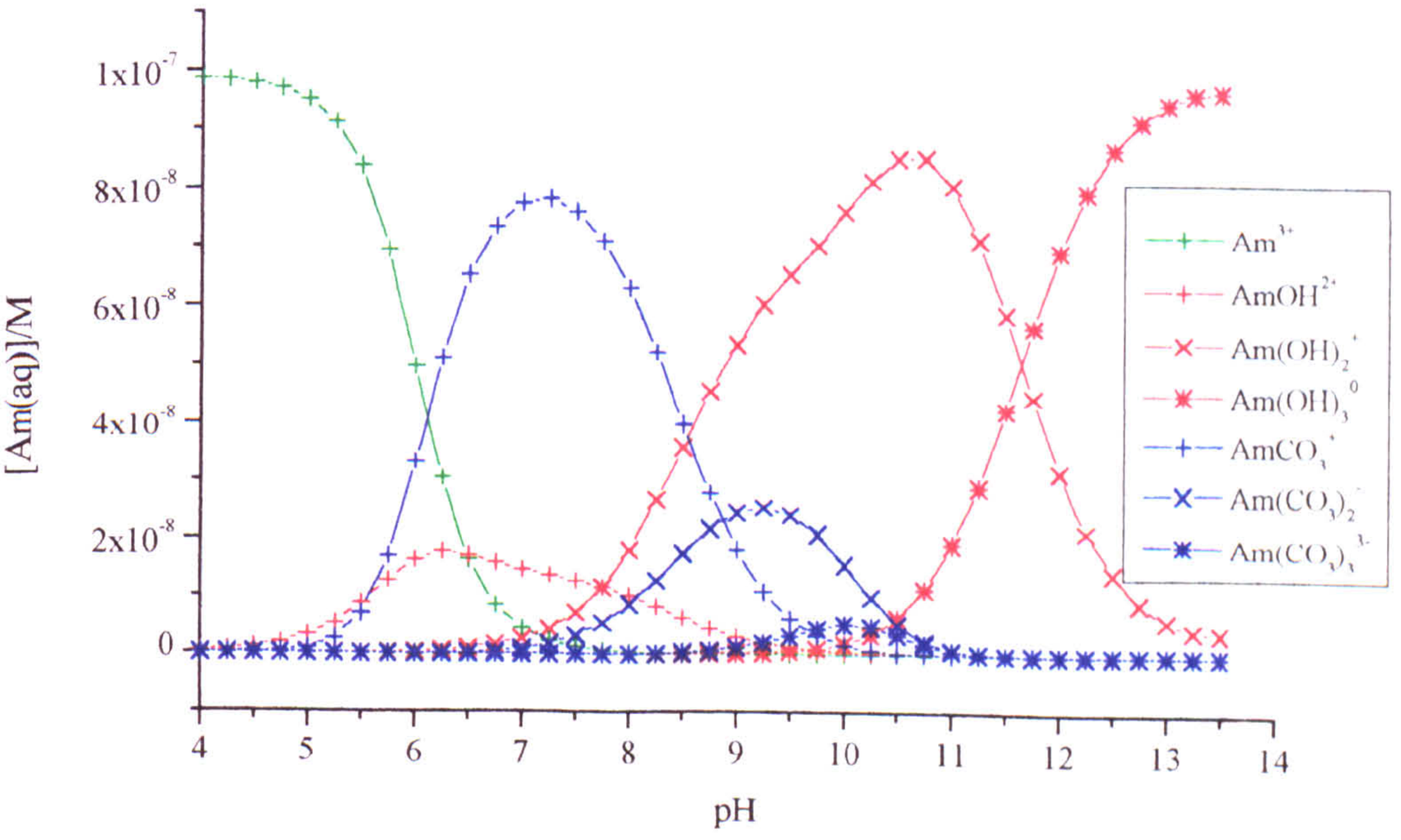

Appendix 7.5c The speciation of 10^{-7}M Am in 0.1mM TIC solution (after Silva *et al.*, (1995)/NEA 9)

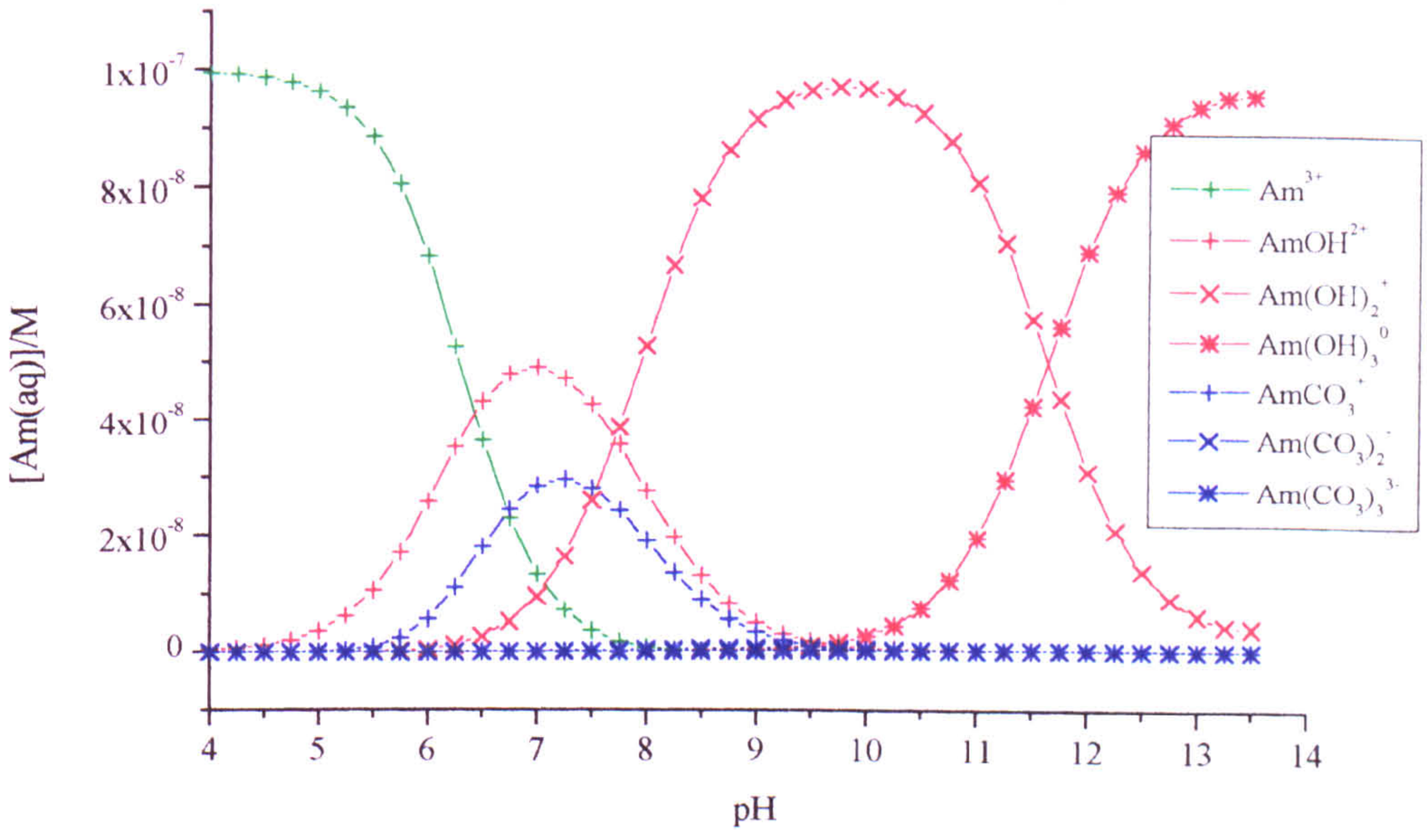

Appendix 7.5d The speciation of 10^{-7}M Am in 0.01mM TIC solution (after Silva *et al.*, (1995)/NEA 9)

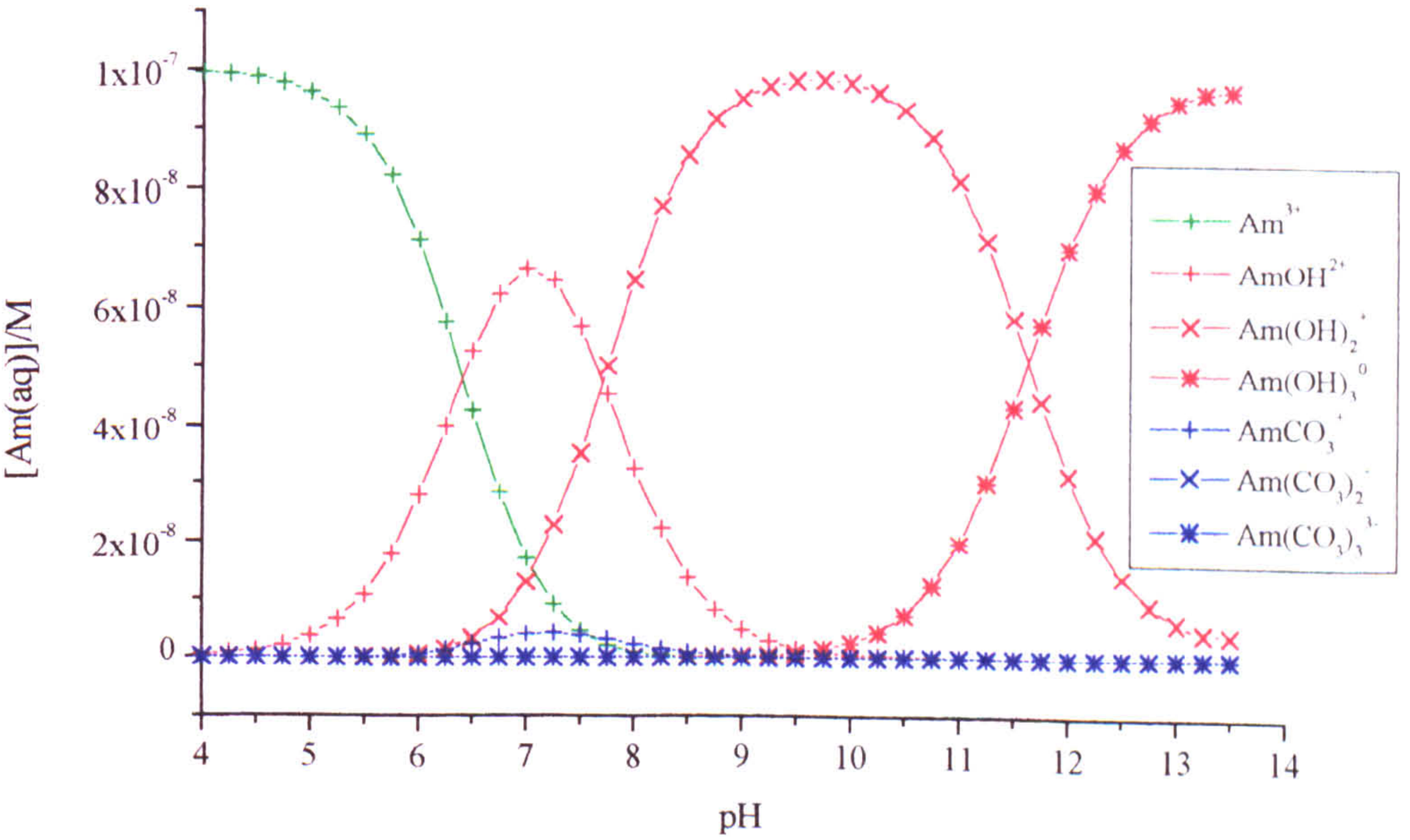

Appendix 7.6a The aqueous speciation of 10^{-7}M Nd in 10^{-3}M TIC (after NEA database)

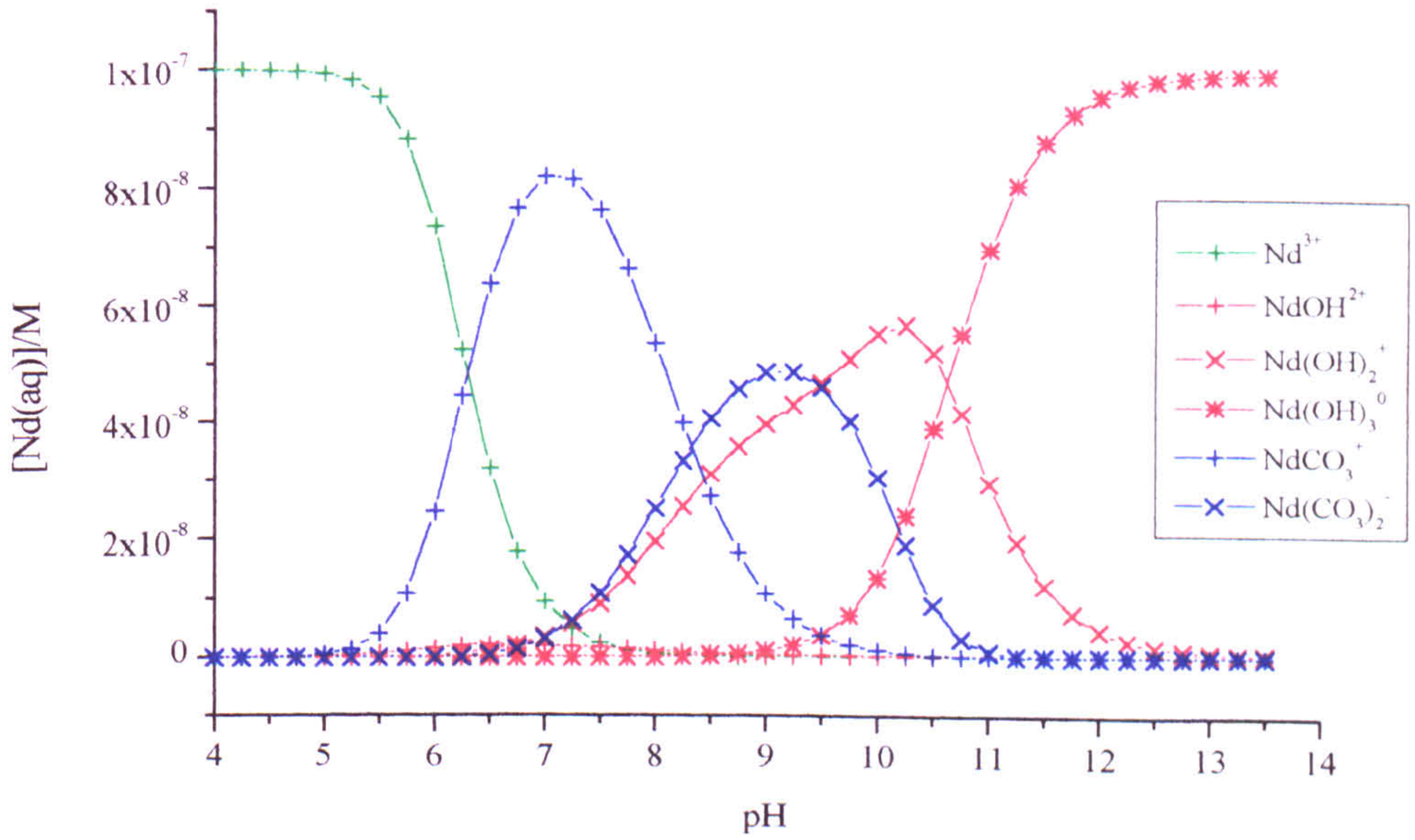

Appendix 7.6b the aqueous speciation of 10^{-7}M Nd in 10^{-5}M TIC (after NEA database)

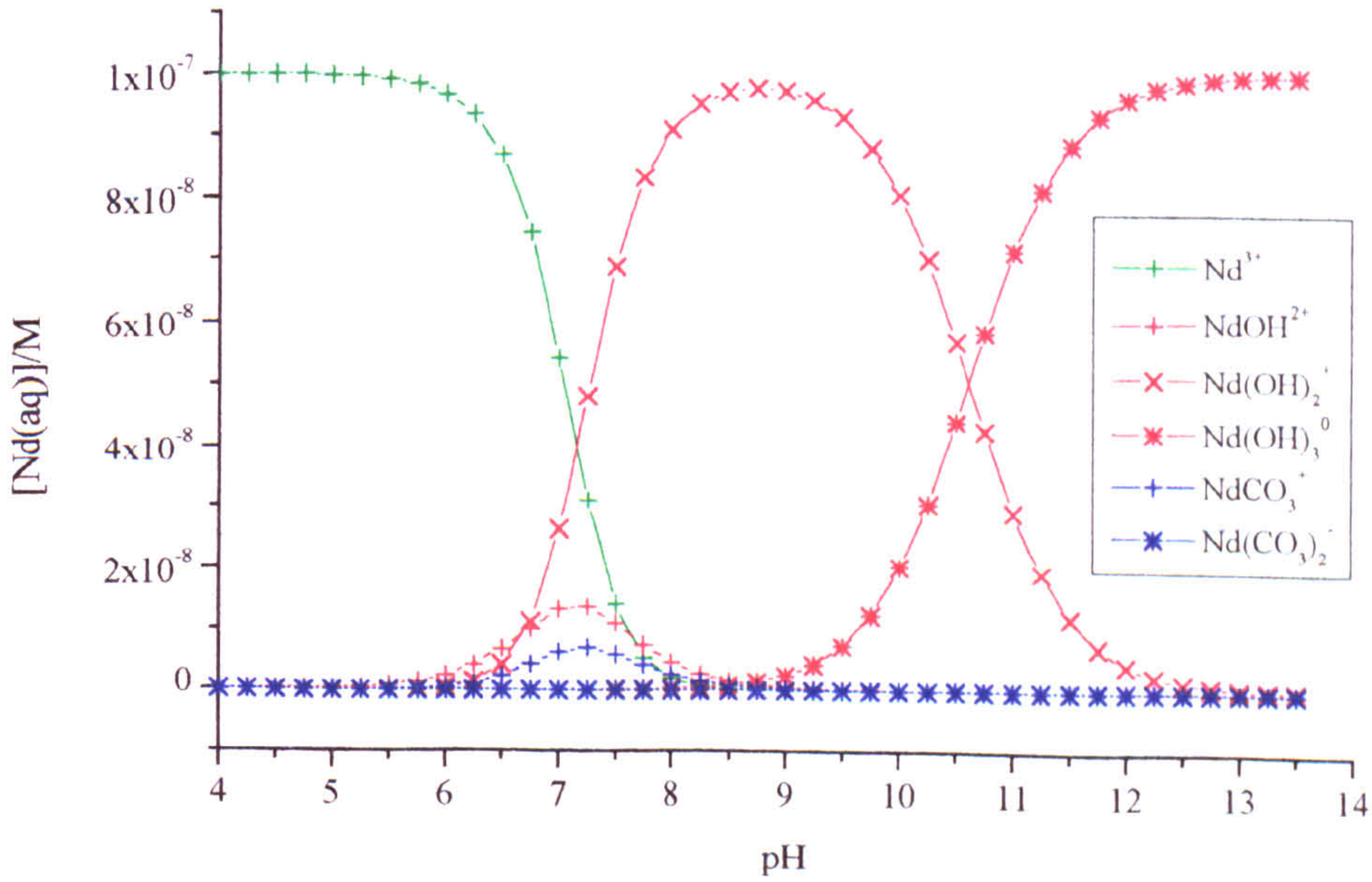

Appendix 7.6c The aqueous speciation of 10^{-7}M Nd in 10^{-2}M TIC assuming $Nd(CO_3)_3^{3-}$ log = K 15.2 (after NEA database)

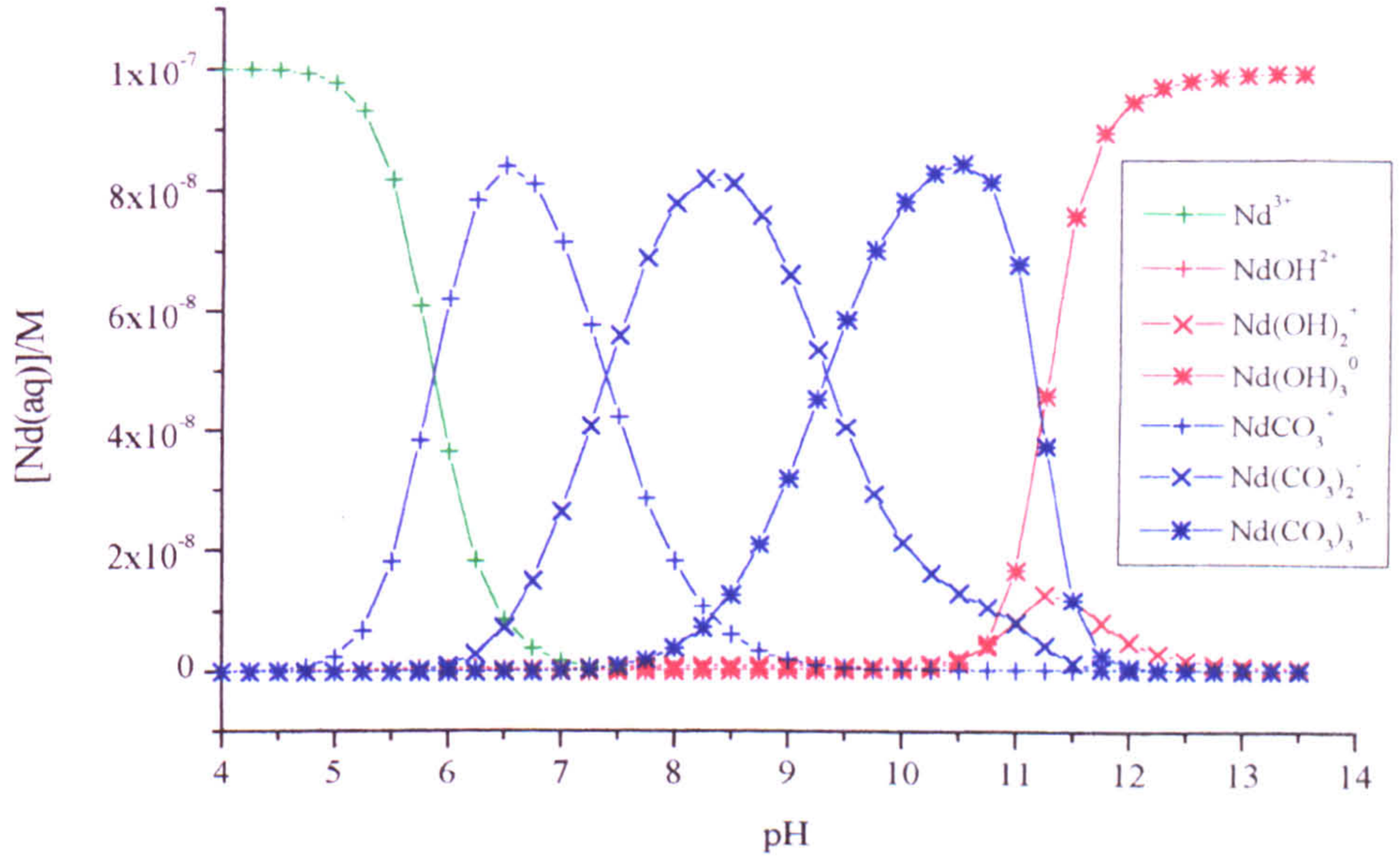

Appendix 7.6d The aqueous speciation of 10^{-7}M Nd in 10^{-3}M TIC assuming $Nd(CO_3)_3^{3-}$ log K = 15.2 (after NEA database)

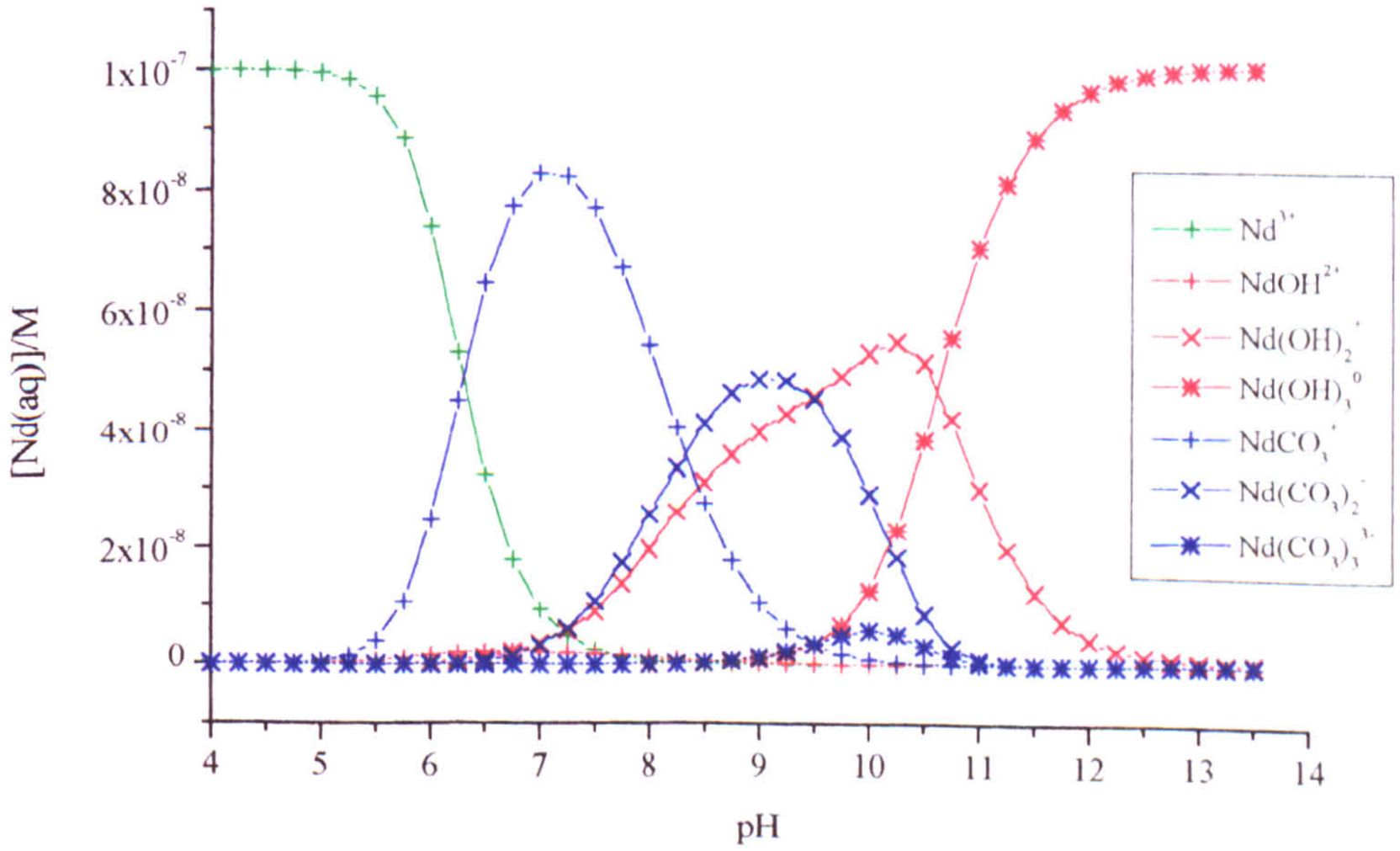

Appendix 7.7a Nd solubility in 1mM TIC and 1mM SO_4^{2-} solution calculated with Lee and Byrne (1992 & 1993) aqueous species constants at 298.15K and 1 atm pressure

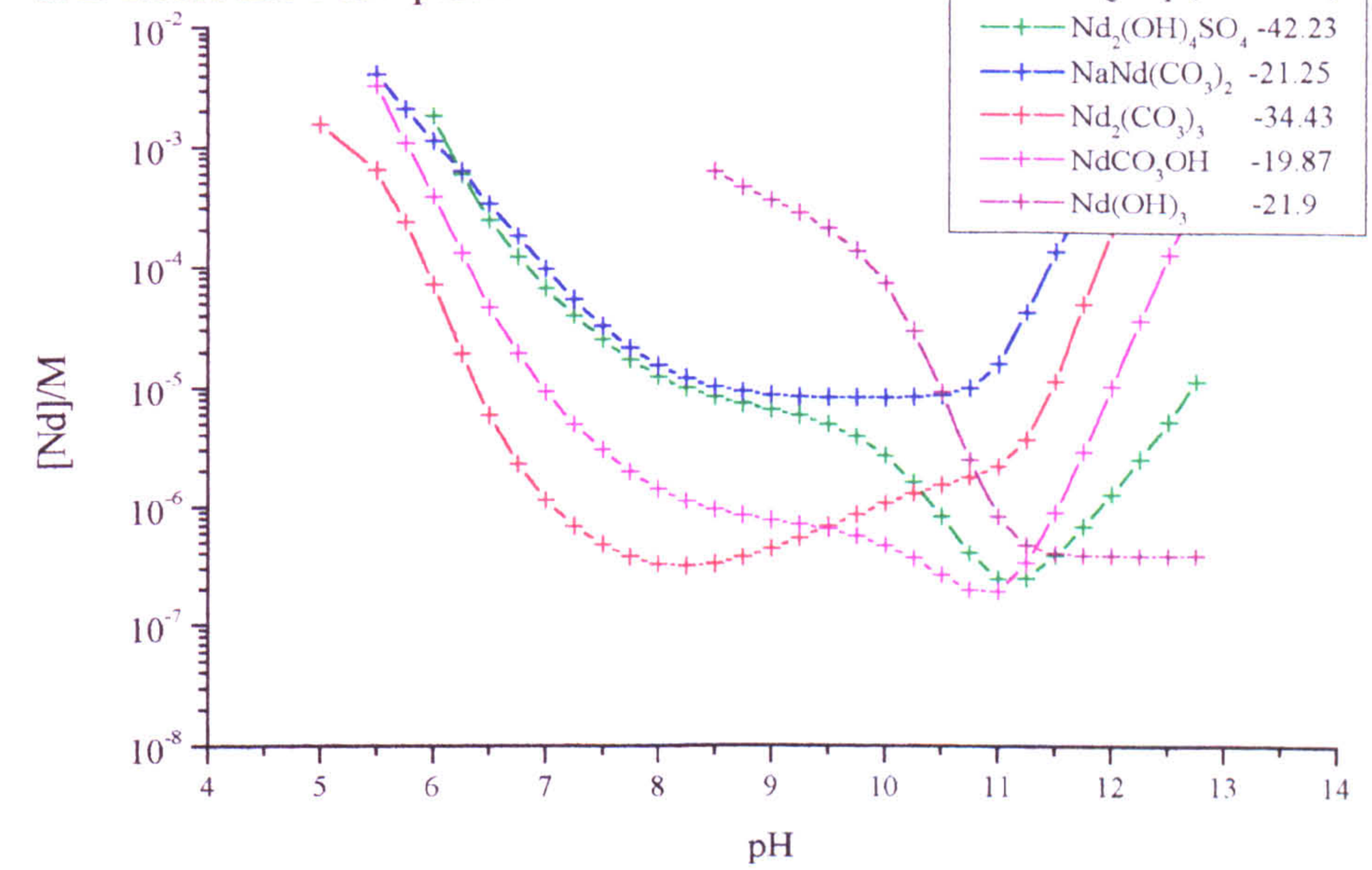

Appendix 7.7b Nd solubility in 1mM TIC and 1mM SO_4^{2-} solution calculated with NEA 9 (Table 7.1) aqueous species constants at 298.15K and 1 atm pressure

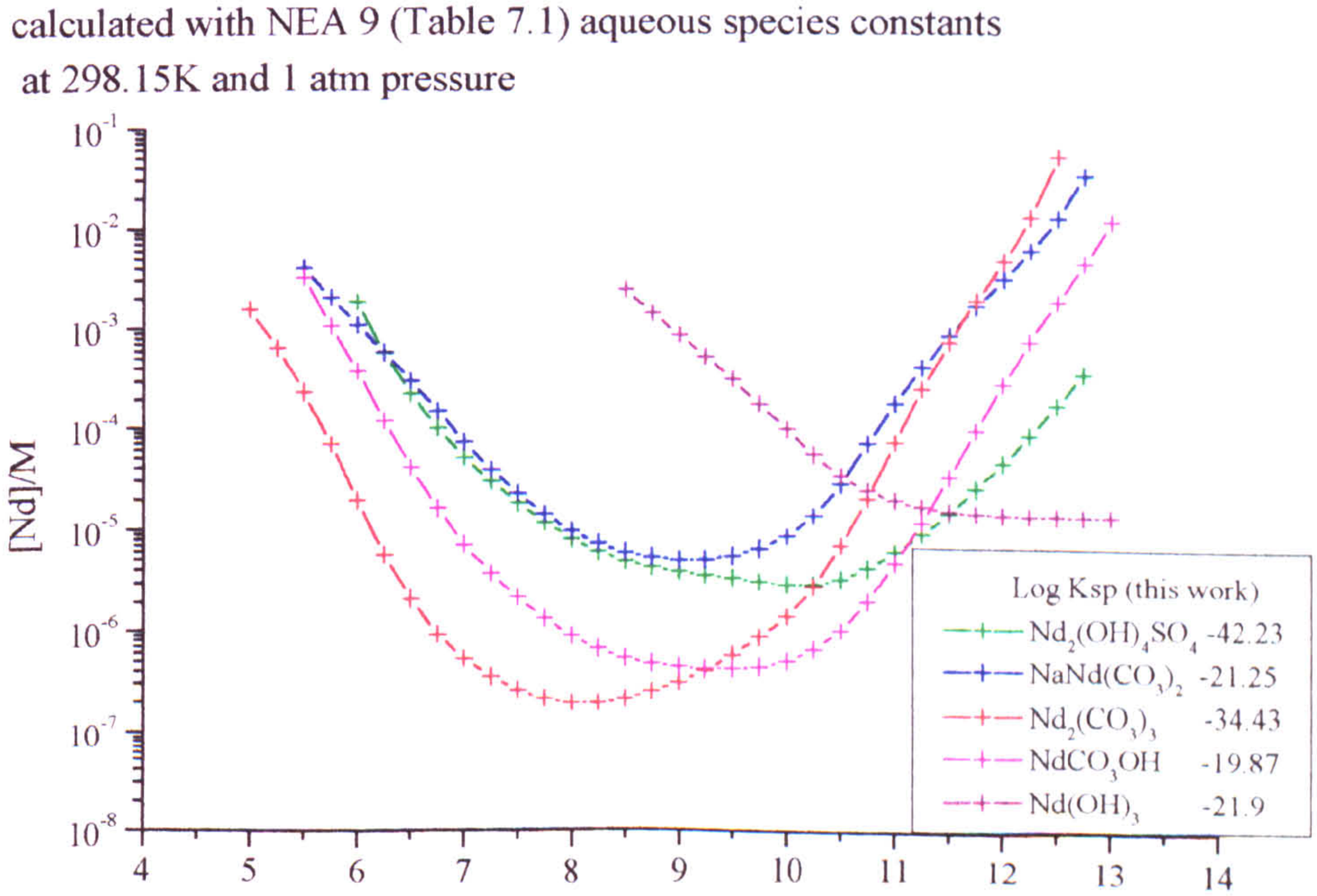

Appendix 7.8 Stability field diagram for the Nd-TIC-pH-Na system (This work) at [Na^+] = 1mM, 298.15K and 1 atm pressure

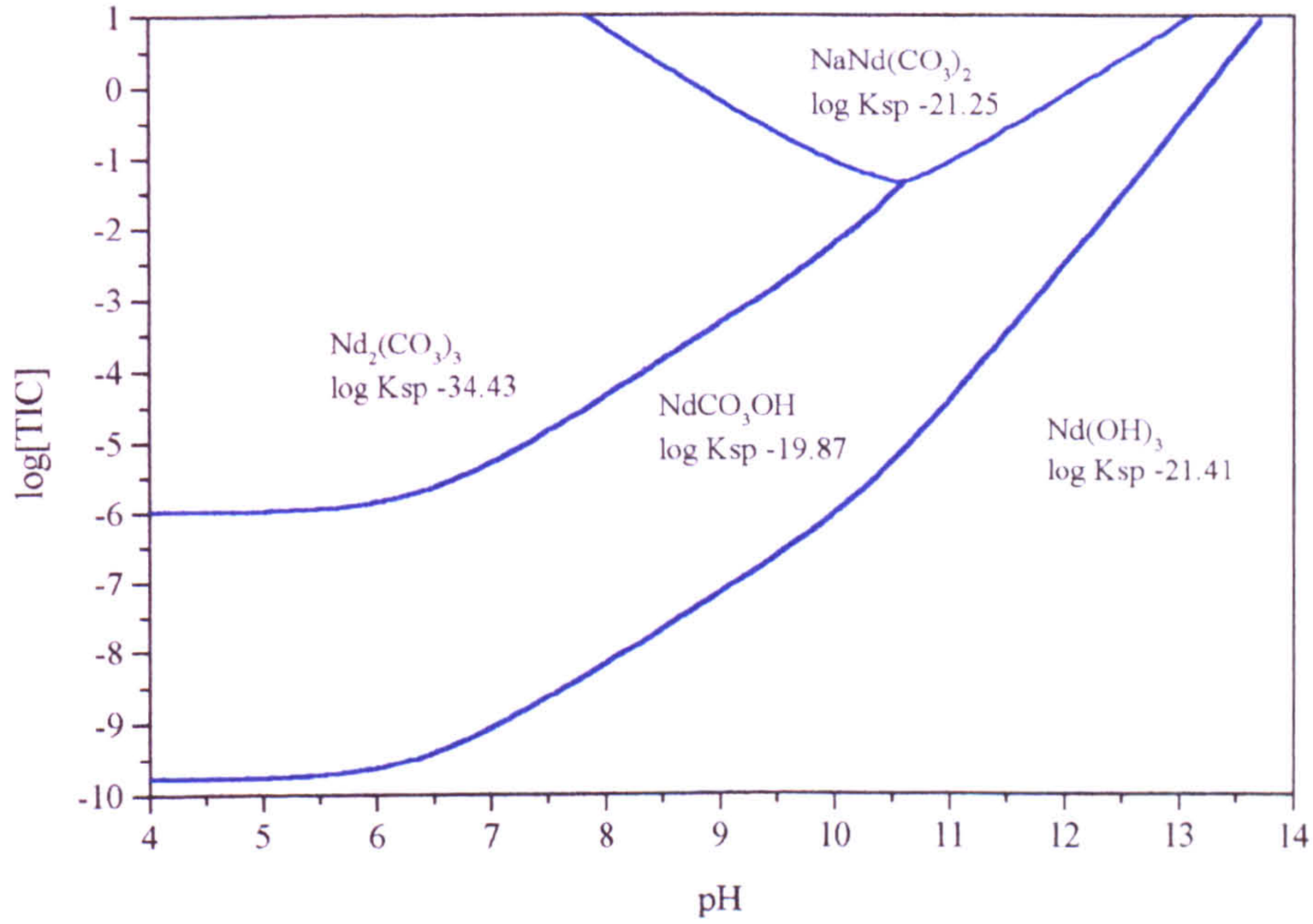

Appendix 7.9 Stability field diagram with data from [1]Runde *et al* and [2,3]Rai *et al*

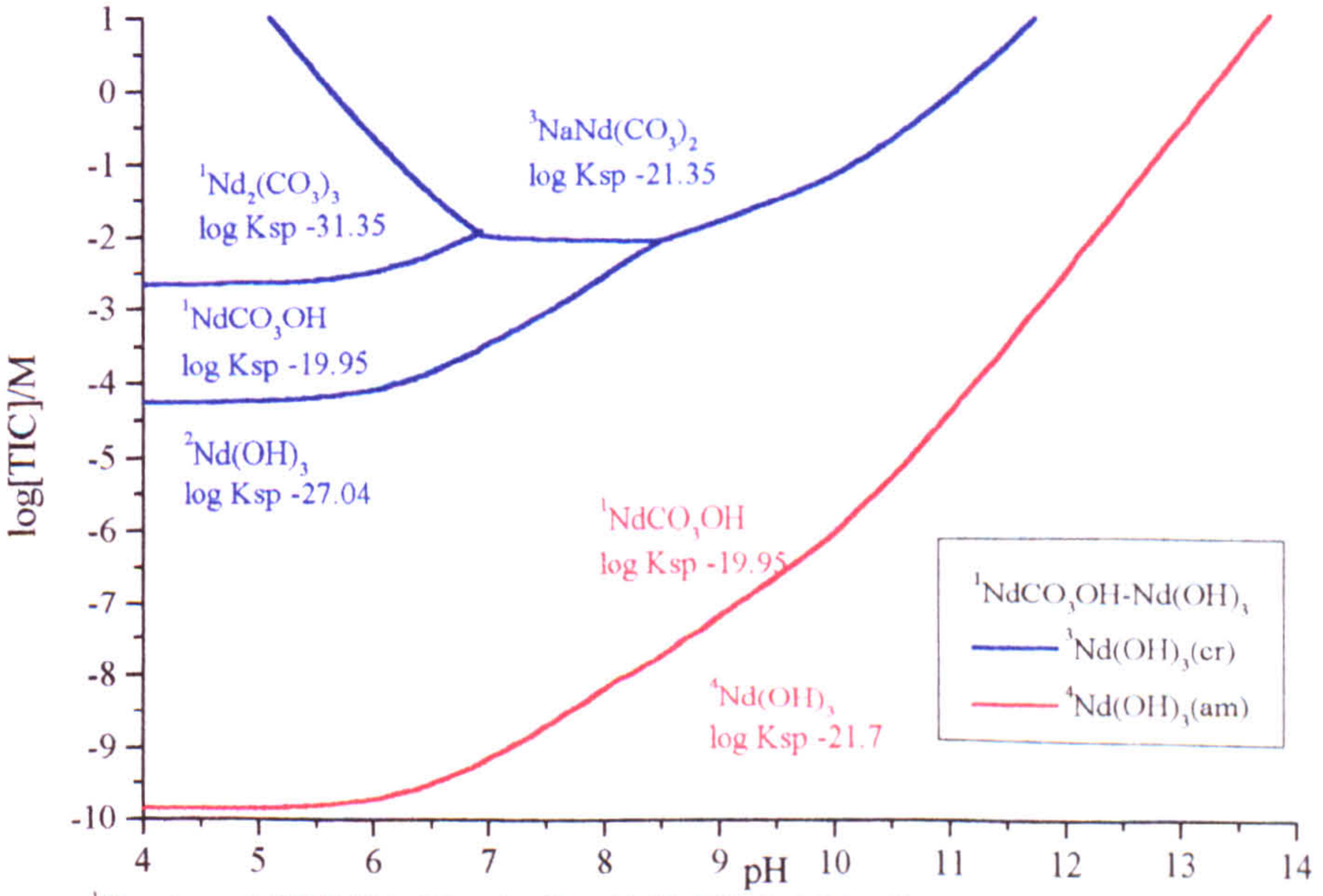

[1] Runde *et al* (1992) $Nd_2(CO_3)_3$ log Ksp-31.35, $NdCO_3OH$ log Ksp -19.95

[2]Rai *et al* (1996a) $NaNd(CO_3)_2$ -21.39, [3]Rai *et al* (1996b) $Nd(OH)_3$ -27.0, [4]This work $Nd(OH)_3$ -21.9

Appendix 7.10a Nd solubility in 10mM Na^+ and 10mM TIC solution calculated from modal solubility products (Table 7.6) using aqueous data from Lee & Byrne (1992 & 1993) at 298.15K and 1 atm pressure

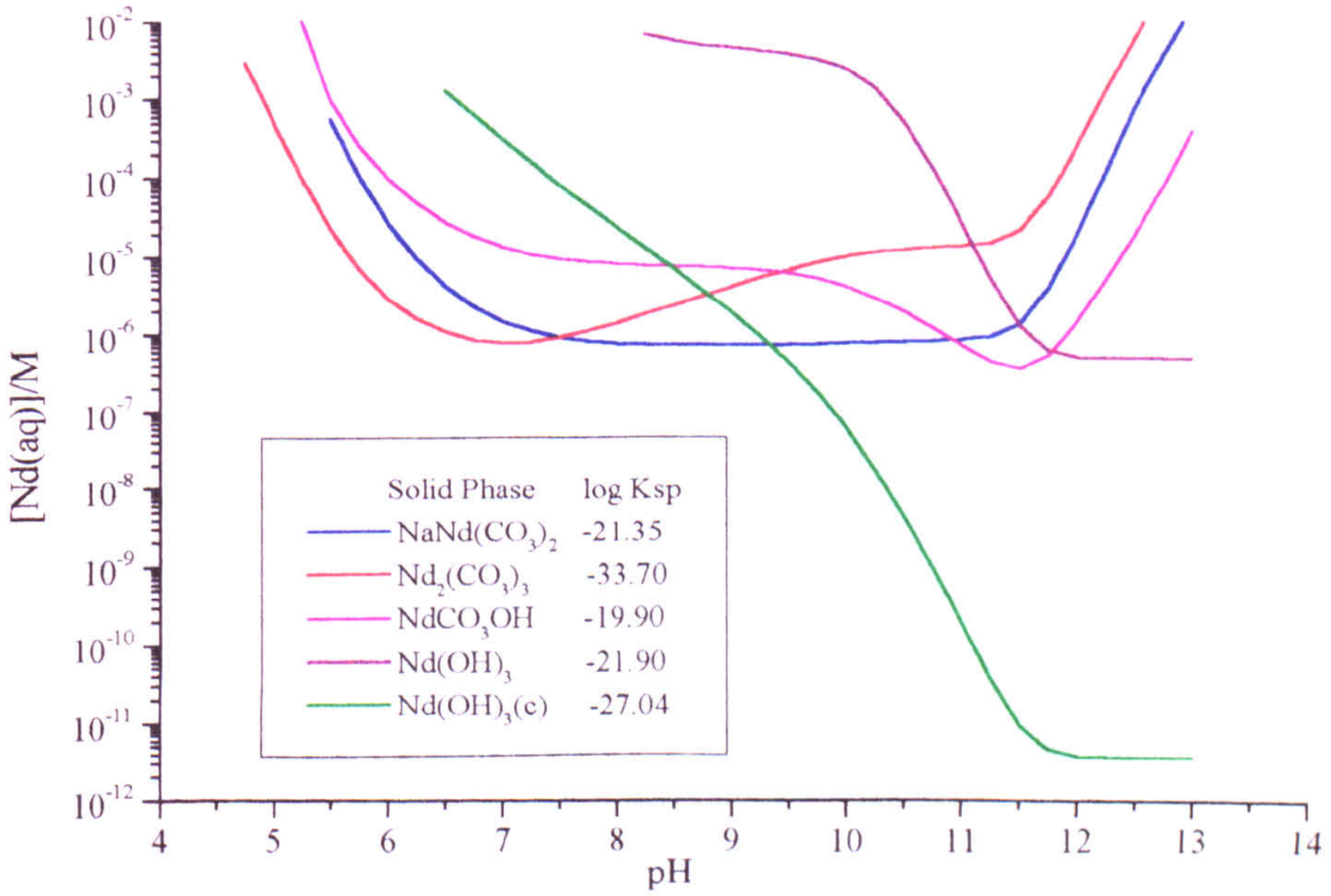

Appendix 7.10b Nd solubility in 10mM Na^+ and 10mM TIC with various solubility products (Table 4.7) aqueous data from Lee & Byrne (1992 & 1993)

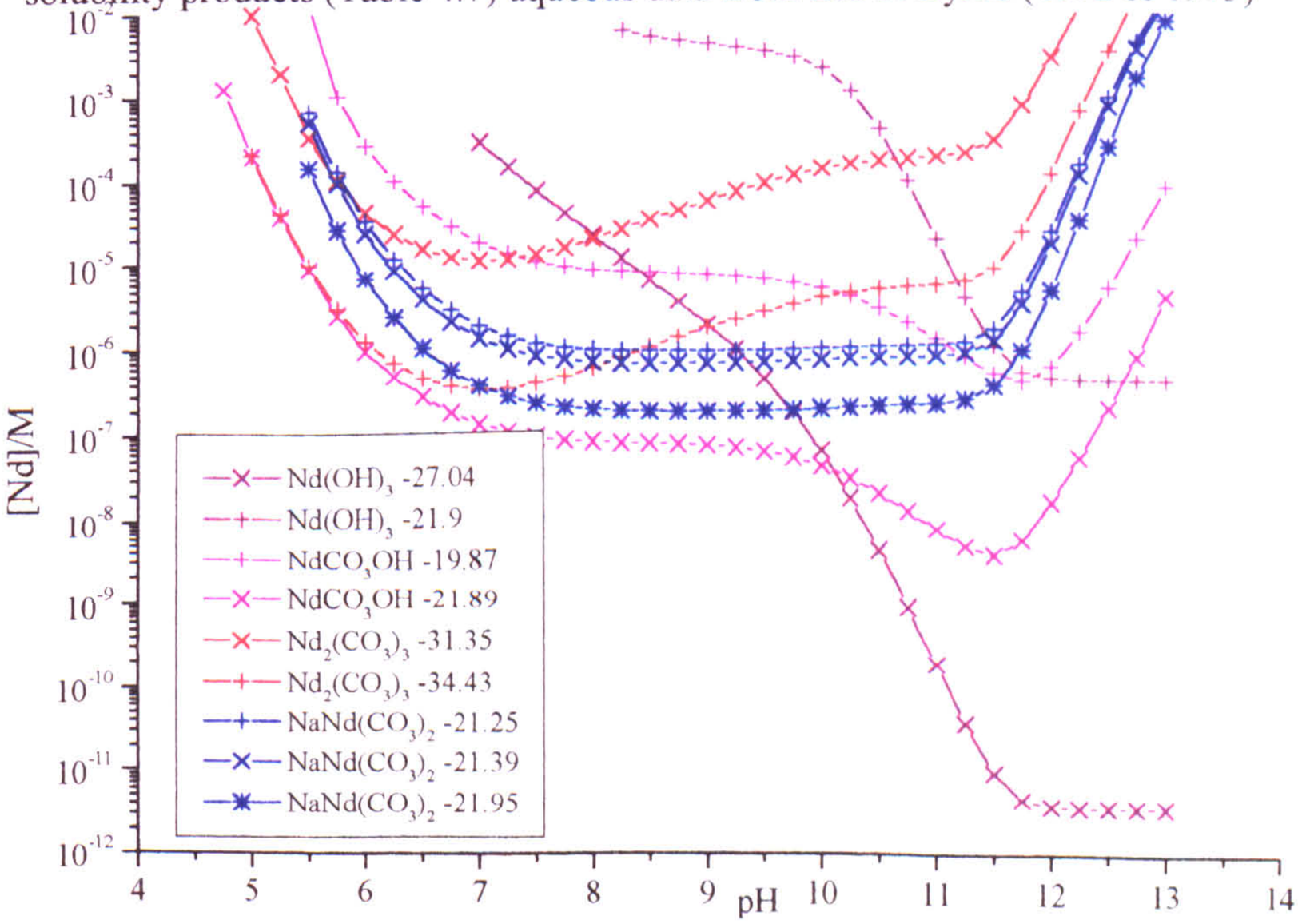

Appendix 7.11 Stability field diagram this work at $[Na^+]$ = 1mM including the $Eu_2(CO_3)_3$-crystalline $Eu(OH)_3$ boundary

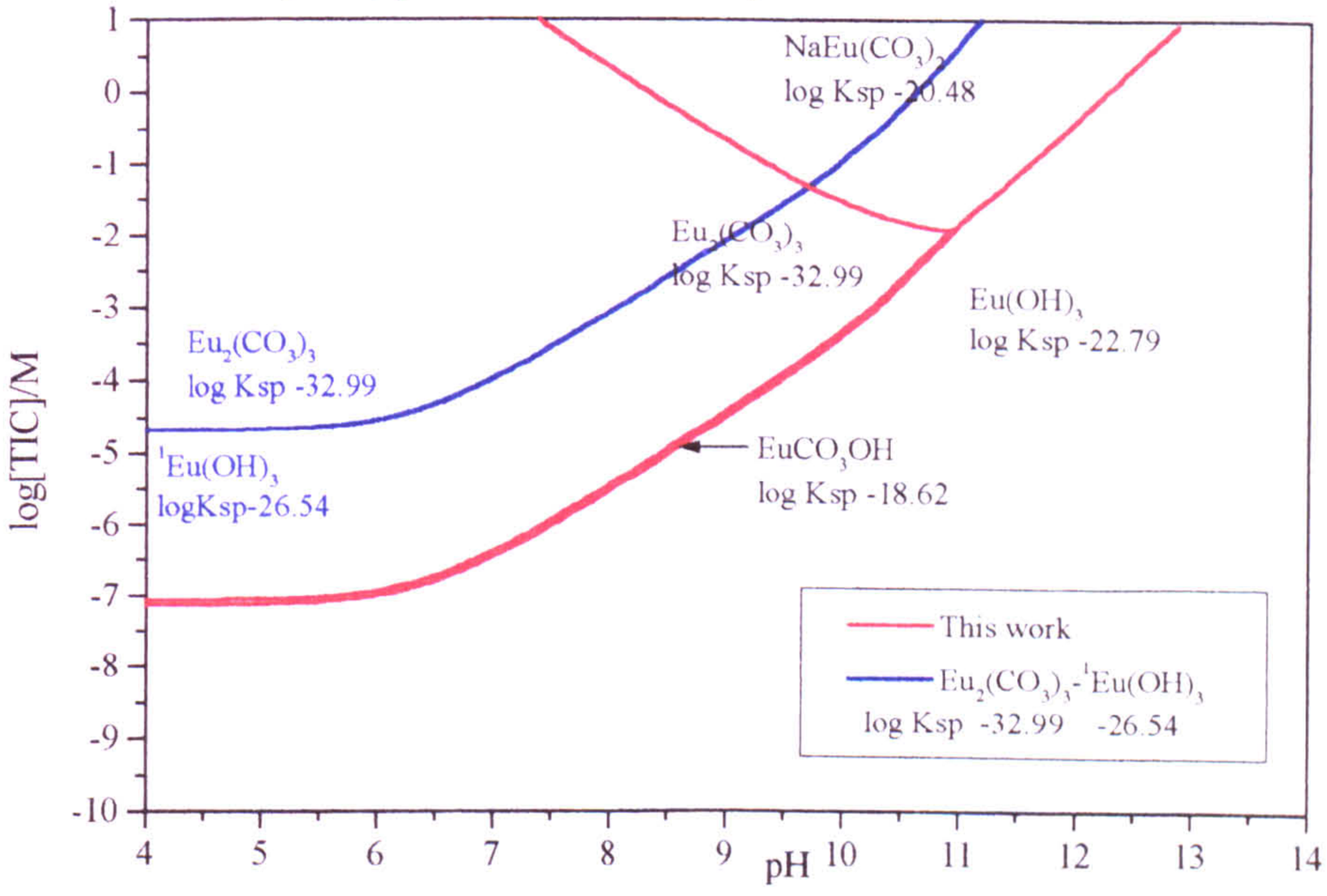

all phases this work except [1]Diakonov *et al* (1998)

Appendix 7.12 Stability field diagram after Runde et al (1992) at $[Na^+]$ = 1mM indicating the effects of increasing $Eu(OH)_3$ crystallinity

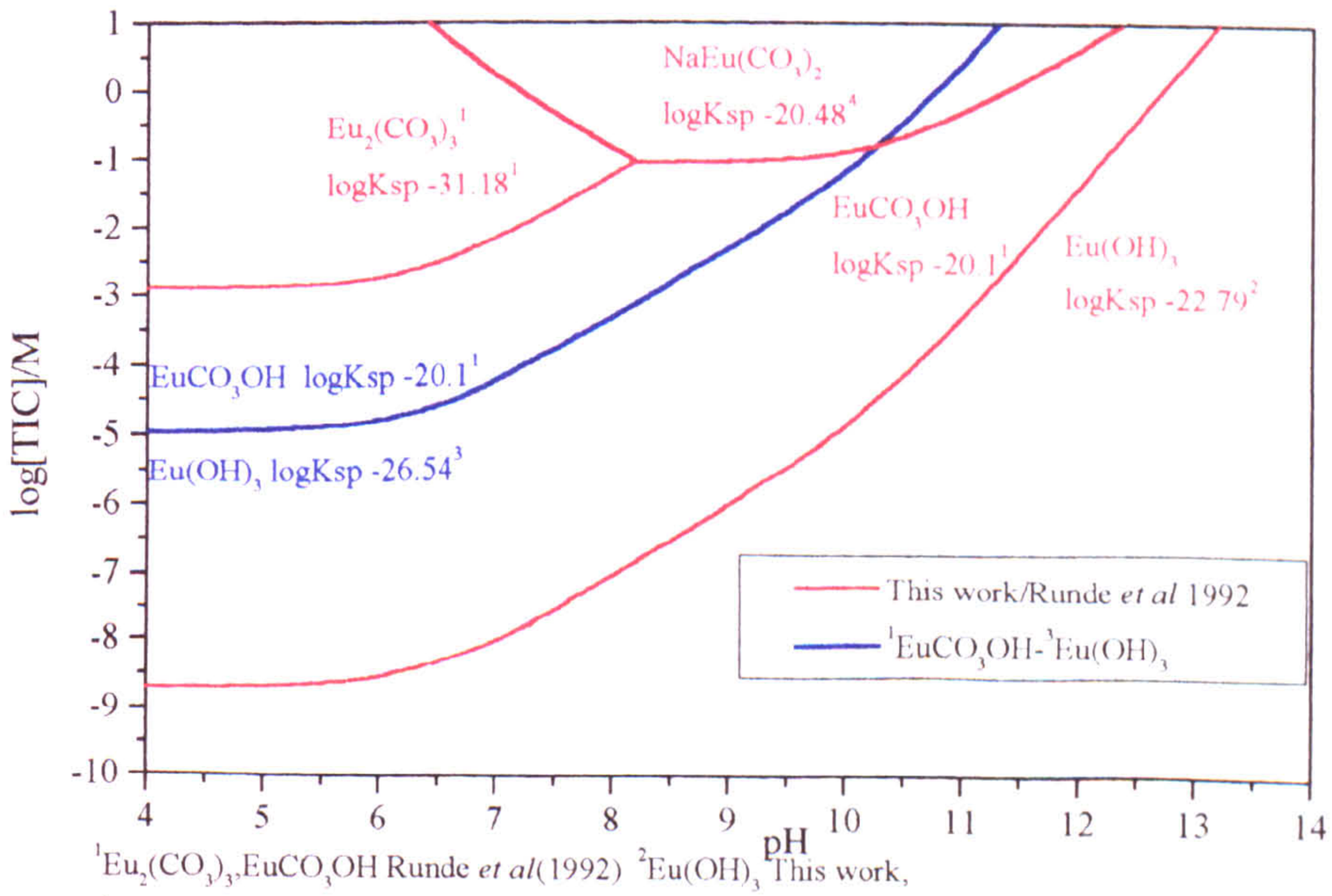

[1]$Eu_2(CO_3)_3$,$EuCO_3OH$ Runde *et al*(1992) [2]$Eu(OH)_3$ This work,
[3]$Eu(OH)_3$ Diaonov *et al*(1998), [4]$NaNd(CO_3)_2$ This work

Appendix 7.13a Eu solubility in 10mM Na^+ and 10mM TIC solution calculated from modal solubility products (Table 7.6) using aqueous data from Lee & Byrne (1992 & 1993) at 298.15K and 1 atm pressure

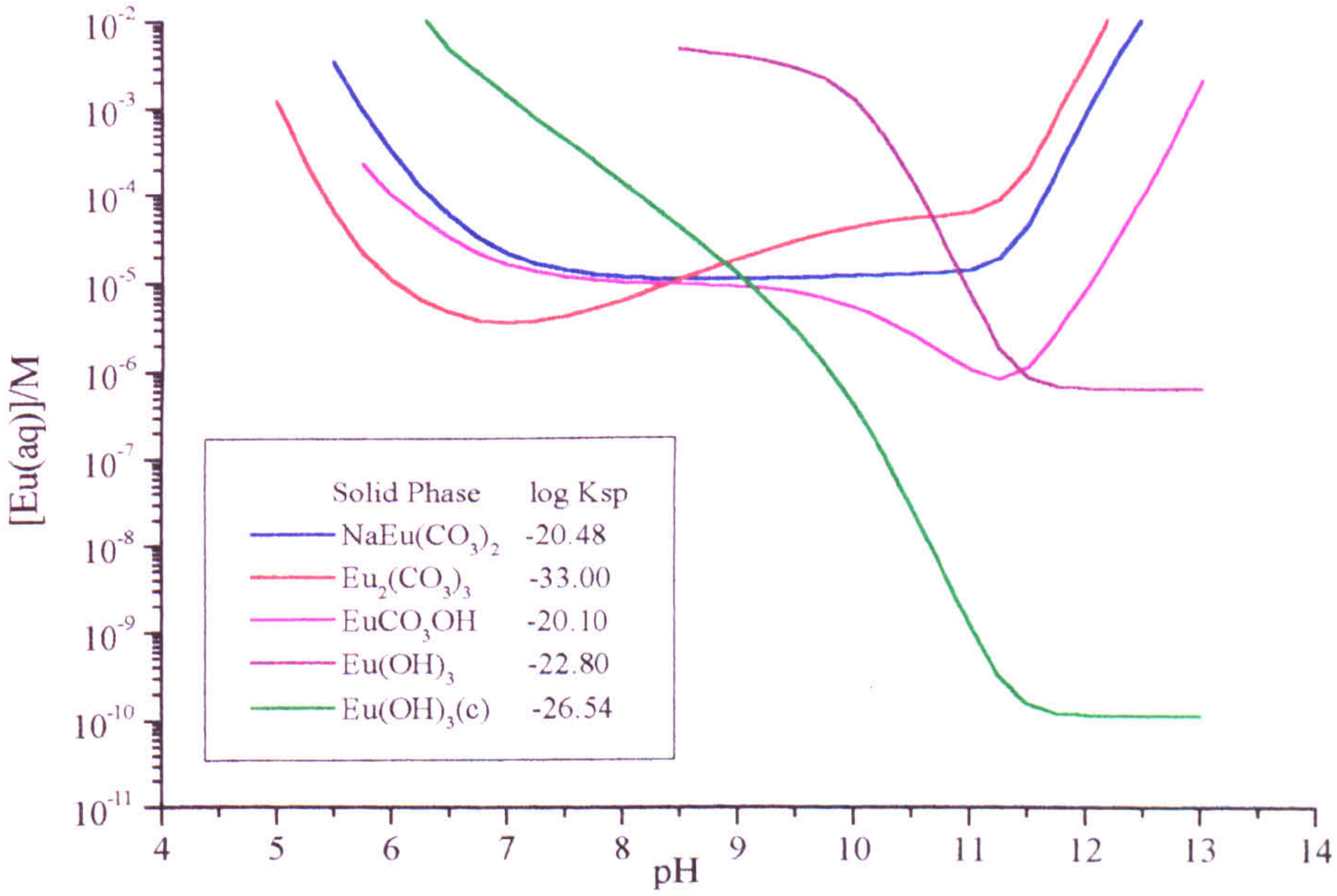

Appendix 7.13b Eu solubility in 10mM Na^+ and 10mM TIC solution with various solubility products (Table 4.7) using Lee & Byrne (1992 & 1993) aqueous data

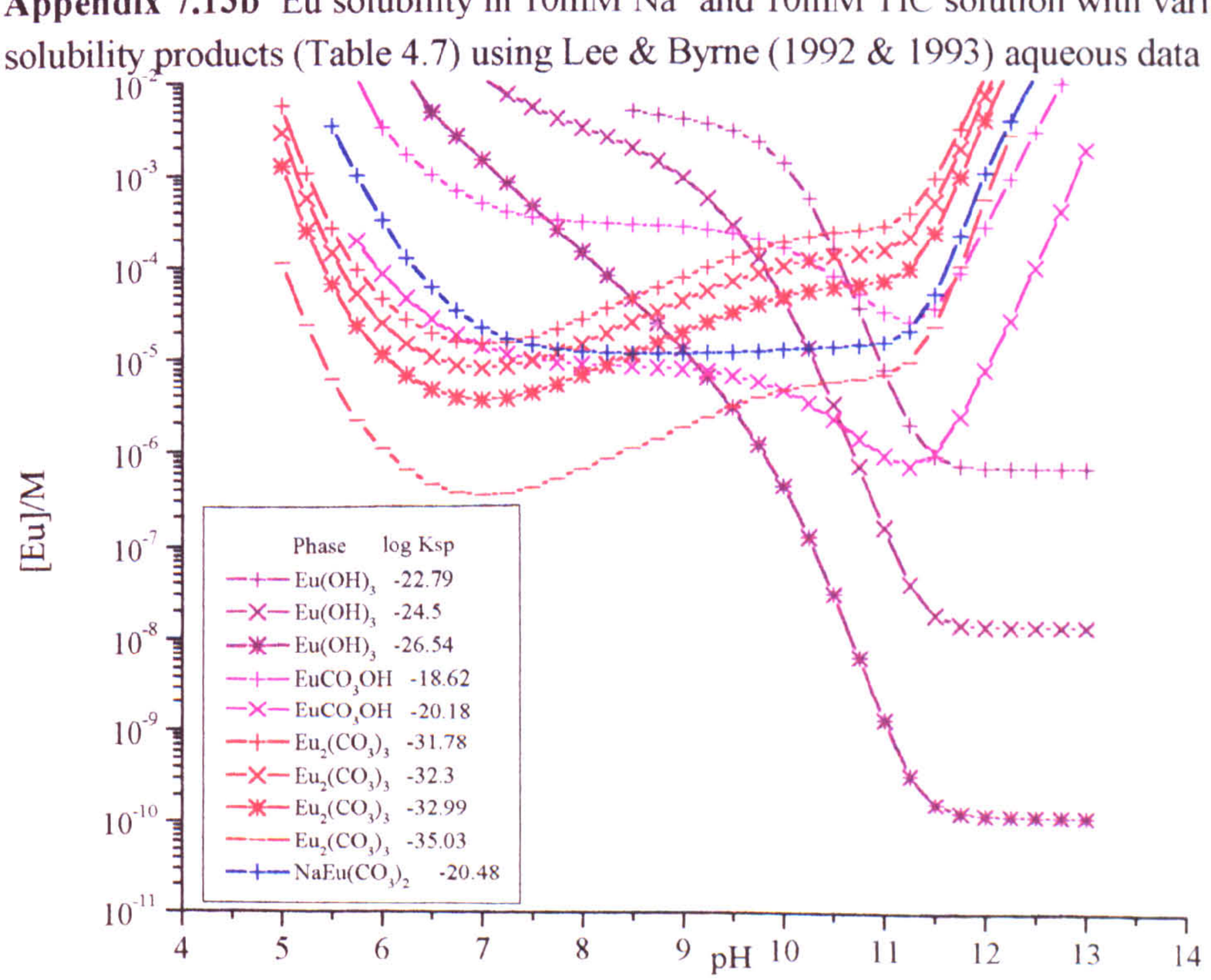

Appendix 7.14 Stability field diagram for the Ce-TIC-pH system at varied pe and 298.15K and 1 atm pressure CeO_2 log K 30.66

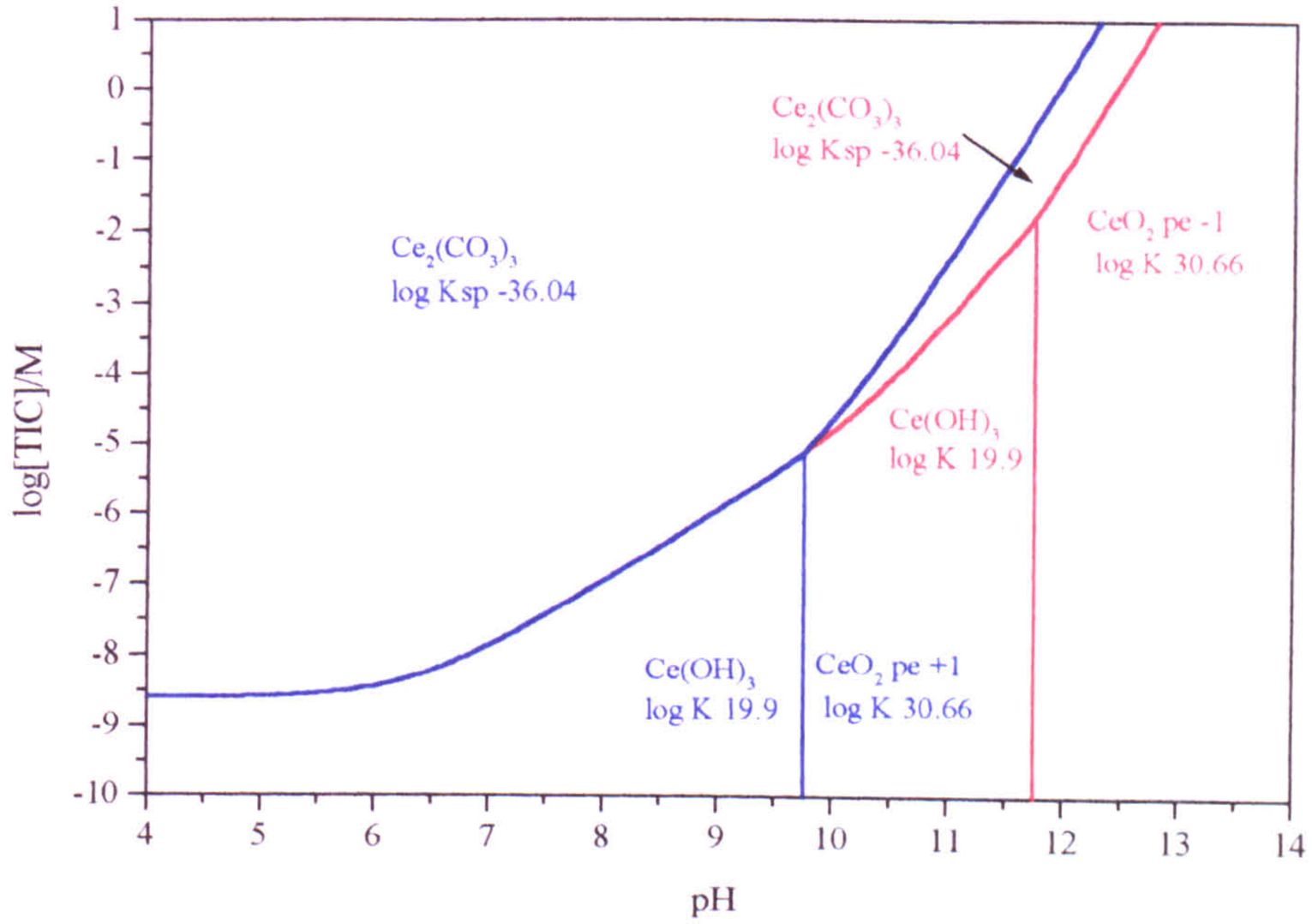

Appendix 7.15 Stability field diagram for the Ce-TIC-pH system at varied pe at 298.15K and 1atm pressure CeO_2 log K 21.12

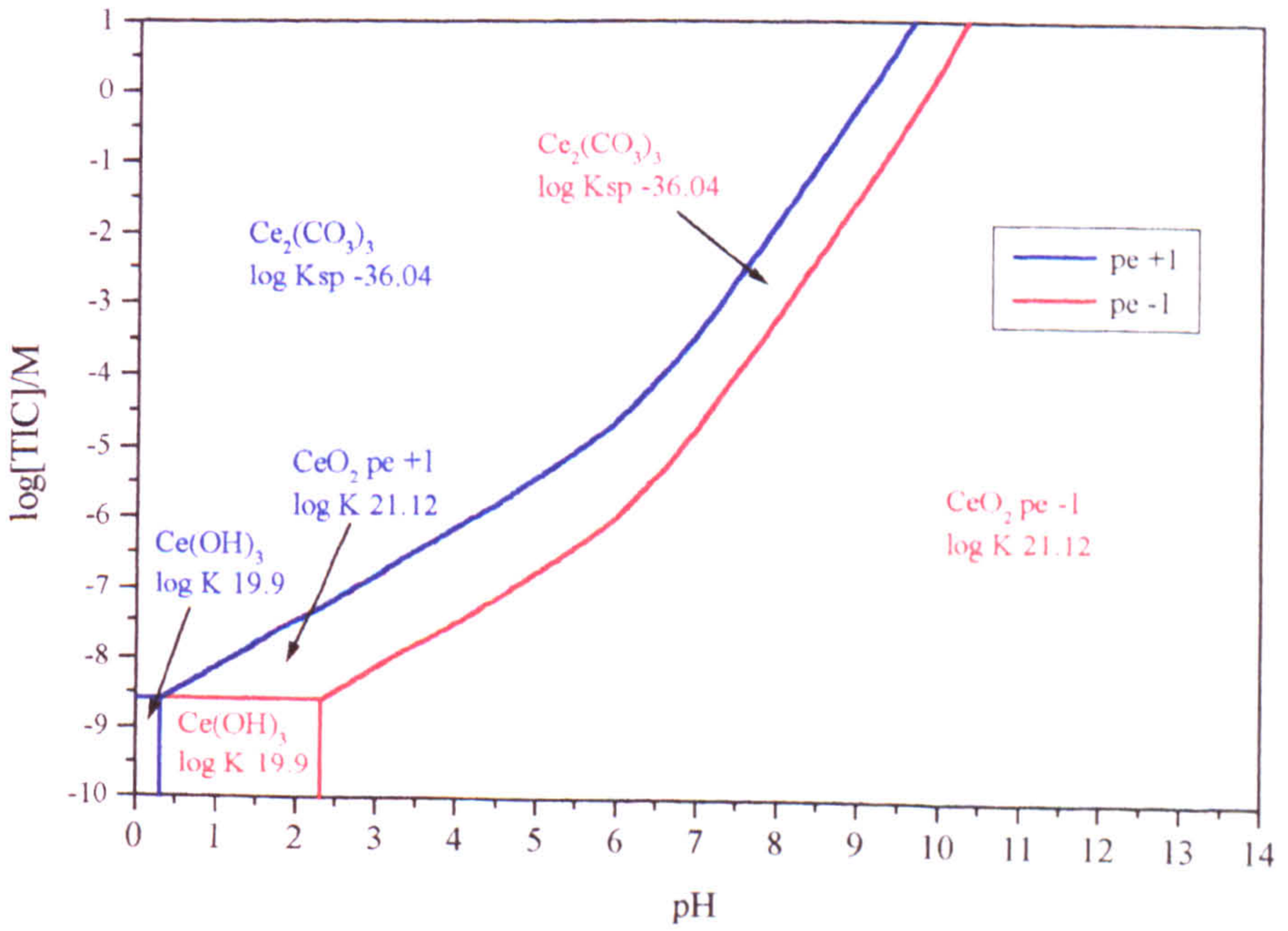

Appendix 7.16a Nd solubility in high F^-/low SO_4^{2-} groundwater
(after Wood 1990, Table 7.7)

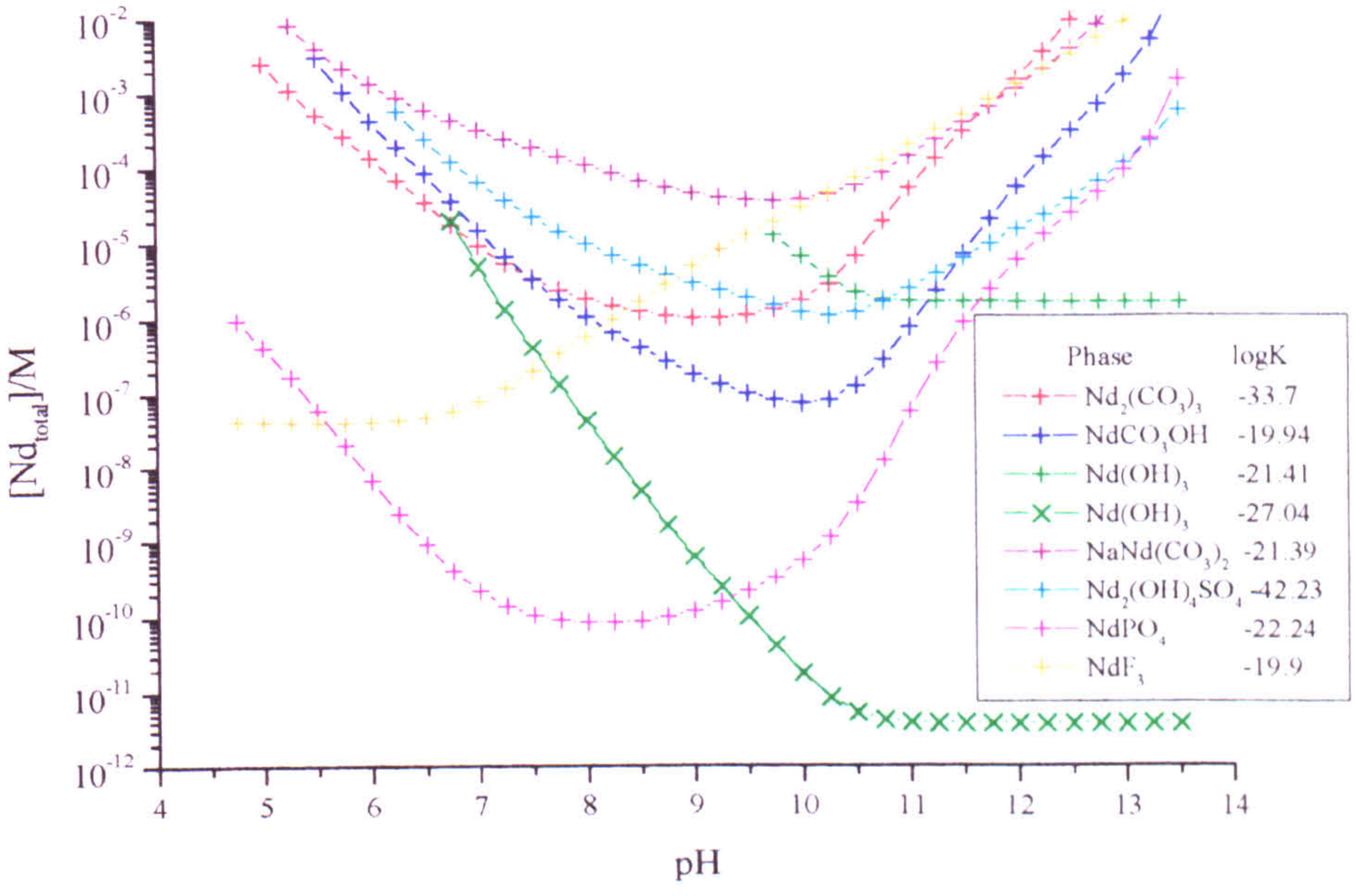

Appendix 7.16b Nd solubility in high TIC/low SO_4^{2-} groundwater
(after Wood 1990, Table 7.7)

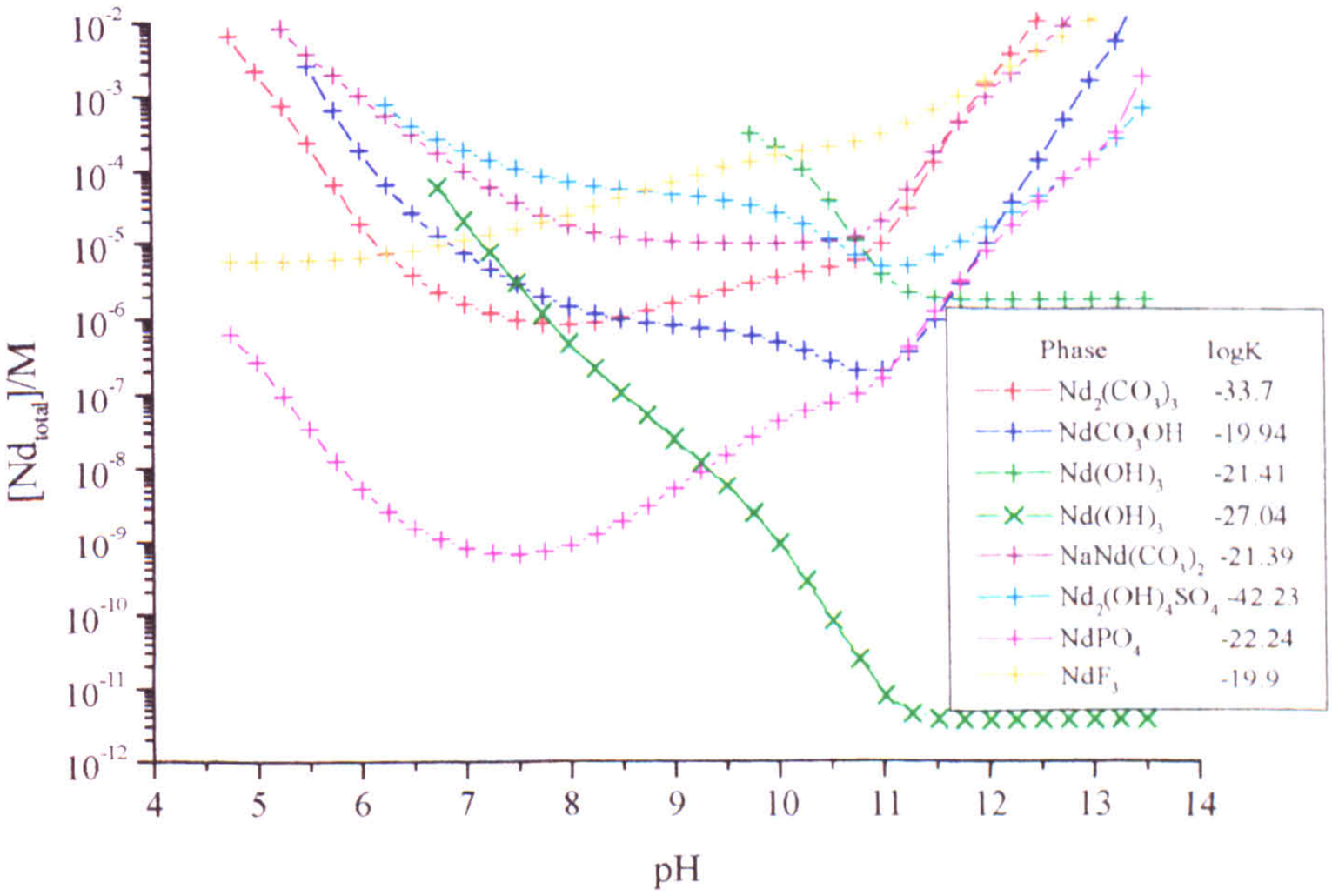

Appendix 7.17a Ce solubility in modal groundwater at pe 0
(after Wood 1990, Table 7.7)

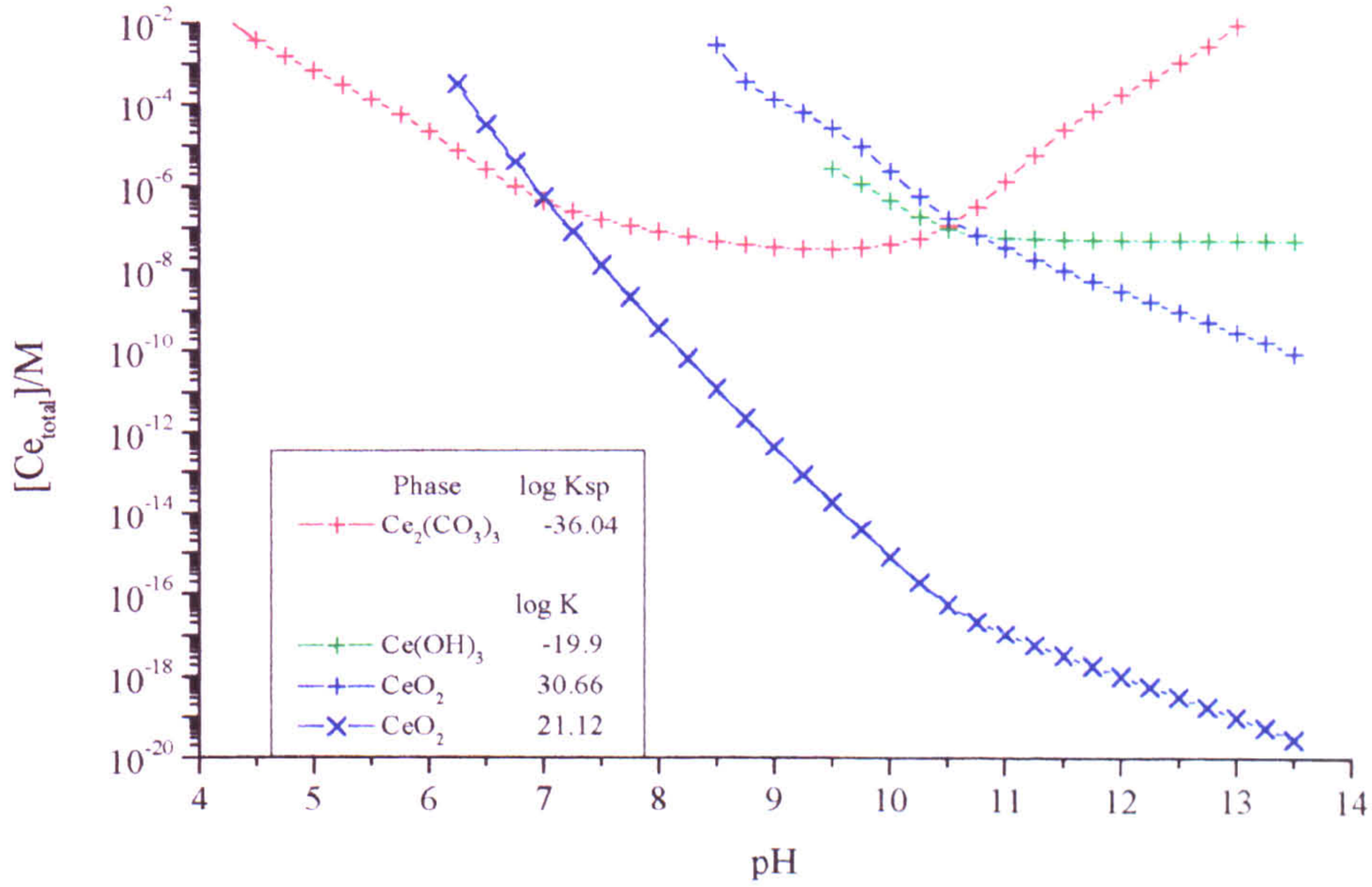

Appendix 7.17b Ce solubility in high TIC/low SO_4^{2-} groundwater at pe 0
(after Wood 1990, Table 7.7)

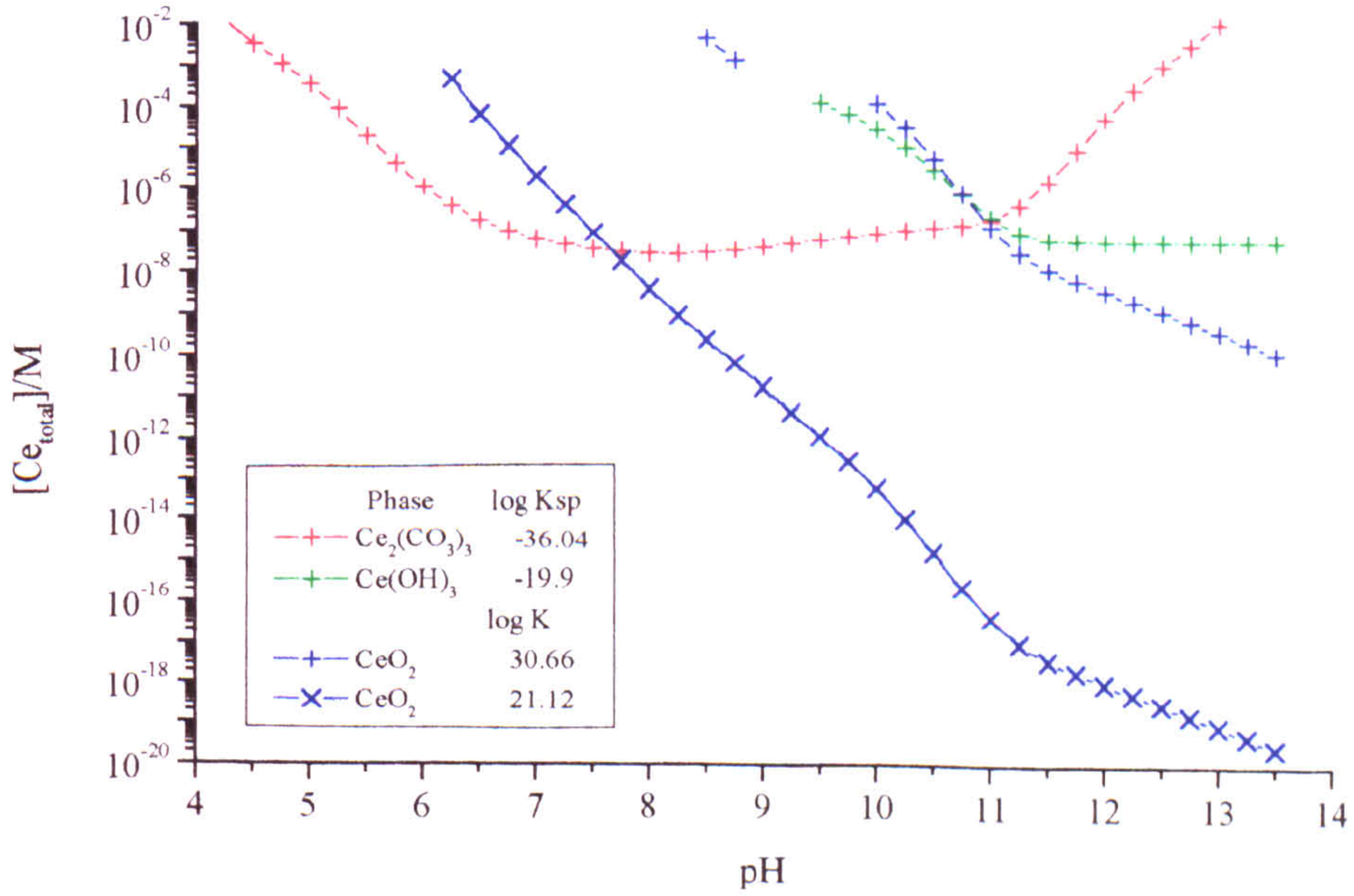

Appendix 7.18a Nd Solubility in groundwater (after Randall 1998, Table 7.8) aqueous speciation after Lee & Byrne, 1992 and 1993)

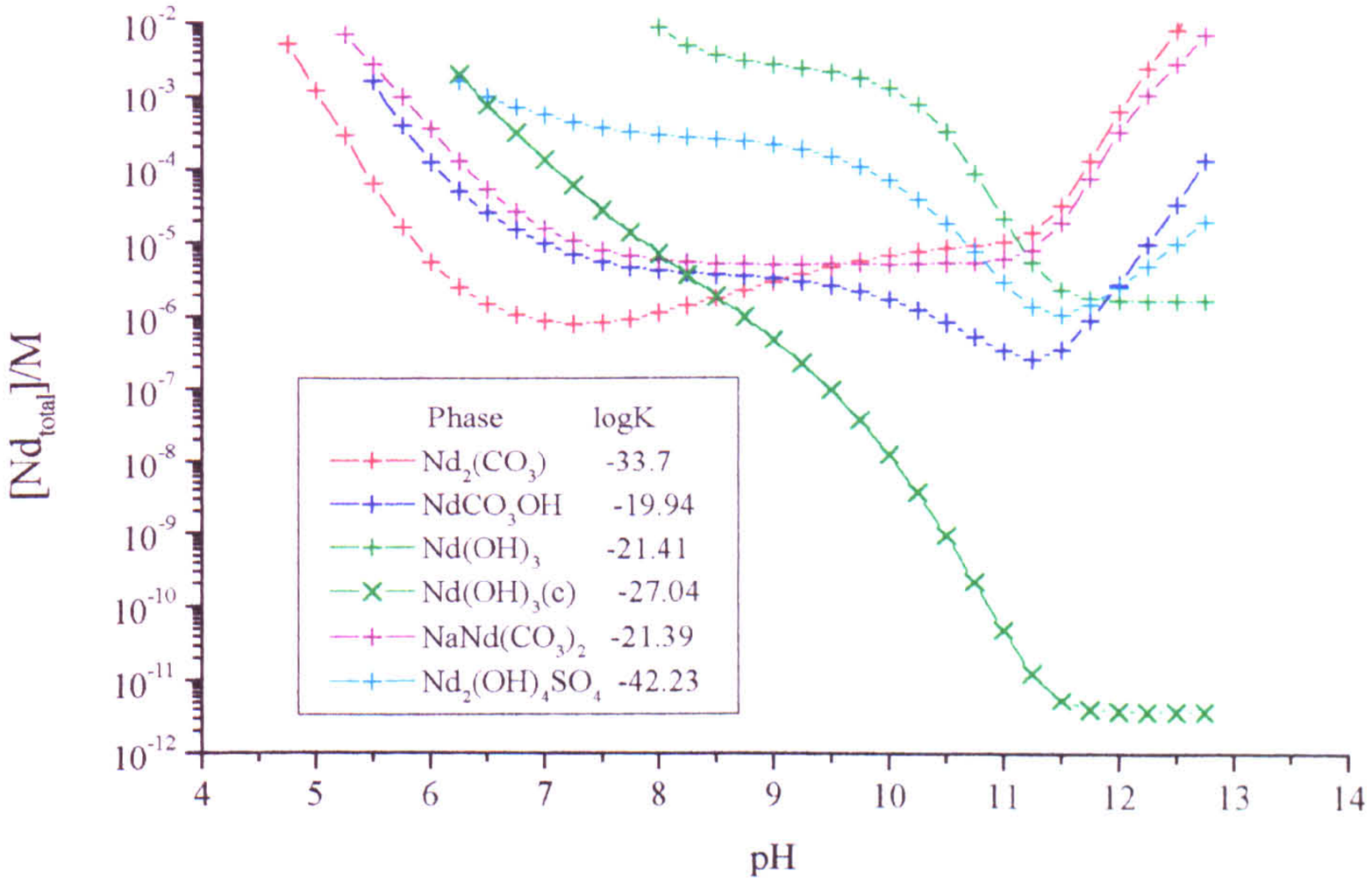

Appendix 7.18b Am solubility in groundwater (after Randall 1998, Table 7.8) aqueous species after Silva., *et al* 1995

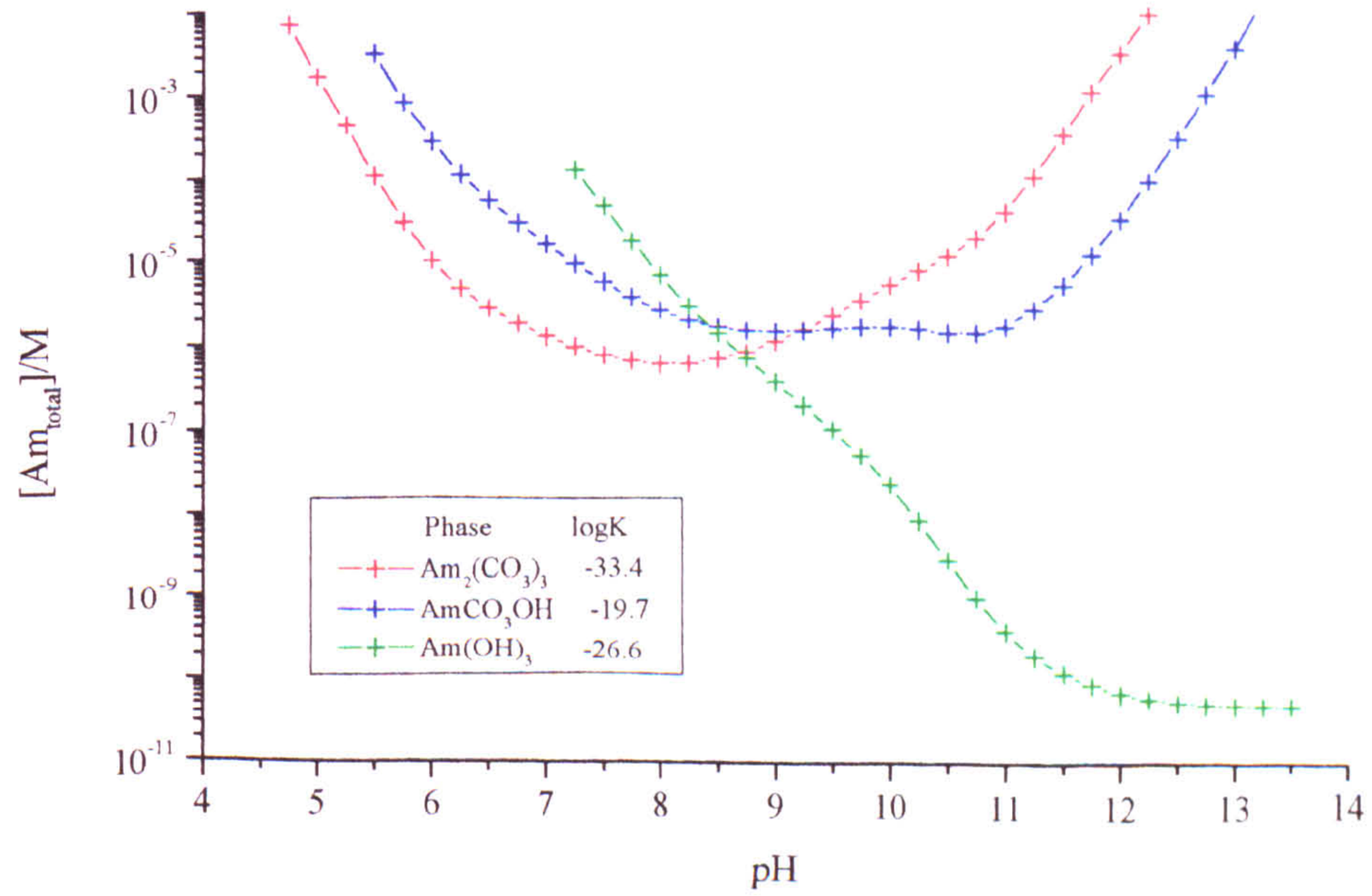

Appendix 7.18c Ce solubility in groundwater at pe 0 (after Randall 1998, Table 7.8) aqueous speciation after Lee & Byrne, 1992 and 1993)

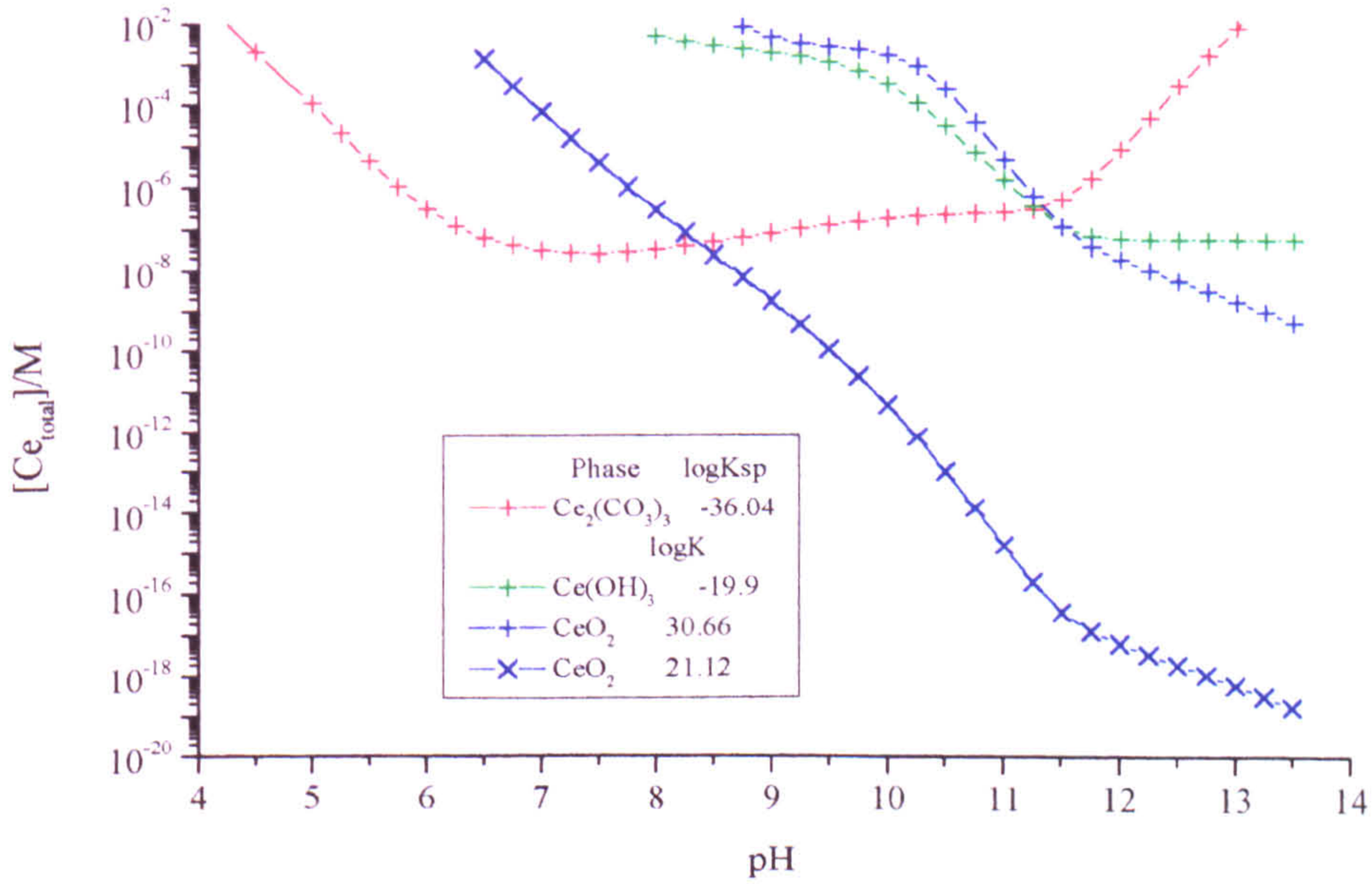

Appendix 8.1 Timed Ce adsorption onto goethite over time (Figure 8.3)

$5x10^{-7}M$ $CeCl_3$ onto 0.2g goethite

Time	$[Ce^{3+}$ (aq)]	mass goethite/g	% adsorbed
0 mins	5.52E-06	0	0
1 min	7.60E-07	0.1994	86.23
2 mins	6.47E-07	0.2002	88.28
3 mins	3.50E-07	0.1995	93.66
5 mins	6.50E-07	0.2004	88.22
10 mins	3.20E-07	0.1986	94.20
15 mins	2.43E-07	0.1989	95.60
20 mins	6.27E-07	0.2000	88.64
3 hrs	6.00E-07	0.1994	89.13

Appendix 8.2 Ce adsorption onto various masses of goethite (Figures 8.4 & 8.5)

pH	[Ce]/M	% Uptake	mass/g	mols(aq)	mols(solid)	mols/ml	mols/g	Kd(ml/g)	log Kd
Start	8.95E-06	0.00	0.0000	4.48E-07	0	8.95E-09	0	0	
7.72	1.10E-06	87.71	0.5064	5.50E-08	8.90E-06	1.10E-09	1.76E-05	1.60E+04	4.20
7.27	2.80E-07	96.87	0.5024	1.40E-08	8.94E-06	2.80E-10	1.78E-05	6.35E+04	4.80
7.66	9.00E-07	89.94	0.4960	4.50E-08	8.91E-06	9.00E-10	1.80E-05	1.99E+04	4.30
7.57	2.50E-07	97.21	0.3535	1.25E-08	8.94E-06	2.50E-10	2.53E-05	1.01E+05	5.00
6.36	4.00E-07	95.53	0.3544	2.00E-08	8.93E-06	4.00E-10	2.52E-05	6.30E+04	4.80
7.22	1.35E-06	84.92	0.2000	6.75E-08	8.88E-06	1.35E-09	4.44E-05	3.29E+04	4.52
7.17	1.70E-07	98.10	0.2040	8.50E-09	8.94E-06	1.70E-10	4.38E-05	2.58E+05	5.41
6.74	2.70E-07	96.98	0.1020	1.35E-08	8.94E-06	2.70E-10	8.76E-05	3.24E+05	5.51
6.82	1.00E-06	88.83	0.1034	5.00E-08	8.90E-06	1.00E-09	8.61E-05	8.61E+04	4.93
6.52	9.20E-07	89.72	0.1058	4.60E-08	8.90E-06	9.20E-10	8.42E-05	9.15E+04	4.96
6.37	1.00E-06	88.83	0.0516	5.00E-08	8.90E-06	1.00E-09	1.72E-04	1.72E+05	5.24

Appendix 8.3a Nd adsorption to goethite between pH 2 and 10 (Figure 8.6)

pH	[Nd]/M	Start	% Uptake	mass goethite /g	mols(aq)	mols(solid)	mols/ml	mols/g	Kd(ml/g)	log Kd
Start	2.17E-06	2.17E-06	0.00	0.0000	1.09E-07	0.00E+00	2.17E-09	0.00E+00	0	
5.57	3.29E-07	2.17E-06	84.88	0.0510	1.64E-08	9.26E-08	3.29E-10	1.82E-06	5522.20	3.74
5.57	3.28E-07	2.17E-06	84.90	0.0510	1.64E-08	9.26E-08	3.28E-10	1.82E-06	5530.00	3.74
6.41	3.44E-08	2.17E-06	98.42	0.0498	1.72E-09	1.07E-07	3.44E-11	2.15E-06	62707.22	4.80
6.41	3.40E-08	2.17E-06	98.44	0.0498	1.70E-09	1.07E-07	3.40E-11	2.15E-06	63418.75	4.80
6.39	2.80E-08	2.17E-06	98.71	0.0497	1.40E-09	1.08E-07	2.80E-11	2.16E-06	77347.88	4.89
6.39	2.64E-08	2.17E-06	98.79	0.0497	1.32E-09	1.08E-07	2.64E-11	2.17E-06	82187.62	4.91
6.40	3.30E-08	2.17E-06	98.48	0.0492	1.65E-09	1.07E-07	3.30E-11	2.18E-06	66068.28	4.82
6.40	3.39E-08	2.17E-06	98.44	0.0492	1.69E-09	1.07E-07	3.39E-11	2.18E-06	64392.88	4.81
6.61	8.60E-09	2.17E-06	99.60	0.0487	4.30E-10	1.09E-07	8.60E-12	2.23E-06	259327.70	5.41
6.61	8.78E-09	2.17E-06	99.60	0.0487	4.39E-10	1.09E-07	8.78E-12	2.23E-06	253977.44	5.40
6.60	2.45E-08	2.17E-06	98.87	0.0481	1.23E-09	1.08E-07	2.45E-11	2.24E-06	91284.83	4.96
6.60	2.36E-08	2.17E-06	98.91	0.0481	1.18E-09	1.08E-07	2.36E-11	2.24E-06	94866.54	4.98
7.04	2.03E-08	2.17E-06	99.07	0.0499	1.02E-09	1.08E-07	2.03E-11	2.16E-06	106578.20	5.03
7.04	2.08E-08	2.17E-06	99.04	0.0499	1.04E-09	1.08E-07	2.08E-11	2.16E-06	104225.73	5.02
6.97	3.62E-08	2.17E-06	98.33	0.0493	1.81E-09	1.07E-07	3.62E-11	2.17E-06	60077.19	4.78
6.97	3.66E-08	2.17E-06	98.31	0.0493	1.83E-09	1.07E-07	3.66E-11	2.17E-06	59340.69	4.77
7.10	4.15E-08	2.17E-06	98.09	0.0504	2.07E-09	1.07E-07	4.15E-11	2.12E-06	51179.30	4.71
7.10	4.07E-08	2.17E-06	98.13	0.0504	2.03E-09	1.07E-07	4.07E-11	2.12E-06	52152.03	4.72
7.02	7.73E-09	2.17E-06	99.64	0.0515	3.87E-10	1.09E-07	7.73E-12	2.11E-06	272783.22	5.44
7.02	8.35E-09	2.17E-06	99.62	0.0515	4.18E-10	1.09E-07	8.35E-12	2.11E-06	252398.55	5.40
9.72	5.73E-08	2.17E-06	97.37	0.0506	2.86E-09	1.06E-07	5.73E-11	2.10E-06	36634.60	4.56
9.72	5.76E-08	2.17E-06	97.35	0.0506	2.88E-09	1.06E-07	5.76E-11	2.10E-06	36388.77	4.56
9.70	6.22E-08	2.17E-06	97.14	0.0486	3.11E-09	1.06E-07	6.22E-11	2.18E-06	35038.38	4.54
9.70	5.88E-08	2.17E-06	97.29	0.0486	2.94E-09	1.06E-07	5.88E-11	2.18E-06	37090.91	4.57
10.59	1.15E-07	2.17E-06	94.73	0.0504	5.73E-09	1.03E-07	1.15E-10	2.05E-06	17882.82	4.25
10.59	1.14E-07	2.17E-06	94.75	0.0504	5.70E-09	1.03E-07	1.14E-10	2.05E-06	17964.30	4.25
10.68	8.08E-08	2.17E-06	96.28	0.0511	4.04E-09	1.05E-07	8.08E-11	2.05E-06	25407.48	4.40
10.68	8.06E-08	2.17E-06	96.29	0.0511	4.03E-09	1.05E-07	8.06E-11	2.05E-06	25479.58	4.41
10.96	2.17E-07	2.17E-06	90.03	0.0494	1.08E-08	9.82E-08	2.17E-10	1.99E-06	9167.15	3.96

10.96	2.18E-07	2.17E-06	89.97	0.0494	1.09E-08	9.81E-08	2.18E-10	1.99E-06	9105.38	3.96
11.27	4.50E-08	2.17E-06	97.93	0.0506	2.25E-09	1.07E-07	4.50E-11	2.11E-06	46849.34	4.67
11.27	4.47E-08	2.17E-06	97.94	0.0506	2.23E-09	1.07E-07	4.47E-11	2.11E-06	47224.08	4.67

Appendix 8.3b Nd adsorption to goethite between pH 2 and 10 (Figure 8.6)

pH	[Nd]/M	Start	% Uptake	mass goethite /g	mols(aq)	mols(solid)	mols/ml	mols/g	Kd(ml/g)	log Kd
Start	5.17E-07	5.17E-07	0.00	0.0000	2.58E-08	0.00E+00	5.17E-10	0	0	
4.62	4.45E-07	5.17E-07	13.95	0.0503	2.22E-08	3.56E-09	4.45E-10	7.08E-08	159.12	2.20
4.62	4.39E-07	5.17E-07	15.09	0.0503	2.19E-08	3.85E-09	4.39E-10	7.66E-08	174.57	2.24
5.25	3.57E-07	5.17E-07	30.85	0.0482	1.79E-08	7.93E-09	3.57E-10	1.64E-07	460.00	2.66
5.25	3.56E-07	5.17E-07	31.08	0.0482	1.78E-08	7.99E-09	3.56E-10	1.66E-07	465.10	2.67
7.24	3.59E-09	5.17E-07	99.31	0.0494	1.79E-10	2.56E-08	3.59E-12	5.19E-07	144,485.75	5.16
7.24	3.56E-09	5.17E-07	99.31	0.0494	1.78E-10	2.56E-08	3.56E-12	5.19E-07	145,846.38	5.16
6.71	1.51E-08	5.17E-07	97.08	0.0498	7.55E-10	2.50E-08	1.51E-11	5.03E-07	33,318.80	4.52
6.71	1.40E-08	5.17E-07	97.30	0.0498	6.99E-10	2.51E-08	1.40E-11	5.04E-07	36,074.39	4.56
7.10	7.91E-08	5.17E-07	84.70	0.0516	3.96E-09	2.18E-08	7.91E-11	4.23E-07	5,350.84	3.73
7.10	7.43E-09	5.17E-07	98.56	0.0516	3.71E-10	2.54E-08	7.43E-12	4.93E-07	66,357.23	4.82
7.11	3.20E-08	5.17E-07	93.81	0.0497	1.60E-09	2.42E-08	3.20E-11	4.87E-07	15,205.68	4.18
7.11	3.06E-08	5.17E-07	94.09	0.0497	1.53E-09	2.43E-08	3.06E-11	4.88E-07	15,978.32	4.20
7.05	1.12E-08	5.17E-07	97.84	0.0507	5.58E-10	2.52E-08	1.12E-11	4.98E-07	44,645.75	4.65
7.05	9.59E-09	5.17E-07	98.15	0.0507	4.79E-10	2.53E-08	9.59E-12	4.99E-07	52,088.40	4.72
7.29	8.70E-09	5.17E-07	98.32	0.0502	4.35E-10	2.54E-08	8.70E-12	5.05E-07	58,057.68	4.76
7.29	8.79E-09	5.17E-07	98.30	0.0502	4.40E-10	2.54E-08	8.79E-12	5.05E-07	57,460.45	4.76
7.56	7.17E-08	5.17E-07	86.12	0.0494	3.59E-09	2.22E-08	7.17E-11	4.50E-07	6,267.79	3.80
7.56	6.97E-08	5.17E-07	86.52	0.0494	3.49E-09	2.23E-08	6.97E-11	4.52E-07	6,480.48	3.81
9.27	1.44E-08	5.17E-07	97.22	0.0517	7.18E-10	2.51E-08	1.44E-11	4.85E-07	33,786.66	4.53
9.27	1.35E-08	5.17E-07	97.39	0.0517	6.74E-10	2.51E-08	1.35E-11	4.86E-07	36,068.46	4.56
7.20	2.87E-08	5.17E-07	94.44	0.0506	1.44E-09	2.44E-08	2.87E-11	4.81E-07	16,761.37	4.22
7.20	2.74E-08	5.17E-07	94.71	0.0506	1.37E-09	2.44E-08	2.74E-11	4.83E-07	17,647.44	4.25
10.10	5.15E-08	5.17E-07	90.03	0.0504	2.58E-09	2.32E-08	5.15E-11	4.61E-07	8,938.86	3.95
10.10	4.67E-08	5.17E-07	90.97	0.0504	2.33E-09	2.35E-08	4.67E-11	4.66E-07	9,978.27	4.00

10.10	4.60E-08	5.17E-07	91.11	0.0504	2.30E-09	2.35E-08	4.60E-11	4.66E-07	10,141.71	4.01
10.10	4.59E-08	5.17E-07	91.12	0.0504	2.30E-09	2.35E-08	4.59E-11	4.66E-07	10,155.89	4.01
11.04	5.95E-08	5.17E-07	88.49	0.0485	2.97E-09	2.28E-08	5.95E-11	4.71E-07	7,913.36	3.90
11.04	6.01E-08	5.17E-07	88.37	0.0485	3.01E-09	2.28E-08	6.01E-11	4.70E-07	7,816.97	3.89
10.59	6.22E-08	5.17E-07	87.97	0.0496	3.11E-09	2.27E-08	6.22E-11	4.57E-07	7,357.18	3.87
10.59	6.01E-08	5.17E-07	88.38	0.0496	3.00E-09	2.28E-08	6.01E-11	4.60E-07	7,651.67	3.88
11.54	1.99E-09	5.17E-07	99.61	0.0501	9.96E-11	2.57E-08	1.99E-12	5.13E-07	257,502.51	5.41
11.54	1.74E-09	5.17E-07	99.66	0.0501	8.68E-11	2.57E-08	1.74E-12	5.13E-07	295,671.52	5.47
11.57	1.49E-08	5.17E-07	97.12	0.0502	7.43E-10	2.51E-08	1.49E-11	4.99E-07	33,572.21	4.53
11.57	1.44E-08	5.17E-07	97.21	0.0502	7.21E-10	2.51E-08	1.44E-11	5.00E-07	34,653.55	4.54
10.59	2.28E-08	5.17E-07	95.59	0.0496	1.14E-09	2.47E-08	2.28E-11	4.97E-07	21,830.22	4.34
10.59	5.44E-08	5.17E-07	89.48	0.0496	2.72E-09	2.31E-08	5.44E-11	4.65E-07	8,552.52	3.93
11.54	2.15E-09	5.17E-07	99.58	0.0501	1.08E-10	2.57E-08	2.15E-12	5.13E-07	238,478.69	5.38
11.54	4.58E-09	5.17E-07	99.11	0.0501	2.29E-10	2.56E-08	4.58E-12	5.10E-07	111,550.02	5.05

Appendix 8.3c Eu adsorption onto goethite (Figure 8.6)

pH	[Eu]/M	%uptake	mass Fe	mols (aq)	mols (solid)	mols/ml	mols/g	K_d (ml/g)	log K_d
Start	4.78E-07	4.49	0.0000	2.39E-08	0	4.57E-10	0	0.00	
3.51	4.61E-07	3.53	0.0502	2.31E-08	8.34E-10	4.61E-10	1.66E-08	36.02	1.56
3.51	4.80E-07	-0.36	0.0502	2.40E-08	-9.72E-11	4.80E-10	-1.94E-09	-4.04	
7.01	9.73E-09	97.97	0.0510	4.86E-10	2.34E-08	9.73E-12	4.59E-07	47198.45	4.67
7.01	9.94E-09	97.92	0.0510	4.97E-10	2.34E-08	9.94E-12	4.59E-07	46162.00	4.66
7.07	1.10E-08	97.70	0.0480	5.51E-10	2.33E-08	1.10E-11	4.86E-07	44131.80	4.64
7.07	1.23E-08	97.43	0.0480	6.15E-10	2.33E-08	1.23E-11	4.85E-07	39451.82	4.60
6.9	1.07E-08	97.76	0.0509	5.35E-10	2.34E-08	1.07E-11	4.59E-07	42892.95	4.63
6.9	1.15E-08	97.59	0.0509	5.76E-10	2.33E-08	1.15E-11	4.58E-07	39803.00	4.60
7.72	3.62E-09	99.24	0.0515	1.81E-10	2.37E-08	3.62E-12	4.61E-07	127069.91	5.10
7.72	3.83E-09	99.20	0.0515	1.91E-10	2.37E-08	3.83E-12	4.60E-07	120230.89	5.08
9.87	1.62E-08	96.61	0.0510	8.11E-10	2.31E-08	1.62E-11	4.53E-07	27928.03	4.45
9.87	1.71E-08	96.41	0.0510	8.57E-10	2.30E-08	1.71E-11	4.52E-07	26345.21	4.42

10.38	3.25E-08	93.20	0.0525	1.63E-09	2.23E-08	3.25E-11	4.24E-07	13037.54	4.12
10.38	3.48E-08	92.72	0.0525	1.74E-09	2.22E-08	3.48E-11	4.22E-07	12127.61	4.08
10.81	1.95E-08	95.93	0.0500	9.73E-10	2.29E-08	1.95E-11	4.59E-07	23561.60	4.37
10.81	1.96E-08	95.90	0.0500	9.80E-10	2.29E-08	1.96E-11	4.58E-07	23395.13	4.37

Appendix 8.4a Nd adsorption to goethite between pH 2 and 10 in 1mM $CaCl_2$ solution (Figure 8.7)

pH	[Nd]/M	% Uptake	mass goethite/g	mols(aq)	mols(solid)	mols/ml	mols/g	Kd(ml/g)	log K_d
Start	6.16E-08	0.00	0.0000	3.08E-09	0.00E+00	6.16E-11	0	0	
5.52	2.42E-08	60.73	0.0552	1.21E-09	1.87E-09	2.42E-11	3.39E-08	1,400.99	3.15
5.52	2.50E-08	59.39	0.0552	1.25E-09	1.83E-09	2.50E-11	3.31E-08	1,324.85	3.12
5.59	2.51E-08	59.32	0.0504	1.25E-09	1.83E-09	2.51E-11	3.63E-08	1,446.58	3.16
5.59	2.65E-08	56.92	0.0504	1.33E-09	1.75E-09	2.65E-11	3.48E-08	1,310.70	3.12
6.96	1.10E-08	82.17	0.0485	5.49E-10	2.53E-09	1.10E-11	5.22E-08	4,749.68	3.68
6.96	1.09E-08	82.25	0.0485	5.47E-10	2.53E-09	1.09E-11	5.22E-08	4,775.61	3.68
7.05	1.80E-08	70.79	0.0489	9.00E-10	2.18E-09	1.80E-11	4.46E-08	2,478.20	3.39
7.05	1.73E-08	71.88	0.0489	8.66E-10	2.21E-09	1.73E-11	4.53E-08	2,613.94	3.42
6.57	3.30E-09	94.65	0.0552	1.65E-10	2.92E-09	3.30E-12	5.28E-08	16,022.84	4.20
6.57	3.30E-09	94.64	0.0552	1.65E-10	2.91E-09	3.30E-12	5.28E-08	16,002.23	4.20
7.03	7.04E-09	88.57	0.0493	3.52E-10	2.73E-09	7.04E-12	5.53E-08	7,861.62	3.90
7.03	7.78E-09	87.37	0.0493	3.89E-10	2.69E-09	7.78E-12	5.46E-08	7,018.57	3.85
7.66	3.14E-09	94.90	0.0556	1.57E-10	2.92E-09	3.14E-12	5.26E-08	16,724.03	4.22
7.66	2.77E-09	95.51	0.0556	1.38E-10	2.94E-09	2.77E-12	5.29E-08	19,123.46	4.28
7.09	4.86E-09	92.11	0.0526	2.43E-10	2.84E-09	4.86E-12	5.39E-08	11,093.29	4.05
7.09	4.25E-09	93.09	0.0526	2.13E-10	2.87E-09	4.25E-12	5.45E-08	12,812.39	4.11
7.93	5.52E-09	91.04	0.0504	2.76E-10	2.80E-09	5.52E-12	5.56E-08	10,075.61	4.00
7.93	6.08E-09	90.12	0.0504	3.04E-10	2.78E-09	6.08E-12	5.51E-08	9,051.69	3.96
7.37	5.44E-09	91.16	0.0521	2.72E-10	2.81E-09	5.44E-12	5.39E-08	9,899.88	4.00
7.37	5.43E-09	91.18	0.0521	2.72E-10	2.81E-09	5.43E-12	5.39E-08	9,921.91	4.00
9.53	2.94E-09	95.23	0.0532	1.47E-10	2.93E-09	2.94E-12	5.51E-08	18,763.20	4.27
9.53	3.23E-09	94.76	0.0532	1.61E-10	2.92E-09	3.23E-12	5.49E-08	17,009.47	4.23

9.84	3.72E-09	93.96	0.0548	1.86E-10	2.89E-09	3.72E-12	5.28E-08	14,183.24	4.15
9.84	3.64E-09	94.09	0.0548	1.82E-10	2.90E-09	3.64E-12	5.29E-08	14,527.08	4.16
10.65	2.75E-08	55.33	0.0519	1.38E-09	1.70E-09	2.75E-11	3.28E-08	1,193.37	3.08
10.65	2.71E-08	55.99	0.0519	1.36E-09	1.72E-09	2.71E-11	3.32E-08	1,225.50	3.09
10.71	1.06E-09	98.28	0.0528	5.29E-11	3.03E-09	1.06E-12	5.73E-08	54,162.35	4.73
10.71	1.06E-09	98.29	0.0528	5.28E-11	3.03E-09	1.06E-12	5.73E-08	54,335.41	4.74
11.15	4.31E-09	93.00	0.0497	2.15E-10	2.86E-09	4.31E-12	5.76E-08	13,375.56	4.13
11.15	1.22E-08	80.15	0.0497	6.11E-10	2.47E-09	1.22E-11	4.97E-08	4,062.85	3.61
11.31	1.40E-08	77.25	0.0516	7.01E-10	2.38E-09	1.40E-11	4.61E-08	3,289.93	3.52
11.31	1.40E-08	77.30	0.0516	6.99E-10	2.38E-09	1.40E-11	4.61E-08	3,299.94	3.52

Appendix 8.4b Nd adsorption to goethite in 1mM $CaCl_2$ solution (Figure 8.7)

pH	[Nd]/M	Start	% Uptake	mass goethite/g	mols(aq)	mols(solid)	mols/ml	mols/g	Kd(ml/g)	log Kd
Start	6.34E-07	6.34E-07	0.00	0.0000	3.17E-08	0	6.34E-10	0	0	
4.35	6.24E-07	6.34E-07	1.53	0.0497	3.12E-08	4.87E-10	6.24E-10	9.80E-09	15.71	1.20
4.35	6.18E-07	6.34E-07	2.53	0.0497	3.09E-08	8.04E-10	6.18E-10	1.62E-08	26.17	1.42
5.18	3.74E-07	6.34E-07	40.94	0.0483	1.87E-08	1.30E-08	3.74E-10	2.69E-07	717.69	2.86
5.18	3.73E-07	6.34E-07	41.15	0.0483	1.87E-08	1.30E-08	3.73E-10	2.70E-07	723.88	2.86
6.34	1.06E-08	6.34E-07	98.33	0.0495	5.28E-10	3.12E-08	1.06E-11	6.30E-07	59657.63	4.78
6.34	1.04E-08	6.34E-07	98.36	0.0495	5.20E-10	3.12E-08	1.04E-11	6.30E-07	60576.32	4.78
6.91	6.66E-09	6.34E-07	98.95	0.0511	3.33E-10	3.14E-08	6.66E-12	6.14E-07	92133.32	4.96
6.91	6.42E-09	6.34E-07	98.99	0.0511	3.21E-10	3.14E-08	6.42E-12	6.14E-07	95585.15	4.98
7.18	8.52E-09	6.34E-07	98.66	0.0505	4.26E-10	3.13E-08	8.52E-12	6.19E-07	72655.45	4.86
7.18	8.41E-09	6.34E-07	98.67	0.0505	4.20E-10	3.13E-08	8.41E-12	6.19E-07	73686.62	4.87
7.30	1.57E-08	6.34E-07	97.52	0.0517	7.86E-10	3.09E-08	1.57E-11	5.98E-07	38054.04	4.58
7.30	1.58E-08	6.34E-07	97.50	0.0517	7.92E-10	3.09E-08	1.58E-11	5.98E-07	37748.14	4.58
10.37	1.56E-08	6.34E-07	97.54	0.0504	7.81E-10	3.09E-08	1.56E-11	6.13E-07	39265.47	4.59
10.37	1.49E-08	6.34E-07	97.65	0.0504	7.45E-10	3.10E-08	1.49E-11	6.14E-07	41198.34	4.61
10.73	2.42E-09	6.34E-07	99.62	0.0518	1.21E-10	3.16E-08	2.42E-12	6.10E-07	252224.18	5.40
10.73	2.51E-09	6.34E-07	99.60	0.0518	1.25E-10	3.16E-08	2.51E-12	6.10E-07	242930.92	5.39

Appendix 8.4c Nd adsorption to goethite in 10mM $CaCl_2$ solution (Figure 8.7)

pH	[Nd]/M	Start	% Uptake	mass goethite/g	mols(aq)	mols(solid)	mols/ml	mols/g	Kd(ml/g)	log Kd
Start	6.98E-07	6.98E-07	0.00	0.0000	3.49E-08	0	7.0E-10	0	0	
4.75	6.94E-07	6.98E-07	0.51	0.0506	3.47E-08	1.78E-10	6.9E-10	3.52E-09	5.07	0.71
6.28	2.36E-08	6.98E-07	96.61	0.0502	1.18E-09	3.37E-08	2.4E-11	6.72E-07	28,408.38	4.45
6.28	2.40E-08	6.98E-07	96.56	0.0502	1.20E-09	3.37E-08	2.4E-11	6.71E-07	27,969.18	4.45
7.16	1.74E-08	6.98E-07	97.50	0.0489	8.72E-10	3.40E-08	1.7E-11	6.96E-07	39,915.28	4.60
7.16	1.88E-08	6.98E-07	97.31	0.0489	9.38E-10	3.40E-08	1.9E-11	6.95E-07	37,001.03	4.57
7.01	2.30E-07	6.98E-07	67.10	0.0506	1.15E-08	2.34E-08	2.3E-10	4.63E-07	2,014.98	3.30
7.01	2.27E-07	6.98E-07	67.47	0.0506	1.14E-08	2.35E-08	2.3E-10	4.65E-07	2,049.48	3.31
7.49	2.05E-08	6.98E-07	97.06	0.0495	1.03E-09	3.39E-08	2.1E-11	6.84E-07	33,354.85	4.52
7.49	1.97E-08	6.98E-07	97.17	0.0495	9.87E-10	3.39E-08	2.0E-11	6.85E-07	34,693.46	4.54
10.42	6.91E-09	6.98E-07	99.01	0.0516	3.45E-10	3.46E-08	6.9E-12	6.70E-07	96,975.91	4.99
10.42	7.83E-09	6.98E-07	98.88	0.0516	3.92E-10	3.45E-08	7.8E-12	6.69E-07	85,388.55	4.93
10.65	2.68E-09	6.98E-07	99.62	0.0485	1.34E-10	3.48E-08	2.7E-12	7.17E-07	267,027.81	5.43
10.65	2.38E-09	6.98E-07	99.66	0.0485	1.19E-10	3.48E-08	2.4E-12	7.17E-07	301,385.89	5.48

Appendix 8.4d Eu adsorption onto goethite in the presence of 1mM $CaCl_2$ solution (Figure 8.7)

pH	[Eu]/M	% uptake	mass Fe	mols (aq)	mols (solid)	mols/ml	mols/g	Kd (ml/g)	log K_d
Start	5.17E-07	0	0	2.39E-08	0	5.02E-10	0	0.00	
4.34	9.62E-09	98.14	0.0486	4.81E-10	2.34E-08	9.62E-12	4.82E-07	50080.34	4.70
4.34	9.33E-09	98.19	0.0486	4.66E-10	2.34E-08	9.33E-12	4.82E-07	51681.44	4.71
6.69	4.65E-09	99.10	0.0500	2.32E-10	2.37E-08	4.65E-12	4.73E-07	101817.36	5.01
6.69	4.80E-09	99.07	0.0500	2.40E-10	2.37E-08	4.80E-12	4.73E-07	98560.11	4.99
6.7	4.83E-09	99.07	0.0511	2.42E-10	2.37E-08	4.83E-12	4.63E-07	95815.56	4.98
6.7	4.72E-09	99.09	0.0511	2.36E-10	2.37E-08	4.72E-12	4.63E-07	98204.01	4.99
7.26	5.33E-09	98.97	0.0492	2.67E-10	2.36E-08	5.33E-12	4.80E-07	90064.37	4.95
7.26	5.51E-09	98.93	0.0492	2.76E-10	2.36E-08	5.51E-12	4.80E-07	87107.77	4.94
10.29	2.81E-09	99.46	0.0494	1.41E-10	2.38E-08	2.81E-12	4.81E-07	171041.89	5.23

10.29	6.96E-09	98.65	0.0494	3.48E-10	2.36E-08	6.96E-12	4.77E-07	68483.61	4.84
10.73	2.82E-09	99.46	0.0510	1.41E-10	2.38E-08	2.82E-12	4.66E-07	165438.59	5.22
10.73	2.77E-09	99.46	0.0510	1.39E-10	2.38E-08	2.77E-12	4.66E-07	167918.21	5.23

Appendix 8.4e Eu adsorption onto goethite in the presence of 10mM $CaCl_2$ solution (Figure 8.7)

pH	[Eu]/M	% uptake	mass Fe	mols (aq)	mols (solid)	mols/ml	mols/g	Kd (ml/g)	log K_d
Start	5.71E-07	0	0	2.39E-08	0	5.51E-10	0	0.00	
6.32	7.38E-09	98.71	0.0487	3.69E-10	2.35E-08	7.38E-12	4.83E-07	65480.84	4.82
6.32	7.44E-09	98.70	0.0487	3.72E-10	2.35E-08	7.44E-12	4.83E-07	64967.93	4.81
6.91	4.77E-09	99.16	0.0513	2.38E-10	2.37E-08	4.77E-12	4.61E-07	96746.88	4.99
6.61	5.28E-09	99.08	0.0513	2.64E-10	2.36E-08	5.28E-12	4.61E-07	87315.70	4.94
6.74	6.60E-09	98.84	0.0519	3.30E-10	2.36E-08	6.60E-12	4.54E-07	68841.92	4.84
6.74	6.81E-09	98.81	0.0519	3.41E-10	2.36E-08	6.81E-12	4.54E-07	66612.49	4.82
6.94	3.73E-09	99.35	0.0497	1.86E-10	2.37E-08	3.73E-12	4.77E-07	128019.41	5.11
6.94	5.96E-09	98.96	0.0497	2.98E-10	2.36E-08	5.96E-12	4.75E-07	79638.92	4.90
7.88	4.27E-09	99.25	0.0504	2.13E-10	2.37E-08	4.27E-12	4.70E-07	110149.52	5.04
7.88	4.76E-09	99.17	0.0504	2.38E-10	2.37E-08	4.76E-12	4.69E-07	98633.78	4.99
10.02	3.74E-09	99.34	0.0496	1.87E-10	2.37E-08	3.74E-12	4.78E-07	127675.89	5.11
10.02	4.20E-09	99.26	0.0496	2.10E-10	2.37E-08	4.20E-12	4.78E-07	113630.47	5.06
10.74	3.96E-09	99.31	0.0484	1.98E-10	2.37E-08	3.96E-12	4.90E-07	123668.61	5.09
10.74	4.43E-09	99.22	0.0484	2.21E-10	2.37E-08	4.43E-12	4.89E-07	110464.00	5.04

Appendix 8.5a Nd adsorption to goethite between pH 2 and 10 in 0.1mM $KHCO_3$ solution (Figure 8.8)

pH	[Nd]	% Uptake	mass goethite /g	mols(aq)	mols(solid)	mols/ml	mols/g	Kd(ml/g)	log Kd
Start	2.78E-07	0.0	0.0	1.39E-08	0	2.78E-10	0	0	
6.25	2.67E-08	90.37	0.050	1.34E-09	1.25E-08	2.67E-11	2.52E-07	9,444.88	3.98
6.25	2.43E-08	91.23	0.050	1.22E-09	1.27E-08	2.43E-11	2.55E-07	10,465.30	4.02
7.39	4.82E-09	98.26	0.050	2.41E-10	1.36E-08	4.82E-12	2.71E-07	56,226.42	4.75
7.39	5.02E-09	98.19	0.050	2.51E-10	1.36E-08	5.02E-12	2.71E-07	54,008.52	4.73

7.41	8.50E-09	96.94	0.050	4.25E-10	1.35E-08	8.50E-12	2.70E-07	31,800.64	4.50
7.41	8.19E-09	97.05	0.050	4.09E-10	1.35E-08	8.19E-12	2.70E-07	33,039.45	4.52
7.65	5.79E-09	97.91	0.051	2.90E-10	1.36E-08	5.79E-12	2.67E-07	46,111.88	4.66
7.65	5.47E-09	98.03	0.051	2.73E-10	1.36E-08	5.47E-12	2.67E-07	48,910.47	4.69
7.64	1.04E-08	96.24	0.048	5.22E-10	1.34E-08	1.04E-11	2.76E-07	26,425.82	4.42
7.64	1.12E-08	95.95	0.048	5.62E-10	1.33E-08	1.12E-11	2.75E-07	24,458.82	4.39
7.56	1.68E-09	99.39	0.052	8.41E-11	1.38E-08	1.68E-12	2.67E-07	158,954.16	5.20
7.56	1.74E-09	99.37	0.052	8.68E-11	1.38E-08	1.74E-12	2.67E-07	153,931.79	5.19
7.82	3.42E-09	98.77	0.051	1.71E-10	1.37E-08	3.42E-12	2.67E-07	77,875.24	4.89
7.82	3.36E-09	98.79	0.051	1.68E-10	1.37E-08	3.36E-12	2.67E-07	79,423.06	4.90
8.30	3.16E-09	98.86	0.049	1.58E-10	1.37E-08	3.16E-12	2.79E-07	88,338.49	4.95
8.30	3.39E-09	98.78	0.049	1.70E-10	1.37E-08	3.39E-12	2.79E-07	82,291.83	4.92
9.49	1.32E-08	95.24	0.049	6.61E-10	1.32E-08	1.32E-11	2.69E-07	20,329.16	4.31
9.49	1.34E-08	95.19	0.049	6.68E-10	1.32E-08	1.34E-11	2.69E-07	20,094.88	4.30
10.35	1.33E-07	52.08	0.050	6.65E-09	7.23E-09	1.33E-10	1.46E-07	1,095.73	3.04
10.35	1.31E-07	52.67	0.050	6.57E-09	7.31E-09	1.31E-10	1.47E-07	1,121.93	3.05
10.72	1.45E-08	94.77	0.050	7.26E-10	1.32E-08	1.45E-11	2.63E-07	18,120.43	4.26
10.72	1.49E-08	94.62	0.050	7.47E-10	1.31E-08	1.49E-11	2.63E-07	17,572.06	4.24
11.09	5.73E-09	97.94	0.051	2.86E-10	1.36E-08	5.73E-12	2.68E-07	46,805.67	4.67
11.09	5.72E-09	97.94	0.051	2.86E-10	1.36E-08	5.72E-12	2.68E-07	46,857.57	4.67

Appendix 8.5b Nd adsorption to goethite between pH 2 and 10 in 1mM $KHCO_3$ solution (Figure 8.8)

pH	[Nd]/M	% Uptake	mass goethite/g	mols(aq)	mols(solid)	mols/ml	mols/g	Kd(ml/g)	log Kd
Start	3.44E-07	0.00	0	1.72E-08	0	3.44E-10	0	0	
7.33	3.78E-09	98.64	0.0506	1.89E-10	1.70E-08	3.78E-12	3.36E-07	89050.87	4.95
7.33	3.93E-09	98.59	0.0506	1.96E-10	1.70E-08	3.93E-12	3.36E-07	85597.29	4.93
7.31	1.86E-09	99.33	0.0499	9.29E-11	1.71E-08	1.86E-12	3.43E-07	184499.24	5.27
7.31	1.68E-09	99.39	0.0499	8.40E-11	1.71E-08	1.68E-12	3.43E-07	204199.02	5.31
8.04	2.09E-09	99.25	0.0487	1.04E-10	1.71E-08	2.09E-12	3.51E-07	168061.67	5.23
8.04	1.58E-09	99.43	0.0487	7.91E-11	1.71E-08	1.58E-12	3.52E-07	222299.65	5.35
8.03	1.13E-08	95.92	0.0501	5.67E-10	1.66E-08	1.13E-11	3.32E-07	29291.17	4.47

8.03	1.10E-08	96.03	0.0501	5.52E-10	1.66E-08	1.10E-11	3.32E-07	30121.30	4.48
8.10	3.07E-09	98.89	0.0521	1.54E-10	1.70E-08	3.07E-12	3.27E-07	106479.83	5.03
8.10	3.35E-09	98.79	0.0521	1.67E-10	1.70E-08	3.35E-12	3.27E-07	97729.33	4.99
8.19	1.64E-09	99.41	0.0490	8.21E-11	1.71E-08	1.64E-12	3.49E-07	212804.03	5.33
8.19	1.55E-09	99.44	0.0490	7.75E-11	1.71E-08	1.55E-12	3.49E-07	225412.11	5.35
8.48	2.24E-09	99.19	0.0490	1.12E-10	1.71E-08	2.24E-12	3.49E-07	155481.70	5.19
8.48	2.32E-09	99.16	0.0490	1.16E-10	1.71E-08	2.32E-12	3.49E-07	150108.69	5.18
8.64	1.79E-09	99.36	0.0484	8.94E-11	1.71E-08	1.79E-12	3.54E-07	197800.16	5.30
8.64	1.64E-09	99.41	0.0484	8.19E-11	1.71E-08	1.64E-12	3.54E-07	215862.61	5.33
9.45	8.68E-09	96.87	0.0497	4.34E-10	1.68E-08	8.68E-12	3.37E-07	38880.60	4.59
9.45	8.74E-09	96.85	0.0497	4.37E-10	1.68E-08	8.74E-12	3.37E-07	38599.64	4.59
9.41	3.41E-09	98.77	0.0506	1.71E-10	1.70E-08	3.41E-12	3.37E-07	98585.63	4.99
9.41	3.74E-09	98.65	0.0506	1.87E-10	1.70E-08	3.74E-12	3.36E-07	90020.51	4.95
10.37	2.89E-08	89.59	0.0487	1.44E-09	1.58E-08	2.89E-11	3.24E-07	11194.27	4.05
10.37	5.74E-08	79.34	0.0487	2.87E-09	1.43E-08	5.74E-11	2.94E-07	5130.94	3.71
10.79	5.11E-08	81.59	0.0506	2.56E-09	1.46E-08	5.11E-11	2.89E-07	5662.70	3.75
10.79	4.85E-08	82.54	0.0506	2.42E-09	1.48E-08	4.85E-11	2.92E-07	6023.64	3.78
11.26	3.61E-08	87.00	0.0509	1.80E-09	1.54E-08	3.61E-11	3.02E-07	8384.73	3.92
11.26	3.74E-08	86.52	0.0509	1.87E-09	1.53E-08	3.74E-11	3.01E-07	8046.17	3.91
11.16	1.15E-08	95.87	0.0486	5.73E-10	1.66E-08	1.15E-11	3.42E-07	29853.21	4.47
11.16	1.14E-08	95.88	0.0486	5.71E-10	1.66E-08	1.14E-11	3.42E-07	29938.68	4.48

Appendix 8.5c Nd adsorption to goethite between pH 2 and 10 in 10mM $KHCO_3$ solution (Figure 8.8)

pH	[Nd]	% Uptake	mass goethite /g	mols(aq)	mols(solid)	mols/ml	mols/g	Kd(ml/g)	log Kd
Start	4.12E-07	0.0	0.0000	2.06E-08	0	4.12E-10	0		
6.93	2.42E-09	99.41	0.0490	1.21E-10	2.05E-08	2.42E-12	4.18E-07	172,793.47	5.24
6.93	2.51E-09	99.39	0.0490	1.26E-10	2.05E-08	2.51E-12	4.18E-07	166,156.52	5.22
6.03	2.25E-08	94.55	0.0495	1.12E-09	1.95E-08	2.25E-11	3.93E-07	17,509.20	4.24
6.03	2.12E-08	94.86	0.0495	1.06E-09	1.95E-08	2.12E-11	3.95E-07	18,634.44	4.27
8.51	2.76E-09	99.33	0.0517	1.38E-10	2.05E-08	2.76E-12	3.96E-07	143,543.52	5.16
8.51	2.29E-09	99.44	0.0517	1.15E-10	2.05E-08	2.29E-12	3.96E-07	172,908.68	5.24

7.60	9.97E-09	97.58	0.0521	4.99E-10	2.01E-08	9.97E-12	3.86E-07	38,691.23	4.59
7.60	1.05E-08	97.45	0.0521	5.26E-10	2.01E-08	1.05E-11	3.85E-07	36,618.66	4.56
8.00	2.70E-09	99.34	0.0520	1.35E-10	2.05E-08	2.70E-12	3.94E-07	145,781.14	5.16
8.00	2.71E-09	99.34	0.0520	1.36E-10	2.05E-08	2.71E-12	3.93E-07	145,017.98	5.16
8.27	1.67E-09	99.59	0.0515	8.37E-11	2.05E-08	1.67E-12	3.98E-07	237,906.82	5.38
8.27	1.90E-09	99.54	0.0515	9.48E-11	2.05E-08	1.90E-12	3.98E-07	209,941.94	5.32
8.64	3.51E-09	99.15	0.0498	1.76E-10	2.04E-08	3.51E-12	4.10E-07	116,692.17	5.07
8.64	4.12E-09	99.00	0.0498	2.06E-10	2.04E-08	4.12E-12	4.09E-07	99,335.00	5.00
8.78	1.27E-07	69.06	0.0486	6.37E-09	1.42E-08	1.27E-10	2.93E-07	2,296.92	3.36
8.78	1.26E-07	69.38	0.0486	6.31E-09	1.43E-08	1.26E-10	2.94E-07	2,331.06	3.37
9.12	2.26E-08	94.52	0.0502	1.13E-09	1.95E-08	2.26E-11	3.88E-07	17,194.09	4.24
9.12	2.20E-08	94.66	0.0502	1.10E-09	1.95E-08	2.20E-11	3.88E-07	17,641.54	4.25
9.27	3.37E-09	99.18	0.0501	1.68E-10	2.04E-08	3.37E-12	4.08E-07	121,079.26	5.08
9.27	2.97E-09	99.28	0.0501	1.49E-10	2.04E-08	2.97E-12	4.08E-07	137,332.11	5.14
10.04	1.13E-08	97.27	0.0485	5.63E-10	2.00E-08	1.13E-11	4.13E-07	36,709.85	4.56
10.04	9.85E-09	97.61	0.0485	4.93E-10	2.01E-08	9.85E-12	4.15E-07	42,082.36	4.62
10.07	3.78E-09	99.08	0.0517	1.89E-10	2.04E-08	3.78E-12	3.95E-07	104,561.48	5.02
10.07	3.21E-09	99.22	0.0517	1.61E-10	2.04E-08	3.21E-12	3.95E-07	123,045.95	5.09
10.93	7.66E-10	99.81	0.0519	3.83E-11	2.06E-08	7.66E-13	3.96E-07	517,351.49	5.71
10.93	4.17E-10	99.90	0.0519	2.08E-11	2.06E-08	4.17E-13	3.96E-07	951,270.69	5.98
10.87	6.32E-09	98.46	0.0488	3.16E-10	2.03E-08	6.32E-12	4.16E-07	65,718.20	4.82
10.87	6.32E-09	98.47	0.0488	3.16E-10	2.03E-08	6.32E-12	4.16E-07	65,751.57	4.82

Appendix 8.5d Nd adsorption to goethite between pH 2 and 10 in1mM K_2SO_4 solution (Figure 8.8)

pH	[Nd]/M	Start	% Uptake	mass goethite /g	mols(aq)	mols(solid)	mols/ml	mols/g	Kd(ml/g)	log Kd
Start	5.70E-07	5.70E-07	0.00	0.000	2.85E-08	0.00	5.70E-10	0.00	0.00	
4.69	5.54E-07	5.70E-07	2.85	0.049	2.77E-08	5.42E-07	5.54E-10	1.12E-05	20148.26	4.30
4.69	5.46E-07	5.70E-07	4.23	0.049	2.73E-08	5.43E-07	5.46E-10	1.12E-05	20453.23	4.31
3.83	6.59E-08	5.70E-07	88.44	0.050	3.30E-09	5.67E-07	6.59E-11	1.13E-05	170940.24	5.23
3.83	7.85E-08	5.70E-07	86.23	0.050	3.92E-09	5.66E-07	7.85E-11	1.13E-05	143374.53	5.16
6.55	1.34E-08	5.70E-07	97.65	0.050	6.71E-10	5.69E-07	1.34E-11	1.14E-05	850552.19	5.93

6.55	1.07E-08	5.70E-07	98.12	0.050	5.37E-10	5.69E-07	1.07E-11	1.14E-05	1063069.36	6.03
6.58	1.20E-08	5.70E-07	97.90	0.050	6.00E-10	5.69E-07	1.20E-11	1.14E-05	951434.61	5.98
6.58	1.21E-08	5.70E-07	97.87	0.050	6.06E-10	5.69E-07	1.21E-11	1.14E-05	941249.92	5.97
7.07	1.81E-08	5.70E-07	96.83	0.049	9.03E-10	5.69E-07	1.81E-11	1.17E-05	645851.88	5.81
7.07	1.69E-08	5.70E-07	97.04	0.049	8.44E-10	5.69E-07	1.69E-11	1.17E-05	690616.49	5.84
7.02	3.82E-08	5.70E-07	93.30	0.050	1.91E-09	5.68E-07	3.82E-11	1.13E-05	296792.00	5.47
7.02	1.40E-07	5.70E-07	75.36	0.050	7.02E-09	5.63E-07	1.40E-10	1.12E-05	80008.32	4.90
6.93	5.62E-09	5.70E-07	99.01	0.050	2.81E-10	5.70E-07	5.62E-12	1.13E-05	2017975.63	6.30
6.93	5.58E-09	5.70E-07	99.02	0.050	2.79E-10	5.70E-07	5.58E-12	1.13E-05	2032695.14	6.31
6.99	1.54E-08	5.70E-07	97.30	0.051	7.70E-10	5.69E-07	1.54E-11	1.12E-05	729388.16	5.86
6.99	1.60E-08	5.70E-07	97.20	0.051	7.99E-10	5.69E-07	1.60E-11	1.12E-05	702663.11	5.85
7.13	1.29E-08	5.70E-07	97.73	0.050	6.47E-10	5.69E-07	1.29E-11	1.13E-05	872722.66	5.94
7.13	1.21E-08	5.70E-07	97.88	0.050	6.05E-10	5.69E-07	1.21E-11	1.13E-05	934258.39	5.97
7.24	5.92E-09	5.70E-07	98.96	0.050	2.96E-10	5.70E-07	5.92E-12	1.14E-05	1930803.16	6.29
7.24	6.08E-09	5.70E-07	98.93	0.050	3.04E-10	5.70E-07	6.08E-12	1.14E-05	1880178.45	6.27
7.72	7.08E-09	5.70E-07	98.76	0.050	3.54E-10	5.70E-07	7.08E-12	1.15E-05	1623283.31	6.21
7.72	6.95E-09	5.70E-07	98.78	0.050	3.47E-10	5.70E-07	6.95E-12	1.15E-05	1652918.10	6.22
9.17	9.00E-09	5.70E-07	98.42	0.051	4.50E-10	5.70E-07	9.00E-12	1.11E-05	1233992.53	6.09
9.17	8.84E-09	5.70E-07	98.45	0.051	4.42E-10	5.70E-07	8.84E-12	1.11E-05	1256393.34	6.10
10.79	3.55E-08	5.70E-07	93.77	0.051	1.77E-09	5.68E-07	3.55E-11	1.12E-05	315830.15	5.50
10.79	3.45E-08	5.70E-07	93.95	0.051	1.72E-09	5.68E-07	3.45E-11	1.12E-05	325202.13	5.51
10.79	2.70E-08	5.70E-07	95.27	0.051	1.35E-09	5.69E-07	2.70E-11	1.11E-05	411160.64	5.61
10.79	2.54E-08	5.70E-07	95.54	0.051	1.27E-09	5.69E-07	2.54E-11	1.11E-05	436305.87	5.64
11.32	2.75E-08	5.70E-07	95.18	0.050	1.37E-09	5.69E-07	2.75E-11	1.13E-05	413198.15	5.62
11.32	2.64E-08	5.70E-07	95.37	0.050	1.32E-09	5.69E-07	2.64E-11	1.14E-05	430070.80	5.63
11.32	5.07E-08	5.70E-07	91.11	0.050	2.53E-09	5.67E-07	5.07E-11	1.14E-05	224760.48	5.35
11.32	5.03E-08	5.70E-07	91.18	0.050	2.52E-09	5.67E-07	5.03E-11	1.14E-05	226519.91	5.36
6.96	1.42E-08	5.70E-07	97.51	0.059	7.11E-10	5.69E-07	1.42E-11	9.62E-06	676556.05	5.83
6.96	1.36E-08	5.70E-07	97.62	0.059	6.78E-10	5.69E-07	1.36E-11	9.62E-06	708854.81	5.85

Appendix 8.6a Eu adsorption to goethite in the presence of 0.1mM $KHCO_3$ solution (Figure 8.9)

pH	[Eu]/M	% uptake	mass Fe	mols (aq)	mols (solid)	mols/ml	mols/g	Kd (ml/g)	log Kd
Start	3.54E-07	0	0	1.77E-08	0.00E+00	3.54E-10	0	0.00	
7.43	7.77E-09	97.80	0.0496	3.89E-10	1.73E-08	7.77E-12	3.49E-07	44913.76	4.65
7.43	7.87E-09	97.78	0.0496	3.94E-10	1.73E-08	7.87E-12	3.49E-07	44312.53	4.65
7.25	3.53E-09	99.00	0.0497	1.76E-10	1.75E-08	3.53E-12	3.53E-07	99976.20	5.00
7.25	3.92E-09	98.89	0.0497	1.96E-10	1.75E-08	3.92E-12	3.52E-07	89759.01	4.95
9.83	4.25E-09	98.80	0.0497	2.13E-10	1.75E-08	4.25E-12	3.52E-07	82745.51	4.92
9.83	4.99E-09	98.59	0.0497	2.49E-10	1.75E-08	4.99E-12	3.51E-07	70410.61	4.85
10.3	3.48E-08	90.16	0.0489	1.74E-09	1.60E-08	3.48E-11	3.26E-07	9370.93	3.97
10.3	3.71E-08	89.52	0.0489	1.85E-09	1.58E-08	3.71E-11	3.24E-07	8735.76	3.94

Appendix 8.6b Eu adsorption to goethite in the presence of 1mM $KHCO_3$ solution (Figure 8.9)

pH	[Eu]/M	%uptake	mass Fe	mols (aq)	mols (solid)	mols/ml	mols/g	Kd (ml/g)	log Kd
Start	5.36E-07	0.00	0.000	2.68E-08	0.00E+00	5.21E-10	0	0.00	
6.48	3.93E-09	99.27	0.050	1.97E-10	2.66E-08	3.93E-12	5.30E-07	134739.88	5.13
6.48	4.23E-09	99.21	0.050	2.12E-10	2.66E-08	4.23E-12	5.30E-07	125065.04	5.10
5.22	2.16E-07	59.79	0.049	1.08E-08	1.60E-08	2.16E-10	3.30E-07	1530.06	3.18
5.22	2.33E-07	56.55	0.049	1.16E-08	1.52E-08	2.33E-10	3.12E-07	1339.21	3.13
8.19	3.75E-09	99.30	0.051	1.87E-10	2.66E-08	3.75E-12	5.19E-07	138451.75	5.14
8.19	3.76E-09	99.30	0.051	1.88E-10	2.66E-08	3.76E-12	5.19E-07	138038.18	5.14
8.55	4.39E-09	99.18	0.048	2.19E-10	2.66E-08	4.39E-12	5.51E-07	125684.01	5.10
8.55	4.43E-09	99.17	0.048	2.21E-10	2.66E-08	4.43E-12	5.51E-07	124555.08	5.10
10.02	1.47E-08	97.26	0.052	7.34E-10	2.61E-08	1.47E-11	5.06E-07	34487.19	4.54
10.02	1.46E-08	97.27	0.052	7.32E-10	2.61E-08	1.46E-11	5.06E-07	34572.70	4.54
10.15	4.07E-08	92.41	0.052	2.03E-09	2.48E-08	4.07E-11	4.76E-07	11711.84	4.07
10.15	4.50E-08	91.61	0.052	2.25E-09	2.46E-08	4.50E-11	4.72E-07	10497.13	4.02

Appendix 8.6c Eu adsorption onto goethite in the presence of 10mM $KHCO_3$ solution (Figure 8.9)

pH	[Eu]/M	% uptake	mass Fe	mols (aq)	mols (solid)	mols/ml	mols/g	Kd (ml/g)	log Kd
Start	4.85E-07	0	0	2.43E-08	0	4.62E-10	0	0.00	
7.39	8.14E-09	98.32	0.0518	4.07E-10	2.38E-08	8.14E-12	4.6E-07	56530.30	4.75
7.39	1.25E-08	97.43	0.0518	6.24E-10	2.36E-08	1.25E-11	4.56E-07	36547.08	4.56
8.33	9.77E-09	97.99	0.0493	4.88E-10	2.38E-08	9.77E-12	4.82E-07	49335.56	4.69
8.33	1.03E-08	97.87	0.0493	5.17E-10	2.37E-08	1.03E-11	4.81E-07	46564.54	4.67
8.65	4.35E-09	99.10	0.0504	2.17E-10	2.40E-08	4.35E-12	4.77E-07	109722.54	5.04
8.65	5.63E-09	98.84	0.0504	2.82E-10	2.40E-08	5.63E-12	4.76E-07	84440.08	4.93
8.75	5.61E-09	98.84	0.0492	2.81E-10	2.40E-08	5.61E-12	4.87E-07	86808.54	4.94
8.75	5.67E-09	98.83	0.0492	2.84E-10	2.40E-08	5.67E-12	4.87E-07	85867.71	4.93
8.89	4.71E-09	99.03	0.0498	2.35E-10	2.40E-08	4.71E-12	4.82E-07	102427.96	5.01
8.89	4.88E-09	98.99	0.0498	2.44E-10	2.40E-08	4.88E-12	4.82E-07	98879.65	5.00
9.66	8.04E-09	98.34	0.0503	4.02E-10	2.38E-08	8.04E-12	4.74E-07	58968.54	4.77
9.66	8.58E-09	98.23	0.0503	4.29E-10	2.38E-08	8.58E-12	4.74E-07	55210.87	4.74
10.13	9.94E-09	97.95	0.0494	4.97E-10	2.38E-08	9.94E-12	4.81E-07	48360.04	4.68
10.13	1.04E-08	97.87	0.0494	5.18E-10	2.37E-08	1.04E-11	4.8E-07	46410.54	4.67

Appendix 8.7a Predicted Nd adsorption to goethite in 1mM TIC solution initial solution $[Nd(aq)]_{total}$ $5x10^{-7}$M logK 3.8, (Lee & Byrne aqueous data)

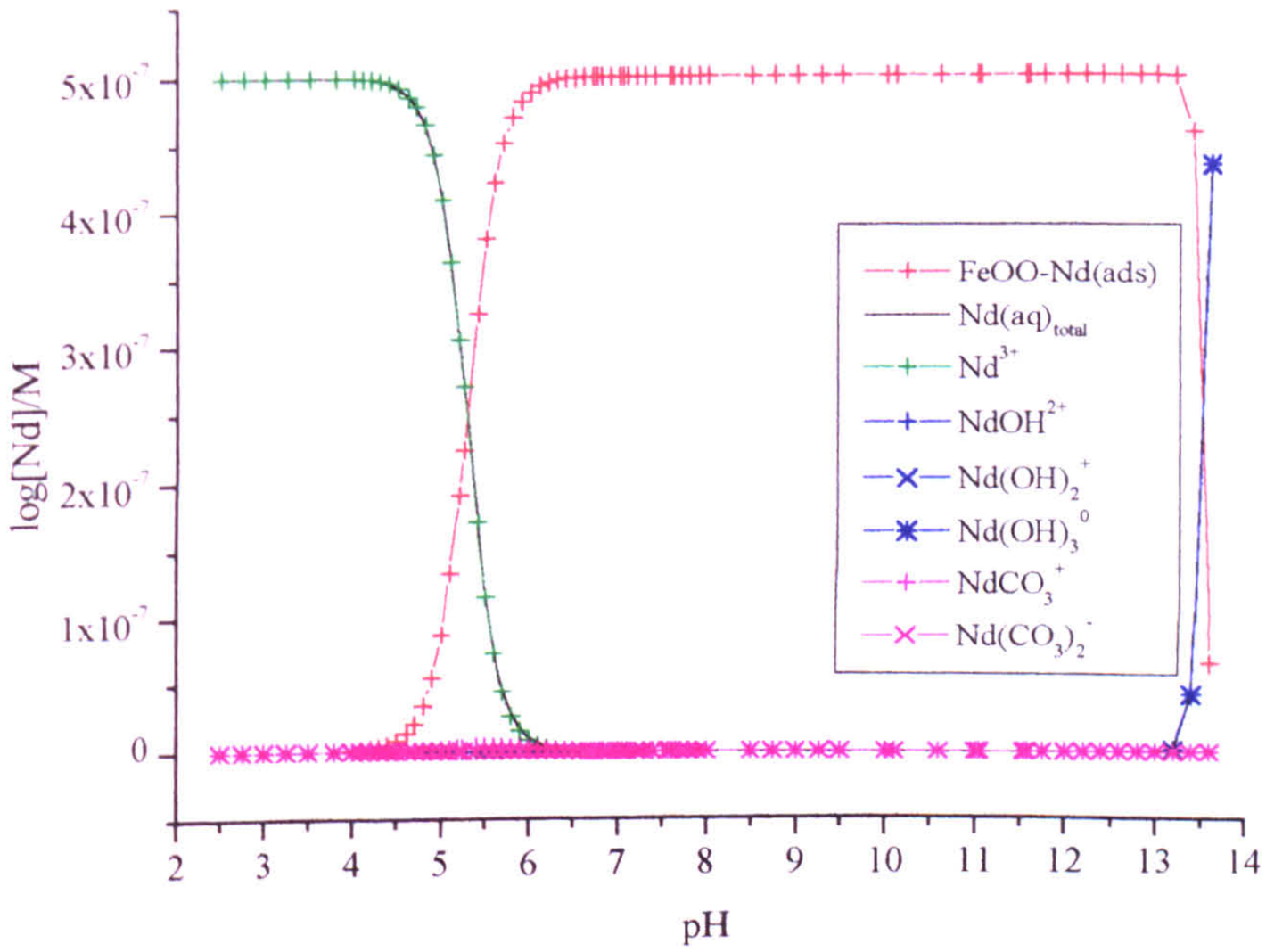

Appendix 8.7b Precited Nd adsorption to goethite in 1mM TIC solution initial solution $[Nd(aq)]_{total}$ $5x10^{-7}$M logK 3.8, (Lee & Byrne aqueous data)

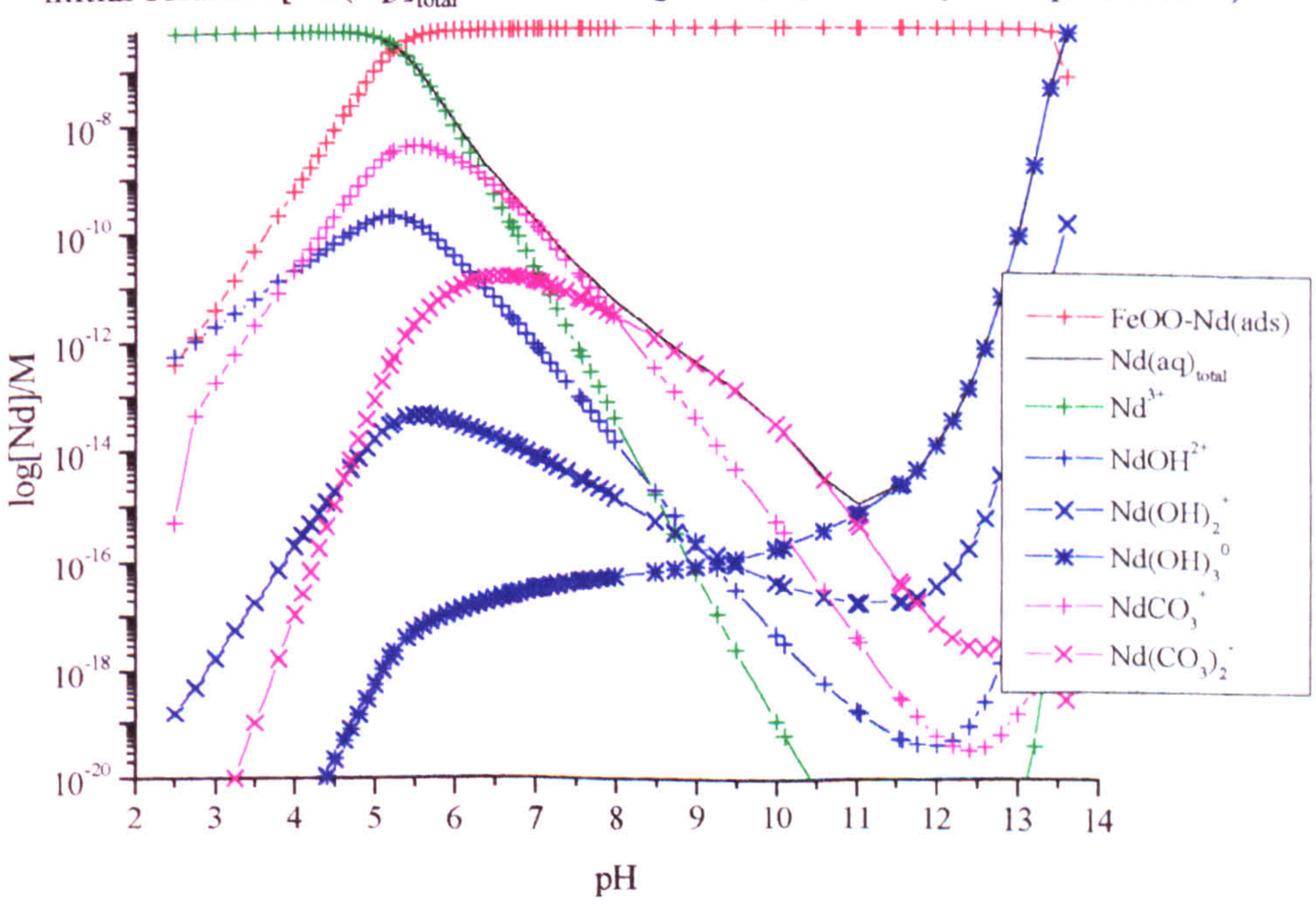

Appendix 8.8a Predicted Nd adsorption to goethite in 0.1mM TIC solution initial solution $[Nd(aq)]_{total}$ $5x10^{-7}$M logK 3.8, (Lee & Byrne aqueous data)

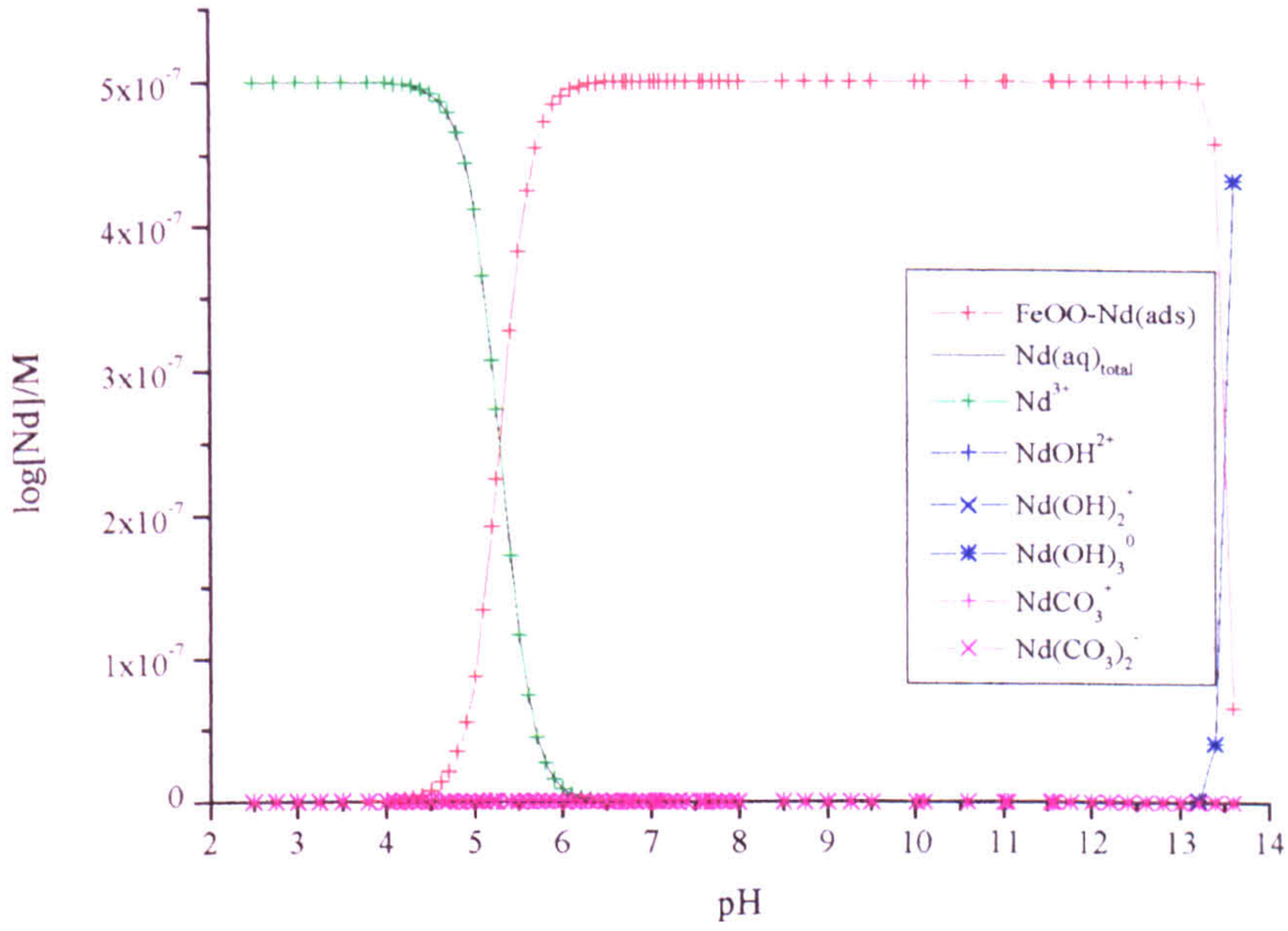

Appendix 8.8b Predicted Nd adsorption to goethite in 0.1mM TIC solution initial solution $[Nd(aq)]_{total}$ $5x10^{-7}$M logK 3.8, (Lee & Byrne aqueous data)